E8643
9/27/94

Seals Flow Code Development–93

Proceedings of a workshop
held at the NASA Lewis Research Center
Cleveland, Ohio
November 3–4, 1993

NASA

Seals Flow Code Development–93

National Aeronautics and
Space Administration

Office of Management

**Scientific and Technical
Information Program**

1994

Preface

Seals Workshop of 1993 continues to provide a forum for information exchange. The program overview presents a series of charts depicting seal configurations studied in 1993 and goals proposed for the out years while calling attention to those requesting information on the use of codes (refs. 1, 2). Codes released include:

SPIRALI - A computer code to calculate leakage and dynamics of incompressible, turbulent, plain and spiral grooved cylindrical and face seal configurations.

IFACE - A computer code to calculate leakage and dynamics of incompressible , isoviscous, face seal configurations with pockets, steps , tapers, turbulence, and cavitation.

GFACE - A computer code to calculate leakage and dynamics of laminar gas lubricated face seals with a variety of "lift pad" configurations.

SCISEAL - A CFD code for analysis of leakage, fluid dynamics for research and design of a variety of seal configurations with a capacity of extension to other classes of problems. The current SCISEAL release is limited to annular, stepped, and tapered cylindrical seals with architecture in place to expand to other seals configurations as well as other classes of problems. The code includes colocated grids higher order schemes (3 in space, 2 in time), rotating and moving grids, and turbulent models.

A description of the GUI (graphical user interface) and the executive shell illustrating features of the code usage was presented. The GUI is very important to any modern code that is to be available to and used by the general seals community and not just by the code developers. Interfacing codes is a difficult task even when the codes are developed within the same organization and requires a very carefully developed GUI to facilitate generalized usage. The GUI represents just one portion of the seals code project development plan.

Sufficient workshop time was devoted to hands on usage of both the industrial (SPIRALI, IFACE, GFACE, others) and scientific code (SCISEAL).

The impact of environmental and customer driven seal requirements was introduced at the workshop providing an initial look at a very complex engineering-social-economic problem for the (generally) customer driven aerospace and legislative driven industrial seals companies and users. Most seal companies have "zero net leak" configurations but in many cases leakage is required for lubrication, cooling, or dynamic stability and presents a major conflict. Environmental considerations, simulation codes, manufacturing, regulation, barrier fluids, aerospace related sealing, and "what's comming" rounds out the presentation.

Some of the more controversial discussions followed the seal code users report where code comparisons to seal leakages were in reasonable agreement but the dynamic data coefficients were not. Codes comparison between CSEAL (Texas A&M University) and GCYL and HSEAL (Mitsubishi) and ICYL, provides an initial look with some industry feedback. EGG (Sealol) and SPIRALG codes are in good agreement with experimental leakage data but the dynamic coefficient predictions differ.

Preceding Page Blank

Comparisons of SPIRALG (a narrow groove laminar code) to turbulent wide groove/land data did not agree. The principal investigaters agreed to iterate the problem to a solution.

NASA Lewis' brush seals program development was discussed. The program includes flow visualization, characterization of flow patterns and quantization, bench testing, T-700 (and T-55) engine testing and materials studies (optical, SEM and XDS) of both bristles and rub runners. Seals that were placed in the turbine environment survived with severe wear (as was expected) and those specifically designed for a compressor discharge seal looked very good after 20 engine hours. A simplistic method that correlates much of the brush seal flow data

$$del\ p = a\ V\ \ + \ b\ \ V**2$$

is discussed. The coefficients are based on flows through porous media.

Cryogenic (fluid nitrogen and hydrogen) seal program at NASA Lewis Research Center tested 4 different rub runner materials with Hayners 25 bristles at surface speeds to 525 fps and 300 psi drop across a 5-seal configuration. Brush spacing and number of brushes alter the leakage with perhaps 0.001 inch grooving of the rub runner. The hot gas facility (NASA/ARMY/USAF) continues to test a variety of brush, labyrinth and advanced seal configurations. Test conditions include pressures to 150 psi, temperatures to 500 F (1200 F potential) at speeds to 30 000 rpm (670 fps). Selected tours were provided to both facilities.

The ceramic seals are being developed and manufactured under contract to Technetics and show significant promise. Several bristle materials (SiC, Al2O3, SiO2), brazing and manufacturing methods were investigated. SiC bristles with metallic side washers was selected for further development under a USAF contract.

Seal companies are working with government organizations to gain testing experience and life of brush seal configuration in a T-407 engine simulation test. The merits of replacing the balance piston labyrinth seals with brush seals was investigated with mixed results. Endurance testing (seal life) with rotor runout tends to be a major problem. Brush seal design revision and new proprietary seal characteristics require investigation.

Analytical/numerical/experimental work continues to provide insights and code validation data for brush seal flows and dynamics characteristics. Work is also continuing on analysis and definition of secondary flows, pocket flow, and thermohydrodynamics of simulated cylindrical and face (bearing/seal) geometries using liquid crystal and full field flow tracking (FFFT) techniques.

The USAF brush seal development program (IHPTET- PRDA II) goals were stated as surface speeds to 900 fps temperatures to 1200 F and pressure drops to 50 psi. The brush was to provide substantially lower leakage than the labyrinth at equivalent operating life. Under PRDA III, the goals increased speed to 1400 fps, temperature to 1400 F, and pressure drops to 150 psi/stage with the brush seal providing enhanced stability. To date, over 40 seals have been tested to maximum conditions of 1200 F, 1080 fps, 60 psid, and 0.0045 inch rotor runout with excursions to 0.019 inch. Test rigs for seals to 20 inches in diameter are available. Tribological pairing and bristle relief geometries have been integrated into the program and test data are presented.

Testing and code validation for pocket and plain bearing seal geometries at Techische Universitat Braunschweig were discussed.

The use and some results from a set of codes CSTEADY and CTRANS were presented by John Crane Inc. These codes deal with face seal analyses and consider the thermohydromechanical effects in face seals, materials, asperites, and seal geometries for optimization of design including balance ratio. The code appeared expedient, fast, with a convenient GUI.

A variety of face and brush seal testing at Allison Gas Turbines was presented for wide dam face seals. Sketches of seal geometry and performance data (leakage, torque, stiffness) were discussed for three basic geometries: 8-pad Rayleigh-Step; Tapered spiral groove (3 tapers); hydrostatic, inherently (no pocket) and orifice (with pocket) compensated. Test conditions included, temperatures to 1200 F, pressures to 665 psia; and surface speeds to approximately 1000 ft/sec with a leakage goal of 10 scfm. Spiral groove and Rayleigh step seal configurations are most promising.

The USAF secondary gas path seals and mainshaft air/oil seals program was presented. The IHPTET program and testing leads to F119 engine applications. Leakage and performance goals for military engines are double thrust/weight, decrease SFC by 40 percent, decrease secondary air flow leakage by 60 percent with a 50 percent increase in mainshaft speed. Seal rotordynamics and R and D programs are presented for brush seals. Generally brushes are more than 20 percent better than labyrinth seals in the long term. Mainshaft air/oil seals programs were also presented as well as future technology needs.

GM presented a new high speed test facility capable of testing a variety of bearing and seal configurations and essentially invited customer testing.

Hypersonic engine seal characteristics are delineated (materials and geometry), leakage models cited, and test results provided illustrating good agreement between data and theory at temperatures to 1350 C and pressures to over 40 psi with and without surface motion.

New dynamic test data for spiral groove (wide lands and grooves) and smooth annular seals with eccentric operation was presented. With increasing eccentricity (e) Kxx decreases, Kyx increases, Cxx increases; whirl frequency ratio (stability indicator (WFR)) at 16 000 rpm shows little dependence on eccentricity up to e = 0.5, the testing limit.

$$Keq = (KxxCyy + KyyCxx - CyxKxy - CxyKyx)/ (Cxx + Cyy)$$

$$WFR **2 = ((Keq-Kxx)(Keq-Kyy) - KxyKyx)/((CxxCyy - CxyCyx) omeg**2)$$

The pressure measurements of a three-wave journal bearing were presented and are in good agreement with theoretical predictions. The advantage of such a bearing is its stability and enchanced load carrying capacity.

To conclude the 1993 Workshop, future activites will move toward face, lip, and some proprietary seals as low leakage with supportive dynamics. The next Seals Flow Code Development Workshop is set for Spring 1995.

1. Liang, A.D. and Hendricks, R.C.: Seals Flow Code Development - 92 , NASA CP 10124, 1992.

2. Liang, A.D. : Designing Seals with the Experts. Machine Design, Feb. 1993, pp 32 37.

TABLE OF CONTENTS

INTRODUCTION/PROGRAM OVERVIEW

Anita Liang
NASA Lewis Research Center
Cleveland, Ohio

REPORT ON NASA CONTRACT NAS3-25644
"NUMERICAL/ANALYTICAL/EXPERIMENTAL STUDY OF FLUID DYNAMIC FORCES IN SEALS"

SPONSORED BY

THE SPACE PROPULSION TECHNOLOGY DIVISION
NASA LEWIS RESEARCH CENTER

FUNDED BY

EARTH-TO-ORBIT PROPULSION PROGRAM
OFFICE OF ADVANCED CONCEPTS AND TECHNOLOGY
NASA HEADQUARTERS

CONTRACT INITIATED IN 1990

CONTRACTOR: MECHANICAL TECHNOLOGY INCORPORATED (MTI)
               LATHAM, NEW YORK

SUBCONTRACTOR: CFD RESEARCH CORPORATION (CFDRC)
                  HUNTSVILLE, ALABAMA

PROGRAM MANAGER: WILBUR SHAPIRO

PRINCIPAL INVESTIGATORS: BHARAT AGGARWAL, MTI
                         JED WALOWIT, INDEPENDENT
                         ANDRZEJ PRZEKWAS, CFDRC
                         MAHESH ATHAVALE, CFDRC

1

NASA TEAM MEMBERS

CONTRACTING OFFICER: LINDA KENDRICK
CONTRACT MANAGER: ANITA LIANG
TECHNICAL MANAGER: BOB HENDRICKS

SEALS RESEARCH: GENE ADDY
MARGARET PROCTOR
JIM WALKER

BEARINGS RESEARCH: GENE ADDY
FLORIN DIMOFTE
JIM WALKER

SYSTEM ENGINEERING: CHRIS FULTON

PEER REVIEW MEMBERS
(PRESENT AT THE WORKSHOP)

PRIT BASU, EG&G SEALOL
DARA CHILDS, TEXAS A&M
CHUCK MERKLE, PENN STATE UNIVERSITY
JOHN MINER, PRATT & WHITNEY
JOHN MUNSON, ALLISON GAS TURBINE
JOE SCHARRER, ROTORDYNAMICS-SEAL RESEARCH
BILL VOORHEES, U.S. NAVY

PAST YEAR ACTIVITIES

CODE DISSEMINATION (PC VERSION)

MACHINE DESIGN ARTICLE

PEER REVIEW COMMENTS

CONTRACT MODIFICATIONS

RELEASE OF CONFERENCE PROCEEDINGS

CODE DISSEMINATION

Prithwish Basu - EG&G Sealol
Jack Braun - University of Akron
Berci Cherpician - Torrington Company
Dan Cornell - Westinghouse
David Elrod - Sverdrup/MSFC
Carl Grala - Navy
William Fohey - Williams International
Robert Hibbs - Rocketdyne
Ralph Gabriel - Durametallics
V. Kadambi - Textron Lycoming
Roger Ku - Conner Perpherals
Richard Jones - Stein Seal
Chester Lee - Solar Turbines
Victor O'Beid - Rotor Bearing Technology
Mark Makhobey - Car-Graph Inc.
John Miner - Pratt & Whitney
Bahram Movahed - Sundstrand
A. Parmar - John Crane
Eugene Ruddy - John Crane
Norman Samurin - Dresser Rand
Peter Withers - Rolls Royce

Barry Bixler - Rolls Royce
Shou-Hao Chen - Quantum Corp
Dara Childs - Texas A&M University
Ronald Dayton - Air Force
Robert Evenson - Revovle Technologies
Alston Gu - Allied Signal Aerospace
Wes Franklin - Bentley
George Hosang - Sundstrand Power System
Harold Greiner - EG&G Sealol
Meng Kann - Ingersoll Rand
Frank Kushner - Elliott Company
John Leary - The Trane Company
Simon Leefe - BHR Group Ltd
Mike O'Brien - Textron Lycoming
Ellen Mayhew - Air Force
Vijay Modi - Columbia University
John Munson - Allison Gas Turbine
John Radford - Kardon Ring and Seal
Richard Salant - George Inst. of Tech
John Waggott - Dressler Rand
Shifeng Wu - John Crane Seal

DESIGN SEALS WITH THE EXPERTS
MACHINE DESIGN
FEBRUARY 12, 1993

Fredric Aichele - NWD Technology

Paris Altidis - Powertrain Engineering

N.K. Bhardwaj - Solar Turbines

Berci Cherpician - Torrington Corp
(Received Codes)

Ralph Gabriel - Durametallic
(Received Codes)

Eric Hao - Dorr-Oliver

Frank Olsofka - Ingersoll-Rand

Shu Peng - Parker Seal
(Received Codes)

Frank Savel - TRW Valve Division
(Cooperative efforts)

Richard Van Slooten - Praxair, Inc.

Peter Allen - Martin Marietta

Peter Amos - Advanced Products

Shuo-Hao Chen - Quantum Corp
(Received Codes)

Dan Cornell - Westinghouse
(Received Codes)

William Giesler - Allied Signal

John Leary - Trane Company
(Received Codes)

Kermit Paul - Fuller Kovako Corp

Eugene Ruddy - John Crane
(Received Codes)

Elizabeth Seidman - U of Cincinnati
(Received Literature)

CONTRACT MODIFICATIONS

TWO YEAR STRETCH

PROGRAM SCOPE REVISION

Task Description	Task Number	Fiscal Year 1993											
		O	N	D	J	F	M	A	M	J	J	A	S
Complete SPIRALI FORTRAN	9												
Install SPIRALI in OS/2 KBS	8												
Convert SPIRALG, GCYL, and ICYL to UNIX	8												
Complete IFACE FORTRAN	9												
Complete GFACE FORTRAN	9												
Convert Scientific Code to UNIX	8												
Rotordynamics and Revised Turbulence	2												
Install IFACE and GFACE on OS/2 KBS	8												
Validation	5												
Workshop	10												
Interim Report	10												
Administration and Monthly Reports	10												

93318A(N)

Figure 1. Fiscal Year 1993 Plans

Task Description	Task Number	Fiscal Year 1994											
		O	N	D	J	F	M	A	M	J	J	A	S
Complete FORTRAN FACEDY	9												
Complete FORTRAN RINGDY	9												
Complete FORTRAN KTK	9												
Modify SPIRALI to Include Local Loss Coefficients	9												
Interface to OS/2 KBS	8												
Multidomain Capability	2												
Validation	5												
Workshop	10												
Administration and Monthly Reports	10												

93318B(N)

Figure 2. Fiscal Year 1994 Plans

4

Task Description	Task Number	Fiscal Year 1995											
		O	N	D	J	F	M	A	M	J	J	A	S
Thermoelastic Distortion Code	9												
Labyrinth and Damping Seal Scientific Code	2												
Convert Distortion to OS/2 KBS	8												
Validation	5												
Workshop	10												
Interim Report	10												
Administration and Monthly Reports	10												

93318C(N)

Figure 3. Fiscal Year 1995 Plans

Task Description	Task Number	Fiscal Year 1996											
		O	N	D	J	F	M	A	M	J	J	A	S
Face Seal (Contact)	9												
Advanced Compressible	9												
Scientific Face Seal	2												
Convert to OS/2 KBS	8												
Validation	5												
Workshop	10												
Administration and Monthly Reports	10												

93318G

Figure 4. Fiscal Year 1996 Plans

5

Task Description	Task Number	Fiscal Year 1997											
		O	N	D	J	F	M	A	M	J	J	A	S
Brush Seals	9												
Conversion to OS/2 KBS	8												
Workstation Conversion Plan	8												
Scientific Face Seals	3												
Scientific Shrouded Tip Seals	4												
Validation	5												
Seal Designs	6												
Workshop	10												
Administration and Monthly Reports	10												

93318E(N)

Figure 5. Fiscal Year 1997 Plans

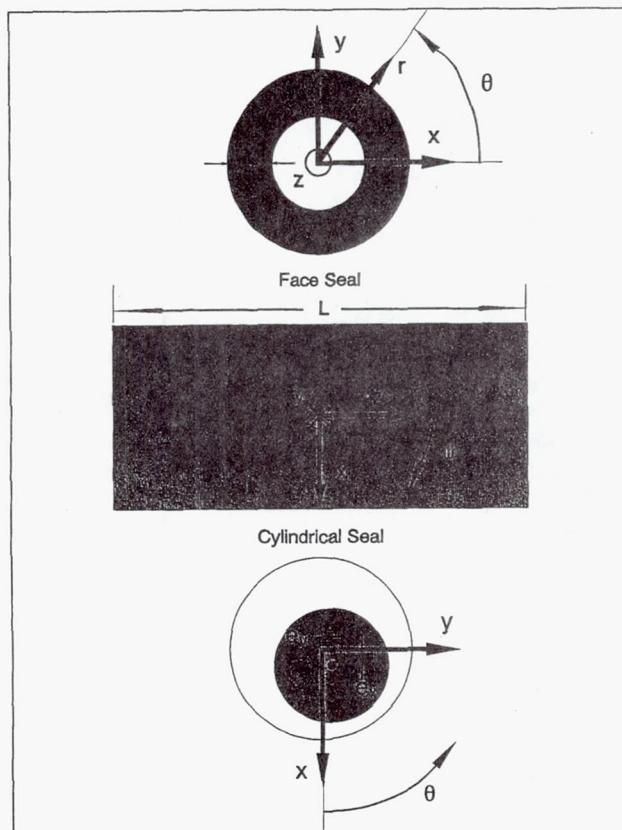| Task Description	Task Number	Fiscal Year 1998											
		O	N	D	J	F	M	A	M	J	J	A	S
Test Data Feedback	7												
Scientific Unshrouded Tip Seals	4												
Update OS/2 KBS	8												
KBS Workstation Conversion													
Final Report	10												
Administration and Monthly Reports	10												
Workshop	10												

93318F(N)

Figure 6. Fiscal Year 1998 Plans

6

PRESENTATION OF COMPUTER CODE SPIRALI FOR INCOMPRESSIBLE, TURBULENT, PLANE AND SPIRAL GROOVED CYLINDRICAL AND FACE SEALS
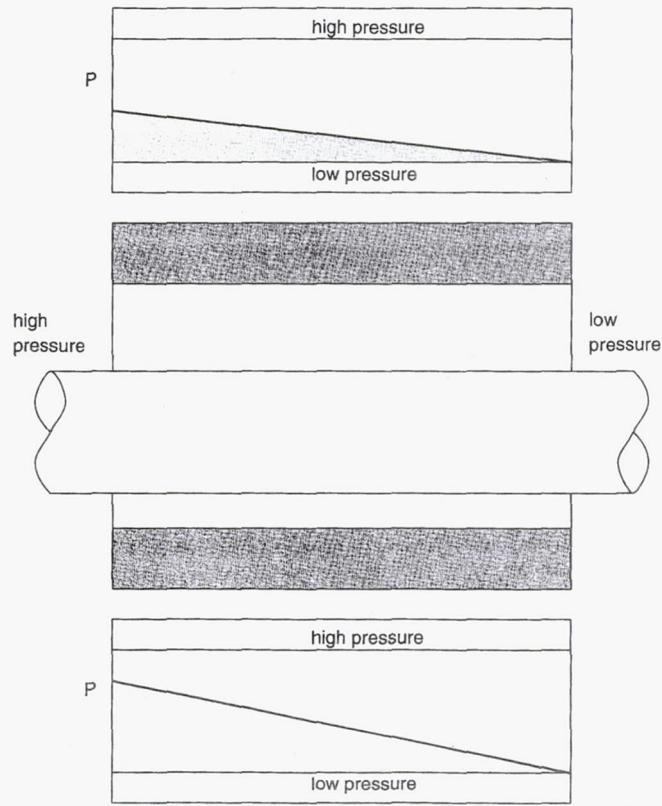
Jed A. Walowit
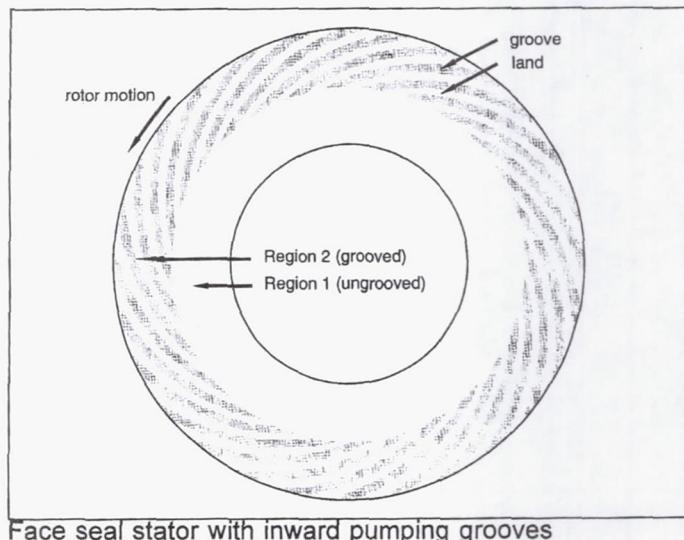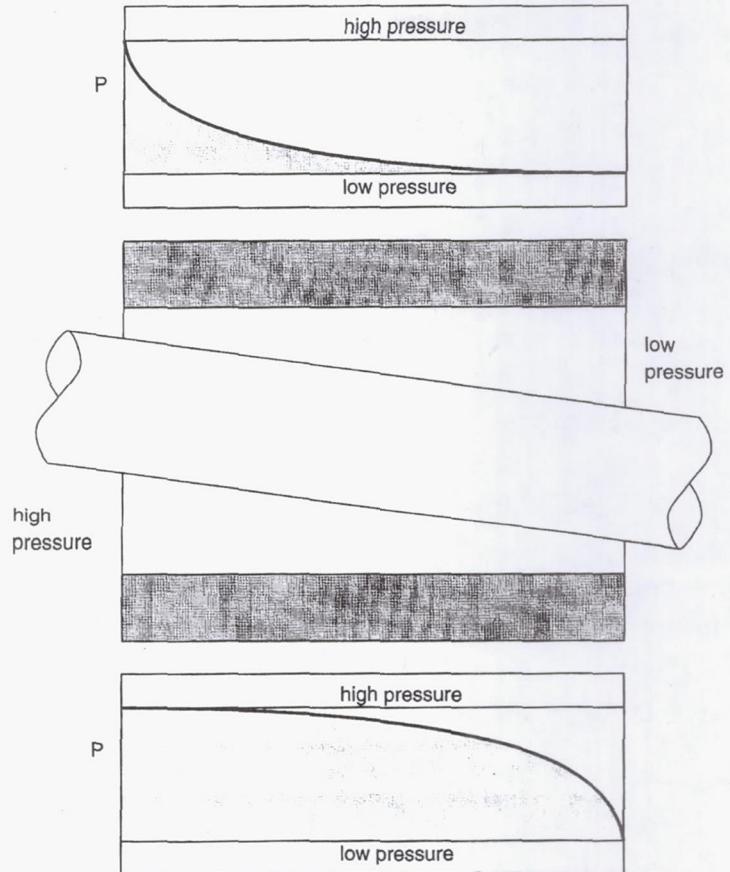Jed A. Walowit, Inc.
Clifton Park, New York

OVERALL CAPABILITIES OF PROGRAM

- Computes rotordynamic coefficients, flow and power loss for cylindrical and face seals

- Treats turbulent and laminar, Couette and Poiseuille dominated flows

- Fluid inertia effects included

- Rotordynamic coefficients in 3 (face) or 4 (cylindrical) degrees of freedom

- Includes effects of spiral grooves

- User definable transverse film geometry including circular steps and grooves

- Independent user definable friction factor models for rotor and stator

- User definable loss coefficients for sudden expansions and contractions

Face Seal

Cylindrical Seal

Coordinate system for seal analysis.

high pressure

P

low pressure

high pressure

low pressure

high pressure

P

low pressure

high pressure

P

low pressure

low
pressure

high
pressure

high pressure

P

low pressure

groove
land

rotor motion

Region 2 (grooved)
Region 1 (ungrooved)

Face seal stator with inward pumping grooves

9

ASSUMPTIONS

- Incompressible and isothermal flow

- Film thickness small in comparison with other geometric parameters

- Bulk flow turbulence model

- Loss coefficients used to treat inertia effects at film discontinuities

- Axisymmetric primary flow with small perturbations theory used for transient and circumferential effects

- Narrow groove theory used for spiral grooves with inertia treated globally

- No cavitation
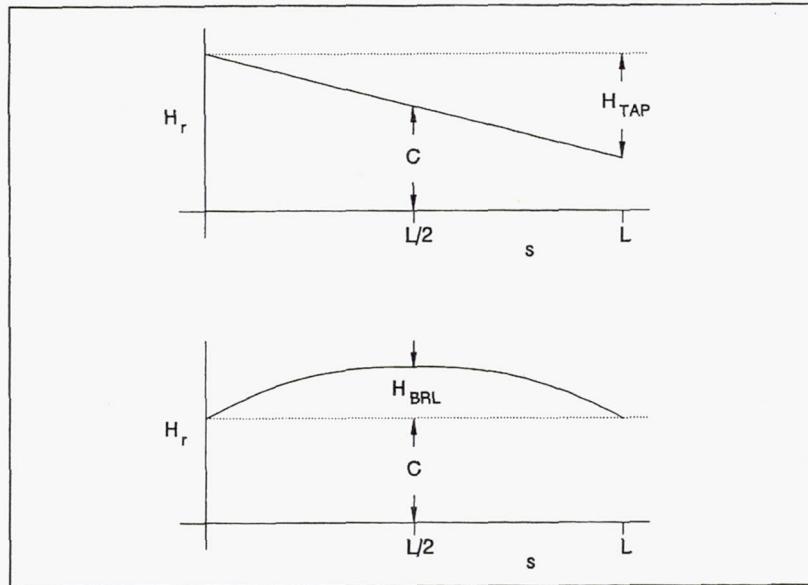
Parameters for characterizing quadratic film variation.
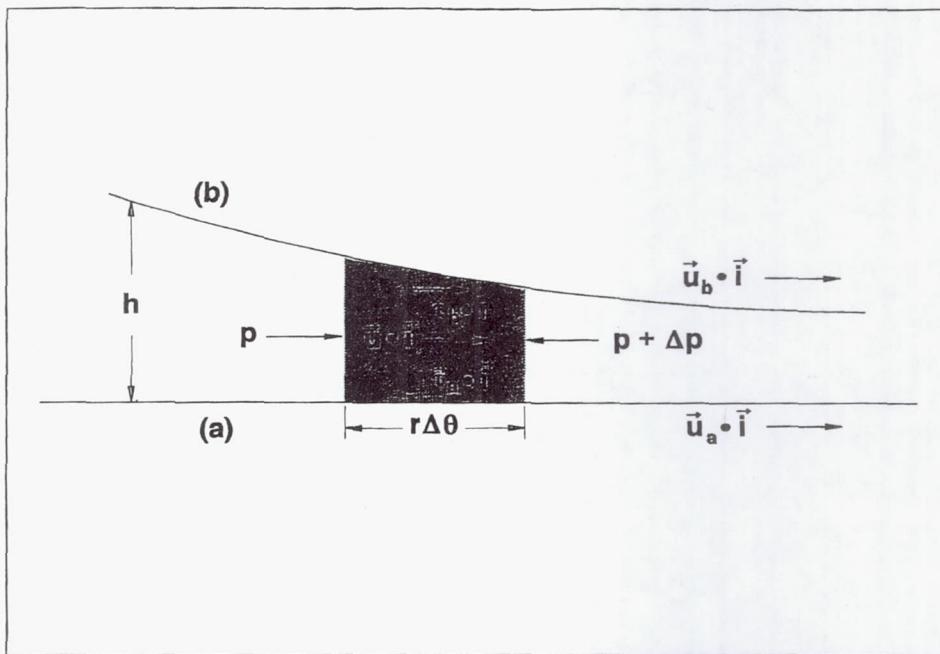
BULK FLOW EQUATIONS FOR TURBULENT FLOW

integrated momentum

$$\rho h \left(\frac{\partial u}{\partial t} + v \frac{\partial u}{\partial s} + \frac{u}{r} \frac{\partial u}{\partial \theta} + \frac{uvl_f}{r} \right) = -\frac{h}{r} \frac{\partial p}{\partial \theta} + (\vec{\tau}_b - \vec{\tau}_a) \cdot \vec{i} \quad ,$$

$$\rho h \left(\frac{\partial v}{\partial t} + v \frac{\partial v}{\partial s} + \frac{u}{r} \frac{\partial v}{\partial \theta} - \frac{u^2 l_f}{r} \right) = -h \frac{\partial p}{\partial s} + (\vec{\tau}_b - \vec{\tau}_a) \cdot \vec{j} \quad .$$

integrated continuity

$$\frac{1}{r} \frac{\partial}{\partial s} (rvh) + \frac{1}{r} \frac{\partial}{\partial \theta} (uh) + \frac{\partial h}{\partial t} = 0 \quad .$$

Velocities and forces on a differential element in the θ direction.

11

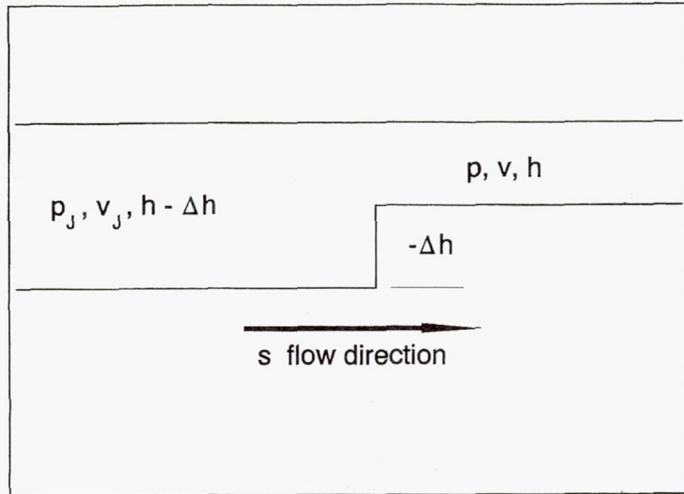## SHEAR STRESS AND FRICTION FACTOR RELATIONSHIPS

$$\vec{\tau}_a = \frac{1}{2}\rho\,|\vec{u} - \vec{u}_a|\,f_a\!\left(\frac{2h\rho\,|\vec{u} - \vec{u}_a|}{\mu}\right)(\vec{u} - \vec{u}_a) = \frac{1}{4}\frac{\mu}{h}R_a f_a(R_a)\,(\vec{u} - \vec{u}_a)\quad,$$

$$\vec{\tau}_b = -\frac{1}{2}\rho\,|\vec{u} - \vec{u}_b|\,f_b\!\left(\frac{2h\rho\,|\vec{u} - \vec{u}_b|}{\mu}\right)(\vec{u} - \vec{u}_b) = -\frac{1}{4}\frac{\mu}{h}R_b f_b(R_b)\,(\vec{u} - \vec{u}_b)\quad,$$

$$R_a = 2h\,|\vec{u} - \vec{u}_a|\,\rho/\mu\quad,\qquad R_b = 2h\,|\vec{u} - \vec{u}_b|\,\rho/\mu\quad.$$
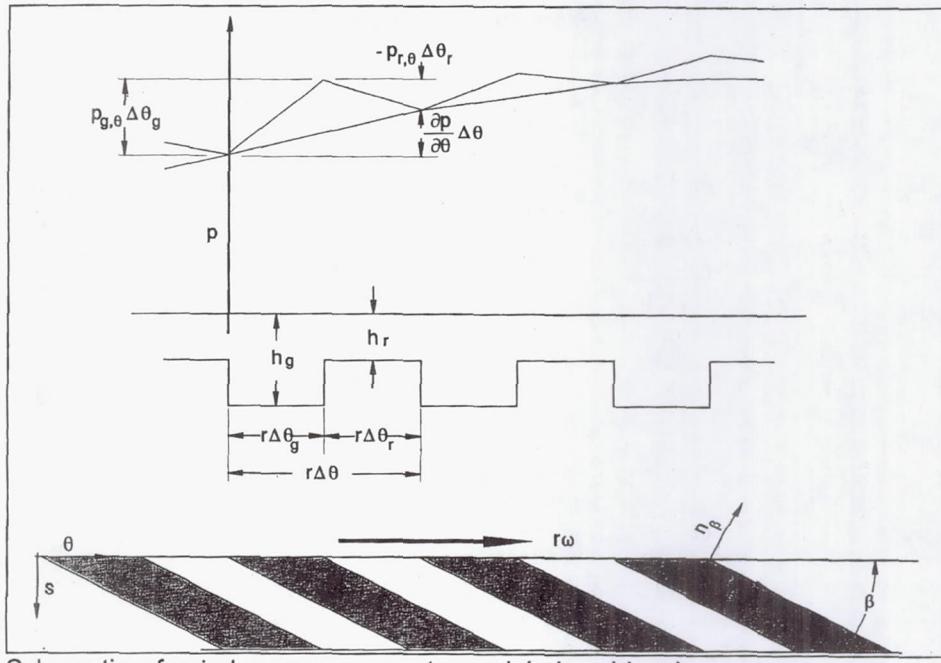
$$f_a(R_a) = n_0 R_a^{\,m_0}\,,\quad f_b(R_b) = n_0 R_b^{\,m_0}\,,\quad \text{Hirs – Blasius}$$

$$f_{a,b} = 0.001375\left[1 + \left(10^4\frac{k_{a,b}}{h} + \frac{10^6}{R_{a,b}}\right)^{\frac{1}{3}}\right]\quad,\quad \text{Moody}$$
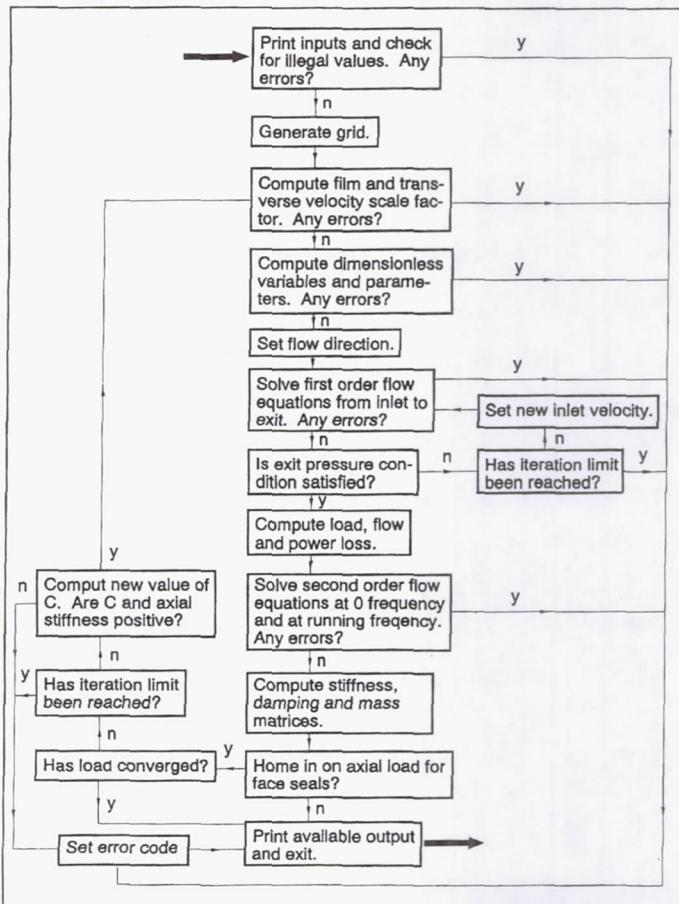

$$p_J + \frac{1}{2}\rho v_J^2 = p + \frac{1}{2}\rho v^2(1 + \xi)\quad @\ s = s_J\quad.$$

$$\xi = \begin{cases} \zeta(R,\tilde{h},\tilde{v}) & ,\ \Delta\tilde{h} < 0 \ \text{(contraction)} \\[2ex] \left(1 - \dfrac{\tilde{h}}{\tilde{h} - \Delta\tilde{h}}\right)^2 & ,\ \Delta\tilde{h} \geq 0 \ \text{(expansion)} \end{cases}$$

Schematic of spiral groove parameters, global and local pressures.

Flow diagram for overall logic used in computations

13

(CASE 1) Cylindrical seal with grooves, laminar, no press. grad.

```
&INPUTS
   TITLE  =  'Cylindrical seal with grooves, laminar, no press. grad.'
   IFACE  =  0              ISIUN  =  0
   IGROT  =  0              NOI    =  2            IFLOW  =  1
   RO     =  1.0000E+00     EL     =  5.0000E-01   C      =  1.0000E-03
   RPM    =  5.0000E+04     RPMO   =  2.5000E+04   RPMD   =  0.0000E+00
   PLEG   =  0.0000E+00     PRIG   =  0.0000E+00   FZD    =  0.0000E+00
   VISC   =  3.0000E-08     DENS   =  0.0000E+00
   EMA    = -2.5000E-01     ENA    =  7.9100E-02
   EMB    = -2.5000E-01     ENB    =  7.9100E-02
   HTAP   =  0.0000E+00     HBRL   =  0.0000E+00
   TOLH   =  1.0000E-04     TOLV   =  1.0000E-05   DUT    =  1.0000E-06
   IHOME  =  0              NITH   =  10           NITV   =  30
   NREG   =  2              NRSUB  =  50  50
   ELFR   =  5.0000E-01  5.0000E-01
   ALPI   =  5.0000E-01  0.0000E+00
   BETI   =  2.5000E+01  0.0000E+00
   DELT   =  2.0000E-03  0.0000E+00
   ZET    =  0.0000E+00  0.0000E+00
```

CYLINDRICAL SEAL, INERTIA NEGLECTED

LENGTH, DIAMETER, CLEARANCE = 5.0000E-01, 2.0000E+00, 1.0000E-03 (IN)

ROTOR, SWIRL AND DIST. SPEEDS = 5.0000E+04, 2.5000E+04, 0.0000E+00 (RPM)

PRESSURE AT START, END AXIAL BOUNDARIES = 0.0000E+00, 0.0000E+00 (PSI)

VISCOSITY = 3.0000E-08 (PSI-SEC),   DENSITY = 0.0000E+00 (LB-SEC/IN4)

ERROR CODE = 0,   ITERATIONS IN PRIMARY FLOW = 2

FLOW = 1.1506E+00 (IN**3/SEC)

TORQUE = 4.3909E-01 (IN-LB),   FILM POWER LOSS = 3.4835E-01 (HP)

AXIAL REYNOLDS NUMBER   = 0.0000E+00
CIRC. REYNOLDS NUMBERS FOR ROTOR AT SEAL ENDS = 0.0000E+00, 0.0000E+00

DYNAMIC COEFFICIENTS (FORCE UNIT / DISP. UNIT)

DISP.	x (IN)	y (IN)	phi (RAD)	psi (RAD)	FORCE UNIT
Kx	2.7021E+04	1.3511E+04	-6.3081E+02	-1.2959E+03	LB
Ky	-1.3511E+04	2.7021E+04	1.2959E+03	-6.3081E+02	LB
Kphi	2.3387E+02	-6.5242E+01	1.6699E+02	8.6419E+01	IN-LB
Kpsi	6.5242E+01	2.3387E+02	-8.6419E+01	1.6699E+02	IN-LB
Bx	5.1297E+00	7.8477E-11	-2.0242E-02	1.3973E-01	LB-SEC
By	-7.8477E-11	5.1297E+00	-1.3973E-01	-2.0242E-02	LB-SEC
Bphi	-2.0242E-02	-1.3973E-01	3.0437E-02	3.8319E-13	IN-LB-SEC
Bpsi	1.3973E-01	-2.0242E-02	-3.8319E-13	3.0437E-02	IN-LB-SEC
Ax	4.7708E-19	4.0552E-18	7.4544E-20	-1.7891E-19	LB-SEC2
Ay	-4.0552E-18	4.7708E-19	1.7891E-19	7.4544E-20	LB-SEC2
Aphi	1.1927E-19	5.4045E-20	-1.8636E-20	3.3545E-20	IN-LB-SEC2
Apsi	-5.4045E-20	1.1927E-19	-3.3545E-20	-1.8636E-20	IN-LB-SEC2

Comparison with results published by D. W. Childs (1983)

	$u_{in}=r_0\omega/2$, $L/D=.2$		$u_{in}=r_0\omega/2$, $L/D=1$		$u_{in}=0$, $L/D=.2$		$u_{in}=0$, $L/D=1$	
	SPIRALI	Childs	SPIRALI	Childs	SPIRALI	Childs	SPIRALI	Childs
Q (cm^3/s)	4006.	4019.	1771.	1779.	3989.	4019.	1767.	1779.
K_{xx} (MN/m)	18.90	18.65	10.79	9.756	18.58	18.52	13.25	12.48
K_{xy} (MN/m)	4.127	4.213	91.78	94.05	-.3027	-.3000	75.18	77.61
B_{xx} (KN-s/m)	21.89	22.35	487.2	500.6	21.89	22.47	489.5	502.2
B_{xy} (KN-s/m)	1.140	1.206	102.9	107.5	.8518	.8932	89.26	93.39
A_{xx} (kg)	3.020	3.200	272.6	285.3	3.003	3.189	272.1	285.3

DEFINITIONS OF COEFFICIENTS

Overall Seal Discharge Coefficient

$$C_d = \frac{\Delta P}{\frac{1}{2}\rho V^2}$$

Radial Force Coefficient

$$-f_r = K + c\omega - M\omega^2 = K_{ef} - M_{ef}\omega^2$$

Tangential Force Coefficient

$$-f_\theta = C\omega - k = C_{ef}\omega$$

15

```
TITLE  =  'Childs,Nolan & Kilgore Stator 1, 25% swirl, 1000 RPM'
IFACE  =  0              ISIUN  =  1
IGROT  =  0              NOI    =  0              IFLOW  =  0
R0     =  5.0800E-02     EL     =  5.0800E-02     C      =  3.5600E-04
RPM    =  1.0000E+03     RPMO   =  2.5000E+02     RPMD   =  0.0000E+00
PLEG   =  0.2500E+06     PRIG   =  0.0000E+00     FZD    =  0.0000E+00
VISC   =  1.5400E-04     DENS   =  1.5700E+03
EMA    = -2.5000E-01     ENA    =  7.9100E-02
EMB    = -2.5000E-01     ENB    =  7.9100E-02
HTAP   =  0.0000E+00     HBRL   =  0.0000E+00
TOLH   =  1.0000E-04     TOLV   =  1.0000E-05     DUT    =  1.0000E-06
IHOME  =  0              NITH   =  10             NITV   =  30
NREG   =  19
NRSUB  =  5 5 5 5 5 5 5 5 5 5
          5 5 5 5 5 5 5 5 5
ELFR   =  .1005 .047 .047 .047 .047 .047 .047 .047 .047 .047
          .047 .047 .047 .047 .047 .047 .047 .047 .1005
ALPI   =  1. 1. 1. 1. 1. 1. 1. 1. 1. 1.
          1. 1. 1. 1. 1. 1. 1. 1. 1.
BETI   =  0. 0. 0. 0. 0. 0. 0. 0. 0. 0.
          0. 0. 0. 0. 0. 0. 0. 0. 0.
DELT   =  0. 3.8E-4 0. 3.8E-4 0. 3.8E-4 0. 3.8E-4 0. 3.8E-4 0. 3.8E-4
          0. 3.8E-4 0. 3.8E-4 0. 3.8E-4 0.
ZET    =  0. 0. 0. 0. 0. 0. 0. 0. 0. 0.
          0. 0. 0. 0. 0. 0. 0. 0. 0.
```
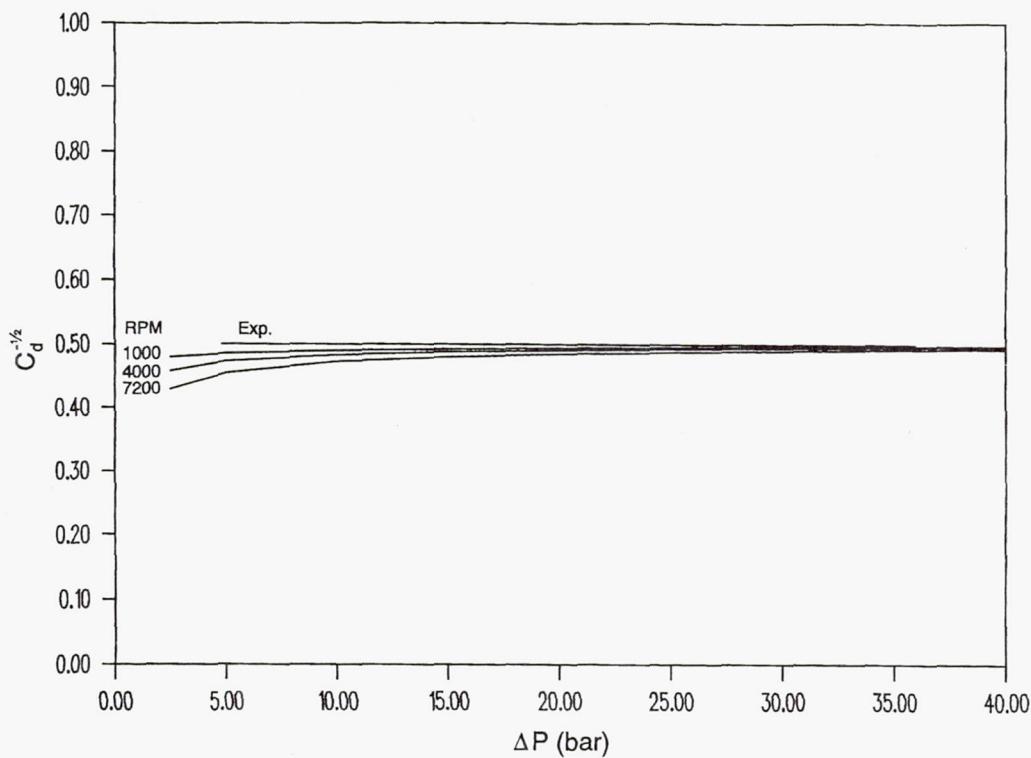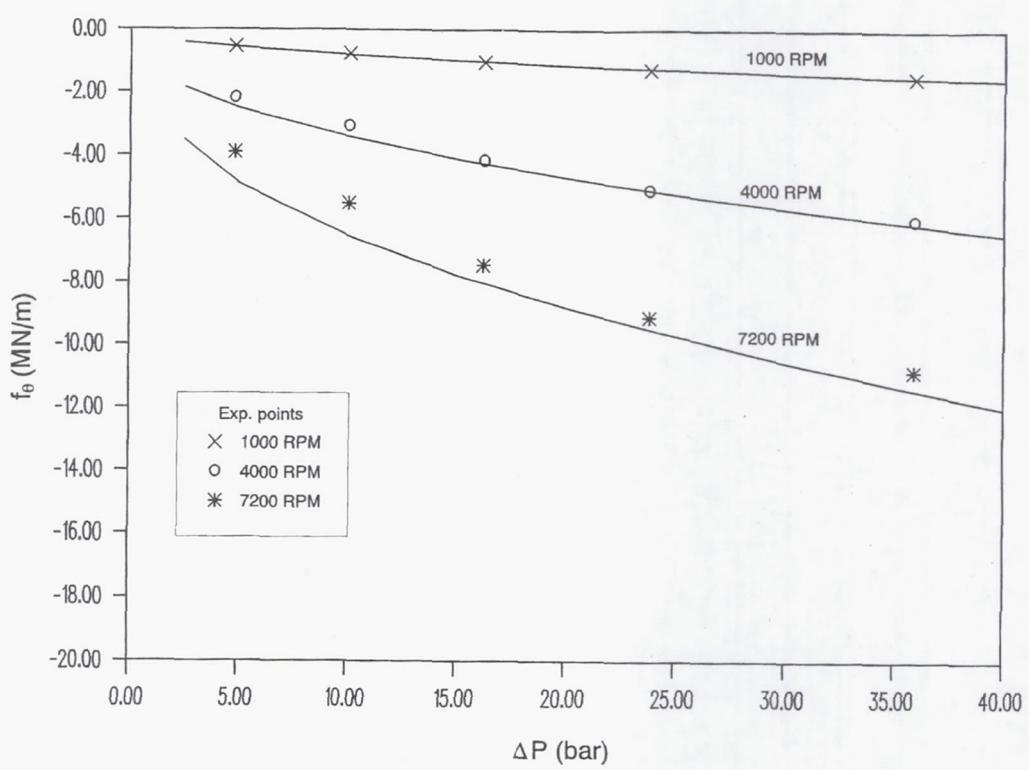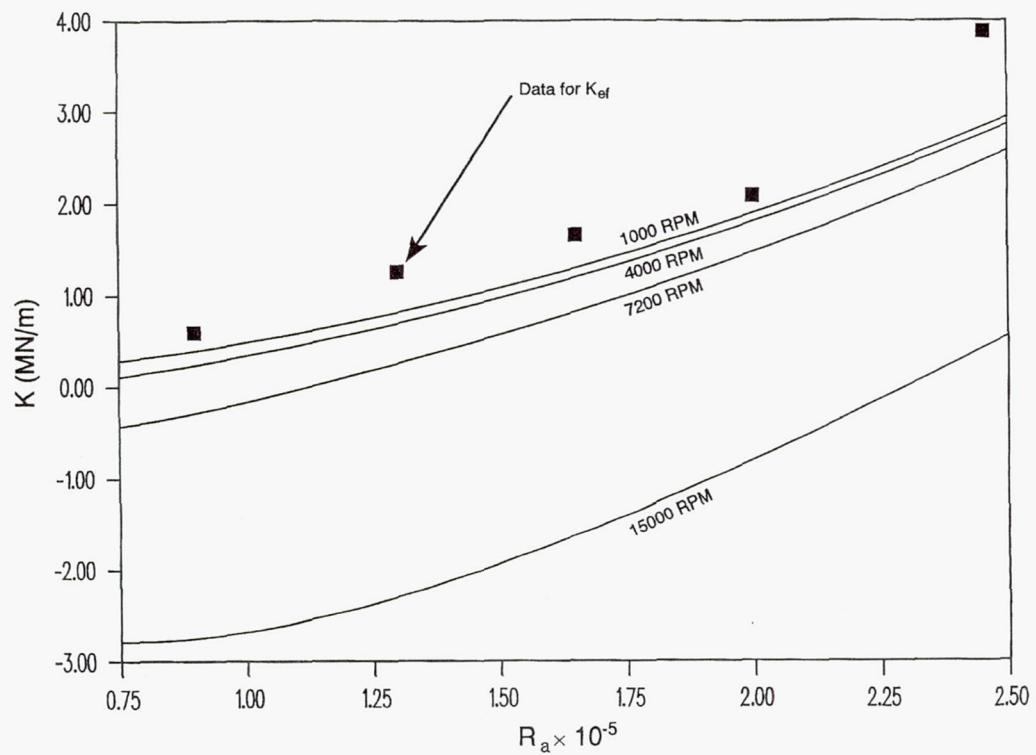

Dimensionless axial flow rates
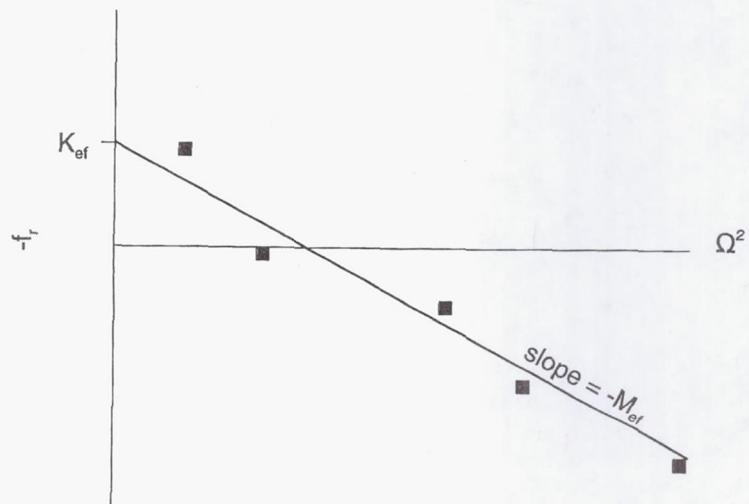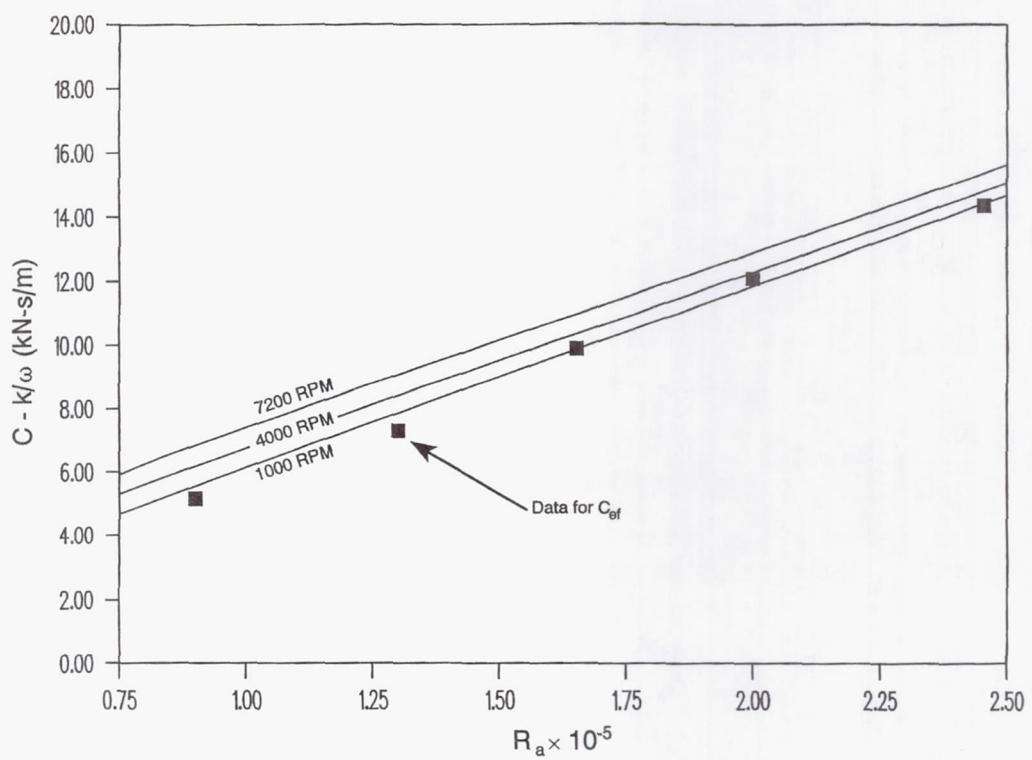
Extraction of effective stiffness and added mass
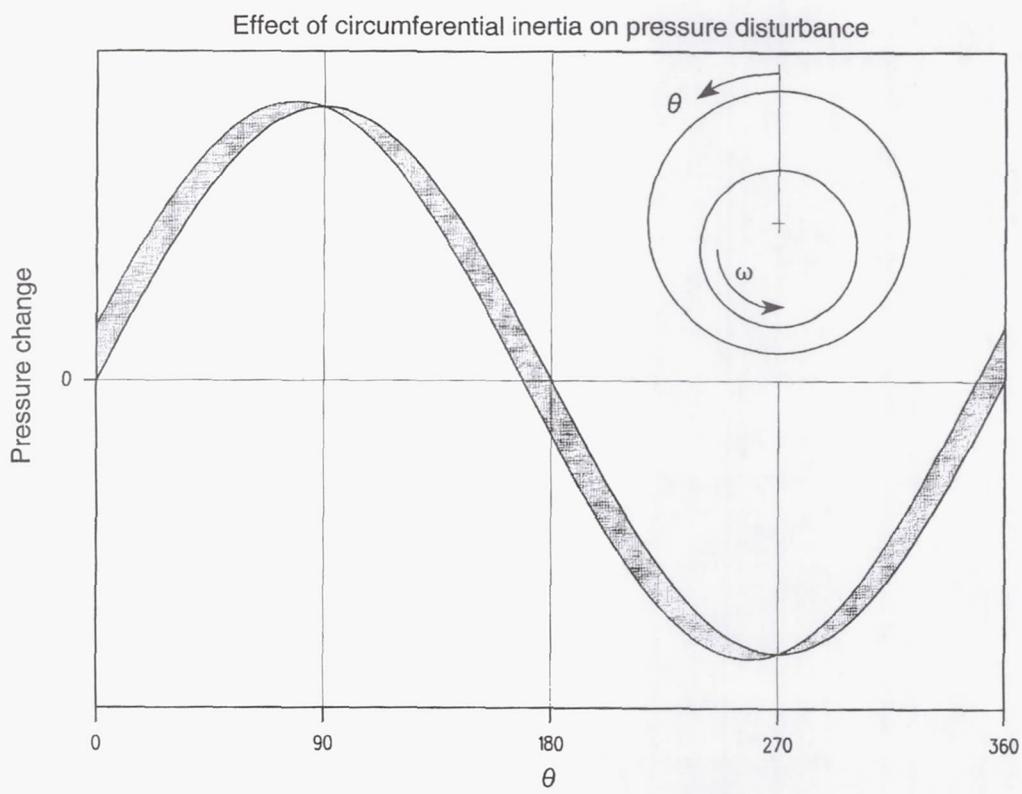

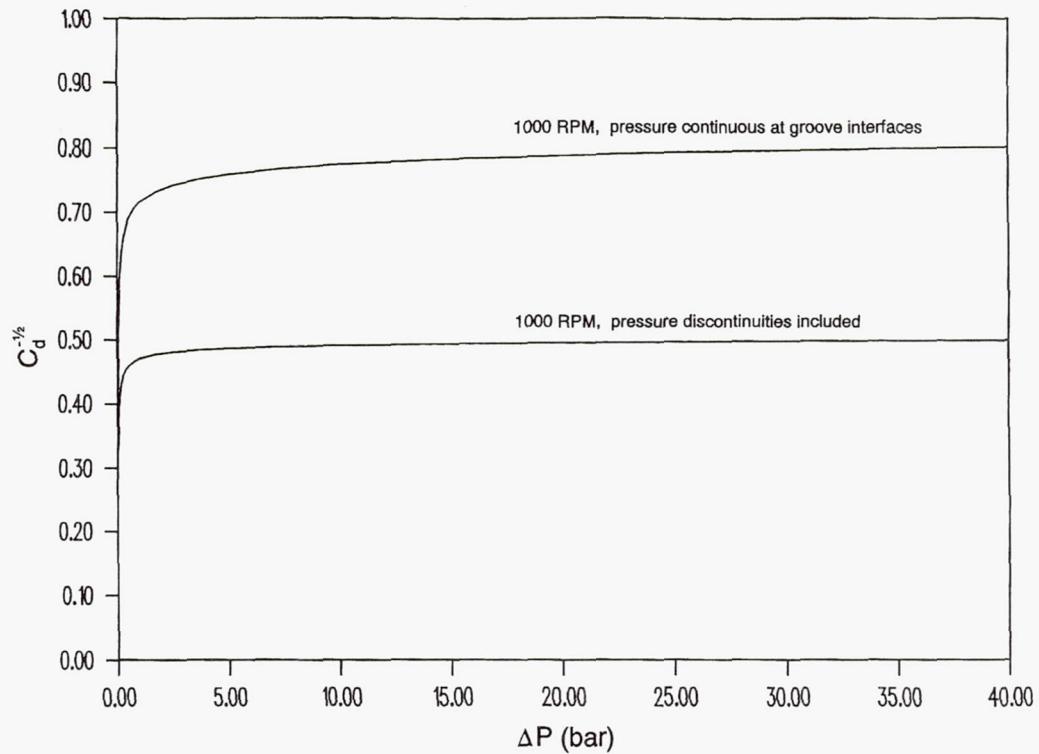Tangential force coefficients
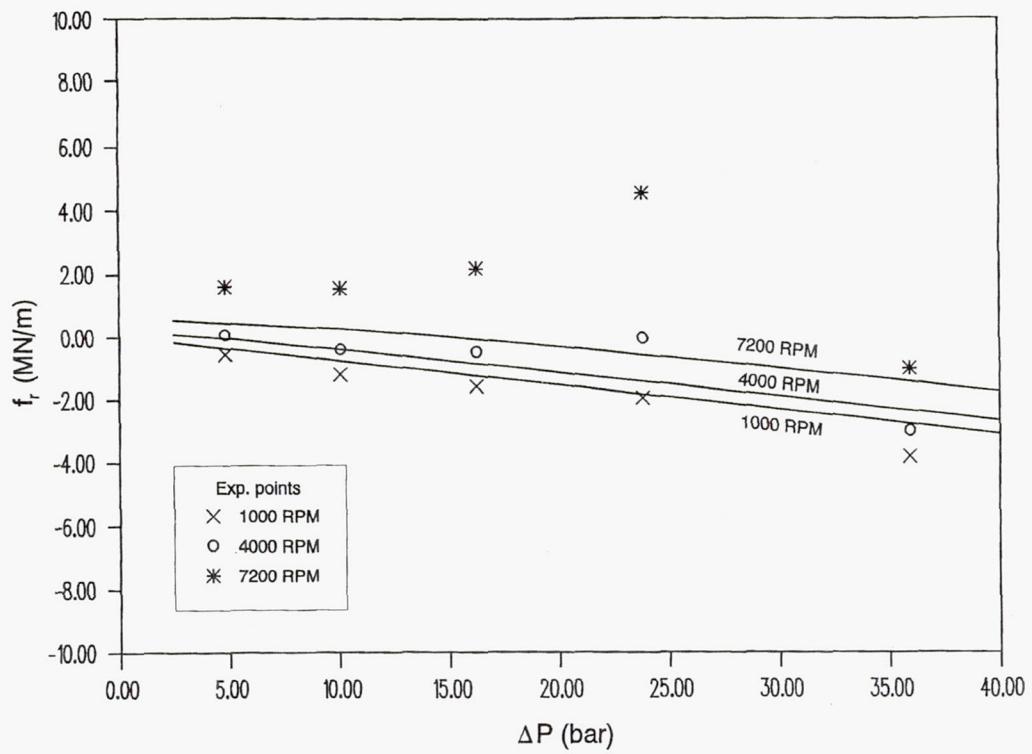
Radial force coefficients

Comparison between K and K$_{ef}$ at various rotating speeds

18

Comparison between C - k/ω and C_{ef} at various rotating speeds

Effect of circumferential inertia on pressure disturbance

Effect of local pressure discontinuities on predicted axial flow rates

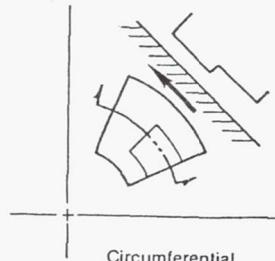Wilbur Shapiro
Mechanical Technology Incorporated
Latham, New York

GFACE Capabilities

- **Varying Geometries-Rayleigh-step, Tapered Land, Hydrostatic**
- **Variable Grid**
- **Z, X-X, Y-Y, Degrees of Freedom**
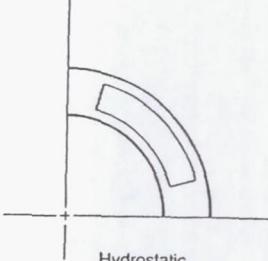- **Can determine position as a function of load**
- **English or SI Units**
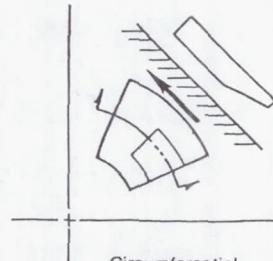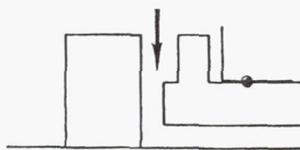
GFACE Configurations
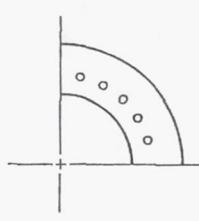
Hydrostatic

Circumferential Rayleigh Step

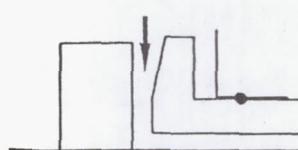Hydrostatic Recess

Circumferential Tapered Land

Radial Rayleigh Step

Radial Tapered Land

GFACE Configurations

Section A-A
- Radial Taper: Type 1

- Radial Taper: Type 2

Section D-D
- Circumferential Taper

Section B-B
- Rayleigh Step

Section C-C
- Rayleigh Step
- Section E - E
- Hydrostatic Recess

67907-1
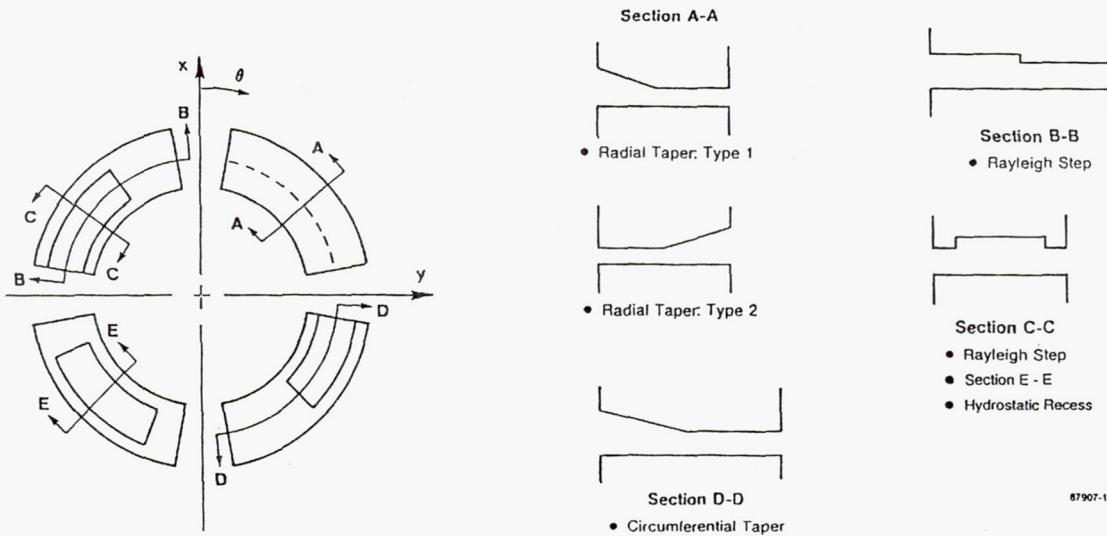
GFACE Output

- **Clearance Distribution**
- **Pressure Distribution**
- **Leakage along specified flow paths**
- **Interface load**
- **Righting Moments**
- **Viscous Dissipation**
- **Frequency dependent stiffness and Damping**
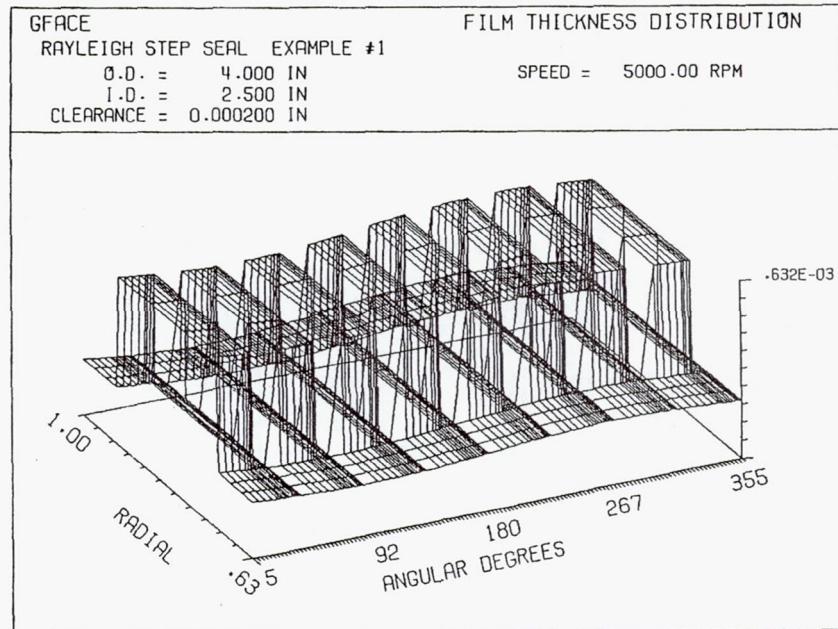- **Plotting Routines**

22

GFACE Examples

- **Rayleigh-step seal with Misalignment**
- **Tapered Land Seal, Option 2**
- **Hydrostatic Recess**
- **Hydrostatic Recess, Periodic Pads**
- **Inherently Compensated Hydrostatic Seal**
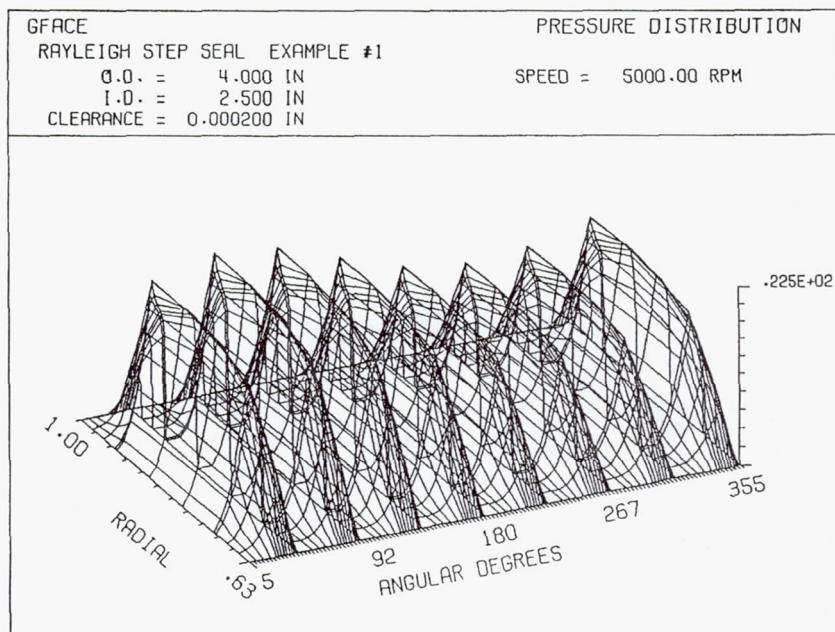- **Radial Tapered Seal**

Rayleigh Step Seal Input

Number of pads, NPAD	8
Outer diameter	4.0 inch
Inner diameter	2.5 inch
Angular extent of pad	35 degrees
Starting angle of first pad	5 degrees
Given displacement, find load. OPTION	1
Compute stiffness at synchronous frequency	5000
Apply variable grid	
Clearance	0.0002 inch
Misalignment angle about the X-axis	-0.001 degree
Number of steps in grid	1
Step depth	0.0004 inch
Location of step	
Lower left corner	I=5, J=1
Upper right corner	I=8, J=8
Specific heat ratio	1.4
Gas constant	246,900 in.^{2}/s^2/°R
Absolute temperature	1460°R
Viscosity	5.35 x 10^{-9} lbs-s/in^2
Speed	5000 rpm
Convergence tolerance	0.01
Ambient (reference) pressure	14.7 psi

Rayleigh-Step Seal Clearance Distribution

GFACE   FILM THICKNESS DISTRIBUTION
  RAYLEIGH STEP SEAL   EXAMPLE #1
        O.D. =   4.000 IN   SPEED =   5000.00 RPM
        I.D. =   2.500 IN
  CLEARANCE = 0.000200 IN

.632E-03

1.00

RADIAL

.635   92   180   267   355
                   ANGULAR DEGREES

Rayleigh-Step Seal Pressure Distribution

GFACE   PRESSURE DISTRIBUTION
  RAYLEIGH STEP SEAL   EXAMPLE #1
        O.D. =   4.000 IN   SPEED =   5000.00 RPM
        I.D. =   2.500 IN
  CLEARANCE = 0.000200 IN

.225E+02

1.00

RADIAL

.635   92   180   267   355
                   ANGULAR DEGREES

Rayleigh-Step Seal Pressure Distribution

GFACE
RAYLEIGH STEP SEAL   EXAMPLE #1
        O.D. =   4.000 IN
        I.D. =   2.500 IN
   CLEARANCE = 0.000200 IN

PRESSURE DISTRIBUTION

SPEED =   5000.00 RPM

.225E+02

| 5 | 92 | 180 | 267 | 355 |

ANGULAR DEGREES

Tapered-Land Seal Grid Geometry

V ⟶

Slope = 0.0509

Section A - A

High Pressure

Inlet Region

14, 21   14, 35

Tapered Region

8, 17   8, 21   7, 37 Constant Pressure

6, 1

Low Pressure

I, R

J, θ

93593

25
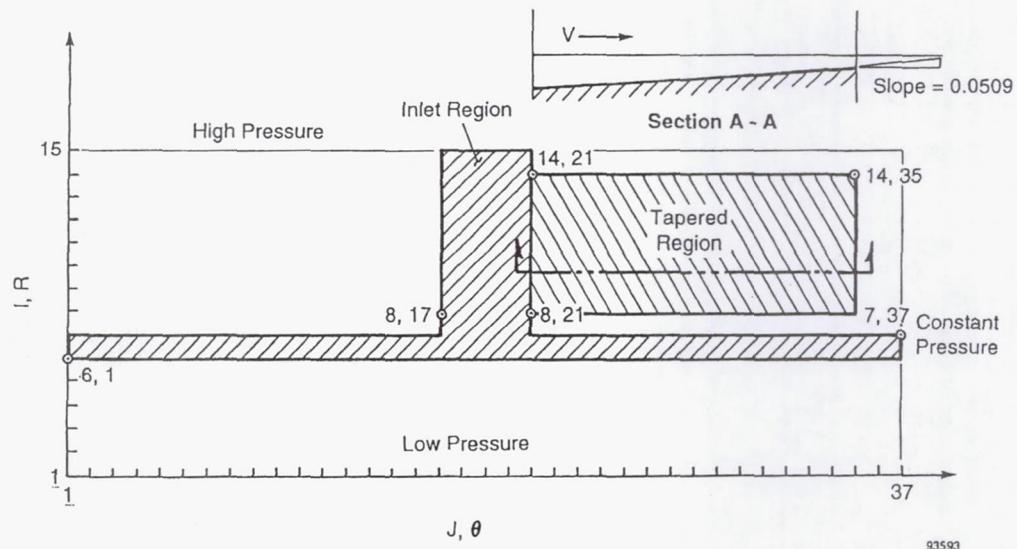
Tapered-Land Seal Input

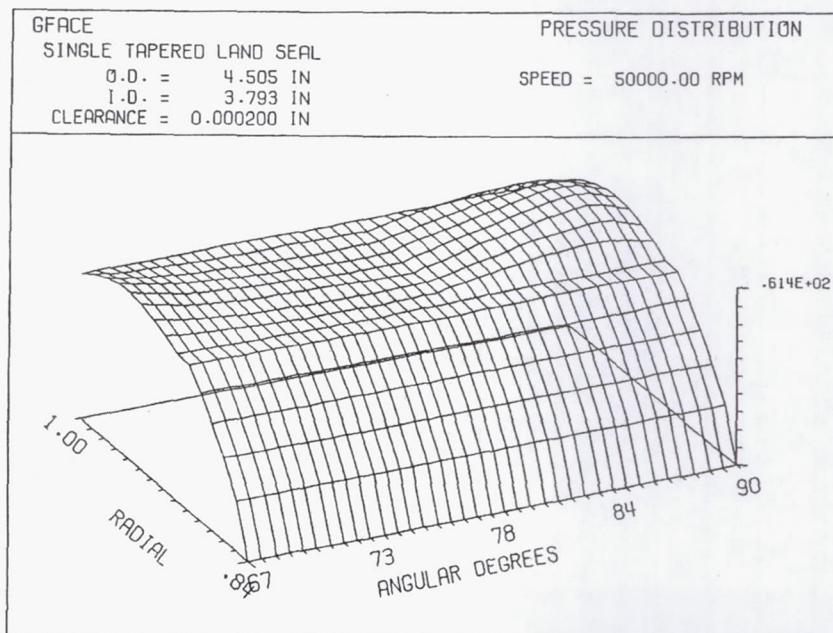|	
OPTION	2 Signifies that the load will be supplied and the axial position determined.
LOAD	13 lbs is the load to be balanced
STIFFNESS	0.0001 A non synchronous, frequency independent stiffness is desired.
NPAD	1 One of the 16 pads is modeled, with periodic conditions along the radial boundaries.
OUTER	4.5 = the outer diameter ,in.
INNER	3.793 = the inner diameter, in.
CLEARANCE	= 0.0002 in. = Initial guess at the axial clearance to support the given load.
START	= 67.5 degrees = start angle of pad
PADANGLE	= 22.5 degrees = angular extent of pad
GRIDN	= 37 = number of grid points in the θ direction
GRIDM	= 15 = Number of grid points in the radial direction
CTAPER	= 1 = Number of circumferential tapers in the grid
	Slope of taper = 0.05209
	Lower left corner of taper, I = 8, J=21
	Upper right corner of taper, I=14, J=35

Tapered-Land Seal Input

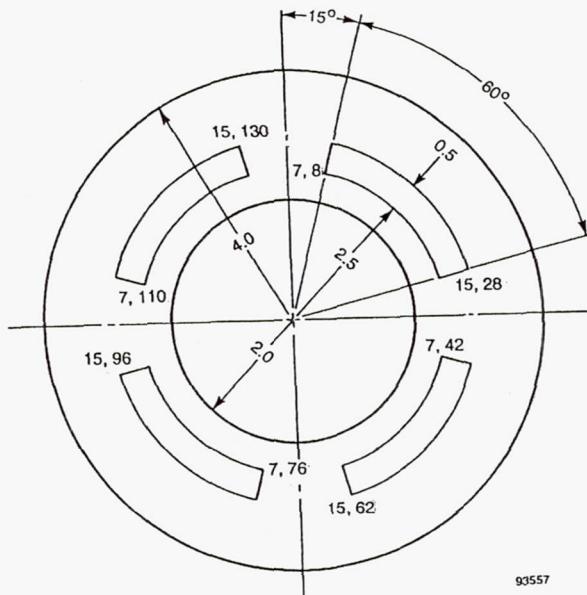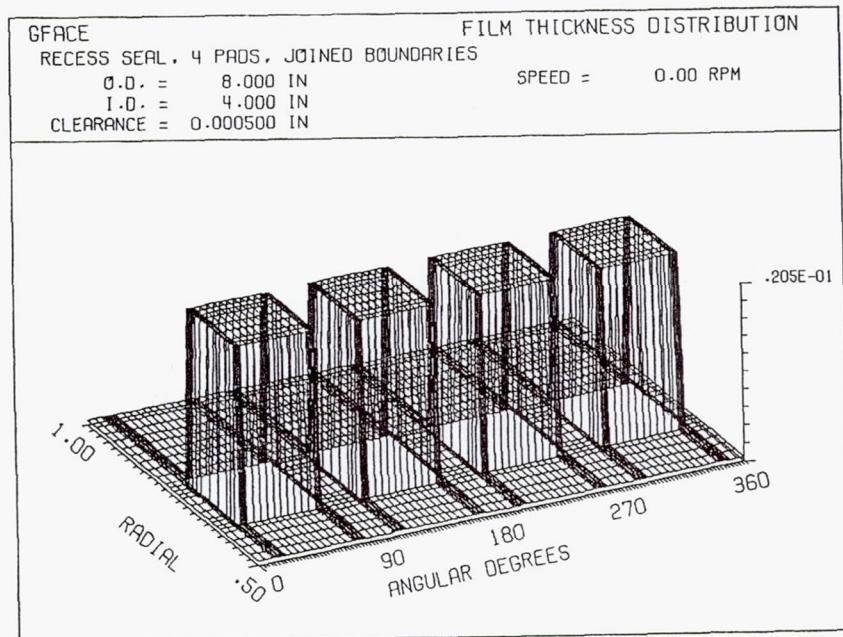|	
VISCOSITY	1.75×10^{-9} lb-s/in^2
GASCONST	= gas constant = 423,184 in^2/s^2/^{o}F
JOINED	Periodic boundaries apply
ITERATION	= 15, 15 = maximum iterations for pressure and load convergence
TOLERANCE	.020, .020 = tolerances on pressure and load convergence
SPEED	50,000 rpm
PO	= 14.7 = reference or ambient pressure, psig
PLEFT	= 0. = Pressure on left radial boundary. Since periodic boundary conditions apply PLEFT has no consequence.
PRITE	= 0. = Pressure on right radial boundary. Since periodic boundary conditions apply PRITE has no consequence.
PTOP	= 50 psig = pressure boundary at outer radius, I=M
PBOT	= 0 psig = pressure boundary at inner radius, I=1

Tapered-Land Seal Clearance Distribution

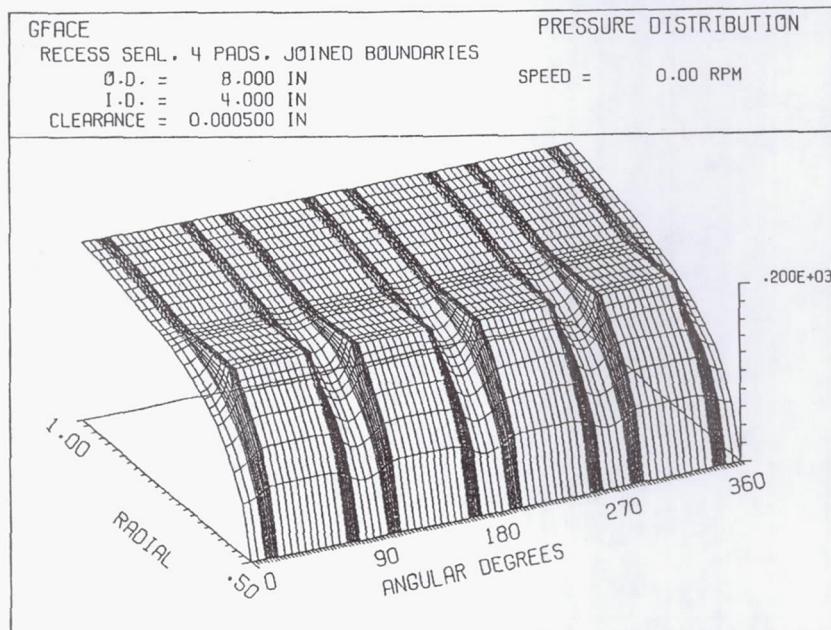GFACE   FILM THICKNESS DISTRIBUTION

SINGLE TAPERED LAND SEAL

O.D. = 4.505 IN   SPEED = 50000.00 RPM
I.D. = 3.793 IN
CLEARANCE = 0.000200 IN

.610E-03

1.00

RADIAL   .867   73   78   84   90

ANGULAR DEGREES
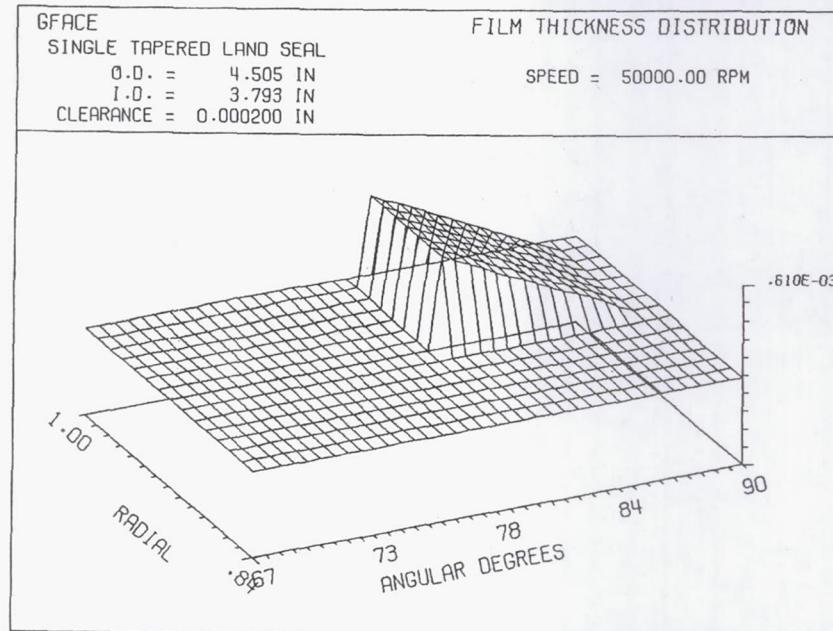
Tapered-Land Seal Pressure Distribution

GFACE   PRESSURE DISTRIBUTION

SINGLE TAPERED LAND SEAL

O.D. = 4.505 IN   SPEED = 50000.00 RPM
I.D. = 3.793 IN
CLEARANCE = 0.000200 IN

.614E+02

1.00

RADIAL   .867   73   78   84   90

ANGULAR DEGREES

Hydrostatic Recess Seal

Hydrostatic Recess Seal Clearance Distribution

Hydrostatic Recess Seal Pressure Distribution


```
GFACE                                          PRESSURE DISTRIBUTION
  RECESS SEAL, 4 PADS, JOINED BOUNDARIES
        O.D. =      8.000 IN              SPEED =      0.00 RPM
        I.D. =      4.000 IN
  CLEARANCE =  0.000500 IN
```
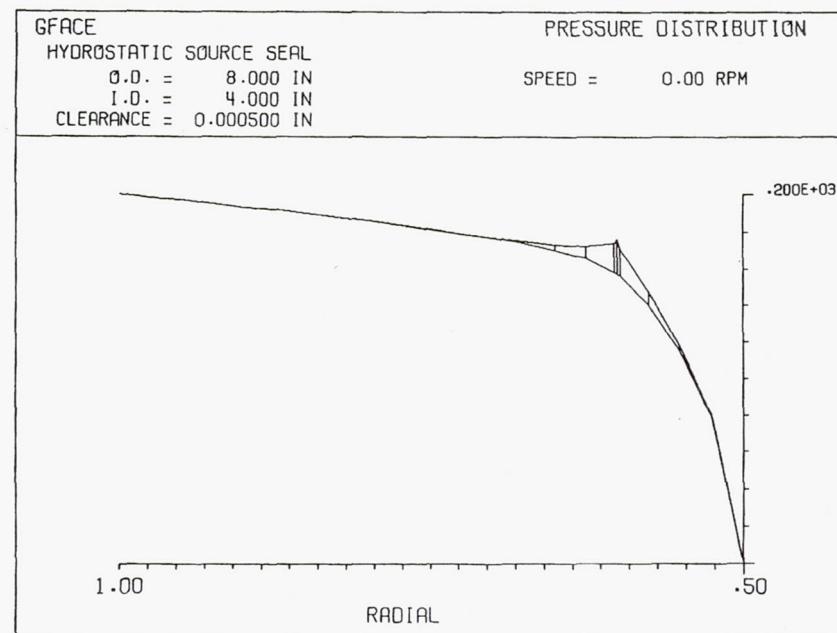
Hydrostatic Recess Seal Pressure Distribution


```
GFACE                                          PRESSURE DISTRIBUTION
  RECESS SEAL, 4 PADS, JOINED BOUNDARIES
        O.D. =      8.000 IN              SPEED =      0.00 RPM
        I.D. =      4.000 IN
  CLEARANCE =  0.000500 IN
```

Hydrostatic Source Seal
Pressure Distribution

GFACE
HYDROSTATIC SOURCE SEAL
    O.D. =   8.000 IN
    I.D. =   4.000 IN
CLEARANCE = 0.000500 IN

PRESSURE DISTRIBUTION

SPEED =   0.00 RPM

.200E+03

RADIAL

1.00

.50 0   90   180   270   360

ANGULAR DEGREES

Hydrostatic Source Seal
Pressure Distribution

GFACE
HYDROSTATIC SOURCE SEAL
    O.D. =   8.000 IN
    I.D. =   4.000 IN
CLEARANCE = 0.000500 IN

PRESSURE DISTRIBUTION

SPEED =   0.00 RPM

.200E+03

1.00   .50

RADIAL

Tilted Slider Comparison

Λ	ε	ζ degrees	N rpm	W' GFACE	W' Etsion & Fleming	Δ%
Table 6-1 Comparisons of GFACE with Etsion and Fleming Load Capacity						
1	2.5	.0143	133.69	0.00476	0.0047	1.27
10	2.5	.0143	1,336.9	0.0466	0.0460	1.30
25	3.0	.0172	3,342.25	0.1086	0.1080	0.56
50	3.5	.0201	6,684.5	0.1897	0.1850	2.5
100	4.5	.0258	13,369	0.3014	0.2950	2.17

Etsion I, D. P. Fleming, *An Accurate Solution of the Gas Lubricated Flat Sector Thrust Bearing, Trans. ASME, J. Lubr. Technology, 99:, 82-88*

Tilted Slider Power Loss

Λ	ε	PLC GFACE	PLC Etsion
Table 6-2 Comparison of GFACE with Etsion and Fleming Power Loss			
1	2.5	49.4	12
10	2.5	12.86	12
25	3.0	12.987	13
50	3.5	14.193	15
100	4.5	16.15	17

$$PLC = \frac{F}{W \omega h_2} \quad where:$$

$$F = Power\ Loss,\ in\text{-}lbs\,/\,s$$

Etsion I, D. P. Fleming, *An Accurate Solution of the Gas Lubricated Flat Sector Thrust Bearing, Trans. ASME, J. Lubr. Technology, 99:, 82-88*

Rayleigh Step References

■ **Ausman, J. S. *An Approximate Analytical Solution for Self-Acting Gas Lubrication of Stepped Sector thrust Bearings,* ASLE Transactions 4: 304-314**

■ **Gross, W. A., et. al *Fluid-Film Lubrication,* John Wiley & Sons, copyright 1980**

GFACE Comparison with Ausman

Table 6-3 GFACE Comparison with Ausman Rayleigh-step Pad					
Λ	n	W	W' GFACE	W' Ausman	$\Delta\%$
10	8	0.7539	0.0456	0.046	-.87
20	7	1.821	0.0957	0.103	-7
40	7	3.701	0.1946	0.219	-11
80	6	7.766	0.3479	0.397	-12
160	6	11.71	0.5246	0.572	-8

$$\Lambda = \frac{6\mu a r_2^2}{P_a h_2^2}; \quad n = number\ of\ pads, \ \frac{r_1}{r_2} = 0.5$$

Load vs. Step height
Step Validation, Gross

Chart: Load (lbs) vs Step Height x 10**4

Gross

GFACE

38 degree pad, 15 deg. step

Ambient Pressure = 42.6 psia

Viscosity = 5 x 10^{-9} Reyns

R_i = 1.05 in, R_o = 1.75 in

Speed = 36,000 rpm

Number of pads = 9
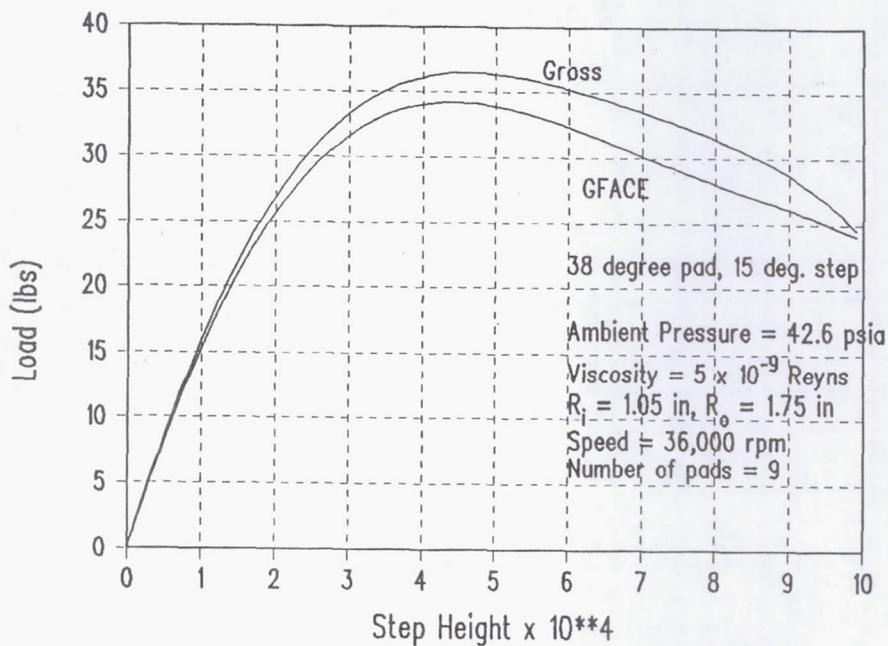
Load/Power vs. Step Height
Step Validation, Gross

Chart: Load/Power X 1000 Lbs/w vs Step Height x 10**4

Gross

GFACE

38 degree pad, 15 deg. step

Ambient Pressure = 42.6 psia

Viscosity = 5 x 10^{-9} Reyns

R_i = 1.05 in, R_o = 1.75 in

Speed = 36,000 rpm

Number of pads = 9

33
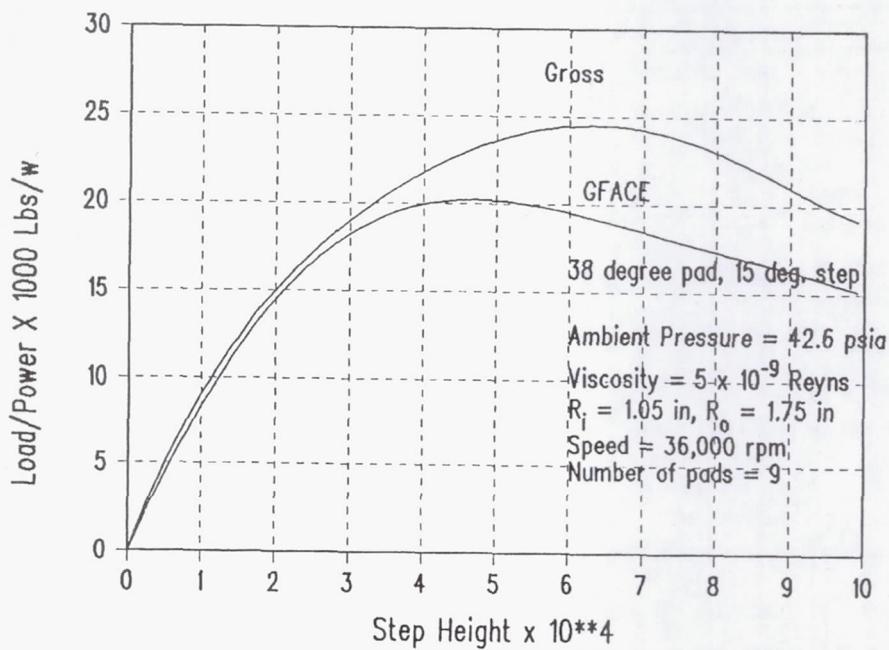
Automatic and Manual Stiffness Comparison

<table>
<tr><td colspan="3">Table 6-5
Stiffness Comparisons Between Automatic and Manual Computed Values
Rayleigh-step Pad
$\delta z = 0.0001$ in, $\delta\alpha = 0.0001$ deg., $\delta\beta = 0.0001$ deg</td></tr>
<tr><td>K_{zz}</td><td>$K_{\alpha z}$</td><td>$K_{\beta z}$</td></tr>
<tr><td>34,570</td><td>27,930</td><td>-48,980</td></tr>
<tr><td>33,000</td><td>26,700</td><td>-46,700</td></tr>
<tr><td></td><td></td><td></td></tr>
<tr><td>$K_{z\alpha}$</td><td>$K_{\alpha\alpha}$</td><td>$K_{\beta\alpha}$</td></tr>
<tr><td>39,900</td><td>31,750</td><td>-57,150</td></tr>
<tr><td>40,107</td><td>34,377</td><td>-57296</td></tr>
<tr><td></td><td></td><td></td></tr>
<tr><td>$K_{z\beta}$</td><td>$K_{\alpha\beta}$</td><td>$K_{\beta\beta}$</td></tr>
<tr><td>-44,200</td><td>-35,840</td><td>62,710</td></tr>
<tr><td>-45,836</td><td>-34,337</td><td>63,025</td></tr>
</table>

Hydrostatic Flow Comparisons

Calculated Flow	Computer Flow
$$f = 386.4\, A_o\, C_D\, G_1\, P_s \left\{ \left(\frac{P_r}{P_s}\right)^{\frac{2}{\gamma}} \left[1 - \left(\frac{P_r}{P_s}\right)^{\frac{\gamma-1}{\gamma}} \right] \right\}^{\frac{1}{2}}$$ $A_o = orifice\ area = \dfrac{\pi d_o^{\ 2}}{4} = \dfrac{\pi 0.010^2}{4} = 7.854\ x\ 10^{-5}$ $C_D = Coefficient\ of\ Discharge = 0.9$ $\dfrac{P_r}{P_s} = \dfrac{recess\ pressure}{supply\ pressure} = \dfrac{131+14.7}{200+14.7} = 0.678621$ $G_1 = \sqrt{\dfrac{2\gamma}{G_c \Theta(\gamma-1)}}$ $where\ \gamma = ratio\ of\ specific\ heats = 1.4$ $G_c = gas\ constant = 246,900\ \dfrac{in^2}{s^2 - °R}$ $\Theta = absolute\ temperature = 1460°R$ $f = 386.4 x 7.854x10^{-5} x 0.9 x 1.3935x10^{-4} x 214.7$ $x\left\{(0.678621)^{\frac{2}{1.4}}\left[1-(0.678621)^{\frac{0.4}{1.4}}\right]\right\}^{\frac{1}{2}} = 2.006x10^{-4}\ \dfrac{lbs}{s}$	$2.0022\ x\ 10^{-4}$ lb/s

Mahesh Athavale and Andrzej Przekwas
CFD Research Corporation
Huntsville, Alabama

OUTLINE

- **Objectives**

- **Status Report**

- **Code Capabilities**

- **Test Results**

- **Concluding Remarks and Future Plans**

OBJECTIVES (CFDRC)

- **Develop Verified CFD Code for Analyzing Seals**

- **Required Features Include:**

  - **Applicability to a Wide Variety of Seal Configurations such as: Cylindrical, Labyrinth, Face, and Tip Seals**

  - **Accuracy of Predicted Flow Fields and Dynamic Forces**

  - **Efficiency (Economy) of Numerical Solutions**

  - **Reliability (Verification) of Solutions**

  - **Ease-of-Use of the Code (Documentation, Training)**

  - **Integration with KBS**

SCIENTIFIC CODE DEVELOPMENT

Task 1:   Develop a 3D CFD Code (SCISEAL) for Cylindrical Seals

- for Annular, Tapered, Stepped
- Verification of Code Accuracy
- Rotordynamic Coefficient Calculations

Future Tasks: Augmentation of SCISEAL

- Incorporation of Multi-Domain Capabilities
- Extension to Labyrinth, Damper, Face, and Tip Seals

Note: Starting CFD Code = REFLEQS (developed by CFDRC under a contract from NASA MSFC/ED32)

STATUS: 1992 WORKSHOP

- **Numerical Methods in 3D Code**

  - Colocated Grids
  - High-Order Schemes
  - Rotating and Moving Grid Systems

- **Rotordynamic Coefficient Calculation Methods (CFD Solutions)**

  - Circular Whirl
  - Moving Grid (numerical shaker)

- **Seal Specific Interface**

  - Grid Generation
  - Pre-Processing

36

CURRENT STATUS

Augmentation Effort on SCISEAL:

- Implementation of Small Perturbation Model for Rotordynamics

    - Treat Eccentric as well as Centered Seals
    - Efficient, Economic Solutions

- Addition of 2-Layer Turbulence Model

    - Very Small Seal Clearances $\rightarrow$ Very Small y^+
    - Standard k-ε Model Inaccurate, Low Re Model Stiffness Problems, etc
    - 2-Layer Model Overcomes this Difficulty to Significant Extent

- Code Validation

    - Rotordynamics: Long & Short Annular Seals, Eccentric Seals
    - Labyrinth Seal Flow Computations
    - Entrance Loss Coefficients

CURRENT CODE CAPABILITIES

- Seals Code has:

    - Finite Volume, Pressure-Based Integration Scheme
    - Colocated Variables with Strong Conservation Approach
    - High-Order Spatial Differencing - up to Third-Order
    - Up to Second-Order Temporal Differencing
    - Comprehensive Set of Boundary Conditions
    - Variety of Turbulence Models (k-ε, Low Re k-ε, multiple scale k-ε, 2-Layer Model), Surface Roughness Treatment
    - Moving Grid Formulation for Arbitrary Rotor Whirl
    - Rotordynamic Coefficient Calculation Methods, CFD Based Centered Seals: (i) Circular Whirl (ii) Numerical Shaker
    - Small Perturbation: Centered & Eccentric Seals

SEAL SPECIFIC CAPABILITIES

- GUI and Preprocessor - Geared for Seals Problems

- Easy, Quick Geometry Definition and Grid Generation

- Four Types of Cylindrical Seals:

  - Annular, Axial Step-Down, Axial Step-Up, and Tapered

- Pull-Down Menus for Problem Parameter Specification

- One Line Commands for

  - Automatic Grid Generation
  - Integrated Quantities: Rotor Loads, Torque, *etc.*
  - Rotordynamic Coefficients

ROTORDYNAMIC COEFFICIENTS

- Relation Between Fluid Reaction Forces and Rotor Motion

$$
-\begin{bmatrix} F_y \\ F_z \end{bmatrix} = \begin{bmatrix} K_{yy} & K_{yz} \\ -K_{zy} & K_{zz} \end{bmatrix}\begin{bmatrix} y \\ z \end{bmatrix} + \begin{bmatrix} C_{yy} & C_{yz} \\ -C_{zy} & C_{zz} \end{bmatrix}\begin{bmatrix} \dot{y} \\ \dot{z} \end{bmatrix} + \begin{bmatrix} M_{yy} & M_{yz} \\ -M_{zy} & M_{zz} \end{bmatrix}\begin{bmatrix} \ddot{y} \\ \ddot{z} \end{bmatrix}
$$

Stiffness   Damping   Inertia (mass)
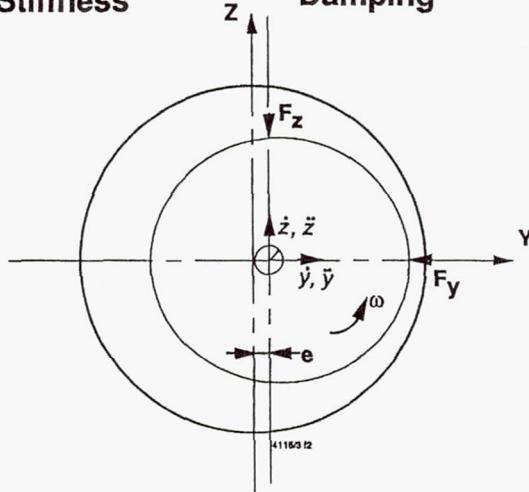
ROTORDYNAMIC COEFFICIENT METHODS

- **Circular Whirl Orbit Method**

  - Rotor Undergoes Circular Whirl
  - Rotating Frame → Quasi-Steady Solution
  - CFD Solutions at Several Whirl Frequencies
  - Pressure Integration to Yield Rotor Loads
  - Curve Fit to Force vs Whirl Frequency

*For Centered Rotor with Skew Symmetry Coefficient Matrices
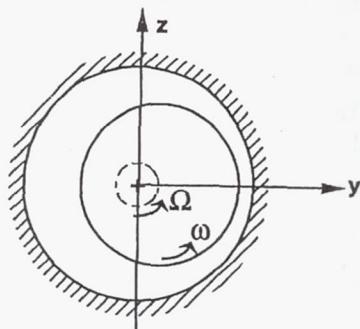
ROTORDYNAMIC COEFFICIENTS

- **Numerical Shaker Method**

  - Rotor Motion Along a Radial Direction
  - Time-Dependent Solutions
  - Moving Grid Algorithm for Grid Deformation
  - Time-Dependent Pressure Loads → Rotordynamic Coefficients
  - Can Treat Centered as well as Eccentric Seals
  - Time Accurate Solutions → Computationally Slower
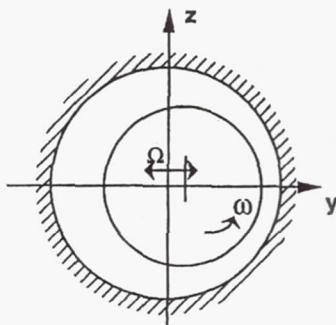
ROTORDYNAMIC COEFFICIENT
CALCULATIONS

- **Small Perturbation Method**

  - **For Centered or Eccentric/Misaligned Seals**
  - **Rotor Undergoes Circular Whirl with Very Small Radius**
  - **Resulting Perturbations in Flow Variables:**
    $$\phi = \phi^0 + \varepsilon\phi^1$$
  - **Generate 0th and 1st Order Flow Equations**
  - **Use Fournier Series in Time for Perturbations:**
    - -- **Complex Form of 1st Order Variables;**
    - -- **Flow Equations are Quasi-Steady**
  - **Complex Flow Perturbations Solved at Several Whirl Frequencies**
  - **Integrate Pressure Perturbations for Rotor Loads**
  - **Curve Fit for Rotordynamic Coefficients**

| $t = nT$ | $t = nT + T/8$ | $t = nT + T/4$ | $t = nT + 3T/8$ |

| $t = nT + T/2$ | $t = nT + 5T/8$ | $t = nT + 3T/4$ | $t = nT + 7T/8$ |
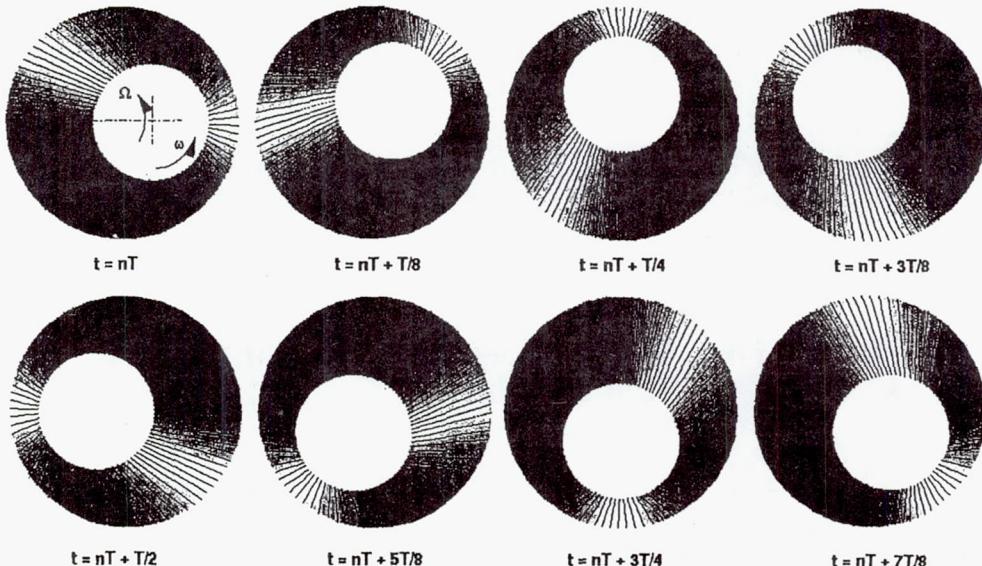
Time–dependent solutions of the perturbation pressure

$\varepsilon = 0.0$, Plane at half seal length, $\Omega = 2.0\omega$
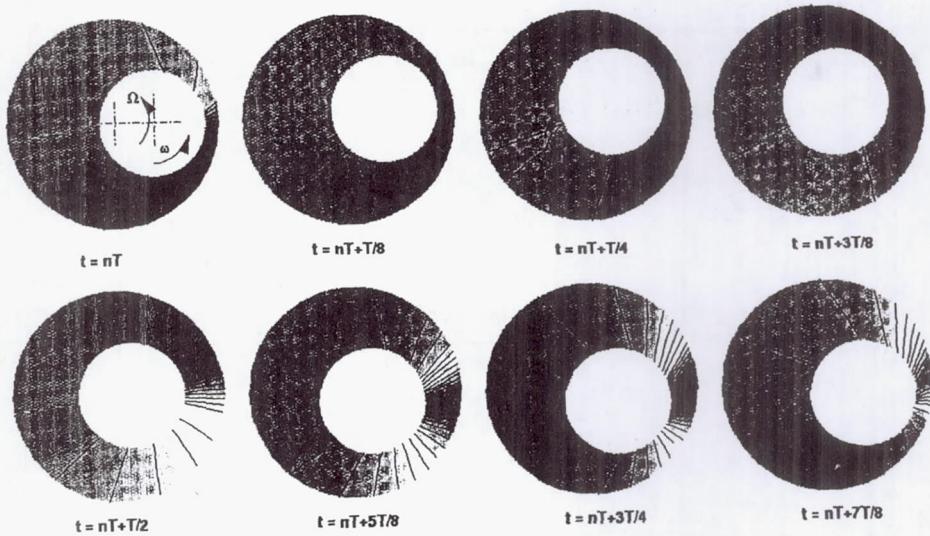
Time–dependent solutions of the perturbation pressure
$\varepsilon = 0.7$, Plane at half seal length, $\Omega \approx 2.5\omega$

2-LAYER TURBULENCE MODEL

- **Small Seal Clearances $\rightarrow$ very Low y^+ Values**

- **Standard Wall Functions $\rightarrow$ Inaccurate**

- **Low Re k-ε Model for Very Low y^+**
  - **can generate very stiff systems**

- **2-Layer Model Uses**
  - **wall functions for large y^+**
  - **Low Re k-ε model for very low y^+**

- **A Buffer Zone Used to Smoothly Merge the Two Treatments**

- **Model has been Tested for a Number of Seal and Rotating Flow Problems**

*Work Performed by Drs. Avva and Lai of CFDRC

41

SAMPLE RESULTS

- ## Computation of Flow in Enclosed Rotor System (Dailey and Nece)
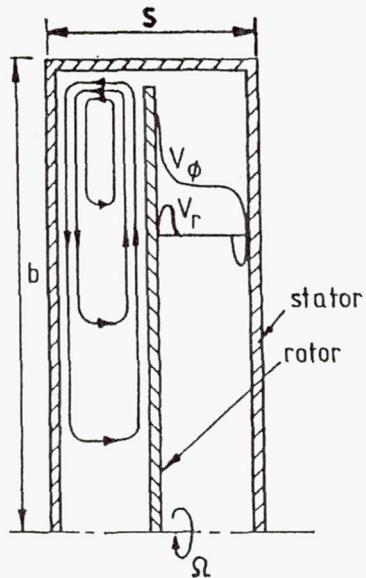
Torque coefficients,
Experimental value ~ 4×10^{-3}

k-ε with wall function		2-layer model	
near wall y^+	c_m	near wall y^+	c_m
16	3.58×10^{-3}	21	3.9×10^{-3}
0.7	5.28×10^{-3}	0.7	4.64×10^{-3}
0.04	5.59×10^{-3}	0.04	4.25×10^{-3}

CODE VALIDATION AND DEMONSTRATION

- ## Code has been Validated for a Large Number of Benchmark Problems

    - A List of 29 Relevant Problems Included in the Interim Report

- ## Extensive Validation Effort Conducted for Practical Seals:

    - Annular and Tapered Seals
    - Labyrinth Seals

- ## Annular Incompressible Seals (Dietzen and Nordmann, 1987)
- ## Long Incompressible Seals (Kanemori & Iwatsubo, 1992)
- ## Eccentric Annular Seal (Simon & Frene, 1991)
- ## Annular and Tapered Gas Seal (Nelson, 1985)
- ## Labyringth Seals Planar, (Wittig et al, 1987)
- ## Labyrinth Seals, Tapered Knives; stepped (Tipton et al, 1986)

VALIDATION CASES

1. Fully-developed flow in a pipe and channel.

2. Developing laminar flow in a narrow annulus between two cylinders. Slug flow at inlet, fully-developed flow at outlet.

3. Laminar flow between rotating cylinders. Below critical Taylor number, tangential flow only.

4. Flow between two cylinders, rotating inner cylinder. Taylor vortex flow, Laminar and turbulent.

5. 2-D driven cavity flow, Reynolds number up to 10,000. Comparisons with numerical results by Ghia et.al.

6. 3-D driven cavity flow.

7. Couette flow under different pressure gradients. With and without heat transfer.

8. Planar wedge flow in a slider bearing.

9. Laminar flow over a back step. Reattachment length comparison with experiments by Armaly and Durst.

10. Laminar flow in a square duct with a 90° bend. Comparison with experimental data by Taylor et.al.

11. Shock reflection over a flat plate.

12. Turbulent flow in a plane channel. Fully-developed solution at exit compared with experiments by Laufer.

13. Turbulent flow induced by rotating disk in a cavity. Comparison with experiments by Daily and Nece.

14. Centripetal flow in a stator-rotor configuration. Comparison with experiments by Dibelius et.al.

15. Flow between stator and whirling rotor of a seal. 2-D results for 0, 0.5, and synchronous whirl frequencies

VALIDATION CASES

16. Flow over a bank of tubes.

17. Turbulent flow in an annular seal. Comparison with experiments by Morrison et.al.

18. Turbulent flow in a 7-cavity labyrinth seal. Comparison with experiments by Morrison et.al.

19. Turbulent compressible flow and heat transfer in turbine disk cavities Athavale et.al.

20. 3-D driven cavity flow with lid clearance and axial pressure gradient. Control of flow through vortex imposition.

21. Flow in cavities on a rotor for an electrical motor. Interaction of Taylor vortices with driven cavity flow.

22. Flow in infinite and finite length bearings (without cavitation). Comparison of calculated attitude angles with theory.

23. Flow and rotordynamic coefficient calculation for straight, incompressible seals. Comparison with results from other numerical and analytical solutions; Dietzen and Nordmann.

24. Flow and rotordynamic coefficients in tapered compressible flow seals. Comparison with bulk-flow theory results; Nelson.

25. Rotordynamic Coefficients in a long annular incompressible flow seal. Comparison with experimental data; Kanemori and Iwatsubo.

26. Calculation of entrance loss coefficients in the entrance region of a generic seal. Effect of flow and geometry on the loss coefficient values; Athavale et.al.

27. Flow coefficient and pressures in a 5 cavity, straight knife, look-through labyrinth seal. Comparison with experimental data ; Witting et.al.

28. Flow coefficients and pressures in a 3 cavity, tapered knife, look-through labyrinth seal. Comparison with experimental data; Tipton et.al.

29. Flow coeffients and pressures in a 2 cavity, straight-knife, stepperd labyyrinth seal. Comparison with experimental data; Tipton et.al.

LONG ANNULAR SEALS

- **Experimental Data by Kanemori & Iwatsubo (1992)**

- **R = 39.656 mm, L = 240 mm, Rotor Speed = 600-3000 rpm**
  Clearance = 0.394 mm, Δp = 20 kPa - 900 kPa
  Specified Inlet Loss Coefficient, Ra = 1000-18000

- **Various Models Checked:**

  - **Whirl Method, Perturbation Method**
  - **Low Re k-ε Model, 2-Layer Model**
  - **20x15x30 grid**

DIRECT & CROSS-COUPLED STIFFNESS
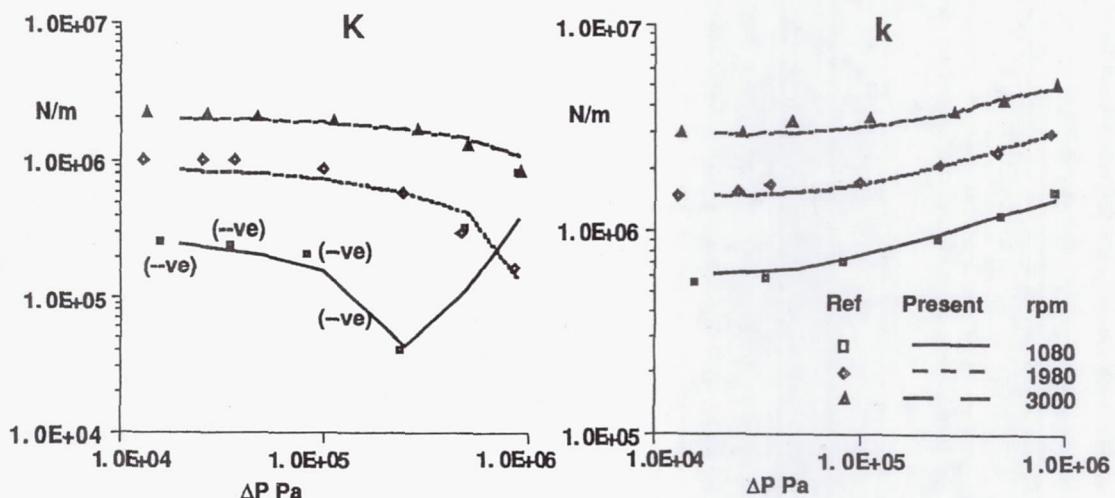
Symbols: Experimental Data by Kanemori and Iwatsubo
Lines: Numerical Results from SCISEAL

45

DIRECT & CROSS-COUPLED DAMPING

C

1.0E+05
Ns/m
1.0E+04
1.0E+03

Ref	Present	rpm
□	——	1080
◆	— —	1980
▲	— —	3000

1.0E+04   1.0E+05   1.0E+06
ΔP Pa

C

1.0E+05
Ns/m
1.0E+04
1.0E+03

Ref	Present	rpm
□	——	1080
◆	— —	1980
▲	— —	3000

1.0E+04   1.0E+05   1.0E+06
ΔP Pa

DIRECT MASS (INERTIA)

M

1.0E+03
kg
1.0E+02
1.0E+01

Ref.	Present	rpm
□	——	1080
◇	·······	1980
△	— ·· — ··	3000
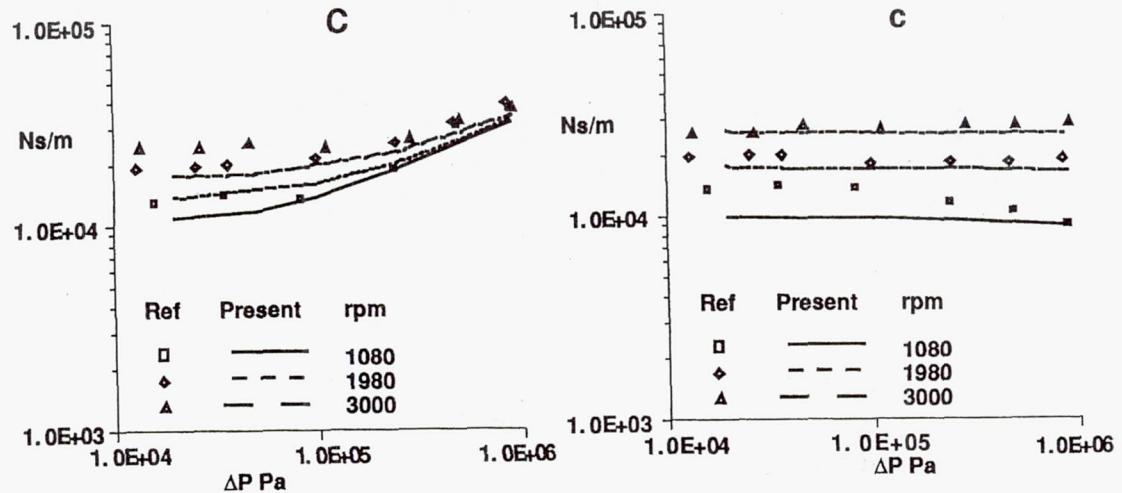
1.0E+04   1.0E+05   1.0E+06
ΔP Pa
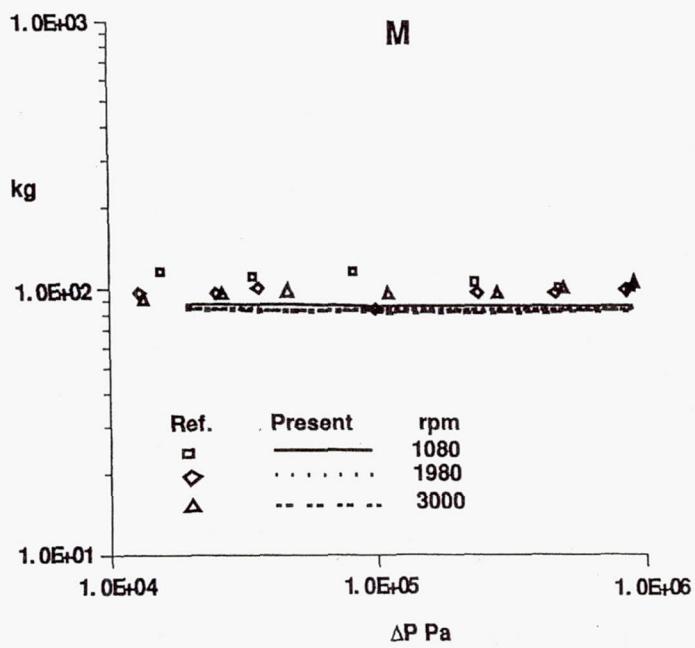
ECCENTRIC SEAL

- Experimental Data by Falco et al (1984)
  Numerical Data by Nordmann (1987), Simon & Frene (1991)

- Radius = 80 mm, Length = 40 mm, ε = 0. 1$\rightarrow$ 0.7
  4000 rpm, Δp = 1MPa, Entrance Loss Coefficient = 0.5

- Physical Models

  - Standard k-ε Model
  - Small Perturbation Method
  - 12x6x30 grid

DIRECT STIFFNESS COEFFICIENT, K_{yy}, K_{zz}

CROSS-COUPLED STIFFNESS, K_{yz}, K_{zy}

K_{yz}

K_{zy}

- ○ Experiment, Falco
- —— SCISEAL
- – — Nelson and Nguyen
- - - - - Simon and Frene
- – – Nordmann

DIRECT DAMPING, C_{yy}, C_{zz}

C_{yy}

C_{zz}

- —— SCISEAL
- – — Nelson and Nguyen
- - - - - Simon and Frene
- – – Nordmann

48
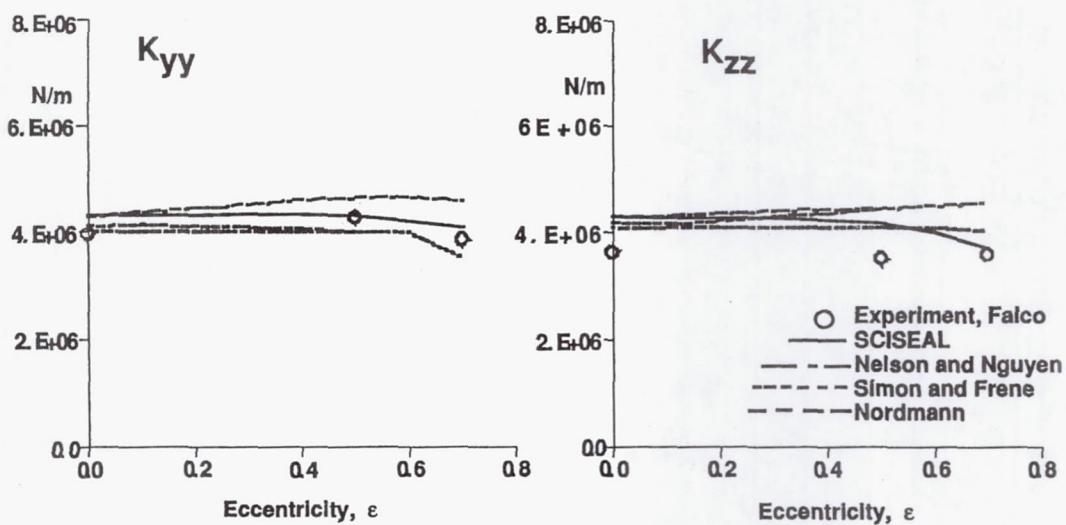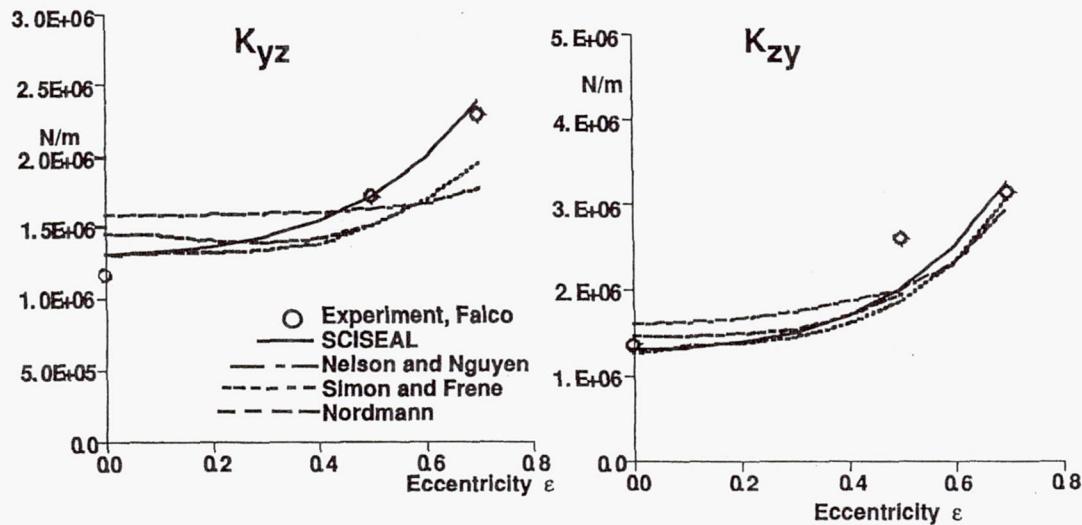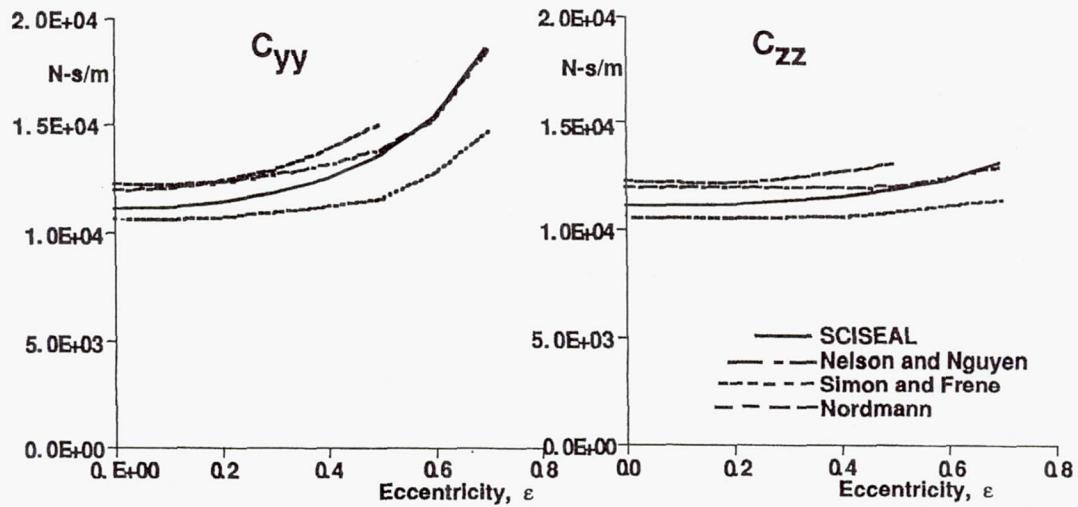
CROSS-COUPLED DAMPING, C_{yz}, C_{zy}
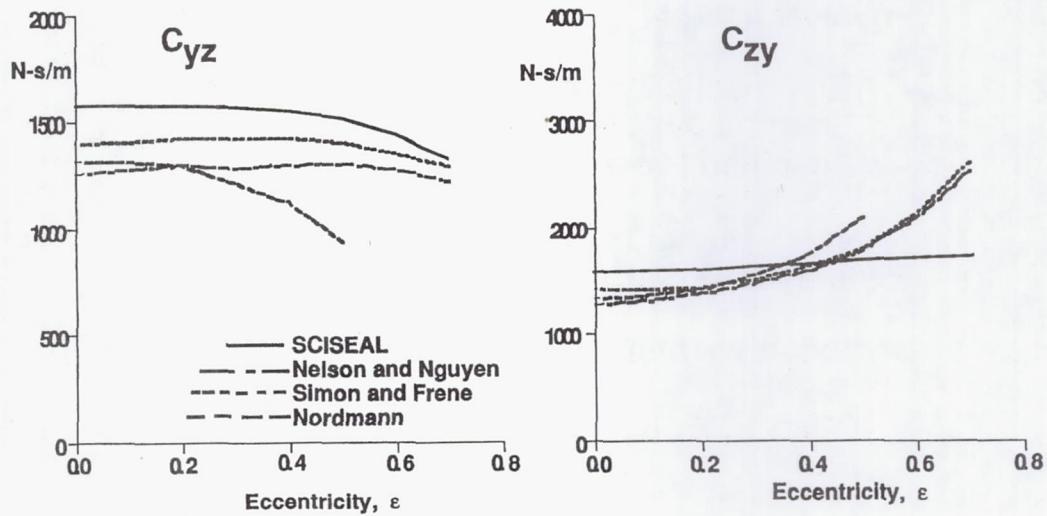
DIRECT INERTIA M_{yy}, M_{zz}

49
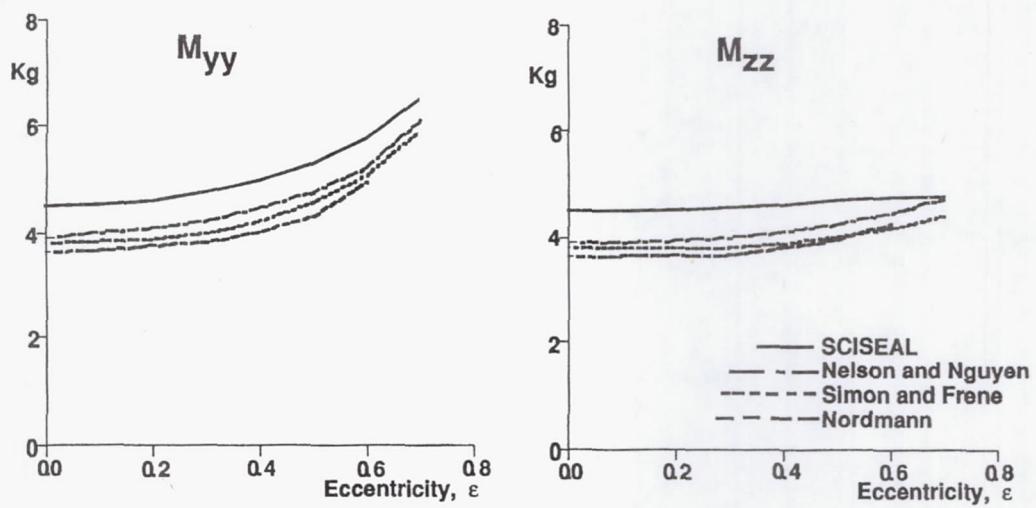
STRAIGHT LABYRINTH SEAL

- Experimental Data by Wittig et al (1987)

- 5 Cavity, Planar Look Through Seal

- Physical Models

  - 30x30 Cells in each Cavity, 8/12 Cells in Gap
  - Compressible Flow, Standard k-ε Model
  - Specified Pressure Ratio Across Seal

- Results: Numerical Results Compared with Experimental Data

  - Pressure Along the Seal Length for Different Tip Gaps
  - Mass Flow Rates at Different Tip Gaps and Pressure Ratios

RESULTS FOR STRAIGHT LABYRINTH SEAL

Pressure

Experimental data
Symbols:
- tip gap = 0.5 mm
- tip gap = 1.02 mm
- tip gap = 1.51 mm
- tip gap = 2.52 mm

$1 - \dfrac{\Delta p}{\Delta p_{max}}$

cavity number

Mass Flow

Experimental data
Symbols:
- seal gap = 0.5 mm
- seal gap = 1.51 mm
- seal gap = 2.52 mm

ϕ

seal pressure ratio
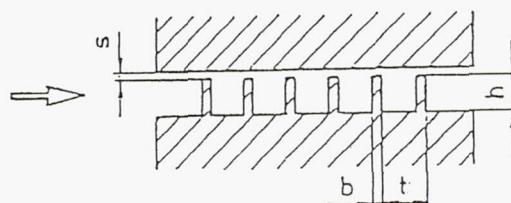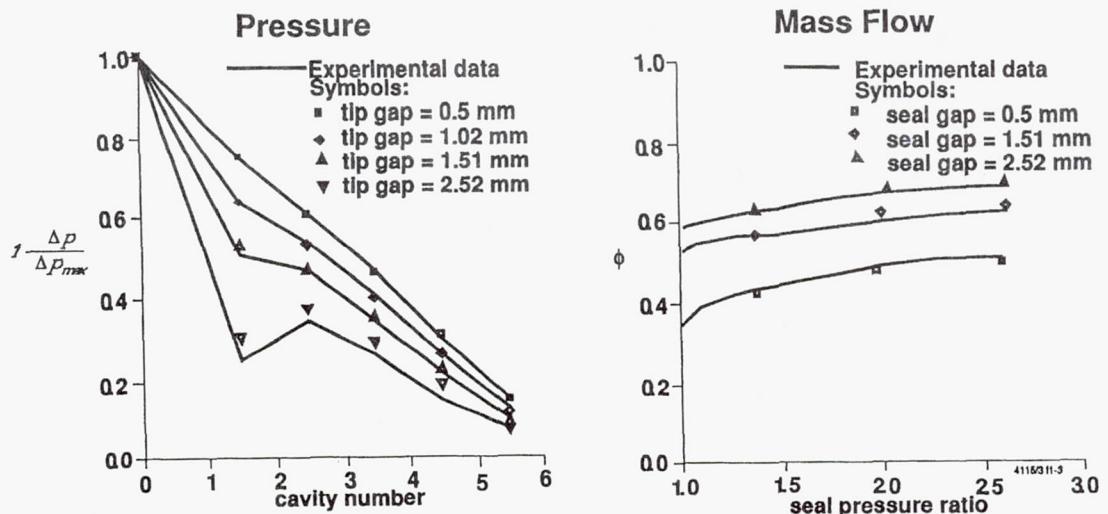
STEPPED LABYRINTH SEAL

- Experimental Data by Tipton et al (1986)

- 2 Cavity, Planar, Stepped Labyrinth Seal

- Physical Models:

  - Compressible Flow, Specified Pressure Ratio
  - Standard k-ε Model
  - 26x53, 26x62 Cells in Cavities; 10 Cells in Tip Gap

- Results: Numerical Results Compares with
  Experimental Data

  - Pressure Along Stator and Rotor Surfaces at One
    Pressure Ratio
  - Mass Flow Rates at Different Pressure Ratios

*Work Performed by Dr. Makhijani of CFDRC

RESULTS FOR STEPPED LABYRINTH SEAL

51
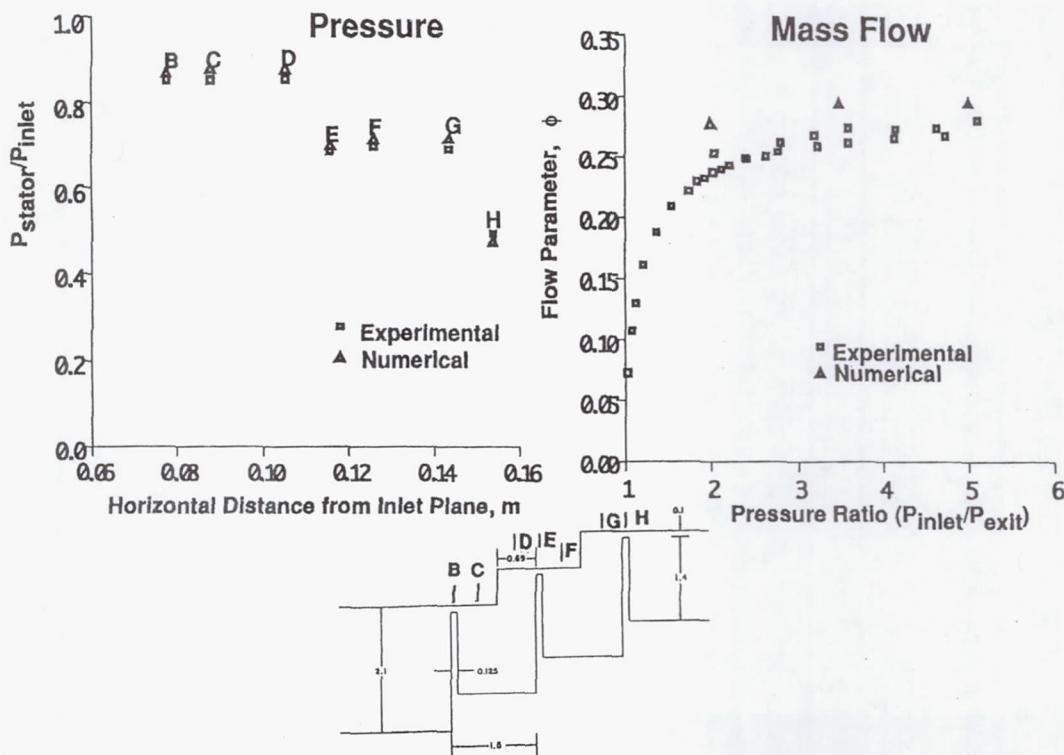
ENTRANCE LOSS COEFFICIENTS

- **Measure of Flow Losses at Entrance Region**

- **SCISEAL Used to Compute ξ with CFD Solution**

- **Variation of ξ with**

    - **Axial Reynolds Number**
    - **Seal Clearance-to-Radius Ratio**
    - **Entrance Gap-to-Clearance Ratio**

- **Physical Models**

    - **Incompressible Flow, Standard k-ε Model**
    - **Fully Developed Flow Upstream, Pressure Downstream**
    - **50 Cells in Axial Direction, 5 in Clearance, 30 or 50 in Entrance Region**
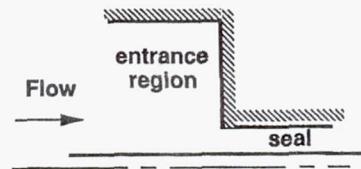
FLOW GEOMETRY FOR ENTRANCE LOSS
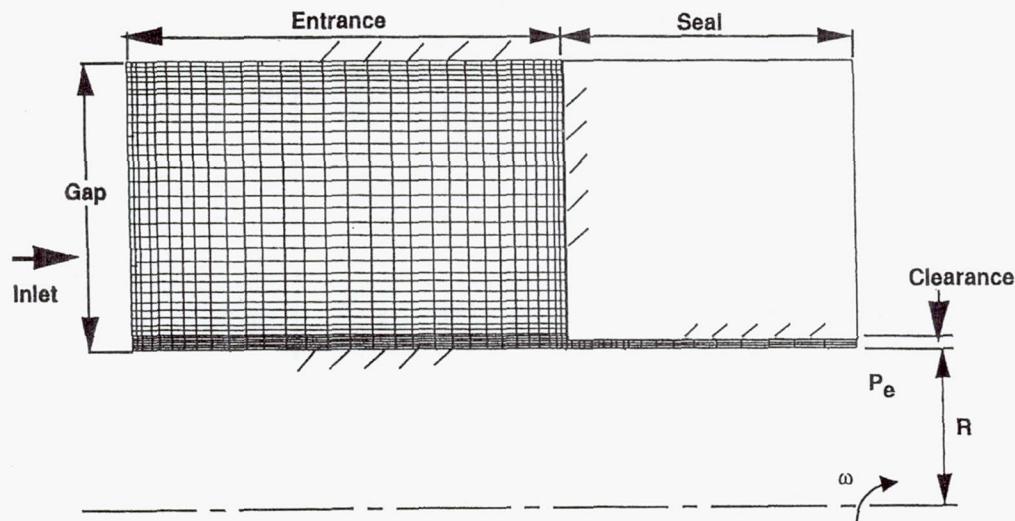
RESULTS

Table 1. Entrance Loss Coefficients, Radius/Clearance = 50

Entrance Gap/Clearance = 50			Entrance Gap/Clearance = 100		
u_{ax} m/s	Re_{ax}	ξ	u_{ax} m/s	Re_{ax}	ξ
10.814	10377	0.471	10.82	10384	0.490
16.232	15484	0.431	10.24	15584	0.488
21.619	20746	0.414	21.66	20785	0.482
26.942	25854	0.406	27.06	25970	0.48

PA-92-24 t2

Table 2. Entrance Loss Coefficients, Radius/Clearance = 100

Entrance Gap/Clearance = 50			Entrance Gap/Clearance = 100		
u_{ax} m/s	Re_{ax}	ξ	u_{ax} m/s	Re_{ax}	ξ
10.80	5181	0.562	10.797	5167	0.567
16.56	7945	0.54	16.176	7761	0.558
21.595	10361	0.526	21.55	10339	0.55
26.67	12796	0.51	26.934	12664	0.54
32.27	15484	0.493	32.24	15469	0.537
43.062	20667	0.478	42.533	20408	0.524

PA-92-24 t3

Table 3. Entrance Loss Coefficients, Radius/Clearance = 150

Entrance Gap/Clearance = 50			Entrance Gap/Clearance = 100		
u_{ax} m/s	Re_{ax}	ξ	u_{ax} m/s	Re_{ax}	ξ
10.82	3461	0.66	10.75	3438	0.68
16.19	5178	0.65	16.09	5146	0.66
21.49	6874	0.647	21.47	6874	0.65
26.74	8553	0.637	26.81	8553	0.648
32.25	10315	0.628	32.176	10292	0.64
48.33	15461	0.606	47.87	15315	0.63
64.487	20630	0.595	64.165	20630	0.624

RELATED CFD RESULTS

- **REFLEQS-3D Used for Rotating Flows**

  - **Flows in Inducer & Centrifugal Impeller (For MSFC Pump Consortium)**
  - **REFLEQS-3D & SCISEAL have Similar Numerical Techniques**

- **SCISEAL in Narrow, Long Channels**

  - **Suitable for Cooling Channels in Rocket Nozzles**
  - **Heat Transfer & Flow Calculations**
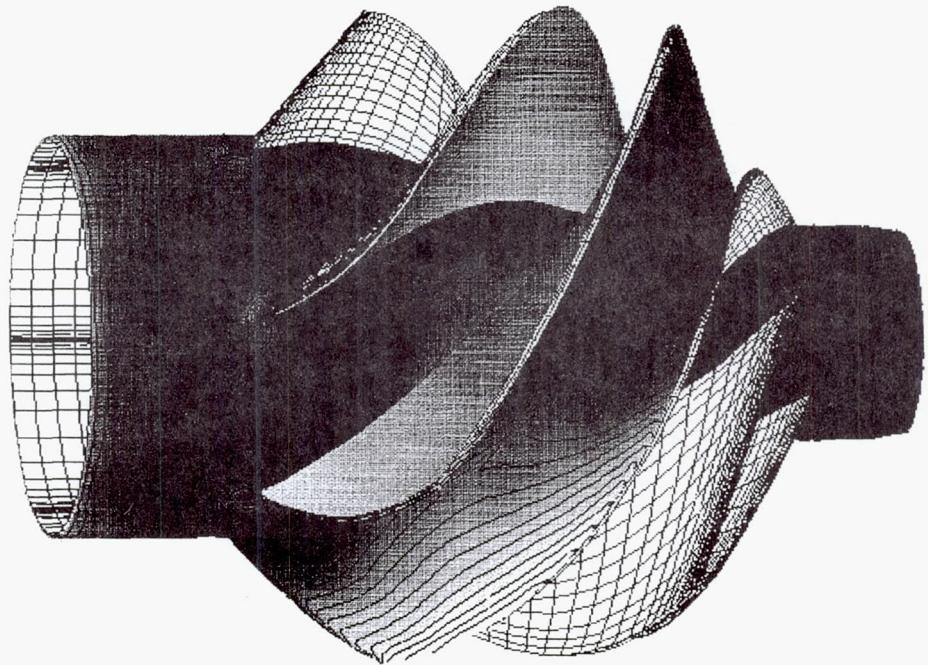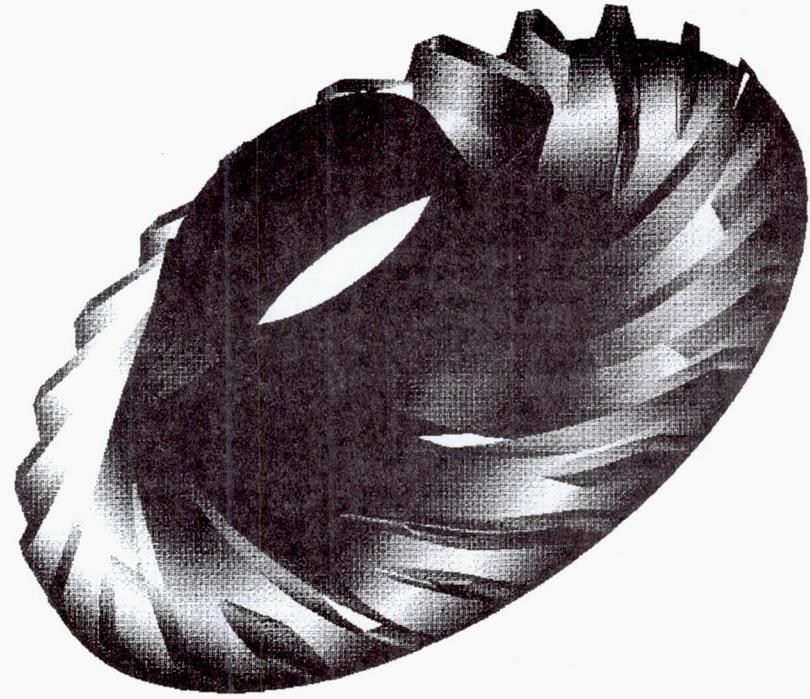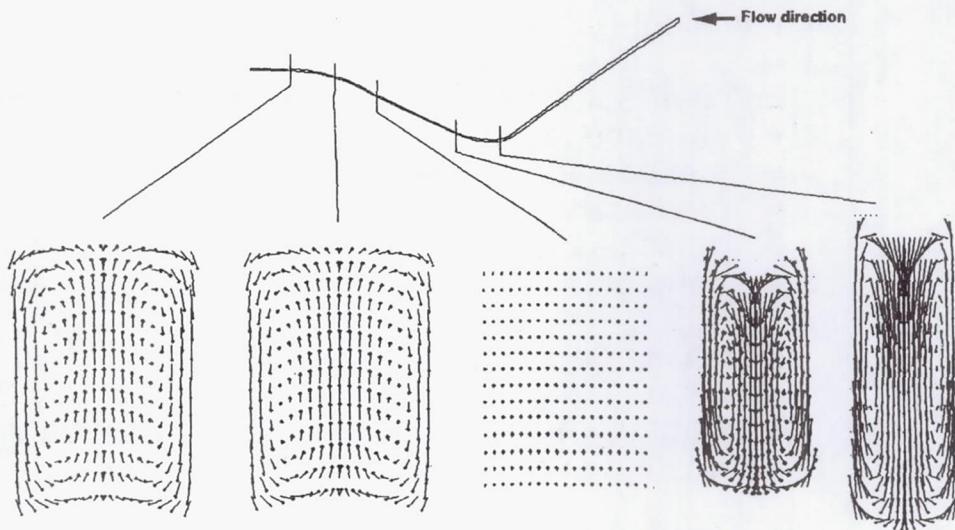
Secondary flow patterns in a long, narrow channel

(Velocity vector size and cross-section sizes not to scale)

CONCLUDING REMARKS

- A 3D CFD Code, SCISEAL, Being Developed and Validated

  - Current Capabilities Include Cylindrical Seals

- State-of-the-Art Numerical Methods

  - Colocated Grids
  - High-Order Differencing
  - Turbulence Models, Wall Roughness (in progress)

- Seal Specific Capabilities

  - Rotor Loads, Torques, etc

- Rotordynamice Coefficient Calculations

  - Full CFD Based Solutions - Centered Seals
  - Small Perturbations Method - Eccentric Seals

- Extensive Validation Effort

WORK PLANS FOR NEXT YEAR

- **Consolidate Current Models**

- **Include Multi-Domain Solution Methodology**

  - **Efficient Solutions for Complicated Flow Geometries**
    -- entrance region & seal clearance
    -- stepped and straight labyrinth seals
    -- face seals
    -- tip seals
    -- conjugate heat transfer

  - **Increases Code Flexibility**

  - **Technology Already Developed but Requires Adaptation and Testing for Seals**

- **Continue Work on Labyrinth Seals**

- **Validation/Demonstration for Practical Seal Configurations**

Entrance Loss Calculations
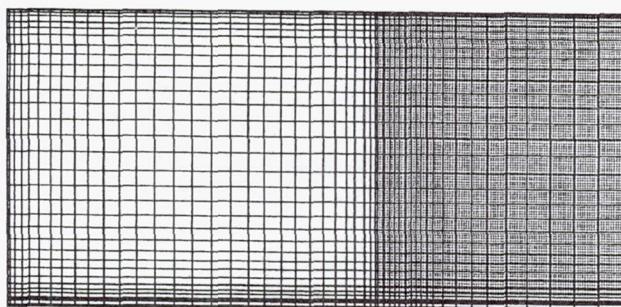
Single Domain Grid
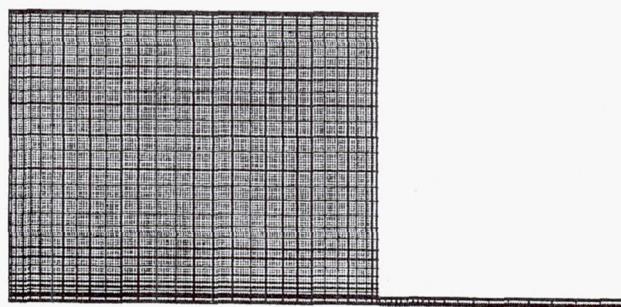
Multidomain Grid

Stepped Labyrinth Seal grids
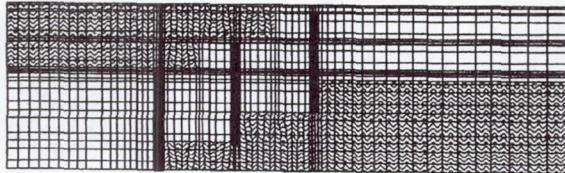
Single Domain grid
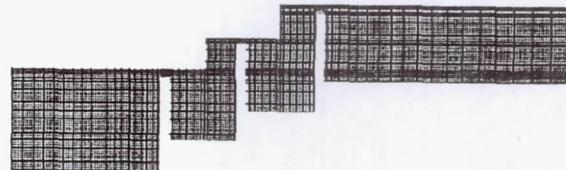
Multidomain grid

USER INTERFACE DEVELOPMENT

Bharat Aggrawal
Mechanical Technology, Inc.
Latham, New York

Current Status

User interface complete for the OS/2 version of the following components:

- Executive Shell

- Spiral Groove Gas Cylindrical Seals (SPIRALGC)

- Spiral Groove Gas Face Seals (SPIRALGF)

- Spiral Groove Face Seal Optimization (FACE)

- Gas Cylindrical Seals (GCYL)

- Gas Face Seals (GFACE)

- Incompressible Cylindrical Seals (ICYL)

- Incompressible Face Seals (IFACE)

- Fluid Properties Calculation (FLUID)

- Plotting Program for GCYL, GFACE, ICYL, and IFACE.

- Cylindrical Seals Configurations for SCISEAL

New Features

Features added since the last workshop based on user feedback:

- Units conversion between SI and English units from the **Analysis Options** menu item

- A **Set Defaults** menu option to set all input values to program defaults

- A **Batch Mode** option in the **Analysis** menu to run multiple test cases

- Automatic handling of data files from a previous test case

- Deletion of Input and Output files from the **File** menu in the Executive

- All analysis codes built using a 32-bit FORTRAN compiler for OS/2. Codes run at least twice as fast as the previous versions. Users must have OS/2 2.0 or later versions.

- New, easy to use installation program

- Several internal enhancements to improve performance and reduce development time

Preceding Page Blank

System Executive

```
┌─────────────────────────────────────────────────────────────────┐
│ CFD Industrial Codes Executive                              ⇧   │
│ File  Setup  Help                                                │
│                                                                  │
│                    CFD Seal Categories                           │
│                                                                  │
│     ┌──────────────────────┐      ┌──────────────────────┐      │
│     │ Bushing and Ring Seals│      │     Damping Seals    │      │
│     └──────────────────────┘      └──────────────────────┘      │
│                                                                  │
│     ┌──────────────────────┐      ┌──────────────────────┐      │
│     │      Face Seals      │      │     Brush Seals      │      │
│     └──────────────────────┘      └──────────────────────┘      │
│                                                                  │
│     ┌──────────────────────┐      ┌──────────────────────┐      │
│     │    Labyrinth Seals   │      │  Electro-Fluid Seals │      │
│     └──────────────────────┘      └──────────────────────┘      │
│                                                                  │
│     ┌──────────────────────┐  ▶   ┌──────────────────────┐      │
│     │      Tip Seals       │      │     Smart Seals      │      │
│     └──────────────────────┘      └──────────────────────┘      │
│                                                                  │
│                                    ┌──────────────────────┐      │
│                                    │   Utility Programs   │      │
│                                    └──────────────────────┘      │
│  Click On A Seal Category                                        │
└─────────────────────────────────────────────────────────────────┘
```

Bushing and Ring Seal Codes

```
┌─────────────────────────────────────────────────────────────────┐
│ ▦                                                           ⇧   │
│ File  Setup  Help                                                │
│        ┌────────────────────────────────────────────────┐       │
│        │ Bushing and Ring Seals                          │       │
│        │  CFD Industrial Codes                           │       │
│    B   │  ┌──────────────────────────────────────────┐  │       │
│        │  │ Gas Lubricated Spiral Groove Seal Analysis│  │       │
│        │  │             Program                       │  │       │
│        │  └──────────────────────────────────────────┘  │       │
│        │  ┌──────────────────────────────────────────┐  │       │
│        │  │ Gas Lubricated Cylindrical Seal Analysis │  │       │
│        │  │             Program                       │  │       │
│        │  └──────────────────────────────────────────┘  │       │
│        │  ┌──────────────────────────────────────────┐  │       │
│        │  │ Incompressible Cylindrical Seal Analysis │  │       │
│        │  │             Program                       │  │       │
│        │  └──────────────────────────────────────────┘  │       │
│        │  ┌──────────────────────────────────────────┐  │       │
│        │  │ Incompressible Spiral Groove Seal Analysis│  │       │
│        │  │             Program                       │  │       │
│        │  └──────────────────────────────────────────┘  │       │
│        │                                                 │       │
│        │   ┌──────────┐           ┌──────────┐           │       │
│        │   │   HELP   │           │   EXIT   │           │       │
│        │   └──────────┘           └──────────┘           │       │
│  Click On A Seal Category ───────────────────────────────┘       │
└─────────────────────────────────────────────────────────────────┘
```

Using an Industrial Code: FILE menu

Gas Lubricated Cylindrical Seal Analysis

File Input Analysis View Help

Read Input Data...
Save Input Data...

Data Set Title: Default input values for GCYL program
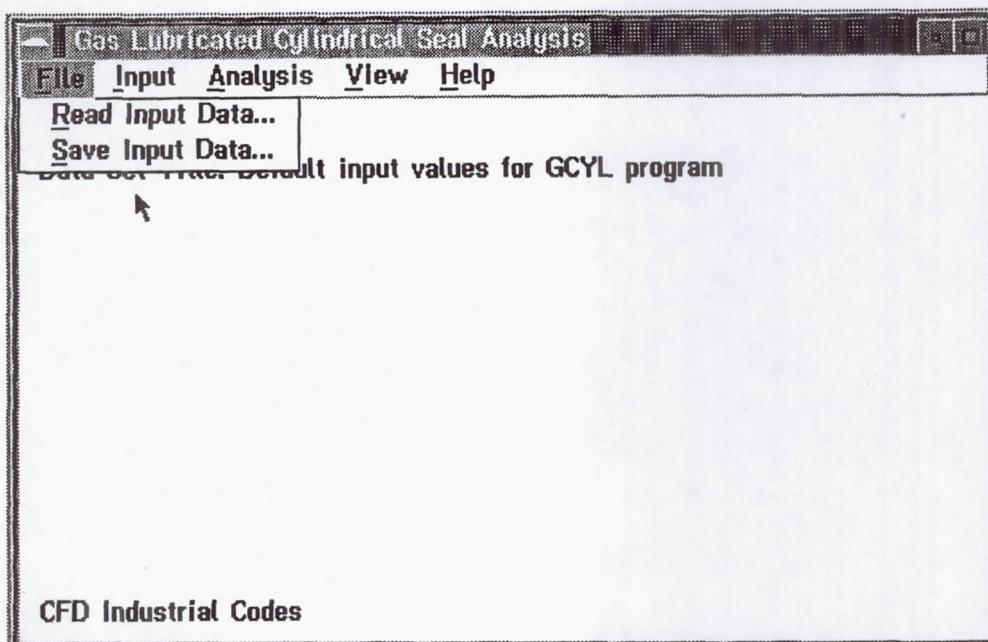
CFD Industrial Codes

Using an Industrial Code: INPUT menu

Gas Lubricated Cylindrical Seal Analysis

File Input Analysis View Help

Analysis Options...
Seal Geometry...
Data Operating Conditions...   les for GCYL program
Seal Configuration   →   Flow Lines...
Grid Definition...   Constant Pressure...
Properties...   Fluid Sources...
Solution Control...   Rayleigh Steps...
                                  Recesses...
Set Defaults...   Spot Recesses...

CFD Industrial Codes

Analysis Options

Descriptions Default input values for GCYL program

Type of Seal
- ● pads
- ○ sectored

Boundary Conditions
- ☐ symmetric
- ☐ periodic

Initial Values for Pressure
- ● User Input
- ○ From file

Calculate Stiffness?
- ○ yes
- ● no

Calculate Position?
- ○ yes
- ● no

Units
- ○ SI
- ● English

[Accept]   [Discard]

Help

Services Options Help

Stiffness Calculations

You can elect to have the analysis include cross coupled, frequency dependent stiffness calculations. The program provides the option of determining stiffnesses in two or four degrees of freedom. Two degrees of freedom include the x and y mode of the center of the journal while four degrees of freedom include the two orthogonal angular modes about the mass center. The Default is not to calulate stiffness.

[Previous] [Search...] [Print...] [Index]

GCYL program

Calculate Stiffness?
- ○ yes
- ● no

Calculate Position?
- ○ yes
- ● no

Units
- ○ SI
- ● English

Seal Geometry

Value	Label
1.00000	Seal Length - in
1.00000	Seal Diameter - in
0.00100000	Seal Clearance - in

1	Number of Sectors	0.000000	Starting Angle - deg
0.000000	Sector Pressure for each Sector - psia
0.000000	Projected Area for each Sector - in×2

1	Number Pads
0.000000	Start of First Pad Region - deg
10.0000	End of First Pad Region - deg
0.000000	Taper Angle - deg	1	Axial Node Number

Accept   Discard

Using an Industrial Code: Array Input

File   In

Flow Lines

Data Se

Number Flow Lines   6

	X1	X2	Y1	Y2
1	1	1	1	1
2	1	1	1	1
3	1	1	1	1
4	1	1	1	1

Accept   Discard

CFD Industrial Codes

63

Using an Industrial Code: Analysis menu
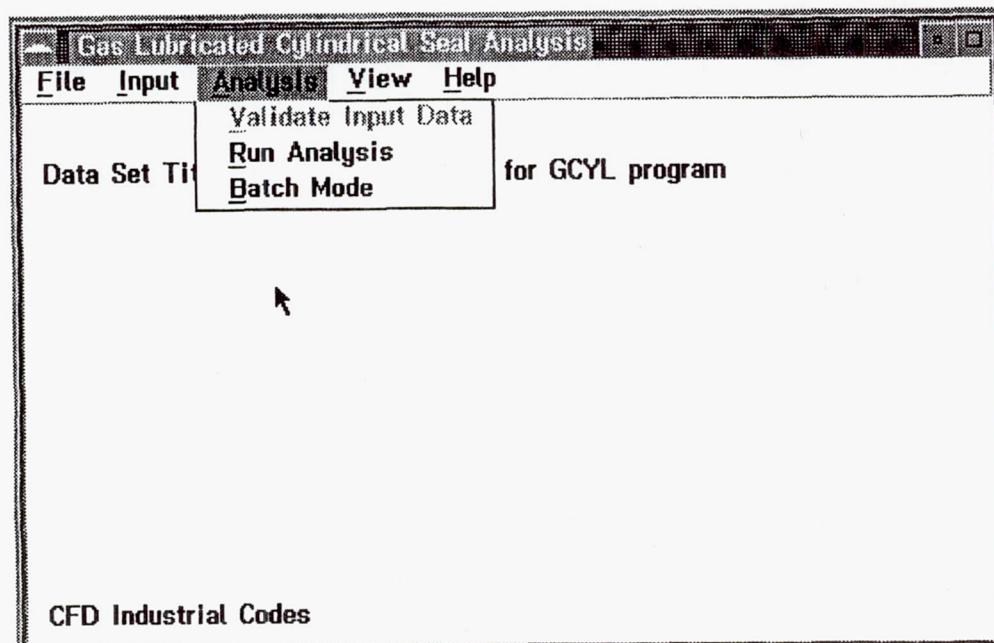
Using an Industrial Code: Batch Mode

Gas Lubricated Cylindrical Seal Analysis

File Input Analysis View Help

Program Input
Program Output
Plots...

Data Set Title: Default   YL program

▶
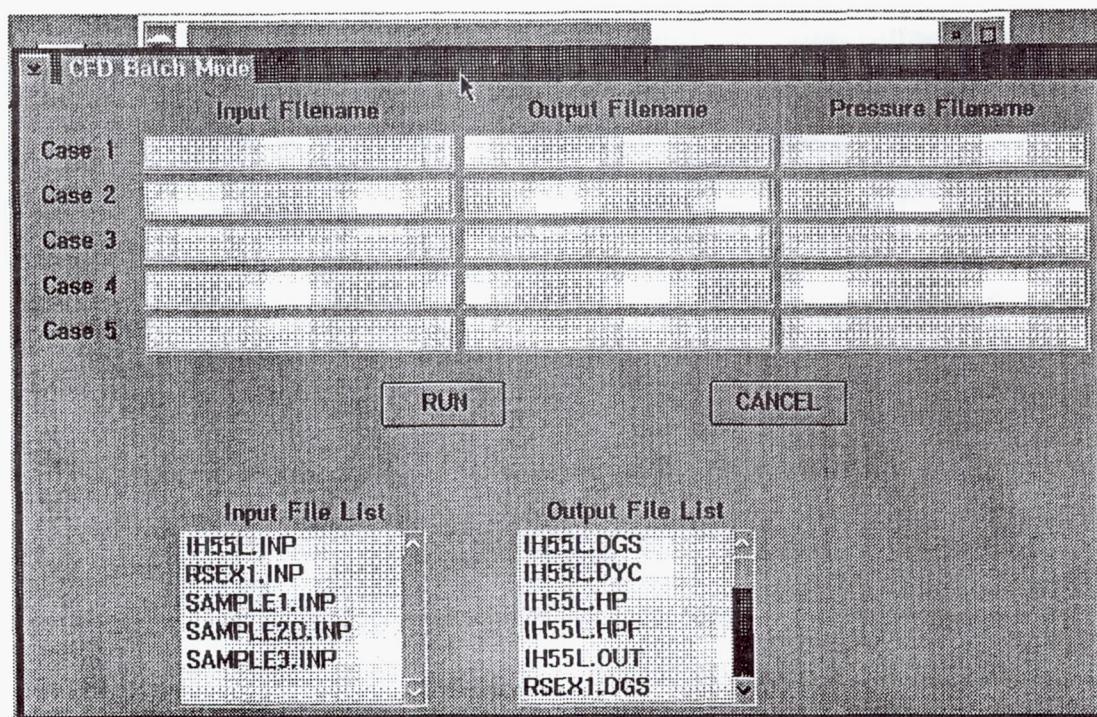
CFD Industrial Codes
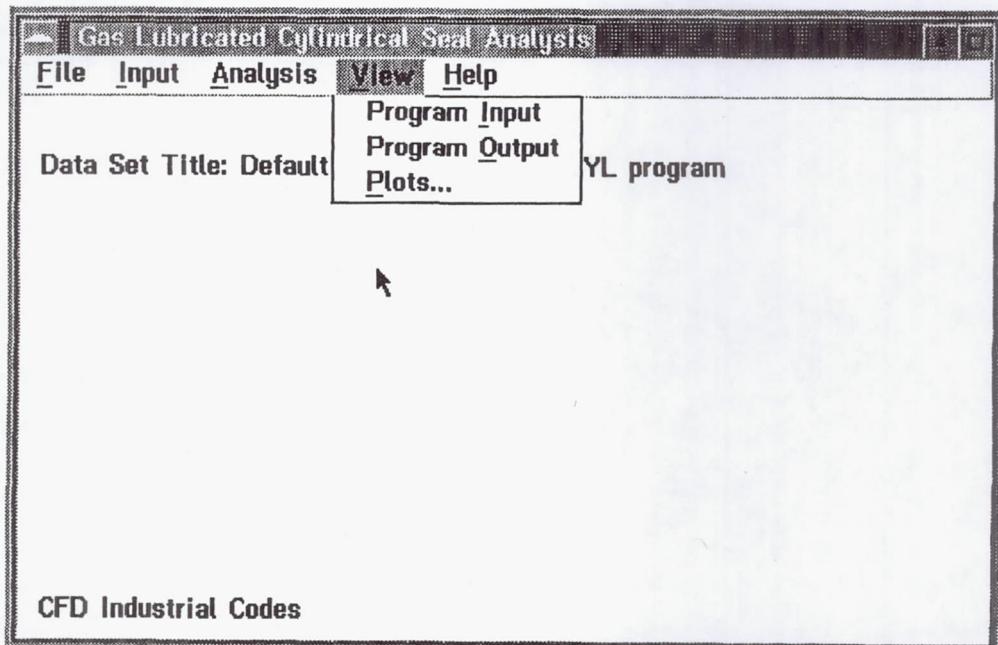
CFD Browse Utility

Browsing File: C:\CFD\OUTPUT\GCYL\IH55L.OUT

```
Q GCYL     MTI     Sample 4:  T-Shaped Sectored Seal


ECHO OF INPUT


OPTION    =   2          GIVEN LOAD, LOAD ANGLE FIND EX, EY
UNIT      =   1.         ENGLISH UNIT
ISTIF     =   1          STIFFNESS CALCULATION
DEGREES OF FREEDOM =   4.
EXCITATION SPEED, RPM  =        .0010
NPAD      =   1          NUMBER OF PADS
START     =   30.00      STARTING ANGLE OF PAD # 1
PAD ANGLE =   120.00         PAD ANGLE OF PAD # 1
DIAMETER  =   2.6790     BEARING DIAMETER
LENGTH    =   .0000      BEARING LENTH
CLEARANCE =   .001000    BEARING CLEARANCE
VISCOSITY =   .2900E-08  ABSOLUTE VISCOSITY
ABS TEMP  =   528.00     ABSOLUTE TEMPERATURE
SPECIFIC  =   1.6600     SPECIFIC HEAT RATIO
GAS CONST =  1790000.0   GAS CONSTANT
```

OK   PRINT

65

File   Plot   Views   Setup   Help

GCYL   PRESSURE DISTRIBUTION

Sample 4: T-Shaped Sectored Seal

DIAMETER = 2.400 IN   SPEED = .00 RPM

LENGTH = 1.027 IN

CLEARANCE = .001000 IN

ANGULAR DEGREES
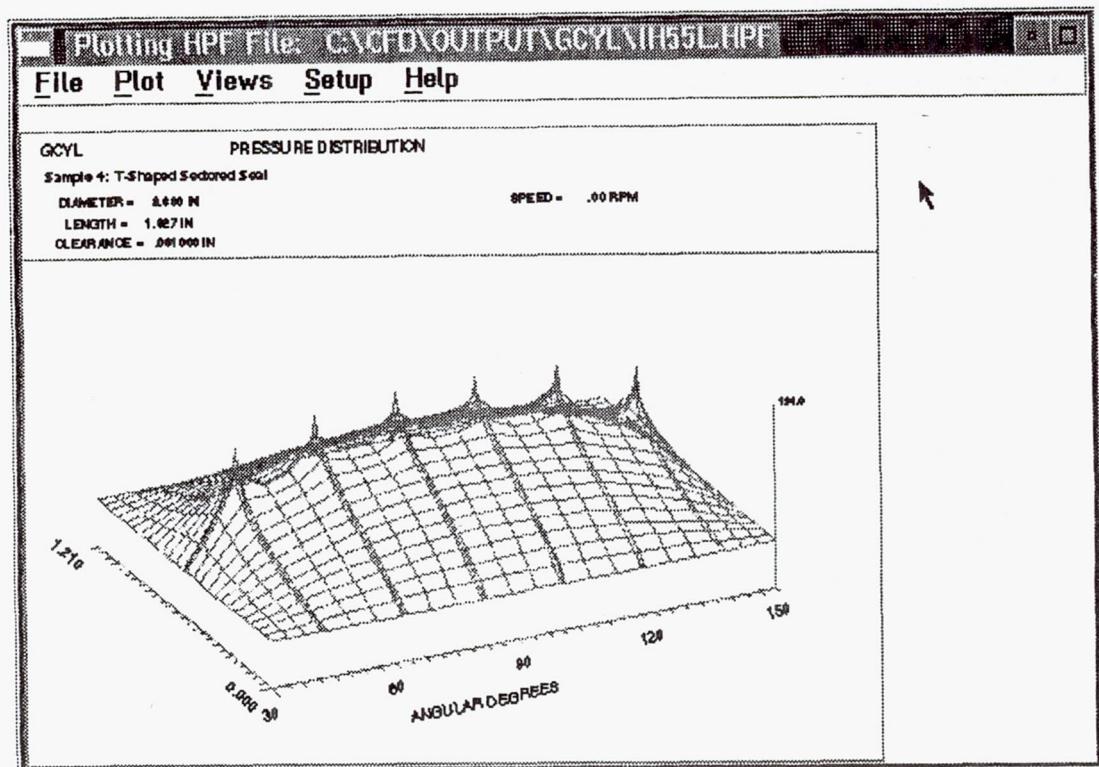
Work in Progress - Future Plans

New components to be added to the system:

- Labyrinth Seal Analysis (KTK) from the Air Force. Work about 70% complete.

- Seal Dynamics Code (Face and Cylindrical Seals)

- Expert systems

- Enhancement of SPIRALI to include loss coefficients for spiral grooves

Operating System Considerations:

- Problems with conversion of user interface code to Unix

- Distributed Computing Environment (DCE) makes it possible to run programs on an OS/2 machine from a Unix workstation

- OS/2 to be available for Power PC RISC machines in April-May 1994.

- Ability to run both Unix and OS/2 on the same machine at the same time on systems based on OSF Mach 3 kernel

66

ENVIRONMENTAL AND CUSTOMER-DRIVEN SEAL REQUIREMENTS

Robert C. Hendricks
NASA Lewis Research Center
Cleveland, Ohio

SUMMARY

Public awareness of environmental hazards, well-publicized effects of hazardous leakages (Three Mile Island, *Challenger*), and a general concern for planet Earth have precipitated emission limits that drive the design requirements for seals applications. Types of seals, barrier fluids, and the necessity of thin lubricating films and stable turbomachine operation to minimize leakage and material losses generated by rubbing contact are discussed.

ENVIRONMENTAL CONSIDERATIONS

Ludwig and Greiner (refs. 1 and 2) pointed out that in technical societies the fluids which must be sealed range from the familiar fluids, such as water and oil, to unfamiliar fluids, such as oxygen, hydrogen, and toxic chemicals. The seals developed for these applications have many diverse forms, from low-cost automotive water pump seals to very sophisticated seals for liquid oxygen and liquid hydrogen turbopumps, such as those used in the space shuttle main engines. It is also recognized that seals have a significant cost impact in regard to maintenance, downtime, and health hazards. Personnel exposure to even low levels of some substances can have serious health consequences, with airborne debris (fibers, metals, bleed fluids, and combustion byproducts) being one form of most interest. The insidious aspect is that the health damage does not become manifest until late in life.

In regard to chemicals that may be a health hazard, Wegman (ref. 3) pointed out that one source of worker exposure comes from leaks in valves and pumps and stated that preventing such health hazards (occupational diseases) is highly desirable because they tend to be chronic, untreatable, and fatal and may go unnoticed if not resulting in an unusual group of clinical manifestations. Industrial carcinogens cause an excess risk that does not appear to drop after exposure ends. Specifically, Spivey (ref. 4) listed numerous substances that appear to be associated with excessive lung cancer mortality, among these are polycyclic aromatic hydrocarbons, bis chloromethyl ether (BCME), and chloromethyl methyl ether (CMME).

Other health hazard sources include the insidious nature of lost, forgotten, and buried toxic chemical and hazardous wastes from strategic manufacturing facilities; storage depots for fuels, chemicals, and bombs; nuclear wastes stored on site; and "abandoned" nuclear and refinery facilities. Many sites were established during World War II when other considerations took precedence. Some areas are so toxic that current technology offers no solution, and the unsettling potential for mishaps and contamination of the soil, the water table, and the atmosphere is significant.

These hazards and increasing world concern about the presence and use of noxious, toxic, and hazardous compounds on planet Earth has prompted legislation at nearly every level of government. The Occupational Safety and Health Administration (OSHA) and the Environmental Protection Agency (EPA) have developed exposure limits for hundreds of substances, with additional substances added daily (e.g., ref. 5). Regulators have gone from a position of little or no concern to one of severely restricting all hazardous emissions.

In order to assist planners and regulatory agencies, simulation programs are being employed to determine cleanup procedures and to evaluate the impact of hazardous materials on the planet and its inhabitants. For example, SIMSITE deals with the cleanup of toxic, radioactive, biological, or foul waste sites; SIMEARTH allows one to simulate the global impact of managing the Earth's resources; SIMREFINERY simulates the production and marketing of, for example, a refinery product from the crude oil state; and SIMPOWER simulates the production and distribution of power over a large power grid such as on the west coast. (Private communication, Tom Cochran of Yosemite Inc.)

For manufacturers and users of valves, pumps, compressors, and other processing devices the focus has been on volatile organic compound emissions (e.g., the California South Coast Air Quality Management District (SCAQMD) limits fugitive emissions to 1000 parts per million (ppm)).

New sealing requirements are set out in American Petroleum Institute API–610 and American National Standards Institute ANSI–B73 standards dealing with new sealing chamber design requirements.

It is especially important to realize that wear debris contributes to emissions (e.g., asbestos in brake linings) and that seal dynamics plays a major role in the control of rubbing and wear debris generation. Not only are the tribological properties of seal materials essential to the performance of a low-emissions seal, but the wear debris must be benign.

Sealing by low-emissions mechanical face seals centers on thin lubricating films and barrier fluids. Three types of seal technology to control emissions are (refs. 1, 2, and 6) single-seal systems and both tandem and double dual-seal systems.

Single-Seal Systems

A properly designed and operating single mechanical seal (fig. 1) can limit emissions to less than 500 ppm, with emissions to the atmosphere limited further by the vapor recovery and disposal technique.

Dual-Seal Systems

A tandem mechanical seal (fig. 2) is made up of two seal assemblies and a barrier fluid that isolates the process fluid from the atmosphere (i.e., a zero-process-fluid emissions seal when attention is paid to vapor pressures and miscibility). The inboard assembly seals the process fluid and the outboard assembly seals the barrier fluid. Emissions to the atmosphere are limited by the recovery and disposal techniques. Examples of common barrier fluids are given in table I and are discussed later.

The double mechanical seal (fig. 3) has two assemblies operating in a barrier fluid that is circulated at a higher pressure than the process fluid and may be internally or externally pressurized. Again zero emissions can be met with proper filtering and disposal.

Emission limits for these seal systems are set in table II (adapted from ref. 6).

MANUFACTURE

The manufacture of seals requires the use of hazardous materials and machining procedures. For example, the rub runner for the brush seal system requires a hardened smooth-running surface. Such a

surface can be built up by plasma spraying, electroplating, ion implanting, CVD/PVD (chemical/physical vapor deposition), sol-gel methods, and filtered arc and laser methods. It is costly and time consuming for manufacturing facilities using these techniques to satisfy the requirements as established by local and Federal environmental laws covering airborne emissions; external radiation levels; noise; water-based effluents; solid liquid and bulk waste disposal procedures; and the handling and storage of toxic, radio-active, and other hazardous materials. Consequently, alternative methods are sought; for example, iron coating solutions generate low amounts of toxic byproducts in a relative sense.

REGULATIONS

For regulations applicable to the control of volatile organic compound emissions from process pumps and compressors, see title 40, part 60, of the Code of Federal Regulations (abbreviated 40 CFR 60). Method 21 (in appendix A of 40 CFR 60) specifies measurement equipment and procedures for these emissions. In California the Bay Area Air Quality Management District has issued regulation 8, rule 25, covering pumps and compressors in refineries and chemical plants, and SCAQMD has issued rules 466 and 1173 with similar coverage (ref. 6).

The definitions of leaks in reference 6 are of some interest:

(1) Leak definition: Instrument reading of 10 000 ppm or greater or visible drip, spray, or mist

(2) Inspection schedule:
   Visual, each calendar week
   Instrument, monthly

(3) Repair schedule: First attempt within five calendar days; repair not later than 15 calendar days after leak is detected.

Perhaps the torte system will be invoked to resolve environmental situations (i.e., a party sues another, giving the person the right to prove his complaints rather than setting standards in terms of parts per billion). For example, suits may be brought over who controls aerospace vehicle fuel dumps in regulated areas and the intentional or emergency disposal of hazardous waste sprayed in unregulated areas from an aerospace vehicle.

BARRIER FLUIDS

Isolation of hazardous fluids (e.g., hydrogen and oxygen, acids, and radioactive gases) is often achieved by introducing into tandem, dual, or multiple seals or other seals a barrier fluid that is "drained" for treatment or disposal. Emission restraints and restrictions on the use of volatile hazardous air pollutants can be eased by using barrier fluids.

Air and water are common barrier fluids. Although the choice of a barrier fluid is application specific, parameters to be considered are (ref. 7)

(1) Compatibility of barrier and process fluids
(2) Cost and availability
(3) Lubrication, corrosiveness, and degradation with time (under load)
(4) Environmental compatibility and ease of recycling

69

(5) Steady-state rise and fluctuations in seal face temperature

(6) Post-test arithmetic average Ra of the absolute value of the unfiltered roughness profile

Inert gases (e.g., noble gases, nitrogen, and carbon dioxide) are effective barrier and purge gases. For example, helium barrier gas effectively isolates hot, hydrogen-rich steam from oxygen in space shuttle main engine applications (fig. 4, refs. 8 and 9). However, it is costly in terms of mission payload, and more efficient designs are being pursued.

Common barrier fluids and the results from testing with a 42.7-mm-diameter cartridge type of bellows seal operating at 3600 rpm are shown in table I. The seal inboard face was silicon carbide (SiC) versus SiC, and the outboard face was carbon versus SiC. The process fluid was 10 wt hydraulic oil. For these tests water showed low face temperature rise, low fluctuations, and low post-test Ra but may not be the barrier fluid of choice because of incompatibility (refs. 8 and 9).

The memory and reality of the Three Mile Island nuclear mishap are clear, and the stringent sealing requirements established by the Nuclear Regulatory Commission dictate a special class of compliant foils and compliant face seals. Face seals have very thin films and special materials to minimize thermo-mechanical distortion. They must operate with a large stability margin. Nuclear seal packages are usually staged seals or multiple seals to prevent the working fluid leaking to the environment. All leakage is collected, processed, and disposed of or returned to the system. For example, for a multiple-seal system operating at 3600 rpm and 2500 psi the first face seal configuration operates with a mating ring flatness of 3.5×10^{-4} in., or three light bands, and leaks about 3 gal/min of brackish water. The second face contacting seal operates near 30 psi. The third contacting seal dam, face seal, or emergency seal operates near 5 psi and is a single-dam bellows type with scraper rings to remove contaminant buildup before the working fluid is returned to the system.

In another application the U.S. Army decreased a tank's specific fuel consumption (sfc) by slowing the compressor at idle but failed to recognize that the compressor air buffered the oil sump labyrinth seal. Occasional blowby occurred and smoke entered the cabin. Because it would have cost millions to reprogram the sfc controller, a decrease in oil pressure was sought as the solution. The point is that both the overall system and the environmental effects must be considered when changes are made either in the field or on the drawing board.

Similar problems are reported in small aircraft turbomachines during startup and shutdown where oil leakage (smoke) may cause an oil sump redesign; this problem is further discussed in the next section.

Automotive engines, and other terrestrial-based engines, are more focused on EPA requirements. For example, valve stem sealing requirements for 98 standards show the need for redesign.

AEROSPACE-RELATED SEALING

Perhaps the aerospace industry is unique in that rather than having an agency dictate the leakage standards, it is the customer who drives requirements (e.g., for the cabin air system in commercial aircraft, where customers pay significant sums of money to be afforded creature comforts and are unwilling to put up with the smell of kerosene in the cabin). Because the cabin air is bled from the compressor, it becomes essential that this air be made as free of contaminants as possible, including the effects of recycled cabin air.

Further, the sealing required to maintain spacecraft environments (e.g., Apollo and shuttle) entails complete life support systems that are sealed to the hostile environment of space. Here the astronauts put up with orders of magnitude more difficult environments than the commercial aircraft customer, but there are limits (Grissom cabin fire). The *Challenger* is probably one of the most publicized seal failure incidents in history and led to many design and philosophical changes.

In early aircraft engines a significant amount of smoke would be discharged upon startup and sometimes during operations owing to unspent fuel mixtures and oil being dumped into the exhaust. Smoke, which implied fire, was of concern to the passengers, who demanded changes, and most of today's engines are nearly smoke free. A low-smoke, low-emissions engine requires interface seals to prevent hazardous materials from reaching the atmosphere. Thus, the need is for low-leakage interface seals, such as a face seal or a leaf seal or some form of contacting seal. The cabin and local environmental problems are more acute at startup and shutdown, as during normal operations the engine is at altitude, where dilution air abounds. However, the upper atmosphere is probably the worst place to put polluted materials. They can reduce the effective sunlight, alter the atmosphere, and deposit thin contaminant layers all over the face of the Earth.

Aircraft and stationary gas turbines generating power for utilities must deal with dilution air leakages including oxides of nitrogen (NO_x). New static brush and rope seals are being tested or considered to minimize the leakage between the compressor and the combustors. It is important to recognize that not only are these leakages objectionable to the "customer," but they also imply losses that decrease the performance of the turbomachine. For example, the high-speed civil transport (HTSC) goal, 5 g NO_x/kg fuel burned, requires combustor sealing. It is also recognized that a 1-percent decrease in turbomachine efficiency results in a 6-percent increase in gross HSCT takeoff weight.

Surface wear can generate debris that can enter the combustion system and form oxides as it passes through the engine tailpipe. Further, upon the impact of a hard landing the rotors can be displaced and rub into the seals. These materials can be released into the combustion stream or into bleed air (hopefully not into the cabin air). The toxicology of these products is not well known and further studies are required.

Some seal configurations are held open during the startup and shutdown transients to decrease rubbing contact, and it is important to bypass cabin air during these periods and flush the system (e.g., the smell of jet fuel due to faulty sealing and buffering) prior to bleeding cabin air.

Further, the toxicology of environmental air coupled with engine bleed air is poorly defined. Although most airports are at some distance from civic centers (e.g., the new Tokyo airport), the building trend is to surround the airport with civic activities. Certainly, the environmental problems at the Hong Kong airport are unique to the world because the volume handled is large and the airport is situated within a heavily populated area. In a sense it is like New York's Laguardia airport, where large amounts of debris darken the shoreline, the result of improper consumption of fuel and oil where leaking seals can commit excessive amounts to engine airflow.

Current sealing concerns center on EPA non-point-source discharge permits. For example, at New York's Kennedy airport, runway runoff effluent, such as oil and fuel spills, deicing agents, and engine exhaust products, are to be collected and treated chemically and biologically prior to release as a result of a 1980's suit. The cost is borne by the customer through airport use taxes. The regulation covers anything "leaked" onto the runway or apron. One may recall that early flights of the Blackbird involved large fuel spills over the hangar floor, apron, and runway. The key here is how much effluent reaches a regulating point where it can be measured. Furthermore, as any tracker knows, when there are no tracks, only man could have been there.

Potential sources of aerospace regulation (manned and unmanned vehicles) include

(1) EPA, which is currently involved in ground effluent control and has a program with the National Oceanic and Atmospheric Administration (NOAA) at Boulder, Colorado, to model atmospheric diffusion

(2) OSHA, which may move to regulate cabin air requirements

(3) RCRA, which covers the operations of every working industry

(4) The Clean Air Act, which may be extended to regulate the exhaust products

One should remember that Queen Elizabeth's decree that all the unsightly soot be removed from the smokestacks led to the creation of sulfur dioxide and hence acid rain in England, implying that regulation may not be the answer.

GROOVED COMPLIANT FACE SEALS

The very low leakage requirements dictated by environmental considerations and the quest for high performance at increased efficiency dictate thin lubricating films, barrier fluids, and well-controlled dynamics. Over 10 years ago Larry Ludwig (refs. 1 and 2) invested his life in mechanical seals (fluid film and contacting face and shaft seals), and the industry followed the NASA work closely. Larry predicted that mechanical seals would be the seals of the future in aircraft engines, but original equipment manufacturers (OEM's) were satisfied with labyrinth seals for many gas path and shaft applications.

Since that time, microtechnology, smart configurations, smart controls, and EPA and customer drives for zero net leakage have forced researchers and OEM's back toward mechanical seals. The standard configurations (cylindrical, labyrinth, and tip) continue to be used, with brush seals as an intermediate step between low-leakage and zero-net-leakage seals. New developments in labyrinth seals, brush seals, and hydrostatic and hydrodynamic effects in seals and bearings will continue to expand our current technology and make one type more effective than another—in a leapfrog fashion. Each seal/bearing design must be investigated as to its life, leakage, stability, load transmission, simplicity, cost of mission failure (human and robot, both terrestrial and aerospace), maintainability, cost, effectiveness, etc., and then a selection can be made. Maybe the simple, effective labyrinth seal used in the Hottle engine or some modified form is "best"!

WHAT'S COMING

In the future more microetched seals and bearings with specially tailored grooving to transmit loads and active control of surfaces and dynamics will replace many "low cost" seals and bearings but never entirely. The high-end cost will be magnetic bearings, which will require no seals and no bearing contact—essentially providing very long life and very low dissipation. The hybrid magnetic-foil bearing promises stability and load capacity at low rpm (magnetic capability) and at high rpm (hydrodynamic capability). Turbomachines and rotating machinery in general will have new envelope designs, be more compact and more efficient, tend toward zero net leakage, and operate at higher speeds.

Further on, magnetic "envelopes" and rotating tubular compressors and turbines could evolve and rotate at very high speeds (perhaps over 1 million rpm, depending on diameter). The exterior envelope will compress the rotating members to mitigate the excessive hoop stresses.

Seals must mature to the point that orifice metering of cooling fluid rather than unreliable seal leakages would be used to supply cooling requirements. However, simple cost-effective solutions (e.g., the labyrinth seal) will not be made obsolete by expanding high technology.

Actively controlled seals are coming. Those using piezoelectric drivers, shaped-memory alloys, or hydrostatic orifices are evolving but are not yet in engines (refs. 10 to 12 and private communication from M. Braun of University of Akron).

Seal acoustics is being considered in the seals code program along with secondary and power stream flow integration. Turbomachine noise is generated not only by the blade/stator interfaces but at the sealing surfaces as well. Shroud and interstage seals whistle, especially when the interface travels above Mach 1. A rotating shock field has to develop into an axial flow field with attendant dissipation of vortex formations (unattended these formations would dissipate, but they interact with structure and other flows to form unwanted sound). Noise abatement is important to the customer in at least two ways: (1) objectionable sound is reduced and (2) 1-dB sound reduction increases gross takeoff weight for the HTSC by 1.5 percent.

Costing models will be used in terms of design, manufacturing, operations, and life. Costing models will enable the designer to select various contracting options and couple them with operations protocol and manufacturing technology to determine how local or global design changes improve the life and decrease the cost of the seal.

Currently, our NASA seals code development by Mechanical Technologies Incorporated and CFD Research Corporation is on target but needs more consideration of compliant seals, seal acoustics, integrating secondary flow paths with the power stream, the concept of surface microgrooving, and active control to provide load transmission and stability with a minimum of "lubricant" requirements. In combination with the NASA programs Texas A&M has developed seal stability coefficients for a variety of shaft seals, and they need to be extended to the compliant configurations.

CONCLUDING REMARKS

Concern for the uniqueness of planet Earth and the health and welfare of its inhabitants has precipitated a set of rules (laws) regulating the emissions of machines, in particular turbomachines. The original equipment manufacturers, the workers, the users, and the general public are aware that hazardous materials leak from seals and that materials generated during rubbing can be deleterious to their "health and wealth." In the aerospace industry, customer satisfaction, efficiency, and performance rather than regulation have been the drivers to mitigate seal leakages.

Integration of secondary flow paths with the power stream and development of thin-film, stable-operating compliant seals with and without barrier fluids are required to meet the goals. One such class of seal is the compliant foils and compliant face seals. The hybrid magnetic-foil bearing provides stability from liftoff (start/stop transients) throughout the engine operating envelope. Minimizing leakage, loss of rub materials, and cost and optimizing performance, efficiency, noise reduction, and life between overhauls continue to drive aerospace seal requirements and, along with regulations, to drive terrestrial seal requirements.

REFERENCES

1. Ludwig, L.P.; and Greiner, H.F.: Design Considerations in Mechanical Face Seals for Improved Performance. I.: Basic Configurations. ASME Paper 77–WA/LUB–3, 1977.

2. Ludwig, L.P.; and Greiner, H.F.: Design Considerations in Mechanical Face Seals for Improved Performance. II.: Lubrication. ASME Paper 77–WA/LUB–4, 1977.

3. Wegman, D.H., et al.: Vinyl Chloride: Can the Worker be Protected? New England J. Med., vol. 294, Mar. 18, 1976, pp. 653–657.

4. Spivey, G.H.: An Interdisciplinary Perspective of Lung Cancer. I. Epidemiology of Lung Cancer. Curr. Probl. Cancer, vol. 1, Apr. 1977, pp. 3–21.

5. National Emissions Standards for Hazardous Air Pollutants: Announcement of Negotiated Equipment Leaks. Environmental Protective Agency, 40 Code of Federal Regulations, Ch. 1, or Federal Register, vol. 56, no. 44, Mar. 6, 1991, pp. 9315–9339.

6. Guidelines for Meeting Emission Regulations for Rotating Machinery With Mechanical Seals. ASLE Report R1/RD88–235P–1, STLE SP–30, 1990.

7. Young, L.A.; and Key, W.E.: Evaluation of Barrier Fluids for Dual Seal Applications, Part I. Lubr. Eng., vol. 48, no. 9, Sept. 1992, pp. 713–717.

8. Proctor, M.P.: Leakage Predictions for Rayleigh-Step Helium-Purge Seals. NASA TM–101352, 1988.

9. Shapiro, W.; and Hamm, R.: Seal Technology of Liquid Oxygen (LOX) Turbopumps. NASA CR–174866, 1985.

10. Salant, R.: Actively Controlled Shaft Seals for Aerospace Applications. NASA CR–191689, 1992.

11. Palazzolo, A.B., et al.: Piezoelectric Actuator-Active Vibration Control of the Shaft Line for a Gas Turbine Engine Test Stand. ASME Paper 93–GT–262, 1993.

12. Anon.: A Low-Cost, Compact, Non-explosive Pin-Puller for Aerospace Applications. Phase I Final Report (NAS3–26834), TiNi Alloy Co., San Leandro, CA, 1993.

TABLE I.—PROPERTIES OF COMMON BARRIER FLUIDS FOR DUAL SEALS

[Adapted from references 6 and 7.]

Barrier fluid	Practical temperature limits				Comments
	Lower		Upper		
	°F	°C	°F	°C	
Water	40	4	180	82	Use corrosion-resistant material; protect from freezing.
Propylene glycol	−76	−60	368	187	Consult seal manufacturer for proper mixture with water to avoid excessive viscosity.
n-Propyl alcohol	−147	−99	157	69	--
Automatic transmission fluid	55	13	200	93	Contains additives.
Kerosene	0	−18	300	149	--
No. 2 diesel fuel	10	−12	300	149	Contains additives.
Inert gases[a]	Dewpoints		----	----	Can displace oxygen in habitats; low oxygen sensors may be required.
Benign gases[b]	Dewpoints		----	----	Low oxygen sensors may be required.
Air (dry) (ambient)	Dewpoint Dewpoint		----	----	Is combustion compatible with other oxidative-sensitive environments.
Hydrogen	Dewpoint		----	----	Must consider sensitivity to oxidizers along with flame propagation limits.

[a]Noble gases (e.g., helium), nitrogen, and gas mixtures (e.g., a combination of helium and nitrogen).
[b]For example, carbon dioxide.

TABLE II.—EMISSION LIMITS AND APPLICATIONS GUIDE

[Size, to 152 mm (6 in.) diameter; pressure, to 40 bar (600 psi); speed, to 28 m/s (5600 ft/min) surface. Adapted from reference 6.]

Emission limits 1 cm from source, ppm	Specific gravity	Technology
1000 to 10 000	>0.4	Single, double, or tandem seals are acceptable.
500 to 1000	>0.4	Single seals may be acceptable depending on actual operating conditions, seal size, pressure, and temperature. Tandem or double seals may be required to meet emission regulations.
0 to 500	>0.4	Tandem or double seals are acceptable.
0 to 500	<0.4	Double seals are required.

Primary ring properties

a Axial flexibility (spring loaded)
b Secondary-ring sealing diameters
c Angular flexibility (nose will tend to align
   itself to angular misalignment of seat face)
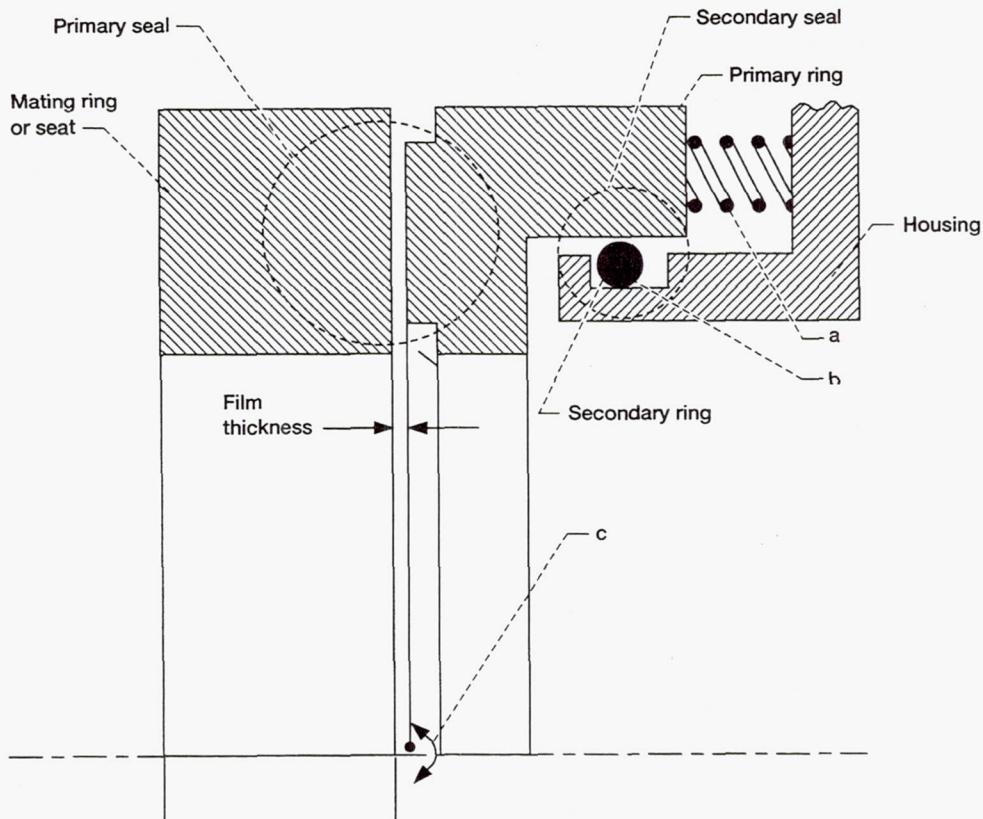
(b) With nonrotating primary ring.
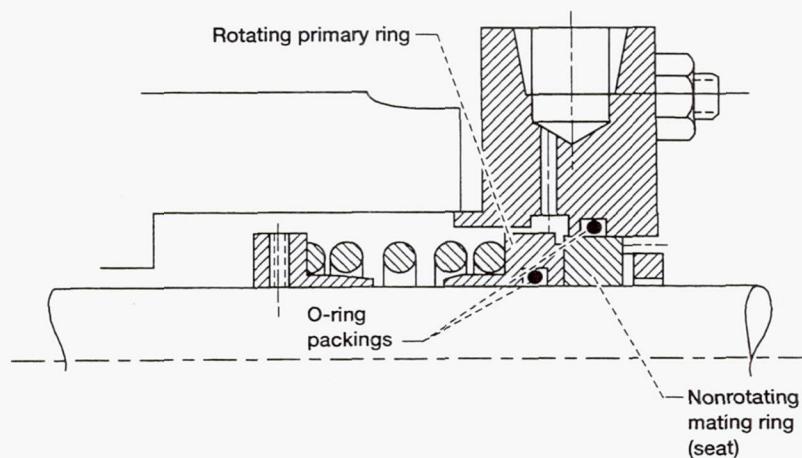
(a) With rotating primary ring.

Figure 1.—Single mechanical face seal.

Process
fluid →

Barrier fluid

Sealed process fluid at OD;
barrier fluid at ID

Sealed barrier fluid at OD
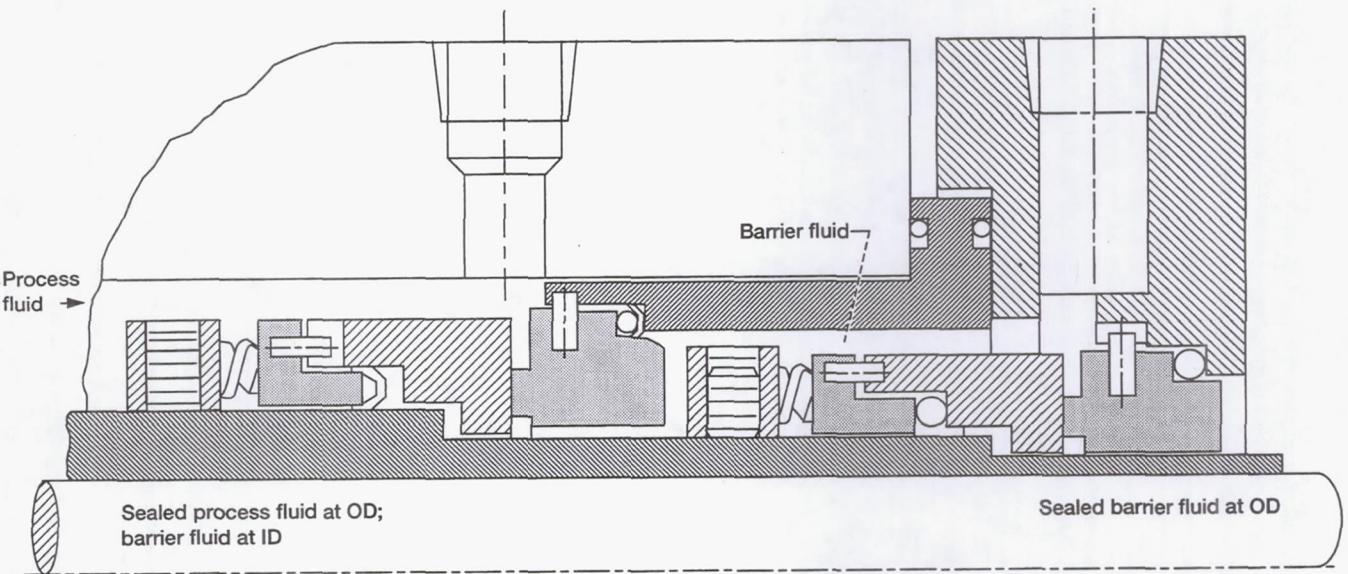
Figure 2.—Tandem seal (rotating-primary-ring type).

Cooling flow

Barrier fluid

Process
fluid →

Sealed process fluid at ID;
barrier fluid at OD

Sealed process fluid at OD
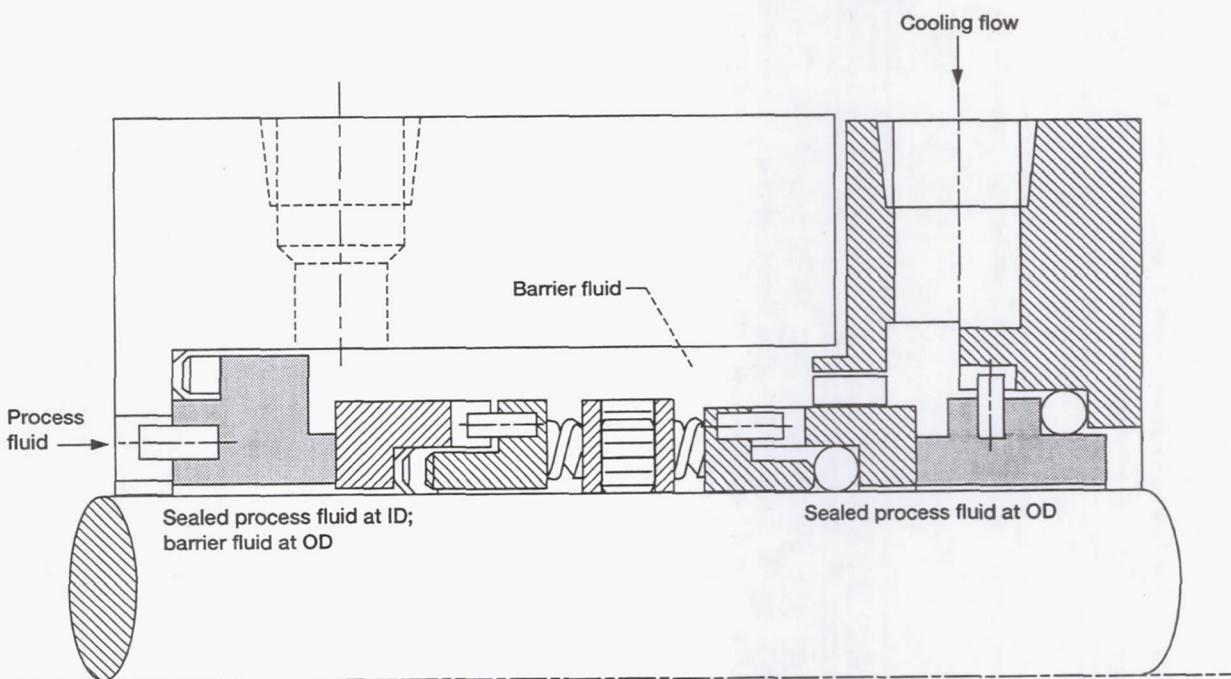
Figure 3.—Double seal (rotating-primary-ring type).
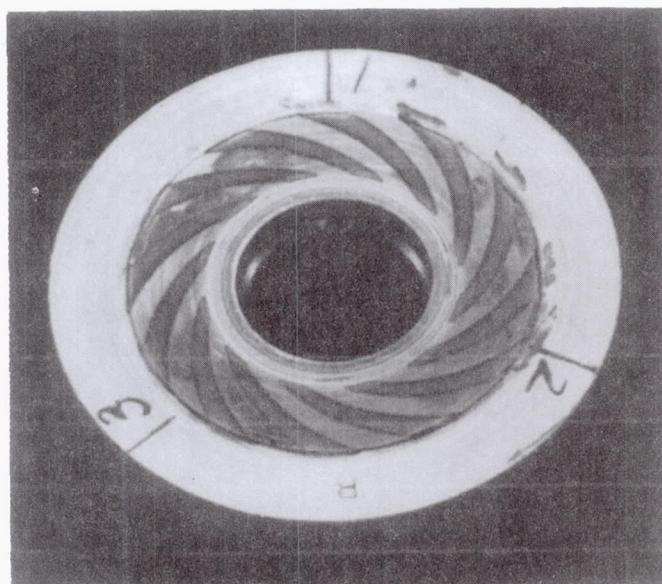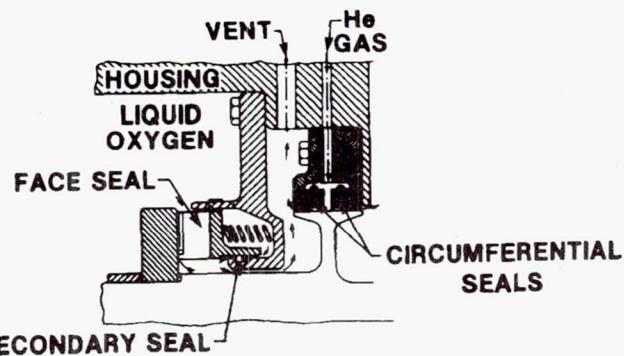
Face-type, spiral-groove, primary liquid oxygen seal.
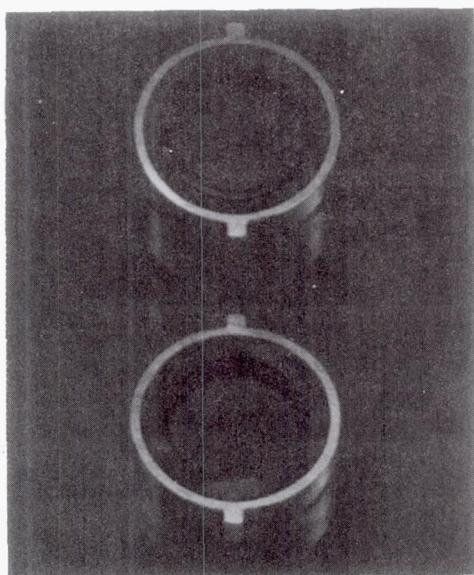
Circumferential-type, Raleigh-lift-pad, helium purge
seal.

Figure 4.—Liquid oxygen turbopump seal with buffer gas.

Joseph Scharrer
RSR Technologies
North Highlands, California

MTI CODE EVALUATION

INTRODUCTION

- **Cylindrical Air and Water Seals Compared**

    - **TAMU Tapered Gas Seal**

        - **CSEAL and GCYL compared**

    - **Mitsubishi Eccentric Water Seal**

        - **HSEAL and ICYL compared**

MTI CODE EVALUATION

GCYL Rudiments

- **Unit Conversion Confusing**

    - **Operating Conditions invariably show English Units**

- **Inlet Tangential Velocity not Input Variable**

CSEAL, GCYL Comparison
Test Data From Elrod
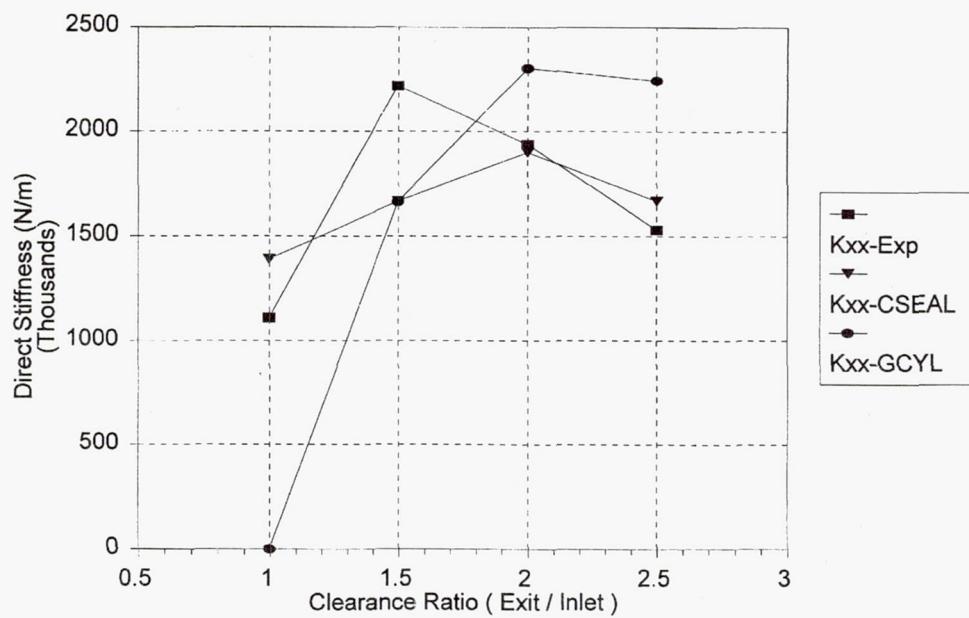
CSEAL, GCYL Comparison
Test Data From Elrod
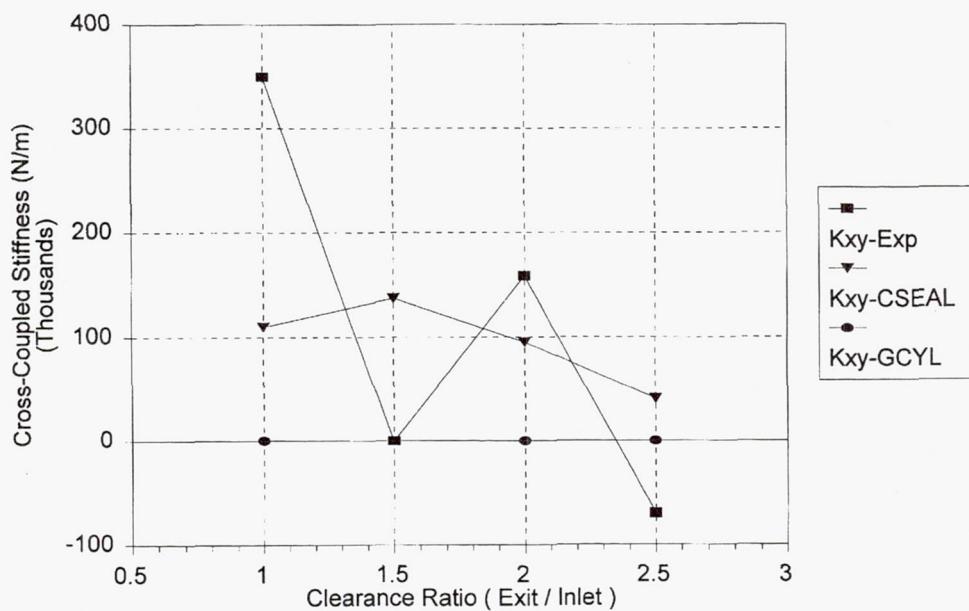
CSEAL, GCYL Comparison
Test Data From Elrod
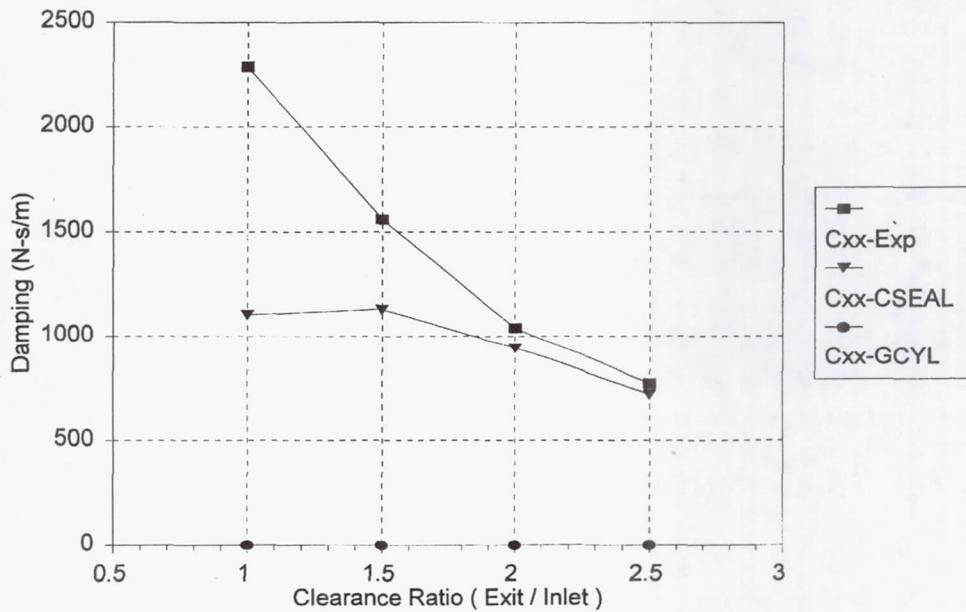
MTI CODE EVALUATION

GCYL and CSEAL Results Compared to TAMU Data

- **Direct Stiffness**

    - **GCYL Comparison Favorable**
    - **CSEAL Closer to experiment at Small and Large Tapers**

- **Cross-Coupled Stiffness**

    - **Neither Code Predicts Trend or Magnitude Well**
    - **GCYL predicts essentially 0**

- **Direct Damping**

    - **CSEAL Predicts trend and Magnitude well**
    - **GCYL Predicts Negligible Damping**

- **Leakage**

    - **GCYL grossly Overpredicts**

MTI CODE EVALUATION

ICYL Rudiments

- **Non-Symmetric Coefficients for Zero Eccentricity**

- **Unit Conversion Confusing**

  - **Operating Conditions invariably show English Units**

- **Inlet Tangential Velocity not Input Variable**

- **No Added Mass Coefficients calculated**

HSEAL Verification
Test Data From Kanki and Kawakami
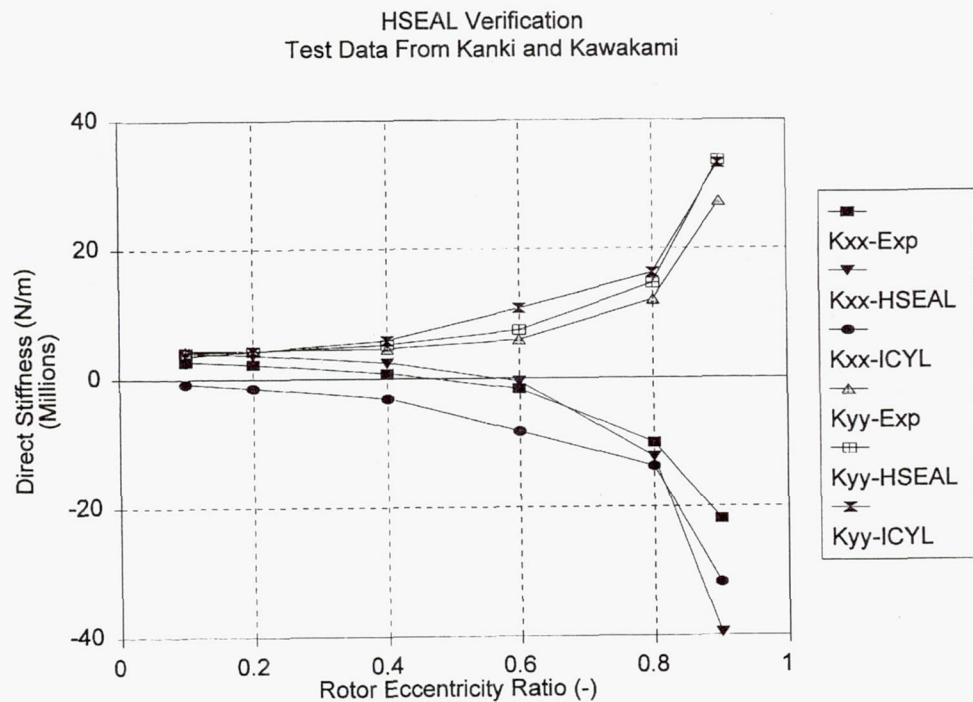
HSEAL Verification
Test Data From Kanki and Kawakami
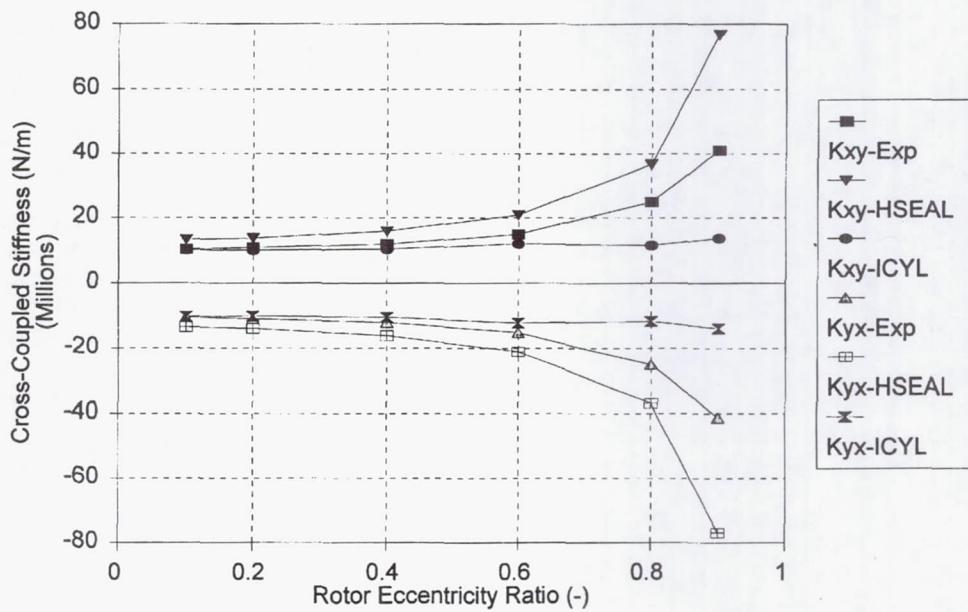
HSEAL,ICYL Verification
Test Data From Kanki and Kawakami
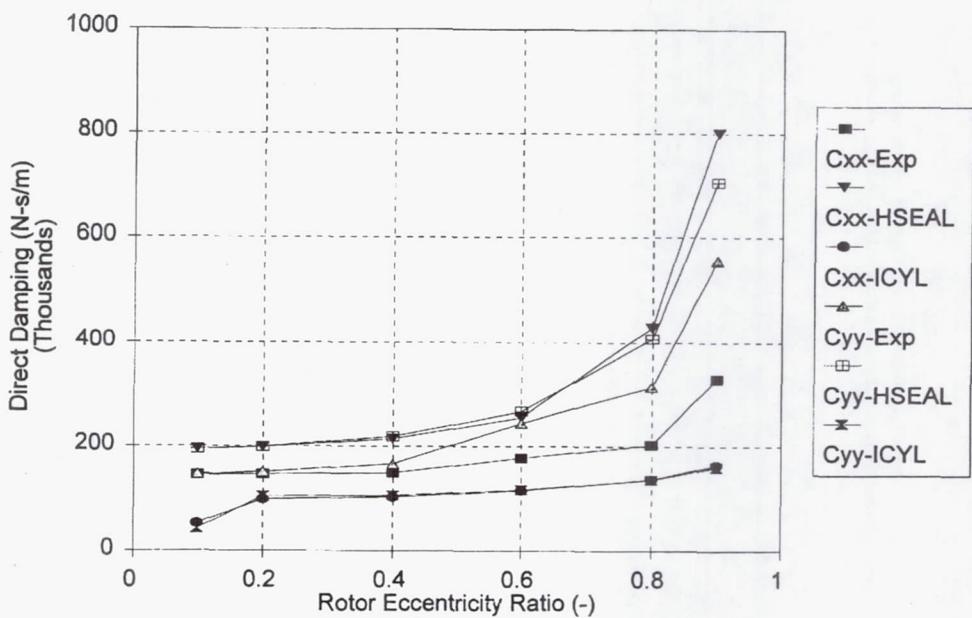
83

HSEAL Verification
Test Data From Kanki and Kawakami
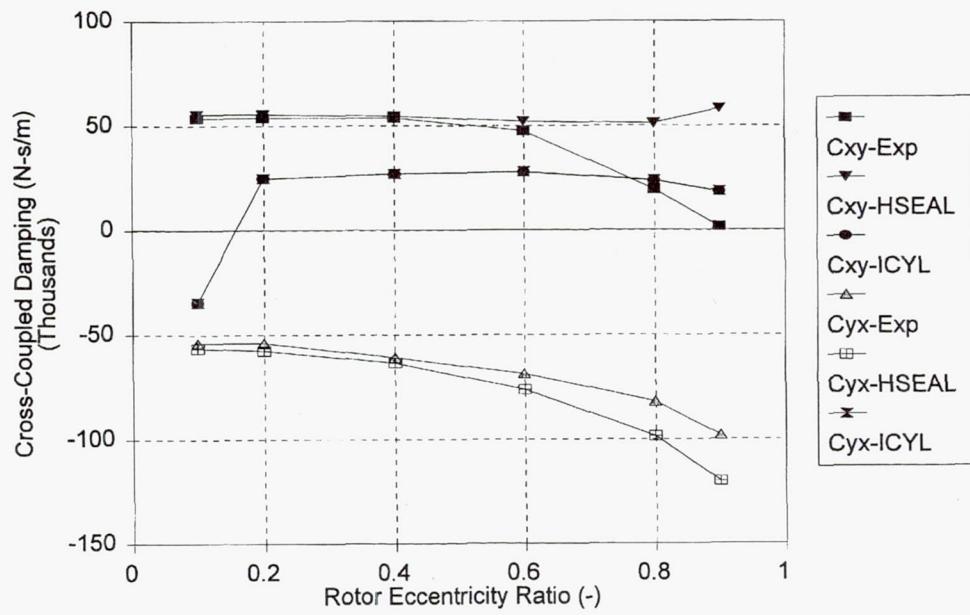
HSEAL Verification
Test Data From Kanki and Kawakami
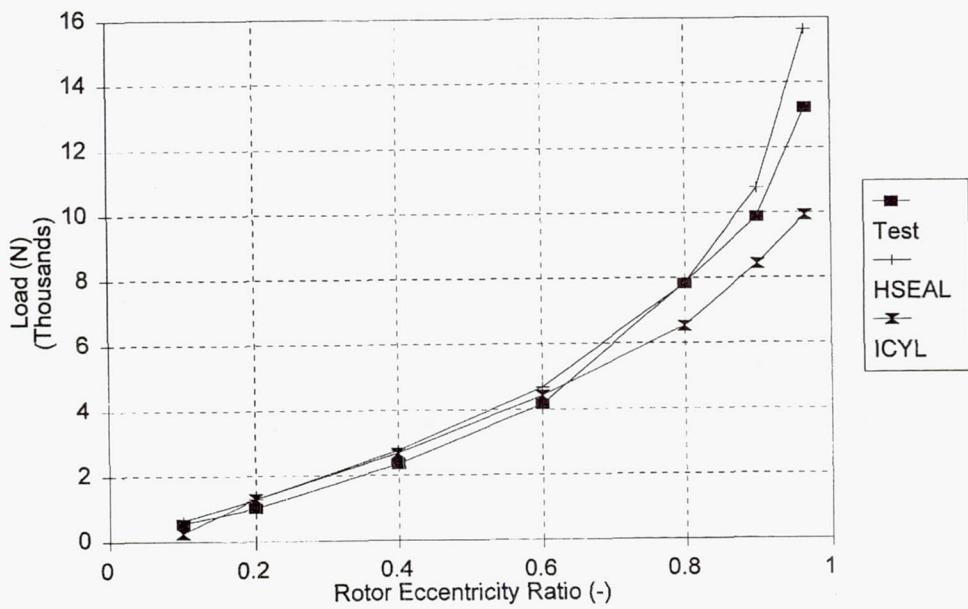
MTI CODE EVALUATION

ICYL and HSEAL Results Compared to Mitsubishi Data

- Direct Stiffness

    - ICYL and HSEAL Comparison Favorable
    - Both Codes Overpredict

- Cross-Coupled Stiffness

    - Neither Code Predicts Magnitude Well
    - ICYL Underpredicts Magnitude
    - HSEAL Overpredicts Magnitude

- Direct Damping

    - HSEAL Overpredicts Magnitude
    - ICYL Underpredicts Magnitude Significantly

(continued)

MTI CODE EVALUATION

ICYL and HSEAL Results Compared to Kanki Data - continued

- Cross-Coupled Damping

    - HSEAL predicts Magnitude and Trend well
    - ICYL misses negative values at large eccentricities

- Loads

    - ICYL and HSEAL predict loads well
    - HSEAL better principally for Long Seal

MTI CODE EVALUATION

SUMMARY

- **ICYL and GCYL Geometry Variations Desirable**

- **Load and Direct Stiffness Calculations Good**

- **Damping and Cross-Coupled Stiffness Predictions Poor**

- **Added Mass Coefficients should be Calculated**

- **Variation in Inlet Tangential Velocity Critical to Design**

EG&G AND NASA FACE SEAL CODES COMPARISON

Prit Basu
EG&G Sealol
Cranston, Rhode Island

• Codes Received from NASA

• **Seal Hardware and Application**

• **Description of EG&G's Code**

• **Description of NASA Code**

• **Results and Discussion**

• **Conclusions and Future Works**

Codes Received from NASA

• **'SPIRALG'** - Gas Lubricated Spiral-Grooved Cylindrical and Face Seals.

• **'GCYL'** - Gas Lubricated Cylindrical.

• **'ICYL'** - Cylindrical Seals Lubricated by Incompressible Fluids.

- Codes Received from NASA

- Seal Hardware and Application

- Description of EG&G's Code

- Description of NASA Code

- Results and Discussion

- Conclusions and Future Works

Schematic Diagram

Carbon Graphite Stator   'Cup-Type' Retainter

Spring Plate

Silicon Carbide Rotor

'Finger Spring' Centering
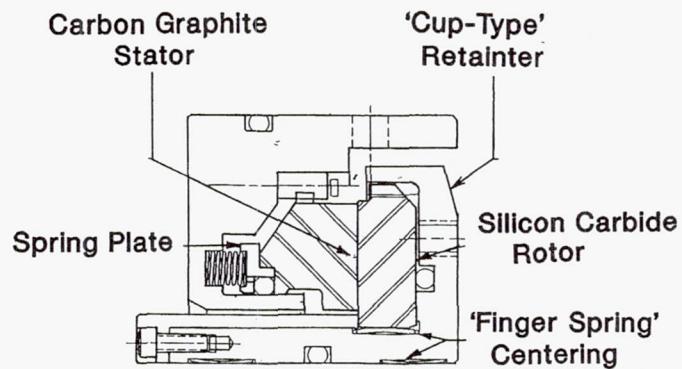
Used in Centrifugal Gas Compressors

88

Spiral-Groove Seal Face
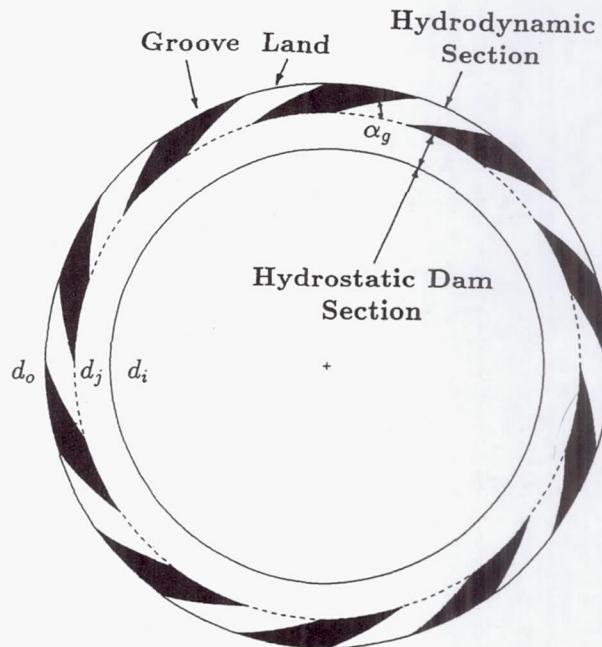
Maximum Operating Conditions

- Pressure - 1500 psig

- Temperature - 400 °F

- Surface Speed - 550 ft/s

89

- Codes Received from NASA

- Seal Hardware and Application

| - Description of EG&G's Code |

- Description of NASA Code

- Results and Discussion

- Conclusions and Future Works

* Seal Face Distortions

- Pressure (Finite Element)
- Thermal
- Centrifugal

Pressure Distortion
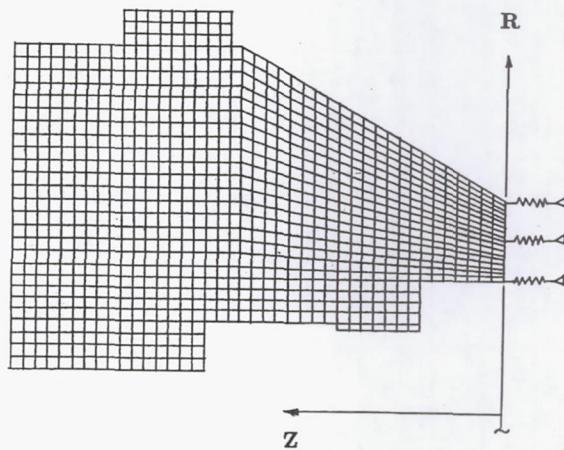
Finite Element Mesh - Stator

* Fluid Pressure Distribution

- Hydrodynamic Section
  2D Compressible Reynolds Eqn

- Hydrostatic Section
  1D Compressible Flow

  • Choking

91

- Codes Received from NASA

- Seal Hardware and Application

- Description of EG&G's Code

| • Description of NASA Code |

- Results and Discussion

- Conclusions and Future Works

"SPIRALG" CODE

Gas Lubricated Spiral-Grooved Cylindrical and

Face Seals

- Narrow Groove Theory. $N_g \gg 2\pi \sin\beta$

- Compressible Reynolds Equation Over

  the Entire Seal Face.

- Inertial Effects Neglected.

- Face Deformations Not Considered.

- Calculates Frequency Dependent Film

  Stiffness and Damping.

92

- Codes Received from NASA

- Seal Hardware and Application

- Description of EG&G's Code

- Description of NASA Code

- **Results and Discussion**

- Conclusions and Future Works

Example Case

Design Parameters :

Seal OD	=	6.0 in
Seal ID	=	4.6 in
Groove Angle	=	*
Groove Depth	=	*
Number of Grooves	=	12
Width Ratio	=	*
(Land/Groove)	=	
Spiral Span	=	*

Operating Parameters :

System Pressures	=	100 - 1500 psig
Discharge Pressure	=	0 psig
Speeds	=	7500, 15000 RPM
Temperatures	=	95, 170 ° F

*Proprietary information of EG&G Sealol.

93

Leakage Correlation

Face Deformations Suppressed in EG&G Code

7500 RPM
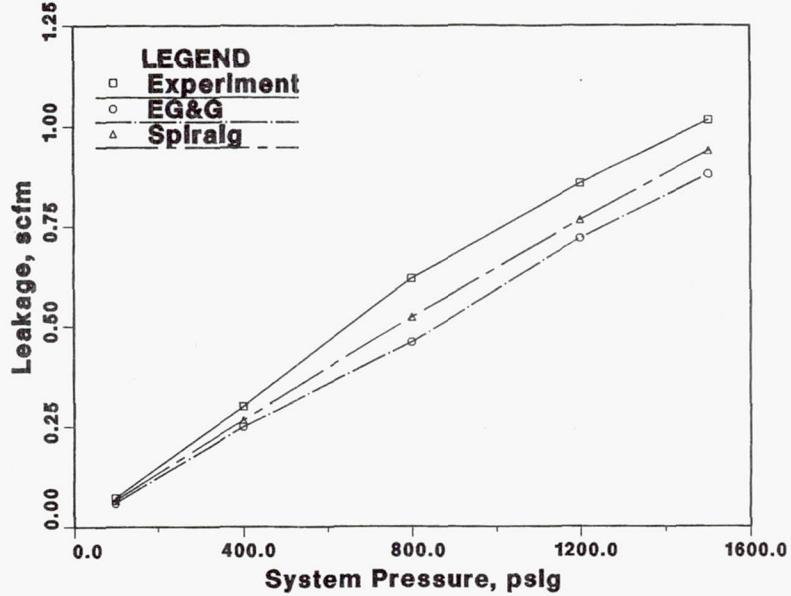
Leakage Correlation

Face Deformations Suppressed in EG&G Code

15000 RPM
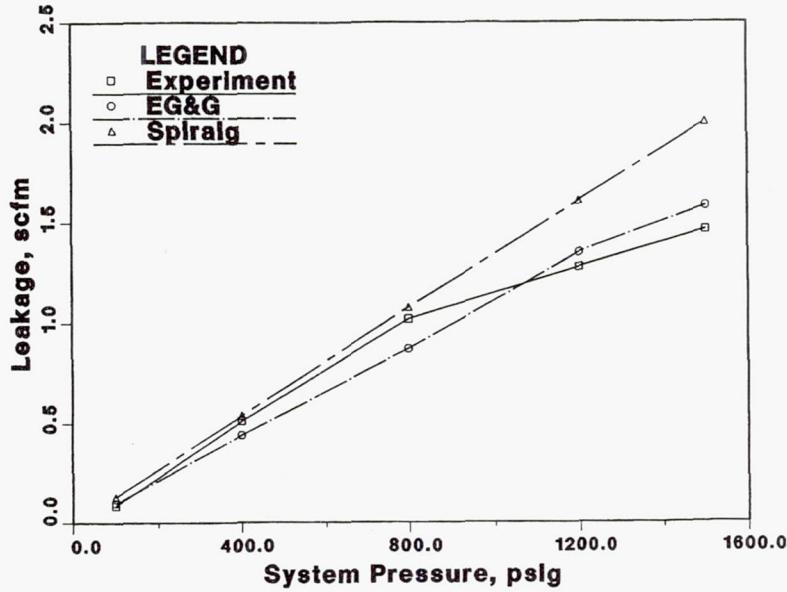
Leakage Correlation

Face Deformations Activated in EG&G Code

7500 RPM
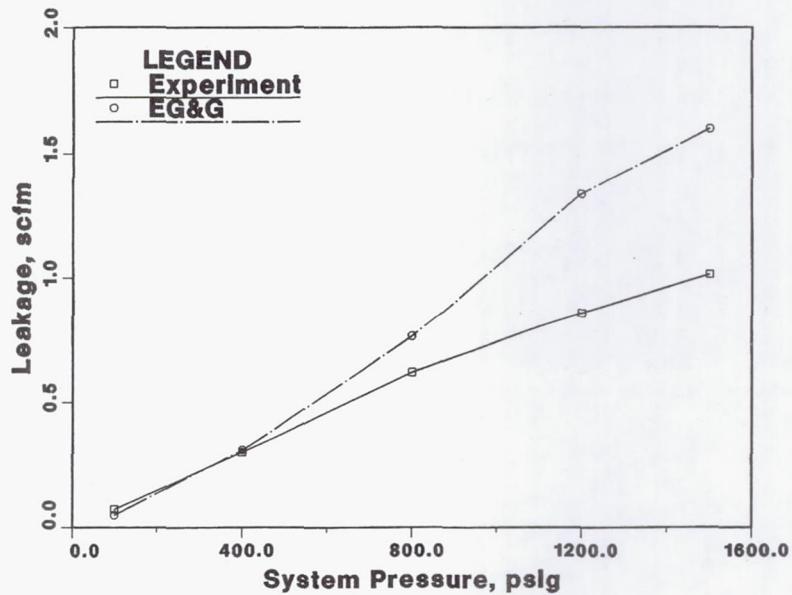
Leakage Correlation

Face Deformations Activated in EG&G Code

15000 RPM
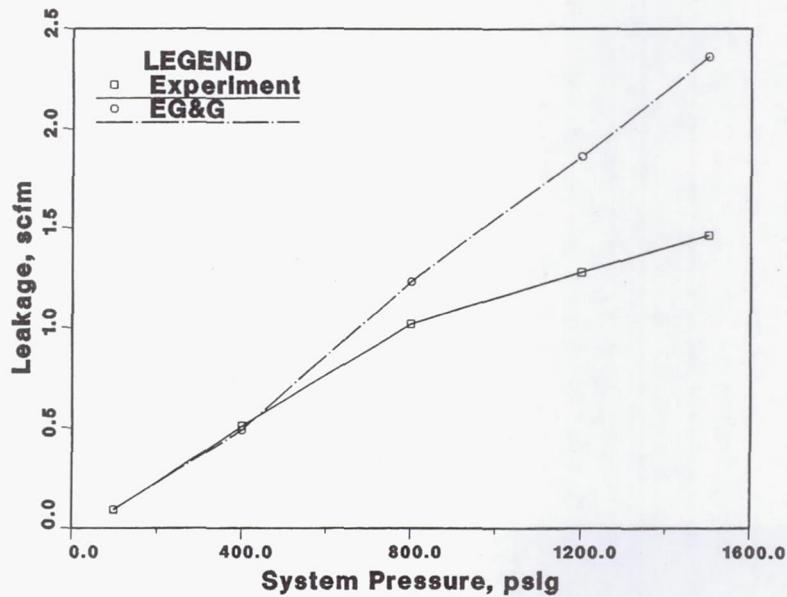
Film Stiffness & Damping

Design & Operating Parameters

h = 100 μin

α_g = 15°

N = 16000 RPM

Stiffness & Damping Data

Inlet Pressure p_o (psia)	EG&G K 0 rpm (lbf/μin)	SPIRALG			
		K 0 rpm (lbf/μin)	C 0 rpm (lbf.s/in)	K 16000 rpm (lbf/μin)	C 16000 rpm (lbf.s/in)
114.7	13.42	26.00	-7087	18.7	-3731
314.7	15.81	28.10	-1312	27.0	-1229
514.7	17.52	29.65	641	30.0	594
1014.7	20.36	33.09	2750	33.9	2670
1514.7	21.68	36.38	3560	37.1	3520

- Codes Received from NASA

- Seal Hardware and Application

- Description of EG&G's Code

- Description of NASA Code

- Results and Discussion

- Conclusions and Future Works

96

Conclusions

For the Example Case :

- EG&G code with face deformations suppressed and "SPIRALG" agree well with each other as well as with the experimental data.

- '0 RPM' stiffness data calculated by EG&G code are about 70-100% lower than that by "SPIRALG".

- Not an appreciable difference between '0 RPM' and '16000 RPM' stiffness and damping coefficients calculated by 'SPIRALG'.

- The film damping above 500 psig calculated by "SPIRALG" is much higher than the O-Ring secondary seal damping (e.g. 50 lbf.s/in).

Future Works

- Annular Seal Analysis with 'GCYL'

DEVELOPMENT OF A BRUSH SEALS PROGRAM LEADING TO CERAMIC BRUSH SEALS

Robert C. Hendricks
NASA Lewis Research Center
Cleveland, Ohio

Ralph Flower
Cross Manufacturing Ltd.
Devizes, U.K.

and

Harold Howe
Technetics Corporation
Deland, Florida

SUMMARY

Some events of a U.S. Army/NASA Lewis Research Center brush seals program are reviewed, and the development of ceramic brush seals is described. Some preliminary room-temperature flow data are given, and the results of testing metallic brushes in cryogenic nitrogen are discussed.

INTRODUCTION

Recognizing the remarkable brush seal accomplishments of John Ferguson of Rolls Royce (ref. 1) and Ralph Flower of Cross Mfg. Ltd. (ref. 2), figure 1, NASA Lewis Research Center embarked on a program to develop the fundamentals characterizing the flow and dynamics of brush seals. The program entailed

1. Developing a heuristic brush seal bulk flow model and code for determining the flow and pressure drop in brush seal systems that would be suitable for both designers and researchers

2. Fabricating simulated brush seal sections with Lucite bristles

3. Utilizing an existing water tunnel facility and fabricating an experimental oil tunnel facility to visualize flows through simulated brush seal sections

4. Setting up an approach for determining rub characteristics, debris, bristle flexure cycles, and seal life associated with long-term operations for the brush seal and rub runner as a system (tribopairing)

5. Integrating observations from an airflow tunnel of the flow through sequences of nylon bristle brushes, such as bristle flexure, flutter, edge loss, and clearance leakage

Toward this end, a bulk flow model and computer code were developed. The model centered on the forces acting on a single bristle and the flow through a porous medium consisting of fibrous materials. Although the details of the brush are proprietary, estimates of its dimensions and allowances for multiple bristles and packing were made and input into the model. By using one data point from Cross Mfg. Ltd., the geometric and flow parameters were established, and predictions of flow and pressure drop followed as illustrated in figure 2.

Preceding Page Blank

A simulated brush seal section with Lucite bristles was fabricated and placed into a water tunnel at NASA Lewis. The flow was seeded with magnesium oxide particles and illuminated with a sheet of laser light. The light provided two-dimensional slices of the flow, revealing a complexity not envisioned (fig. 3). By moving the light beam, the tunnel was surveyed to show flows along the bristles and up and down through the bristles, revealing complex vortex attachments and surface boundary layers. Videotapes of these flow fields were made to illustrate the complexity of brush seal flows (ref. 3).

The program went unsupported by NASA but found support from the U.S. Army Office for further modeling and flow visualization work at the University of Akron. At that time industry and universities were invited to use the program materials, the models, and the limited flow visualization work that was available to begin or supplement their own brush seals programs.

By using the flow visualization methods of Braun et al. (ref. 4), a special oil tunnel was fabricated as well as sets of simulated brush seal sections with Lucite bristles. Because the refraction indices of the Lucite and the oil were matched, these sections could not be seen once they were immersed in the oil, but the magnesium oxide flow tracers illuminated by a sheet of laser light provided two-dimensional slices of flows through the sections that were recorded on videotape. Frame-grabbing techniques and software developed by Braun et al. (refs. 4 and 5) were used to quantify these flows (figs. 4 to 6).

The simple brush seal bulk flow model and code evolved into more complex forms, including extensions to other gases by using the theory of corresponding states. The code still required geometric information and one data point to determine the flow and pressure drop (refs. 6 and 7, fig. 7). Concurrently, a numerical method was developed to characterize the two-dimensional flow patterns about sets of pins simulating flow patterns in brush seals. The code has been validated experimentally and faithfully reproduced the flow patterns associated with a variety of two-dimensional arrays of pins (figs. 8 and 9, refs. 8 and 9).

DEVELOPMENT OF CERAMIC BRUSH SEALS

Testing and modeling brush seal systems (e.g., refs. 10 to 12) including flow, thermal effects, and rubbing effects and projecting the sealing needs of future propulsion systems revealed the need for seals that can withstand high surface speeds and temperatures. Therefore, a brush seal made of silicon carbide bristles and metallic plates and an aluminum oxide brush seal were to be developed. The former is anticipated to operate at 1200 ft/s and 1500 °F and is suitable for configurations now in the design stage. The latter is anticipated to operate at over 1500 ft/s and over 2000 °F and can be used in the next generation of engines. Both types could be used in static sealing applications (ref. 13).

With the assistance of Ralph Flower of Cross Mfg. Ltd., Mel Mitnik of Textron Specialties Co. (silicon carbide fibers), and Saphikon (aluminum oxide fibers), sample brush sections were fabricated and assessed. Although sample brush sections of both silicon carbide and aluminum oxide appeared feasible, NASA Lewis and the U.S. Army Office contracted with Cross Mfg. Ltd. to fabricate the silicon carbide bristle/metallic plate brush seal and to investigate an all-ceramic configuration using aluminum oxide (or other ceramics) with washers of lesser purity purchased from Coors Ceramics to facilitate bristle attachment.

The craftsmanship of the 5.1-in.-diameter silicon carbide bristle/metallic plate brush seal fabricated and delivered by Cross Mfg. Ltd. in February 1992 was superb. Each bristle appeared to be well manufactured and to be placed as well as any metallic bristle with tips ground to a perfect contour to provide the standard 5-mil interference (figs. 10 to 12). Truly a remarkable achievement.

The silicon carbide bristle/metallic plate brush seal was installed for flow testing. At first the rotor could be turned in only one direction. After operation it could be rotated by hand in either direction but rotated freely in one direction only. Upon reinstallation the rotor tended to buckle the bristles, implying that some third-body surface lubrication or preferential surface texturing had developed during operation. The flow rate data at ambient temperatures were consistent (figs. 13 and 14) considering that a brush seal is not a positive seal system and leaks like a porous medium. However, brush seals leak less than labyrinth seals and are dynamically stable (refs. 11 and 14).

Concurrently, a Small Business Innovative Research program was begun by the U.S. Army Office with Technetics Corp. of Deland, Florida, to develop both the silicon carbide/metallic plate and all-ceramic aluminum oxide brush seals (ref. 15). Three fibers were considered feasible: silicon carbide (Textron Specialties), aluminum oxide (Saphikon), and quartz (Dolan Jenner). The layup of the bristles appeared standard, but the braze materials to withstand 1500 °F while not completely wetting the bristles required characterization. Active metal hydrides were effective and the assembly was fabricated into a brush seal capable of 1600 °F operations. The processes are described in reference 15. The progress on the aluminum oxide all-ceramic brush seal was impeded by problems of material instability, excessive shrinkage, and residual stresses. Nevertheless, a methodology for fabricating such a brush seal that centered around a prefired ceramic body with bristle inserts appears able to withstand thermal loads to 2000 °F at high surface speeds.

CRYOGENIC TESTING OF METALLIC BRUSH SEALS

Concurrently, NASA Lewis began an effort to test metallic bristle brush seal systems at cryogenic temperatures under a cooperative agreement with Rocketdyne (ref. 16) in order to determine the feasibility of running brush seals in high-speed turbomachines. The liquid nitrogen flow data were predominantly two phase at the exit and difficult to assess although an initial effort has been described in reference 17 (see also errata). The post-test inspection of the yttria-stabilized-zirconia (YSZ)-coated rub runner and the metallic bristle brush showed them to be pristine (figs. 15 and 16).

OTHER MODELING EFFORTS

In addition to the modeling already cited, several other researchers have developed models to correlate and interpret brush seal flow data. These models also require heuristic information, and many follow the geometric considerations and modeling of the NASA models. In some cases the design methods are characterized, but the details for application are absent (refs. 18 and 19). In other cases the results are simply related to a flow coefficient (ref. 20), and in others they are related to geometric packing (ref. 21) and provide a simple code methodology. Other flexure models (ref. 22) follow the NASA bristle loading model. Still others have provided some results for geometric variations (ref. 23) or for other types of ceramic configurations, such as fiberglass (ref. 24). Although these models and the NASA models provide physical insight into brush seal flow characteristics, the Ergun porous flow model (with modifications for brush seals) could be used to correlate and predict brush seal flows with simplicity (fig. 17). Two data points would be required to establish geometric and flow parameters, and the gaseous results for simple corresponding-states fluids appear to fit quite well. The effects of surface speed are not well established.

$$\Delta P = a \left(\frac{\mu}{\mu_0} \right) \dot{V} + b \left(\frac{\rho}{\rho_0} \right) \dot{V}^2$$

Laminar   Turbulent

For the seal configuration and data described in reference 7,

$$a = 25\sqrt{M}$$

$$a = 25M \quad \text{For helium}$$

$$b = 0.00015\, M \times F(f_0)$$

where

ΔP pressure drop, Pa

$\dot{V} = A_0 u_0$ volumetric flow rate at standard conditions (1 bar and 300 K), cm^3/s

A_0 flow area without bristles (shaft to fence), cm^2

u_0 flow velocity in flow area without bristles, cm/s

M molecular weight of gas

f_0 turbulent friction factor

μ_0 viscosity at reference conditions

ρ_0 density at reference conditions

where the subscript 0 refers to the reference conditions used to evaluate a and b; usually these are standard conditions, such as 1 bar and 300 K.

    Note that $\dot{w} = \rho\,\dot{V}$, the mass flow rate in grams per second, can be used in the relation by substituting for $\dot{V}$; and usually $F(f_0) \rightarrow$ constant $= 1$ is assumed but has not been verified. Also note that for gaseous helium the linear coefficient becomes proportional to M rather than to $\sqrt{M}$, which also requires verification as helium is a quantum fluid with viscous effects nearly equivalent to those of air.

    Ideally, the coefficients a and b are related to brush porosity e, thickness $\langle t \rangle$, and bristle diameter d, with a also related to viscosity μ and b related to density ρ and to the turbulent friction factor f_0.

$$\phi = \frac{\langle t \rangle / d}{e^3}, \quad a = 2\phi\mu/(A_0 d), \quad b = \phi\rho f_0/A_0^2$$

    For geometries other than described in reference 7, coefficients a and b have to be recalculated or ratioed; for example,

$$a = \left[\frac{\dfrac{\phi\mu}{A_0 d}}{\left(\dfrac{\phi\mu}{A_0 d}\right)_0}\right] \times \begin{cases} 25\sqrt{M} \\ 25\,M \quad \text{For helium} \end{cases}$$

$$b = 0.00015\, M \left[\frac{\phi\rho f_0/A_0^2}{\left(\phi\rho f_0/A_0^2\right)_0}\right]$$

CONCLUSIONS

Recognizing the propulsion system requirements of next-generation engines, the NASA Lewis Research Center and the U.S. Army Office have successfully developed, fabricated (using two different methodologies), and flow checked a silicon carbide bristle/metallic plate brush seal system.

The success of the brush seals program and the successful operation of brush seals in cryogenic fluids under a cooperative agreement have led to a technology test bed demonstration program for brush seals in high-speed turbomachines.

ACKNOWLEDGMENT

REFERENCES

1. Ferguson, J.G.: Brushes as High Performance Gas Turbine Seals. ASME Paper 88–GT–182, 1988.

2. Flower, R.: Brush Seal Development Systems. AIAA Paper 90–2143, 1990.

3. Braun, M.J.; Hendricks, R.C.; and Canacci, V.A.: Flow Visualization in a Simulated Brush Seal. ASME Paper 90–GT–217, 1990.

4. Braun, M.J.; et al.: A Non-Invasive Laser Based Method in Flow Visualization and Evaluation in Bearings. International Conference on Tribobology Friction, Lubrication and Wear, The Institution of Mechanical Engineers, London, Paper C 347/143, 1987, pp. 37–45.

5. Braun, M.J.; Hendricks, R.C.; and Canacci, V.A.: Flow Visualization and Quantitative Velocity and Pressure Measurements in Simulated Single and Double Brush Seals. Tribol. Trans., vol. 34, Jan. 1991, pp. 70–80.

6. Hendricks, R.C.; Carlile, J.A.; and Liang, A.D.: Some Sealing Concepts — A Review. Part A: Industrial, Proposed and Dynamic, and Part B: Brush Seal Systems. Presented at ISROMAC–4, Fourth International Symposium of Transport Phenomena and Dynamics of Rotating Machinery, Honolulu, HI, Apr. 5–8, 1992.

7. Carlile, J.A.; Hendricks, R.C.; and Yoder, D.A.: Brush Seal Leakage Performance With Gaseous Working Fluids at Static and Low Rotor Speed Conditions. ASME Paper 92–GT–304, 1992. (Also, NASA TM–105400, 1992.)

8. Braun, M.J.: Experimental and Analytical Investigation of Brush Seals. Seals Flow Code Development–92, A.D. Liang and R.C. Hendricks, eds., NASA CP–10124, 1993, pp. 181–196.

9. Kudriavtsev, V.V.: Numerical and Analytical Study of Flows in Cylindrical Arrays. Ph.D. Thesis, Submitted to Moscow Aviation Institute, 1993.

10. Hendricks, R.C.; et al.: Integrity Testing of Brush Seal in Shroud Ring of T–700 Engine. NASA TM–105863, 1992.

11. Hendricks, R.C.; et al.: A Bulk Flow Model of a Brush Seal System. ASME Paper 91–GT–325, 1991.

12. Hendricks, R.C.; Braun, M.J.; and Mullen, R.L.: Brush Seal Configurations for Cryogenic and Hot Gas Applications. 1990 Conference on Advanced Earth-to-Orbit Propulsion Technology, NASA CP–3092–VOL–2, R.J. Richmond and S.T. Wu, eds., 1990, pp. 78–90.

13. Hendricks, R.C.; et al.: Static Brush Seals for Propulsion System Interfaces. 1992 Conference on Earth-to-Orbit Propulsion Technology, NASA CP–3174–VOL–1, R.J. Richmond and S.T. Wu, eds., 1992, pp. 432–439.

14. Conner, K.J.; and Childs, D.W.: Brush Seal Rotordynamic Damping Characteristics. AIAA Paper 90–2139, 1990.

15. Howe, H.; Jarrabet, G.; and Tolokan, R.: Ceramic Brush Seals. SBIR Final Report NAS3–26319, 1993.

16. Scharrer, J.K.; and Hendricks, R.C.: Results of Cryogenic Brush Seal Testing. Seals Flow Code Development–92, A.D. Liang and R.C. Hendricks, eds., NASA CP–10124, 1993, pp. 215–216.

17. Carlile, J.A.; et al.: Preliminary Experimental Results for a Cryogenic Brush Seal Configuration. AIAA Paper 93–2535, 1993.

18. Holle, G.; and Krishnan, M.: Gas Turbine Engine Brush Seal Applications. AIAA Paper 90–2142, 1990.

19. Chupp, R.: Evaluation of Brush Seals for Limited Life Gas Turbine Engines. AIAA Paper 90–2140, 1990.

20. Chupp, R.; and Dowler, C.: Flow Coefficients for Brush Seals. AIAA Paper 91–3390, 1991.

21. Holle, G.; Chupp, R.; and Dowler, C.: Leakage Flow Correlations for Brush Seals. Presented at ISROMAC–4, Fourth International Symposium of Transport Phenomena and Dynamics of Rotating Machinery, Honolulu, HI, Apr. 5–8, 1992.

22. Modi, V.: Modelling Bristle Lift-Off in Idealized Brush Seal Configurations. Presented at ISROMAC–4, Fourth International Symposium of Transport Phenomena and Dynamics of Rotating Machinery, Honolulu, HI, Apr. 5–8, 1992.

23. Gorelov, G.M.; Reznik, V.E.; and Tsibizov, V.I.: An Experimental Study of the Rate Characteristics of Brush Seals in Comparison With Labyrinth Seals. Aviats. Tekh., no. 4, 1988, pp. 43–46.

24. Hendricks, R.C.; et al.: Investigation of Flows in Bristle and Fiberglass Brush Seal Configurations. Presented at ISROMAC–4, Fourth International Symposium of Transport Phenomena and Dynamics of Rotating Machinery, Honolulu, HI, Apr. 5–8, 1992.
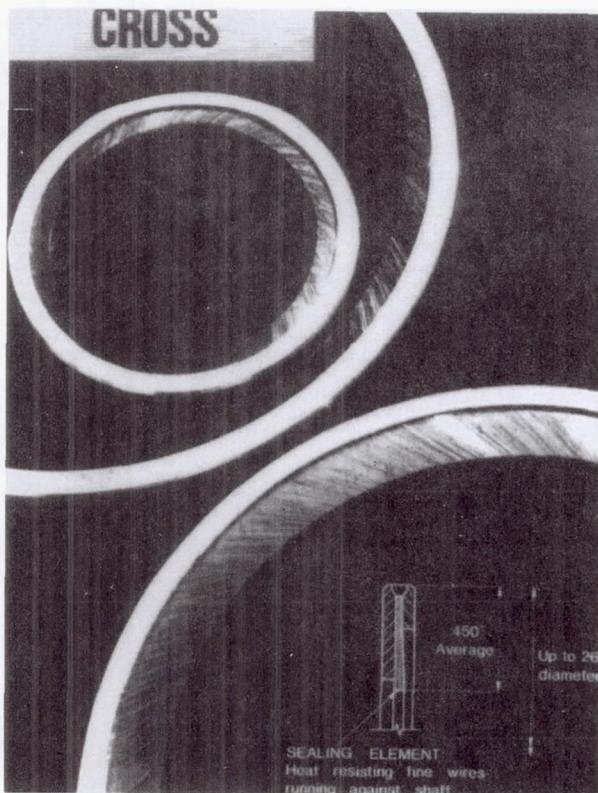
Figure 1.—Circular brush seal. (Courtesy of Cross Mfg. Ltd.)
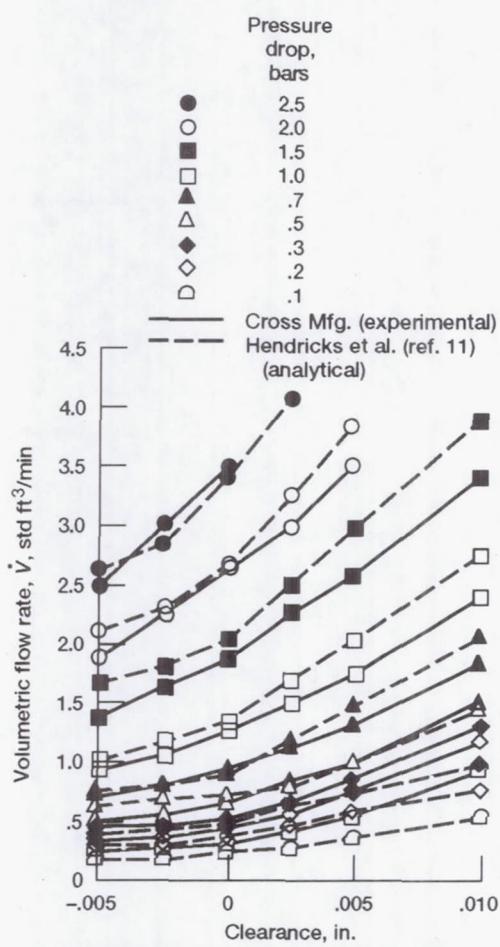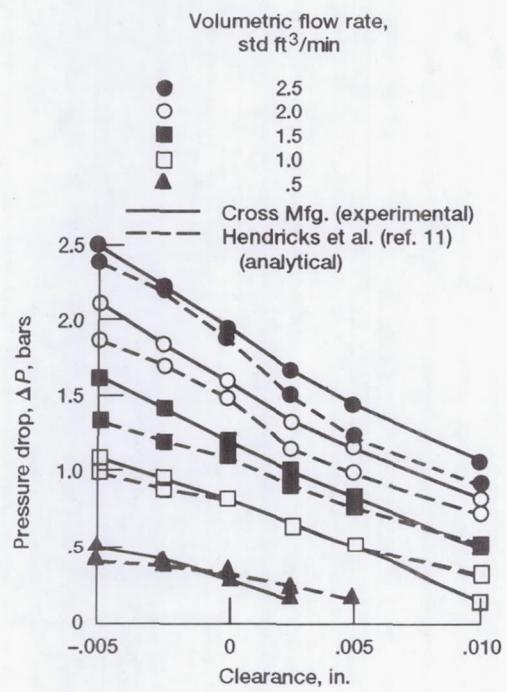
Figure 2.—Comparison of brush seal bulk flow model with experimental data of Cross Mfg. Ltd. Brush seal diameter, 5.1 in.

105
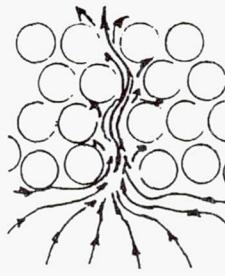
(a) Rivering.
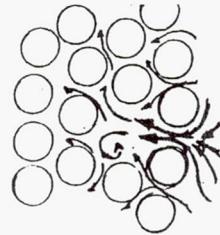
(b) Jetting.
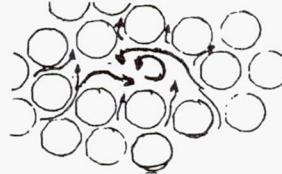
(c) Vortical flow.
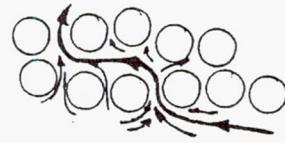
(d) Lateral and parallel flow.
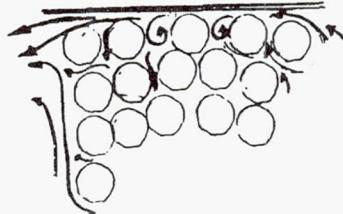
(e) End-wall flow.
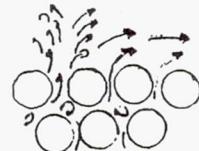
(f) Flow at bristle tips.
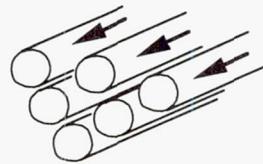
(g) Radial flow.

Figure 3.—Observed flow patterns in brush seals.
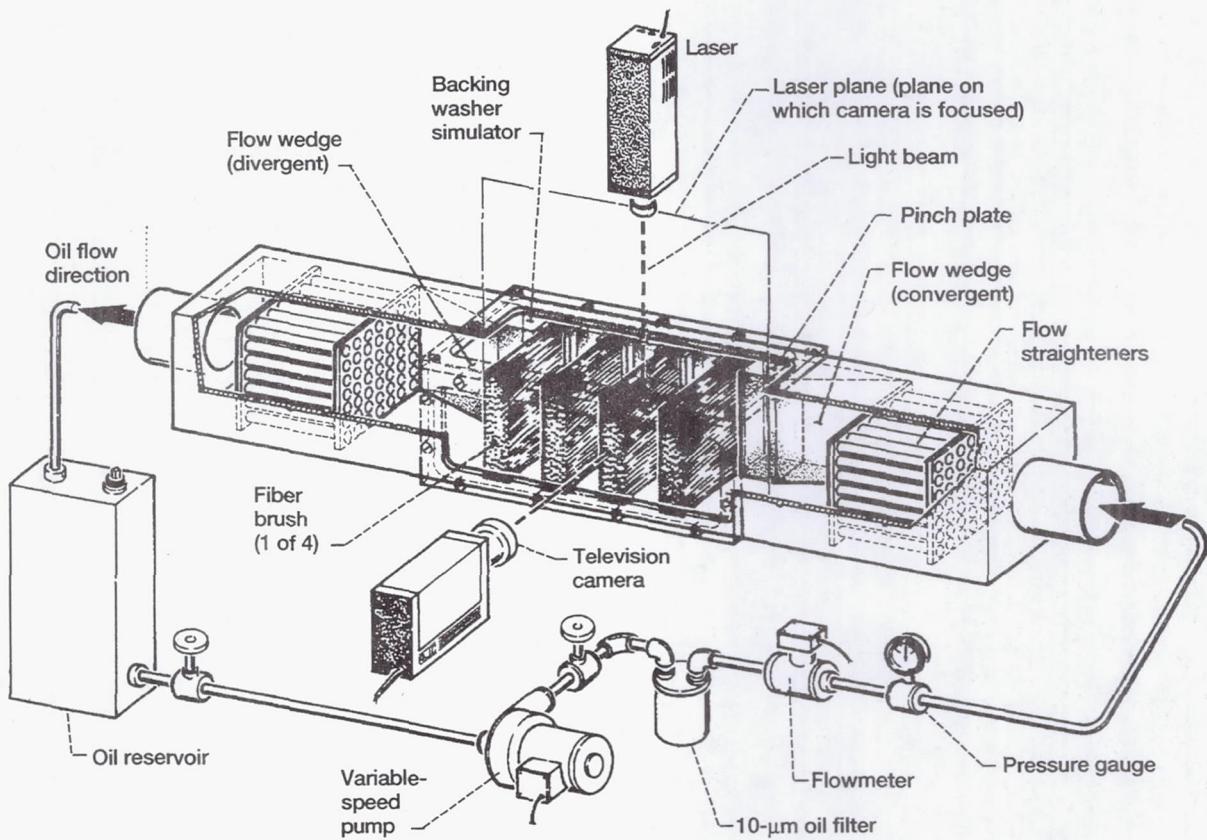
Figure 4.—Two-dimensional oil flow visualization facility.
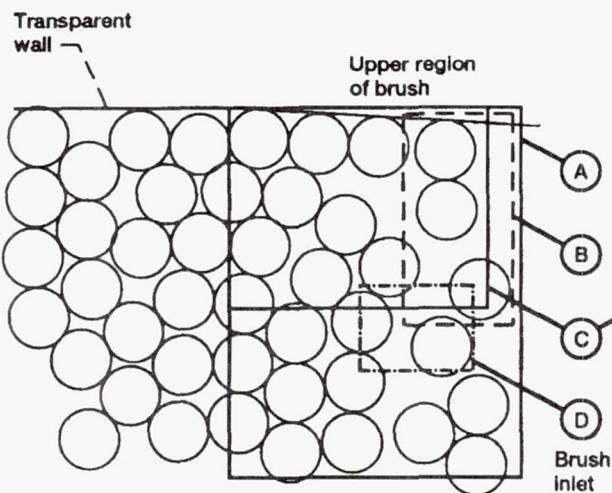
(a) Map of upper region of brush (2-mm bristles).
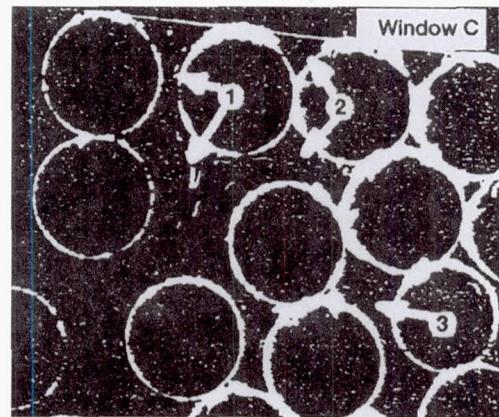
(b) Flow visualization in window C.
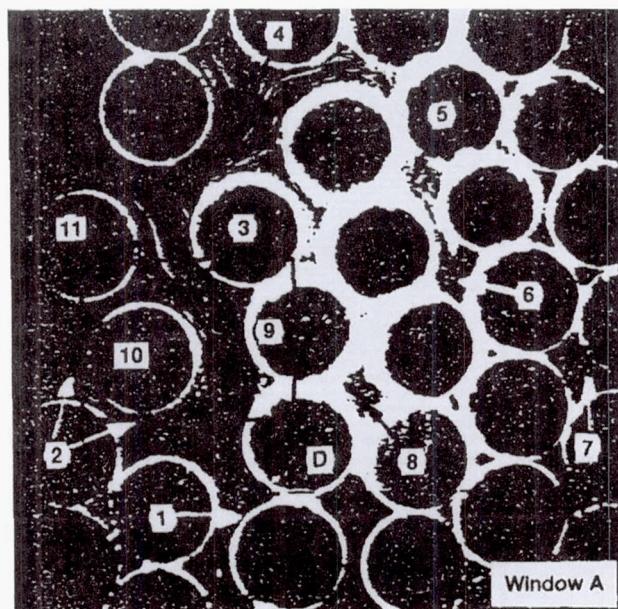
(c) Flow visualization in window A.
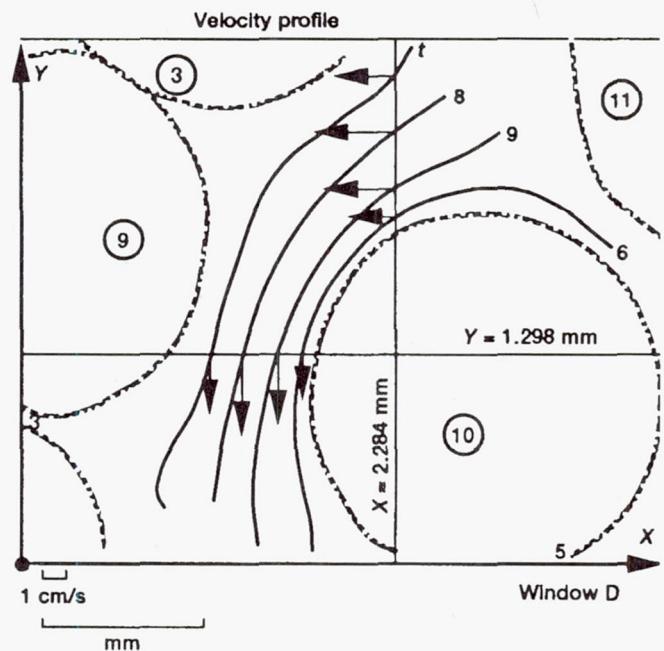
(d) Quantification of flow trajectories and velocities in window D.

Figure 5.—Qualitative and quantitative flow assessment in inlet section of brush seal (oil tunnel).

108
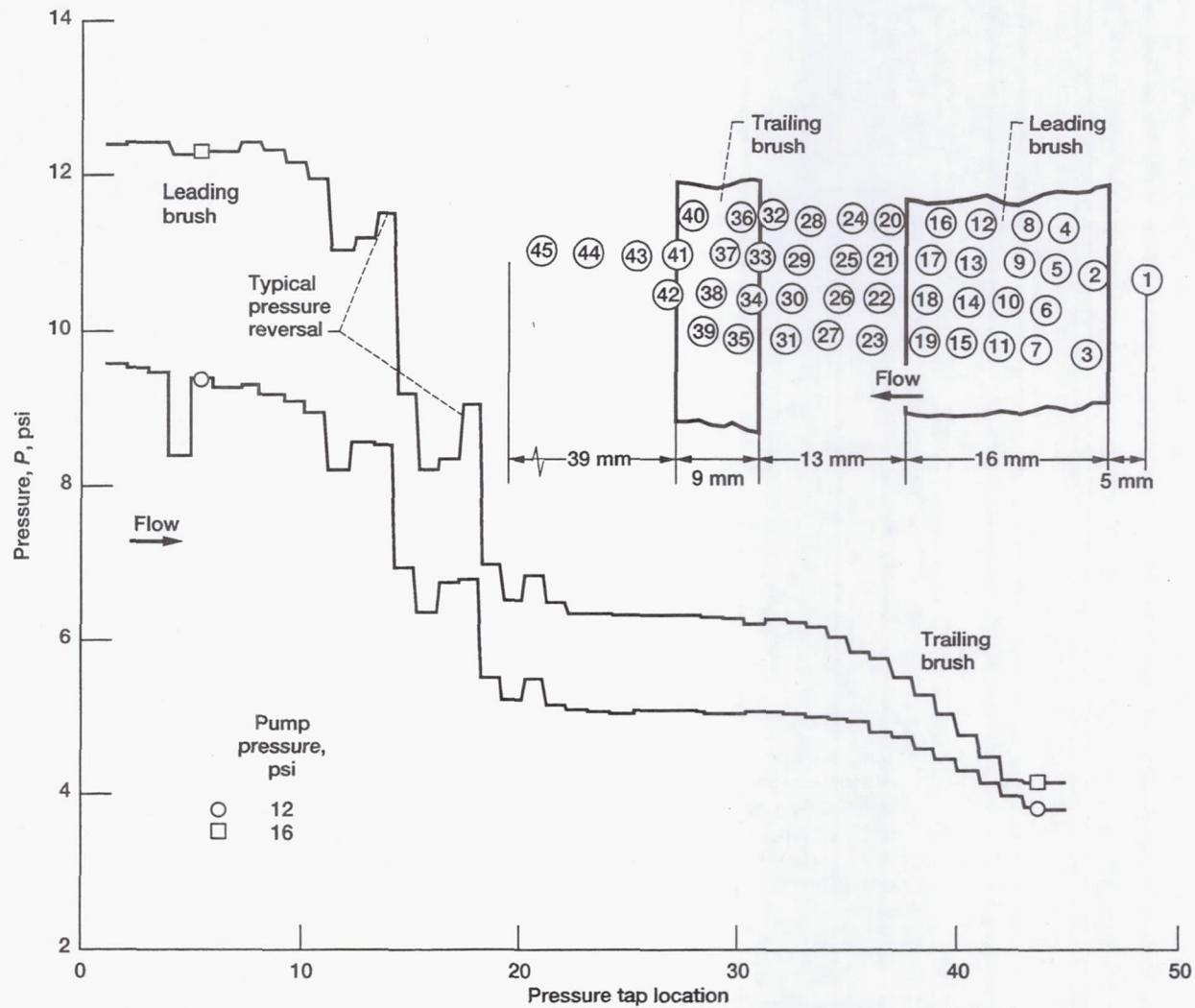
Figure 6.—Pressure drop patterns through sequence of two brushes. Bristle diameter: leading brush, 2 mm; trailing brush, 1 mm.

109
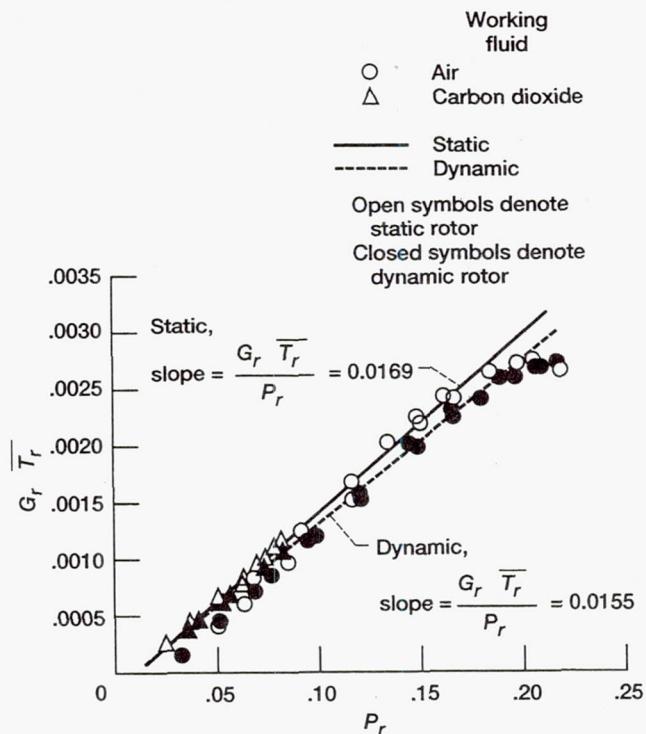
Figure 7.—Normalized brush seal performance data at static and low-speed dynamic rotor conditions in air and carbon dioxide. Radial interference, 0.0024 in. (G_r = reduced mass flux; T_r = reduced temperature; P_r = reduced pressure, P_{in}/P_c, where P_{in} = inlet pressure and P_c = pressure at critical point).
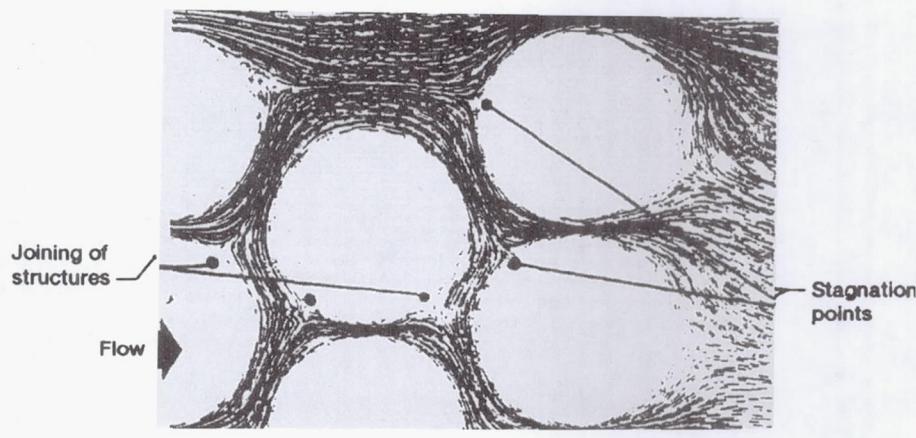
(a) Numerical.
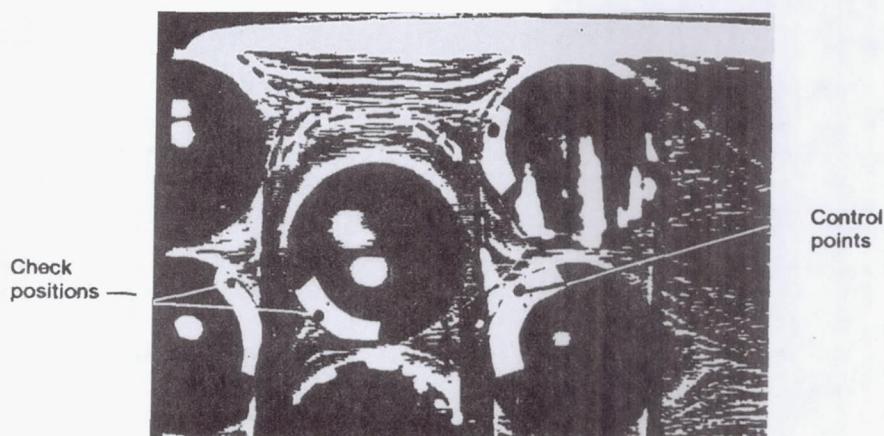
(b) Experimental.
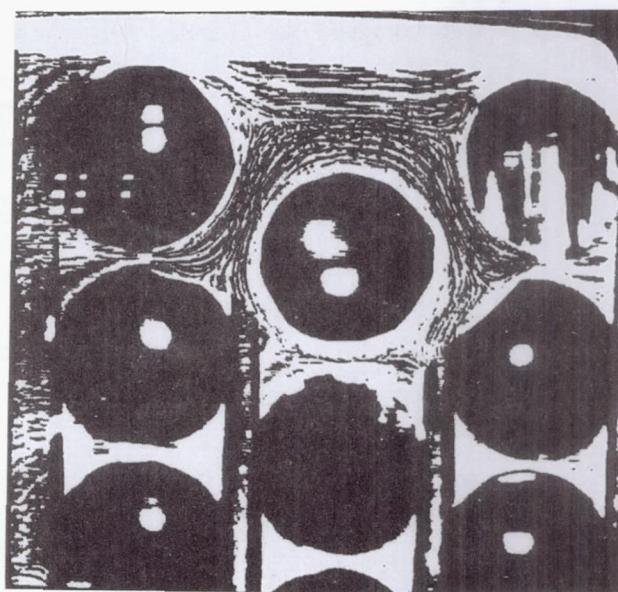
(c) Compositional (a) and (b).

Figure 8.—Comparison of calculated and experimental flow
structures in cylindrical arrays of pins.

111

Rivering jet

Typical recirculation zone

(a) Six rows.

(b) Cascade of two elements (three rows each); clearance spacing, 3 diameters.

Zone A

Zone B

Zone C

(c) Cascade of two elements (three rows each); clearance spacing, 5 diameters.
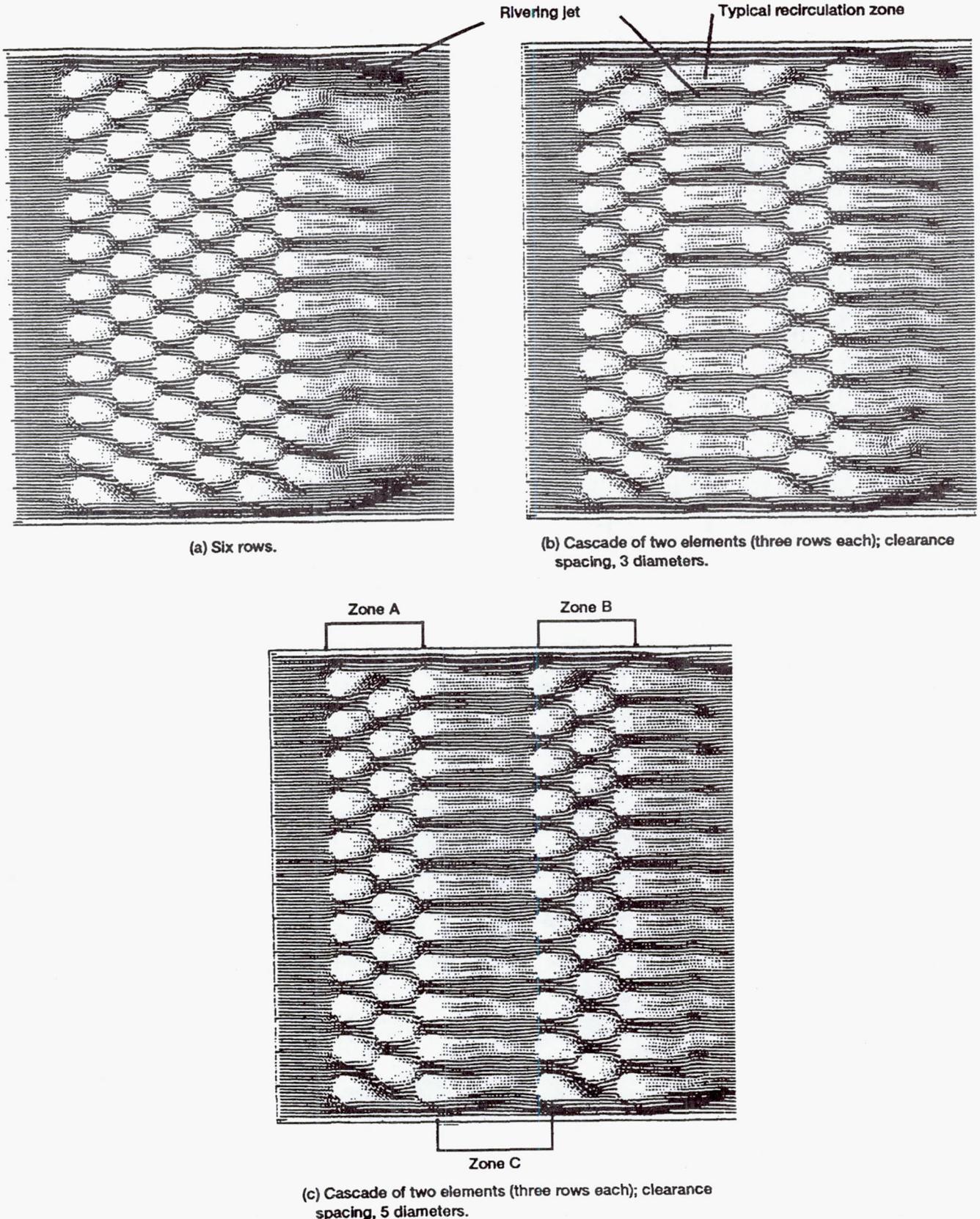
Figure 9.—Calculated flow across cascade of two arrays of cylindrical pins. Reynolds number, 2000.
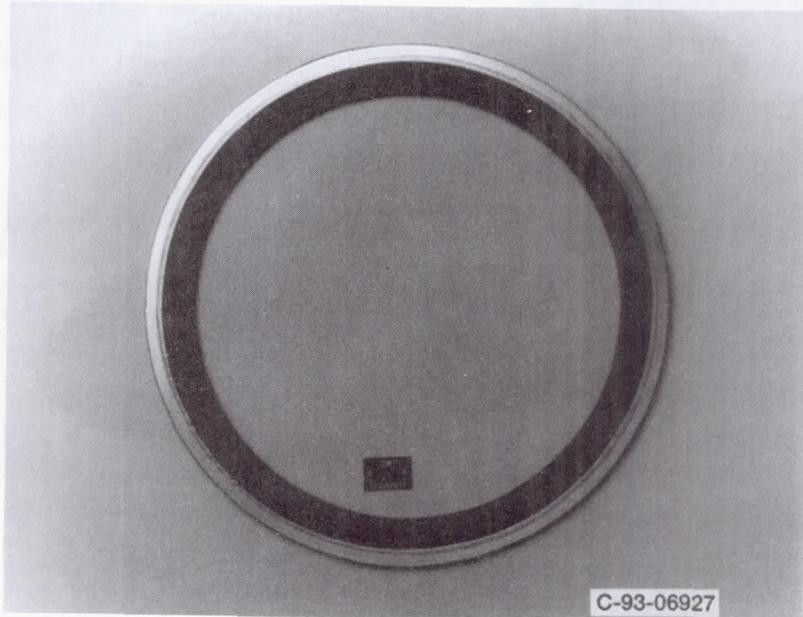
(a) Plan view.
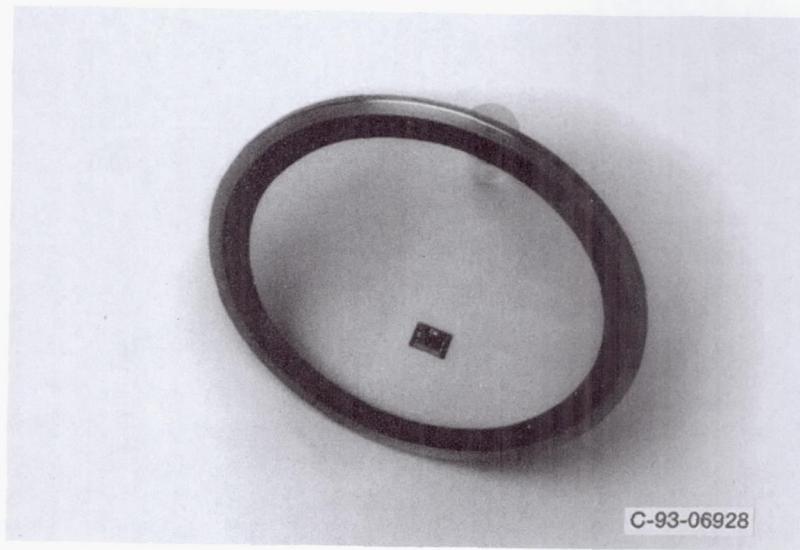
(b) Isometric view.

Figure 10.—Silicon carbide bristle/metallic plate brush seal.
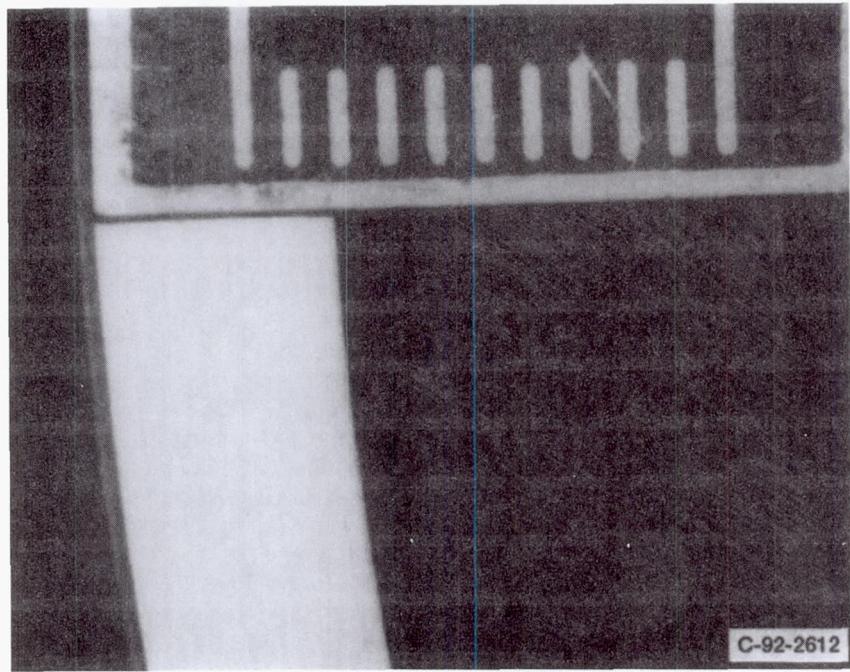
(a) Bristle layup.
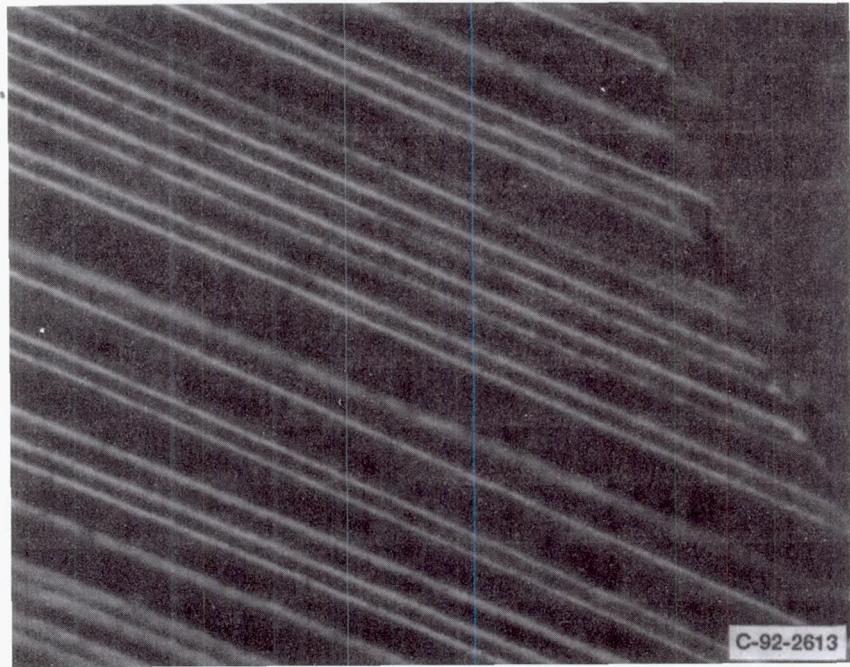
(b) Closeup including bristle tips.

Figure 11.—Details of silicon carbide bristle/metallic plate brush seal configuration.

114
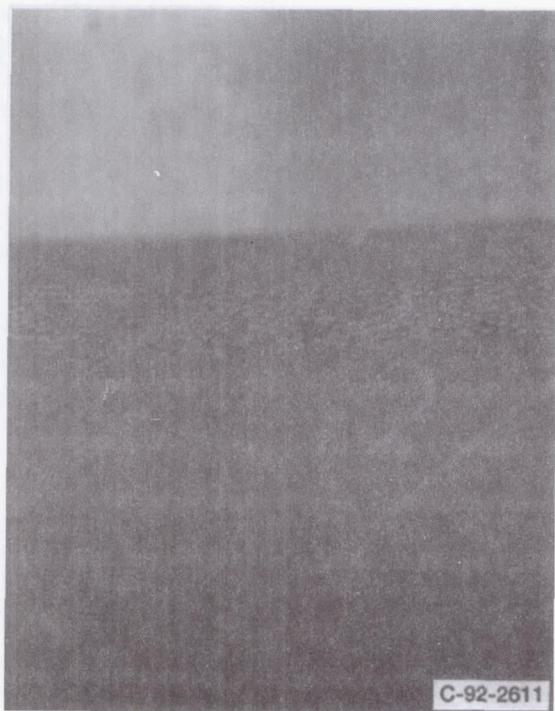
(a) Cored bristles.
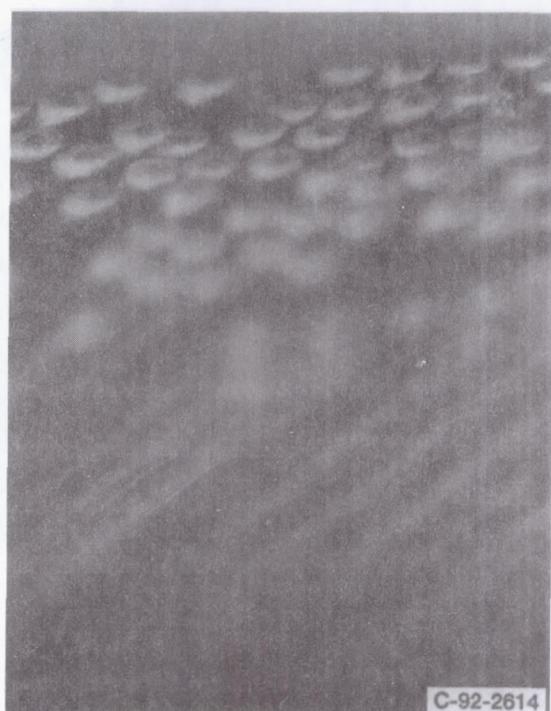
(b) Closeup of bristle tips.
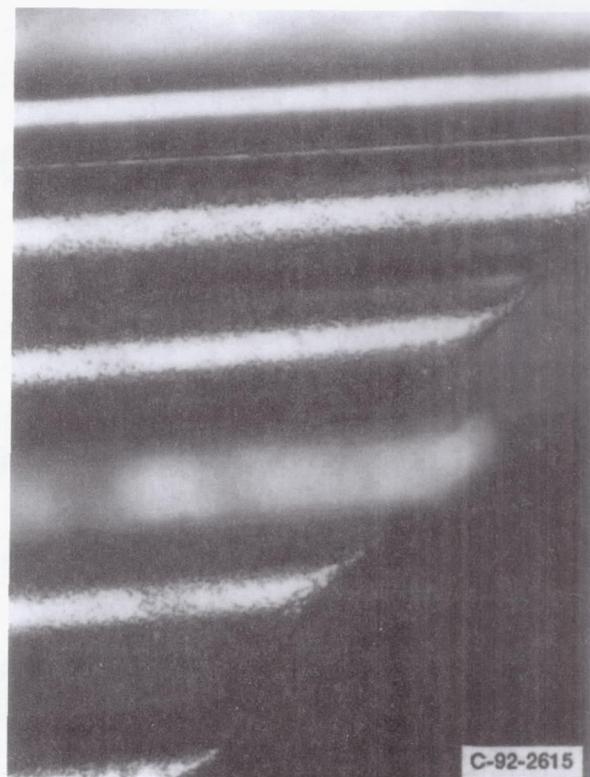
(c) Bristle tip contours.

Figure 12.—Silicon carbide bristle tips.

115
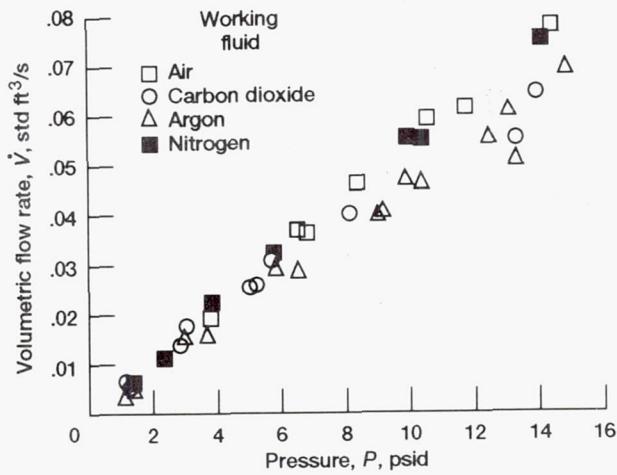
Figure 13.—Flow data for 1.5-in.-diameter silicon carbide bristle/metallic plate brush seal at ambient temperature and 2600 rpm.
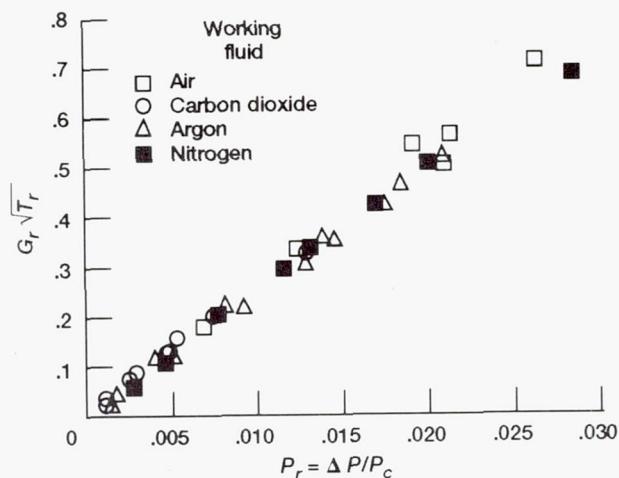
Figure 14.—Normalized flow data for 1.5-in.-diameter silicon carbide bristle/metallic plate brush seal at ambient temperature and 2600 rpm. (See fig. 7 for definition of symbols.)
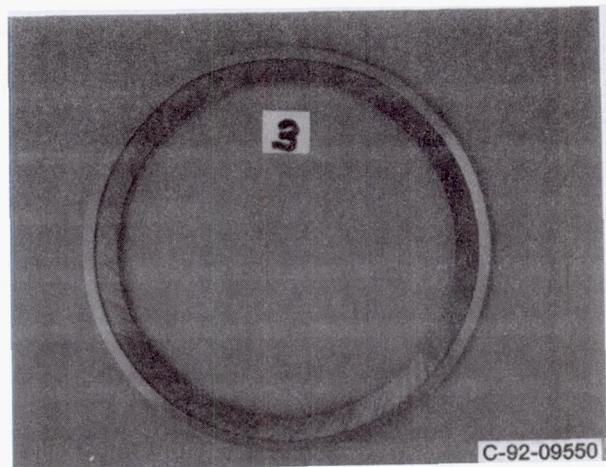
(a) Upstream side.
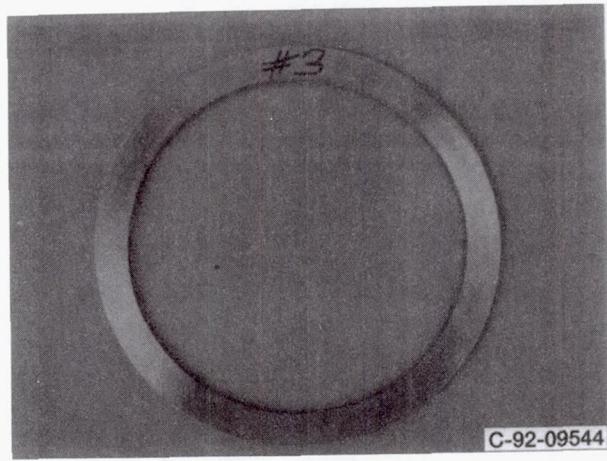
(b) Downstream side.

(c) Bristle interface.

Figure 15.—Metallic brush seal (Cross Mfg. Ltd.) and YSZ-coated rub runner (Technetics Corp.)—single brush typical of five-brush configuration.

116
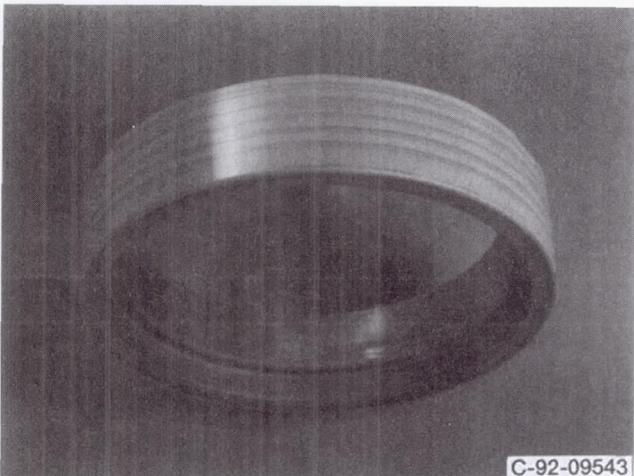
Figure 16.—Post-test photograph of YSZ-coated rub runner from Cross Mfg. Ltd. metallic brush seal, illustrating wear tracks of five-brush configuration.
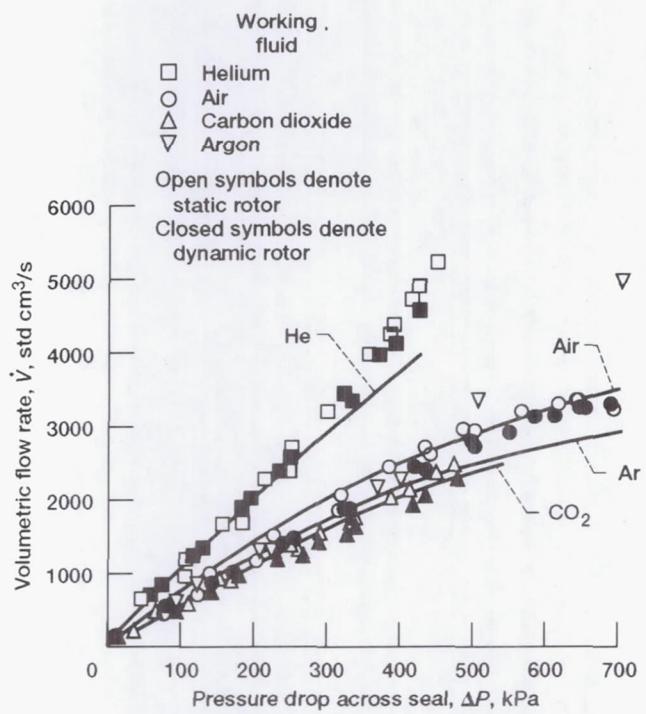
Figure 17.—Simplified brush seal modeling based on Ergun relation, standard volumetric flow rate versus pressure drop across brush seal for gaseous helium, air (or nitrogen or oxygen), argon, and carbon dioxide. $\Delta P = 25 \ \overline{M} \ (\mu/\mu_0) \ \dot{V} + 0.00015 \ M \ (\rho/\rho_0) \ \dot{V}_2$, where M is molecular weight, μ is viscosity, ρ is density, and subscript zero denotes standard conditions (1 bar, 300 K); for helium use M in place of $\overline{M}$.

117

BRUSH SEALS FOR CRYOGENIC APPLICATIONS

Margaret P. Proctor
NASA Lewis Research Center
Cleveland, Ohio
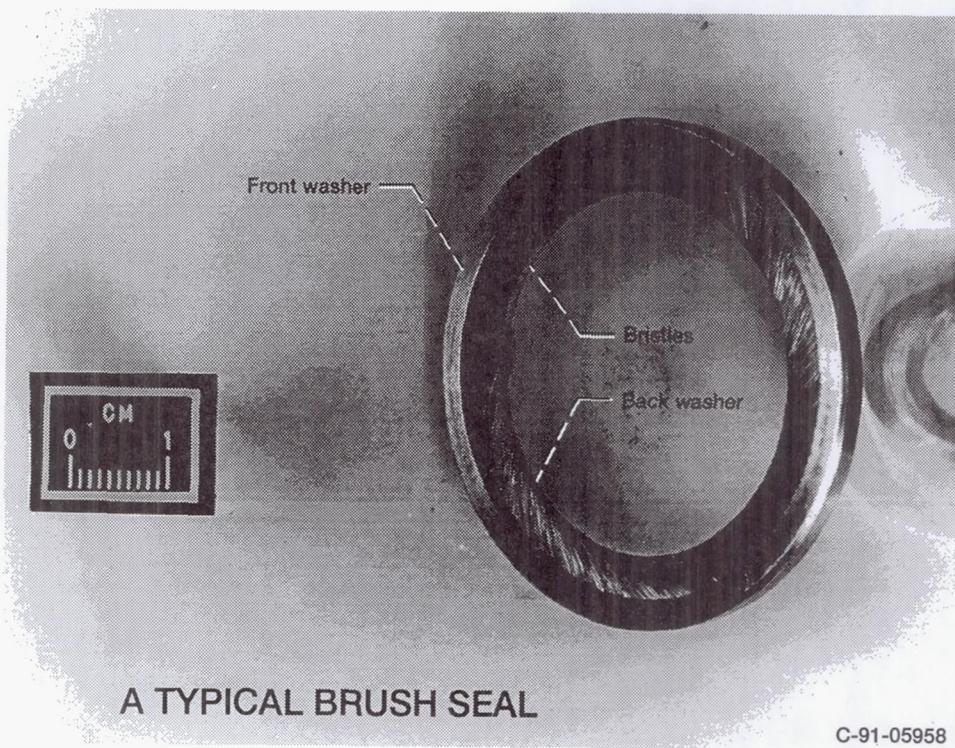
A TYPICAL BRUSH SEAL

C-91-05958

TEST PLAN

LN$_2$:
- CHECKOUT TESTER WITH FIXED CLEARANCE SEALS
- MEASURE LEAKAGE & WEAR PERFORMANCE OF
  SINGLE BRUSH SEAL   up to 40,000 rpm
  2 BRUSH SEALS FAR APART Δp /seal 150 psi max
  2 BRUSH SEALS CLOSE TOGETHER

LH$_2$:
- MEASURE LEAKAGE & WEAR PERFORMANCE OF
  SINGLE BRUSH SEAL - UP TO 62,000 RPM (525 fps)
  5 BRUSHES TIGHTLY PACKED

- MEASURE LEAKAGE & WEAR OF BRUSH SEALS FOR 4 DIFFERENT
  MATERIALS AND 3 DIFFERENT INITIAL INTERFERENCES

  BARE INCONEL
  OXIDE OF AL, MAGNESIA-ZIRCONIA   0.0025 inches
       OR ZIRCONIUM   0.005 inches
  CHROME CARBIDE   0.0075 inches
  SILVER

LN$_2$:
- MEASURE EFFECT OF FENCE HEIGHT, BRISTLE DIAMETER, PACKING
  DENSITY, DEPTH OF SPACES BETWEEN BRUSHES, BRISTLE
  MATERIALS, BRISTLE LENGTH AND ANGLE ON BRUSH SEAL
  PERFORMANCE

Preceding Page Blank

119

LH$_2$ BRUSH SEAL TESTER
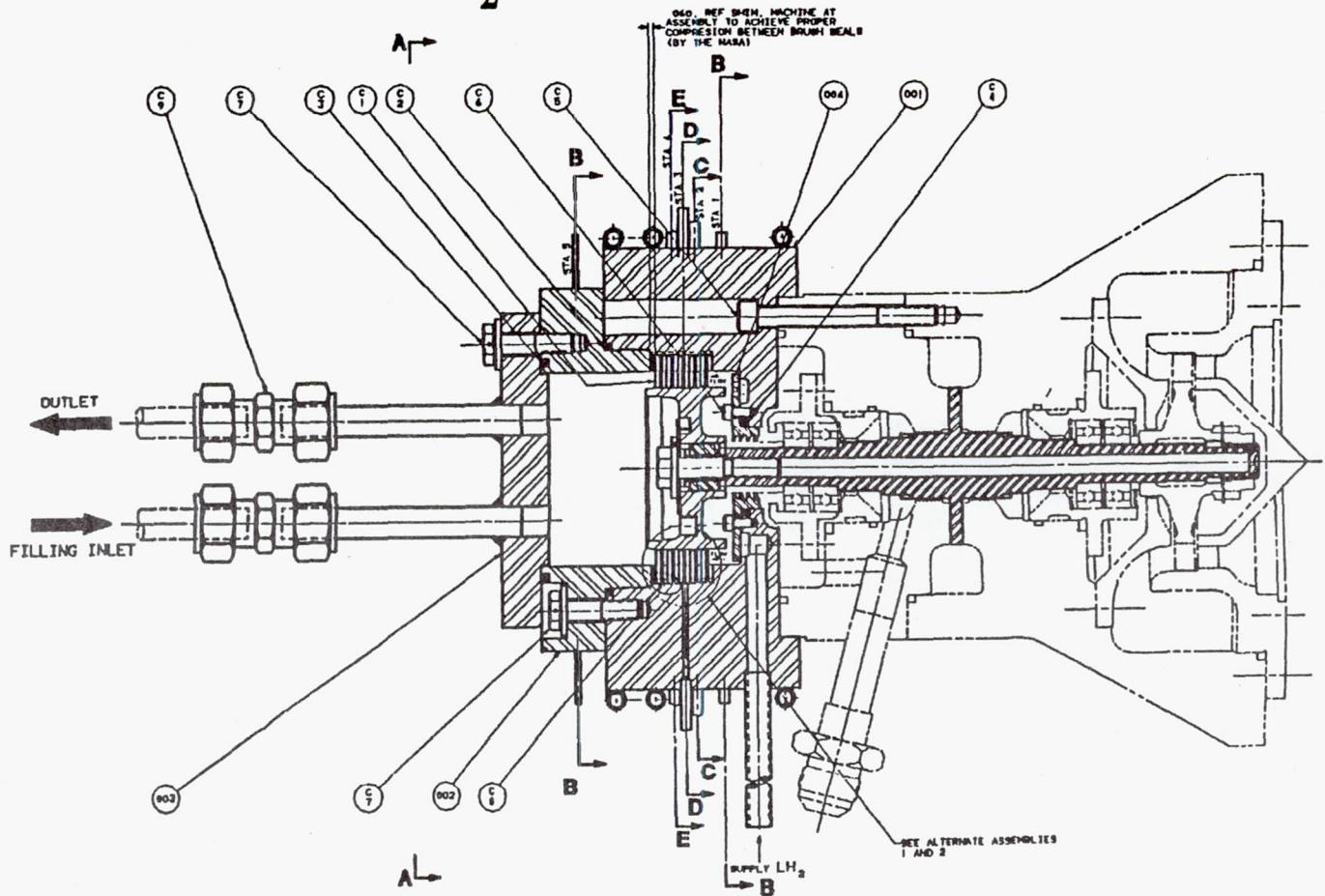
TESTER/FACILITY CAPABILITIES IN LN2

800 PSIG SUPPLY TO TEST SEAL

37,700 RPM AT 0 DELTA-P ACROSS SEAL

300 PSID ACROSS SEAL DURING ROTATION
(LIMIT OF BALANCE PISTON)

INSTRUMENTATION
STATIONS

STA 5   STA 4 STA3 STA 2   STA 1

SEAL HOLDER

SEAL POSITIONS   5   4   3   2   1

← FLOW

RUNNER

C_L

POSITIONS & STATIONS
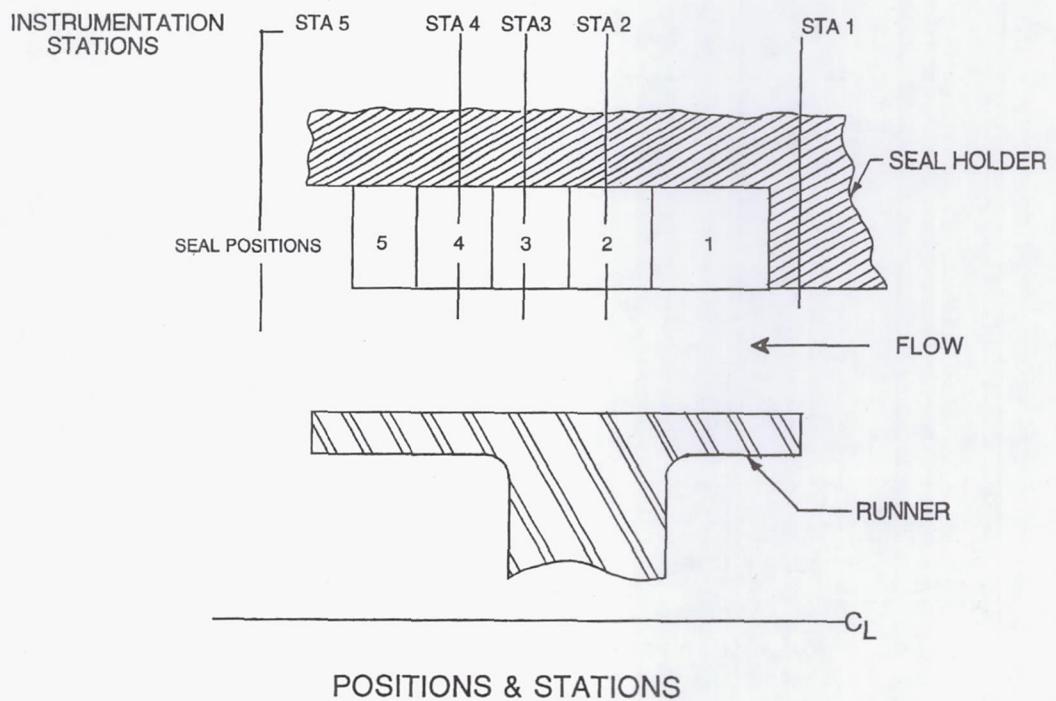
CONFIGURATIONS TESTED IN LN2

NO.	DESCRIPTION
1	12 TOOTH LABYRINTH SEAL (0.00513 IN. RADIAL CLEARANCE)
2	SINGLE BRUSH SEAL (POSITION 1)
3	TWO BRUSHES FAR APART (POSITIONS 2 & 5)
4	TWO BRUSHES TIGHTLY PACKED (POSITIONS 3 & 4)
5	THREE BRUSHES (POSITIONS 1, 3 & 5)
6	TWO BRUSHES (POSITIONS 2 & 5) - PRESSURE TAPS AT SPACER ID
7	THREE BRUSHES (POSITIONS 1, 3, 5) - PRESSURE TAPS AT SPACER ID
8	SINGLE BRUSH (POSITION 1) - BLOWOUT TEST

121

NOMINAL BRUSH GEOMETRY
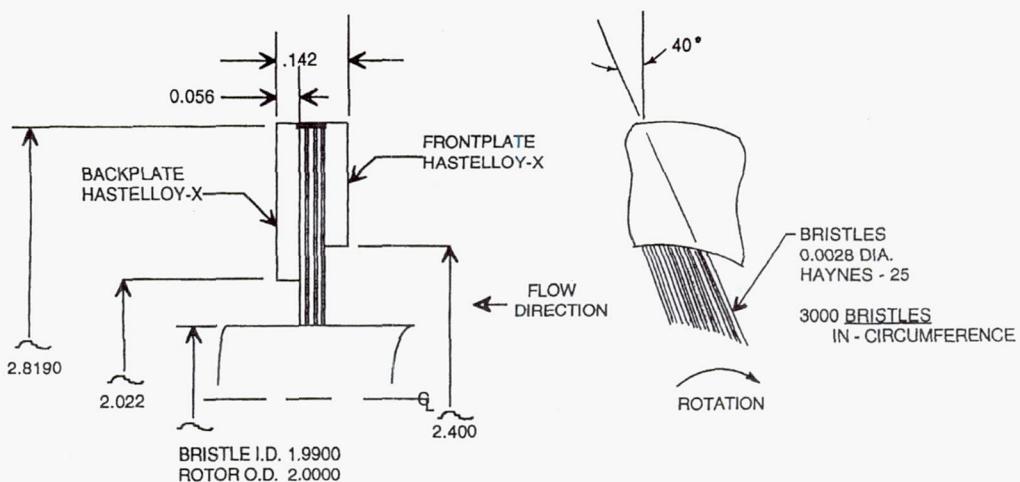
RADIAL INTERFERENCE   0.0050
RADIAL CLEARANCE BETWEEN BACKPLATE AND ROTOR   0.011
RADIAL DISTANCE BETWEEN BACKPLATE AND BRISTLE I.D'S   0.016
RADIAL DISTANCE BETWEEN FRONTPLATE AND BRISTLE I.D.'S   0.205

(NOT TO SCALE; ALL DIMENSIONS ARE INCHES)

12-TOOTH LABYRINTH SEAL IN LN2
0.00513 IN. RADIAL CLEARANCE

SOLID SYMBOLS
ARE PREDICTIONS

SINGLE BRUSH IN LN2
0.004375 IN. RADIAL INTERFERENCE

Shaft Speed, RPM

○ 0
□ 5,000
◇ 0
△ 15,000
▽ 0
◿ 0
⬠ 25,000
⌂ 0
⬡ 35,000
▱ 0

AVERAGE LEAKAGE RATE, LBM/S

INLET DENSITY X PRESSURE DROP, LBM-LBF/FT3-IN2

123
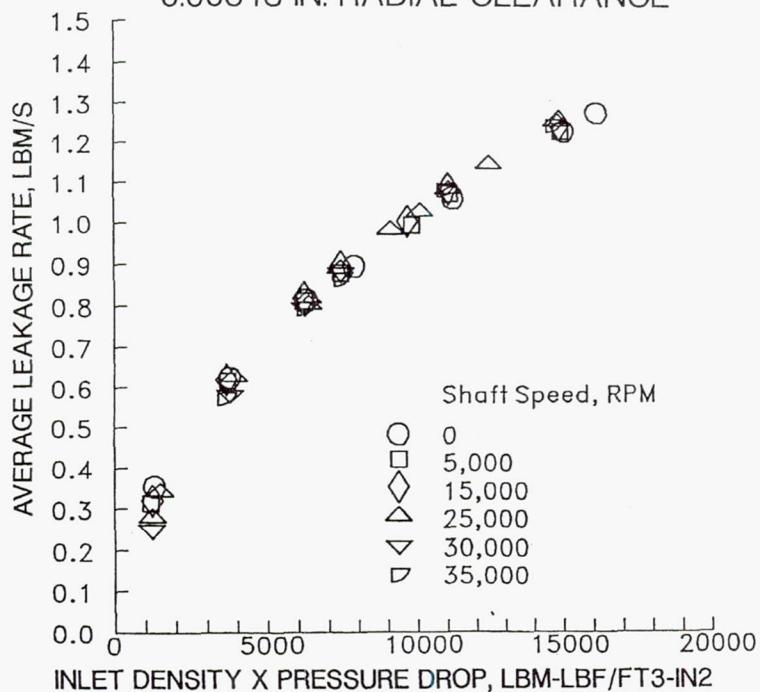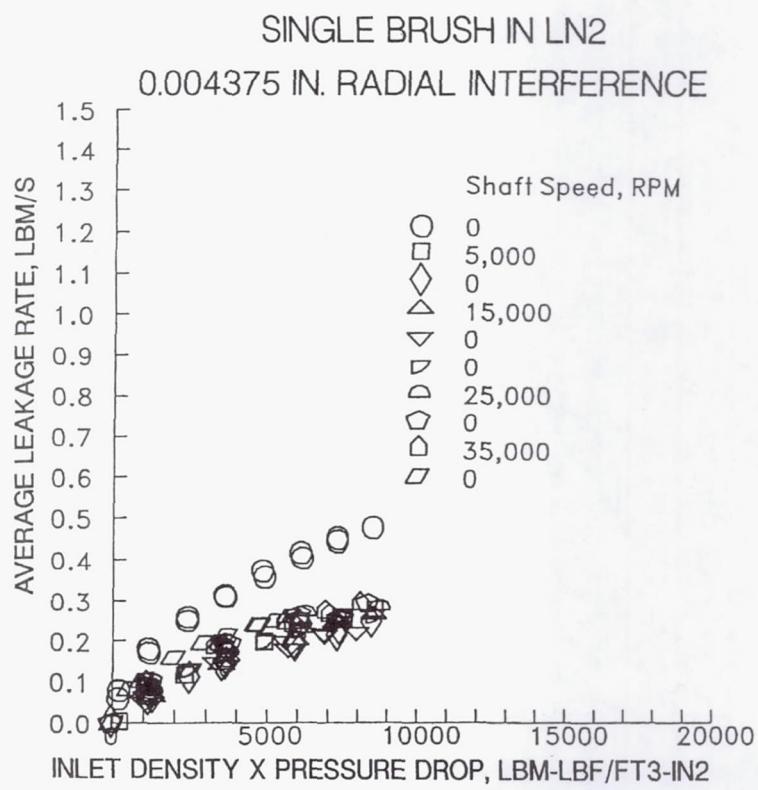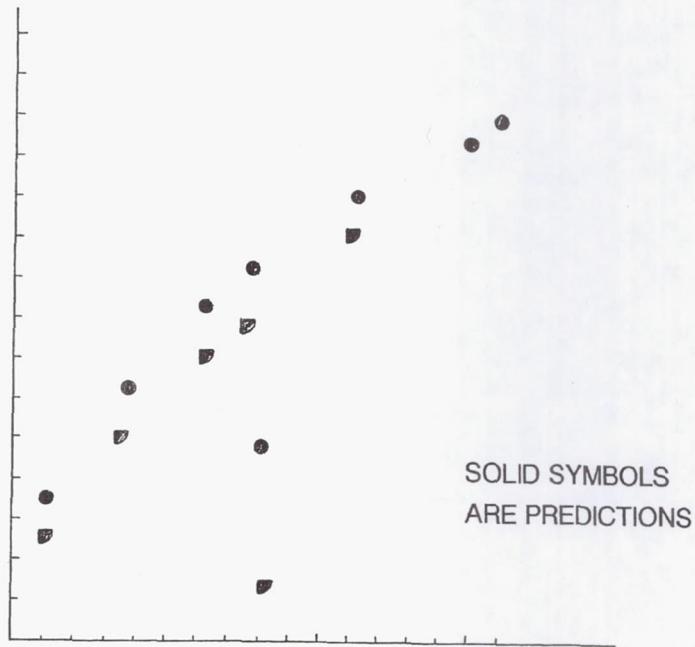
SPEED EFFECTS ON TEMPERATURE
FOR A SINGLE BRUSH IN LN2
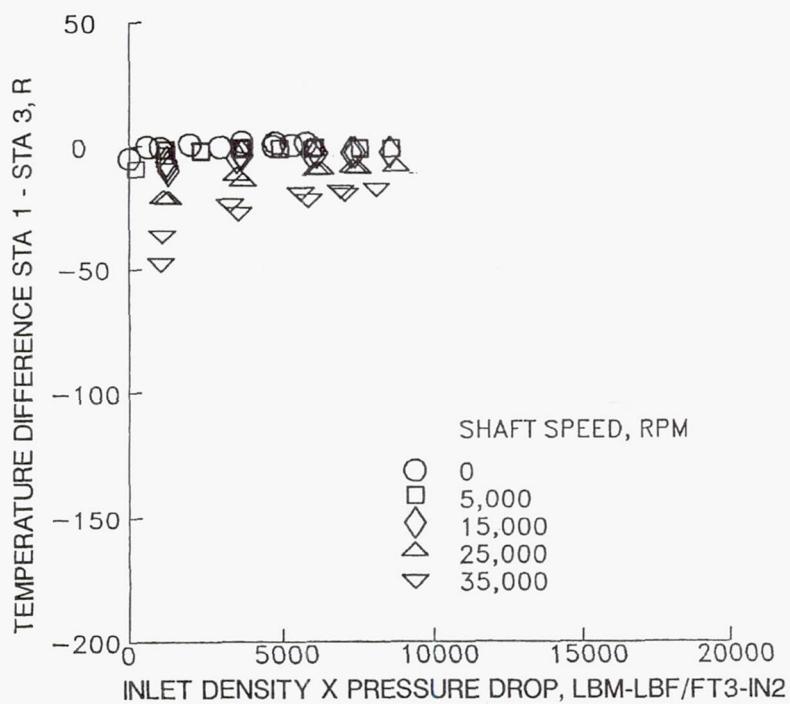
BLOWOUT TEST OF A SINGLE BRUSH IN LN2 AT ZERO RPM
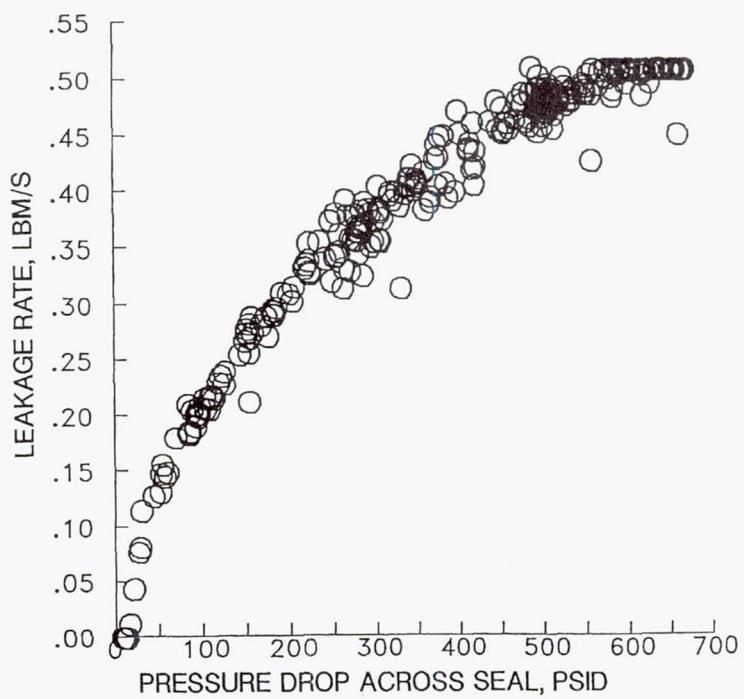
Power Loss vs Shaft Speed for SINGLE BRUSH IN LN2
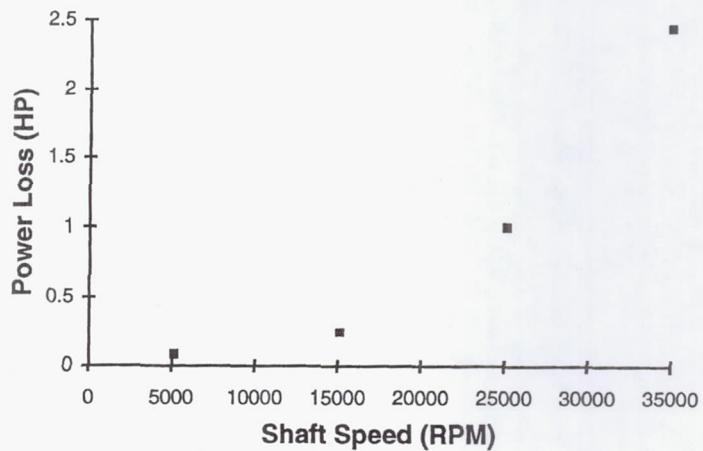
COMPARISON OF LN2 LEAKAGE PERFORMANCE FOR 1 AND 2 BRUSH CONFIGURATIONS AT 5000 RPM

CONFIGURATION

○ 1 BRUSH
□ 2 BRUSHES FAR APART
◇ 2 BRUSHES TIGHT

125
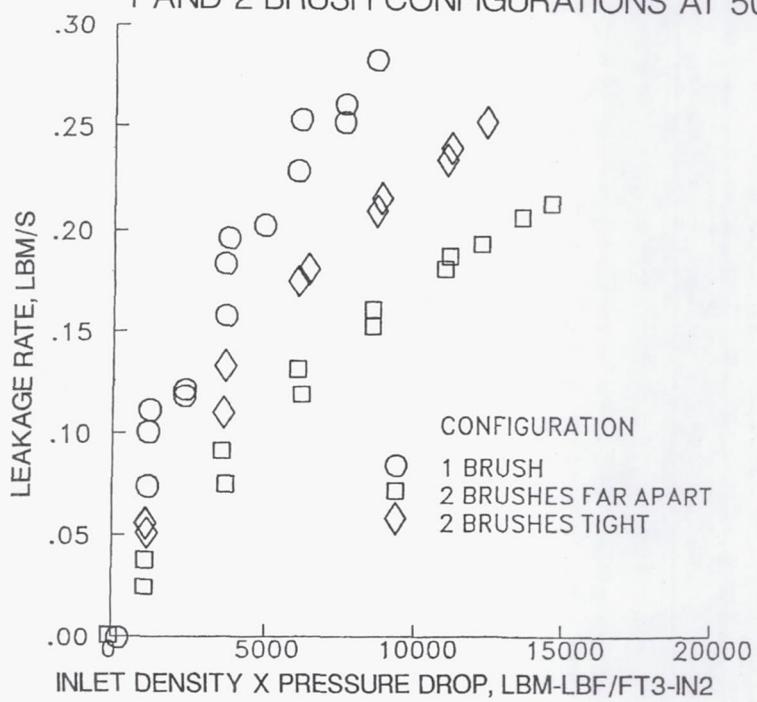
STAGING EFFECTS ON TEMPERATURE
IN LN2 AT 35,000 RPM
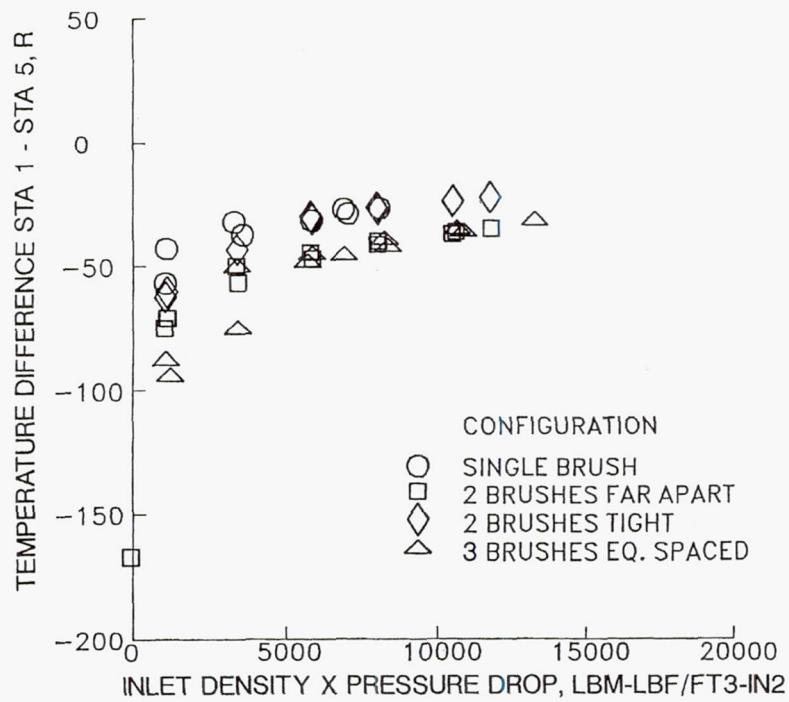
3 BRUSHES EVENLY SPACED IN LN2 AT ZERO RPM

126
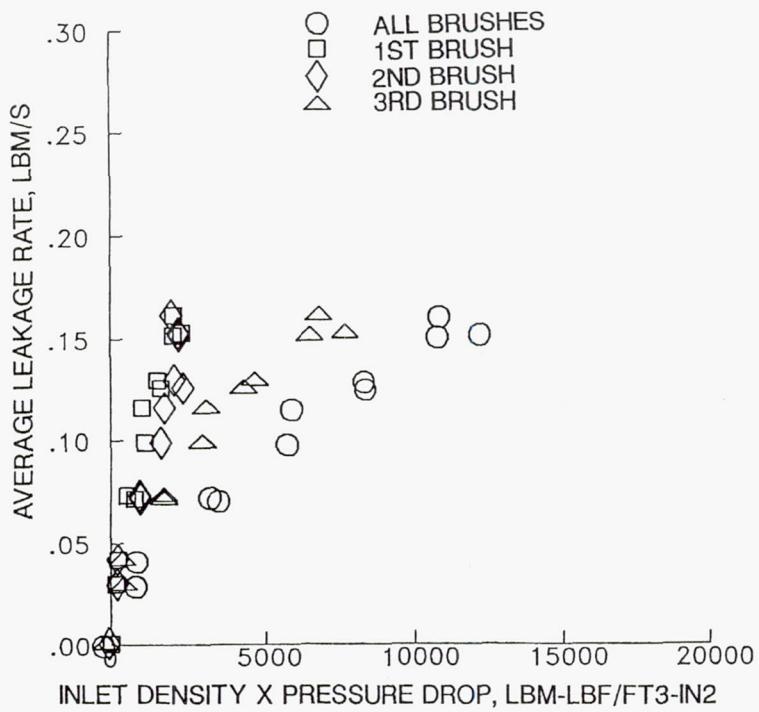
3 BRUSHES EVENLY SPACED IN LN2 AT 35,000 RPM

INLET DENSITY X PRESSURE DROP, LBM-LBF/FT3-IN2
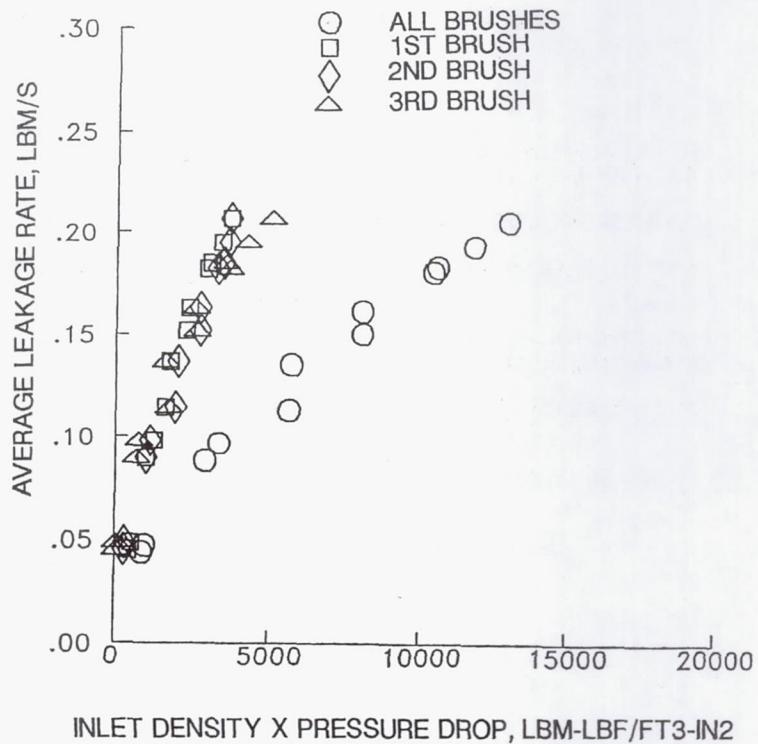
WEAR DATA

CONDITIONS:

INCONEL 718 ROTOR

HAYNES - 25 BRISTLES

SHAFT ROTORDYNAMICS VERY GOOD

- NOMINAL ROTOR ORBITS < 0.2 MILS IN DIAMETER
- MAXIMUM ORBIT WAS 1.0 MIL DIAMETER

MAXIMUM SHAFT SPEED: 35,000 RPM

MAXIMUM SURFACE VELOCITY: 305 FT/S

127

WEAR DATA

ROTOR:

PROFILOMETER TRACES ACROSS AXIAL LENGTH OF ROTOR
TAKEN AT 4 LOCATIONS - 0, 90, 180, AND 270 DEGREES

MAXIMUM GROOVE DEPTH MEASURED: 0.0010 INCH

NOMINAL GROOVE DEPTH MEASURED: 0.00075 INCH

PLOT OF GROOVE AREA SHOWS AN INCREASE WITH TIME
WITH A MAXIMUM VALUE OF 12,361 SQUARE MICRONS

4 -1/2 HOURS OF SHAFT ROTATION ACCUMULATED

WEAR DATA

BRUSHES:

SOME BRISTLE WEAR OCCURRED (1-3 MILS)

BRISTLE WEAR IS DIFFICULT TO QUANTIFY DUE TO UNCERTAINTY
IN BRISTLE BORE I.D. MEASUREMENTS

BORE I.D. CAN VARY BY 7.5 MILS

OPTICAL COMPARATOR USED

SOME MELTING OF BRISTLES DID OCCUR, THOUGH IT WAS
MINIMAL.....APPROXIMATELY 10 BRISTLES

AFTER MELTING WAS FIRST OBSERVED, TEST CONDITIONS
OF ROTATION WITH NO DELTA-P ACROSS THE SEAL WERE
DISCONTINUED

Region A

129
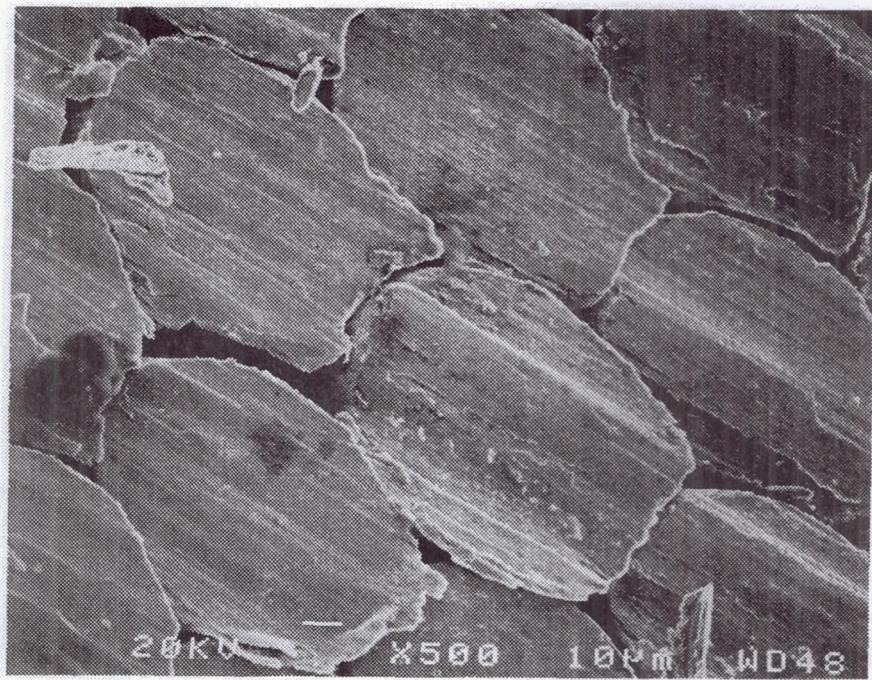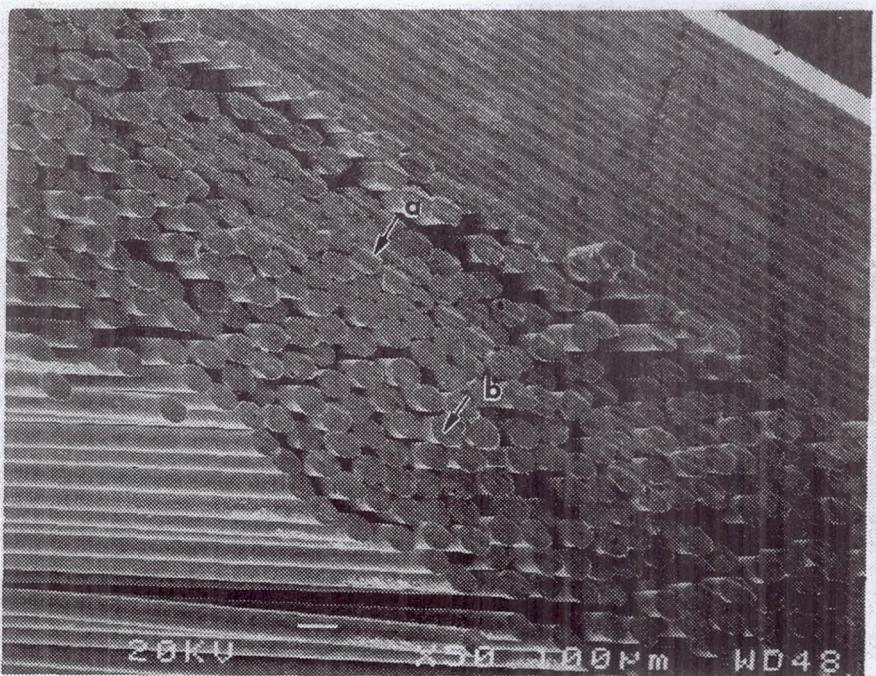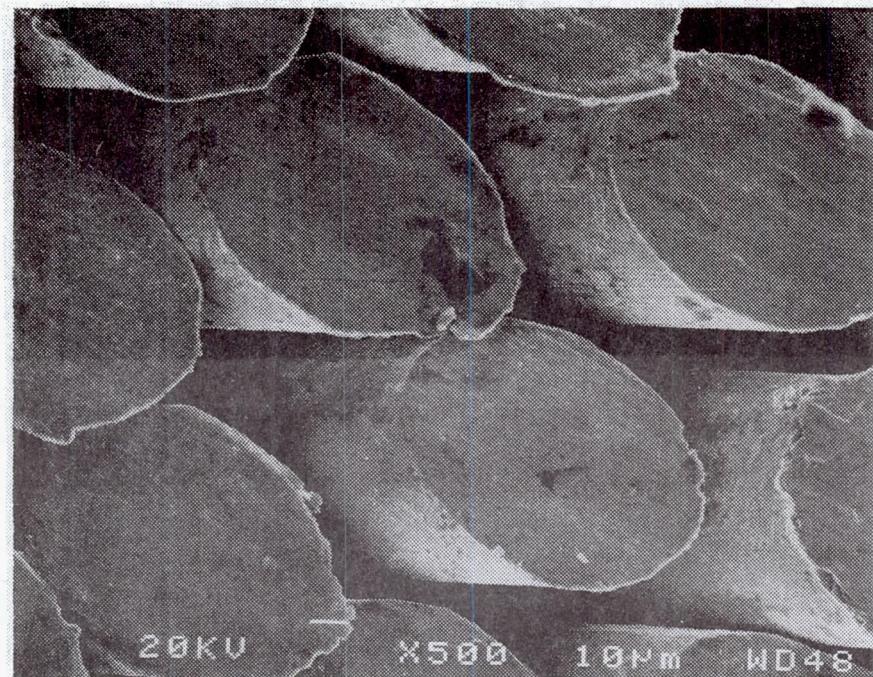
Region B

SUMMARY OF LN2 BRUSH SEAL TEST RESULTS

- LEAKAGE FOR A SINGLE BRUSH SEAL WAS 2-3 TIMES LESS THAN FOR A 12-TOOTH LABYRINTH SEAL.

- THE MAXIMUM TEMPERATURE RISE FOR A SINGLE BRUSH SEAL WAS LESS THAN 50 R AND OCCURRED AT 25 PSID ACROSS THE SEAL AND 35,000 RPM. (THIS TEMPERATURE RISE WOULD BE GREATER AT 0 PSID).

- A STATIC BLOWOUT TEST DEMONSTRATED SEALING CAPABILITY UP TO 550 PSID. THE SEAL LIMIT WAS NOT OBTAINED.

- THE POWER LOSS FOR A SINGLE BRUSH AT 35,000 RPM AND 175 PSID WAS 2.45 HP.

- TWO BRUSHES FAR APART LEAK LESS THAN TWO BRUSHES TIGHT PACKED.

- ROTOR WEAR WAS ~ 0.00075 MILS AND BRISTLE WEAR WAS 1-3 MILS AFTER 4-1/2 HOURS.

HIGH TEMPERATURE SEALS TEST RIG

Harold E. Addy, Jr.
NASA Lewis Research Center
Cleveland, Ohio

The High Temperature Seals Test Rig Program at NASA's Lewis Research Center is a joint effort involving three separate federal government agencies. The U.S. Air Force had the rig built under contract by Teledyne CAE in Toledo, Ohio and a series of brush seal tests (Ref. 1) were conducted at Teledyne as part of the contract. At the conclusion of the contract, the USAF chose to locate the rig at NASA Lewis where Lewis could provide support for continued testing. To help provide this support, NASA is receiving assistance from the Vehicle Propulsion Directorate of the U.S. Army Research Laboratory. The U.S. Army provides primary technical support for rig operation while NASA provides primary research and development capability.

Testing has been underway at Lewis in this test rig since April, 1993. The rig was designed to run tests at temperatures to 800 degrees F at pressures to 200 psia or at temperatures to 1300-1500 degrees F at pressures to 65 psia. Because of the difficulties encountered in attempting to maintain high working gas temperatures at the low leakage rates typical of contact seals, the highest temperature and pressure to which seals have been subjected during a test thus far is 700 degrees F and 120 psia. More insulation will be applied to the rig to attempt to raise the maximum operating temperature. In the event that wear data is of primary importance for a particular seal design, the seal can be tested at temperatures greater than 700 degrees F by opening a rig bypass valve. The hot gas bypass valve was incorporated into the design of the rig to allow for shorter rig warm-up times. This action will, however, preclude the measurement of seal leakage.

The rig was designed to run at speeds of up to 50,000 rpm which, for a 5.1 inch diameter disk, is a surface speed of about 1100 ft./sec. However, it was found that at speeds above 35,000 rpm, undue disk vibrations occur that interfere with testing and could lead to shaft failure. To avoid this problem, testing to date has been limited to 30,000 rpm or a surface speed of about 700 ft./sec. A thinner disk is being designed which will weigh approximately half as much as the current disk thereby increasing the critical speed of the rig such that safe testing may be conducted above 30,000 rpm.

The rig was designed to allow easy replacement of the disks as well as the seals such that different disk materials and coatings may be tested using interchangeable disks. Eight disks made of Inconel 718 are currently available; one has no coating, two have a chromium carbide coating, and five have an aluminum oxide coating.

Figure 1 shows a cross section of the rig with the path of hot air flow during a test depicted by arrows. Hot air enters at the top of the rig then flows through a baffle plate before impinging on the disk and seal in an axial direction. The rig bearings are cooled by both oil and an air purge. Air cooling is also provided to reduce the exhaust air temperature. Figure 2 indicates rig instrumentation.

Air Flow Path During Brush Seal Test
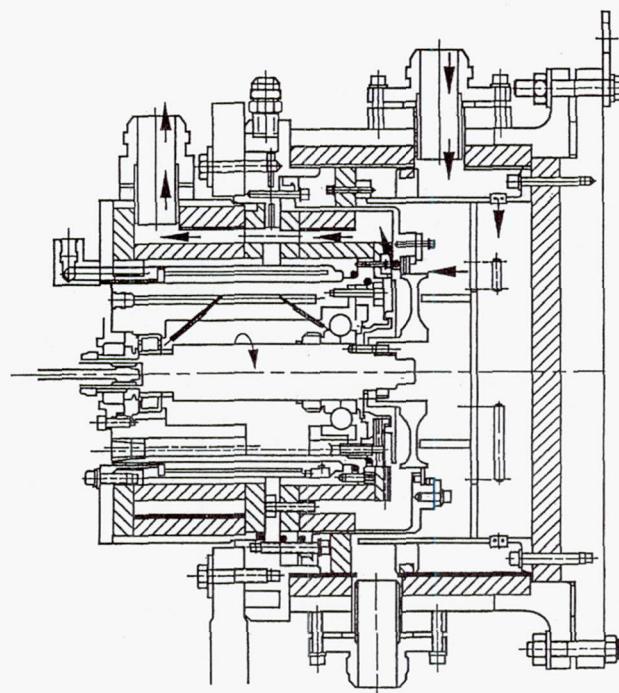
Figure 1. Cross Section of Rig Showing Air Flow

Brush Seal Rig Instrumentation Schematic
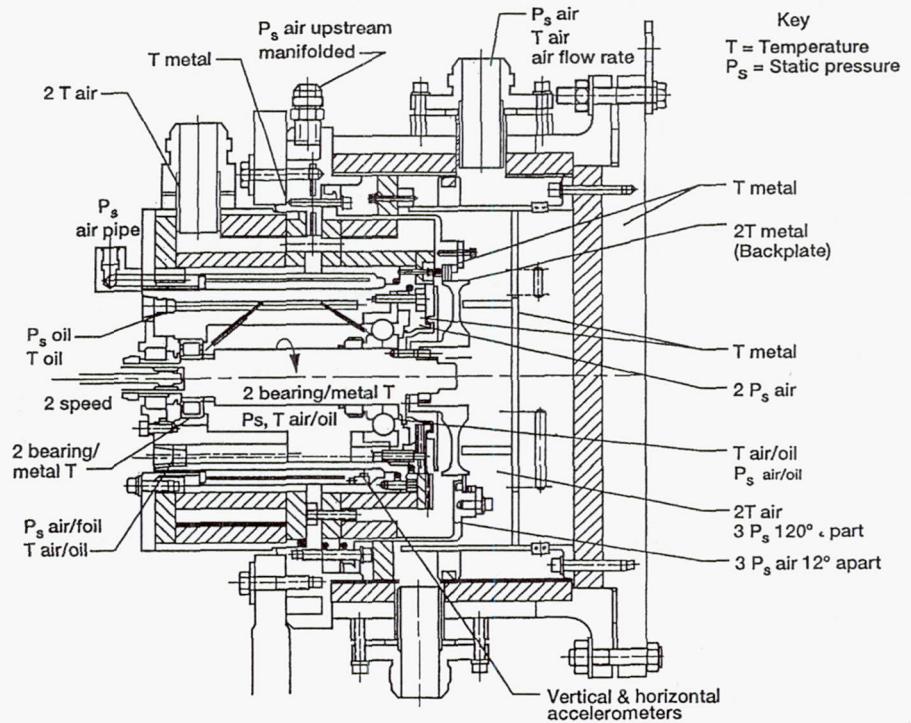
Figure 2. Rig Instrumentation

CERAMIC BRUSH SEALS DEVELOPMENT

Harold Howe
Technetics Corporation
DeLand, Florida

CERAMIC BRUSH SEALS

METALLIC BRUSH SEALS

A. BENEFITS OVER CURRENT SEALS

1. HIGHER EFFICIENCY

2. ABLE TO WITHSTAND SHAFT EXCURSIONS

3. ABLE TO TAKE UP BUILD TOLERANCES

4. REDUCE SECONDARY FLOW LOSSES

B. LIMITATIONS

1. TEMPERATURE

2. LIFE/WEAR

3. OXIDATION

CERAMIC

A. HIGHER TEMPERATURE

B. LOWER WEAR

C. INTERFERENCE FIT BENEFIT

TECHNETICS TEST RIG
2450/36/.003

Legend: □ .3 SCFM   + .6 SCFM   ◇ .8 SCFM   △ 1.0 SCFM   × 1.2 SCFM   ▽ 1.4 SCFM

Y-axis: PRESSURE DROP (bars), X-axis: CLEARANCE (in)
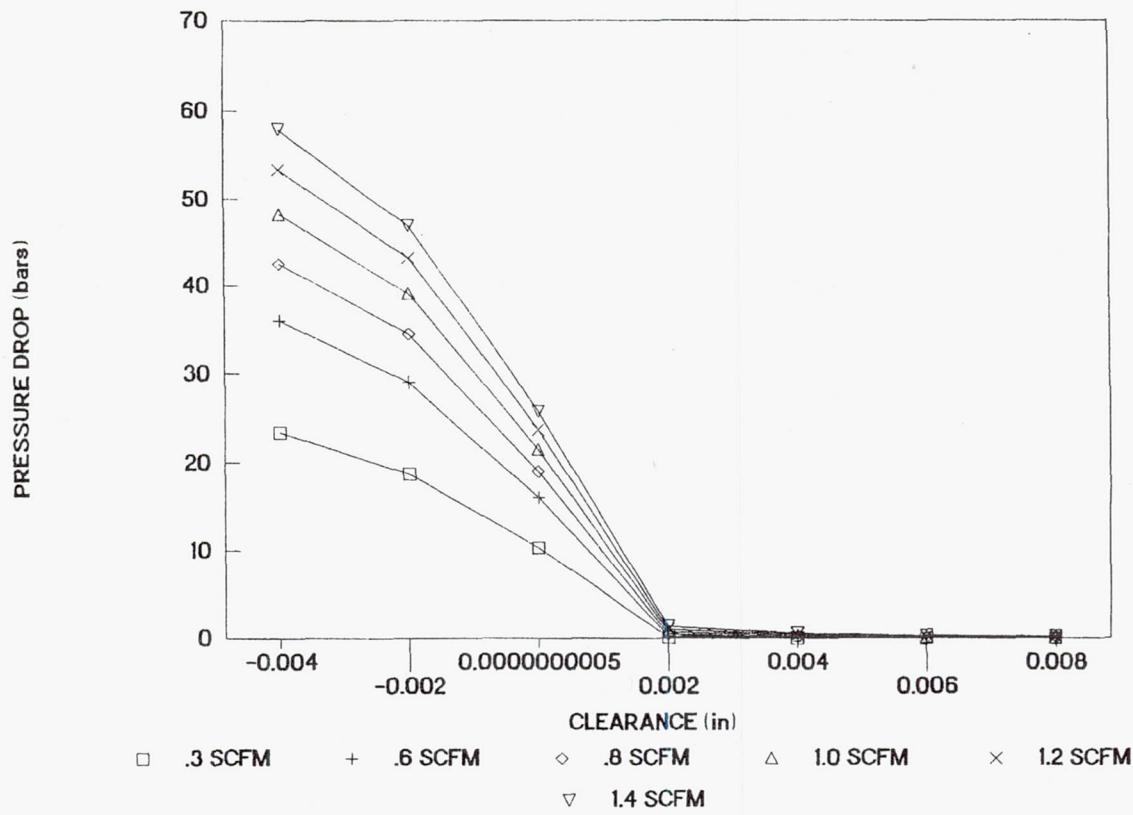
<u>R & D</u>

<u>PURPOSE</u>:

A. INVESTIGATE AND SHOW
    FEASIBILITY

B. BUILD AND INITIAL TEST
    OF CERAMIC BRUSH SEAL

<u>TECHNICAL OBJECTIVES</u>:

A. IDENTIFY MATERIALS

B. DEMONSTRATE
    MANUFACTURABILITY

C. TEST SEAL INTEGRITY

<u>MATERIALS</u>:

INDUSTRY STANDARD MATERIALS

<u>CERAMIC FIBER</u>

A. NEEDS

    1. SIZE (.002"-.006")

    2. FLEXIBLE

    3. QUALITY

    4. PRICE

B. AVAILABLE

    1. ALUMINUM OXIDE

    2. SILICON CARBIDE

    3. TITANIUM DIBORIDE

    4. QUARTZ

AVAILABLE CERAMIC BRISTLE MATERIALS

	AL_2O_3 SINGLE CRYSTAL	SIC CVD FILAMENT	SIO_2 FIBER OPTICS
SIZE	.005	.0056/.0031	.004
MODULUS (MSI)	60	58	10
TENSILE (KSI)	--	500	--
HARDNESS (MOHS)	9	2040-4487 $\frac{KG}{MM^2}$ VICKERS	7-8
BEND RADIUS (IN)	5/16	13/64 / 7/64	1
OPERATING TEMPERATURE (°F)	3632	BELOW 1800	2000

HAYNES 25
COBALT ALLOY

MODULUS (MSI)	25.9 @ 1300°F
TENSILE (KSI)	145-165
OPERATING TEMPEATURE (°F)	1200-1400°F

MANUFACTURING

A.   ALL CERAMIC

   1.   BRISTLES CAST IN PLACE

   2.   BRISTLES PRESSED IN PLACE

   3.   POST FIRING BRISTLE PLACEMENT

B.   BRAZED ASSEMBLY

   1.   METAL BACKING/CERAMIC FIBER

   2.   PLATING PROCESS

   3.   DIRECT BRAZE PROCESS

BRAZED ASSEMBLY DEVELOPMENT

A.   BRAZE ALLOYS

    1.   DUCTILE

    2.   HIGH TEMPERATURE

    3.   OXIDATION RESISTANT

B.   BRAZE METHOD (WETTING OF CERAMIC)

    1.   MOLY-MANGANESE

    2.   ACTIVE METALS
       i.e., Ti, Zr, V, etc. (ABA)

    3.   ACTIVE METAL HYDRIDES
       i.e., TiH_2, ZrH_2, etc.

CONTROLLING BRAZE FLOW

A.   EXCESSIVE WICKING

    1.   ABA ALLOYS (i.e., TiCuSil)

    2.   ACTIVE METAL BRAZING

B.   LIMIT FLOW USING BRAZE BARRIERS (STOP-OFF)

C.   ACTIVE METAL HYDRIDE PROCESS

    1.   ONE STEP

    2.   EASY APPLICATION

    3.   ALLOWS FOR BATCH PROCESSING

    4.   BRAZE ONLY WHERE ACTIVE METAL IS DEPOSITED

BRAZE ALLOYS

NAME	COMPOSITION	LIQUIDUS (°F)	SOLIDUS (°F)
CUSIL	AG - 72 CU - 28	1436	1436
TICUSIL	TI - 4.5 CU - 26.7 AG - 68.8	1562	1526
50% GOLD 50% COPPER	AU - 50 CU - 50	1778	1751
PALMANSIL 5	AG - 75 PD - 20 MN - 5	1962	1846
NIORO (AMS-4787; BAu-4)	AU - 82 NI - 18	1742	1742
PALNIRO 1 (AMS-4784)	AU - 50 PD - 25 NI - 25	2050	2016
PALNIRO 7 (AMS-4786)	AU - 70 PD - 8 NI - 22	1899	1841

FIBER SELECTION

1. QUARTZ (SiO_2)

2. ALUMINUM OXIDE (Al_2O_3)

3. SILICON CARBIDE (SiC)

CONSIDERATIONS

1. AVAILABILITY (Size/Price)

2. BRAZE WETTING

3. USE TEMPERATURE

4. INTEGRITY OF ASSEMBLY

BRAZE RESULTS

1. ALUMINUM OXIDE

2. QUARTZ

3. SILICON CARBIDE/Ni

4. SILICON CARBIDE/CuSil

5. SILICON CARBIDE/Au-Cu

6. SILICON CARBIDE/PALMANSIL

CURRENT CONFIGURATION

1. SiC/CuSil   to   1200°F

2. SiC/Au-Cu   to   1600°F

PRELIMINARY TEST RESULTS

1. LOW WEAR

2. SAME PERFORMANCE AS METALLICS

3. HIGH FRICTIONAL HEATING

CURRENT WORK

1. HIGHER TEMPERATURE
FIBERS

2. HIGHER TEMPERATURE
BRAZE ALLOYS

3. OTHER ACTIVE METAL
HYDRIDES

4. IMPROVING PROCESS

5. TESTING

FUTURE WORK

1. ROTOR COATING

2. FURTHER TESTING

3. ALL-CERAMIC BRUSH SEAL
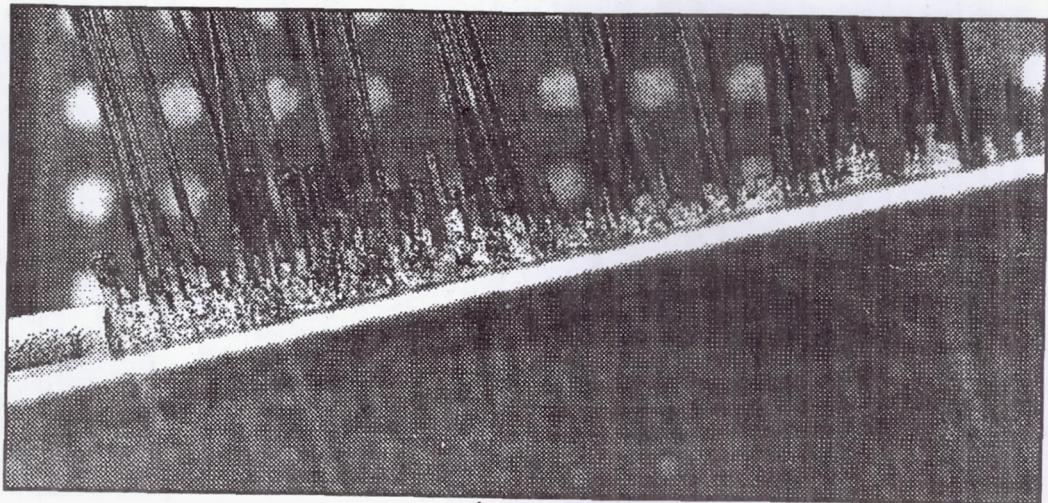
Figure 1
Sic/Palniro 7 Braze Sample
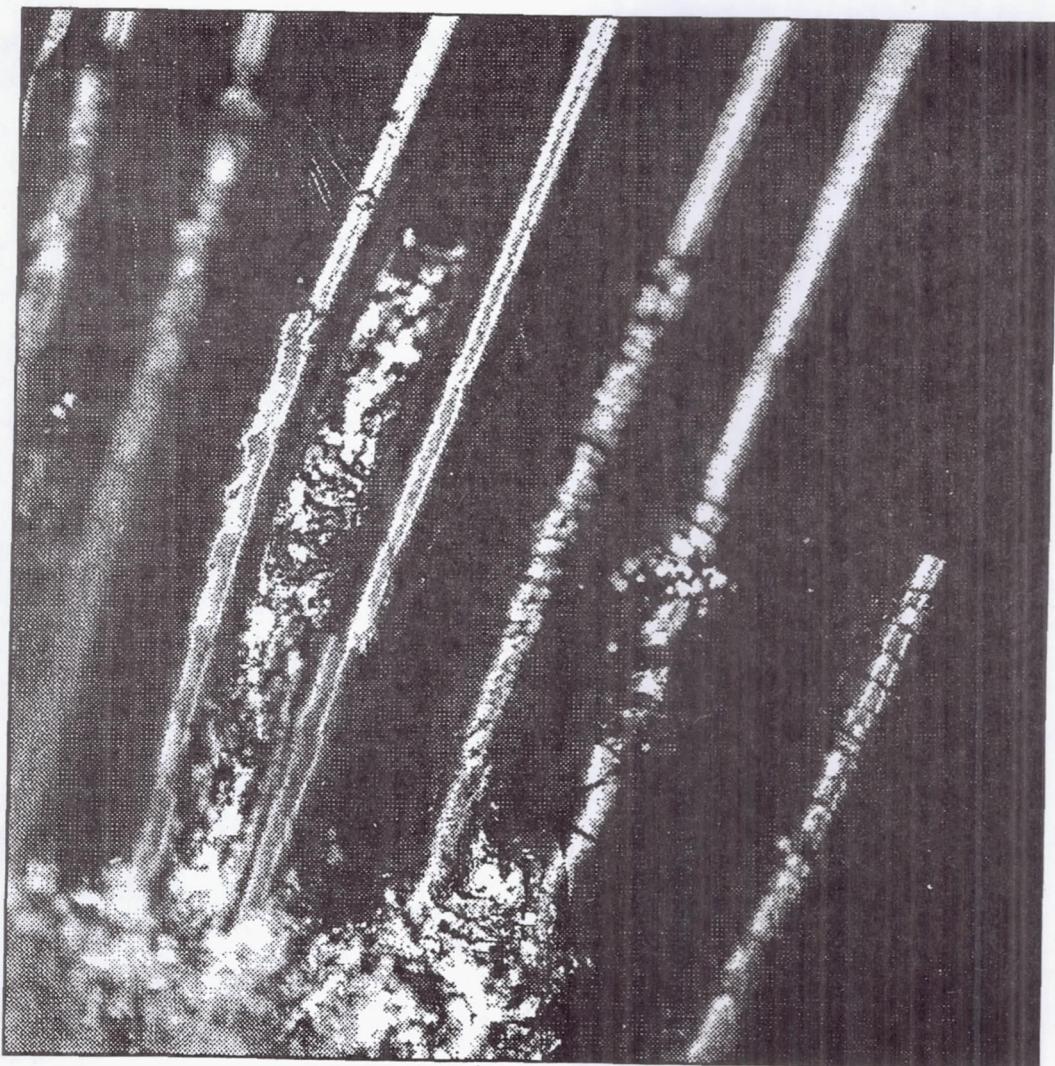
Figure 2
Nickel Attack on SiC Fiber

141
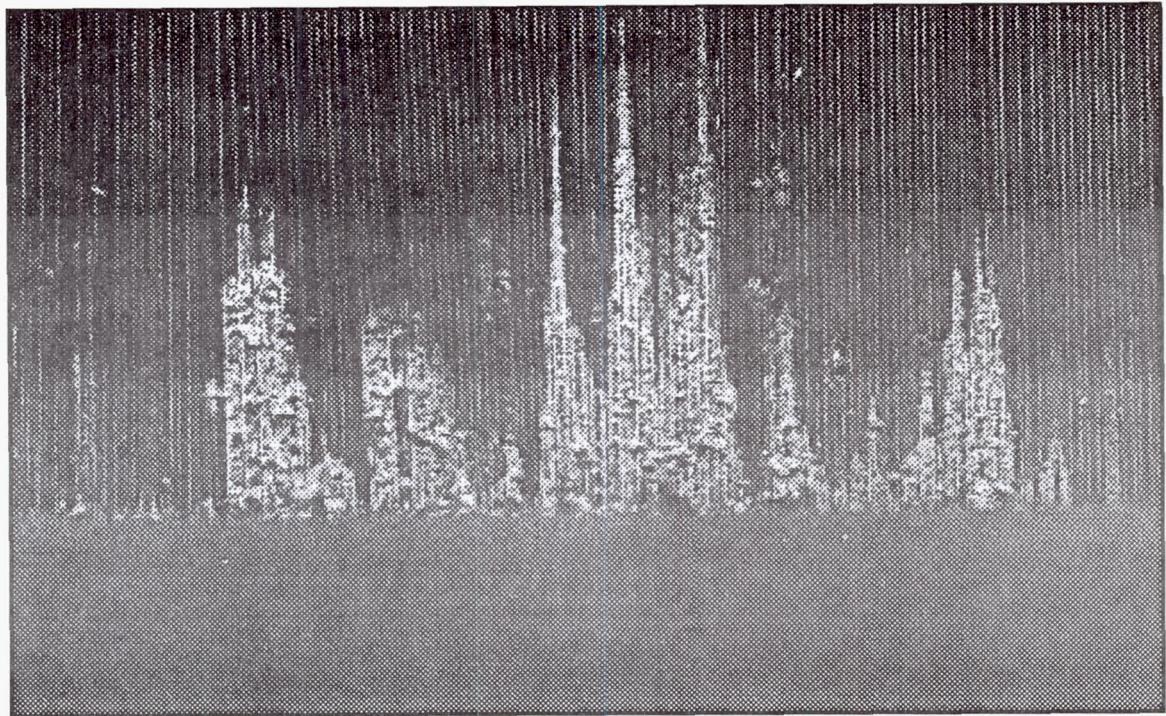
Figure 3
Cusil/Active Metal Wicking
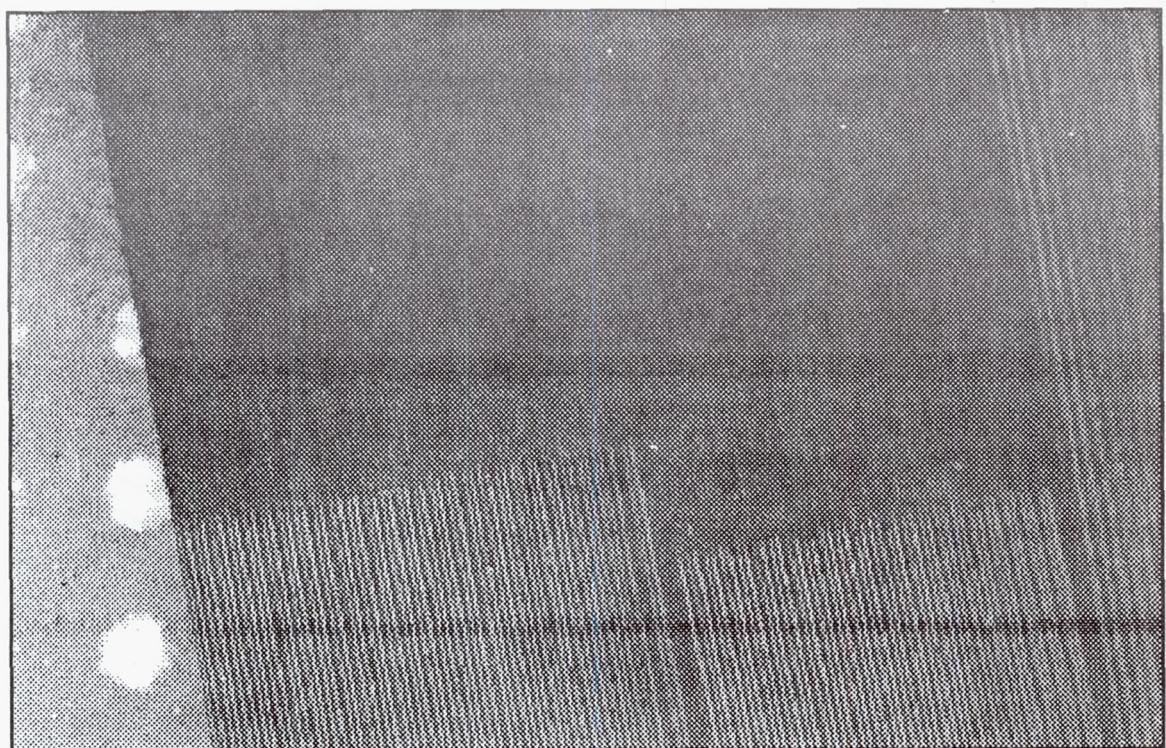
Figure 4
Active Metal Hydride on SiC Fiber
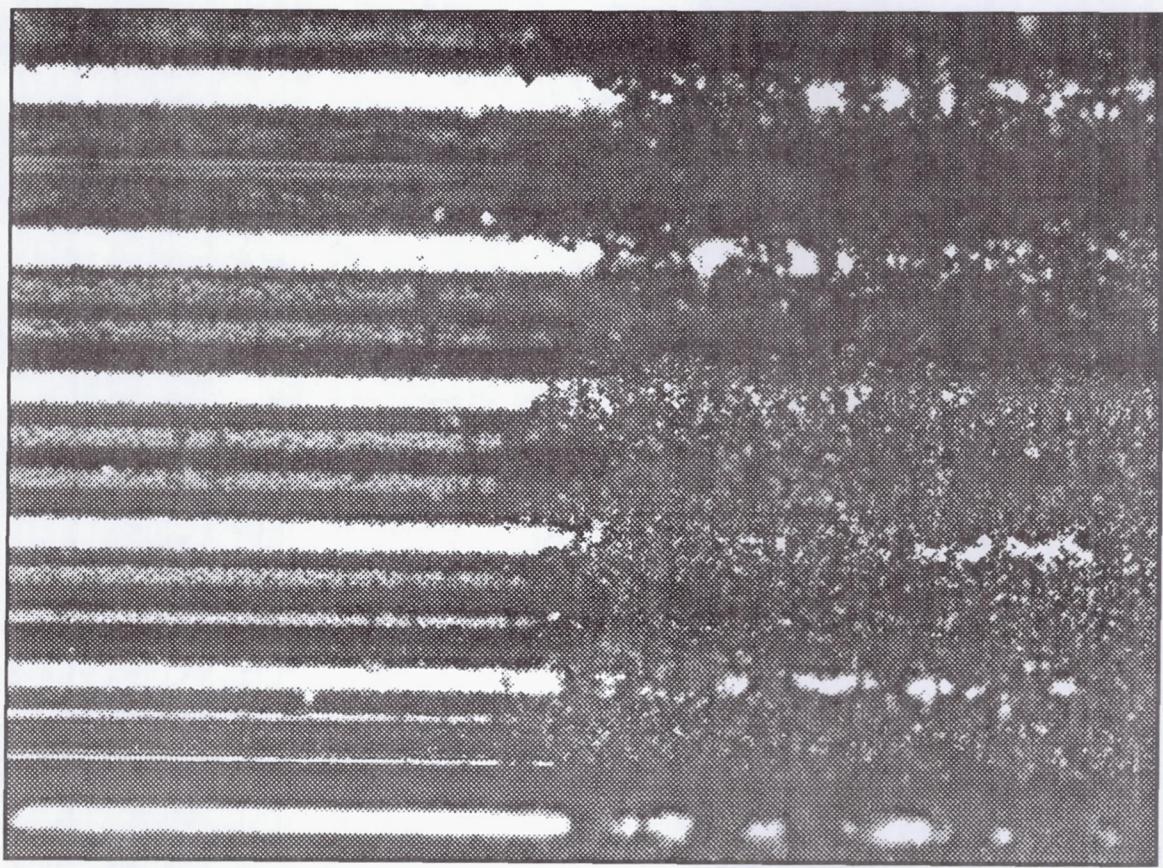
Figure 5
Active Metal Hydide Deposited on SiC Fiber
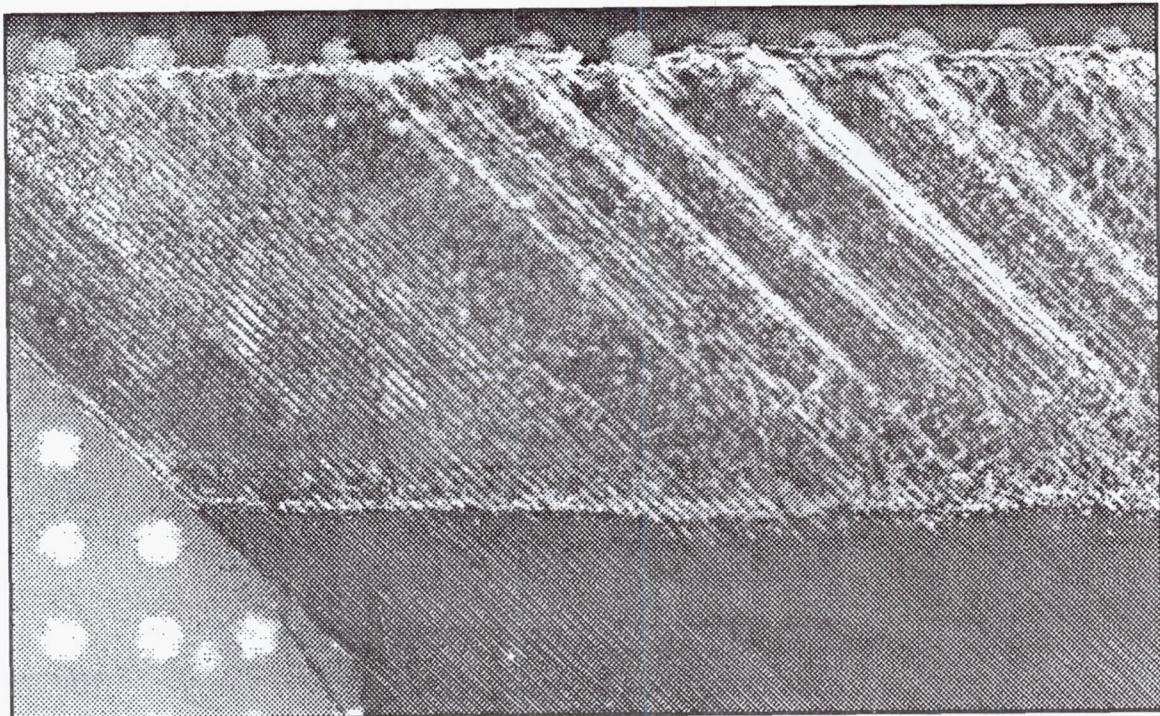
Figure 6
SiC Fiber Braze Sample
Cusil/Active Metal Hydride
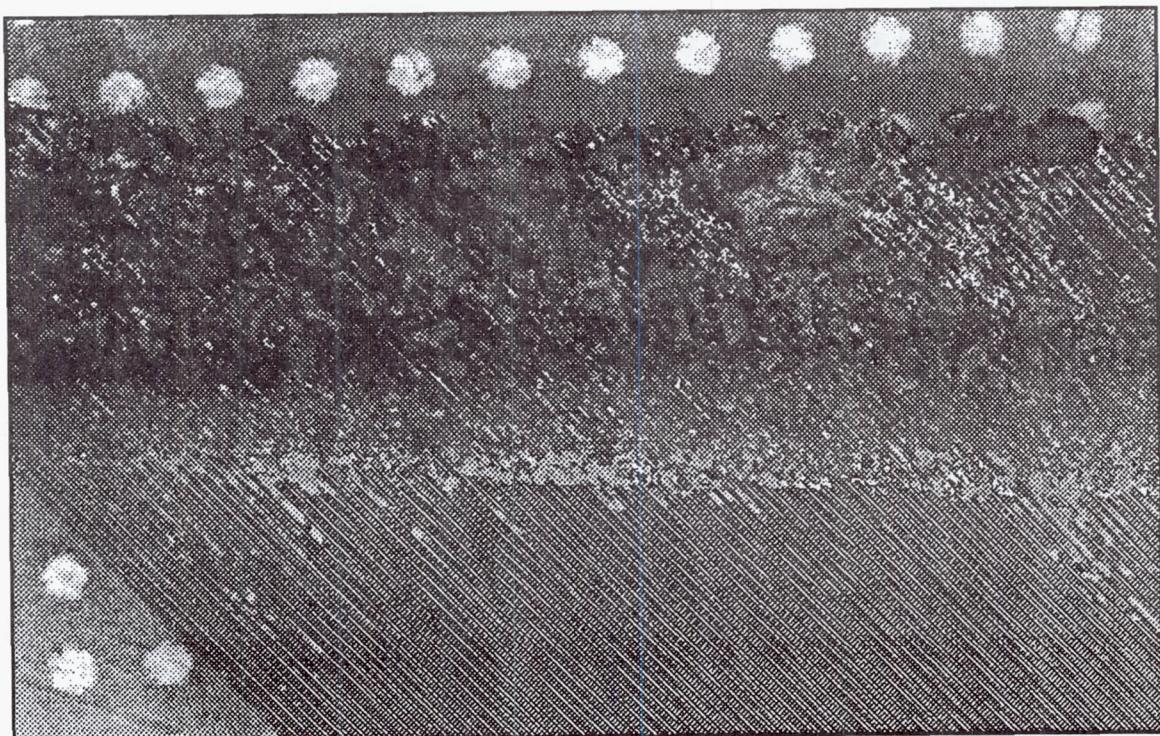
Figure 7
Improper Active Metal Hydride Application Result

144
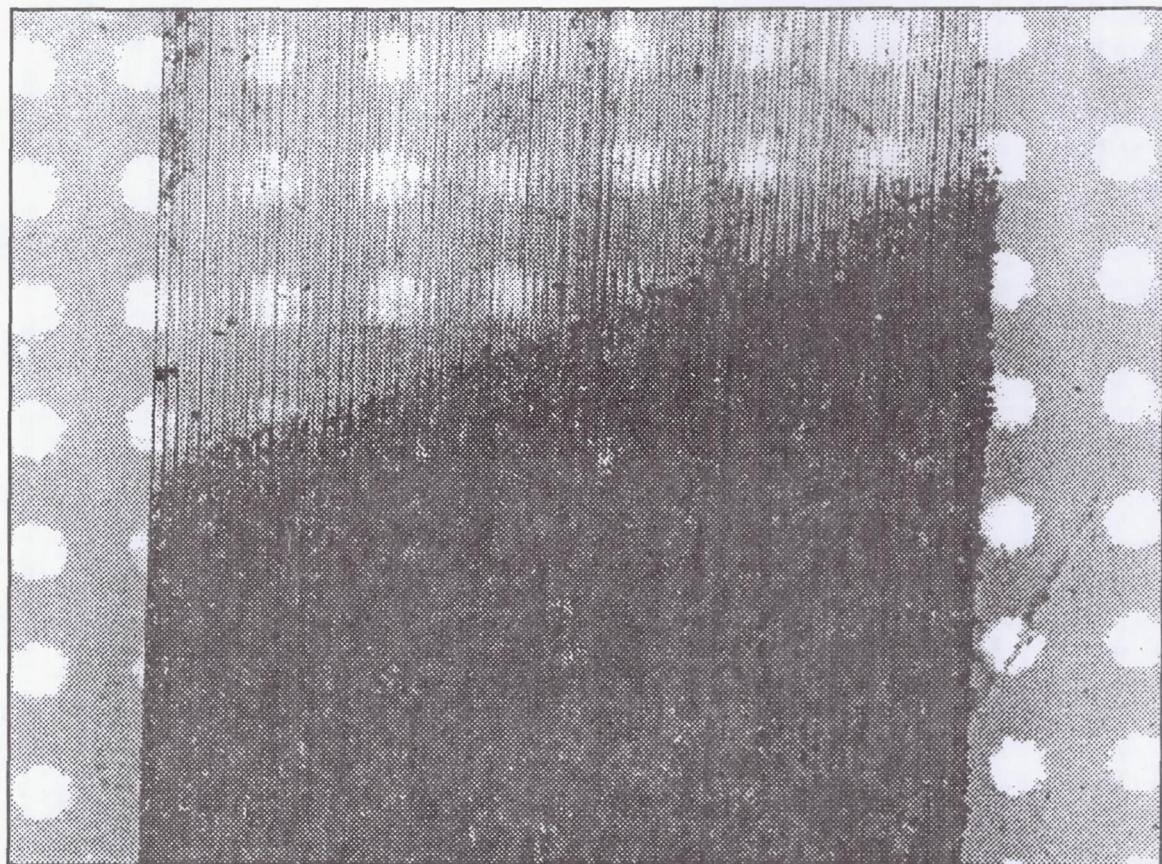
Figure 8
Aluminum Oxide/50% Gold 50% Copper Braze Sample
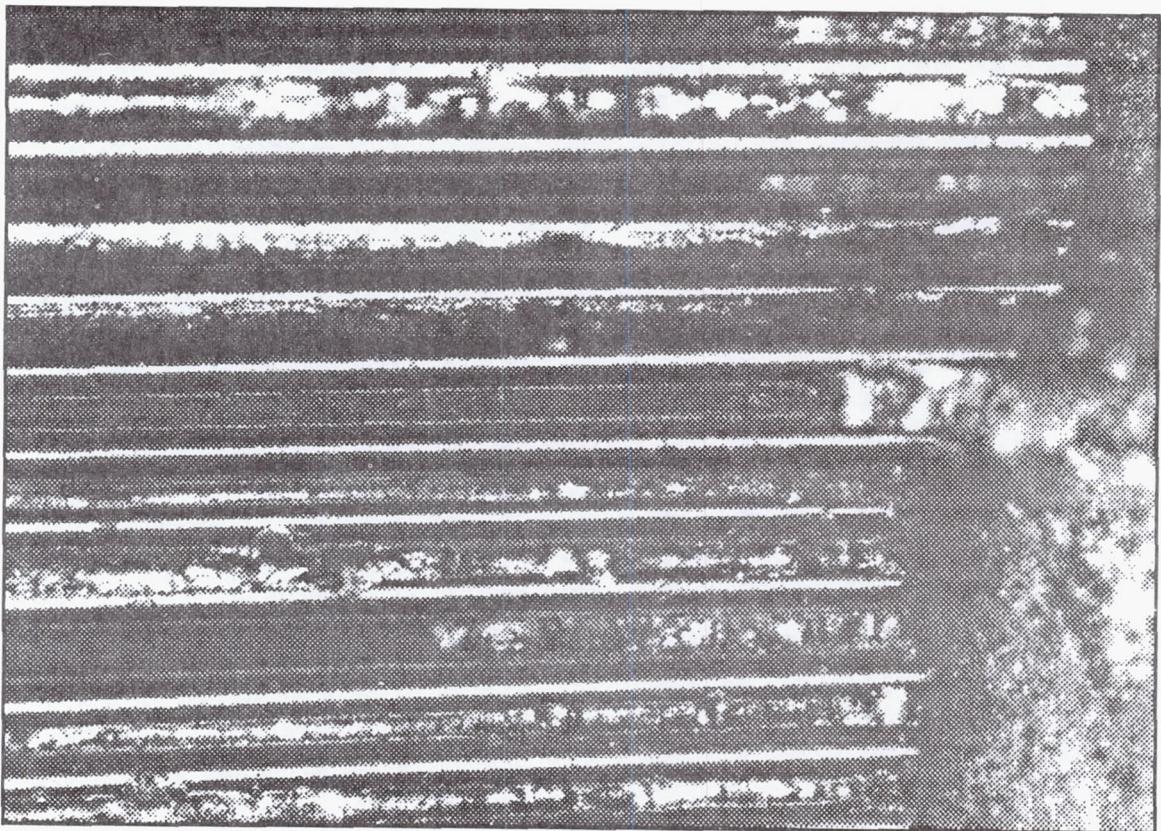
Figure 9
SiC Fiber/Active Metal Hydride
Active Metal Flow

146
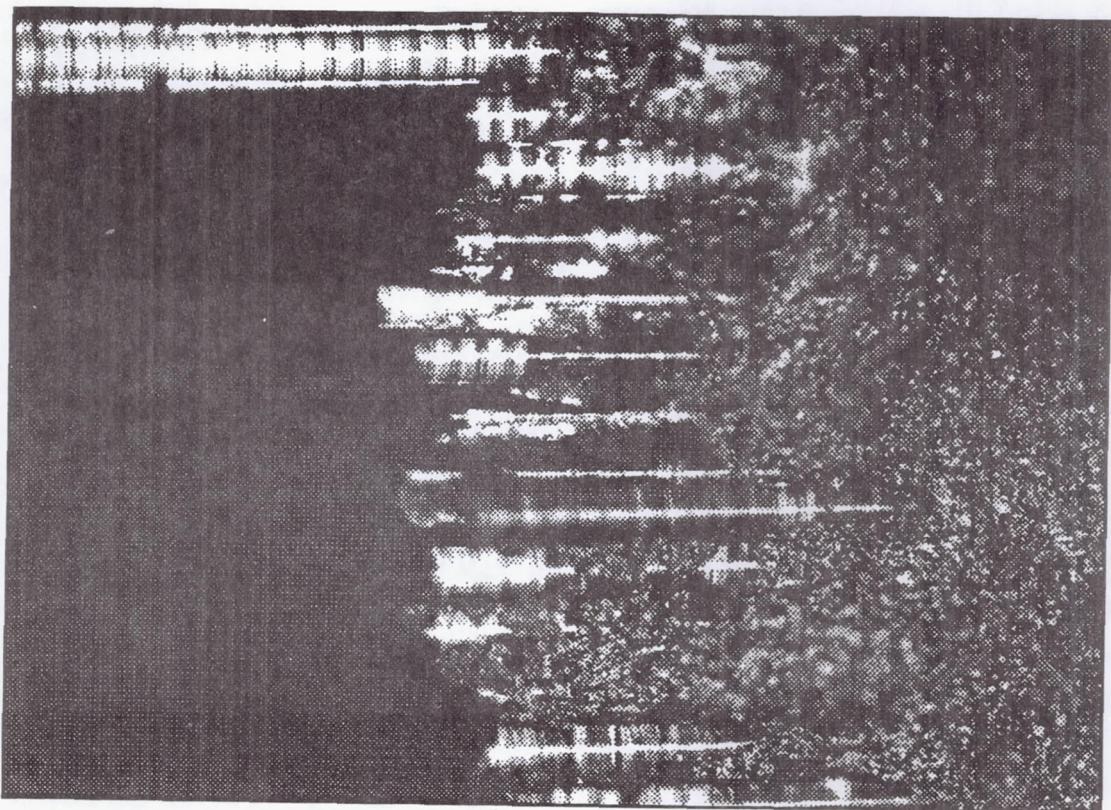
Figure 10
Aluminum Oxide/50% Gold 50% Copper
Dark Field
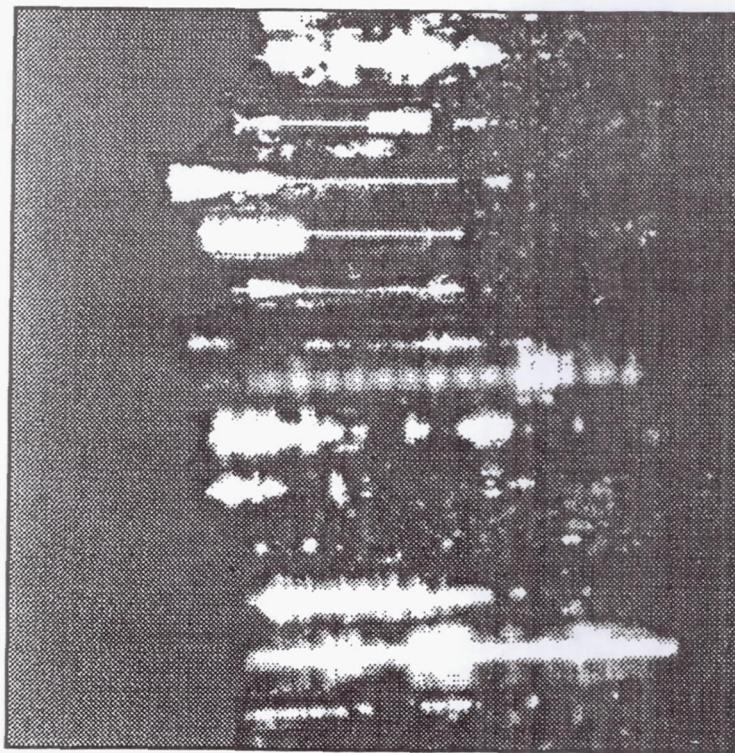
Figure 11
Aluminum Oxide/50% Gold 50% Copper
Light Field
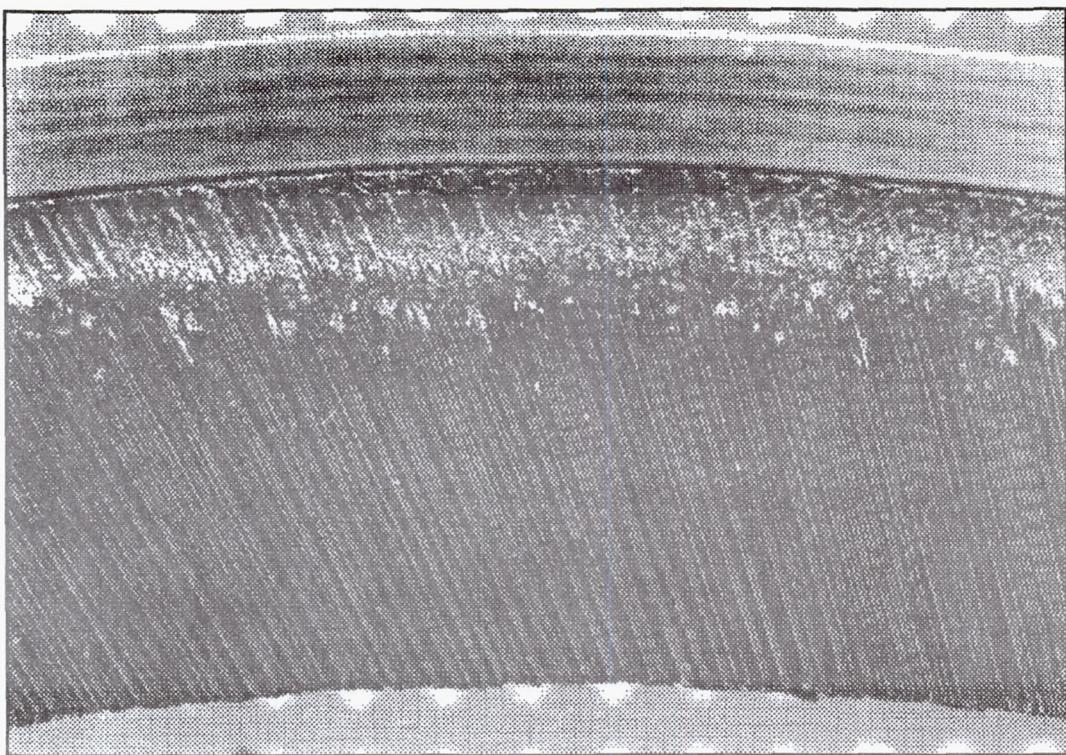
Figure 12
SiC/Cusil/Titanium Hydride - Brush Seal
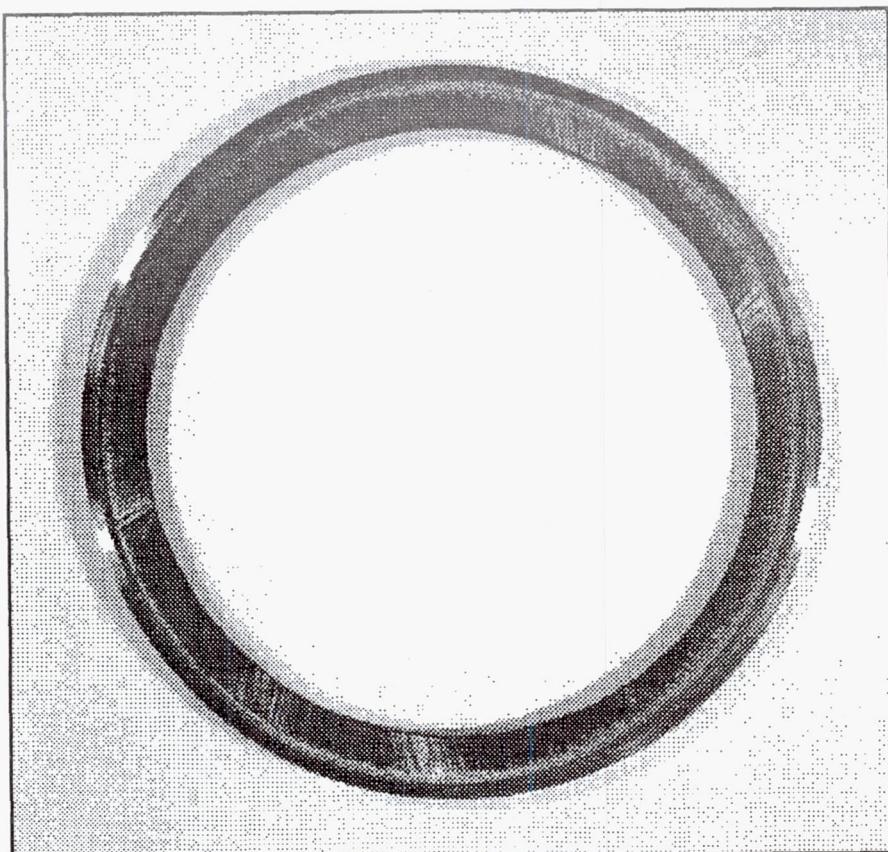
Figure 13
Brazed SiC Fiber/Metal Backing - Brush Seal
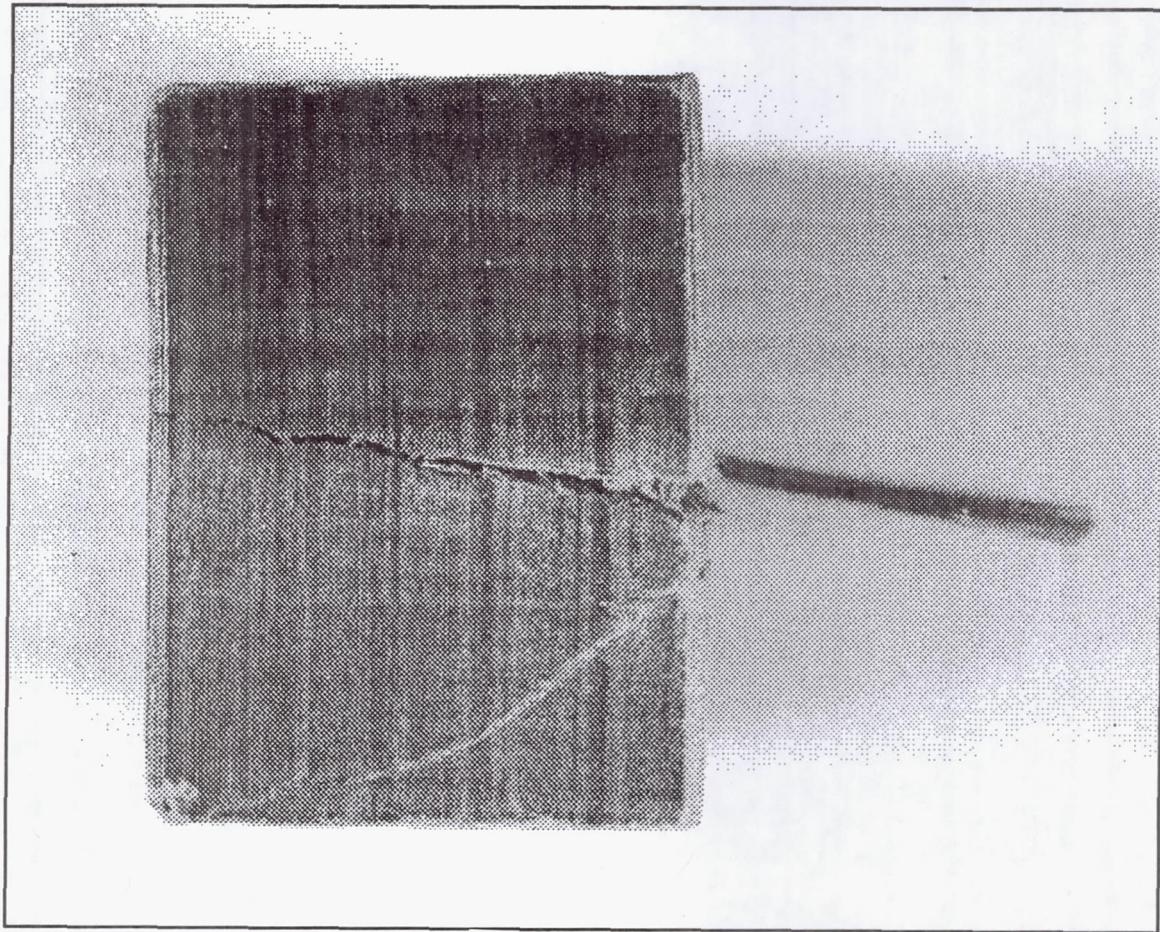
Figure 14
Cracking in Ceramic
Ceramic Powder Pressed Around Fiber

149
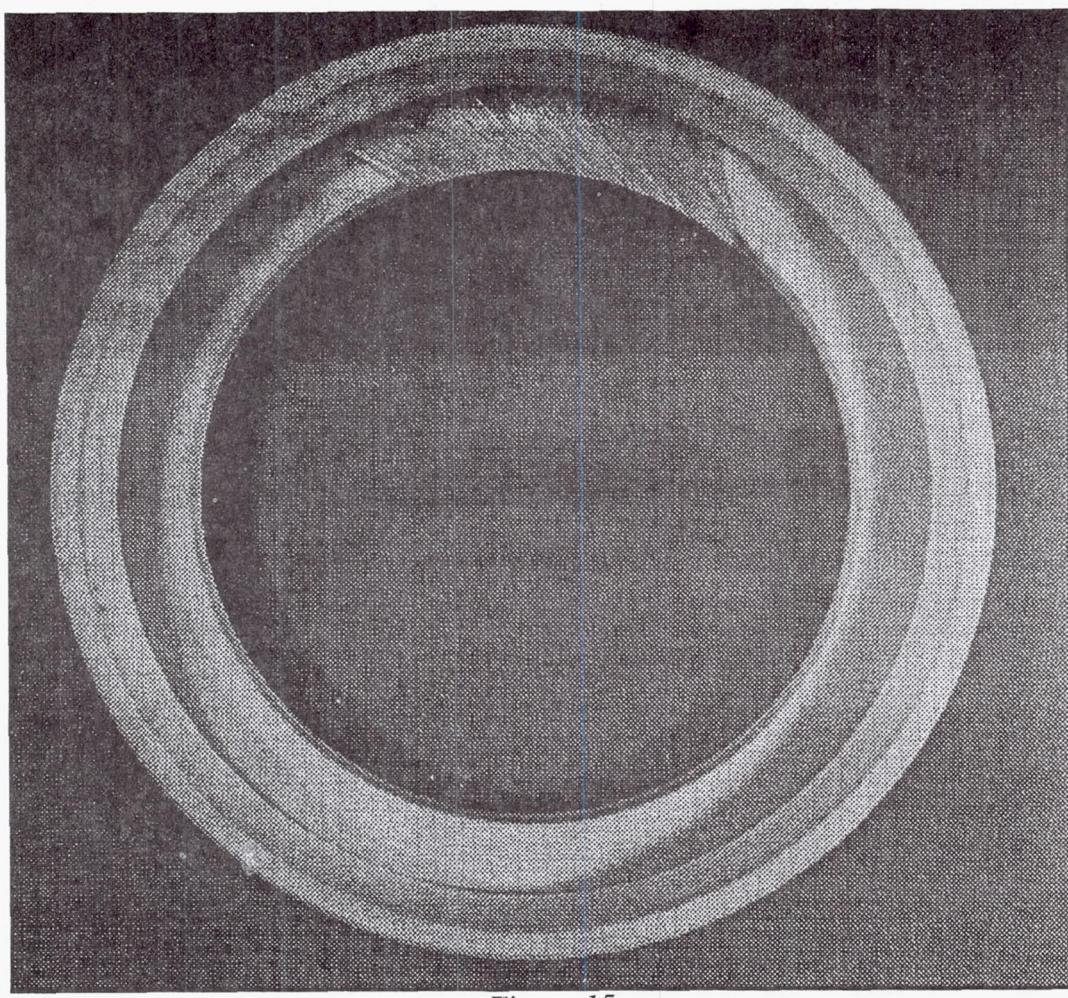
Figure 15
All-Ceramic Brush Seal Concept
Fiber Placed After Firing
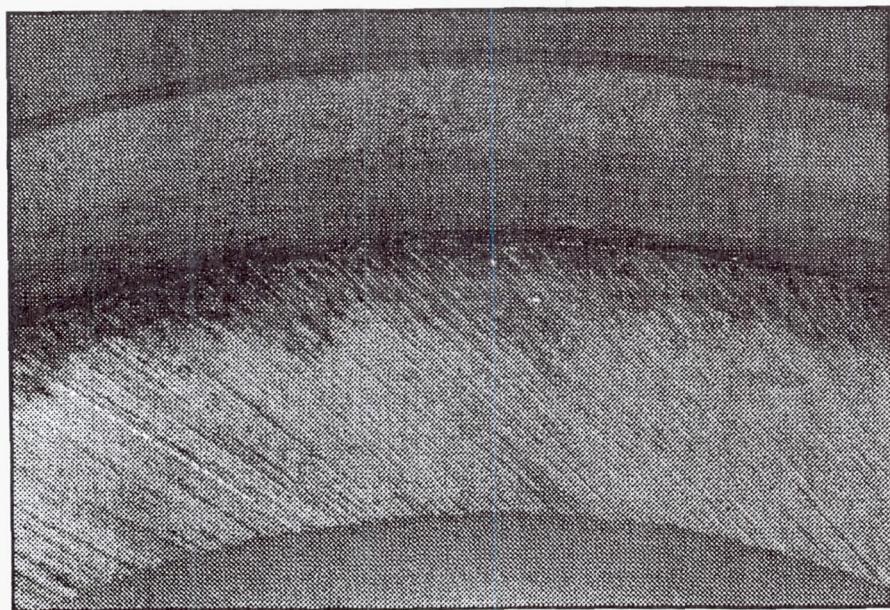
Figure 16
Ceramic Ring with Aluminum Oxide Fiber

BRUSH SEALS FOR TURBINE ENGINE FUEL CONSERVATION

Mike Sousa
General Electric Aircraft Engines
Lynn, Massachusetts

Program Objective

Demonstrate Brush Seals For Replacing
Labyrinth Seals In Turboprop Engines

Program Approach

- Design And Procure Brush Seals With Assistance From Sealol

- Modify And Instrument An Existing T407 Low Pressure Turbine Test Rig

- Replace Inner Balance Piston And Outer Balance Piston Labyrinth Seals With Brush Seals

- Conduct Cyclic Tests To Evaluate Seal Leakage At Operating Pressures And Temperatures

- Evaluate Effect Of Seal Pack Width And Rotor Eccentricity

Project Organization
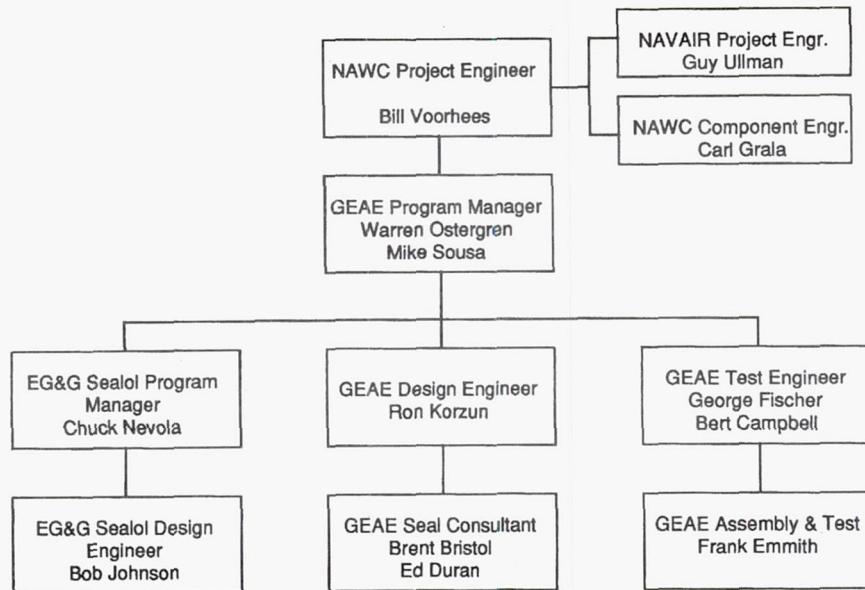
T407 IBP And OBP Brush Seal Dynamic Test Rig
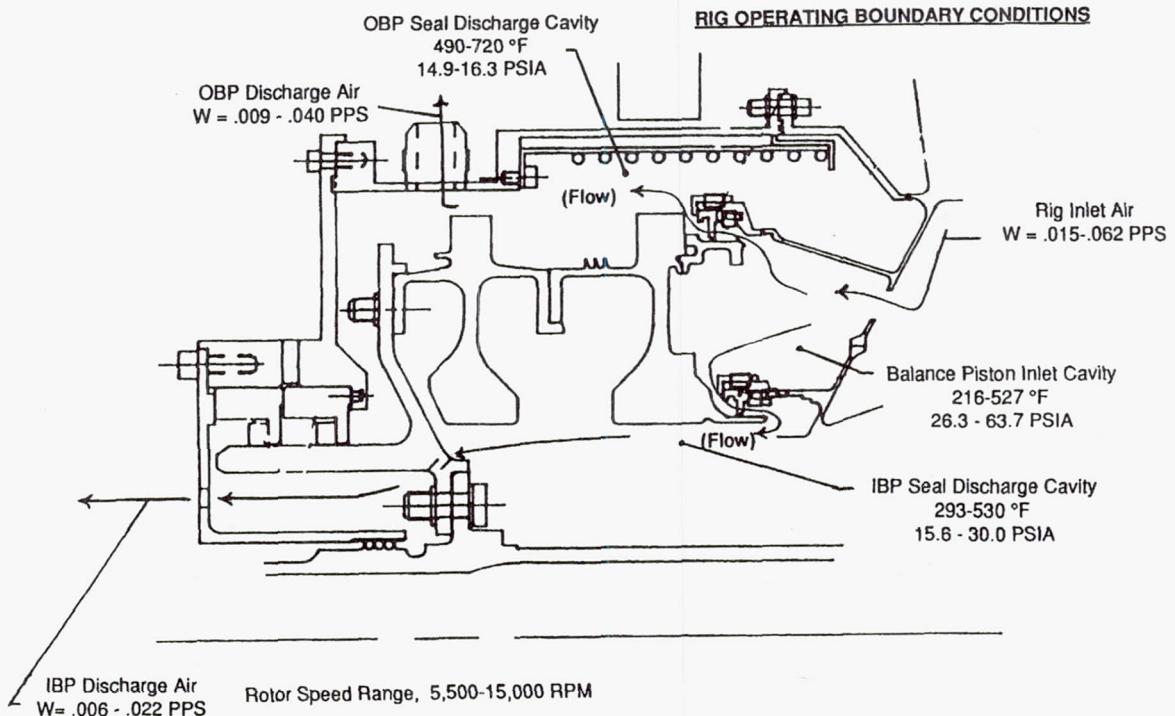
T407 Rig Assembled In Test Platform
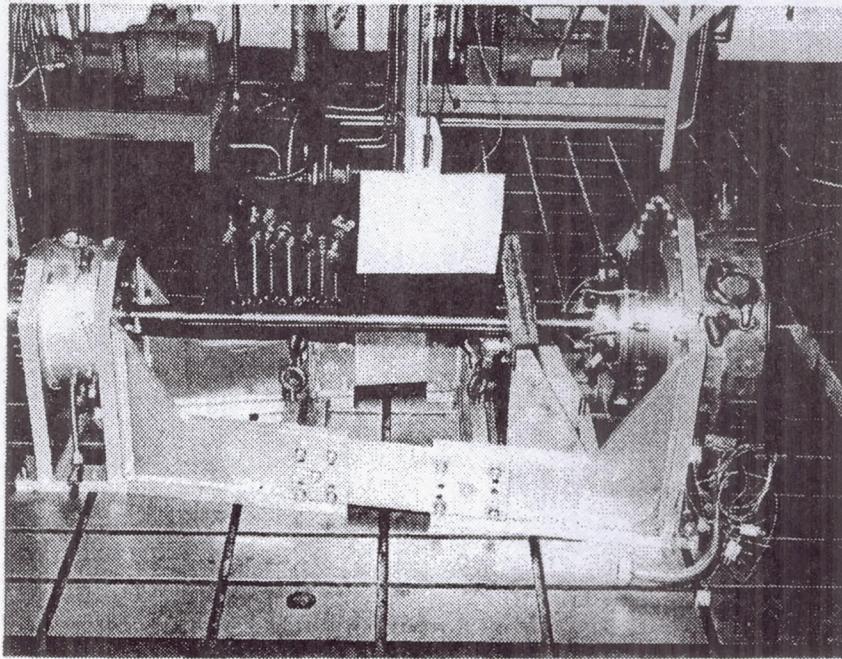
Key Brush Seal/Rig Features

Spacer Arms Used To Position Seals In 2 Locations On Runner

Chromium Carbide Runner Coating Compatible With Haynes 25 Bristles

Axial Retention Sleeves With Locking Pin

INCO 625 Support With HAST-X Brush Seal Backing Plate Gives Best Growth Compatibility To Avoid Errant Rig Leakages
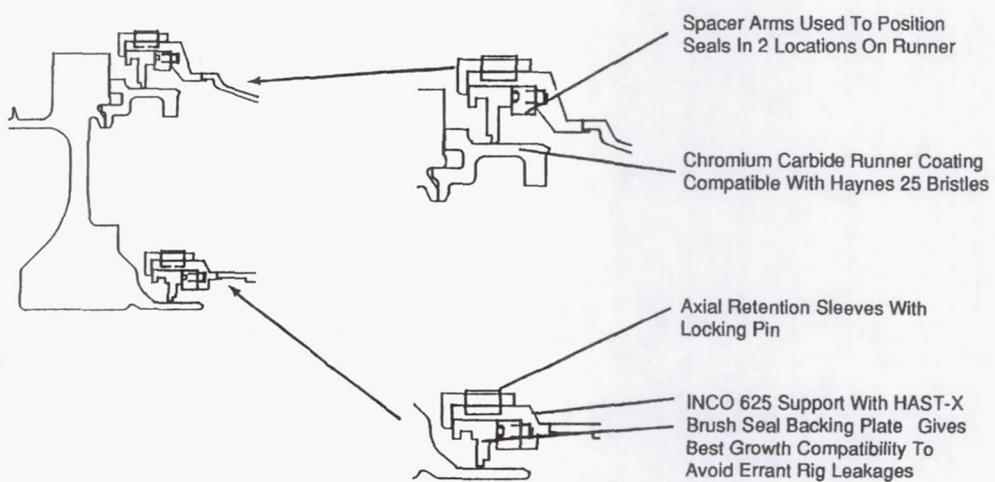
Outer Balance Piston Brush Seal
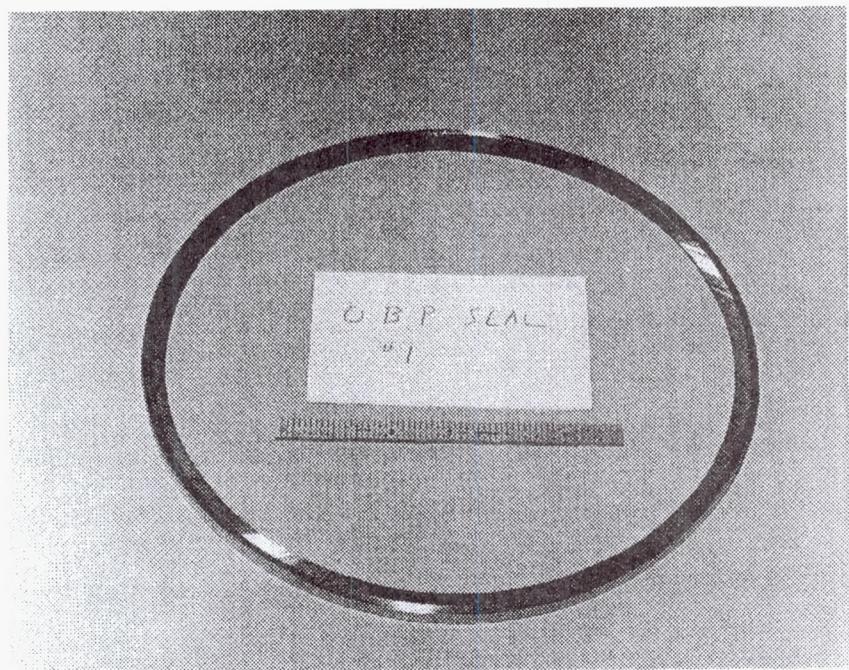
Inner Balance Piston Brush Seal
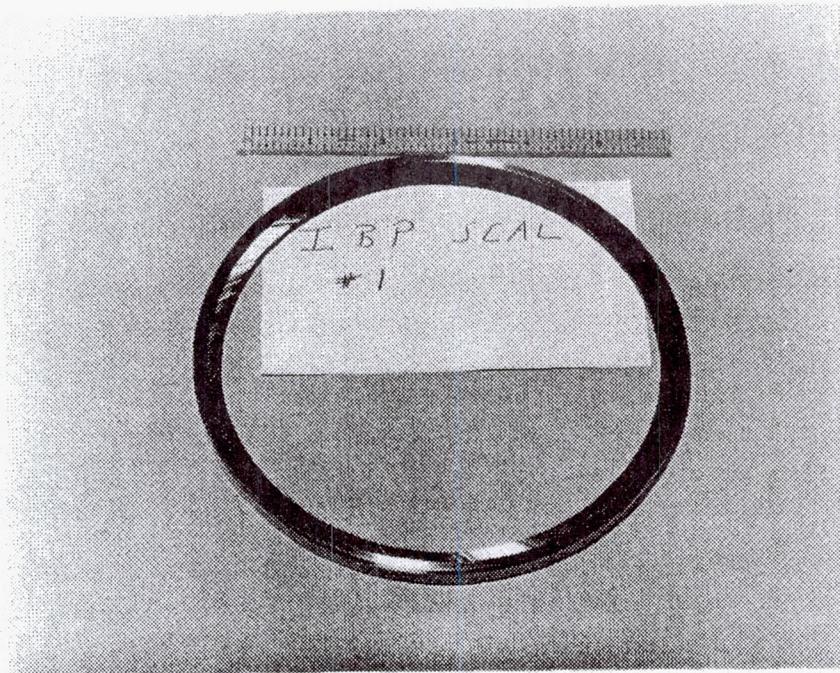
Seal Design and Fit - Ups

Puller Grooves To Facilitate
Removal Of Seals

Anti Rotation Pins

A, B, C, D
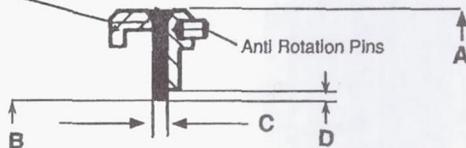
	OBP	IBP
Brush Seal Inner Diameter Cold (B)	10.1"	5.6"
Brush To Runner Diametral Interference - Cold (B)	.006	.008
Brush To Runner Diametral Interference - Hot (B)	.010	.010
Brush Axial Pack Width (C)	.025 (.050)	.050
Backing Plate GAP (D)	.051	.044
Diametral Interference Fit With Stator Support - Cold (A)	.006	.004
*Maximum Stress – Seal Support	18 KSI	25 KSI
*Maximum Stress –Brush Seal	13 KSI	17 KSI

* At SS IRP, Nominal Fit Up

- Brushes Maintain Contact With Rotor At All Operating Conditions
- Backing Plate Distance Sized For 'Worst Case Conditions Expected in Field
- Backing Interference Maintained At All Operating Conditions - Avoid Leakage
- Stress Is Acceptable - Below .2% Yield Strength

Brush Seal Testing

- Build #1 - 75 Hours - (Primarily-Diagnostic Testing)
    - Seal Flows Higher Than Anticipated
    - Tear Down For Review/Inspection

- Build #2 - 175 Hours - 55 Cycles (Still Running)
    - Reduce Rotor Runout
    - OBP
        - Double Pack Width
        - Increase Bristle/Runner Interference
    - IBP
        - Same Seal Endurance

Brush Seal Performance Results

- Mixed Results For IBP And OBP Seals
  - IBP Seal Looks Promising
  - OBP Seal Needs Further Evaluation

- IBP Seal
  - Second Rig Build Demonstrated Better Performance Than Calculated Labyrinth Seal
  - No Apparent Deterioration With Time (>250 Hours And >60 Cycles)

- OBP Seal
  - Second Rig Build Demonstrated Better Max Power Performance Only (Hysteresis Caused Poorer Performance At Part Power)
  - Endurance Testing Appears To Have Increased Seal Flow

IBP Performance Data

T407 IBP/OBP BRUSH SEAL LEAKAGE, RIG BUILD NO. 2

OBP Performance Data

T407 IBP/OBP BRUSH SEAL LEAKAGE, RIG BUILD NO. 2

'OBP' FLOW PARAMETER VS PRESSURE PARAMETER
- -□- INITIAL PERFORMANCE EVAL.   -✕- 1ST BUILD DATA
- -◇- 45TH CYCLE OF ENDURANCE   -○- CALC. LABYRINTH SEAL

Y-axis: FLOW PARAMETER W×(T)·0.5/(P×D)
X-axis: PRESSURE PARAMETER (1-(Pd/Pu)·2)·0.5
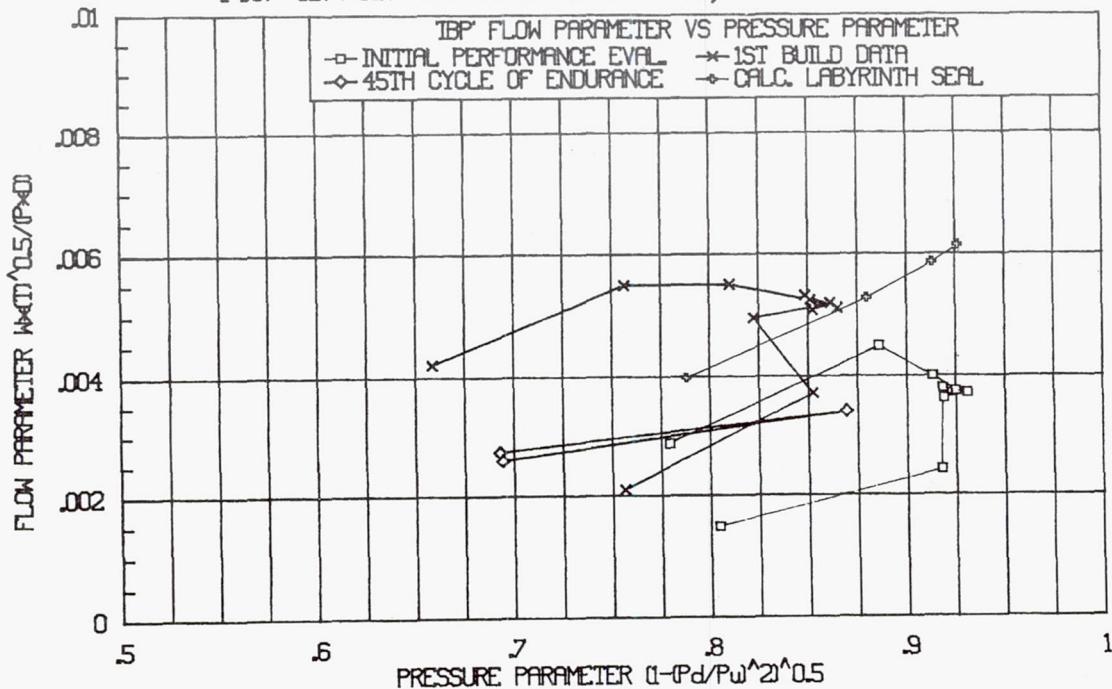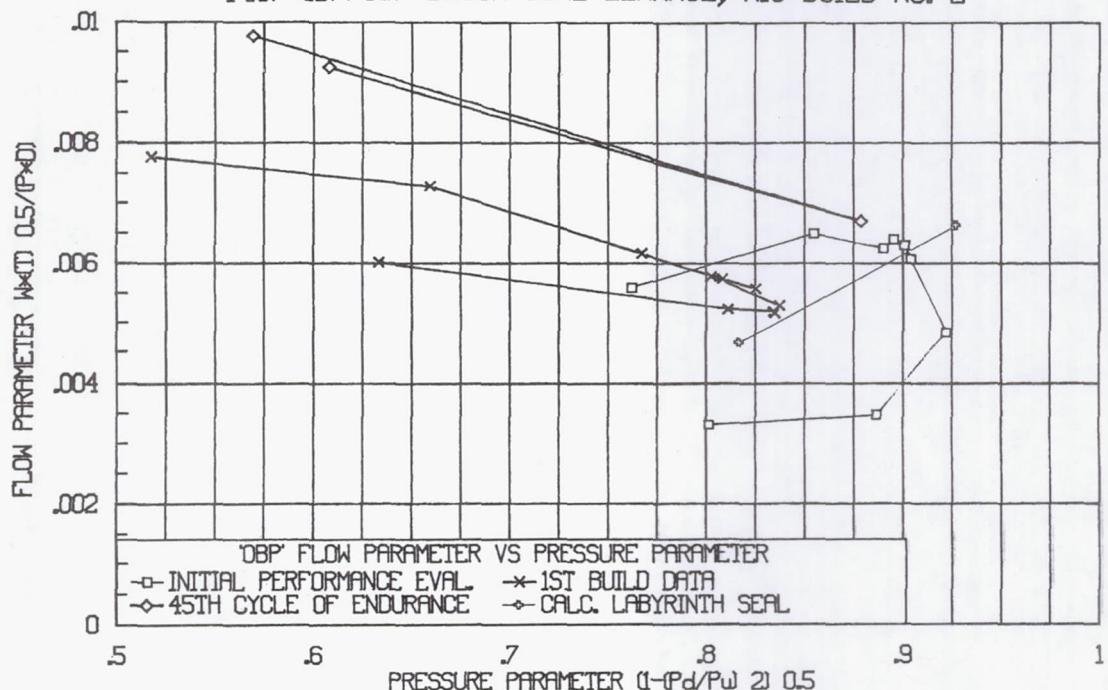
Conclusions

- Seal Designs Currently On Test Were State Of The Art ~2 Years Ago - Seal Designs Have Evolved Since Then - As Demonstrated On Sealol Testing

- Incorporation Of Brush Seals Requires Attention To Design Details
  - Critical Parameters Include Rotor Runout

- Brush Seals Offer Performance Advantages Over Labyrinth Seals And Need To Be Pursued Further

157

BRUSH SEAL NUMERICAL SIMULATION: CONCEPTS AND ADVANCES

M.J. Braun and V.V. Kudriavtsev
Department of Mechanical Engineering
University of Akron
Akron, Ohio

The development of the brush seal is considered to be most promising amongst the advanced type seals that are presently in use in the high speed turbomachinery. The brush is usually mounted on the stationary portions of the engine and has direct contact with the rotating element, in the process of limiting the "unwanted" leakage flows between stages, or various engine cavities. This type of sealing technology is providing high(in comparison with conventional seals) pressure drops due mainly to the high packing density(around 100 bristles/1 mm^2), and brush compliance with the rotor motions. In the design of modern aerospace turbomachinery leakage flows between the stages must be minimal, thus contributing to the higher efficiency of the engine. Use of the brush seal instead of the labyrinth seal reduces the leakage flow by one order of magnitude[1,2]. Brush seals also have been found to enhance dynamic performance, cost less and are lighter than labyrinth seals. Even though industrial brush seals have been successfully developed through extensive experimentation[1,2], there is no comprehensive numerical methodology for the design or prediction of their performance[3,4,5]. The existing analytical/numerical approaches are based on bulk flow models[6,7] and do not allow the investigation of the effects of brush morphology(bristle arrangement), or brushes arrangement(number of brushes, spacing between them), on the pressure drops and flow leakage. An increase in the brush seal efficiency is clearly a complex problem that is closely related to the brush geometry and arrangement, and can be solved most likely only by means of a numerically distributed model.

STATE-OF-THE-ART

★ The reduced leakage, and physical compliance of the brush body to external perturbing factors are features that stand out in turbomachinery applications where there are expected boundary variations due to mass flow, brush fibers' compliance pressure, temperature, and time dependent eccentric shaft motion. All these characteristics have made the brush configuration an especially interesting and worthy candidate.

★ Rolls-Royce(RR), in 1980's, has successfully introduced a brush seal manufactured by Cross Mfg. Ltd.(CML) on a demonstrator engine, and then tested it for several thousand hours, Fergusson[1]. More recently EG&G Sealol, Technetics, Detroit-Allison and others have enabled full programs of study of this type of seal.

★ Conclusions of a recent workshop on code development(1992) indicate that while the brush seals works well, there is a need to improve its performance characteristics. Such a goal can be achieved by using cascades of brushes, nonhomogeneous brush morphology, "non-conventional" brush structure design, and in general, a process of optimization of brush design parameters.

★ The concept employed by the lumped bulk flow numerical models can not predict local brush compliance, associated local flow phenomena and the pressure drops and the transient effects associated with them. The importance of the local flow phenomena in the sealing process is paramount to the global performance of the brush.

CURRENT RESEARCH ACTIVITIES :

• DEVELOPMENT AND VALIDATION OF A NUMERICAL
  ALGORITHM AND COMPUTER CODE THAT UTILIZES
  MATHEMATICAL MODEL WITH DISTRIBUTED PRIMARY
  PARAMETERS(NAVIER-STOKES EQUATIONS),
  UNDER NASA GRANT , NASA LEWIS RESEARCH
  CENTER.

Computer Code Allows: Estimation of the pressure drops (flow
rates) for the typical brush seal segments of different shapes:
i.e. brustles diameters, configurations, packing densities.

APPROACHES:

-Large size characteristic segment: 7-10 rows with 10 pins in one
row in the   transversal   direction

-Brush Partitioning: inflow segment(first 3 rows), central part,
outflow segment(last rows)

• DEVELOPMENT OF THE COMPUTER PROGRAM THAT
  ADRESSES BRISTLES MOTION AND ITS INFLUENCE ON
  THE PRESSURE DROPS AND FLOW RATES.

• FURTHER MODIFICATION OF THE EXPERIMENTAL
  FACILITY FOR THE PURPOSES OF CODE VALIDATION.
  DIFFERENT SHAPES OF THE BRUSH SECTION

OBJECTIVES AND ACCOMPLISHMENTS:

• Develop verified family of CFD codes for Analyzing Brush Seals

    -idealized(uncompliant) 2D configuration   \/
             regular gridding   \/
             variable grid size   \/

    -compliant 2D geometry   under development

• Experimental Facilities for the Adequate Code Verification

    -stationary bristles(cylinders)   \/

    -moving bristles   under development

• Qualitative and quantitative analyses of the Fluid Flow in
  the Brush Seal Configuration

    -flow around one bristle,   level 1   \/
    -flow around several bristles,   level 2   \/
    -flow in deep tube bundles, level 3   \/
     (intermediate pitch-to-diameter ratio)
     7 rows of pins with 11 cyl. in a row

- -

    -flow through uncompliant brush prototypes
    (small pitch-to-diameter ratio), level 4   \/

    -flow through the characteristic brush
    segments, brush partitioning technique   \/
    level 5

PROBLEM DEFINITION

Conclusions of a recent NASA Seal Workshop[5] indicate that while the brush seals work well, there is a need to further improve the performance characteristics. Such a goal can be achieved by using cascades of brushes, nonhomogeneous brush morphology, "non-conventional" brush structure design, and in general, a process of optimization of brush design parameters[18]. The distributed velocity fields(u,v) and the associated pressure maps are of vital importance for the prediction of the average pressure drop, or the possible sudden failure of the brush seal under unexpected local "pressure hikes". The momentum carried by these velocities(or the upstream pressure) can force the brush deformation, and can create favorable conditions for the brush 'opening', followed by seal failure[4,15]. It is in this context that the development and validation of a numerical model with distributed primary parameters(u,v,p) becomes important.

The design goals of the model are to determine the pressure drop for a configuration specified by the designer, i.e. the density of the brush packaging, length, number of rows, bristles sizes(homogeneous or nonhomogeneous), distances between the rows, or brushes respectively(single, double or cascade brush). The systemic goals are a) to develop physically relevant packages of assumptions for the simulation of the brush seal and to implement a robust numerical method(using primitive variables u,v,p) for the calculation of the forced convective flow through dense brush-like cylinder arrays, and b) to analyze numerically different aspects of the flow dynamics in the generic brush prototypes. Achieving the goals set forth in a) and b), will allow usage of predictive design codes with a high level of reliability.

For analysis and classification purposes we identified four different models of the generic brush geometry[19]. The simplest

model(Level 1) assumes flow analysis in the vicinity of a non-moving single brush bristle[20]. The second level(Level 2) model introduces the analysis of a limited cluster that consists of several non-moving bristles[19,20], that do influence jointly the flow field through disturbances generated by the wake vortices. The next level(Level 3) introduces the analysis for a multi-cluster[21], and finally we assemble large numbers of clusters with small pitch to diameter ratio(PTDR) that actually simulate the real brush(Level 4, [22]). Each one of these levels is designed to introduce one additional level of difficulty, help learn more about the physics of the flow, and increase the level of confidence in the final numerical model.

One can see an idealized schematic of a linear brush seal in Fig. 1. In real conditions the flow upstream of the seal exhibits both circumferential and axial components. Reynolds numbers that are typical for the circumferential component are usually in the range 10^4- 10^6, while the Reynolds number of the transversal component component (leakage flow) does not exceed low laminar values that are defined by the design requirements of the seal(an ideal case leakage is equal to zero). A review of the data published by Chupp et al[6], Nelson and Chupp [10], Dowler[11] allowed us to determine the typical ranges of the parameters that are usual for the brush seals tested by the industry. The level of the leakage flow and maximum velocity in the pitch between the bristles were estimated as 3.17 m/s and 76.55m/s respectively. In Fig. 2 one can find an approximate range of Reynolds numbers typical for a brush seal functioning in air. As we can see from this qualitative figure an assumption of laminar and incompressible fluid can be well justified since the Reynolds numbers are not in the turbulent range and the Mach number is M<0.4. The authors have established through their experimental work[4,15] that the major factor contributing to the pressure drop is the longitudinal flow in the X direction in the XOY plane(Fig. 1). Thus, in order to simplify the model we assumed a two dimensional flow, and neglected both curvature effects and flow in the Z direction.
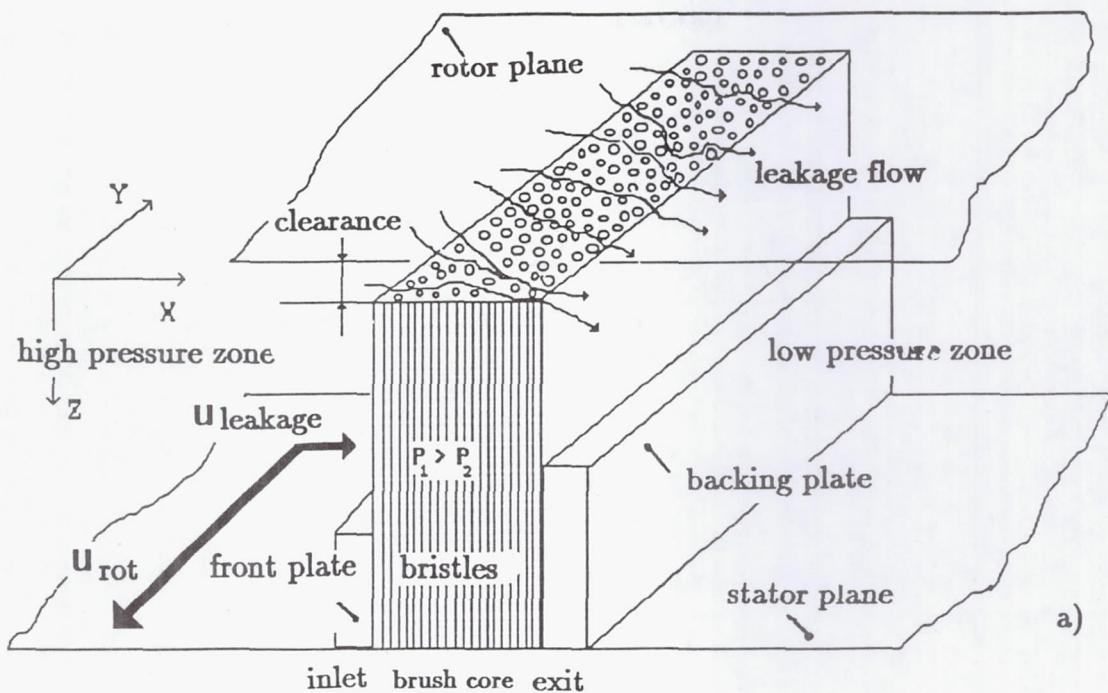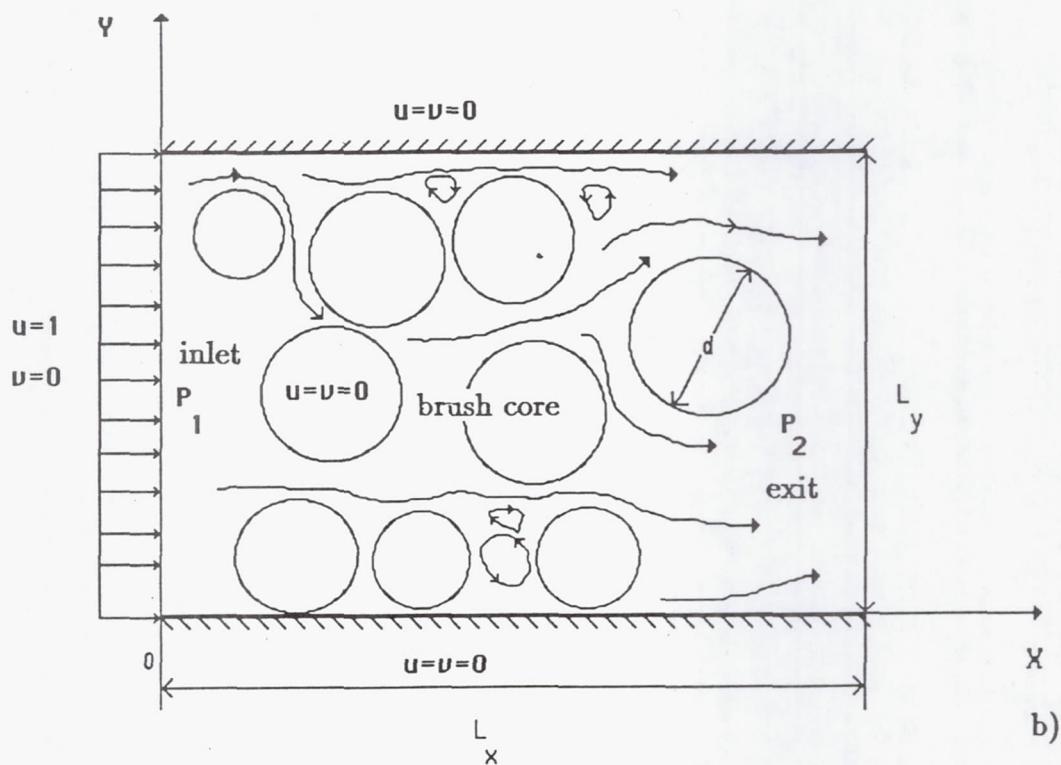
Figure 1(a,b)   Idealized Schematic of the Brush Seal and Flowpath

a) generic seal

b) problem definition

165
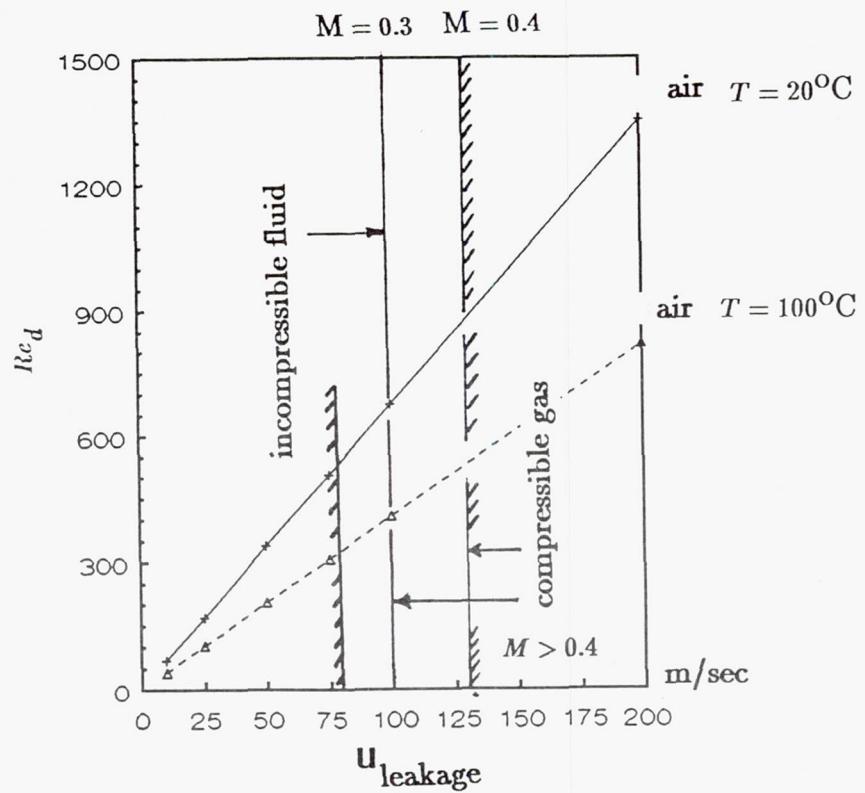
Figure 2. Qualitative Diagram of the Flow Leakage vs Reynolds Number

MATHEMATICAL MODEL

● Characteristic Geometry

The computational domain (with L_x as length and L_y as width) is represented by the horizontal brush cross section restricted by two walls as shown in Fig. 1b. Inside the domain, solid bodies(bristles) of round cross-section are located, thus, creating a structure of (n) rows with (m) elements in each row. The bristle diameter is used as a characteristic length scale(L_0) and the velocity at the entrance, as a characteristic velocity(U_0).

● Governing equations.

It is assumed that the flow is viscous and laminar and it is caused by the pressure difference across the generic brush. The initial velocity distribution $u(x,y)$ and the characteristic pressure at the entrance are assumed known. The influence of the body forces is excluded from the problem definition. We also neglect the influence of heat transfer on the flow structure(isothermal flow). The two-dimensional Navier-Stokes equations for unsteady incompressible viscous flow, can be written in dimensionless conservative form (Cartesian), as

$$\frac{\partial u}{\partial t} + \frac{\partial(uu)}{\partial x} + \frac{\partial(uv)}{\partial y} = -\frac{\partial P}{\partial X} + \frac{1}{Re}\left(\frac{\partial^2 u}{\partial x^2} + \frac{\partial^2 u}{\partial y^2}\right) \tag{1}$$

$$\frac{\partial v}{\partial t} + \frac{\partial(vv)}{\partial y} + \frac{\partial(uv)}{\partial x} = -\frac{\partial P}{\partial Y} + \frac{1}{Re}\left(\frac{\partial^2 v}{\partial x^2} + \frac{\partial^2 v}{\partial y^2}\right) \tag{2}$$

$$\nabla^2 P = -\frac{\partial^2(u^2)}{\partial x^2} - 2\frac{\partial^2(uv)}{\partial X \partial y} - \frac{\partial^2(v^2)}{\partial y^2} + \left\{-\frac{\partial \mathcal{D}}{\partial t} + \right.$$

$$\left. + \frac{1}{Re}\left(\frac{\partial^2 \mathcal{D}}{\partial x^2} + \frac{\partial^2 \mathcal{D}}{\partial y^2}\right)\right\} \tag{3}$$

$$\mathcal{D} = \frac{\partial u}{\partial x} + \frac{\partial v}{\partial y} \tag{4}$$

During calculations, $\mathfrak{D}$(the dilation term) represents the residual that has to shrink to zero if continuity is to be satisfied[23,24]. Previous numerical work of these authors[19,20,21] explored models of Levels 1, 2, and 3 in order to obtain qualitative information about fluid flow in the generic brush configurations.

The new technique that involves brush partitioning proposes the division of the brush in three typical areas(Fig.1): (i)inflow area with the free flow and first several rows of pins with developing flow profile, (ii) a central core that consists of several rows of bristles with symmetric fully-developed flow distribution, and (iii) an outflow zone that includes the last rows of bristles and the area behind the brush where vortices generation is taking place.

Hendricks[25] showed that the <u>first three</u> and <u>last three rows of bristles</u> are usually deflected outward of the main brush core during the experiments. These bristles are located at a considerable distance from each other and thus do not significantly contribute to the overall pressure drop. Since the central core has the highest level of packing density and flow resistance, as a first step we will concentrate our analysis on this region. In general, the total pressure drop in cylinder arrays can be expressed as following:

$$\Delta P = C_z \sum \Delta P_{av} \quad , \quad i=1., \ldots, N_{rows} \tag{5}$$

According to Zukauskas et al.[18], $C_z = 1$, if the number of rows is greater than three. One can conclude that in terms of the pressure field the flow is fully developed as it passed the first three rows.

Assumption of a fully developed flow distribution in the central brush core reduces the size of the computational domain to a characteristic cell of several sequential rows(characterized by a constant ΔP_{av}), if indeed, one supplies proper symmetric conservative boundary conditions.

BOUNDARY CONDITIONS

• Brush Entrance Region

We assume an entrance velocity profile with $u = f(y,t)$ and $v = f(y,t)$, which in most cases can be reduced to $u(x=0)=1$ and $v(x=0)=0$. In the case of lateral solid walls boundary conditions are specified as non-porous and non-slip, i.e. $u=v=0$. In the case of flow symmetry, boundary conditions at the "top" and "bottom" boundaries are given as

a) $\quad \frac{\partial u}{\partial y} = 0 \quad$ and $\quad \frac{\partial v}{\partial y} = 0 \qquad$ (6)

b) $\quad \frac{\partial u}{\partial y} = 0 \quad$ and $\quad v = 0 \qquad$ (7)

Exit boundary conditions can be specified in a similar way:

$$\frac{\partial u}{\partial x} = 0 \quad \text{and} \quad v = 0 \qquad (8)$$

• Brush Core Zone

Inflow velocity condition for this zone are the outflow conditions for the brush entrance zone. In this case:

$$v = 0 \quad \text{and} \quad u = f_1(y,t), \qquad (9)$$

where $f_1(y,t)$ is established from the solution of the Navier-Stokes equations in the entrance region. At the outflow of the computational domain we apply Eq. 8, and at the lateral walls Eqs. 6-7.

BOUNDARY CONDITIONS

• Brush Outflow Zone

Inflow velocity conditions for this area are calculated via the solution of the Navier-Stokes equations at the brush core zone. That implies $v=0$ and $u=f_2(y,t)$. At the lateral walls we employ conditions (6-7). The exit flow is allowed to develop naturally based on boundary conditions situated far downstream. The velocity boundary conditions imposed at the exit are derived from (i) the satisfaction of the continuity equation(specifically in the direction of the U velocity),

$$\frac{\partial u}{\partial x} = -\frac{\partial v}{\partial y} \qquad\qquad (10a)$$

and (ii) the condition for fully developed velocity gradient for the vertical component

$$\frac{\partial v}{\partial x} = 0 \qquad\qquad (10b)$$

• Boundary Conditions for the Poisson Equation

The dynamic pressure P, is determined from the balance of the normal forces with the inertia and viscous forces. This formulation implies Neumann type boundary conditions. The effects of the terms $\frac{\partial u}{\partial t}$ and $\frac{\partial v}{\partial t}$ have been considered negligible. The following formulation of Eqs. 11 and 12 is totally independent of the boundary configuration, and thus applicable with no restrictions.

$$\frac{\partial P}{\partial x} = -[\frac{\partial(uu)}{\partial x} + \frac{\partial(uv)}{\partial y}] + \frac{1}{Re}(\frac{\partial^2 u}{\partial x^2} + \frac{\partial^2 u}{\partial y^2}); \qquad (11)$$

$$\frac{\partial P}{\partial y} = -[\frac{\partial(uv)}{\partial x} + \frac{\partial(vv)}{\partial y}] + \frac{1}{Re}(\frac{\partial^2 v}{\partial x^2} + \frac{\partial^2 v}{\partial y^2}) \qquad (12)$$

In combination with the Dirichlet conditions for the velocity, Eqs. 11 and 12 form a well-posed boundary-value problem with resulting solutions free of odd-even velocity-pressure decoupling as described by Gresho[26] and Patankar[27].

Odd-even Velocity-Pressure Decoupling For the Inline Brush Segment
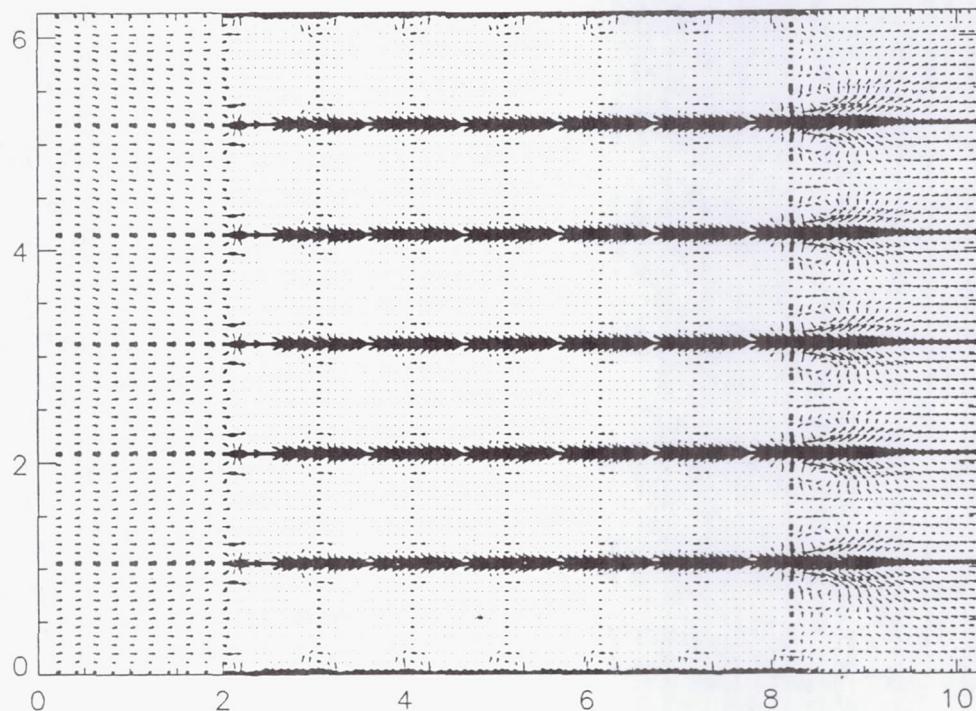
Initial conditions(t=0). The input velocities are given as $u=1$, $v=0$. The pressures are set initially to an arbitrary, operator chosen $P=P_{ref}=$const.

SOLUTION PROCEDURE

The discretization of the system of governing equations introduced above, follows the use of the Alternating Direction Method[28] applied to a collocated grid. The procedure uses the full direct approximation of each term within the differential equation on every half time step, $\Delta\tau/2$. One obtains the following system of linear algebraic equations.

The spatial derivatives, with the exception of the convection terms and cross-derivatives, are approximated by an implicit second order central finite difference. For the convective terms, the implicit form of the third-order deferred correction scheme proposed by Kudriavtsev[30] and Hayase et al.[31] was implemented[4].

After discretization of the boundary conditions we obtain a self sufficient system of linear algebraic equations that is solved using a tridiagonal matrix elimination. The steps of the solution are as follows:
- introduce the initial flow and pressure field at the n time level
- solve in the x direction for U velocity at the n+1/2 time step
- solve in the y direction for the U velocity at the n+1 time step
- solve in the x direction for V velocity at the n+1/2 time step
- solve in the y direction for the V velocity at the n+1 time step
- solve the Poisson's pressure equation at the n+1 time step by means of the pseudo-transient method within the set of internal ADI iterations $n_{it}=1,...n_f$: (i) in the x direction at the s+1/2 pseudo-time step and (ii) in the y direction at the s+1 pseudo-time step
- advance to the next time level .

On each iteration pressure at the reference point $P(1,2)$ is assigned as P^*. Nondimensional pressure at every node is calculated as: $\Delta p_{i,j} = P^* - P_{i,j}$. If steady-state solution is of interest we employ psevdo-transient method as proposed by [28].

RESULTS AND DISCUSSION

● **Pressure and flow patterns for different generic brush formations.**

There is a considerable amount of numerical and experimental work treating the flow around circular or squared cylinders in crossflow. However, only few investigations concentrated their attention on the flow interaction with the tube bundles[32,33,34]. The effects of the cylinders' arrangement and the array size, or morphology on the flow structure and pressure drops has not been extensively studied, especially if the pitch-to-diameter ratio(PTDR) is smaller than 1.

● Braun et al.[21], Kudriavtsev et al.[20], and Kudriavtsev[19] have studied systematically the time-flow, and time-pressure development in arrays of cylinders with PTDR equal and smaller than 1. The database that emerged, showed that the development of flow and pressures around one cylinder, small groups of cylinders, and large groups of cylinders, do not lend themselves to extrapolation from one configuration to another. This is exemplified in Figs. 3 and 4. Figure 3 presents the pressure oscillations at the trailing edge of a single cylinder located in the square channel of Fig. 1. On inspection, it can be seen that in a quasi steady regime the pressures in the wake of the cylinder reach a repetitive oscillatory profile within an envelope of +5%. When the number of cylinders is increased to five, arranged in a staggered formation of two rows, the same envelope is contained between +10%, Fig. 4a. Finally, the increase of the cluster to 72 cylinders, arranged also in a staggered formation of seven rows, generates in the wake of the array oscillatory pressures that can be contained within +2.5% envelope, fig. 4b. These results, when considered in conjunction with the flow patterns already discussed by the authors in previous papers, demonstrate that phenomena indigenous to small arrays do not, as a rule, apply to large formations. Therefore one has to be extremely careful during the analytical/numerical modeling of large arrays. Special methodologies, that involve realistic treatment of

PARAMETRIC STUDIES OF THE FLOW IN THE
BRUSH PROTOTYPES LOCATED IN THE OIL TUNNEL
Re=195

grid 551x1281   qrid 501x1281
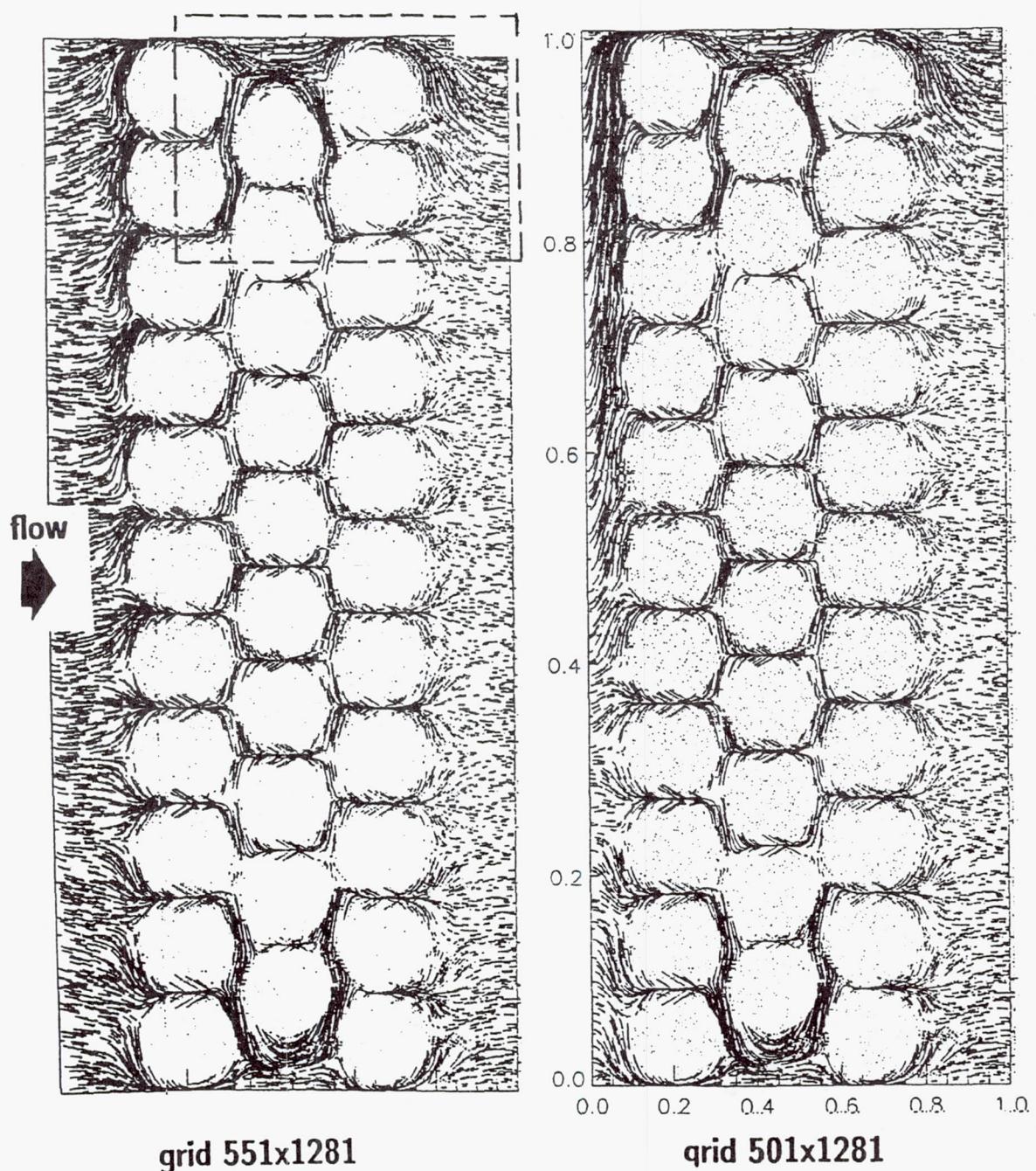
CALCULATED FLOWFIELD

$\Delta P(num) = 4.31$ psi $\Delta P(exp) = 4.02$ psi , error $= 7\%$
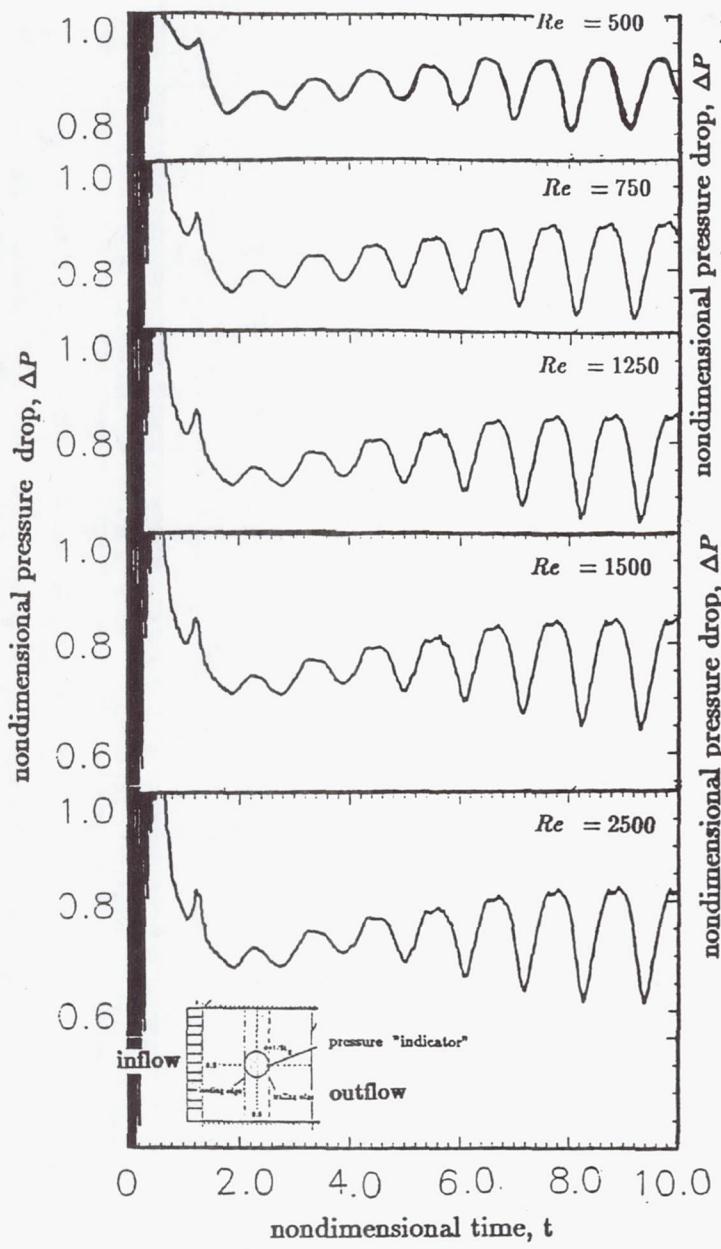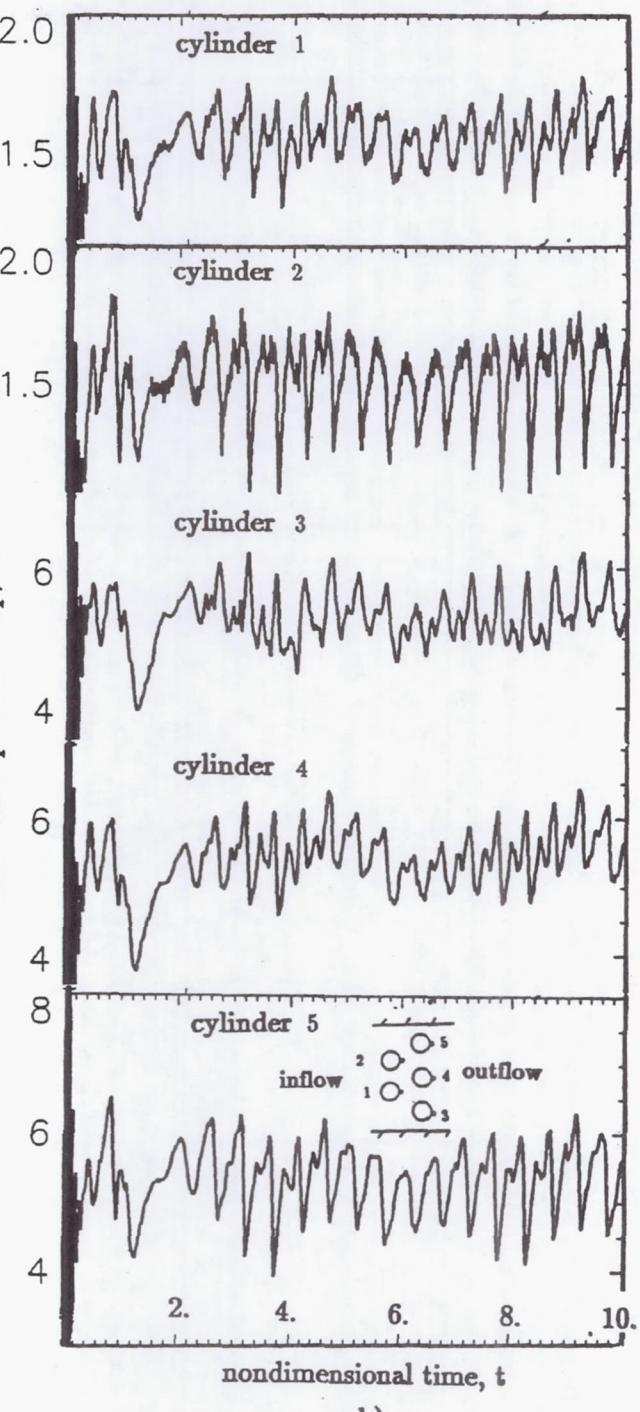
Figure 3(a,b) Pressure Development Behind Single Cylinder(Level 1)
and Small Cluster of Cylinders(Level 2)

a)single sylinder in the square channel

b)small cluster in the square channel

175
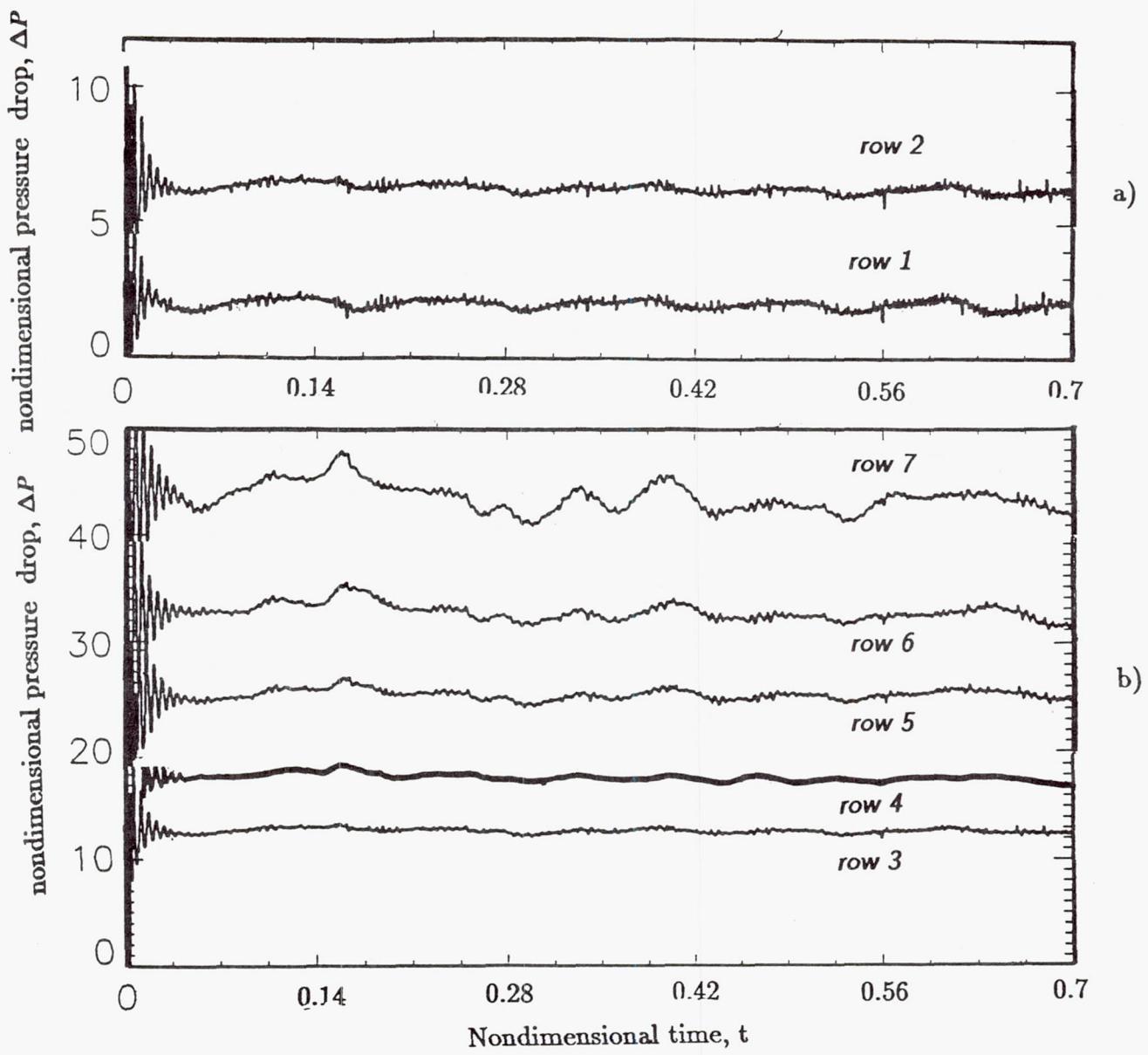
Figure 4(a,b) Pressure Development Behind a Large Cluster of Cylinders(Level 3)

(Locations of the "pressure indicators" are shown in Fig. 5)

176

boundary conditions, have to be applied to small arrays, that can then be assembled (based on these boundary conditions) in large clusters, and render a realistic reproduction of the flow conditions.

Figures 5 present the flow development in an array of 7(rows)x11 round pins with $PTDR_L=PTDR_T=1$. Along the walls, one can clearly observe high velocity rivering jets that engender contiguous regions of lower pressure which attract the flow from the center of the generic brush[21]. The central region appears to be, fortunately, quite repetitive in nature, and indicates that the use of a repetitive cell for the construction of a large brush core is a feasible alternative. Finally the wake region presents the formation of the exit jets, and the incipient formation of meandering vortices.

The same algorithm used to obtain the results presented in Fig. 5($PTDR=1$) has been used for the modeling of the dense array of Fig. 6. The flow, at Re=195, presents a steady-state pattern in this array of three rows with $PTDR_L=PTDR_T=0.084$. This packing density is of significance for the real industrial brush seal applications($1/10 \geq PTDR \geq 1/30$). Modeling of the fluid flow through the pin array with such a PTDR is a challenging computational task that so far has not been addressed in the open computational fluid dynamics(CFD) literature. The flow is dominated by accelerating-decelerating streams formed by the system of converging-diverging nozzles(constituted by the adjacent cylinders). These flows are characterized by extremely high convective gradients at their smallest cross-section. This situation imposes limitations on the computational algorithm in terms of computational stability, resolution and global accuracy. The window marked in Fig. 6a, is shown in detail in Fig. 6b. One can get an appreciation of the complicated flow formations that are at work. In Fig. 6b the rivering, lateral rivering, and the nozzle-jets are quite evident. The formation of the jets at the exit of the array can also be observed. The corresponding experimental results and the successful superposition of these results and the numerical simulation are shown in this sequence(Fig. 6b). For an entire array
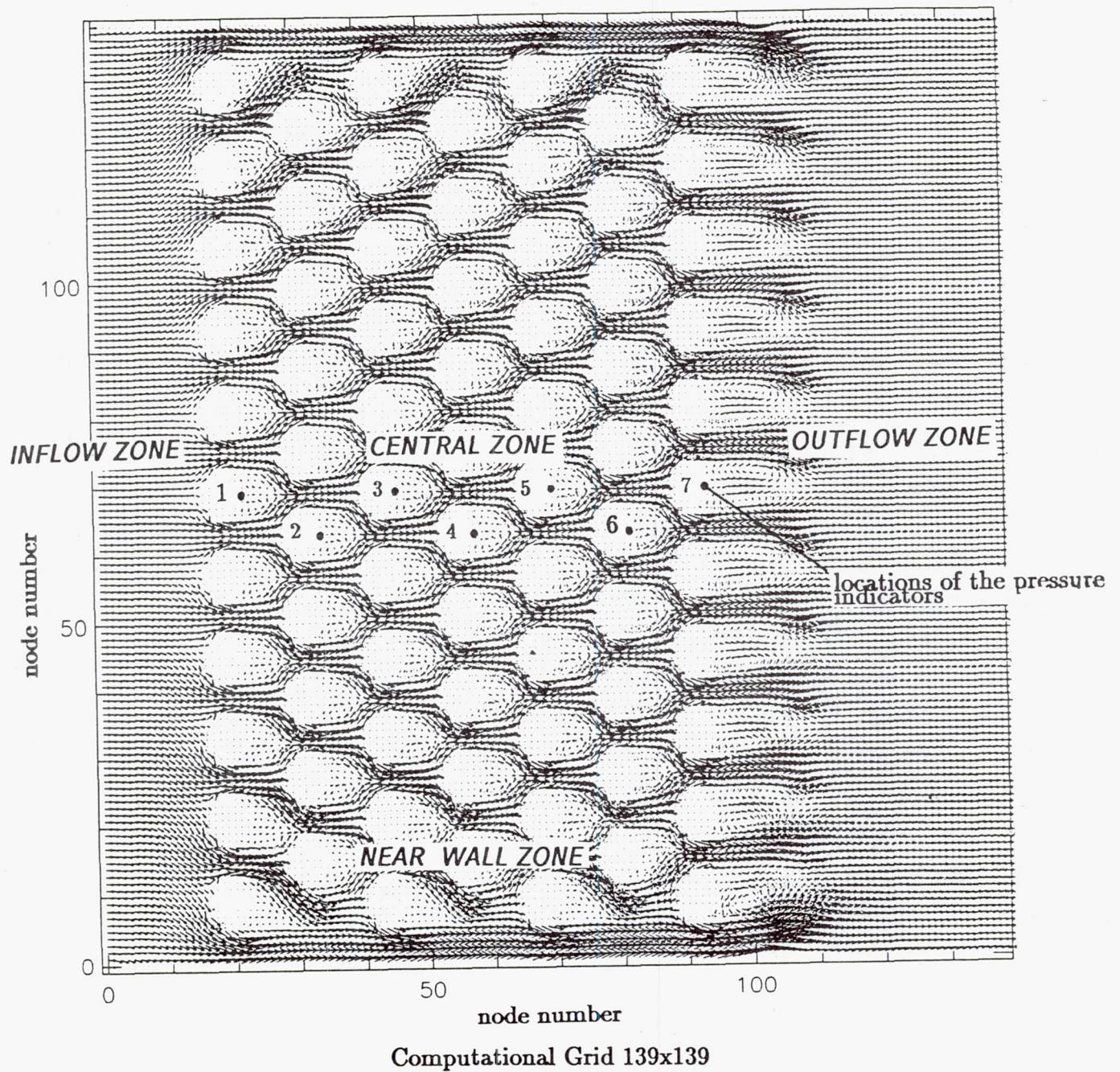
Figure 5. Typical Flow Structure in the Large Cluster of Cylinders(Level 3)

178
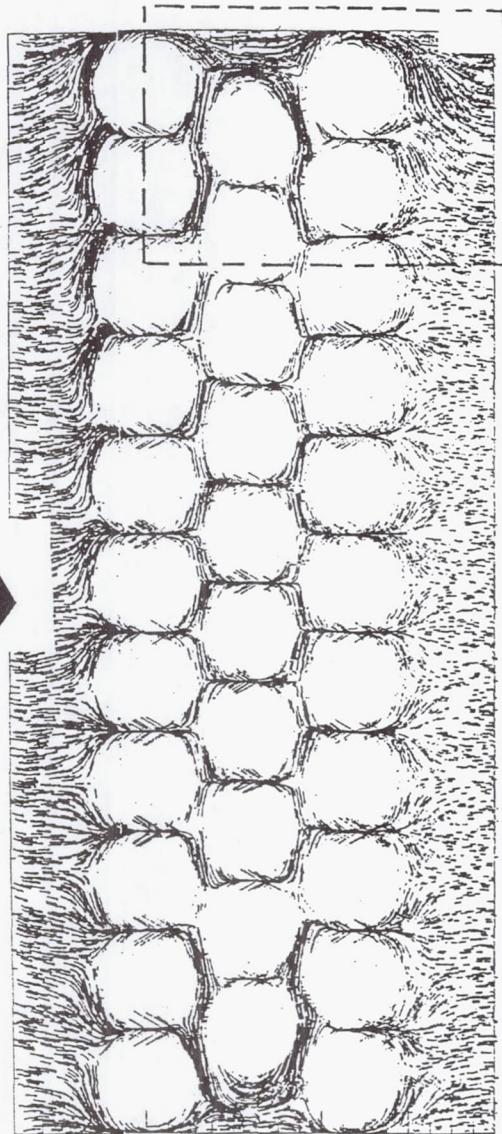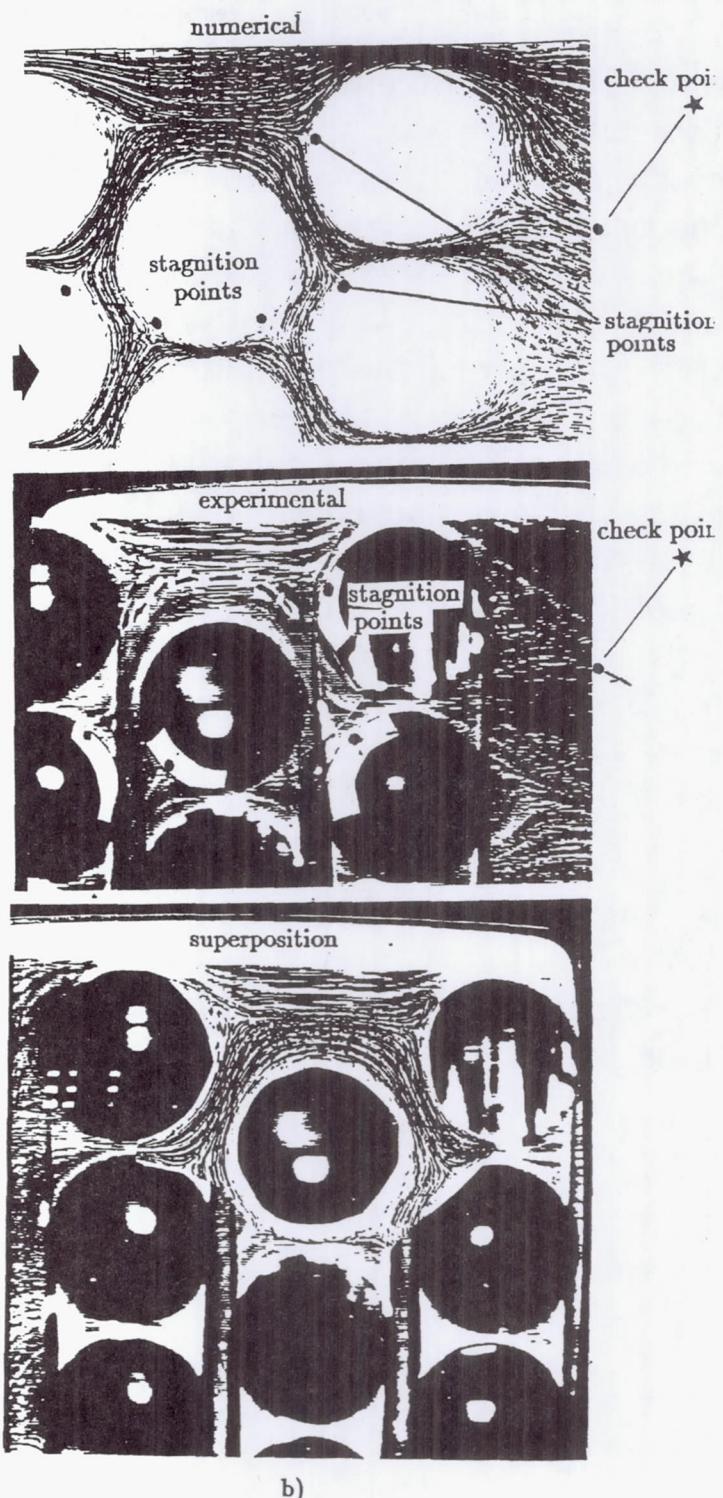
Figure 6(a,b) Large Cluster of Densly Packed Cylinders at Re=195(Level 4)

a)flow through the cylinder's array
b)detail of flow near the wall marked at Fig.6a .

Comparison of numerical and experimental results.

of 3(rows)x11, Fig. 7a, presents experimentally the interaction of 12 convective jets as they interact with each other and with the wall. The experiment was run at Re=1000, and a rather unusual flow formation was observed in the wake of the array. The low pressure region that developed near the walls, in- and outside of the pin array, causes constant jet flow deviation towards the walls. The void created in the wake is associated with a pressure that is lower than the far downstream pressure. This pressure field engenders a recirculation bubble that occupies considerable part of the outflow cross section and consists of the two butterfly like vortices with strong "negative" flow along the centerline of the cross section. The global resulting recirculation structures include numerous vortices and require high computational accuracy in order to obtain any realistic solution. Such solution can be observed in Figs. 7b and 7c. For the numerical results of both Figs. 6 and 7 it has been found that the flow structure, inside the array, converged to a steady solution much faster than the flow in the wake of the array, Figs. 7b, 7c.

For PTDR<0.1, the numerical solution can be obtained only by large scale CFD modeling that requires grid sizes approaching 1000x1000 nodes. Thus a further increase in the size of the array or any further grid refinement becomes rather prohibitive, and appropriate strategies need to be found to handle this situation.

FLOW ➤

a)experimental
Re=1000

◀ "Negative" flow
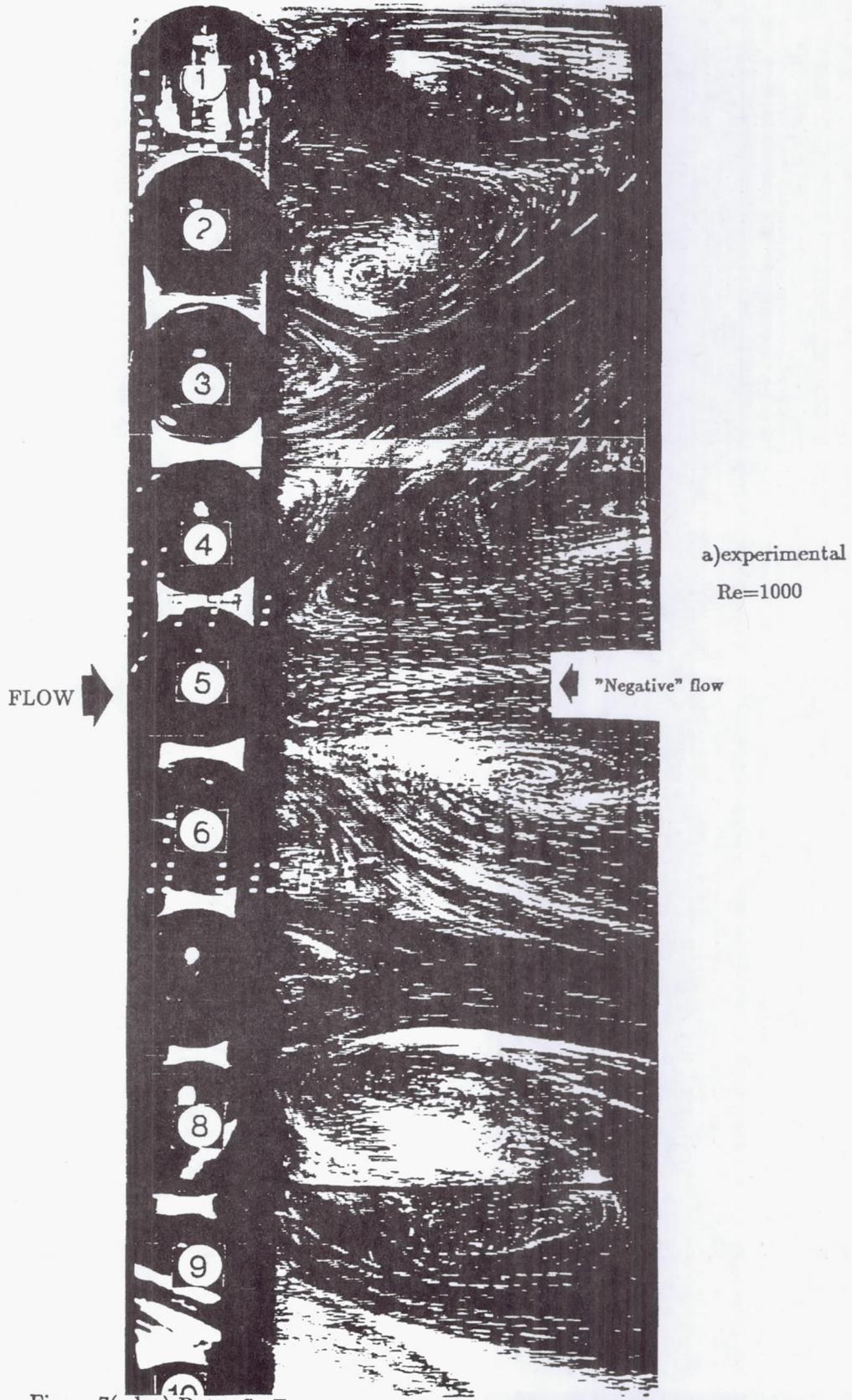
Figure 7(a,b,c) Butterfly Formations in the Wake of the Cylinder's Clusters
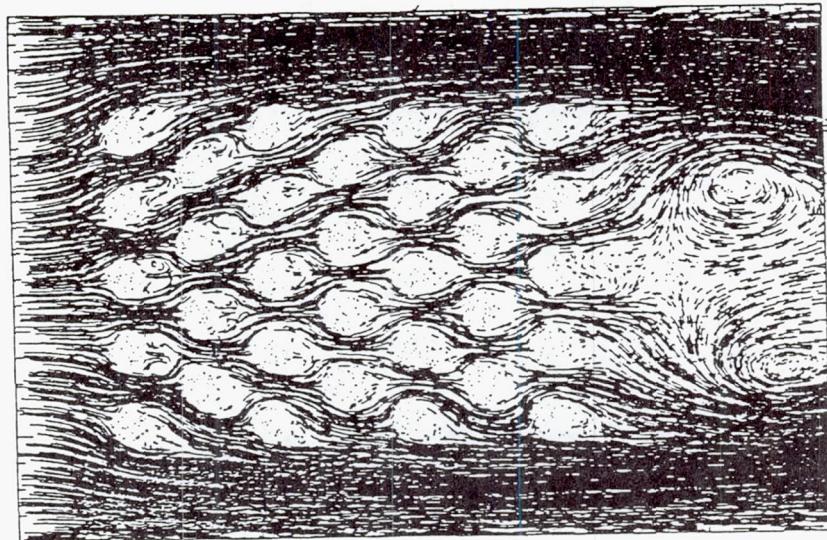
b)numerical(small array)
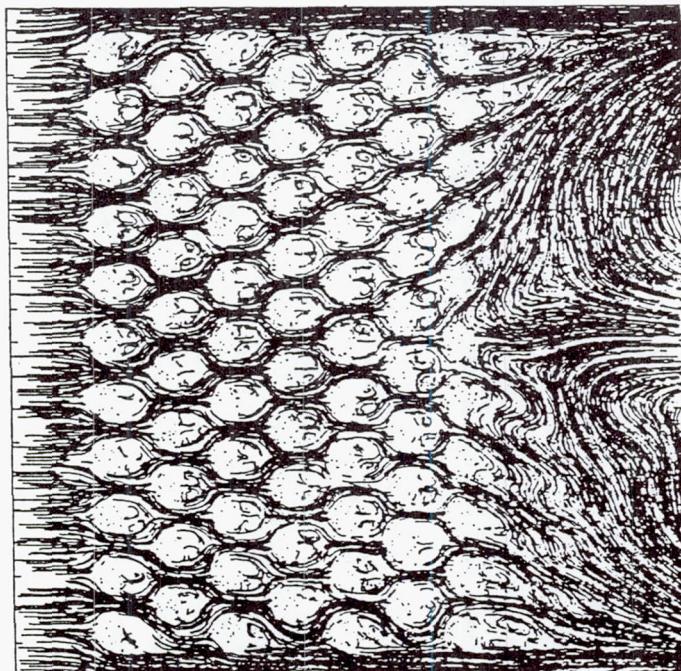
c)numerical(large array)

Figure 7(a,b,c) Butterfly Formations in the Wake of the Cylinder's Clusters
Re=1000

PARAMETRIC STUDIES OF THE FLOW IN AN ARRAY OF FIVE STAGGERED CYLINDERS

- authors have extended their analysis to a representative cell of five staggered cylinders. The longitudinal and transversal pitches are equal to each other, $PTDR_L = PTDR_T = 1$, while the cylinder diameter is $d = 0.143L_0$.

CORRESPONDING BUTTERFLY FLOW FORMATION

Numerical

A

FLOW

JET ZONE

BUTTERFLY FLOW FORMATION

LAST ROW OF PINS
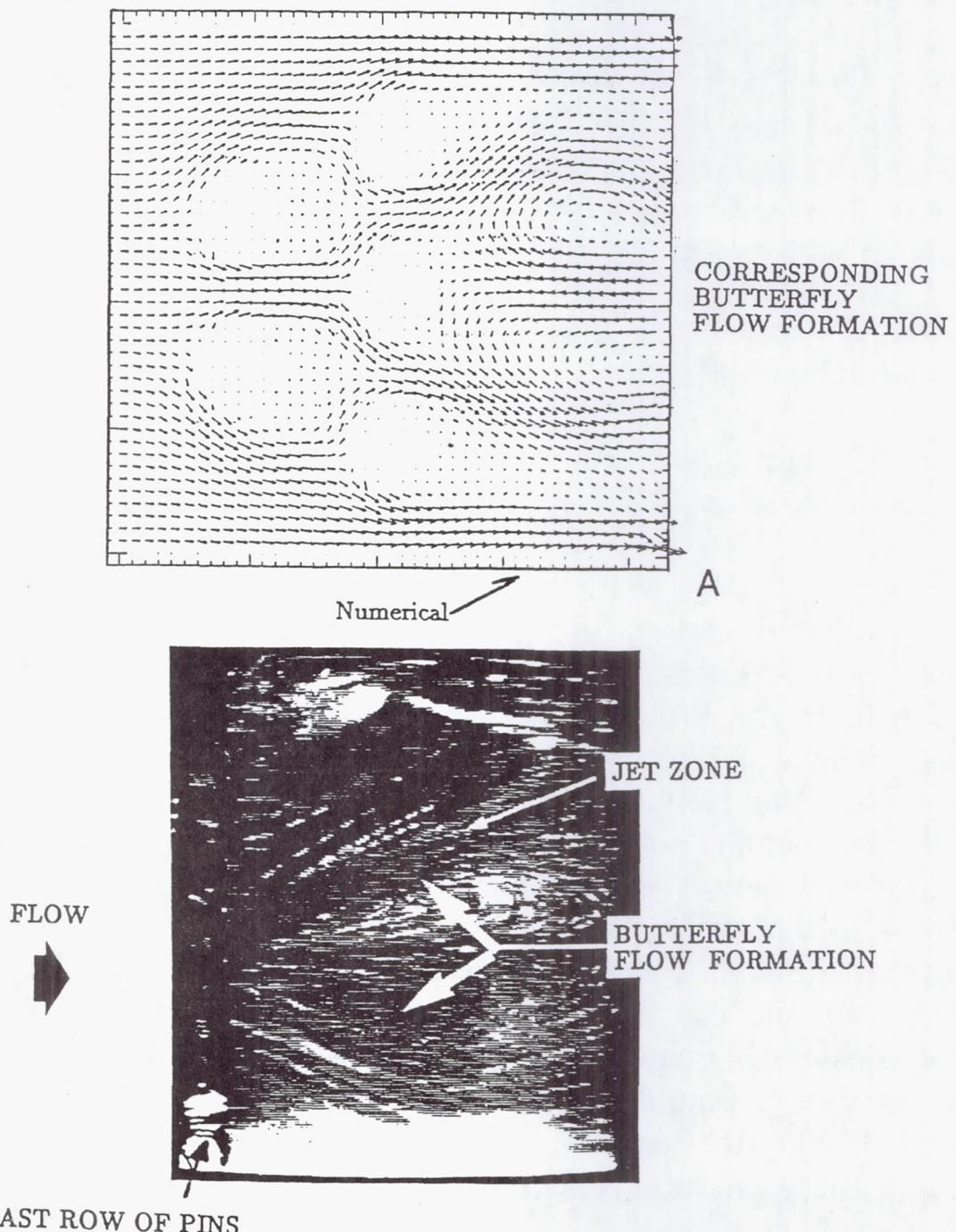
The totality of the numerical and experimental work presented above has led us to the conclusion[19], that we were fastly approaching the limits of our modeling capability from the standpoint of the computer capacity to handle the large arrays necessary to model a full brush. We have learned that

a) the flow inside the brush reaches a convergent solution, much sooner than near the wall boundaries or in the brush wake;

b) in a deep cluster the flow is practically repetitive, as long as it is at least two rows away from the inlet or exit of the generic brush;

c) the pressures fall monotonously in the core portion of the simulated brush[4];

d)the computational time for calculating flow in dense arrays of cylinders(3rows x 11 lines) at moderate Re numbers can become prohibitive.

As mentioned earlier, the brush can be partitioned into several areas. The numerical simulations shown in Figs. 8 explain the rationale of the brush partitioning approach. One of our previous conclusions was that large brush modeling is restrictive, so one tries to reduce the computational domain to a representative cell. In order to define optimally this cell, and its environment, two geometrical setups were chosen. First is the flow in the channel with non-slip walls as boundary conditions. The second setup replaces the wall with symmetry conditions at the boundary. From Fig.8(a,b) one can see that the wall introduces near wall effects that considerably change the flow structure. Thus one has to select the symmetry boundary conditions setup, as the optimal one(see Eqs.7-8,10). At Re=100 in the later time stages of the flow development one observes the incipience of an asymmetric mode in

the outflow zone. This situation induces asymmetry in the central part of this brush segment(Fig. 8b and 8d). In larger(deeper) cylinders bundles this effect does not penetrate to the core(like in Fig. 5). Thus, the core and the outflow segments need to be treated as separate computational domains.

To respond to these physical conditions and the conclusions drawn above in items a) to d) we proceeded to assemble a full brush out of the component segments that were identified in the mathematical model section. The continuity and momentum governing equations remain the same, but the boundary conditions had to be modified in order to take into the account the repetitive nature of the assembly of the brush core. These boundary conditions were described by Eqs. 6-10. For the verification of the concept we have used a partitioned array that contains the segments shown in Fig. 9. Figure 9a, presents a succession of identical core segments that are characterized by the same pressure drops. Figure 9b displays the inflow and outflow segments that are added to the central core in order to form a complete system. The resulting total pressure drop can be calculated as

$$\Delta P_{brush} = \Delta P_{inflow} + N^{seg} \Delta P_{central} + \Delta P_{outflow} \qquad (19a)$$

If one considers the Hendricks[25] report, and if the brush has more than $n \geq 10$ rows, it seems rational that the overall pressure drop can be evaluated with little error by considering only what we defined as the core portion. Thus one can simplify Eq. 19a to

$$\Delta P_{brush} = n \Delta P^{*}_{central} \qquad (19b)$$

where $\Delta P^{*}_{central}$ - average pressure drop per single row.

185
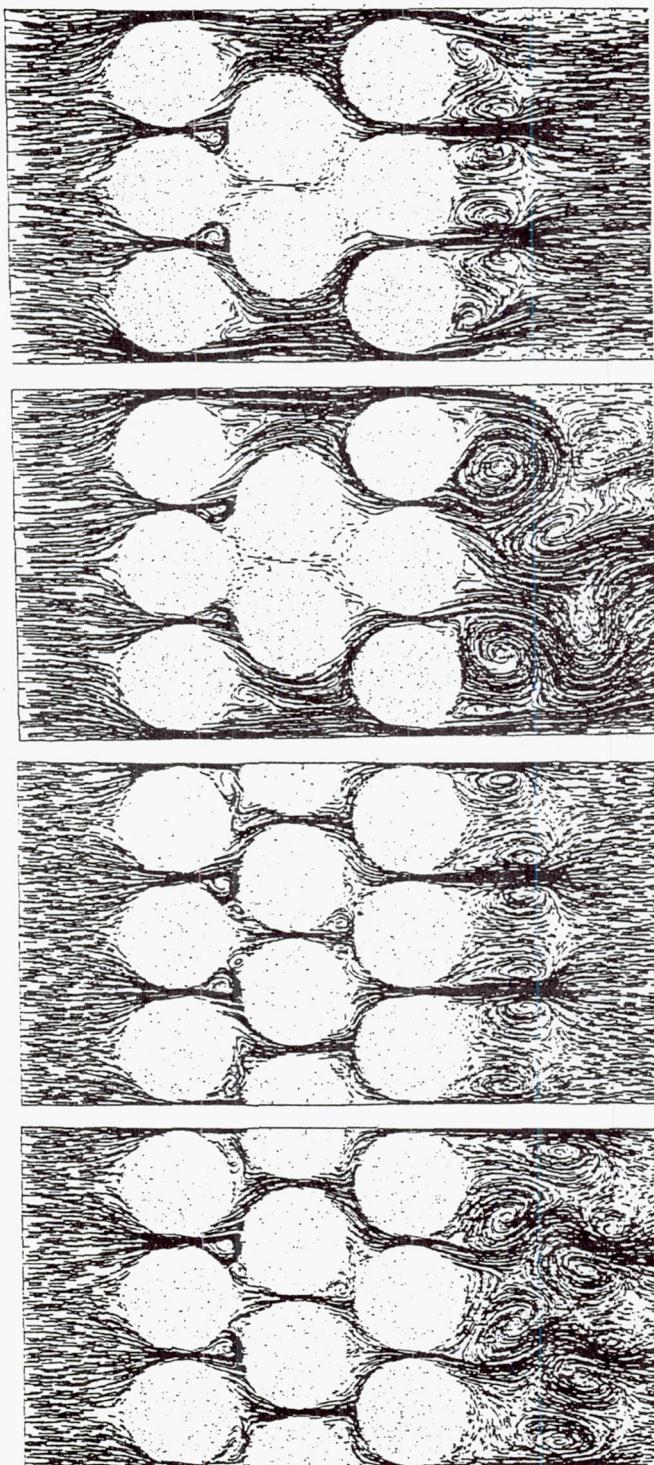
a)

Brush Segment Located
in the Channel

b)

c)

Symmetry boundary conditic
on lateral boundaries

d)

Figure 8(a,b,c,d) Samples of the Fluid Flow in the Brush Segments at Re=100

a)symmetric mode(initial stage of flow development)

b)asymmetric mode(final stage of flow development)

c)symmetric mode(initial stage of flow development)

d) asymmetric mode(final stage of flow development)

186

central core

midsection

inflow

outflow

front brush section

back brush section
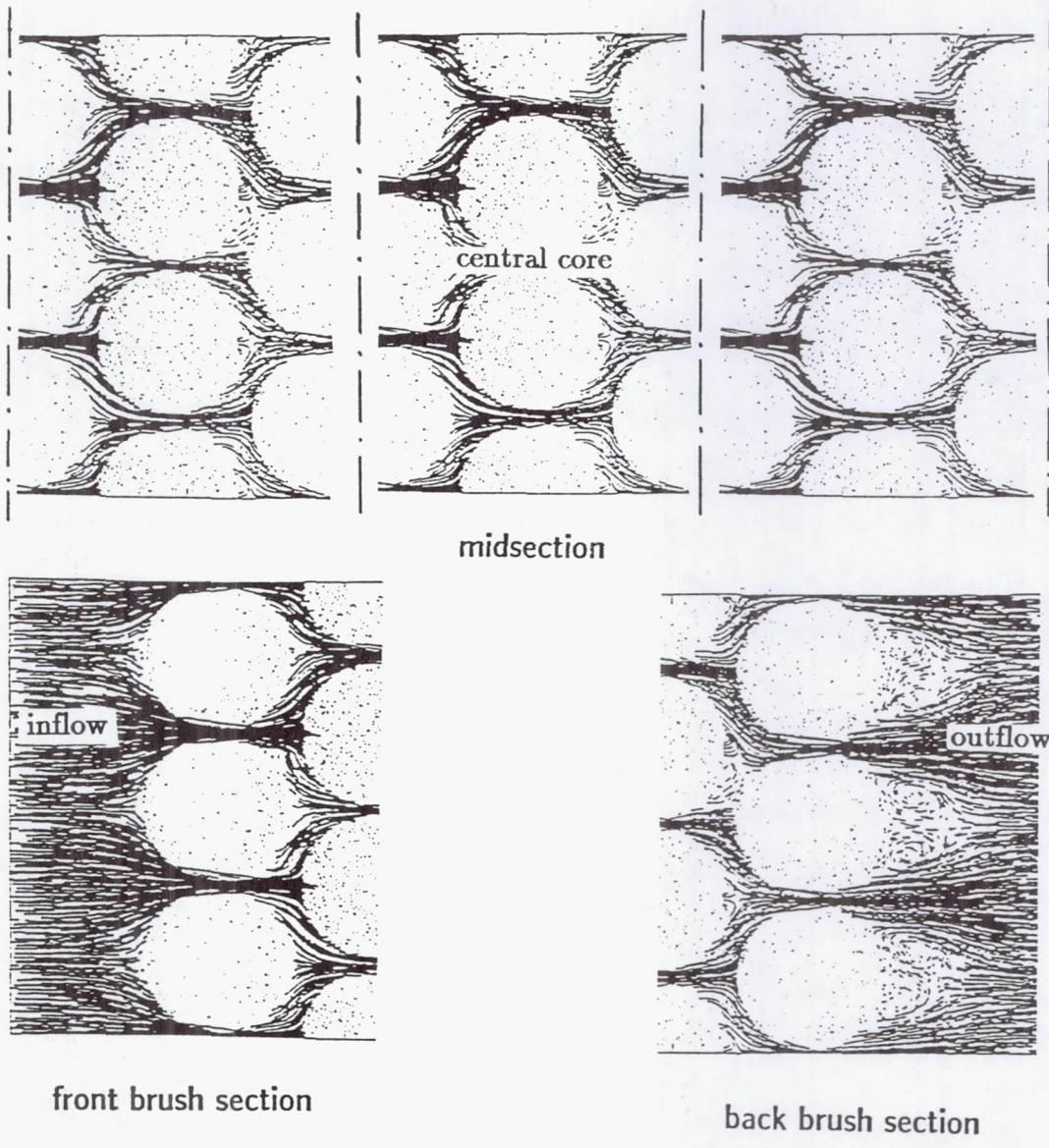
Figure 9. Assembled Brush Cluster at Re=20

STUDIES OF THE FLOW IN THE BRUSH SEGMENTS

Variation in the boundary conditions
$$\partial v/\partial y = U$$

).0   0.2 $\partial v/\partial y = 0$ 0.6   0.8

$$\partial v/\partial y = 0 \cdot$$

.0   0.2 $\partial v/\partial y = 0$ 0.6   0.8
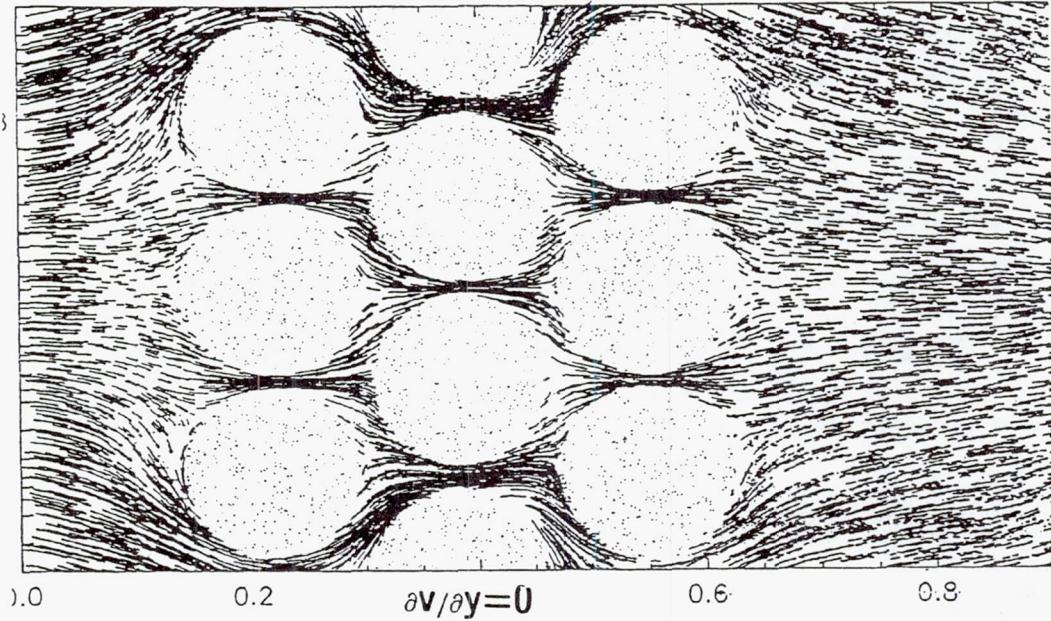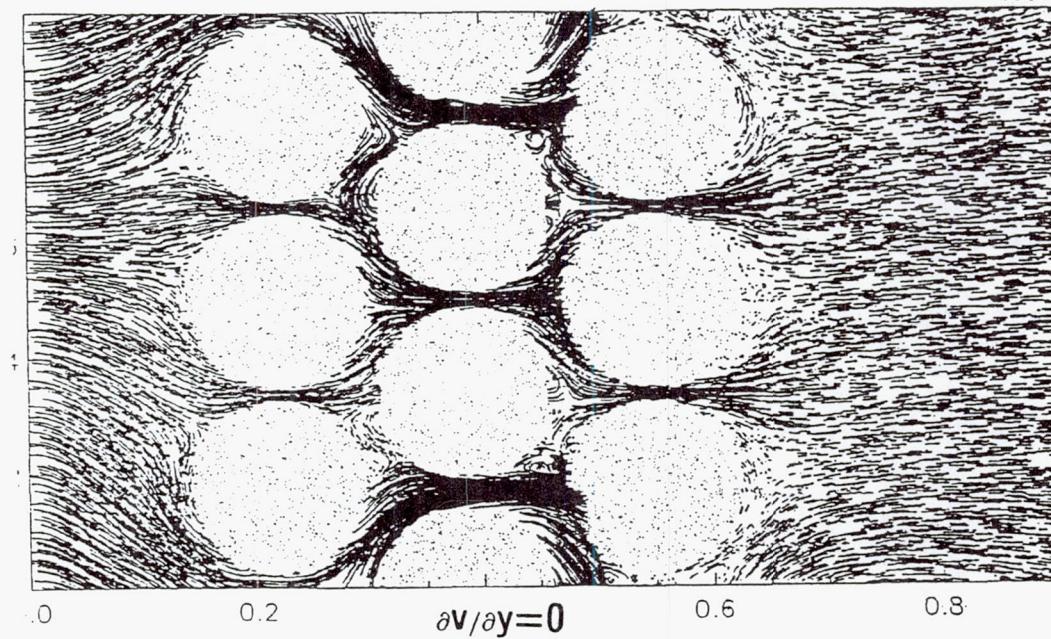
$$Re_d = 20$$

Boundaries are opened to the flow

188

STUDIES OF THE FLOW IN THE BRUSH SEGMENTS

boundary pitch equal to the internal pitch
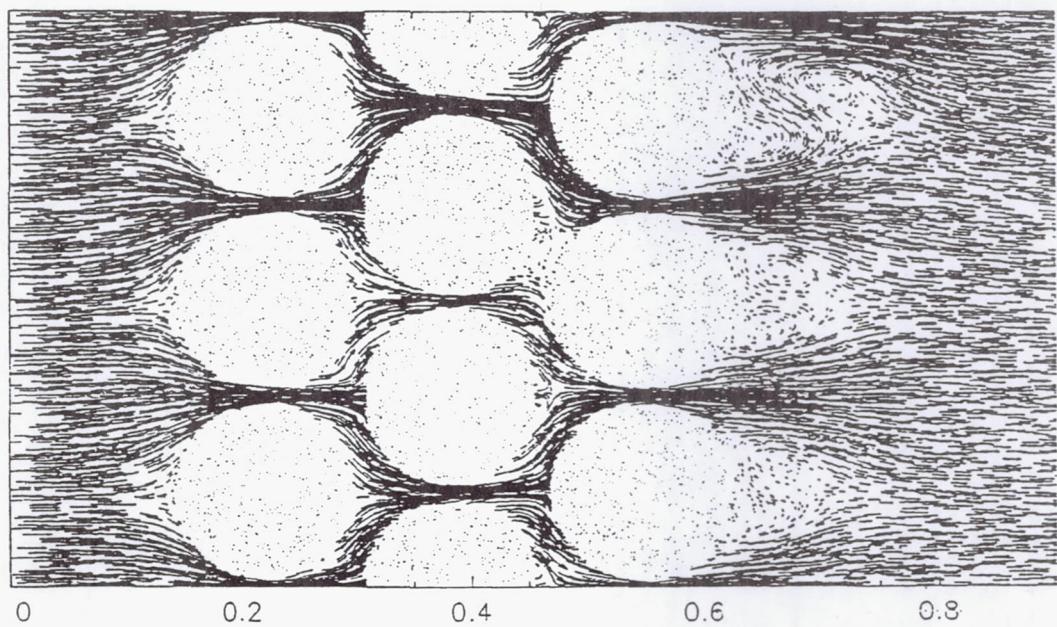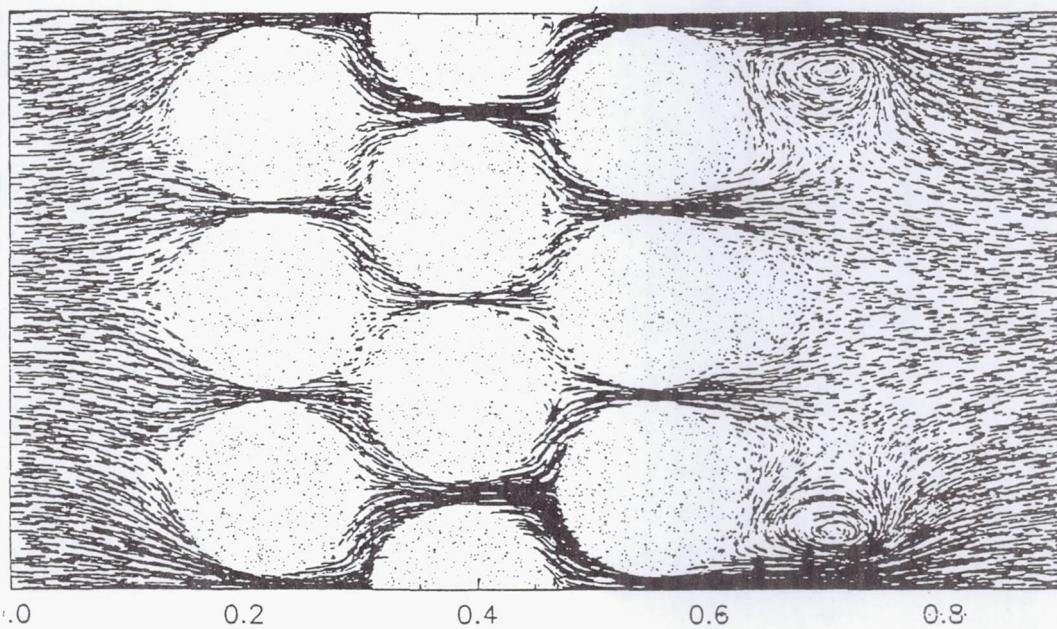
assymetric configuration,   top pitch larger than the bottom one

$Re_d = 20$

t=1.4

189

Scale
1 cm

Partition

Window A

Flow

Window C

Window E

38 mm

Side wall
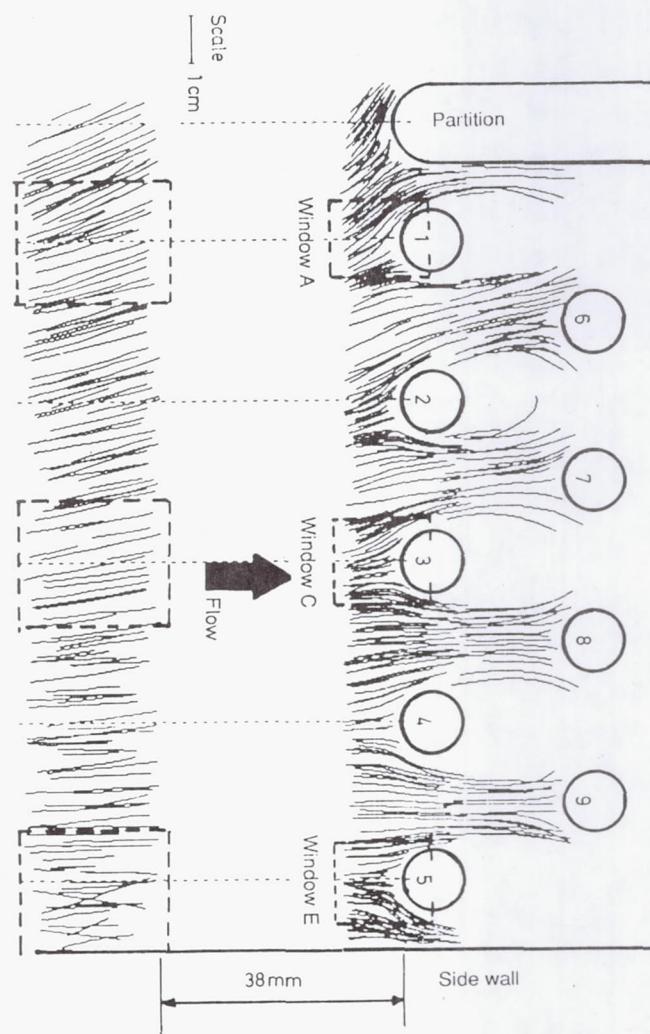
CONCLUSIONS

The authors have presented chronologically the main contributors in the technological development of the brush seals. As one can see, there were three avenues that were followed. The first involved laboratory experiments on simulated brush seals, that led to a better understanding of the flow conditions and flow paths in the brush. The second involved industrial testing of brushes, that yielded real experimental data concerning pressure drops and leakages. These efforts performed within the framework of major industrial manufacturers and users, led to the incorporation of these seals in production jet engines. The third and final avenue was the numerical development of design and predictive tools for the brushes. These codes have used either lumped or distributed codes, as it was shown earlier in this paper. The present paper presents a first attempt at extending the distributed model of Braun and Kudriavtsev to a model where the brush is segmented in inlet, core and exit component. This concept allows the construction of infinitely large brushes with diminished computational penalty. It was shown that this concept predicts correctly the flow in the repetitive segments of the core, as well as in the inlet and exit zones.

REFERENCES

1. Hendricks, R.C., Carlile, G.A., Liang A.D., "Some Sealing Concepts, Part B: Brush Seal Systems", Fourth International Symposium on Transport Phenomena and Dynamics of Rotating Machinery, Honolulu, Hawaii, ISROMAC-4, vol. A, April 5-8, 265, (1992).

2. Withers, P.A., "High Pressure Compressor Delivery Brush Seal of the International Aero Engines (IAE) V2500-A1 Gas Turbine Engine", Proceedings of Seals Flow Code Development-92, NASA CP-10124, pp. 275-279, NASA Lewis Research Center, Cleveland, Ohio August 5-6, 1992.

3. Shapiro,W., Artiles, A., "Industrial Code Development, Seals Flow Code Development-92", NASA CP-10124, Proceedings of a workshop held at NASA Lewis

Research Center, August, 5-6, 1992, pp. 13-67.

4. Braun, M.J., Kudriavtsev, V.V., "A Numerical Simulation of a Brush Seal Section and Some Experimental Results", Int. Gas Turbine and AeroEngine Congress, Cincinnati, 1993, ASME Paper 93-GT-398, pp. 1-12. (Accepted for the publication in the ASME Journal of Turbomachinery).

5. Liang A., (Editor), Seals Flow Code Development, NASA CP-10070, NASA Lewis Research Center, Cleveland, Ohio, March, 1991.

6. Chupp, R.E., Holle, G.F., Dowler, C.A., "Simple Leakage Flow Model for Brush Seals", AIAA Paper 91-1913, AIAA/SAE/ASME/ASEE 27th Joint Propulsion Conference, June 24-26, Sacramento, CA, 1991.

7. Hendricks, R.C., Shlumberger, S., Braun, M.J., Choy, F., Mullen, R.L., "A bulk flow model of a brush seal system", ASME Paper, 91-GT-325, 1991 .

8. Flower, R. "Brush Seal Development Systems", AIAA Paper 90-2140, 1990.

9. Holle, G., Krishnan, M., "Gas Turbine Engine Brush Seals Applications", AIAA Paper 90-2142, 1990.

10. Chupp, R., Nelson, P., "Evaluation of Brush Seals for Limited Life Gas Turbine Engines", AIAA Paper 90-2140, 1990.

11. Dowler, C., "Air Force Brush Seal Programs", Seals Flow Code Development-92, NASA CP-10124, Proceedings of a Workshop held at NASA Lewis Research Center, Aug 5-6, 1992.

12. Basu, P.,

13. Childs, D., "Dynamic Coefficients for Multiple Brush Seals", Seals Flow Code Development-92, NASA CP-10124, Proceedings of a workshop held at NASA Lewis Research Center, August, 5-6, 1992, pp. 211-213.

14. Caroll, P.F., Easter B.P., "Brush Seal Would Impede Flow of Hot Gas", (Rockwell International), NASA Tech Briefs, Vol.17, No.12, Dec. 1993.

15. Cannaci, V.A., Braun, M.J., Hendricks, R.C., "Flow Visualization and Motion Analysis for a Series of Four Sequential Brush Seals", J. of Propulsion and Power, Vol. 8, No. 3, pp. 697-702, 1992.

16. Braun, M.J., Canacci, V.A., Russell, L.M., "Full field flow visualization and computer-aided velocity measurements in a bank of cylinders in a wind tunnel", Experiments in Fluids, vol. 13, pp. 117-127, 1992 .

17. Zukauskas, A., "Heat Transfer from Tubes in Crossflow", Adv. Heat Transfer, Vol. 8, pp. 93-160, 1972.

18. H.F., Griner, "Seal Related Activities at EG&G", NASA CP-10070, Proceedings of a Workshop held at NASA Lewis Research Center, March 26, 1991, pp.113-124 .

19. Kudriavtsev, V.V., "Numerical Studies of the Transient Flows within the Brush Seal Elements of the Aerospace Turbomachinery", Ph.D. Dissertation, Moscow Aviation Institute, School of Engine Technology, Oct., 1993(in Russian).

20. Kudriavtsev, V.V., Braun, M.J., "A Reynolds Number Parametric Numerical Investigation of Flow Structures and Pressure Distributions in a System of Cylinder Arrays", Int. ASME Fluid Engineering Conference, Washington D.C., Separated Flows/FED-Vol.149, Ed. by J.C.Dutton and L.P.Purtell, 1993, pp. 83-95 .

21. Braun, M.J., Kudriavtsev, V.V., "Numerical Visualization of Flow Structures in Dense Banks of Cylinders Located in a Channel", Third Int. Symposium on Experimental and Numerical Flow Visualization, 1993 ASME Winter Annual Meeting, New Orleans, Louisiana, Nov.28-Dec. 3, 1993/Eds. B. Khalighi, M.J. Braun, C.F. Freitas, D.H. Fruman, pp. 1-8. (submitted to the ASME Journal of Fluids Engineering)

22. Braun, M.J., Kudriavtsev, V.V., "Experimental and Analytical Investigation of Brush Seals", Seals Flow Code Development-92, NASA CP-10124, Proceedings of a workshop held at NASA Lewis Research Center, August, 5-6, 1992, pp. 181-195.

23. Ghia, K.N., Ghia, U., Oswald, G.A., "Study of Incompressible Separated Flow Using an Implicit Time-Dependent Technique", AIAA Paper 83-1894, 1, 1983.

24. Roache, P.L., Computational Fluid Mechanics, Hermosa Publishers, 1985.

25. Hendricks R.C., "Integrity Testing of Brush Seal in a T-700 Engine", Seals Flow Code Development-92, NASA CP-10124, Proceedings of a workshop held at NASA Lewis Research Center, August, 5-6, 1992, pp.117-138.

26. Gresho, P.M., Sani, R.L. Lee, R.L., Griffiths, D.F., "The Cause and Cure(?) of the Spurious Pressures Generated by Certain FEM Solutions of the Incompressible Navier-Stokes Equations", Int. J. Num. Meth. in Fluids, 1, No.1, 1981.

27. Patankar, S.V. Numerical Heat Transfer and Fluid Flow,Hemisphere, 1980.

28. Washpress, E.L., Iterative Solution of Elliptic Systems, Prentice-Hall, 1966.

29. Torrance, K.E., "Comparison of Finite-Difference Computations of Natural Convection", Journal Res. NBS: Math. Sci, N72B, 281, 1968.

30. Kudriavtsev, V.V., "New Higher-order Finite difference scheme for Hyperbolic Conservation Law: HYBRID Approach", Proc. Modeling and Simulation Conference, Eds. W.G.Vogt, M.H.Mickle, vol. 23, part 5, Pittsburgh, pp. 2655-2662, 1992.

31. Hayase, T., Humphrey, J.A.C., Grief, R., "A Consistently Formulated QUICK Scheme for Fast and Stable Convergence Using Finite-Volume Iterative Calculation Procedures", Journal of Computational Physics, Vol. 98, pp., 1992.

32. Zdravkovich, M.M., Stonebanks K.L., "Intrinsically Non-Uniform and Metastable Flow in and Behind Tube Arrays", Flow Induced Vibrations in Cylindrical Structures:

Solitary Cylinders and Arrays in Cross-Flow, Vol. 1, pp. 61-73, 1988.

33. Mullen R., Braun, M., Hendricks R., "Numerical modeling in simulated brush seal configurations", AIAA Paper, AIAA-90-2141, 1990.

34. Launder, B.E., and Massey, T.H. "The Numerical Prediction of Viscous Flow and Heat Transfer in Tube Banks", Transactions of the ASME, Journal of Heat Transfer, Vol.100, pp.565-571, Nov. 1978 .

OBTAINED NEW SCIENTIFIC RESULTS :

★ transients are negligible for Re < 1000

★ pressure distribution and flow structure behind the simulated brush(located in the channel) are non-symmetrical. Flow assymetry depends on the Re number.

★ creation of the butterfly-like flow formation behind the simulated brush seal(located in the channel) and observed experimentally and numerically

★ nonlinear behaviour of the pressure coefficient vs Re number for the brush segments located in the channel. Pressure paradox.

★ nonlinear behaviour of the pressure drop vs $PTDR_L$

★ formation of the near wall jets for the multi-row cylinder bundles located within the channel (simulated brush), Coanda effect, flow "expansion" from the center to the walls

CONCLUSIONS

* approximate mathematical model with distributed parameters that is free from the disadvantages associated with porous media assumption

* developed and evaluated a new computational algorithm for the solution of the N-S equations in (u,v,p) formulation

* systematic analyses of the fluid flow in the brush seal components

* Capabilities of calculation of the pressure drop for a given bristle geometry and the flow rate for typical brush segment

CURRENT DEVELOPMENTS IN BRUSH SEALS

Bob Loewenthal
Fluid Components Technology Group
Research and Development
EG&G Sealol
Cranston, Rhode Island
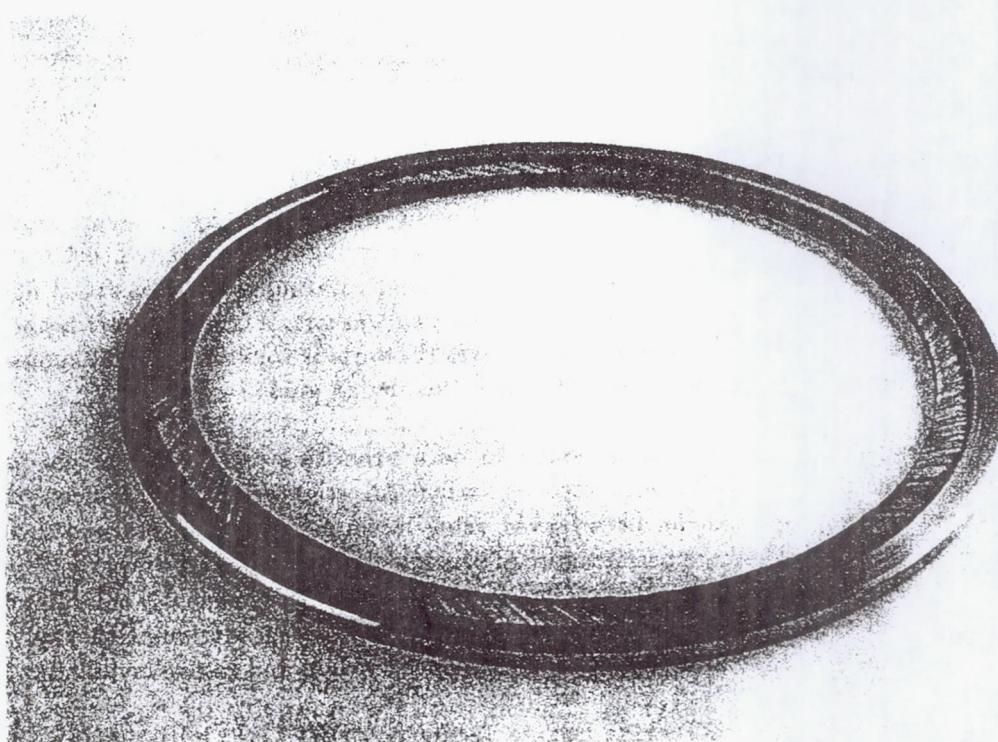
Photograph of an Annular Brush Seal
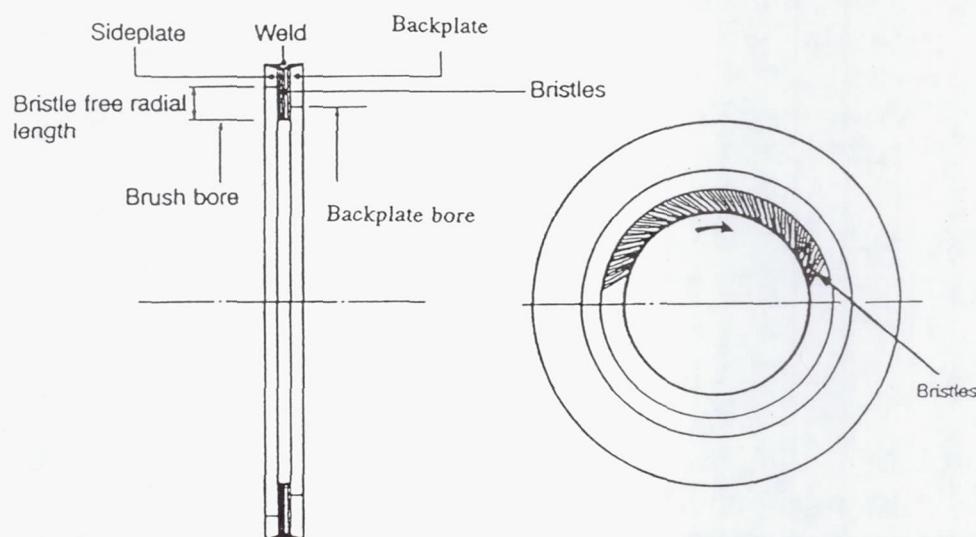
Illustration and Nomenclature of a Typical Brush Seal

199

Brush Seal Development Program

U. S. Air Force - Sponsored Integrated High Performance Turbine Engine Technology (IHPTET) - PRDA-II

- OBJECTIVE: DEVELOP A COMPREHENSIVE DESIGN METHODOLOGY FOR BRUSH SEALS USING:
  - APPLICATION REQUIREMENTS FROM ENGINE MANUFACTURER
  - EXPERIMENTAL CHARACTERIZATION OF SEAL DESIGN AND TRIBOLOGICAL PAIRS
- GOALS:
  - SUBSTANTIALLY LOWER LEAKAGE THAN LABYRINTH SEALS
  - SEAL LIFE CONSISTENT WITH MAN-RATED MISSION REQUIREMENTS
  - INVESTIGATE SINGLE AND MULTIPLE STAGED BRUSH SEALS
  - TEMPERATURE - up to 1200F
  - SURFACE SPEED - up to 900 FPS
  - PRESSURE - $\triangle$P ACROSS THE SEAL, 50 PSID
- PROVIDE:
  - COMPREHENSIVE SEAL DESIGN GUIDE
  - BRUSH SEAL FOR TEST IN A DEMONSTRATOR ENGINE

Brush Seal Development Program

U. S. Air Force - Sponsored Integrated High Performance Turbine Engine Technology (IHPTET) - PRDA-III

Started: October 1992   Will complete: 1995

- OBJECTIVE: DEVELOP DESIGN METHODOLOGY FOR ADVANCED BRUSH SEALS
  - SIMILAR METHODOLOGY TO PRDA-II EXCEPT:

    MORE EXTENSIVE CFD-BASED MODEL BEING DEVELOPED AT TEXAS A&M UNIVERSITY

- TECHNICAL GOALS
  - 1400 FEET PER SECOND - SURFACE SPEED
  - 1400° F
  - 150 PSID PER STAGE

- PROVIDE:
  - COMPREHENSIVE DESIGN GUIDE
  - BRUSH SEAL FOR TEST IN AN IHPTET DEMONSTRATOR ENGINE

Brush Seal Testing at EG&G Fluid Components Technology Group Research and Development

PRDA-II 1990-1993

- Baseline Testing   12 seals   184 hours
- Tribological Evaluation   Ring-on-ring samples
        and 9 small (2") brush seals
- Characterization Testing   17 seals   484 hours
- Design Selection Testing   8 seals   280 hours
- Performance Testing   3 seals   101 hours

PRDA-III 1992-1995

Characterization Testing to date

4 seals - 76 hours

Projected - 20 seals for characterization and performance

» 350 hours more testing

Other Brush Seal Programs

- Various seals   120 hours

Brush Seal Testing at EG&G Fluid Components Technology Group Research and Development

> 1990 to 1993

Maximum Conditions of Testing - to date

- Tested 9 inch diameter seal with 4.5 mil of runout and applied radial excursions of up to 19 mil for 765 cycles, Leakage acceptable for the application

- Highest temperature - 1200°F

- Highest surface speed -14 inch I.D. seal - 1,080 FPS

- Highest $\triangle$ P across seal   60 psid

Brush Seal Testing at EG&G Fluid Components Technology Group Research and Development

- ## Test Rigs used for brush seal programs

  - ### High Speed - High Temperature Tribology Test Rig
    - » 60,000 rpm, small samples, 1200°F

  - ### Gas Seal Test Rig
    - » 16,000 rpm, 2000 psi, 600°F, up to 4 inch diameter runners

  - ### Aerospace Test Rig
    - » 24,000 rpm, 200 psi, 1000°F, up to 20 inch diameter runners
    - » Can set in desired continuous runout and can induce excursions of up to .030 inches (radial) during dynamic testing. Excursions done by moving the seal housing.

Experimental Procedure

Air Cylinder & Guide Mechanism

Dummy Seal

Test Seal

Seal Chamber

End Plate

Rotor

Seal Holder

Housing

Radial Excursion

Dynamic Test

30 mils
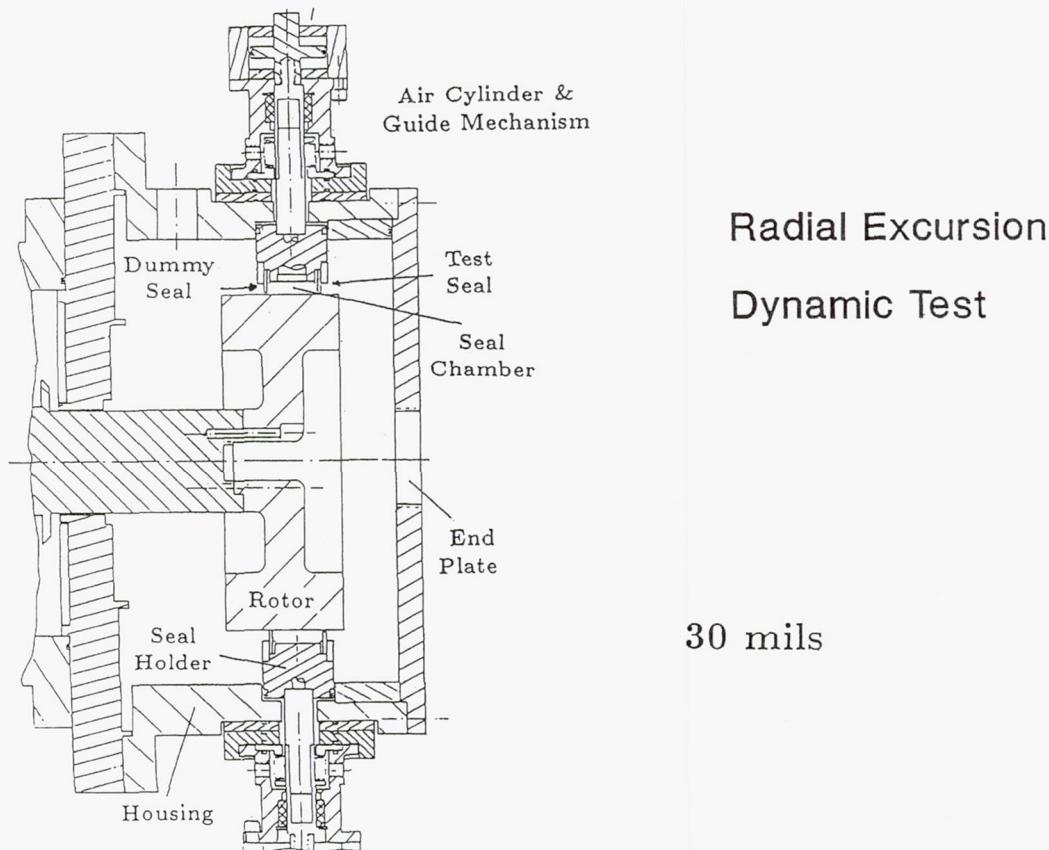
Brush Seal Development Program

- Major Results
  - Developed new design to alleviate "bristle hysteresis" effect
  - Developed tribological pair, bristle material and coating combination, that performs well at required speed and temperature goals
  - Delivered brush seal acceptable to engine manufacturer for test on demonstrator, anticipated to test December 1993
  - Design Guide has been published, U.S. Air Force publication

Note: Copies of AIAA Propulsion Conference papers:

"Hysteresis and Bristle Stiffening Effects of Conventional Brush Seals"

and

"Tribological Evaluation of Brush Seal Applications"

are available in the back of the room.

Brush Seal Development Program

IHPTET - PRDA-III

- **Where we are**
  - Completed initial series of "wear pattern tests"
  - Have new designs for higher pressures being fabricated
  - Have started tribopair work

- **What next**
  - Test higher pressure designs
  - Investigate ceramic brush seal bristle possibilities, as we go to higher temperatures

Test Results

* Bristle Stiffness versus Pressure

* Dynamic Test Leakage Data

    - Concentric Rotor

    - Eccentric Rotor

    - Radial Excursion

Flow Parameter, $\quad \Phi = \dfrac{\dot{m}\,\sqrt{T}}{p_u\,D_i}$

Test Results

Bristle Stiffness versus Pressure
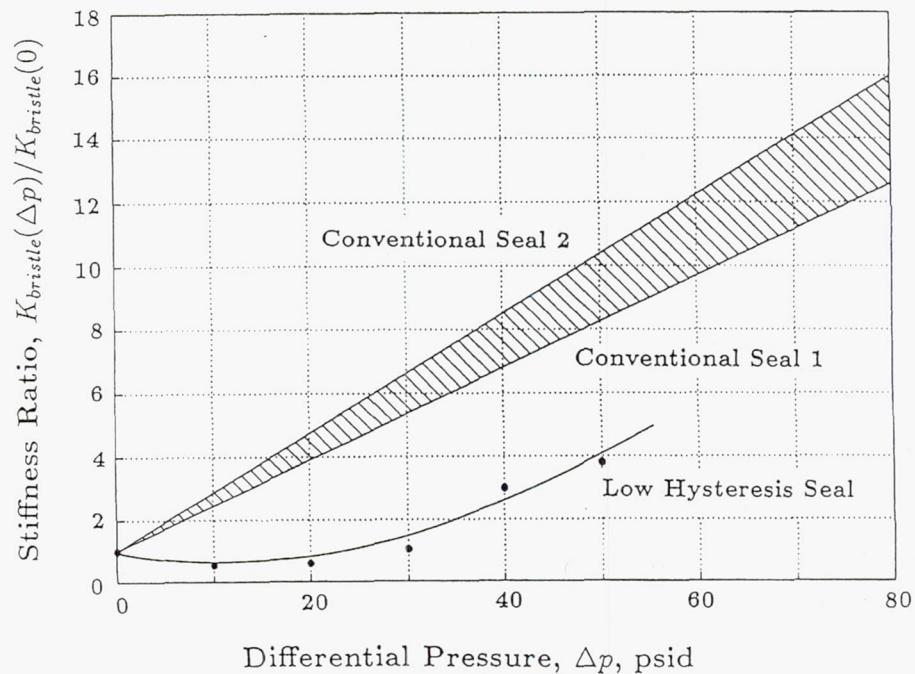
204

Test Results
Dynamic Test with Concentric Rotor

Conventional Seal

$\Delta P = 30$ psid

Chamber de-pressurized completely and then pressurized

Flow Parameter, $\Phi \times 1000$

Speed, RPM

Test Results
Dynamic Test with Concentric Rotor

Low Hysteresis Seal

$\Delta P = 30$ psid

Flow Parameter, $\Phi \times 1000$

Speed, RPM
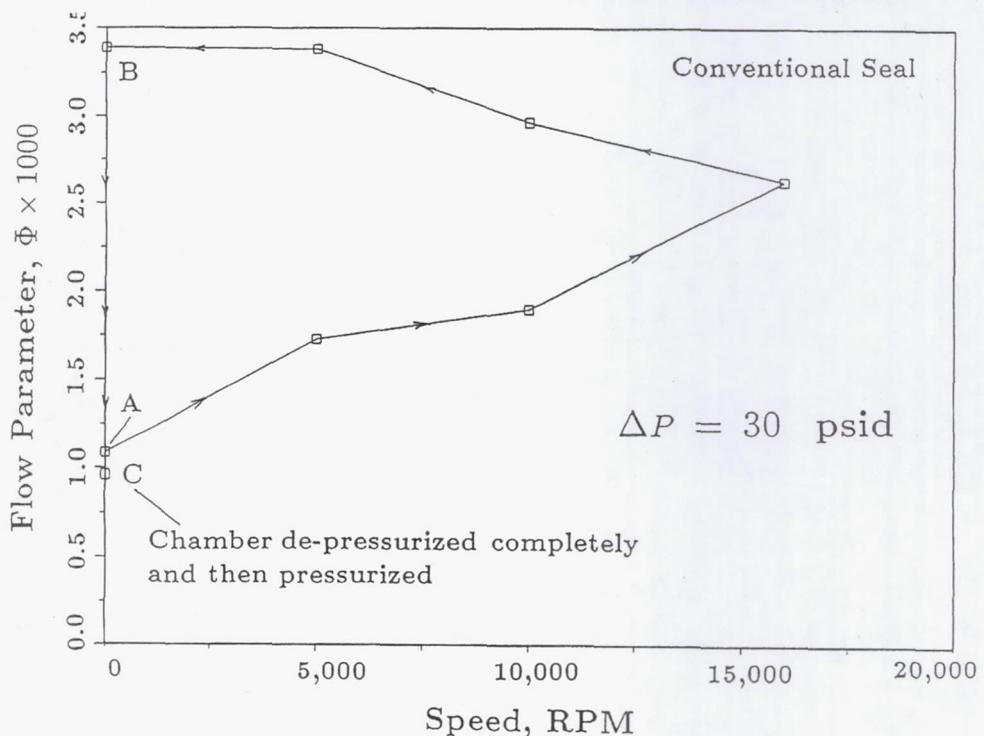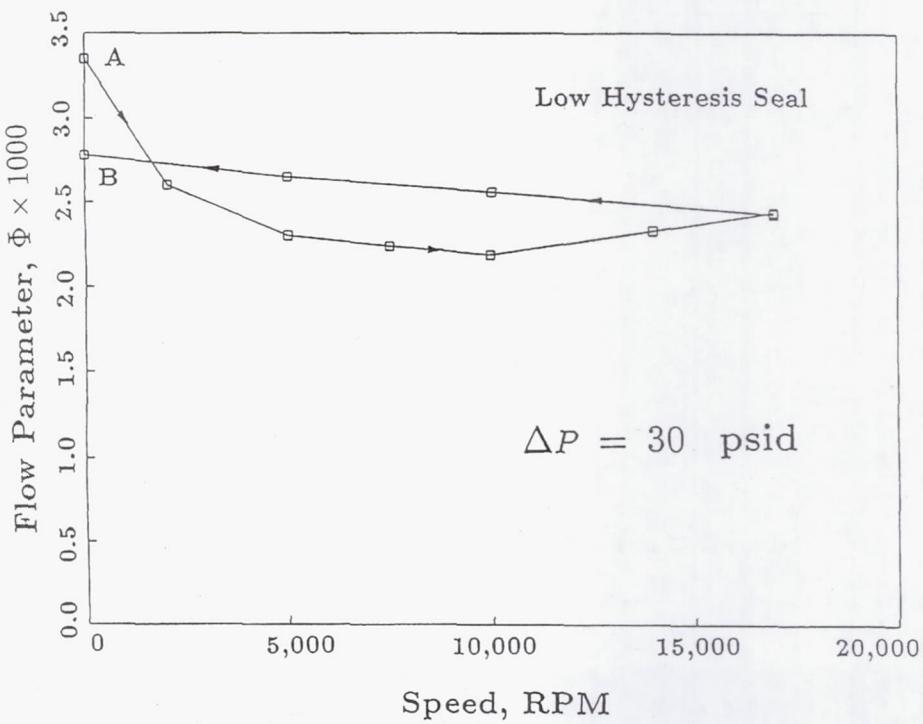
Dynamic Test with Radial Excursion

Flow Factor

Φ_L Φ_H Φ_H^*

Δ_r
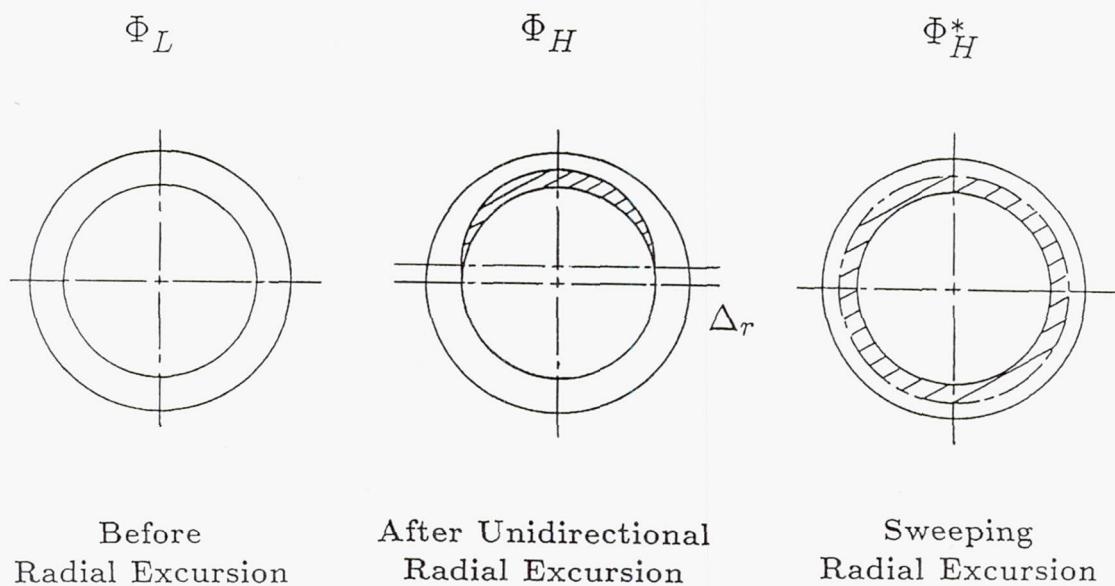
Before
Radial Excursion

After Unidirectional
Radial Excursion

Sweeping
Radial Excursion

Test Results

Dynamic Test with Radial Excursion

Conventional Seal

Φ_H^*

45-25 psid
450 °F
22,000 RPM

Φ_H

Φ_L

Flow Parameter, $\Phi \times 1000$

Excursion Cycles

206
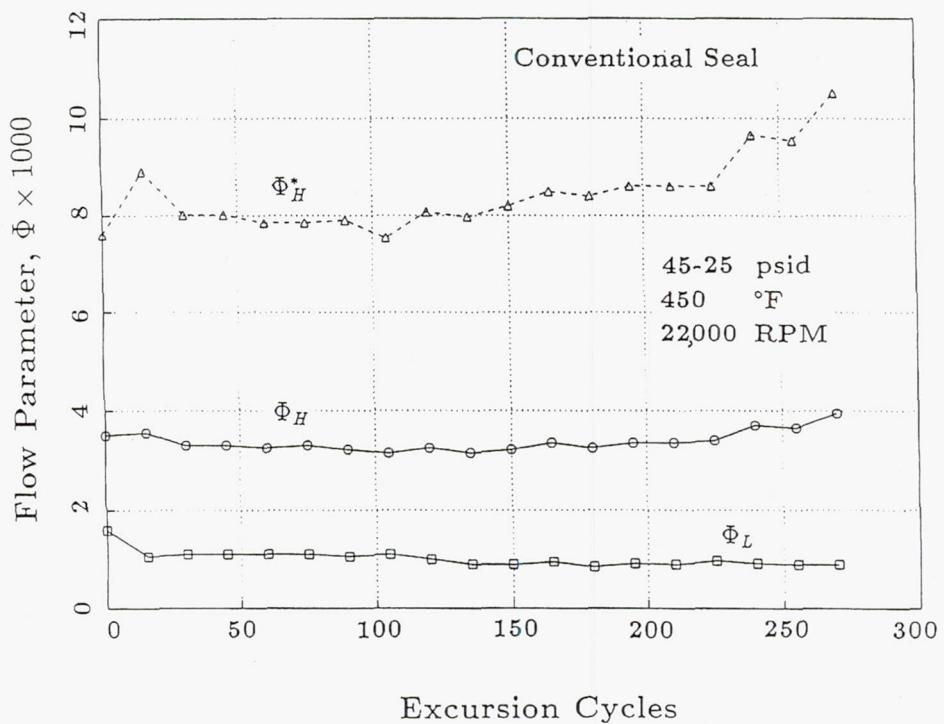
COMPUTER TOOLS FOR FACE SEAL ANALYSES DEVELOPED AT JOHN CRANE

Shifeng Wu
John Crane Inc.
Morton Grove, Illinois

PROGRAM PURPOSES

■ New product optimization

■ Existing seals on new application

■ Existing seals on off-duty conditions

■ Trouble-shooting

PROGRAM FUNCTIONS

■ Take into account the combined effects of pressure, temperature, speed, fluid sealed, materials and seal geometry on seal distortion, temperature distribution, operating film thickness, friction and leakage
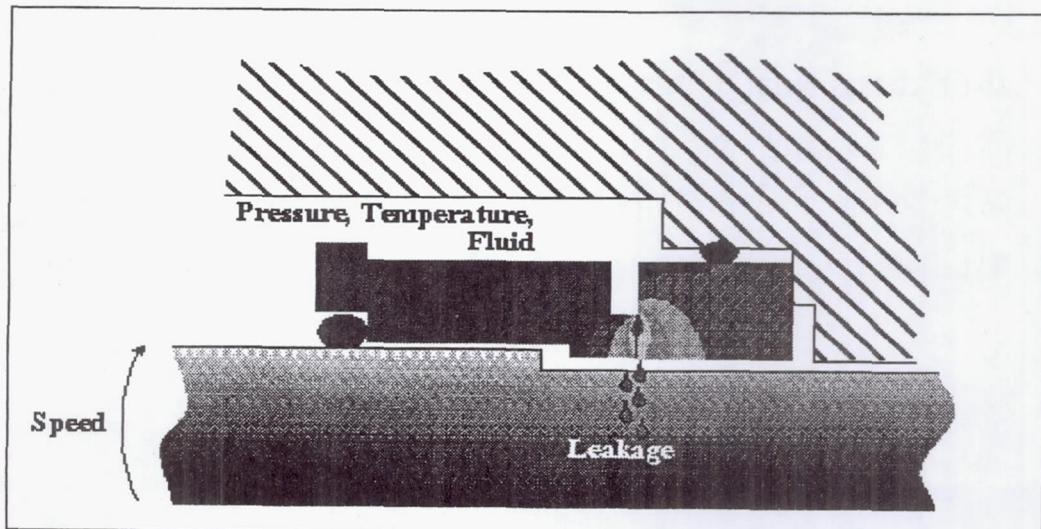
DIFFERENT CODES FOR DIFFERENT APPLICATIONS
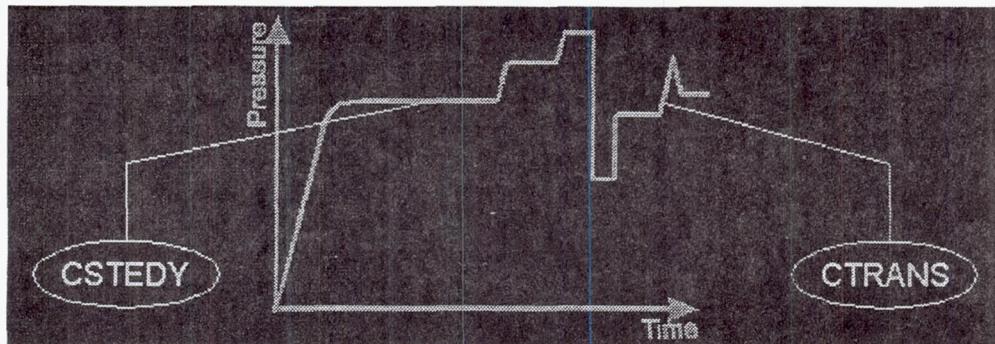
Steady-state	Transient
■ Steady-state	■ Transient
■ Liquids or gas	■ Liquids or gas
■ Conventional flat face	■ Conventional flat face
■ Active lift grooves	■ Active lift grooves

MAJOR ISSUES INVOLVED

■ Interface forces
- Wet seal
- Gas seal

■ Friction / Heat generation

■ Heat transfer / Axisymmetric temperature distribution

■ Axisymmetric pressure / Thermal distortion

■ Leakage

Test Results

Dynamic Test with Radial Excursion

Low Hysteresis Seal 1

30-25 psid
450 °F
22000 RPM

Φ_H^*

Φ_H

Φ_L

Φ_L^*

Flow Parameter, $\Phi \times 1000$

Excursion Cycles

Test Results

Dynamic Test with Radial Excursion

Low Hysteresis Seal 2

Φ_H

Φ_L

27 psid
550 °F
17000 RPM

Flow Parameter, $\Phi \times 1000$

Excursion Cycles

207
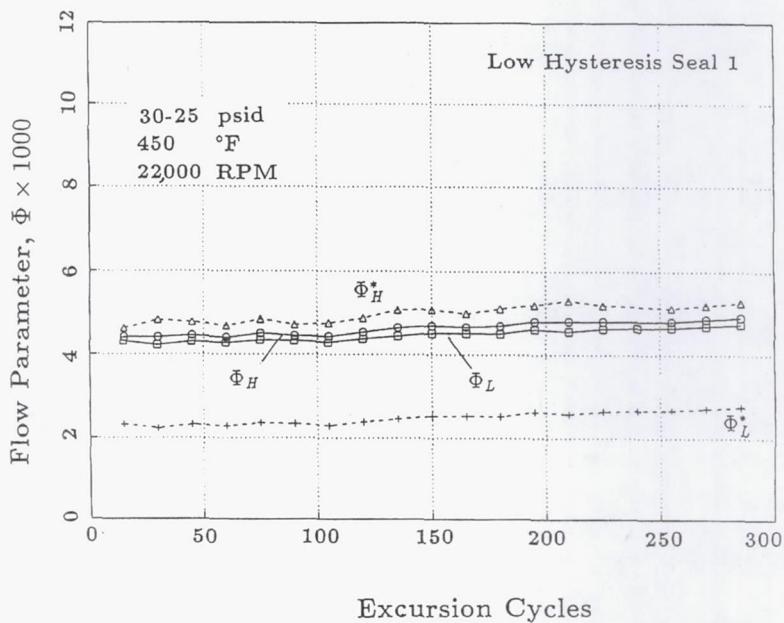
Conclusions

* Conventional Brush Seals

    - Hysteresis : Leakage

    - Bristle Stiffening : Life

* "Low Hysteresis" Brush Seal

    - Above Effects Considerably Reduced

    - Low Leakage over Operating Cycles

    - Potential for Longer Life

INTERFACE FORCES

■ **Force equilibrium**
  – Closing force = Opening force

■ **Hydrostatic pressure**
  – Single liquid phase/Gas film
  – Two phase liquid/vapor

■ **Hydrodynamic pressure**
  – Liquid phase
  – Periodic groove gas film

■ **Contact pressure**

FRICTION / HEAT GENERATION

■ **Viscous shearing**
  – Fluid shear in direction of sliding
  – Isoviscous through film thickness

■ **Asperity sliding**
  – Contact pressure
  – Boundary friction

HEAT TRANSFER / TEMPERATURE DISTRIBUTION

- ■ Heat source at interface only
- ■ Heat normally dissipated through seal components to the product
- ■ Thermal resistance
    - Fluid film negligible
    - Seal components (conduction)
    - Product boundary heat transfer coefficient (convection)
- ■ Axisymmetric temperature distribution

AXISYMMETRIC PRESSURE / THERMAL DISTORTION

- ■ Pressure distortion
    - Face distortion (toroidal, bending, local compression)
- ■ Thermal distortion
    - Face distortion (toroidal, local expansion)
    - Radial expansion
- ■ Centrifugal distortion
    - Distortion and stress significant at high speeds

LEAKAGE

■ Based on Poisseuille flow

$$Q \propto \frac{r \cdot h^3}{12 \cdot \mu} \cdot \frac{\partial P}{\partial r}$$

FULLY INTEGRATED SOLUTION
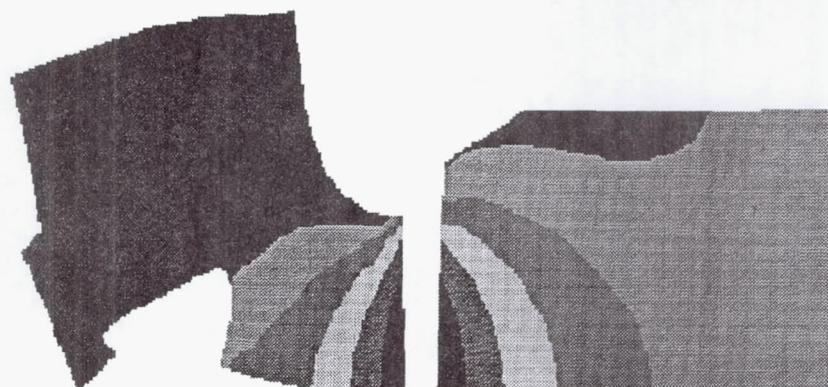
Leakage
Friction power

PROGRAM INTERFACE

Fluid Film Model 2

☒ Geometry   ☒ Mesher   ☒ Solver   ☒ View

                                         ◉ Cstedy1 [High]

                                         ○ Cstedy1 [Low]

                                         ○ Cstedy2 [High]

                                         ○ Cstedy2 [Low]

                                         ○ Cstedy3

Directory   c:\cstedyw   **Options :-**

Filename   *.J **Run Programmes As...**

ourdemo.j ◉ Interactive
t48 us1.j ○ Icons [Faster]
t48-us2.j **Calculate...**
t40-us3.j
[..]   ◉ Stress
[-a-]   ○ No Stress
[-c-]

        Ok   **Cancel**
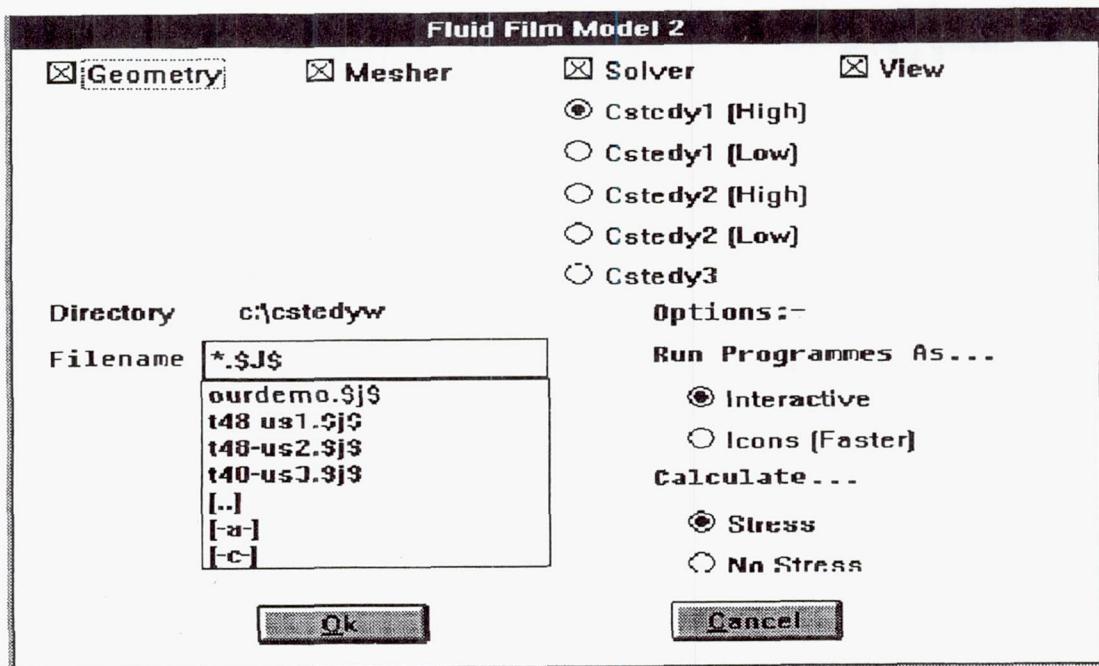
PROGRAM MODULES

■ **CSTEDY**

- Conventional face (no face grooves / hydropads)
- Liquid, vapor and 2-phase films
- Single and multi-component fluid database
- 2D generic face grooves (e.g. spiral grooves)
- Gas film

■ **CTRANS**

- Transient loading and speed
- Liquid or gas films

SOLUTION OUTPUT

- Temperatures
- Distortions
- Film thickness
- Leakage
- Heat generation
- Interface pressures
- Stresses

A CSTEDY EXAMPLE

Po = 500 psia
68 °F
Propane

Carbon Graphite

3600 rpm

Silicon Carbide

Stationary

Ro = 2.033 in
Ri = 1.846 in
σ = 4 μ in
f = 0.10

Pi = 14.7 psia
68 °F
Atmosphere
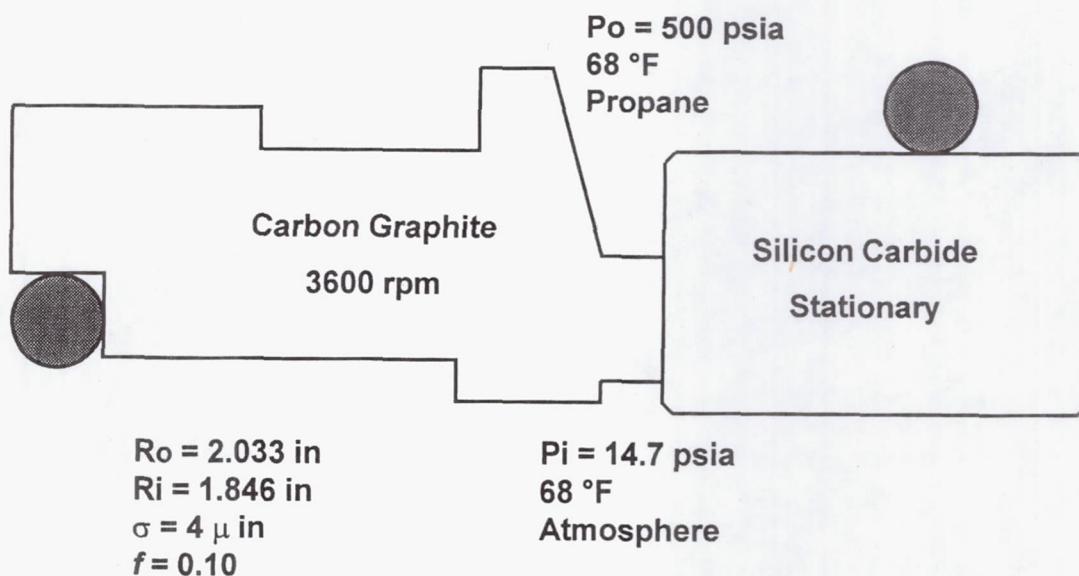
AUTOMESH
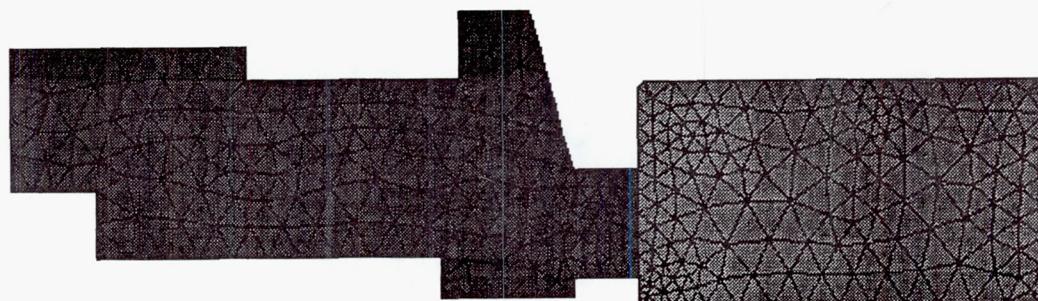
DISTORTION, LEAKAGE AND
TEMPERATURE CONTOUR

Thermal Taper: + 101.6 µRadians
Pressure Taper: - 108.8 µRadians
Total Radial Taper: - 7.2 µRadians

3.56 g/hr

68 106 144 182 219 257 295 333 (°F)
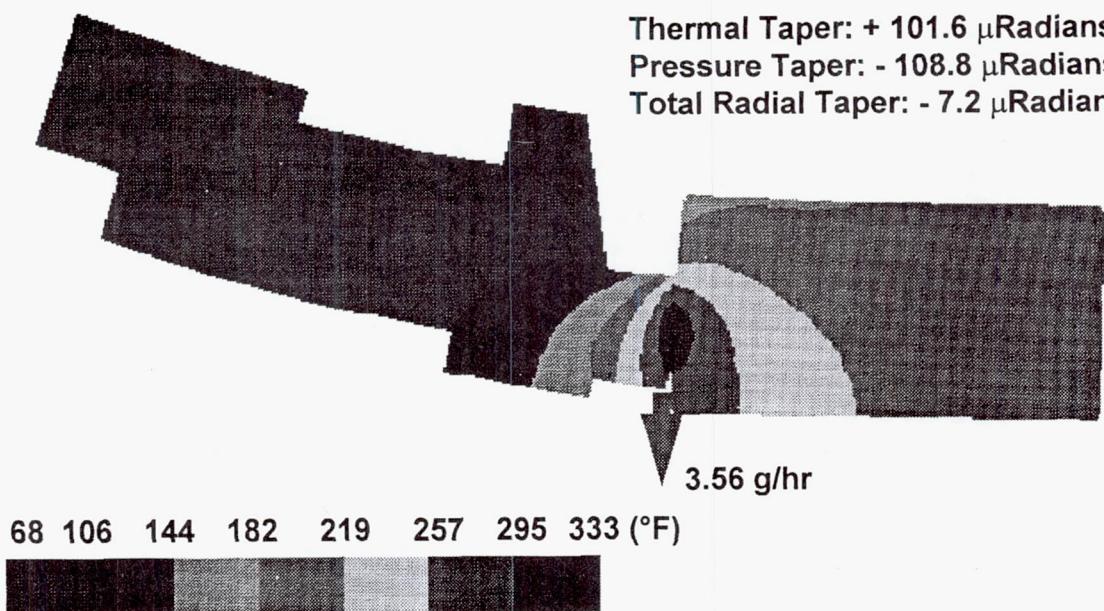
FILM THICKNESS DISTRIBUTION
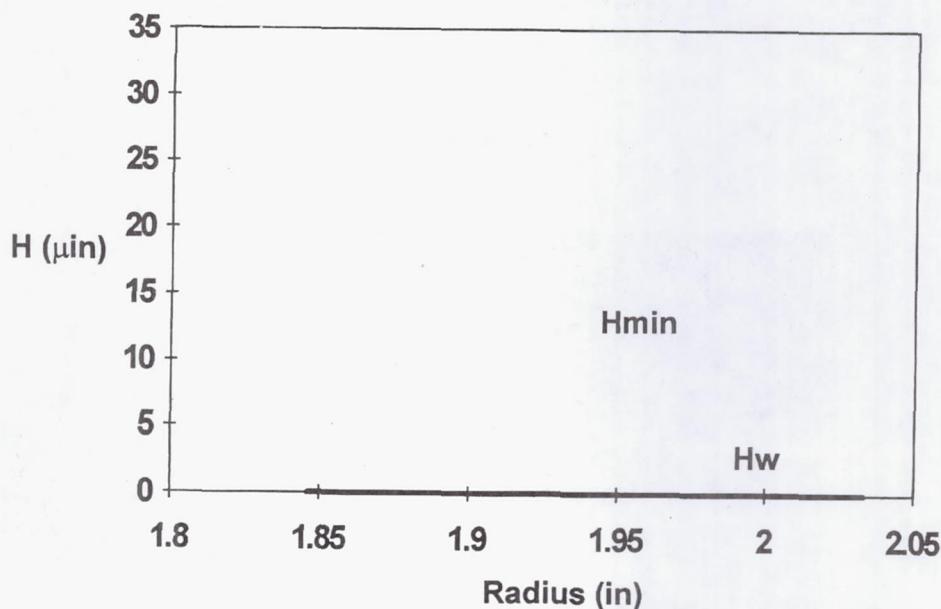
INTERFACE PRESSURE DISTRIBUTIONS
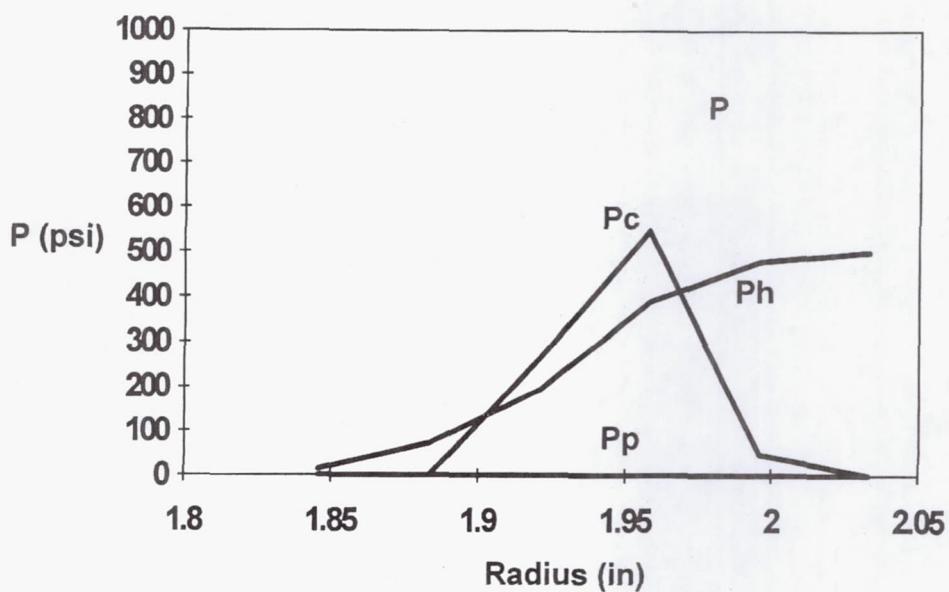
STRESS CONTOUR (P.R.)

Hoop Stress

-4.2 -3.7 -3.2 -2.7 -2.3 -1.8 -1.3 -0.8 (kpsi)
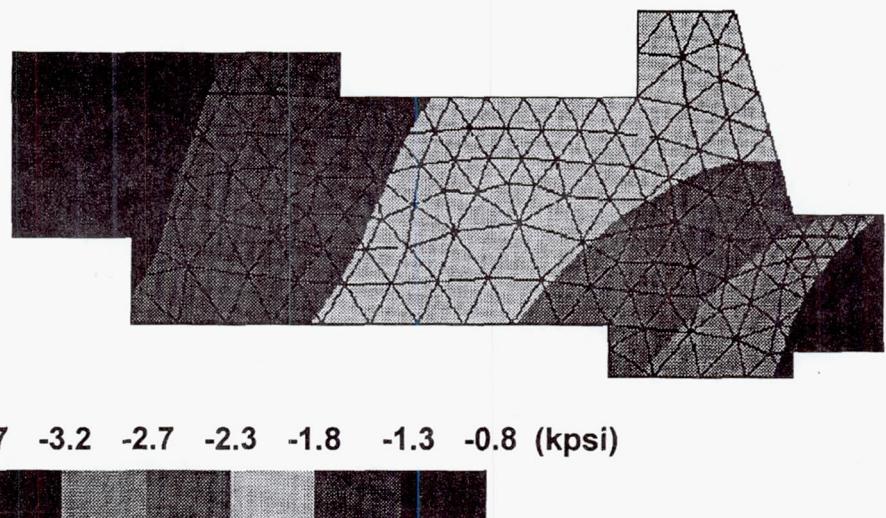
STRESS CONTOUR (M.R.)

Hoop Stress

-1.3 1.9 5.2 8.5 11.8 15.1 18.4 21.7 (kpsi)
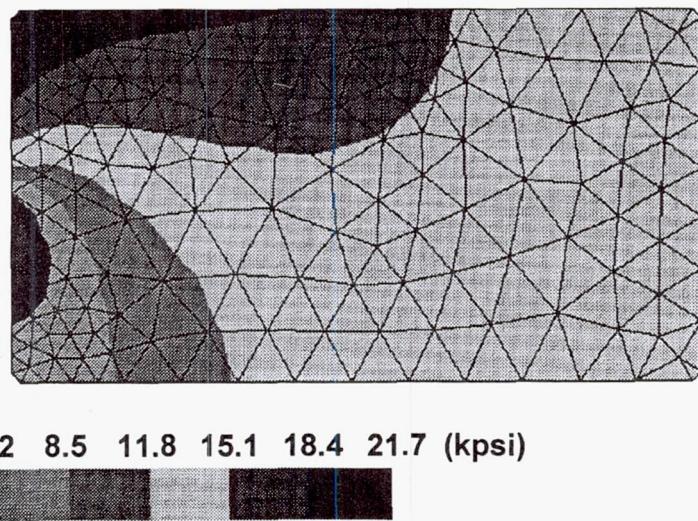
COMPRESSOR DISCHARGE FILM RIDING FACE SEALS

John Munson
Allison Gas Turbine
Indianapolis, Indiana

SEALS EXAMINED

1. 8 PAD RAYLEIGH - STEP

2. TAPERED SPIRAL - GROOVE

   ° 3 TAPERS

3. HYDROSTATIC

   ° INHERENTLY COMPENSATED

   ° ORIFICE COMPENSATED WITH RECESS

CIRCUMFERENTIAL GROOVE CONFIGURATION

SPIRAL - GROOVE PARAMETERS

Direction of Rotation
Providing Pumping
Grooves Rotate

Land Width

Groove Width

R_m R_i

R_o
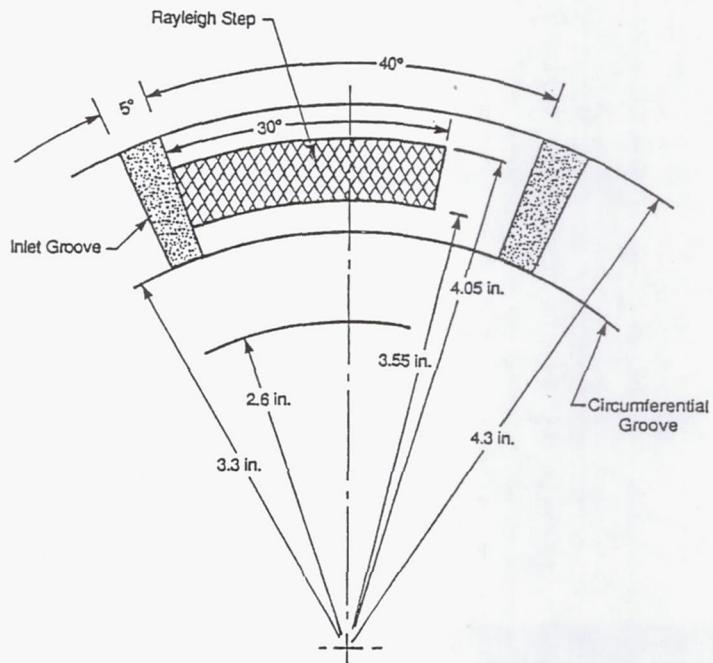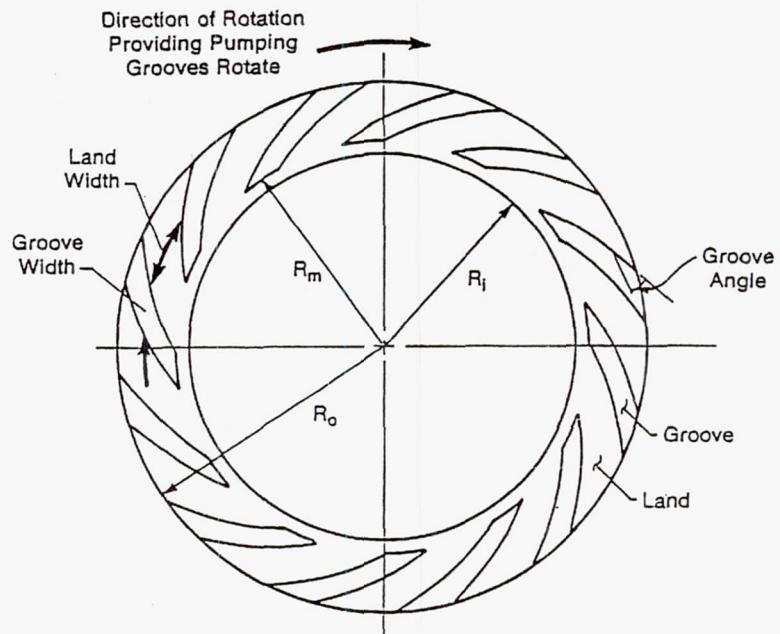
Groove Angle

Groove

Land

Groove Angle $= \alpha$
Groove Depth $=$ GD
Land Width/Groove Width $= \gamma$

$A = \pi d\, h$

INHERENT COMPENSATION

$A = \pi d^2 / 4$

ORIFICE COMPENSATION
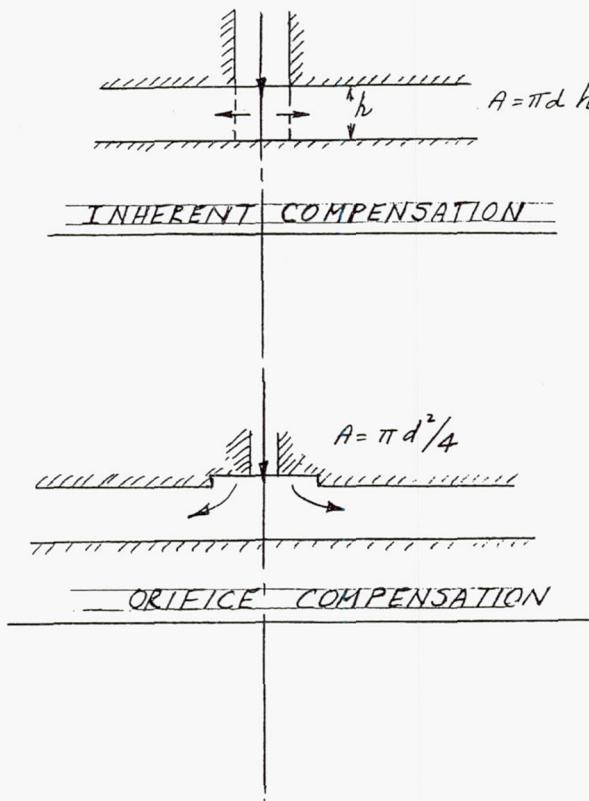
COMMON CONDITIONS

o	GAS TEMPERATURE	$1200^{\circ}F$
o	GAS CONSTANT	$247,420\ in^2/s^2\text{-}^{\circ}R$
o	SPECIFIC HEAT RATIO	1.342
o	VISCOSITY	$5.82\times10^{-9}\ lb\text{-}s/in^2$
o	SPEED	30,000 RPM
o	HIGH PRESSURE	650 PSIG
o	LOW PRESSURE	100 PSIG

PERFORMANCE PARAMETERS PRODUCED AS A FUNCTION OF FILM THICKNESS

o   LEAKAGE

o   STIFFNESS

o   VISCOUS POWER LOSS

o   HYDROSTATIC PRESSURE RATIO

o   ALSO LOOKED AT:

    o   LOAD CAPACITY

    o   ADIABATIC TEMPERATURE RISE

Comparision, Ro=4.3 in, Ri=3.3 in

Stiffness, lb/in x 10-06 vs Film Thickness, mils

+ Rayleigh Step
x Spiral Groove
□ IC Hydrostatic
■ Recess

Comparision, Ro=4.3 in, Ri=3.3 in

Leakage, SCFM vs Film Thickness, mils

+ Rayleigh Step
x Spiral Groove
□ IC Hydrostatic
■ Recess
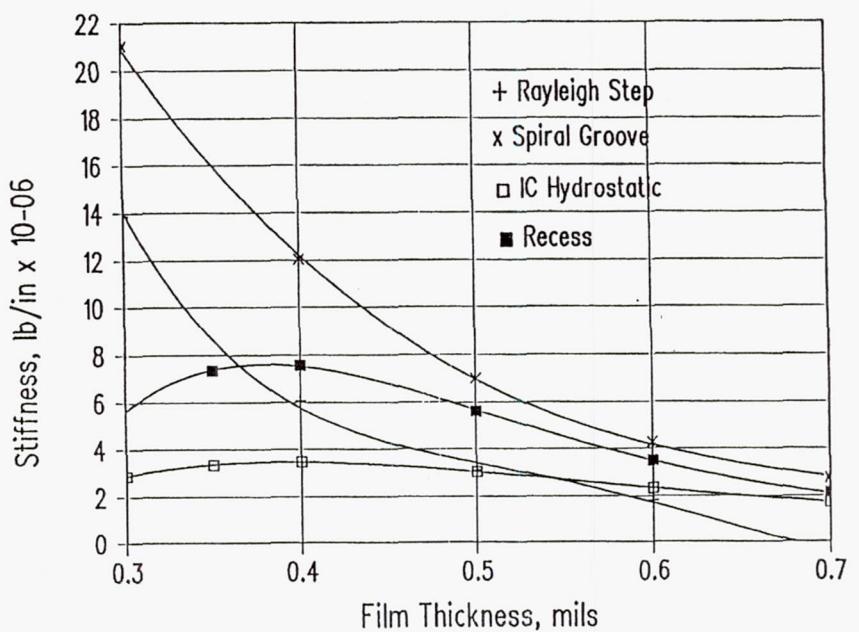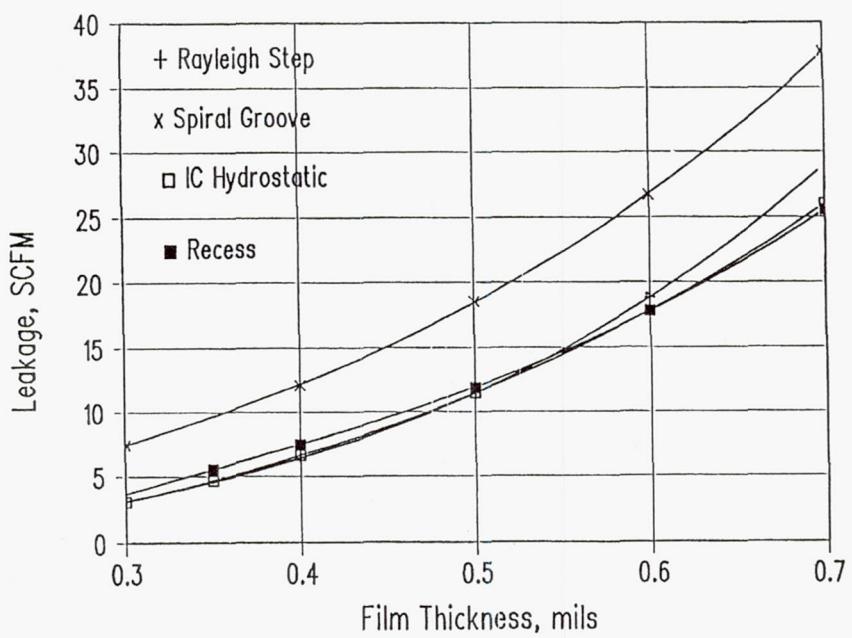
CONCLUSIONS AND RECOMMENDATIONS

o   SPIRAL-GROOVE CONFIGURATION IS PREFERRED CHOICE BECAUSE
     OF SUPERIOR STIFFNESS.

o   SECOND CHOICE IS RAYLEIGH-STEP BECAUSE OF COMBINED HIGHER
     OPERATING FILM THICKNESS AND GOOD STIFFNESS AT LOW CLEARANCE.

o   RECESS HYDROSTATIC HAS REASONABLE PERFORMANCE, BUT STIFFNESS
     FALLS OFF AT LOW CLEARANCE. ALSO, PNEUMATIC HAMMER CHARACTERIS-
     TICS MUST BE INVESTIGATED. EXPERIENCE AT HIGH PRESSURE RATIOS IS
     LIMITED. AN ADVANTAGE IS THAT IT WOULD HAVE GOOD LOW SPEED
     PERFORMANCE. IT MAY BE A GOOD COMPRISE SECOND CHOICE, BECAUSE IT
     OFFERS AN ALTERNATIVE TO A STRICTLY HYDRODYNAMIC CONFIGURATION.

Final Design Parameters For Experimental Seals

	Spiral Groove	Rayleigh Step Pad
Mating Ring OD	7.280 - 7.285	7.280 - 7.285
Pad OD	-	7.030
Pad ID	-	6.470
SG ID	5.940	-
SG angle (deg)	19°	-
No. Grooves/Pads	15	8
Nom. Groove Depth	0.0010 - 0.0015	.002 - .004
Primary Ring OD	6.750	7.600
Primary Ring ID	5.660	5.660
Seal Balance Dia.	5.840	5.981
Secondary Seal Type	3 Ring Circumferential	Piston Ring
Materials		
Mating Ring	INCO 718 Cr2C3 wear face	INCO 718 PS212 wear face
Primary Ring	α – Silicon Carbide carbon / graphite	α – Silicon Carbide carbon / graphite
Secondary Seal	CJPS	CJPS
Housing	INCO 718	INCO 718
Springs	INCO 750-X	INCO 750-X

Control of both Circumferential & Radial Face Flatness Effects Seal Performance

Performance is Reflected in Breakaway Torque Measurements

Spiral Groove Seals
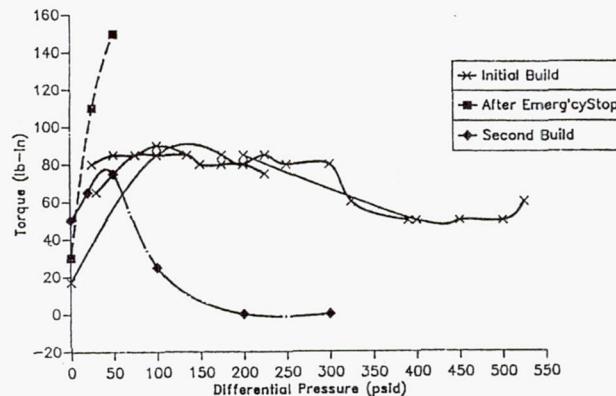
Rayleigh Step Pad Seal
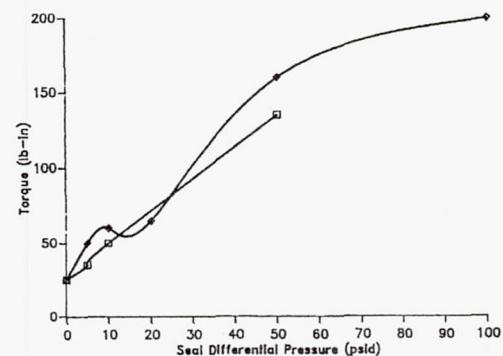
Test Results for Spiral Groove Seal
400 psid Test Results
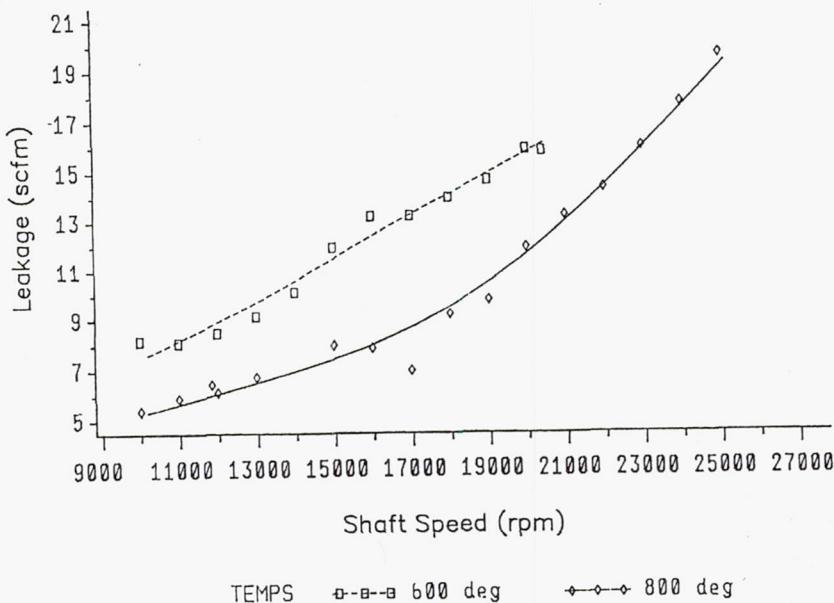
Test Results for Spiral Groove Seal
400 psid Test Results
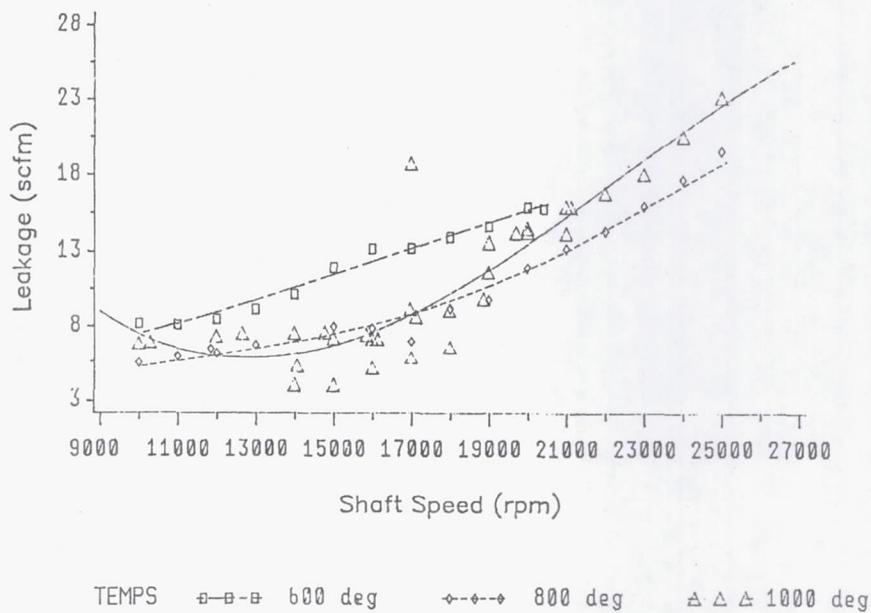
Test Results for Rayleigh Step Pad Seal
20000 rpm Test Results

Seal Starting Characteristics
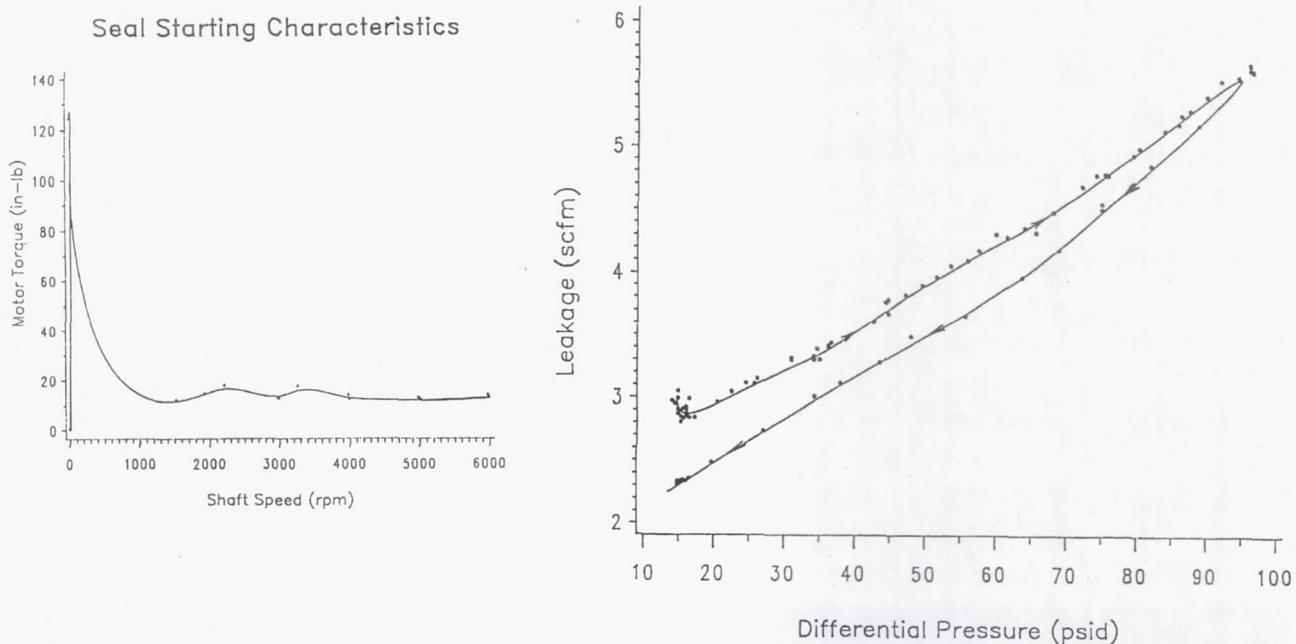
Low Leakage of FRFS will provide substantial reduction in cycle specific fuel consumption:
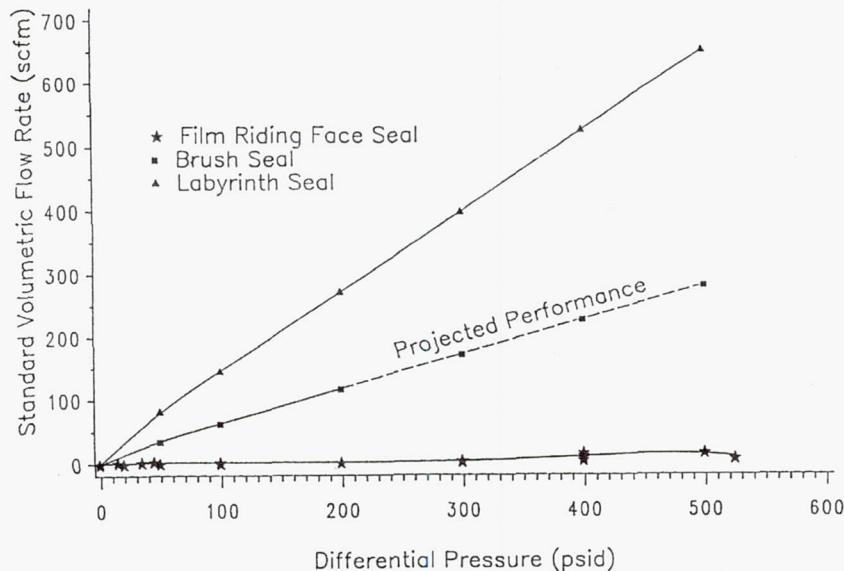
- 1.5% relative to Labyrinth seal system
- 0.5% relative to Projected multi-stage brush seal

Conclusions

- Both seals operated as designed after lift-off had been acheived

- No particular reason to favor either the spiral groove, or Rayleigh step pad design over the other

- Windage may need to be addressed in engine design

- Measured seal leakage very close to design goal of 10 scfm

- Hydrodynamic seals can operate succesfully at either low, or high ΔP

- Seal face taper has strong effect on seal performance

- Analytical design methodology has been proven

AIR FORCE SEAL ACTIVITIES

Ellen R. Mayhew
Aero Propulsion & Power Directorate
Wright Laboratory
Wright-Patterson Air Force Base, Ohio

Seal technology development is an important part of the Air Force's participation in the Integrated High Performance Turbine Engine Technology (IHPTET) initiative, the joint DOD, NASA, ARPA, and industry endeavor to double turbine engine capabilities by the turn of the century. Significant performance and efficiency improvements can be obtained through reducing internal flow system leakage, but seal environment requirements continue to become more extreme as the engine thermodynamic cycles advance towards these IHPTET goals. Brush seal technology continues to be pursued by the Air Force to reduce leakage at the required conditions. Likewise, challenges in engine mainshaft air/oil seals are also being addressed. Counter-rotating intershaft applications within the IHPTET initiative involve very high rubbing velocities. This presentation briefly describes past and current seal research and development programs and gives a summary of seal applications in demonstrator and developmental engine testing.

OUTLINE

* INTRODUCTION - INTEGRATED HIGH PERFORMANCE TURBINE ENGINE TECHNOLOGY (IHPTET) INITIATIVE

* SECONDARY GAS PATH SEALS
  - PAST R&D PROGRAMS
  - CURRENT R&D PROGRAMS
  - DEMONSTRATOR ENGINE APPLICATIONS
  - F119 ENGINE APPLICATIONS

* MAINSHAFT AIR/OIL SEALS
  - PAST R&D PROGRAM
  - CURRENT R&D PROGRAM
  - DEMONSTRATOR ENGINE APPLICATIONS

* TECHNOLOGIES OF FUTURE INTEREST

* SUMMARY

IHPTET INITIATIVE

* GOAL: DOUBLE TURBINE ENGINE PROPULSION CAPABILITY BY THE
  TURN OF THE CENTURY

  - FIGHTER/ATTACK ENGINE GOALS:
    - FN/WT   + 100%
    - FUEL CONSUMPTION   - 40%
  - SIMILAR TURBOSHAFT/PROP AND EXPENDABLE ENGINE GOALS

* SIGNIFICANT SECONDARY FLOW IMPACT ON ENGINE PERFORMANCE
  - HPC: EFF +4.4% ==>   TIT -85F   OR   FN +7.6%
  - HPT: EFF +4.2% ==>   TIT -93F   OR   FN +9.7%
  - REDUCE/ELIMINATE LPT COOLING AIR

* SECONDARY FLOWS GROUPED UNDER COMPRESSOR TECHNOLOGY
  - GOAL OF 60% LEAKAGE REDUCTION
  - NEARLY 20% HPC T/W , 10% HPC FUEL BURN OBJECTIVES

* MAINSHAFT SEAL TECHNOLOGY FOR SHAFT SPEED REQUIREMENTS
  - GOAL OF 50% SPEED INCREASE

SECONDARY GAS PATH SEALS
PAST R&D PROGRAMS

* TEXAS A&M: BRUSH SEAL ROTORDYNAMICS

  - LAST STAGE OF SEAL GROUP DEVELOPS HIGHER DELTA P
  - LEAKAGE INCREASES SLIGHTLY WITH INLET TANGENTIAL
    VELOCITY

  - CROSS-COUPLED STIFFNESS COEFFICIENT VERY STABLE
  - EXTREMELY STABLE WHIRL FREQUENCY RATIO
  - ROTORDYNAMICS INDEPENDENT OF SEAL SPACING/INLET
    TANGENTIAL VELOCITY
  - HOWEVER, BRUSH SEAL DIRECT DAMPING IS LESS THAN LAB SEAL

  - BRUSH SEAL WILL GENERALLY IMPROVE ROTOR DYNAMIC
    CHARACTERISTICS IF LAB SEAL IS DESTABILIZING THE ROTOR DUE
    TO FLUID PRESWIRL
      - LOWER DAMPING OF BRUSH SEALS MUST ALSO BE
        CONSIDERED

  - REPORT #: WL-TR -92-2125 (REVISED)

SECONDARY GAS PATH SEALS
PAST R&D PROGRAMS

• EG&G FCTG: BRUSH SEAL DEVELOPMENT PROGRAM

- BRISTLE ANGLE, LENGTH, STIFFNESS, STAGING, PACKWIDTH
  EFFECTS ON HYSTERESIS, DELTA P, LEAKAGE; TRIBOPAIR WEAR

- INCREASED PACKWIDTH GAVE HIGHER DELTA P/LOWER LEAKAGE

- MULTIPLE STAGE BRUSH SEAL PERFORMANCE
   - LEAKAGE REDUCTION
   - UNEQUAL PRESSURE DISTRIBUTION
      - CONTROL WITH MIXED PACKWIDTHS/STIFFNESSES
      - HIGHER PACKWIDTH SEALS MOST EFFECTIVE

- LOW FRICTION/WEAR/OXIDATION TRIBOPAIRS IDENTIFIED

- TESTING VERIFIED REDUCED HYSTERESIS IN ADVANCED DESIGNS

- FULL SCALE HARDWARE DELIVERED FOR DEMO ENGINE TEST

- REPORT #: WL-TR-93-2029 (DESIGN GUIDE)
- REPORT #: WL-TR-93-2064 (FINAL REPORT)

SECONDARY GAS PATH SEALS
CURRENT PROGRAMS

• EG&G FCTG
   - ADVANCED BRUSH SEAL DEVELOPMENT
     PROGRAM

• PRATT & WHITNEY
   - HIGH SPEED BRUSH SEAL DEVELOPMENT
     PROGRAM

• TECHNETICS CORPORATION
   - CERAMIC BRUSH SEALS

ADVANCED BRUSH SEAL DEVELOPMENT PROGRAM
EG&G FCTG

* OBJECTIVE: DEVELOP A COMPREHENSIVE DESIGN METHODOLOGY FOR APPLICATION OF ADVANCED, HIGH PERFORMANCE BRUSH SEALS IN MAN-RATED ENGINES

* APPROACH:
    - EXPERIMENTAL/CFD CHARACTERIZATION OF SEAL DESIGN
        - MAXIMIZE SINGLE- AND MULTI-STAGE DELTA P CAPABILITY
        - ACCOMMODATE LARGE AXIAL AND RADIAL EXCURSIONS
        - EVALUATE NON-CONTACTING BRUSH SEAL FEASIBILITY
    - TRIBOPAIR TESTING AND EVALUATION AT ELEVATED CONDITIONS

* ACCOMPLISHMENTS:
    - INITIAL WEAR TESTING OF "LOW HYSTERESIS" DESIGNS SUCCESSFUL
        - INITIAL TESTING TOWARD ACCOMMODATION OF EXCURSIONS
        - HIGH SPEED TESTING THIS MONTH
    - FOUR HIGH PRESSURE SEAL DESIGNS BEING FABRICATED
    - BRISTLE MOVEMENT/HYSTERESIS OBSERVED IN OPTICAL VIEWING
    - CFD MODELING OF BRISTLE TIP LIFT-OFF IN PROGRESS

HIGH SPEED BRUSH SEAL DEVELOPMENT PROGRAM
PRATT & WHITNEY

* OBJECTIVE: DEMONSTRATE HIGH-SPEED AND HIGH-TEMPERATURE OPERATION OF ADVANCED BRUSH SEALS FOR IHPTET PHASE II DEMONSTRATOR ENGINES

* APPROACH:
    - APPLICATION STUDY OF IHPTET PHASE II ENGINE/MISSION FLIGHT CYCLE FOR SURFACE SPEED AND TEMPERATURE REQUIREMENTS
    - DESIGN/FABRICATE/RIG TEST BRUSH SEALS TO VERIFY THEIR CAPABILITY TO OPERATE AT IHPTET PHASE II CONDITIONS

* ACCOMPLISHMENTS:
    - APPLICATION STUDY COMPLETED
    - PRELIMINARY DESIGN OF BRUSH SEAL CONCEPTS COMPLETED
    - RIG ADAPTIVE HARDWARE DESIGN IN PROGRESS

CERAMIC BRUSH SEALS
TECHNETICS CORPORATION

* OBJECTIVE: DEVELOP "HYBRID" CERAMIC BRISTLE/METALLIC HOLDER
  BRUSH SEALS FOR GAS TURBINE ENGINES CAPABLE OF OPERATING
  AT IHPTET PHASE II AND PHASE III TEMPERATURES

* APPROACH:
    - PERFECT THE MANUFACTURING METHODS OF THE "HYBRID" SEAL
    - CONDUCT RIG TESTING FOR PERFORMANCE, ROTORDYNAMICS,
      AND WEAR
    - FABRICATE HYBRID SEAL FOR TEST IN A DEMONSTRATOR ENGINE

* PROGRESS:
    - NEW START

SECONDARY GAS PATH SEALS
DEMONSTRATOR ENGINE BRUSH SEALS

* TESTING TO DATE
    - TURBINE AND COMPRESSOR APPLICATIONS
    - HAYNES 25 BRISTLES
    - CHROME CARBIDE OR ALUMINUM OXIDE COATINGS
    - 20-80% REDUCTION IN LEAKAGE OVER LAB SEALS
    - GENERALLY GOOD DURABILITY

* FUTURE TESTING
    - PLANNED FOR ALL DEMO ENGINES (ATEGG, JTDE, JTAGG, JETEC)
    - HIGHER SURFACE SPEEDS, TEMPERATURES
    - EXPANDED ARRAY OF BRISTLE AND COATING MATERIALS
    - ADVANCED CONFIGURATIONS

SECONDARY GAS PATH SEALS
F119 ENGINE BRUSH SEALS

* INITIAL FLIGHT RELEASE
  - 4 STATIC SEALS

* FULL FLIGHT RELEASE
  - HPT (3 LOCATIONS)
  - LPT (4 LOCATIONS)
  - COMPRESSOR DISCHARGE LOCATION

MAINSHAFT AIR/OIL SEALS
PAST R&D PROGRAM

* PRATT & WHITNEY: HIGH SPEED SEAL DEVELOPMENT

  - MODIFIED CONTROLLED GAP CLEARANCE SEAL

  - 1200 FT/SEC PITCH LINE VELOCITY DEMONSTRATED
  - 60 PSID, 450 F
  - AIR LEAKAGE AS LOW AS 54 LBS/HR AT 1050 FT/SEC, 50 PSID
  - SUCCESSFUL 80 HR ENDURANCE TEST WITH VERY LITTLE WEAR

  - REPORT #: WL-TR-92-2102

MAINSHAFT AIR/OIL SEALS
CURRENT PROGRAM

GENERAL ELECTRIC: MAINSHAFT AIR/OIL SEAL PROGRAM

- OBJECTIVE: DEVELOP AN INTERSHAFT SEAL FOR IHPTET PHASE II
  DEMONSTRATOR ENGINE CONDITIONS (900 FPS/900F/50 PSID)

- APPROACH:
  - ESTABLISH PHYSICAL/TRIBOLOGICAL CHARACTERISTICS OF SEAL
    MATERIALS
  - SELECT BEST MATERIALS FOR APPLICATION
  - DESIGN/FABRICATE/RIG TEST AT IHPTET PHASE II CONDITIONS

- ACCOMPLISHMENTS:
  - HIGH STRENGTH CARBON/CARBON COMPOSITES AND
    METALLIC/CERAMIC PAIRS CHARACTERIZED
  - CARBON COMPOSITE MATERIAL CHOSEN
  - DETAILED SEAL DESIGNS COMPLETED
    - HYDROSTATIC GAS BEARING SUPPORTED, CONTINUOUS RING
      CONFIGURATION
  - SEALS FABRICATED/RIG TESTING IN PROGRESS

MAINSHAFT SEALS

DEMONSTRATOR ENGINE APPLICATIONS

- BOTH PROGRAMS TRANSITIONING DIRECTLY INTO THEIR RESPECTIVE
  CONTRACTOR'S DEMONSTRATOR ENGINE PROGRAMS

SUMMARY

* AF COMMITTED TO DEVELOPING AND TRANSITIONING SEAL TECHNOLOGY

* PUSHING FOR INCORPORATION OF ADVANCED SEAL TECHNOLOGY IN ALL DEMONSTRATOR ENGINES

* WORKING WITH PROGRAM OFFICES TO TRANSITION SEAL TECHNOLOGY TO OPERATIONAL AND DEVELOPMENT ENGINES

FUTURE TECHNOLOGIES

* SECONDARY GAS PATH SEALS:

  - RUB-TOLERANT BRUSH SEAL BACKPLATES
    - NO CATASTROPHIC RUNNER DAMAGE DUE TO BACKPLATE CONTACT IN PRIMARY OR SECONDARY FAILURE EVENTS
    - SOME PROPRIETARY/PATENTED CONCEPTS AVAILABLE
    - INCREASED AF ATTENTION IN THIS AREA
  - INCREASED TEMPERATURE REQUIREMENTS
    - ALL-CERAMIC BRUSH SEALS/ADVANCED COATINGS
  - NON-CONTACTING SEALS
    - NON-CONTACTING BRUSH SEALS
    - OTHERS
  - BRUSH SEAL COMPRESSOR SHROUD (PRIMARY GAS PATH)
    - BLADE TIP LEAKAGE REDUCTION FOR INCREASED EFFICIENCY
    - BLADE DAMPING AUGMENTATION
    - STALL MARGIN IMPROVEMENT

* MAINSHAFT SEALS:

  - INCREASED SPEED AND TEMPERATURE REQUIREMENTS
    - CERAMICS
    - NON-CONTACTING GAS-BEARING FEATURES FOR DURABILITY

Jean B. Panos
GM Electro-Motive
Lagrange, Illinois

HIGH SPEED SEAL/BEARING RIG AGENDA

BACKGROUND

PROJECT STATUS

FACILITY FEATURES

RIG CAPABILITIES

EMD ADVANTAGES

FUTURE OPPORTUNITIES

HIGH SPEED SEAL/BEARING RIG BACKGROUND

- **PRIMARY GOAL:** Off—Turbo Measurement of Parasitic Power Losses

- **SECONDARY GOAL:** Validation of Seal and Bearing Calculation Techniques

- **Provide Quick Turnaround Test Bed for Prototype Designs**

- **Design Verification and Continuous Improvement**

- **(Rotor Dynamics Studies Done in Separate Test Facility)**

HIGH SPEED SEAL/BEARING RIG
PROJECT STATUS

AUGUST 1991	**Preliminary Design/ Specification Begins**
JULY 1992	**Contractor Design Begins**
AUGUST 1993	**Installation at EMD Begins**
TODAY	**Checkout/Demo Phase Add-On Modules in Process Inquiries Invited**

HIGH SPEED SEAL/BEARING RIG
FACILITY FEATURES

PRIME MOVER	VFD Controlled 42 HP 28000 RPM Motor
MODULAR SETUP	Separate Test Article Housing Two Independent Lube Systems
AXIAL POSITIONING AT SPEED	Stepper Motor .001" Increments
DATA ACQUISITION	Fluke 2286 With Toshiba EX40 PLC

HIGH SPEED SEAL/BEARING RIG
TEST RIG CAPABILITIES

SEAL CHAMBERS	3 Separately Controlled for Pressure and Temperature
AIR FLOW	100 SCFM to 35 PSIG and 300 F 100 SCFM to 5 PSIG and 600 F
TEST OIL	12 GPM TO 100 PSIG AND 260 F
IN-LINE TORQUE METER	100 LB-IN
RADIAL LOADS	200 LB
AXIAL LOADS	TO 5000 LB

HIGH SPEED SEAL/BEARING RIG
CAPABILITIES, CONTD.

FEATURE	CURRENT DIMENSION	GROWTH TO
BEARING BORES	TO 3"	5-6"
BEARING LENGTH	TO 3"	5-6"
THRUST BEARING OD	TO 7"	13"
SEAL BORE	TO 13"	15"

NEW MODULES POSSIBLE - CASE BY CASE

HIGH SPEED SEAL/BEARING RIG EMD TESTING ADVANTAGES

- Save Capital $ and Startup Costs

- 30 Years EMD Turbo Experience

- Pragmatic Approach – Development Oriented

- Try Out Experimental Designs Without Compromising a Costly Assembly

- Design of Experiments –– Optimize Parameters

- Minimize Mechanical Losses

HIGH SPEED SEAL/BEARING RIG FUTURE OPPORTUNITIES

- Upgrade Prime Mover for Other Applications

- Higher Air Temperatures Based on Safety

- Increase Radial Loads at Lower Speeds

- Upgrade to PC–Based Data Acquisition System

- <u>WE CAN HELP YOU VALIDATE YOUR DESIGN !</u>

HYPERSONIC ENGINE SEAL DEVELOPMENT AT NASA LEWIS RESEARCH CENTER

Bruce M. Steinetz
NASA Lewis Research Center
Cleveland, Ohio

NASA Lewis Research Center is developing advanced seal concepts and sealing technology for advanced combined cycle ramjet/scramjet engines being designed for the National Aerospace Plane (NASP). Technologies are being developed for both the dynamic seals that seal the sliding interfaces between articulating engine panels and sidewalls, and for the static seals that seal the heat-exchanger to back-up structure interfaces.

This paper will provide an overview of the candidate engine seal concepts, seal material assessments, and unique test facilities used to assess the leakage and thermal performance of the seal concepts.

Outline

o   Introduction

o   Flow Modeling

o   High Temperature Material Friction and Wear Tests

o   High Temperature Durability/Flow Assessments

o   High Heat Flux Facility

o   Summary
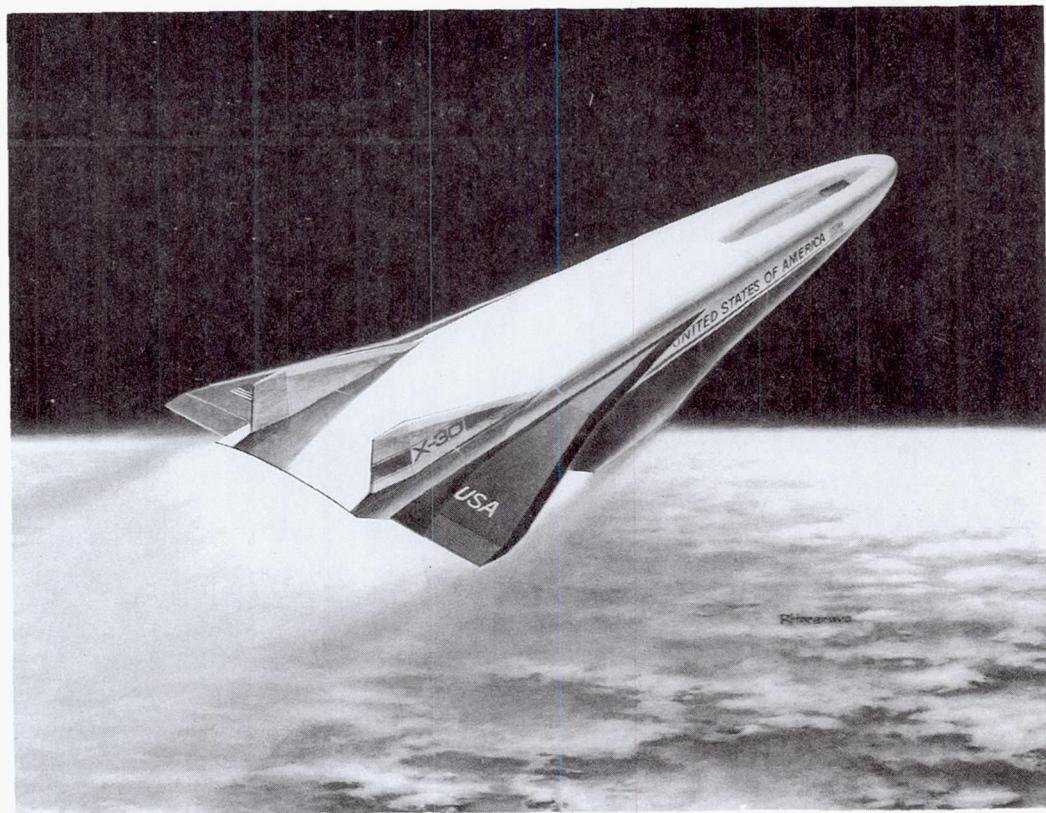
HYPERSONIC ENGINE PANEL-EDGE SEAL

PANEL-
EDGE
SEAL

HIGH
SPEED
FLOW

CD-91- 55195
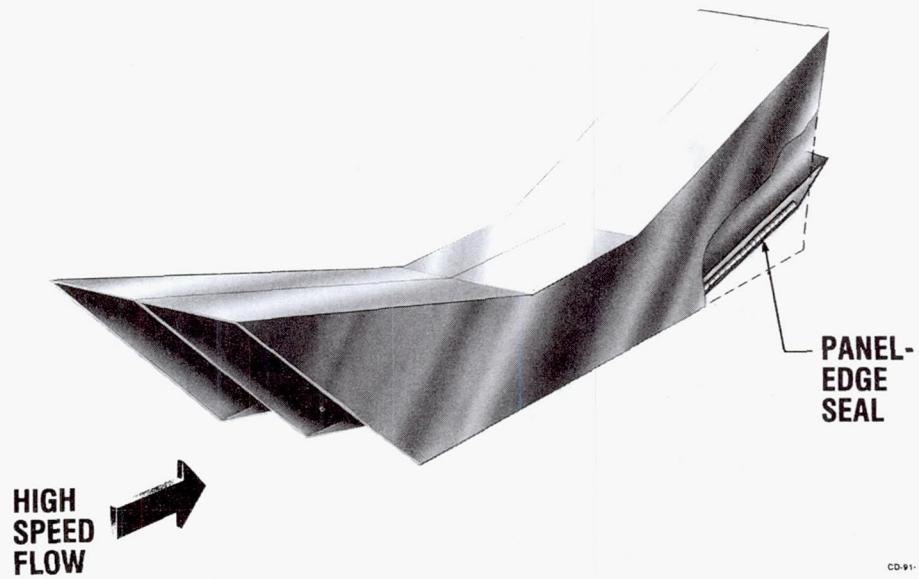
SEAL CONCEPTS UNDER DEVELOPMENT (U)

CERAMIC WAFER SEAL

MOVABLE HORIZONTAL ENGINE PANEL

HOT GAS FLOW

FILM COOLING FOR HIGH HEAT FLUX ENV.

CERAMIC WAFERS

SPLITTER WALL

COOLED PRESSURIZED METAL BELLOWS

BRAIDED CERAMIC ROPE SEAL

MOVABLE HORIZONTAL ENGINE PANEL

HOT GAS FLOW

TRANSPIRATION COOLING

BRAIDED ROPE SEAL

SPLITTER WALL

OPTIONAL COOLED PRESSURIZED METAL BELLOWS
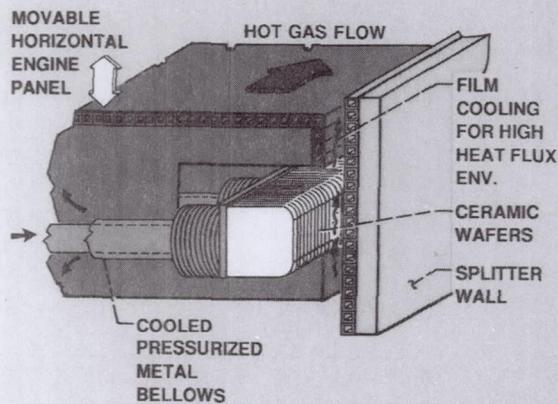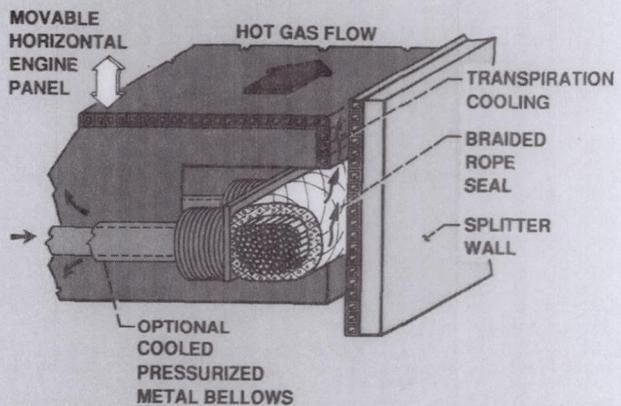
Flow Modeling

Ceramic Wafer Seal Flow Modeling

$$\dot{M}_{TOT} = \underbrace{\dot{M}_1}_{\text{Top}} + \underbrace{\dot{M}_2}_{\text{Nose}} + \underbrace{\dot{M}_3}_{\substack{\text{Between} \\ \text{wafers}}}$$
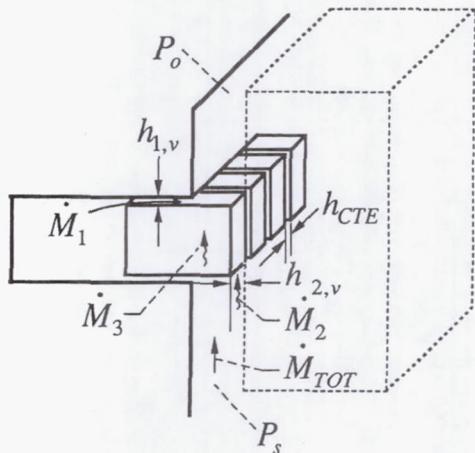
$h_{1,v}; h_{2,v}; h_{CTE}$ - Seal leakage gap heights

$H_1; H_2$ - Seal-to-wall contact dim.

L - Seal length

$P_s; P_o$ - Inlet & outlet pressures

$\mu; \rho; T$ - Gas viscosity, density, temp.

R - Gas constant

241

Ceramic Wafer Seal Leakage vs Temperature
Comparison of Measured & Predicted

$\Delta P = 20$ psi

Leakage rate, lb/s ft

5×10^{-3}

Tentative leakage limit

○ Measured
— — Predicted

4
3
2
1

0   200   400   600   800 1000 1200 1400

Temperature, F

$\Delta P = 40$ psi

Leakage rate, lb/s ft

5×10^{-3}

Tentative leakage limit

○ Measured
— — Predicted

4
3
2
1

0   200   400   600   800 1000 1200 1400

Temperature, F
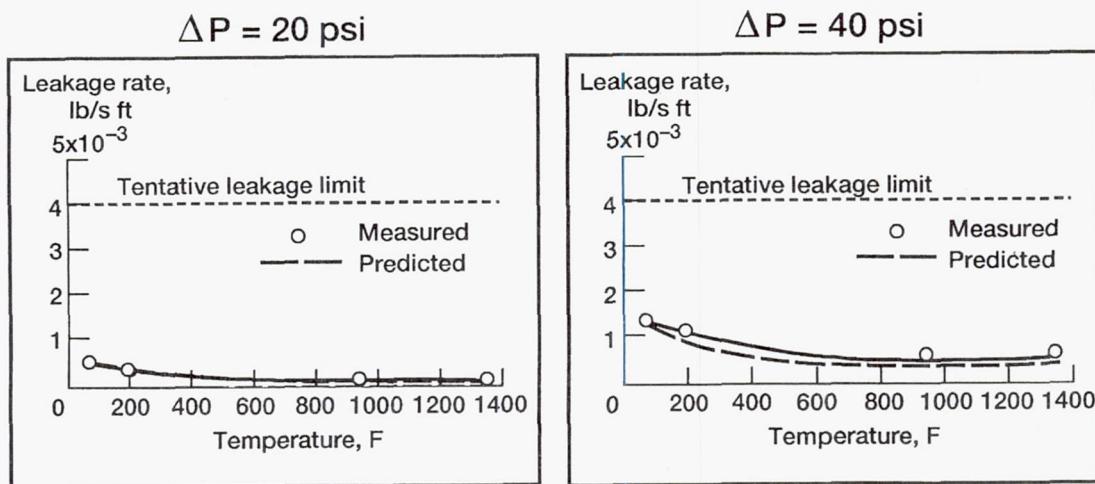
Leakage Path Flow Resistances

$$\dot{M}_{TOT} = \underbrace{\dot{M}_1}_{\substack{\text{Behind} \\ \text{seal}}} + \underbrace{\dot{M}_2}_{\substack{\text{Through} \\ \text{seal}}} + \underbrace{\dot{M}_3}_{\substack{\text{Front of} \\ \text{seal}}}$$

Rope Seal Flow Paths

P_s P_o g
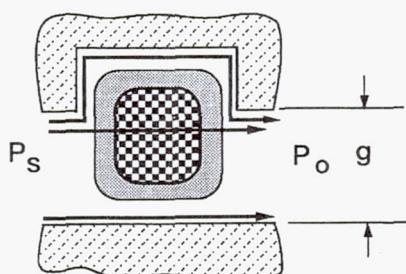
Flow Path	Flow Resistance
$\dot{M}_1$ — 1 —	$R_1 = 9K \dfrac{t}{y_o^3}$
$\dot{M}_2$ — 2 —	$R_2 = 300K \dfrac{tL}{A_c} \dfrac{(1 - \varepsilon_{avg})^2}{\varepsilon_{avg}^3 (\phi D_{f,avg})^2}$
$\dot{M}_3$ — 3 —	$R_3 = 3K \dfrac{t}{y_o^3}$

Where: $\phi D_{f,avg}$ = Characteristic length

$$\varepsilon_{avg} = 1 - \frac{A_y N_c + A_y N_s / \cos \theta}{t^2}$$

242

Braided Ceramic Rope Seal Leakage vs Temperature
Comparison of Measured and Predicted

$\Delta P = 10$ psi

Leakage rate, lb/s ft

14×10^{-3}
12
10
8
6
4
2
0

○ Measured
— — Predicted

$\varepsilon_{avg} = 0.43$
$\varepsilon_{min} = 0.22$
Tentative leakage limit

0   200   400   600   800   1000 1200 1400
Temperature, F

$\Delta P = 35$ psi

Leakage rate, lb/s ft

14×10^{-3}
12
10
8
6
4
2
0

○ Measured
— — Predicted

$\varepsilon_{avg} = 0.43$
$\varepsilon_{min} = 0.22$
Tentative leakage limit

0   200   400   600   800   1000 1200 1400
Temperature, F

HIGH-TEMPERATURE PIN ON DISK TRIBOMETER

THERMOCOUPLE
FURNACE
PYROMETER PORT
NORMAL LOAD SENSOR
FLEXURE
PNEUMATIC LOADER
PIN & DISK SPECIMENS
PULLEY
SPRING PACK
DC MOTOR
BEARING SPINDLE
TORQUE TUBE
PIN LOCKING ROD
SPRING PACK
FRICTION FORCE SENSOR
FLEXURE

CD-87-30923

243

High Temperature

Solid Seal Durability/Flow Studies

High Temperature Dynamic Seal Rig (U)

Left Half

Sabre

Adjustable lateral preload system

A

Test Seals: Rope or wafer seals

Axial Preload

A   1 ft test zone

High watt density surface heaters

Sabre

Simulated wall roughness/waviness

Percent crush (channel depth) or load (bellows) control

Section A-A

Seal Cartridge

Seal Cartridge

Mesh heat exchanger

Hot, pressurized metered supply gas

Temp. and pressure measurement

Hot Dynamic Seal Test Fixture

SOLID SEAL DURABILITY TEST
Hot Dynamic Seal Rig

Haynes 25 (2 mil wire) Hybrid seal _after_ hot durability cycling

SEAL - HY3 - 1

SEAL - HY3 - 2

<u>CONDITIONS:</u>

SEAL ARCH:	HY3(32.8%)-NX312(600/8)-4400/94.8%-H25(172/50)-24x1/10/80° (12.00")
SEAL GAP:	**0.030 inches**
PRELOAD:	Active (20 psi contact pressure)
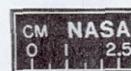
Coolant Panel Braided Ceramic Rope Seal
Potential Alternate to Metal Seal
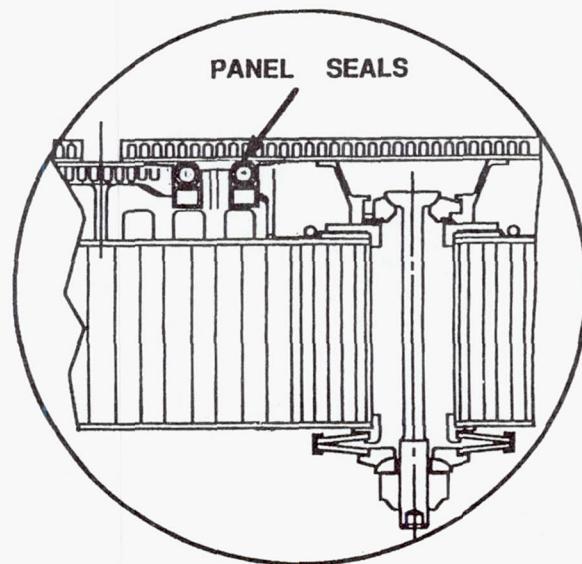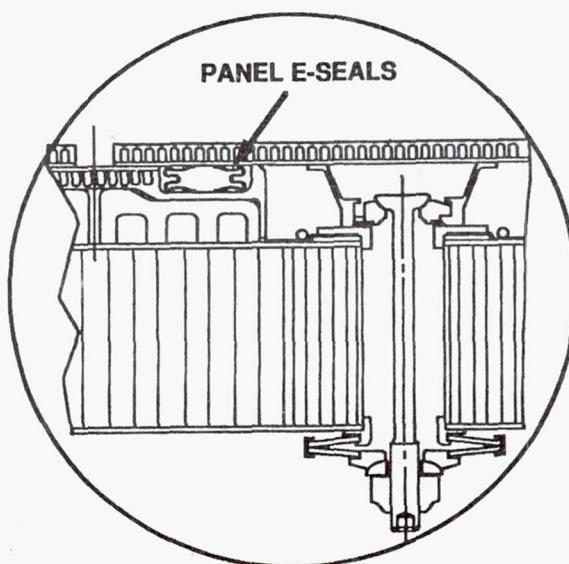
CONTINUOUS LOOP BRAIDED ROPE SEAL

NASA Lewis Research Center

Transpiration Cooled Seal Concepts Tested for National Aero-Space Plane

Braided Rope Seal

Rocket Nozzle Exit
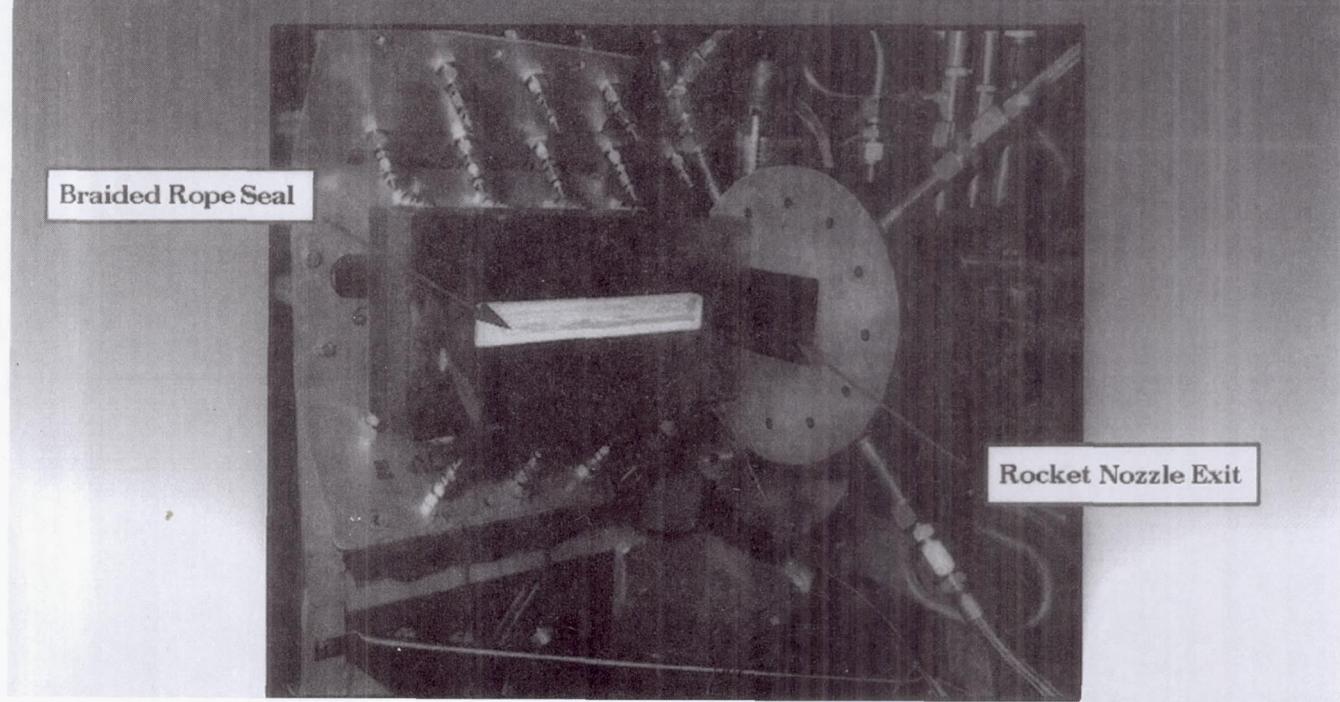
CRL–22 Hot Gas Facility

Summary

o   Hypersonic engines pose unique dynamic seal challenges:
    +   Prevent leakage of combustible hydrogen/oxygen mixtures
    +   Seal highly distorted sidewalls during sliding
    +   Operate hot requiring minimum coolant
    +   Resist mechanical abrasion and supersonic-flow erosion

o   NASA Lewis has developed unique test capabilities for evaluating the
    seal/material performance under engine simulated conditions:
    +   Materials/Lubricant Friction Apparatus
    +   High Temperature Dynamic Seal Rig
    +   High Heat Flux Facility

o   NASA Lewis developed hybrid seal meets the dynamic engine seal life
    requirements at temperatures $\geq$1500 F.

THEORETICAL VERSUS EXPERIMENTAL RESULTS FOR THE ROTORDYNAMIC COEFFICIENTS OF ECCENTRIC, SMOOTH, GAS ANNULAR SEAL ANNULAR GAS SEALS

Dara W. Childs and Chris Alexander
Turbomachinery Laboratory
Texas A&M University
College Station, Texas

INTRODUCTION

ANNULAR GAS SEAL MODEL

- Annular gas seal exhibiting small motion about a centered position

$$-\begin{Bmatrix} F_x \\ F_y \end{Bmatrix} = \begin{bmatrix} K & k \\ -k & K \end{bmatrix} \begin{Bmatrix} X \\ Y \end{Bmatrix} + \begin{bmatrix} C & c \\ -c & C \end{bmatrix} \begin{Bmatrix} \dot{X} \\ \dot{Y} \end{Bmatrix}$$

- Rotordynamic force components acting on a rotor

Forces on a whirling rotor

TEST APPARATUS

- Rotor shaft / Pivot shaft arrangement

- Horizontal excitation through shaker head arrangement

- Load cell / Accelerometer arrangement

- Cross sectional view

Figure 4. Excitation system.

250

PIVOT
SHAFT

SHAKER

ROTOR
HOUSING

RETURN
SPRING

PROXIMITY PROBE

STATOR HOLDER

BACK PRESSURE SEAL

LOAD CELL

THRUST BEARING

SWIRL VANES

TEST SHAFT

FLOW

EXHAUST PORT

TEST STATOR

TEST ROTOR

INLET PORT
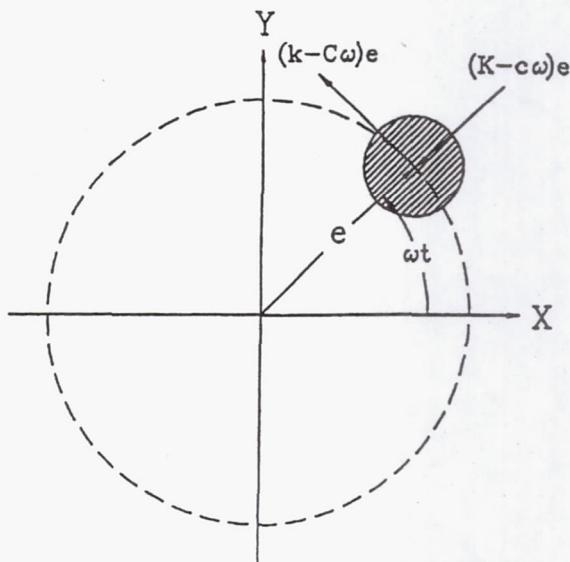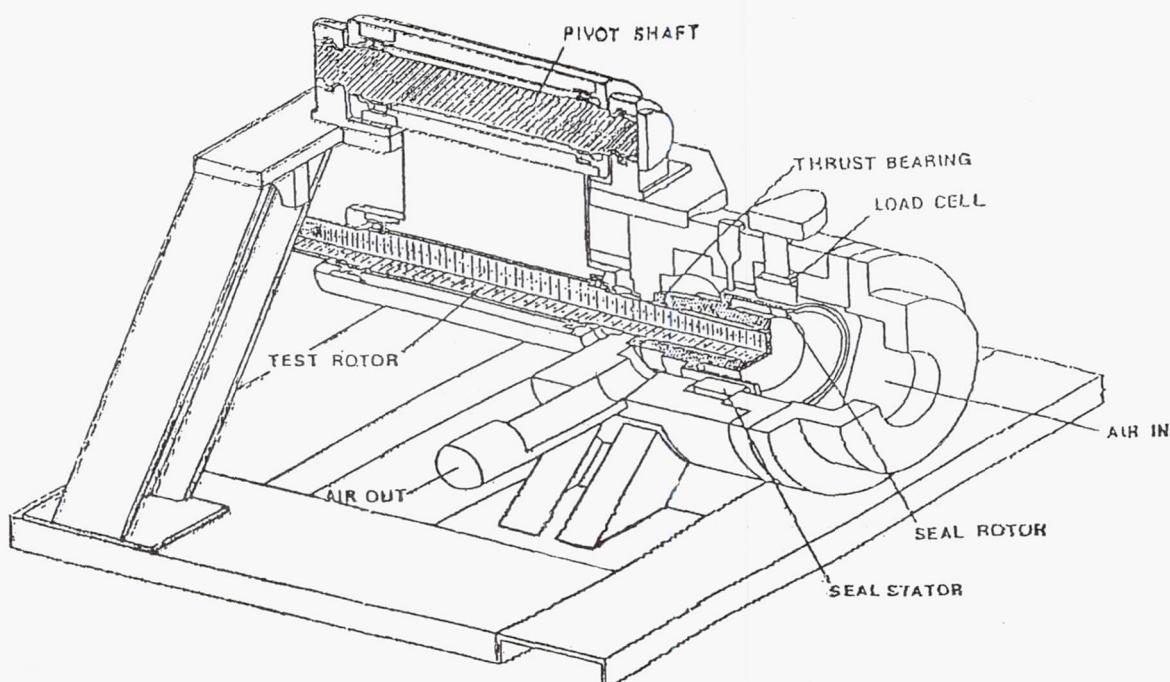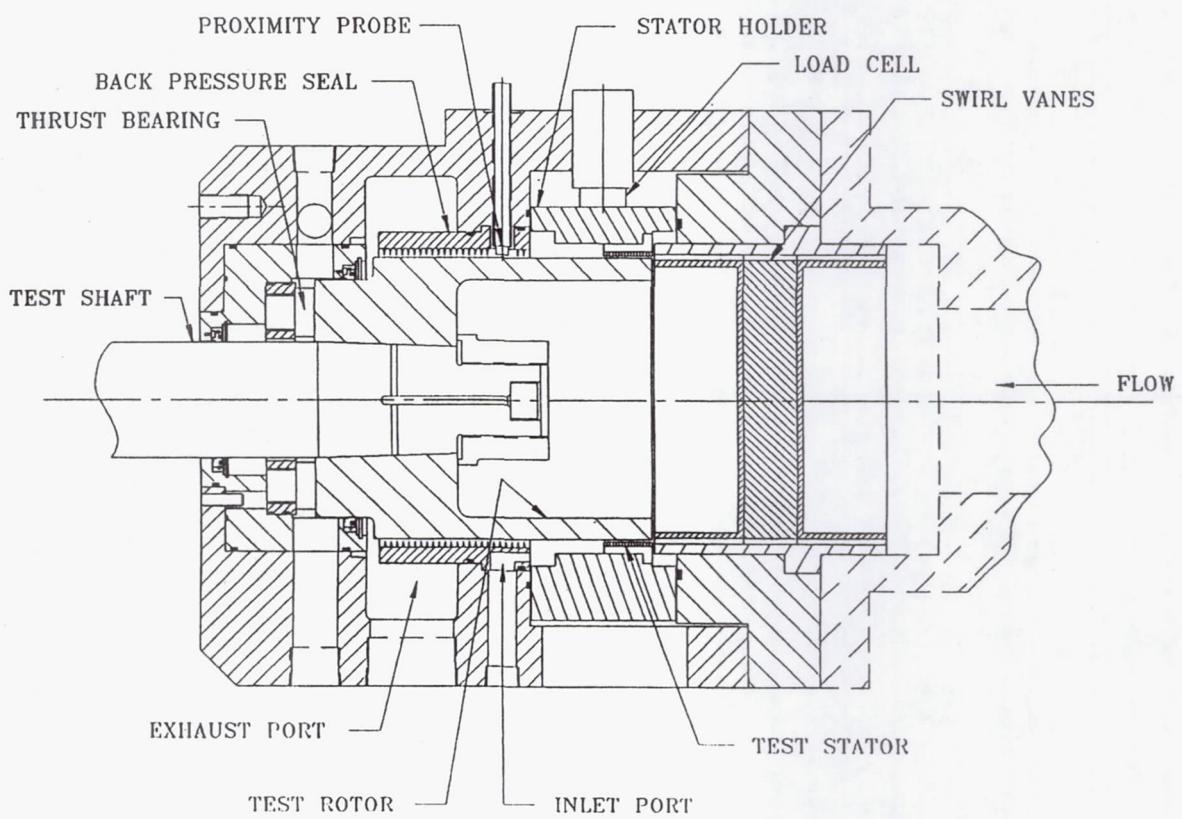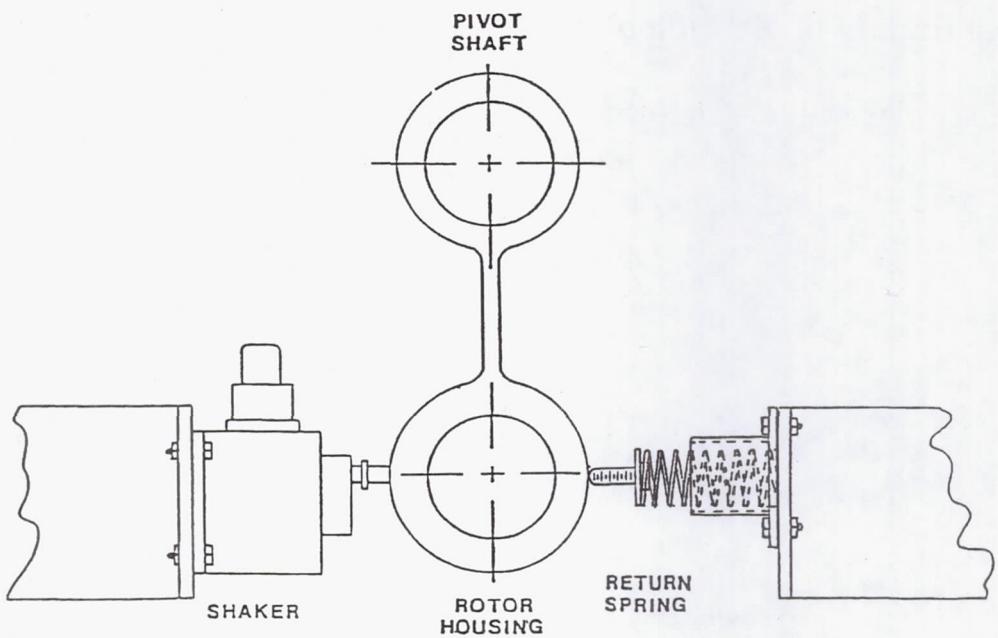
Modifications for Coefficient Identification with Eccentric Operation

Identification of all 8 rotordynamic coefficients requires excitation parallel and perpendicular to the static eccentricity vector. The figure below shows the necessary process.

Total Excitation

Parallel Excitation   Perpendicular Excitation

$$X(0)= e_o \ , Y(0)= 0 \ , \Delta X(t) \quad X(0)= 0 \ , Y(0)= e_o \ , \Delta X(t)$$
$$K_{xx} \ , K_{yx} \ , C_{xx} \ , C_{yx} \qquad K_{xy} \ , K_{yy} \ , C_{xy} \ , C_{yy}$$
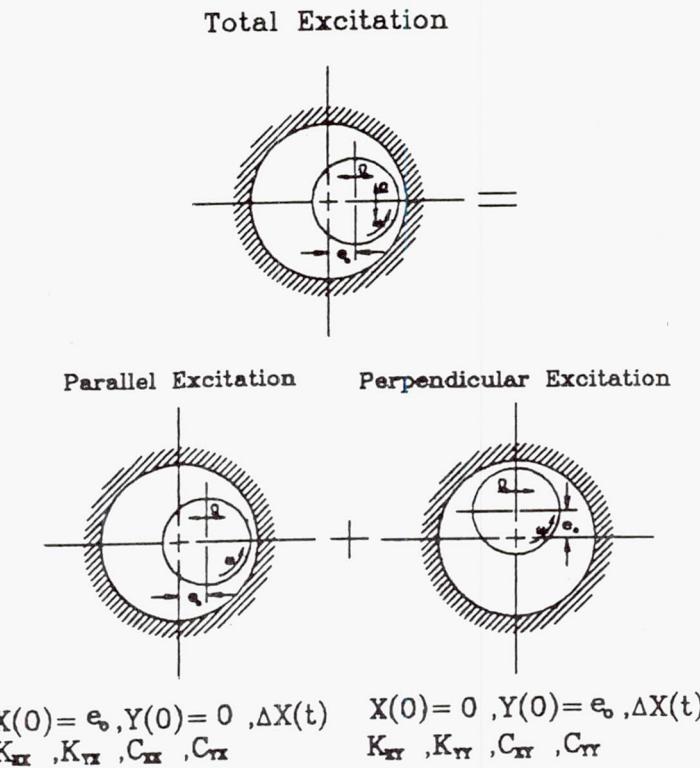
Fig. 6 - Shaking configuration for coefficient identification

Test Parameters

The testing apparatus can determine the effects of the following test parameters on the rotordynamic and leakage rates of a seal:

1) Rotor Speed

2) Inlet Pressure

3) Pressure Ratio

4) Inlet Fluid Rotation

5) Rotor Eccentricity

PRESENTATION OF EXPERIMENTAL VERSUS THEORETICAL RESULTS

The independent parameter is ECCENTRICITY. The results presented also show the effects of:

Speed
Pressure ratio
Inlet pressure
Preswirl

Rotor Speed (rpm) ω	Inlet Pressure (bars) P_r	Pressure Ratio (-) P_{ra}	Inlet Preswirl in the Direction of Rotation
5,000	7.90	0.67	None
16,000	11.4	0.55	Intermediate
	14.8	0.50	High
		0.45	

The following coefficients will be discussed:

DIRECT STIFFNESS
CROSS-COUPLED STIFFNESS
DIRECT DAMPING
WHIRL FREQUENCY RATIO

Also discussed will be:

MASS FLOW RATE
PRESSURE PROFILES
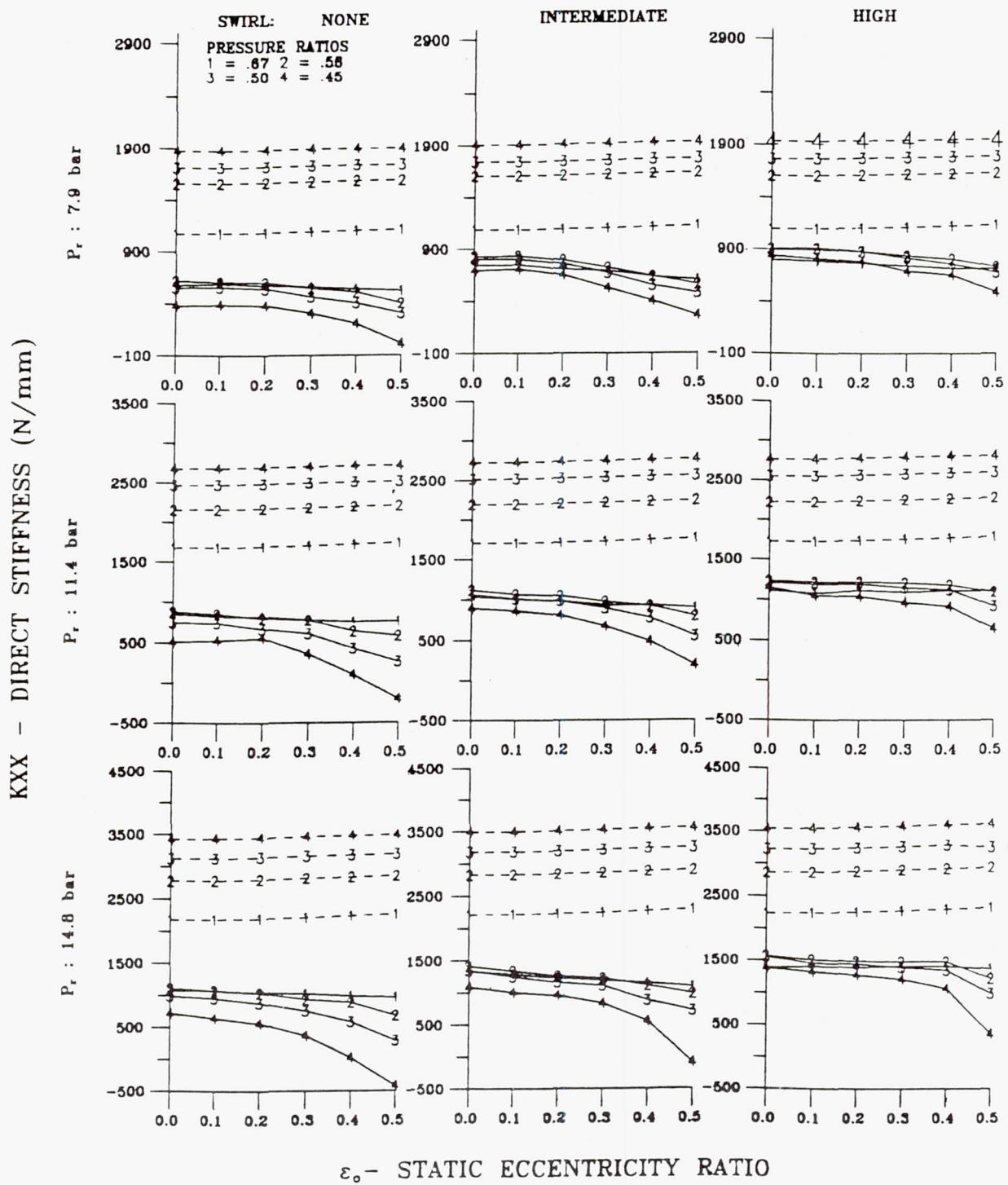
Fig. 9 - Experimental (solid) versus theoretical (dashed) results for direct stiffness, K_{XX}, as a function of the static eccentricity ratio, ε_o, for a smooth seal at 16,000 rpm
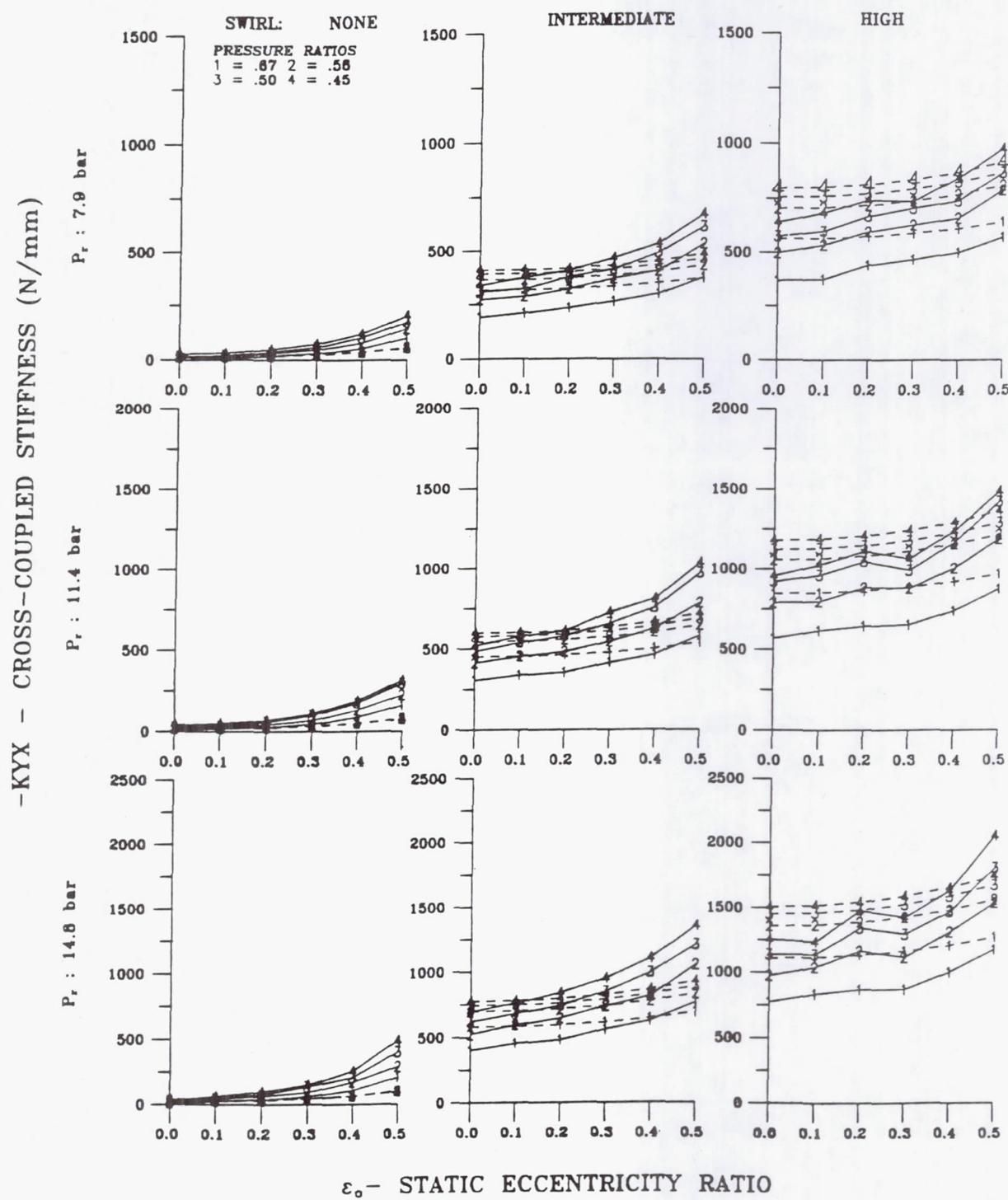
Fig. 10 - Experimental (solid) versus theoretical (dashed) results for cross-coupled stiffness, K_{YX}, as a function of the static eccentricity ratio, ε_o, for a smooth seal at 5,000 rpm
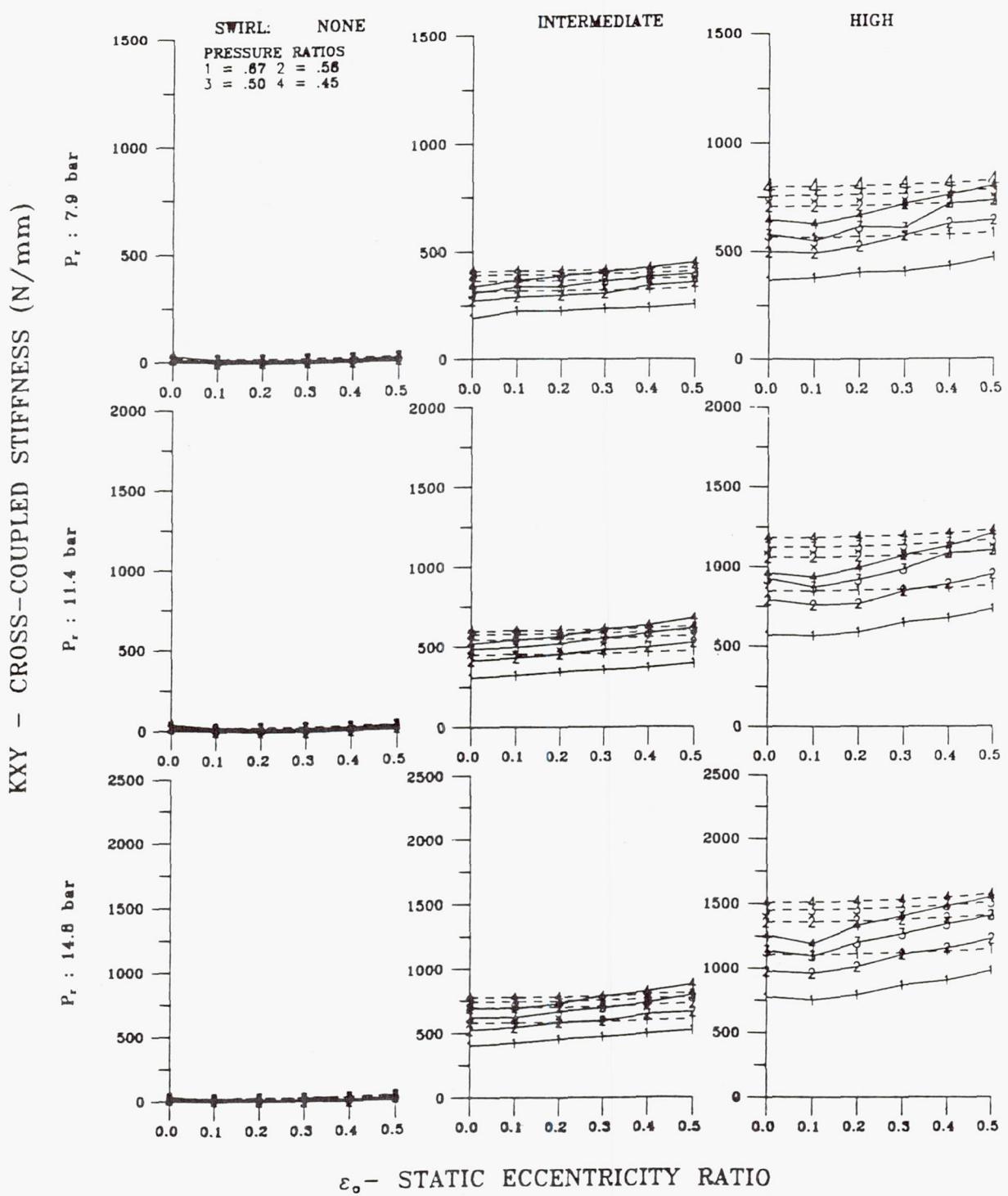
Fig. 11 - Experimental (solid) versus theoretical (dashed) results for cross-coupled stiffness, K_{XY}, as a function of the static eccentricity ratio, ε_o, for a smooth seal at 5,000 rpm
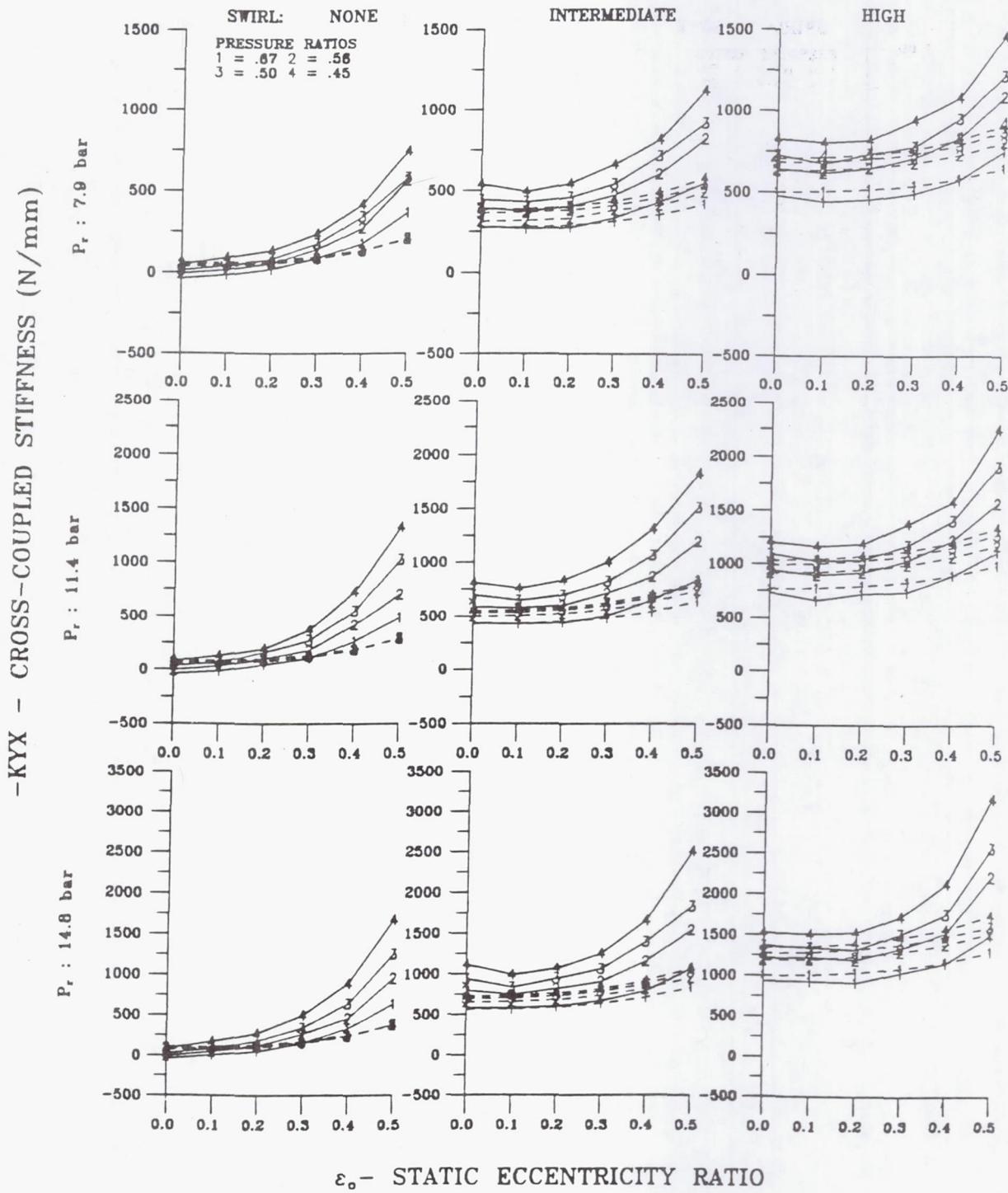
Fig. 12 - Experimental (solid) versus theoretical (dashed) results for cross-coupled stiffness, K_{YX}, as a function of the static eccentricity ratio, ε_o, for a smooth seal at 16,000 rpm
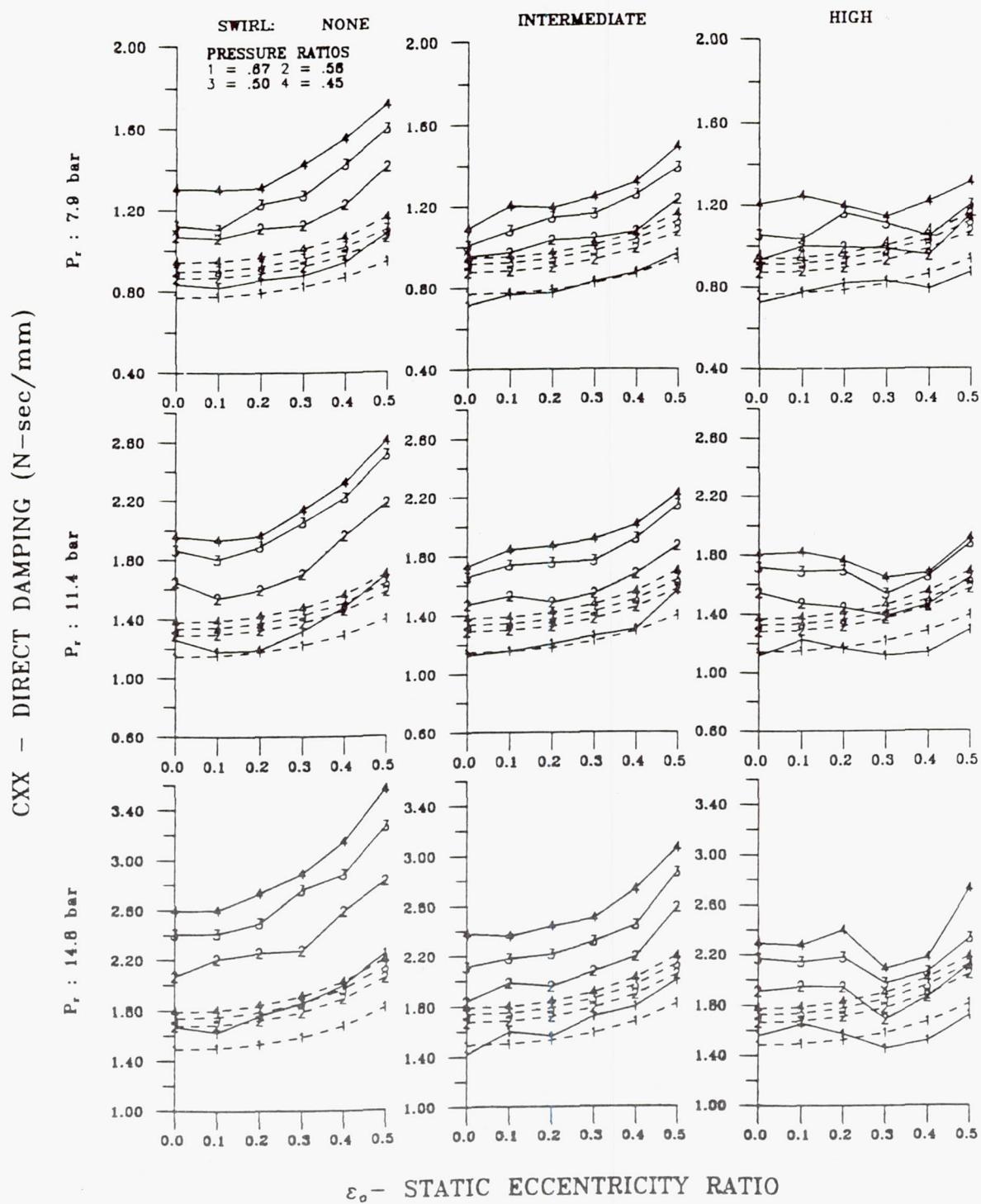
Fig. 13 - Experimental (solid) versus theoretical (dashed) results for direct damping, C_{XX}, as a function of the static eccentricity ratio, ε_o, for a smooth seal at 5,000 rpm
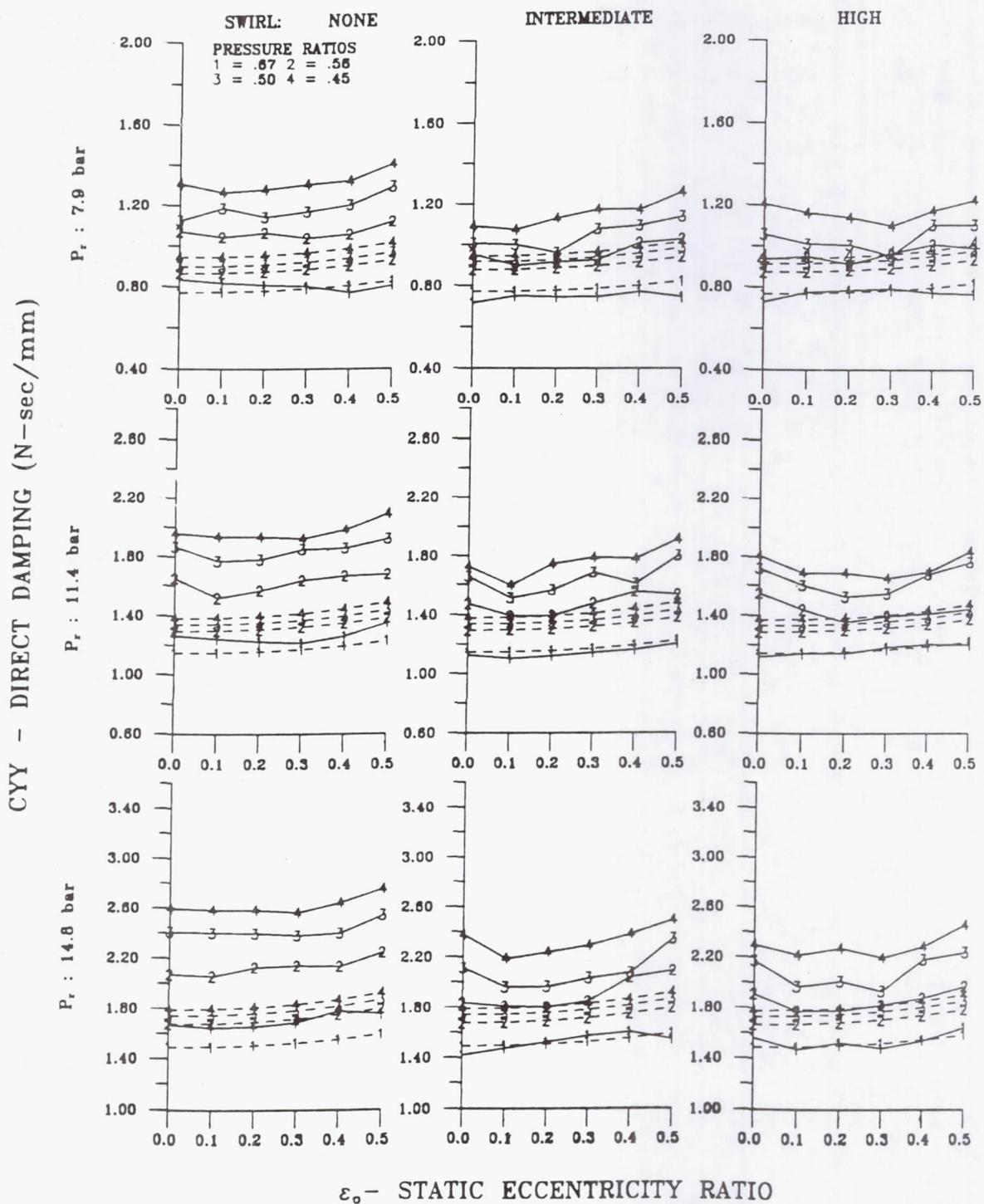
Fig. 14 - Experimental (solid) versus theoretical (dashed) results for direct damping, C_{YY}, as a function of the static eccentricity ratio, ε_o, for a smooth seal at 5,000 rpm

259
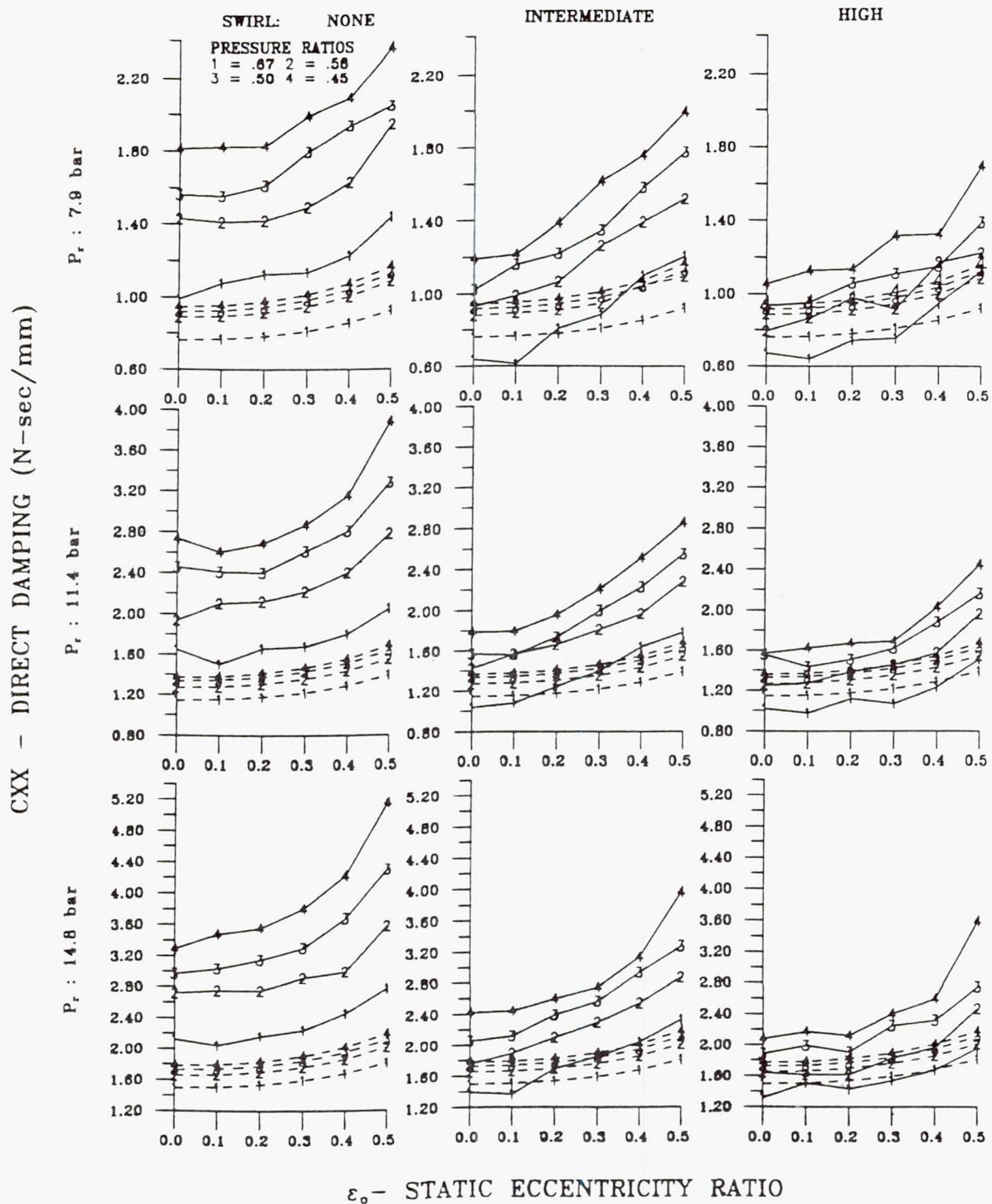
Fig. 15 - Experimental (solid) versus theoretical (dashed) results for direct damping, C_{XX}, as a function of the static eccentricity ratio, ε_o, for a smooth seal at 16,000 rpm

WHIRL FREQUENCY RATIO

The whirl frequency ratio is a means by which to quantitatively determine
the rotordynamic stability of a seal. According to Lund (1965), the whirl frequency
ratio for eccentric operation is obtained by using the following equations.

$$K_{eq} = \frac{K_{XX}C_{YY} + K_{YY}C_{XX} - C_{YX}K_{XY} - C_{XY}K_{YX}}{C_{XX} + C_{YY}}$$

$$WFR^2 = \frac{(K_{eq} - K_{XX})(K_{eq} - K_{YY}) - K_{XY}K_{YX}}{(C_{XX}C_{YY} - C_{XY}C_{YX})\omega^2}$$

The onset speed of instability is defined by the following equation,

$$\omega = \frac{\omega_{nl}}{\Omega_w}$$

where ω_{nl} is the first critical speed of the rotor and Ω_w is the whirl frequency ratio.

261
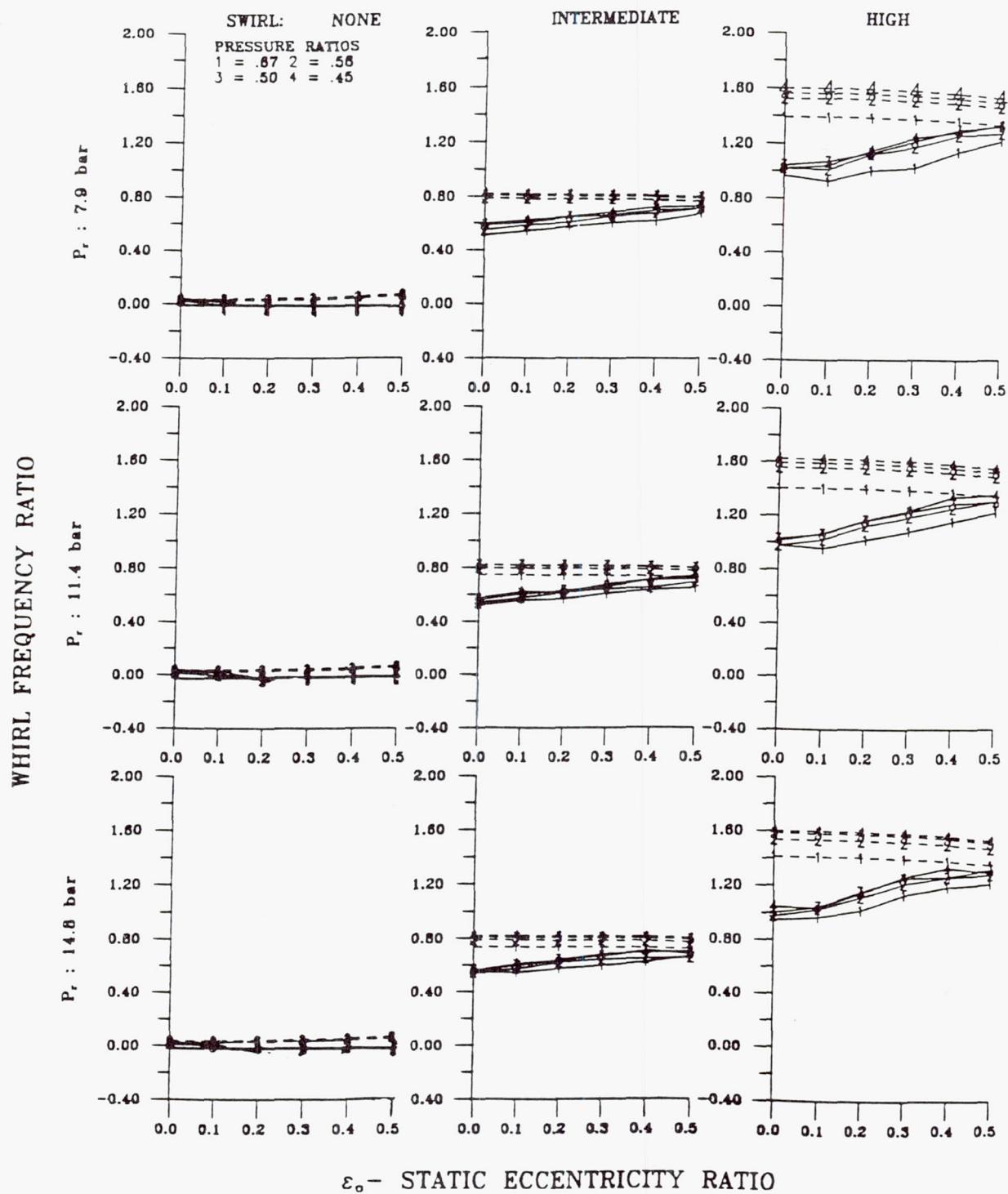
Fig. 16 - Experimental (solid) versus theoretical (dashed) results for the whirl frequency ratio as a function of the static eccentricity ratio, ε_o, for a smooth seal at 5,000 rpm
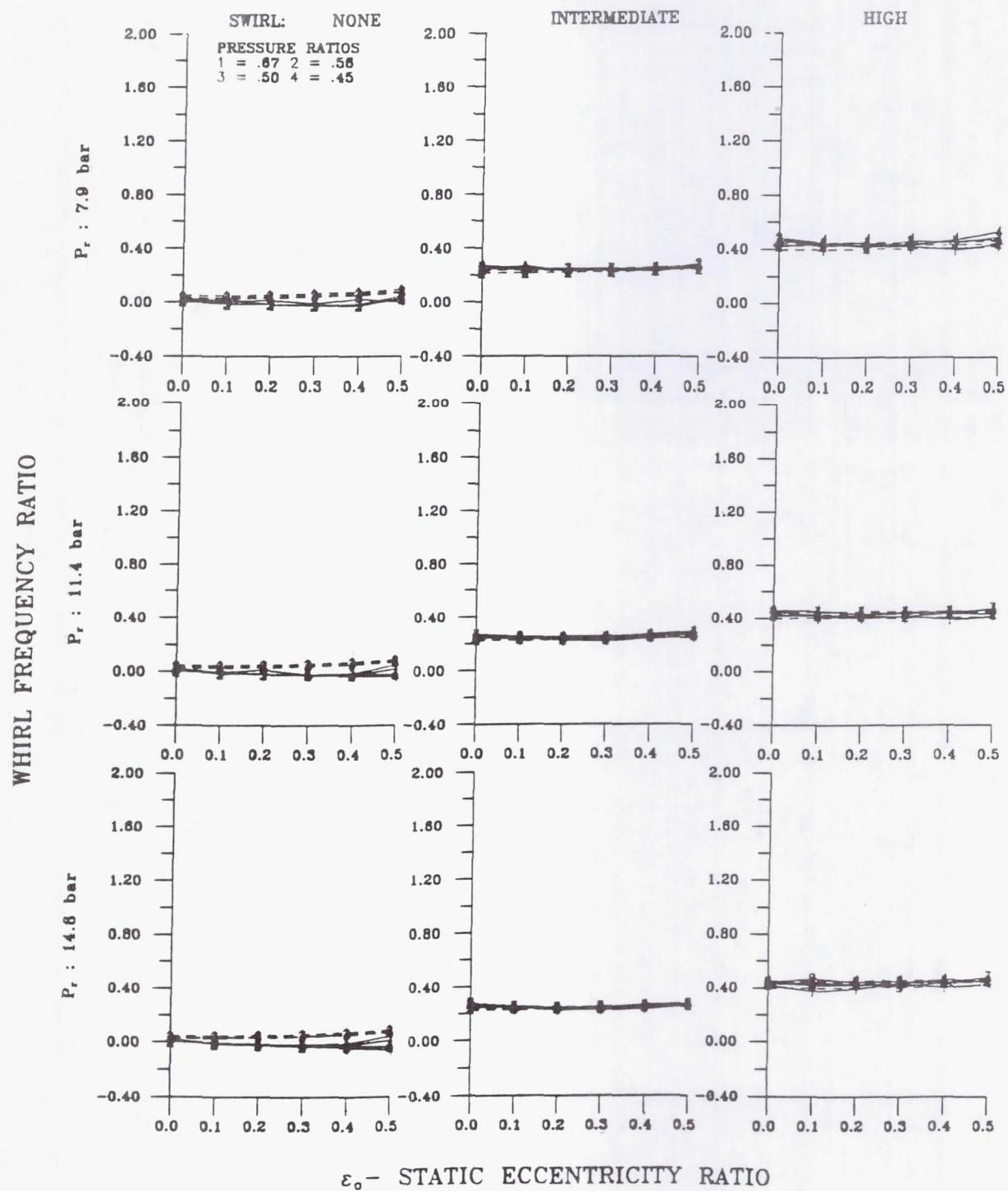
Fig. 17 - Experimental (solid) versus theoretical (dashed) results for the whirl frequency ratio as a function of the static eccentricity ratio, ε_o, for a smooth seal at 16,000 rpm
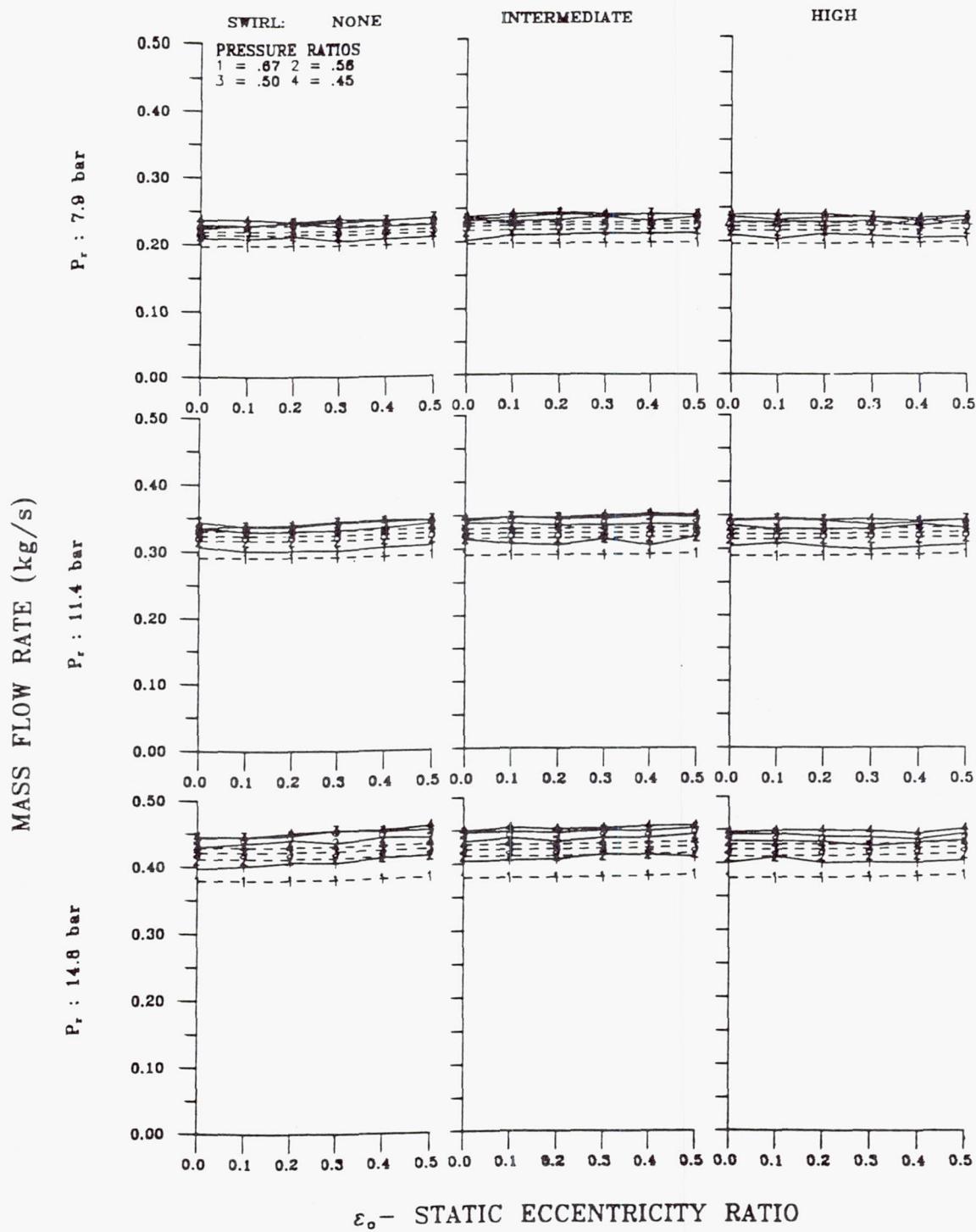
Fig. 18 - Experimental (solid) versus theoretical (dashed) results for mass flow rate as a function of the static eccentricity ratio, ε_o, for a smooth seal at 5,000 rpm
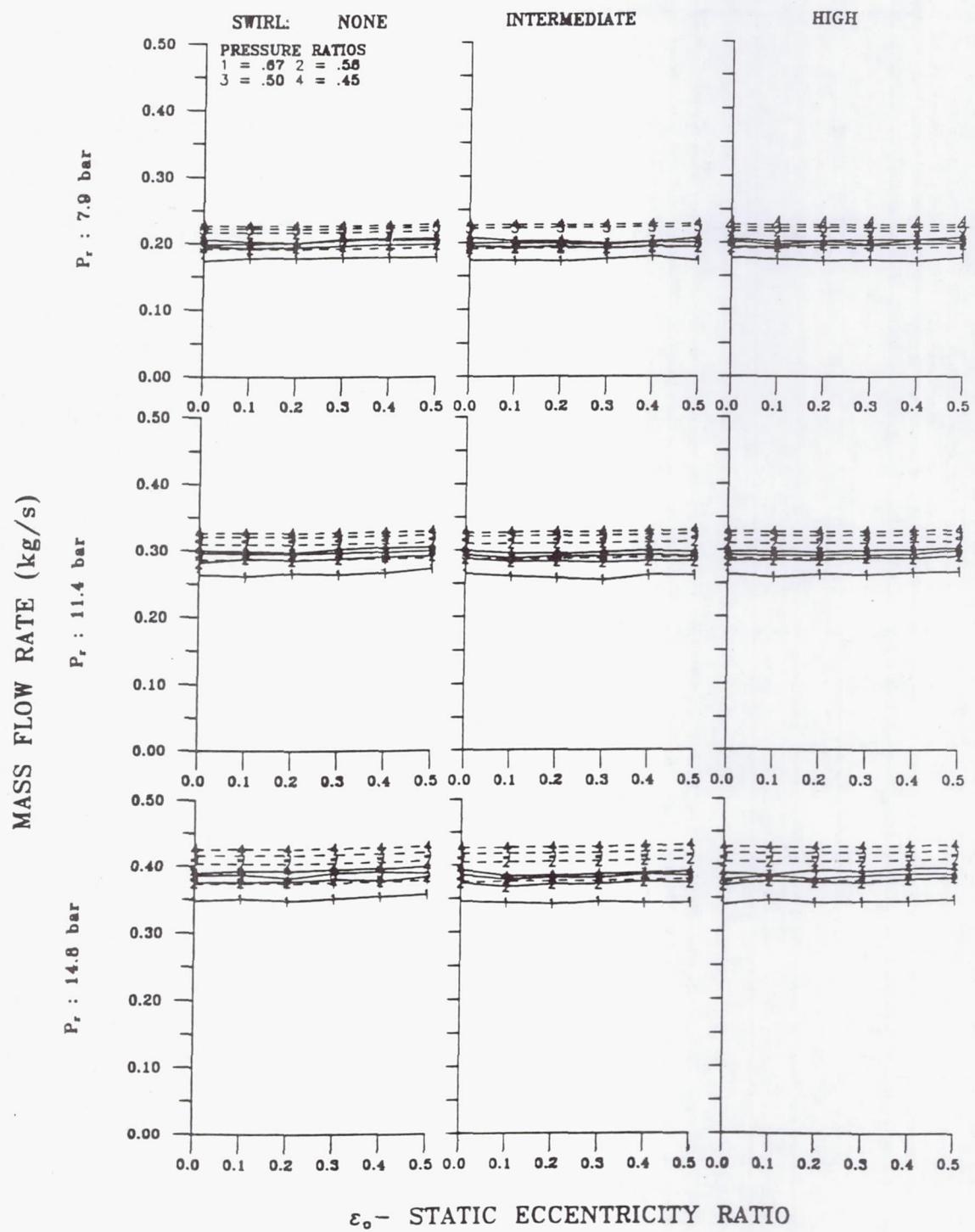
Fig. 19 - Experimental (solid) versus theoretical (dashed) results for mass flow rate as a function of the static eccentricity ratio, ε_o, for a smooth seal at 16,000 rpm

CONCLUSIONS

Experimental Results

• Direct stiffness, K_{XX}, decreases with increasing eccentricity, inlet pressures, and slightly with increasing inlet preswirl

• Cross-coupled stiffness, K_{YX}, increases with increasing eccentricity, preswirl and speed

• Direct damping, C_{XX}, increases with increasing eccentricity, speed, and inlet preswirl

• At 5,000 rpm and no swirl the whirl frequency is basically zero for all eccentric positions. For the configurations with swirl the whirl frequency values increase with increasing eccentricity. At 16,000 rpm the whirl frequency ratio does not change with eccentricity.

• At 5,000 and 16,000 rpm the leakage is invariant to changes in the static eccentricity ratio

• Linear pressure profiles exist for all eccentric positions

Theoretical versus Experimental Results

• The analytical results overpredict the experimental results for the direct stiffness values and incorrectly predict increasing stiffness with decreasing pressure ratios

• Theory correctly predicts increasing cross-coupled stiffness, K_{YX}, with increasing eccentricity and inlet preswirl

• Direct damping, C_{XX}, underpredicts the experimental results, but the analytical results do correctly show that damping increases with increasing eccentricity

• The whirl frequency values predicted by theory are insensitive to changes in the static eccentricity ratio. Although these values match perfectly with the experimental results at 16,000 rpm, the results at the lower speed do not correspond

• Theoretical and experimental mass flow rates match at 5,000 rpm, but at 16,000 rpm the theoretical results overpredict the experimental mass flow rates

• Theory correctly shows the linear pressure profiles and the associated entrance losses with the specified rotor positions

TURBOMACHINERY LABORATORY TEXAS A&M UNIVERSITY RESEARCH
PROGRESS ON ANNULAR GAS SEALS

Dara W. Childs
Turbomachinery Laboratory
Texas A&M University
College Station, Texas

ACCOMPLISHMENTS

* Tested 3 helically-grooved seals and compared results to MTI code SPIRALG

* Tested a smooth annular seal at 6 eccentricity ratios $(0 \rightarrow 0.5)$

* Transferred test apparatus to a new facility. Testing should resume in December 1993.

REMAINING TESTS

* Test 2 long honeycomb seals; $L/D = 1/2, 1$

* Test a short labyrinth or honeycomb seal with and without a reduced inlet cavity.

INTRODUCTION

HELICALLY GROOVED ANNULAR GAS SEAL

- Reduce leakage from high to low pressure side

- Cylindrical seal with groove pattern along face

- α, angle between direction of grooves and rotational velocity
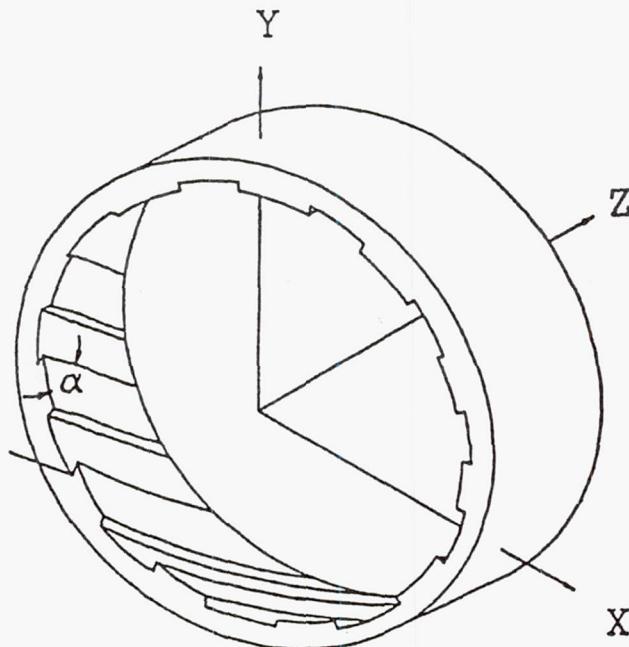
Helically grooved seal

INTRODUCTION

ANNULAR GAS SEAL MODEL

- Annular gas seal exhibiting small motion about a centered position

$$
-\begin{Bmatrix} F_x \\ F_y \end{Bmatrix} = \begin{bmatrix} K & k \\ -k & K \end{bmatrix} \begin{Bmatrix} X \\ Y \end{Bmatrix} + \begin{bmatrix} C & c \\ -c & C \end{bmatrix} \begin{Bmatrix} \dot{X} \\ \dot{Y} \end{Bmatrix}
$$

- Rotordynamic force components acting on a rotor
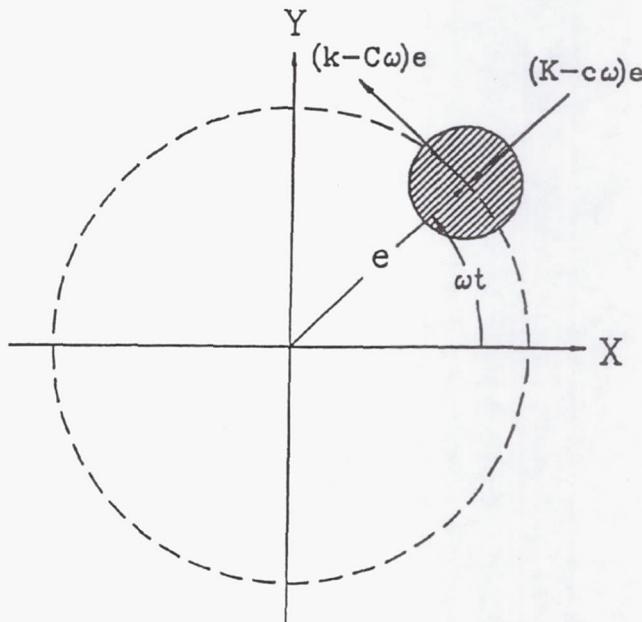
Forces on a whirling rotor

TEST APPARATUS

- Rotor shaft / Pivot shaft arrangement

- Horizontal excitation through shaker head arrangement

- Load cell / Accelerometer arrangement

- Cross sectional view
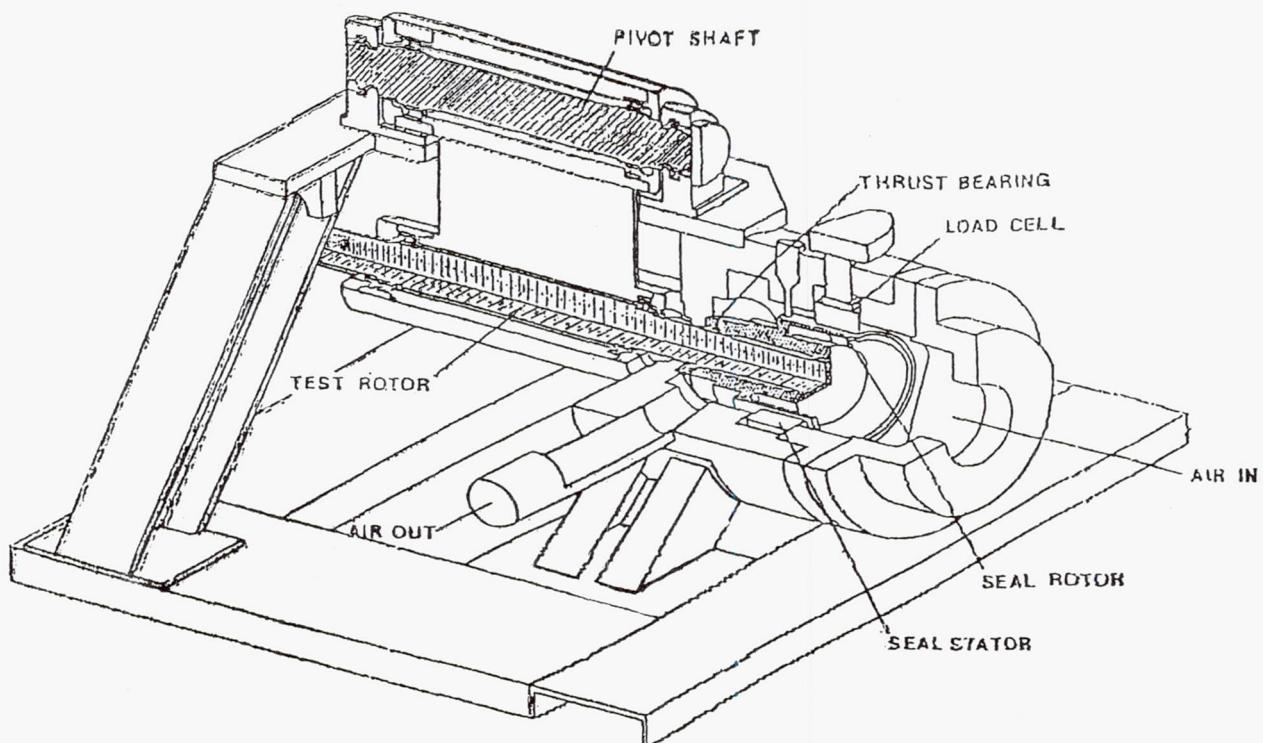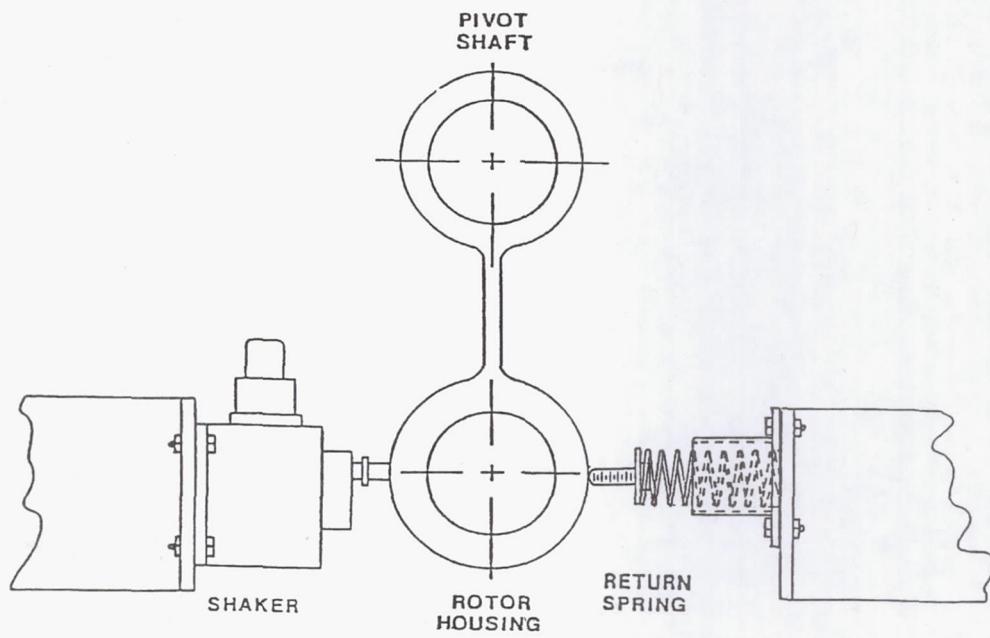
Figure 4. Excitation system.
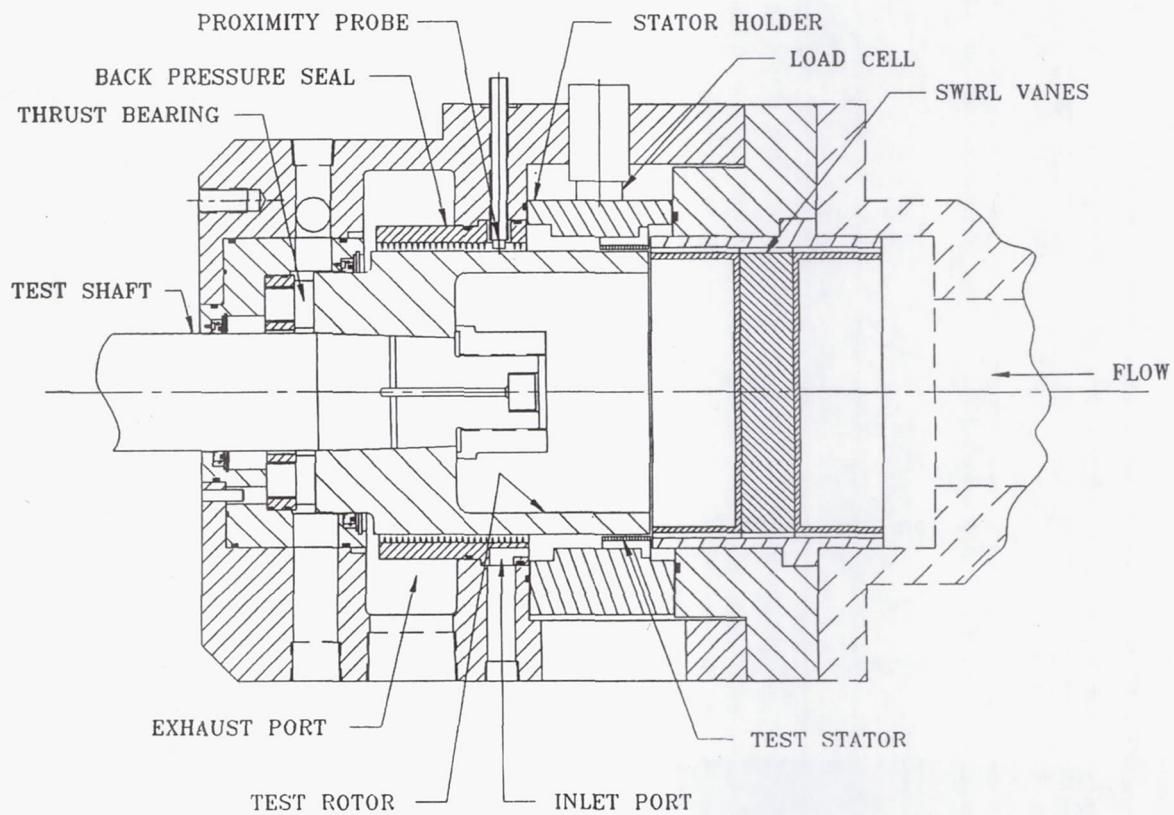
TEST PARAMETERS

TEST POINTS

Rotor Speed (rpm) ω	Inlet Pressure (bar) P_r	Pressure Ratio (-) P_{ra}	Inlet Preswirl in the Direction of Rotor Rotation
1 - 5000	1 - 7.90	1 - 0.67	1 - None
2 - 12000	2 - 13.1	2 - 0.56	2 - Intermediate
3 - 16000		3 - 0.50	3 - High
		4 - 0.45	

- 100 Hp electric motor with belt drive and pulley system

- Only two inlet pressures obtainable

- Pressure ratio controlled through back pressure seal and exhaust ports

TEST PARAMETERS

- Preswirl guide vanes

- Intermediate swirl provides half exit tangential velocity as maximum swirl
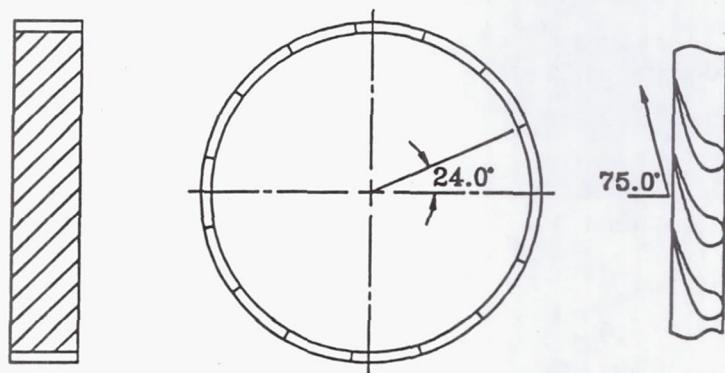
MAXIMUM SWIRL VANES EXIT ANGLE
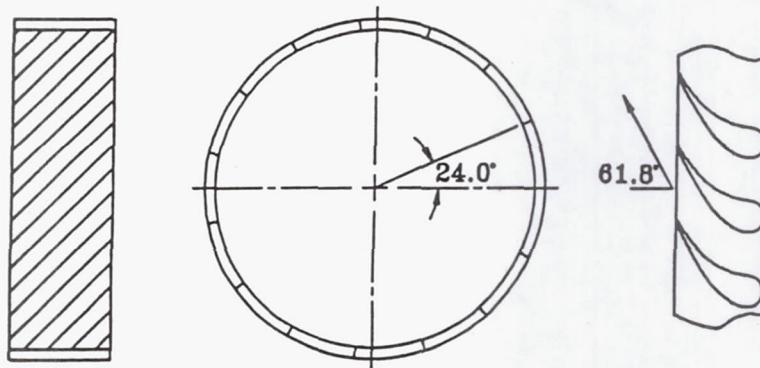
INTERMEDIATE SWIRL VANES EXIT ANGLE

- Exit velocity / Inlet tangential velocity

$$V_{EX} = \frac{\dot{Q}}{N_B \, A_{EX}}$$

$$V_{\theta 0} = V_{EX} SIN\beta$$

273

EXPERIMENTAL RESULTS

- Direct stiffness

- Cross-coupled stiffness

- Direct damping

- Whirl frequency ratio

- Leakage

- Uncertainty analysis using Kline-McClinktock

EXPERIMENTAL RESULTS

LEAKAGE CHARACTERISTICS

- Mass flow rate determined using turbine flow meter, temperature and pressure measurements

- Flow coefficient determined

$$\lambda = \frac{\dfrac{\dot{m}}{2\pi R_0}}{C_r \sqrt{\dfrac{P_i^2 - P_e^2}{R_g T}}}$$

GAS SEAL THEORY

- Analysis based on Smalley (1972)

- Theory

    o Compressible form of Reynold's equation

    o Narrow groove theory with pressure distribution

- Major assumptions

    o Laminar flow

    o No inertial effects

    o Large number of grooves

    o Ideal, adiabatic gas

- Major SPIRALG inputs

    o Seal geometry

    o Shaft speed

    o Inlet and exit pressure

    o Viscosity of working fluid

    o Groove angle

    o User specifications
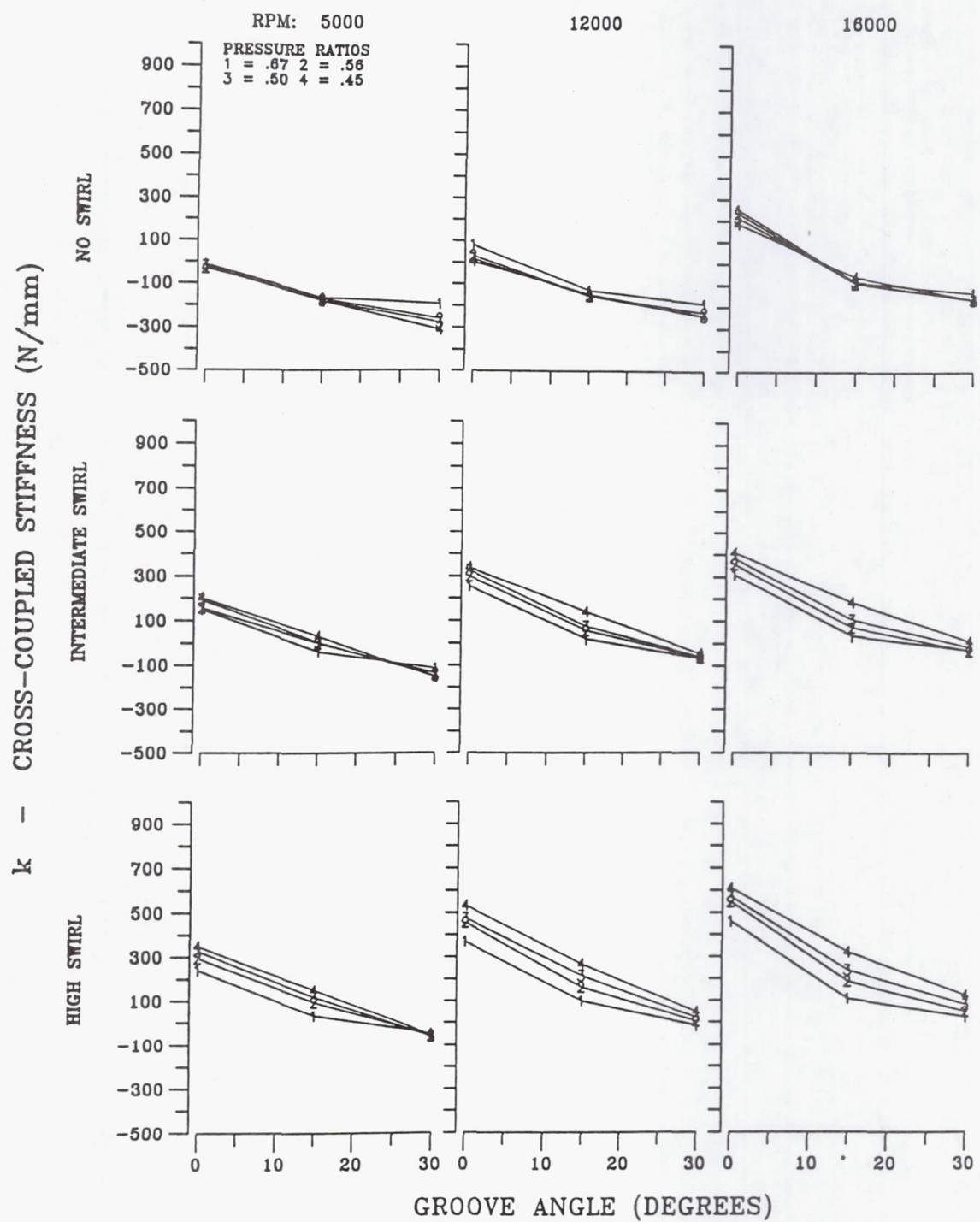
Cross-coupled stiffness, k, as a function of groove angle for $C_r=0.229$ and $P_r=7.9$ bar
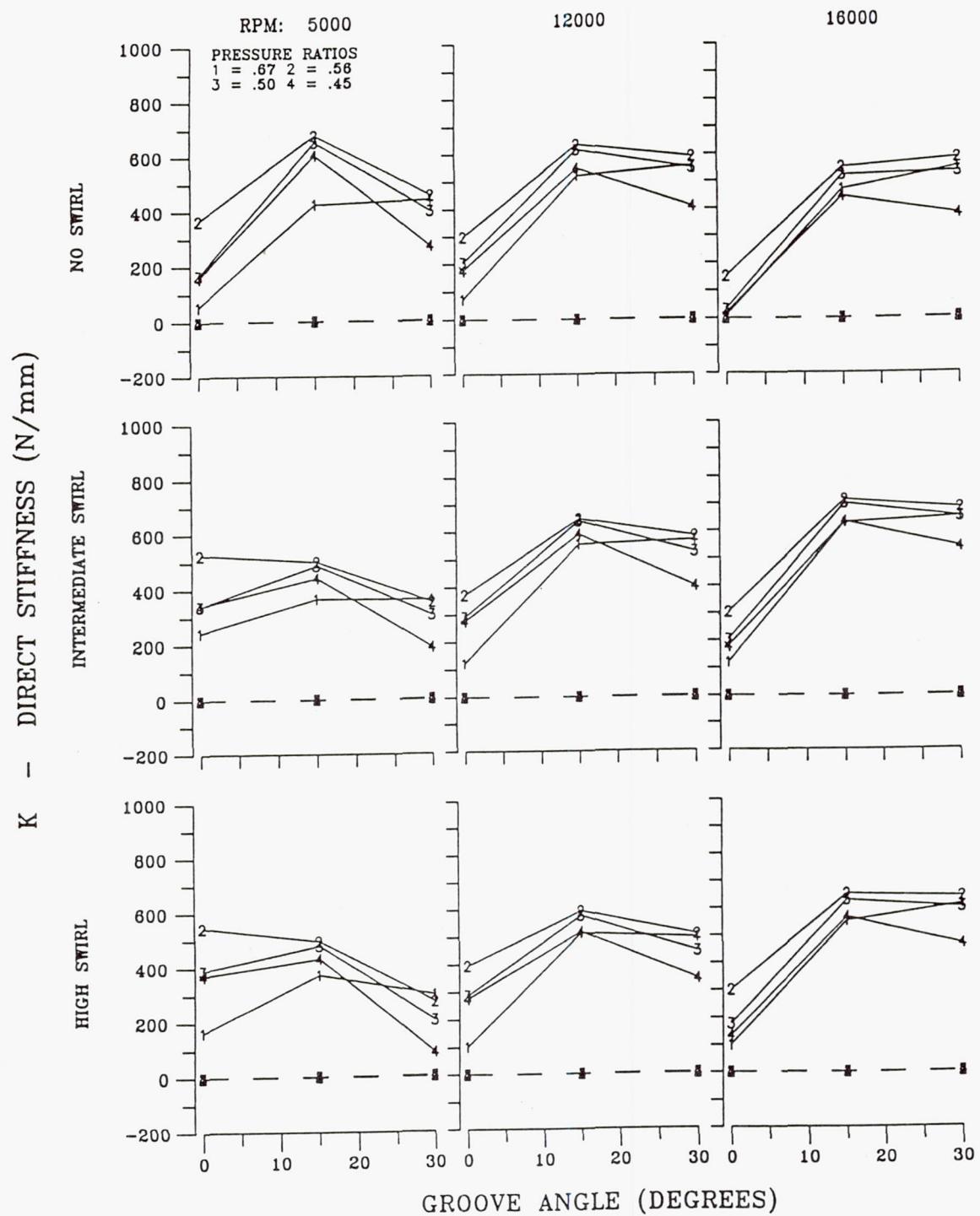
Experimental (solid) versus theoretical (dashed) results for direct stiffness, K, as a function of groove angle for C_r=0.305 mm and P_r=7.9 bar
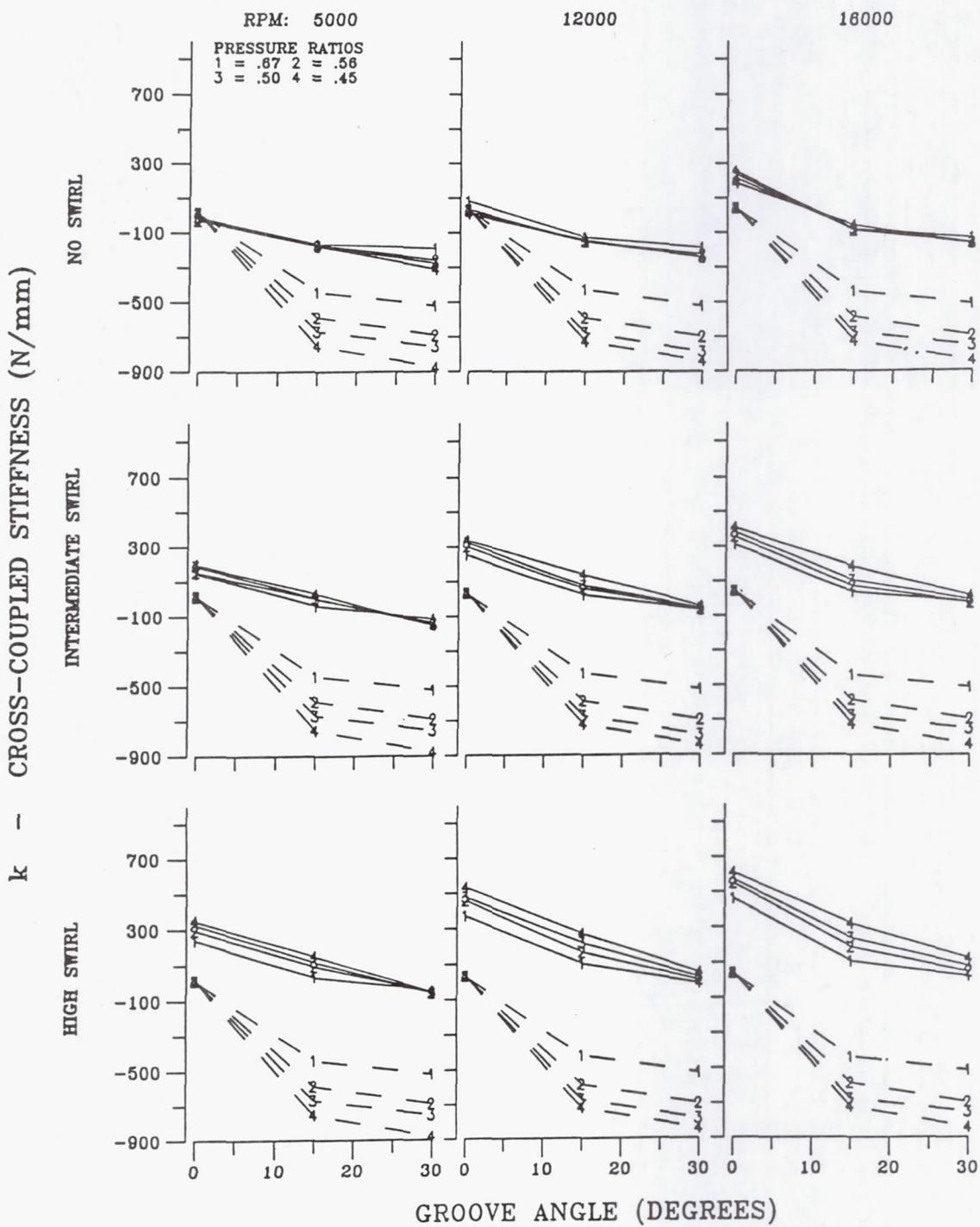
Experimental (solid) versus theoretical (dashed) results for cross-coupled stiffness, k, as a function of groove angle for C_r=0.229 mm and P_r=7.9 bar
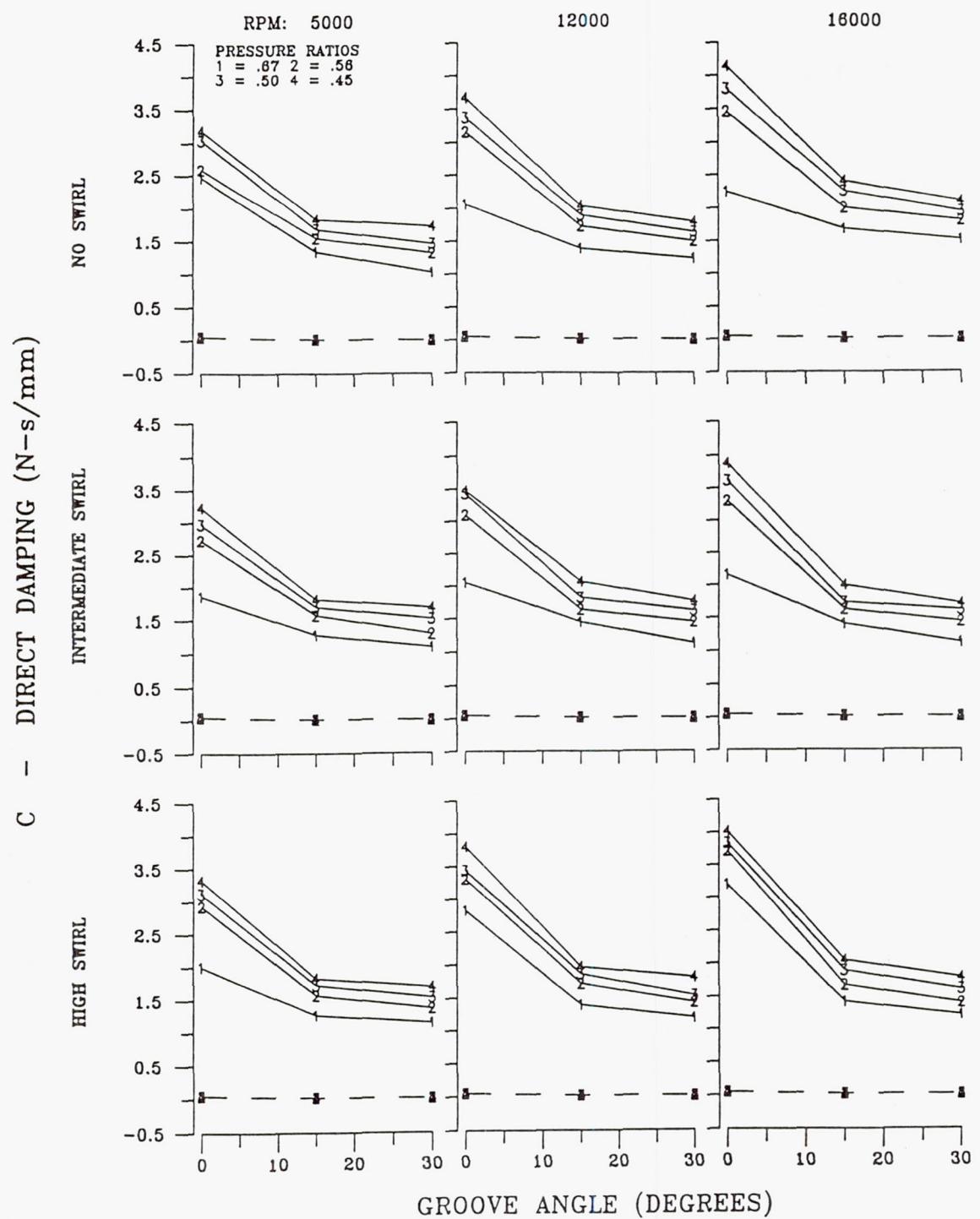
Experimental (solid) versus theoretical (dashed) results for direct damping, C, as a function of groove angle for C_r=0.229 mm and P_r=7.9 bar
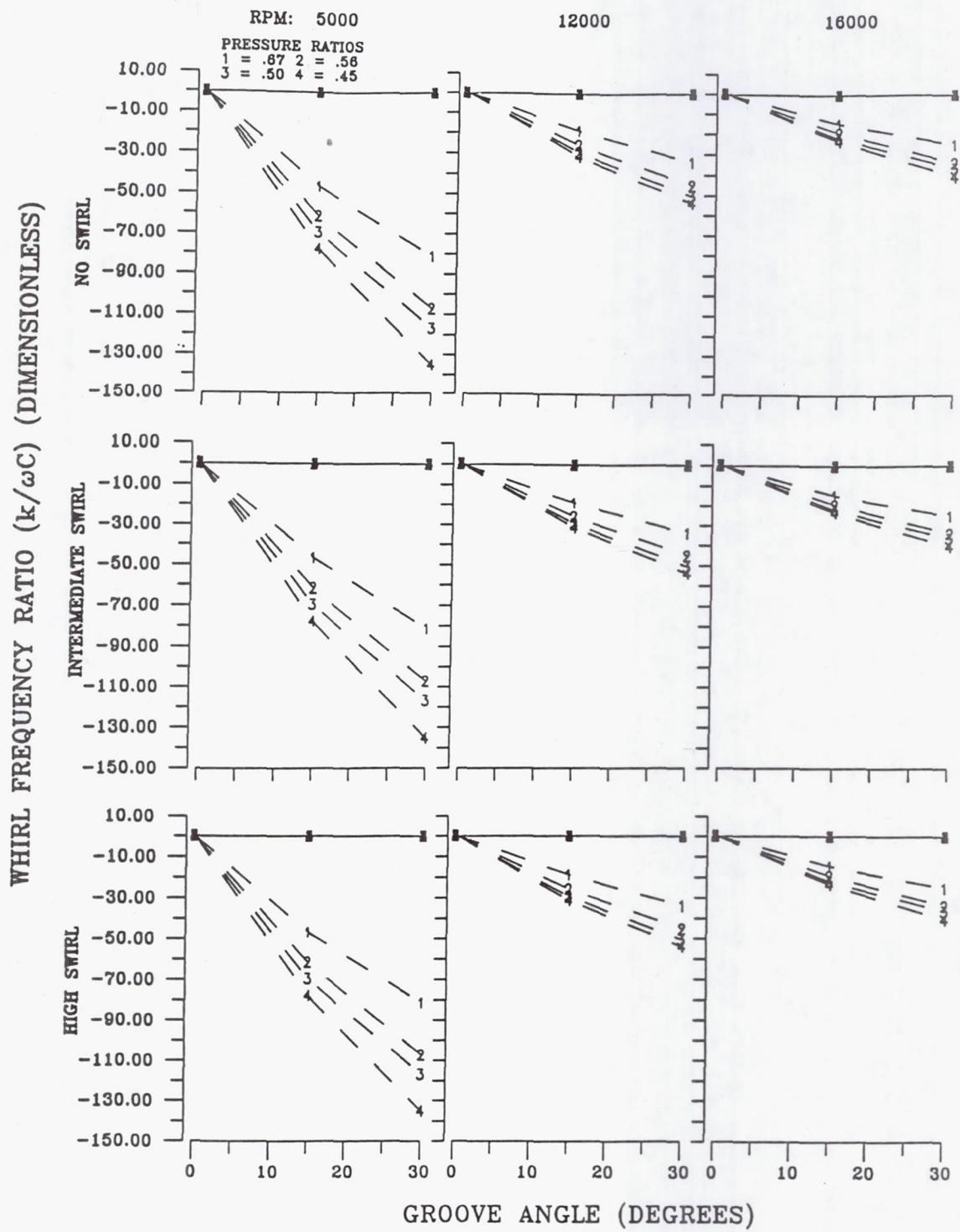
Experimental (solid) versus theoretical (dashed) results for whirl frequency
ratio as a function of groove angle for C_r=0.229 mm and P_r=7.9 bar
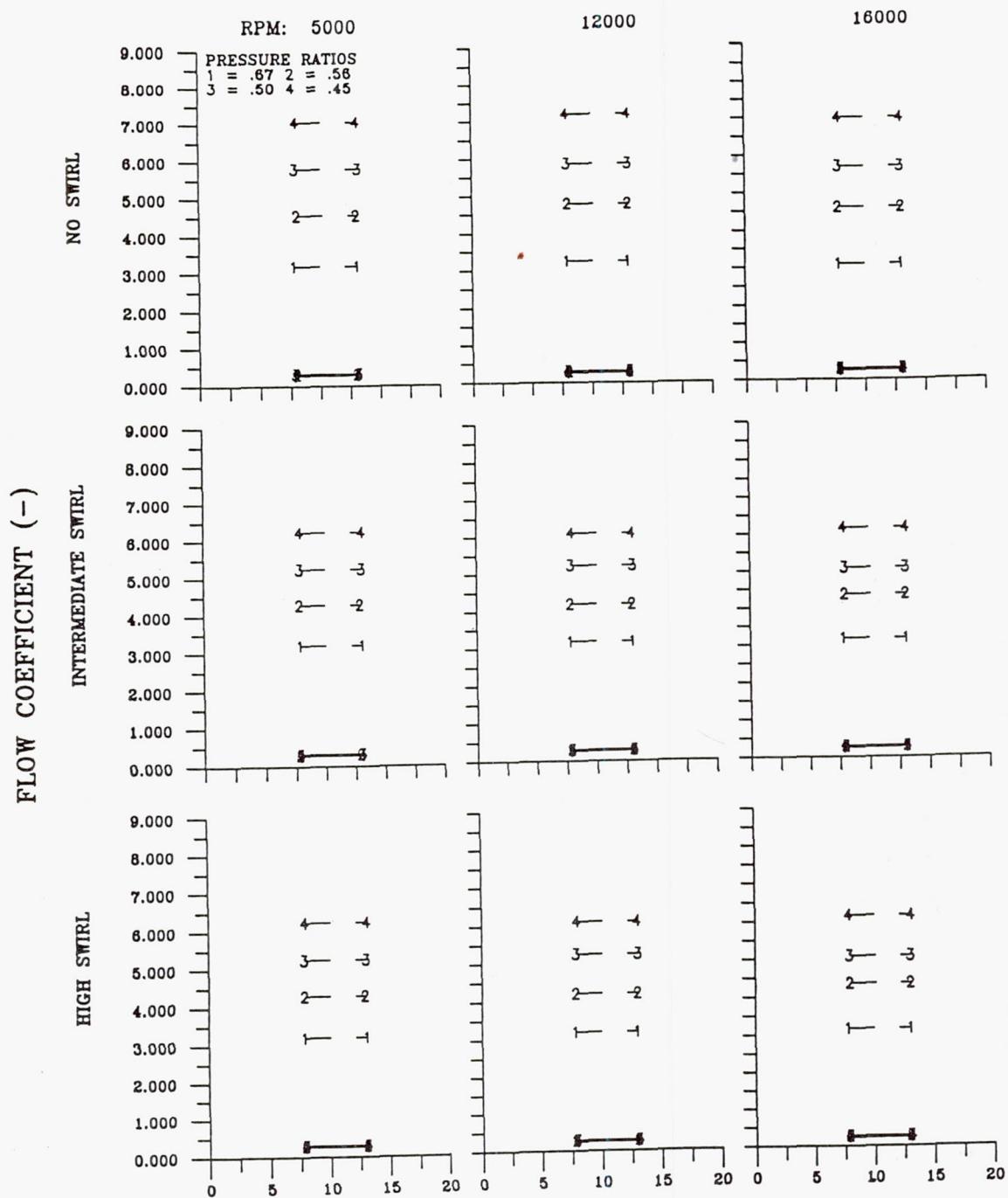
Experimental (solid) versus theoretical (dashed) results for flow coefficient
as a function of absolute inlet pressure for α=15° and C_r=0.305 mm

CONCLUSIONS

*   Helical-grooved seals provide a substantial reduction in cross-coupled stiffness coefficients. Negative k_{xy} values are obtained for no-swirl or low swirl cases.

*   SPIRALG is completely unsuitable for the type of seal tested; namely, turbulent flow, wide grooves and lands, etc.

*   A good analysis code is needed to guide the design of helically-grooved annular seals including groove and smooth sections.

PRESSURE MEASUREMENTS OF A THREE WAVE JOURNAL AIR BEARING

Florin Dimofte[*] and Harold E. Addy, Jr.
NASA Lewis Research Center
Cleveland, Ohio

ABSTRACT:

In order to validate theoretical predictions of a wave journal bearing concept, a bench test rig was assembled at NASA lewis Research Center to measure the steady-state performance of a journal air bearing. The tester can run up to 30,000 RPM and the spindle has a run out of less than 1 micron. A three wave journal bearing (50 mm diameter and 58 mm length) has been machined at NASA Lewis. The pressures at 16 ports along the bearing circumference at the middle of the bearing length were measured and compared to the theoretical prediction. The bearing ran at speeds up to 15,000 RPM and certain loads. Good agreement was found between the measured and calculated pressures.

[*]NASA Resident Research Associate
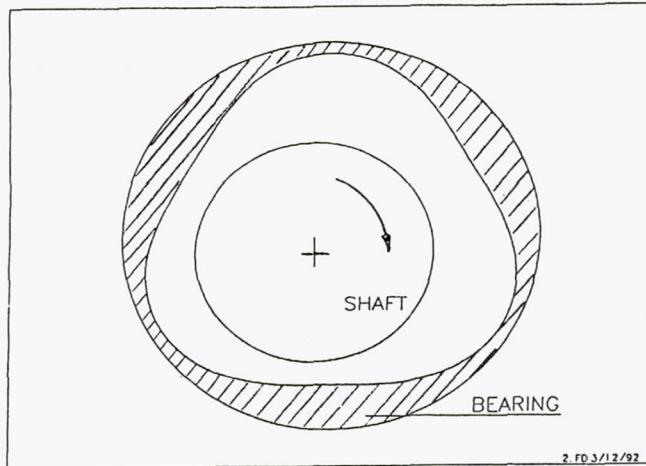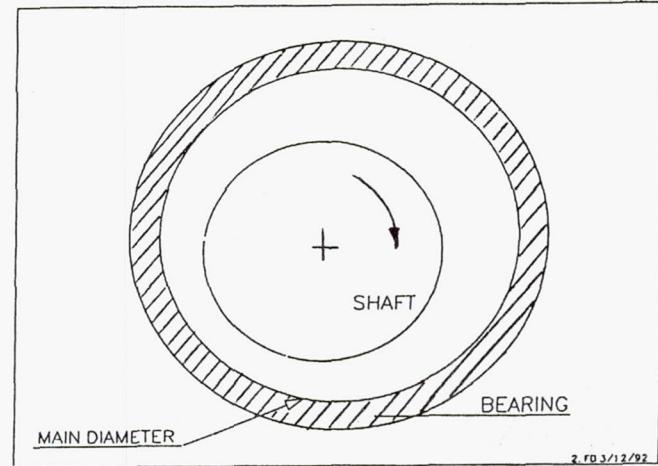
WAVED JOURNAL BEARING　　　　　　　　CONVENTIONAL JOURNAL BEARING

FIGURE 1. WAVED JOURNAL BEARING CONCEPT (Wave height and clearance greatly exaggerated)
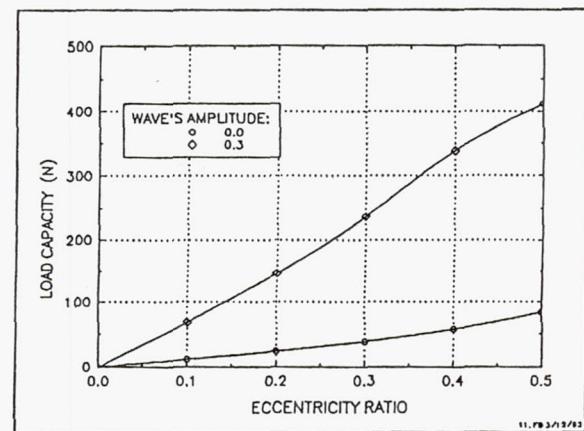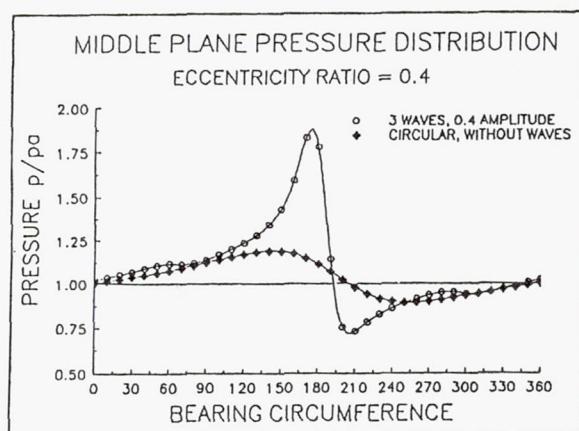
FIGURE 1A. WAVED/CONVENTIONAL BEARING PRESSURE DISTRIBUTION AND LOAD CAPACITY COMPARISON

286

Wave Bearing Advantages:

* The wave journal bearing has increased load (stiffness) compared to the truly circular journal bearing.

* The wave journal bearing offers better stability than the truly circular journal bearing under all operating conditions.

* The wave journal bearing's performance is dependent upon the wave amplitude and increase significantly as the wave amplitude increases.
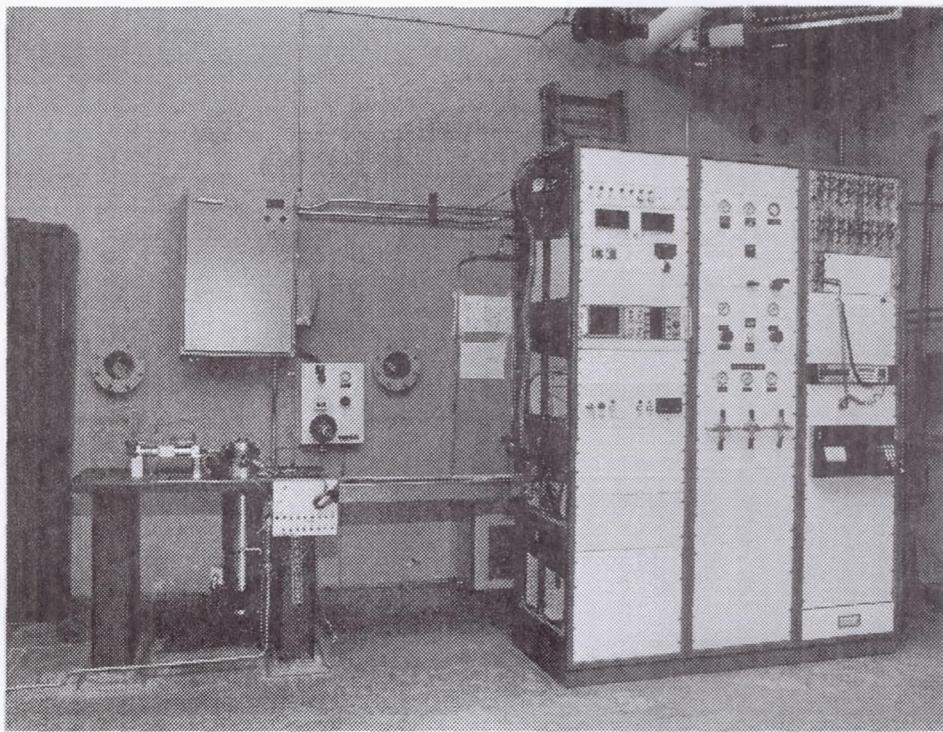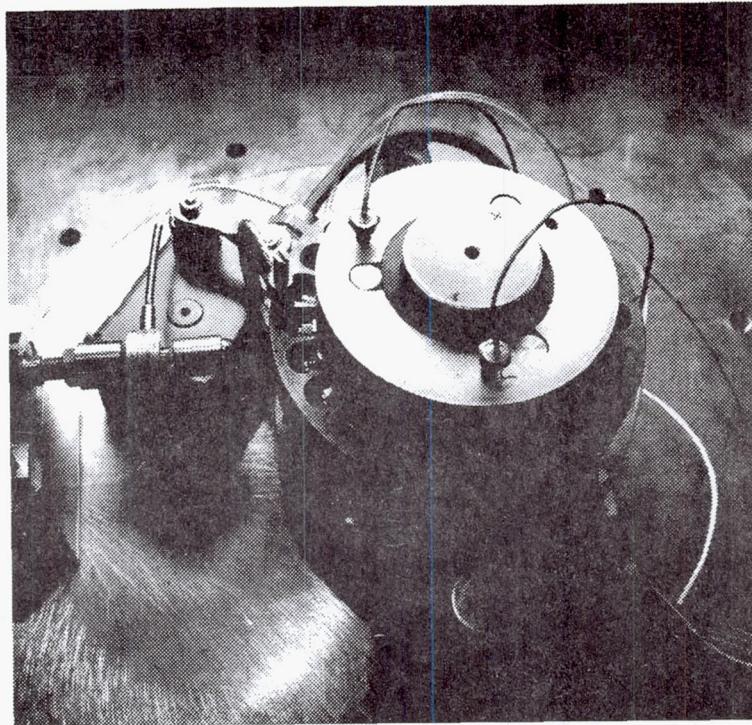
The Journal Bearing Bench Tester

* Lubricant: air

* Spindle: Air Bearing Spindle:

    - Speed: up to 30000 RPM,

    - Run-out less than 1 micron.

* Levitation Thrust Air Bearing Plate with three sectors.

* Instrumentation:

    - Turning Speed Read Out,

    - SOTEC Precision Miniature Load Cell 100 lbs.,

    - Kaman Instrumentation Displacement Sensors,

    - ENDEVCO Piezo-resistive Pressure Transducers,

    - Thermo-couples.
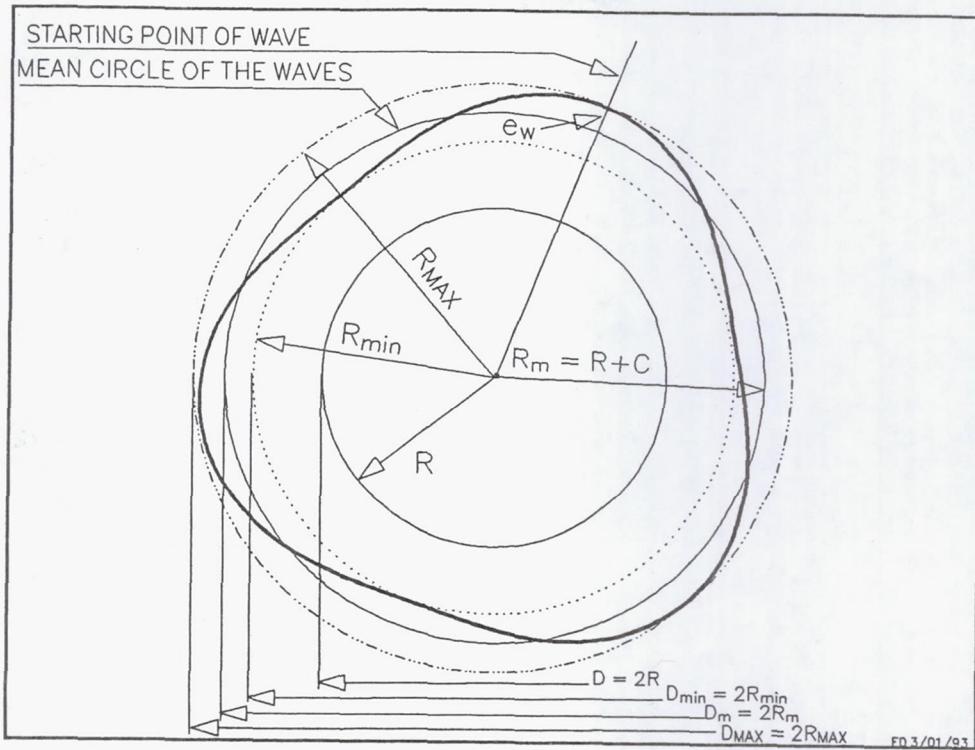
a. Theoretical three wave bearing profile.
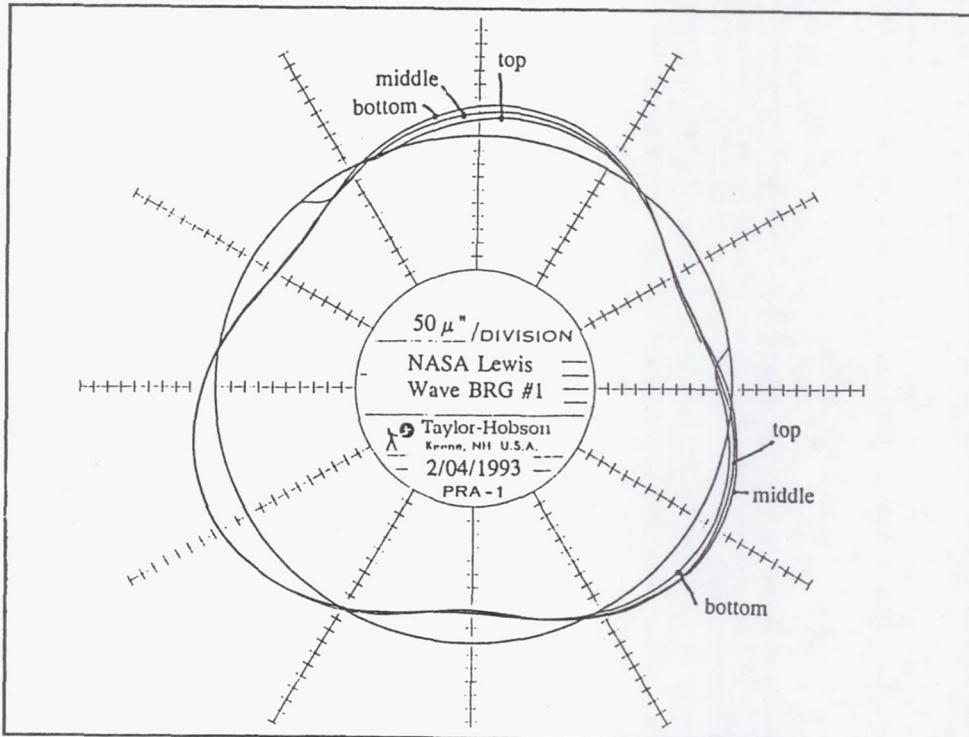
b. NASA Lewis Three Wave Bearing Measured Profile.

Date: 2/04/93 Machine Shope 71° F

Bearing:	D_{min}	D_{MAX} [inchs]	ϵ_w & C [μm]		Shaft: D =2R [inchs]	
Top:	2.0118	2.013	7.62	12.7	2.0114	2.0114
Middle	2.0119	2.0129	6.35	12.065	2.0114	2.0115
Bottom	2.0121	2.0133	7.62	15.24	2.0115	2.0115
	2.011933	2.013067	7.2	13.335	2.01145	

****
D_m =2R_m =2.0125"   Error: 0.0003"/D =3.8 μm /R   Error: .0001"/D =1.2 μm /R
****

Metric:	D_{MAX} =51.132	D_{min} =51.103	D_m =51.1175	D =51.091
[mm]	R_{MAX} =25.566	R_{min} =25.5515	R_m =25.55875	R =25.5455

Radial Clearance: C =(D_m - D)/2 =(R_m - R) =0.01325mm =13.25 μm

Wave Amplitude e_w =(D_{MAX} - D_{min})/4 =(R_{MAX} -R_{min})/2 =0.00725mm =7.25 μm

Wave Amplitude Ratio ϵ_w =e_w/C =.54717

Bearing Length: L =58mm   Bearing Mass: M =2.966 Kg

NASA THREE WAVE JOURNAL TEST BEARING
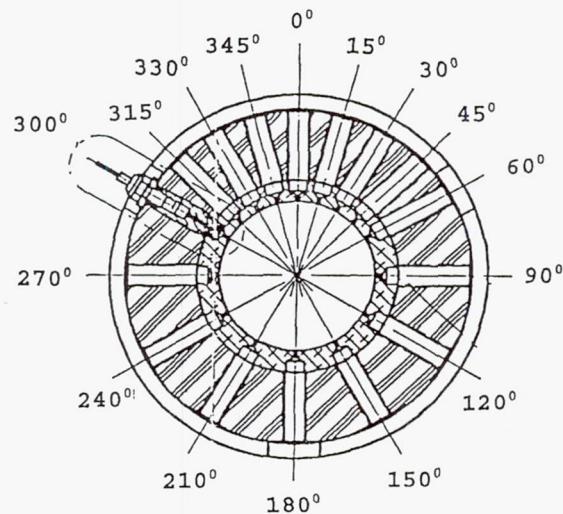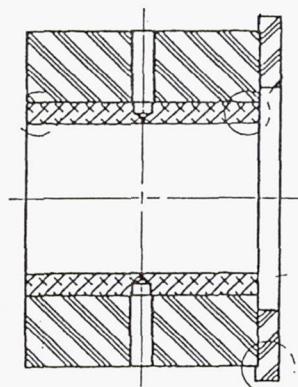
PRESSURE PORT LOCATIONS
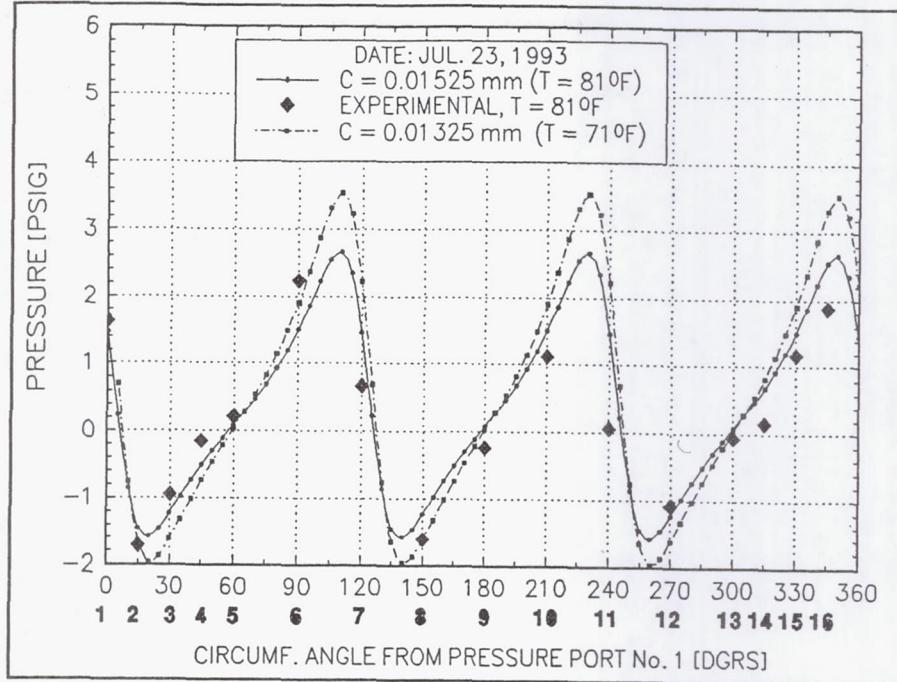
a. Speed 2000 RPM, Load 0..
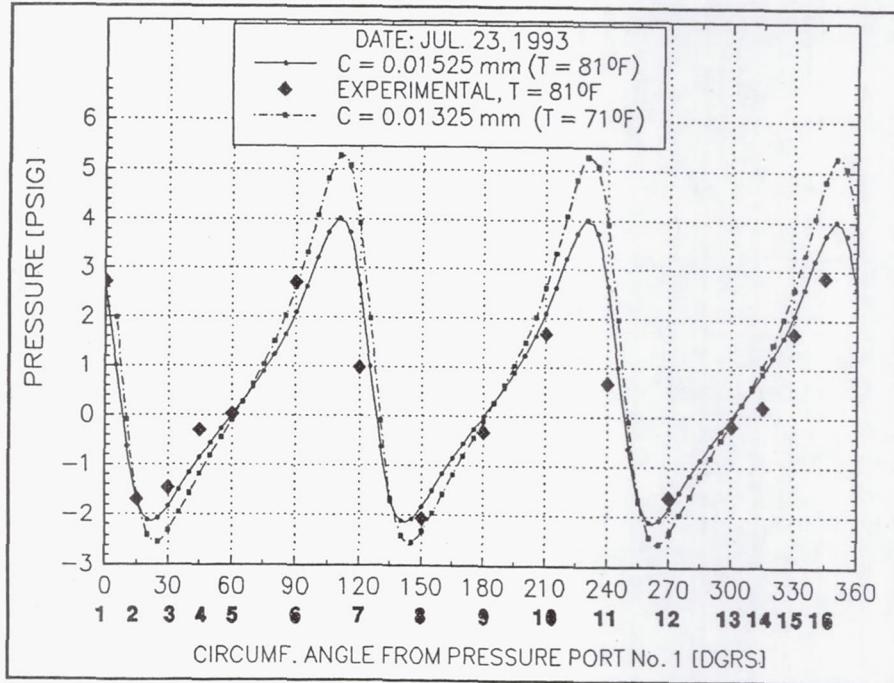
b. Speed 3000 RPM, Load 0..

NASA Test Wave Bearing #1, Predicted and measured pressures in the bearing middle plane. The influence of the bearing temperature over the bearing radial clearance and bearing pressures.

291
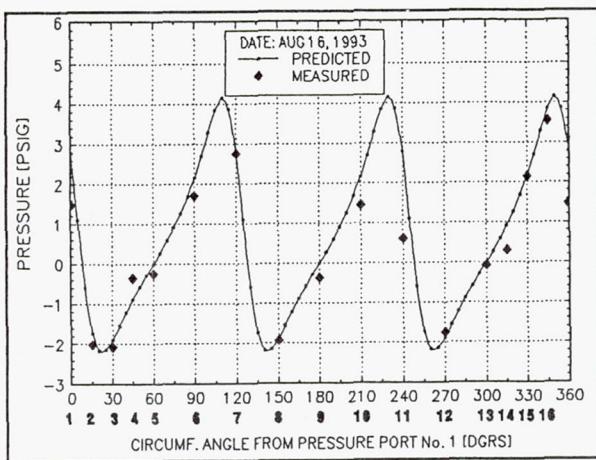
a. 3000 RPM, C=15.0μm, (t=80°F)
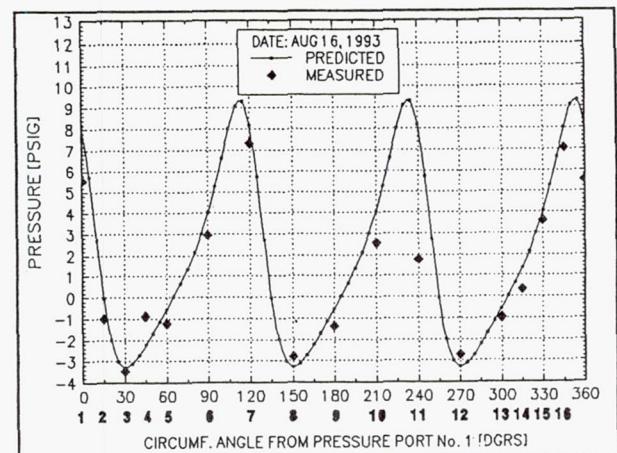
c. 8000 RPM, C=15.8μm, (t=84°F)
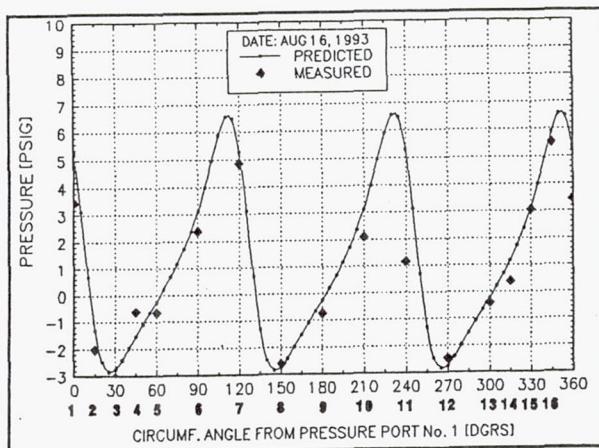
b. 5000 RPM, C=15.1μm, (t=81°F)
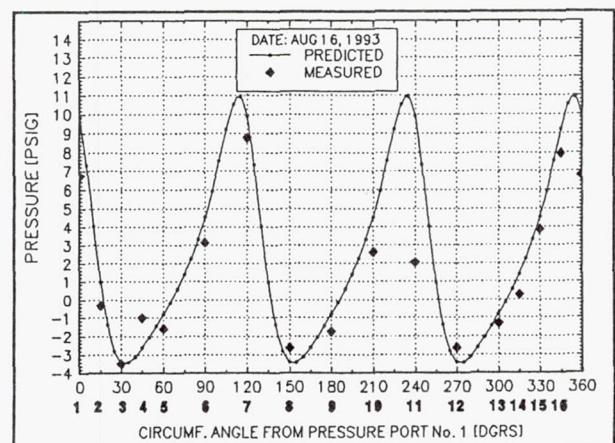
d. 10000 RPM, C=15.9μm, (t=85°F)

NASA LEWIS Test Wave Bearing #1, Predicted and measured pressures in the bearing middle plane at zero load and certain speeds.
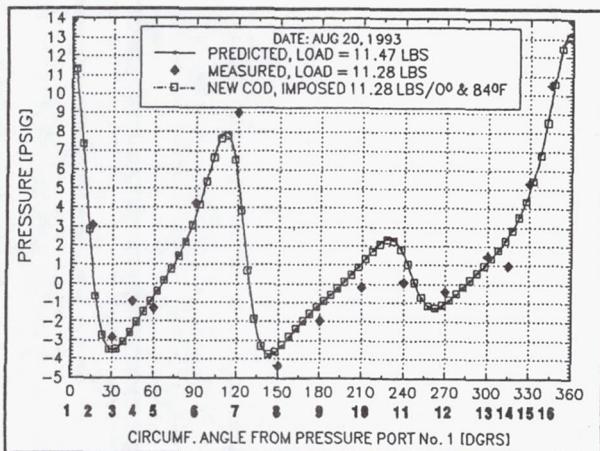
a. 5000 RPM, C=15.8μm, (t=83^{0}F).
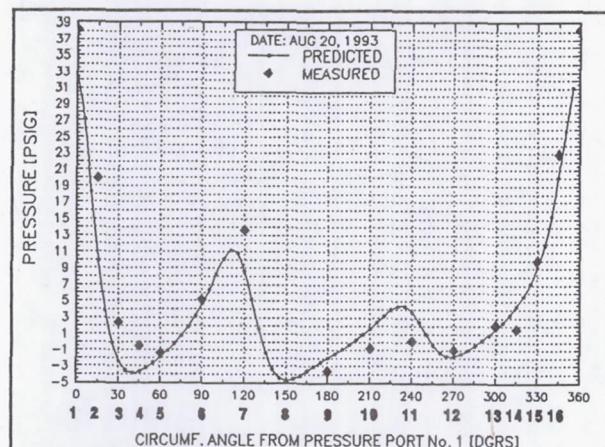
c. 10475 RPM, Load 22.0 lbs., C=15.9μm.
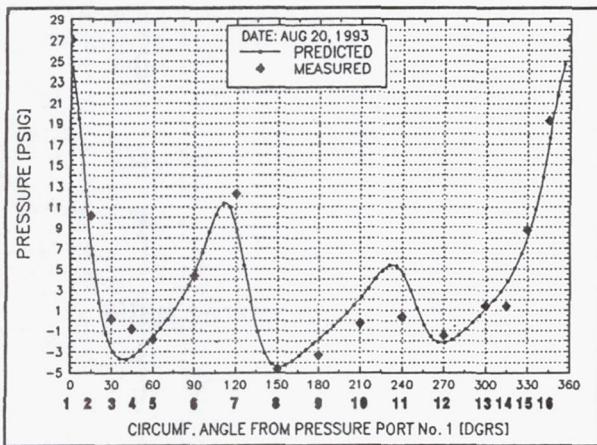
b. 10475 RPM, Load 22.0 lbs., C=15.9μm.
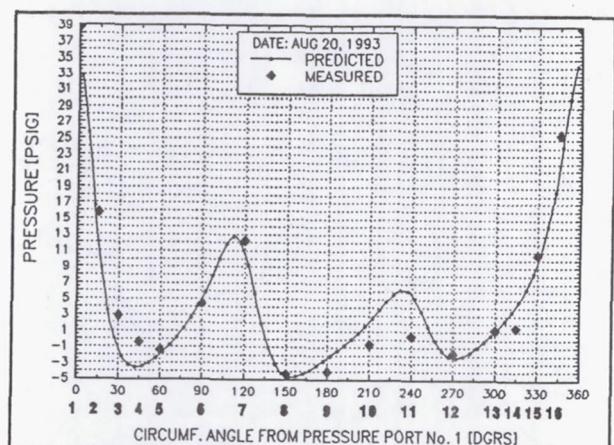
d. 15069 RPM, Load 31.8 lbs., C=19.0μm.

NASA LEWIS Test Wave Bearing #1, Predicted and measured pressures in the bearing middle plane at certain loads and speeds.

CONCLUSIONS:

* Good agreement was found between the measured and calculated pressures. A correction of the bearing clearance due to actual bearing running temperature is necessary.

* The three wave test bearing # 1 can run stable without load up to 6000 RPM when the half frequency whirl instability phenomena occurs. However, the bearing running speed can be increased up to 10000 RPM without any damage of the bearing. The wave bearing can keep the half frequency whirl instability orbit inside its clearance and the bearing runs safely. A small amount of load such as 10 lbs. makes the bearing to run stably without any half frequency whirl phenomena.

Antonio Artiles
Mechanical Technology Incorporated
Latham, New York

Capabilities

- 2-D incompressible isoviscous flow
- Rotation of both rotor and housing
- Roughness in both rotor and housing
- Arbitrary film thickness distribution, including steps, pockets and tapers
- 3 degrees of freedom
- Dynamic coefficients
- Prescribed Force and Moments
- Pocket pressures or orifice size
- Turbulence, Couette and Poiseuille
- Cavitation
- Inertia pressure drops at inlets to film (from seal ends and from pressurized pockets)

Assumptions

- Small film thickness

- Constant pocket pressures

- Isotropic roughness

- Negligible film inertia

Arbitrary Film Thickness
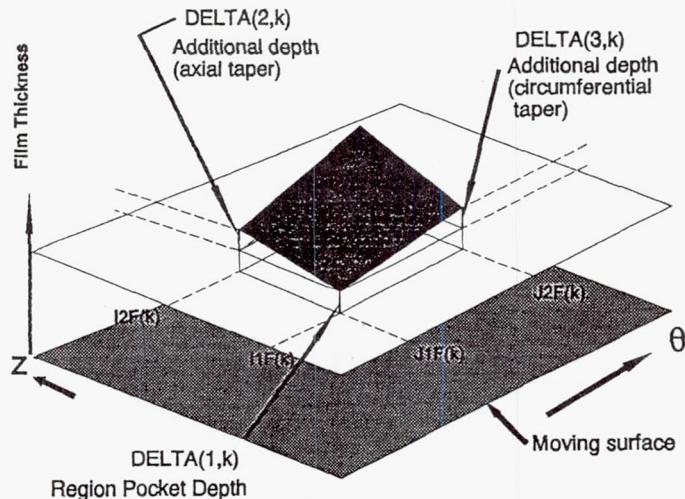
Figure 10   Arbitrary film thickness specification

Friction Factor

Curve Fit by Nelson to Moody's Data*
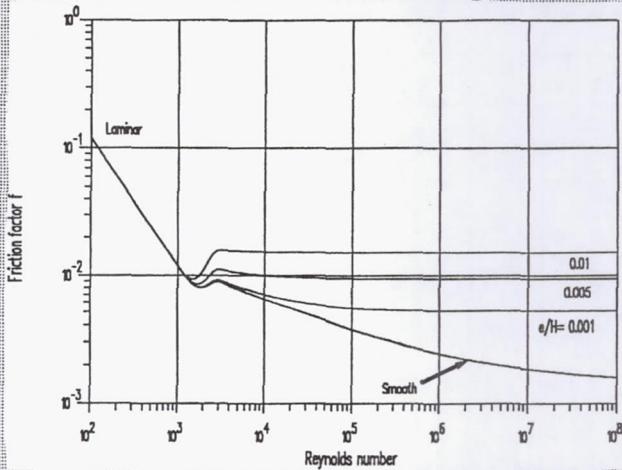
*Nelson, C. C., Ngyen, D. T., *Comparison of Hir's Equation with Moody's Equation for Determining Rotordynamic Coefficients of Annular Pressure Seals*, Trans ASME, Journal of Tribology, Jan. 1987 pp. 144-148

Transition Friction Factor

Cubic polynomial to match values and slopes at both ends
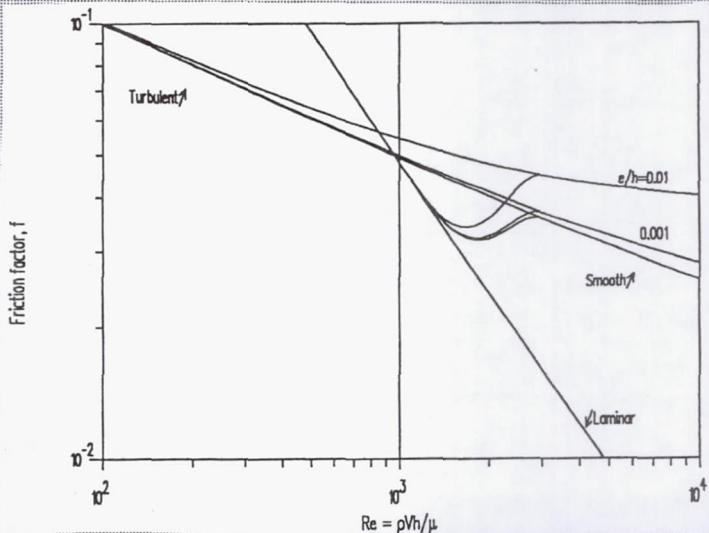
Sample Problems

Case	Mesh size MxN	Variables specified	Variables calculated	NPADS	run time (sec)	features
1	5x11	EX, ALFA			3.75	variable grid, DELTA(1,1)
2A	5x31	FXG, MXG, MYG	EX,ALFA, BETA	3	125	prescribed force & moments, DELTA(5,1)
3A	7x41	PPOCK	DORIF, K,B	4	404	4-pocket, calculation of orifice & coefficients
3B	7x41	DORIF, EX,BETA	PPOCK	4	352	4-pocket, prescribed displacements
3C	7x41	DORIF, FXG, MXG,MYG	PPOCK, EX, ALFA,BETA	4	566	4-pocket, prescribed force & moments, pressures read
13	9x37		K, B	4	1093	preloaded pads, roughness multiple cases, DELTA(4,1)
17	9x65	ALFA		8	103	8 Rayleigh steps
15A	10x61	PPOCK	DORIF, K,B	4	2115	4-pocket with XKE=1
15B	10x61	DORIF, EX, MXG, MYG	ALFA,BETA, PPOCK	4	1368	4-pocket finding angular position, pressures read

Table 3 Summary of sample cases

Sample 13, Effect of Roughness on Torque and Direct Stiffness

roughness (mils)		torque	K_{zz}	$K_{\alpha\alpha} = K_{\beta\beta}$
			(10^8lb/in)	(10^8lb-in/rad)
rotor	housing	(in-lb)		
0.02	0.02	2,900	245	1,956
0.02	0.00	2,354	158	1,153
0.00	0.02	2,366	263	2,035
0.00	0.00	2,006	184	1,337

Table 4   Effect of roughness on torque and direct stiffnesses
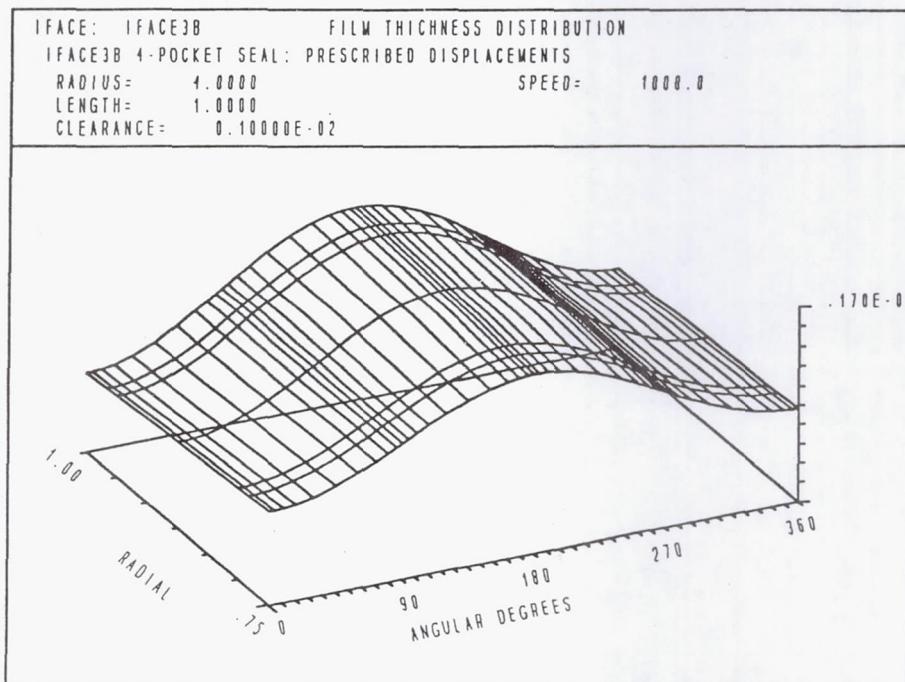
Figure 15   Film thickness distribution for sample 3B
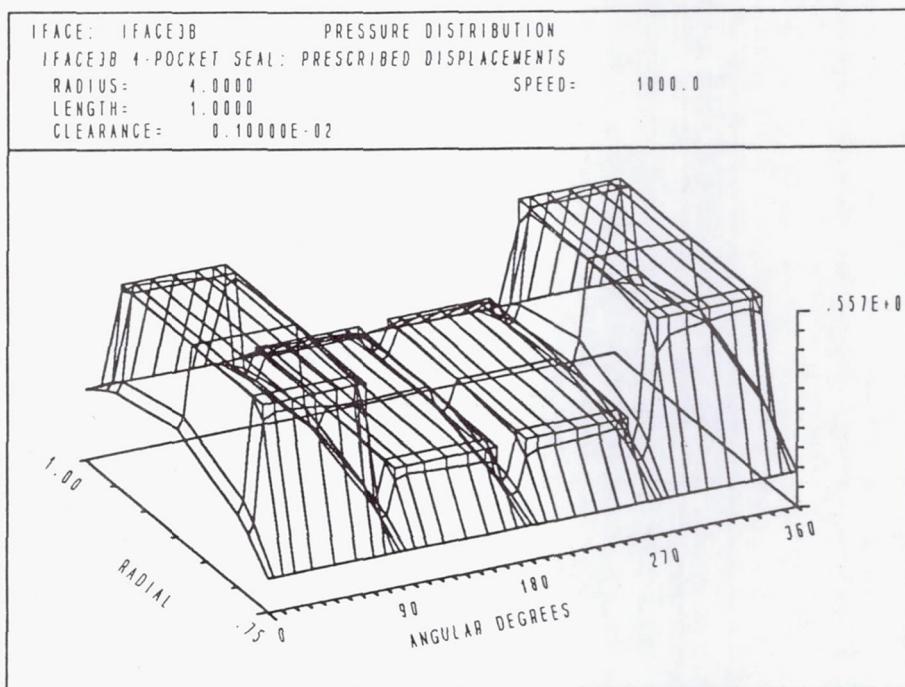
Figure 16   Pressure distribution for sample 3B.

Preloaded Pads With Rough Housing
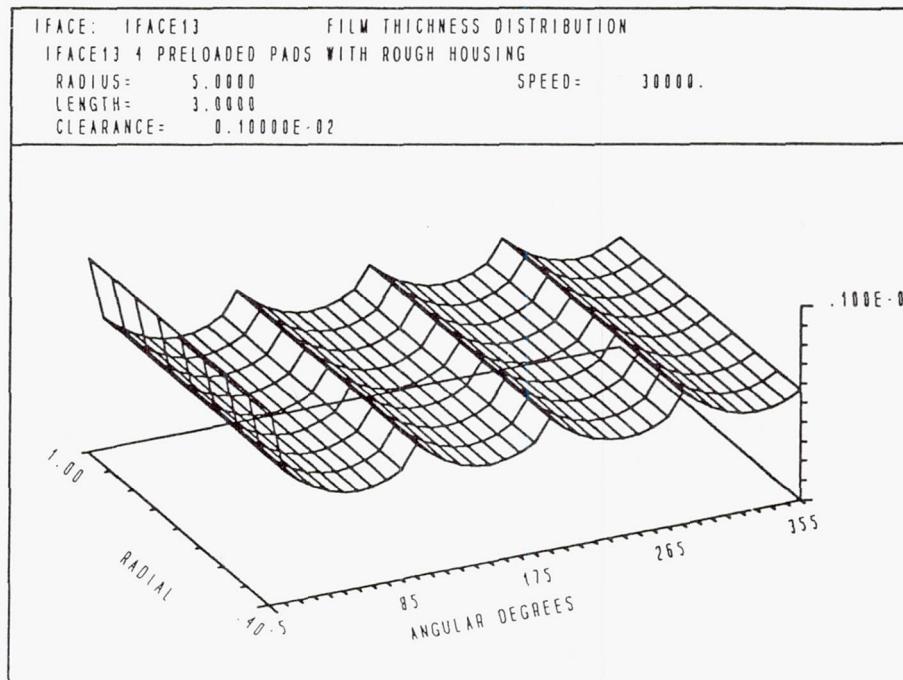
Figure 17 Film thickness distribution for sample 13.
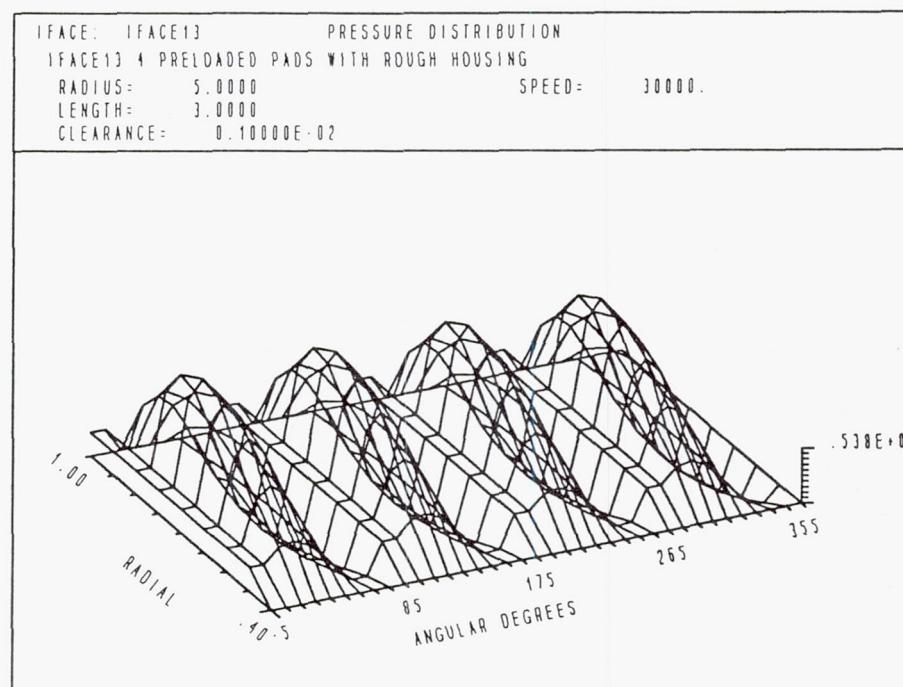
Figure 18 Pressure distribution for sample 13.

Rayleigh-step Seal Fed From Groove I.D.

IFACE: IFACE17   FILM THICKNESS DISTRIBUTION
IFACE17 8 RAYLEIGH STEPS FED FROM GROOVE FROM ID
RADIUS=   5.0000   SPEED=   1600.0
LENGTH=   3.0000
CLEARANCE=   0.10000E-02
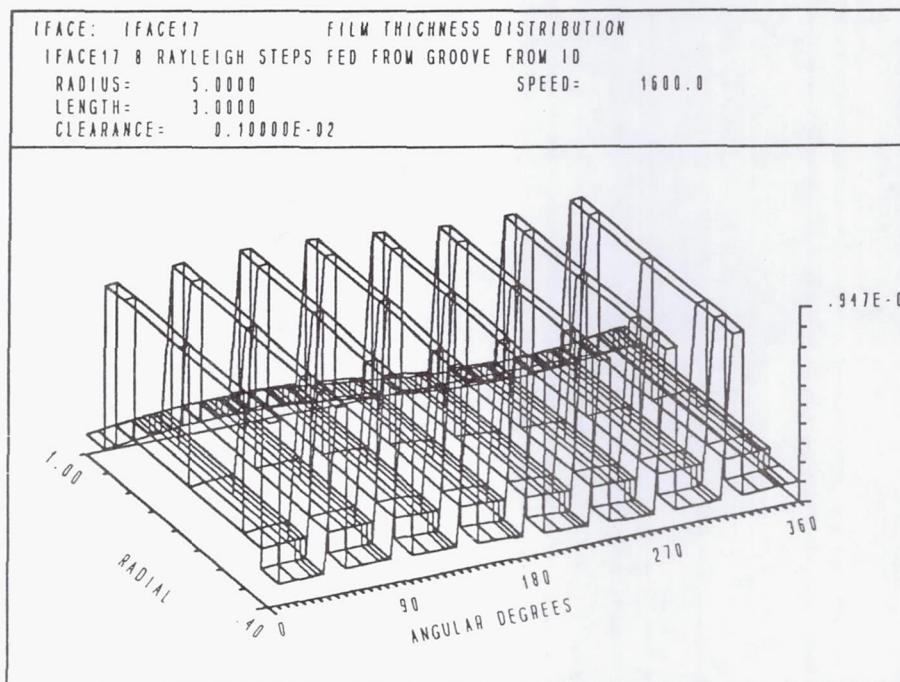
Figure 19   Film thickness distribution for sample 17.

IFACE: IFACE17   PRESSURE DISTRIBUTION
IFACE17 S RAYLEIGH STEPS FED FROM GROOVE FROM ID
RADIUS=   5.0000   SPEED=   1600.0
LENGTH=   3.0000
CLEARANCE=   0.10000E-02
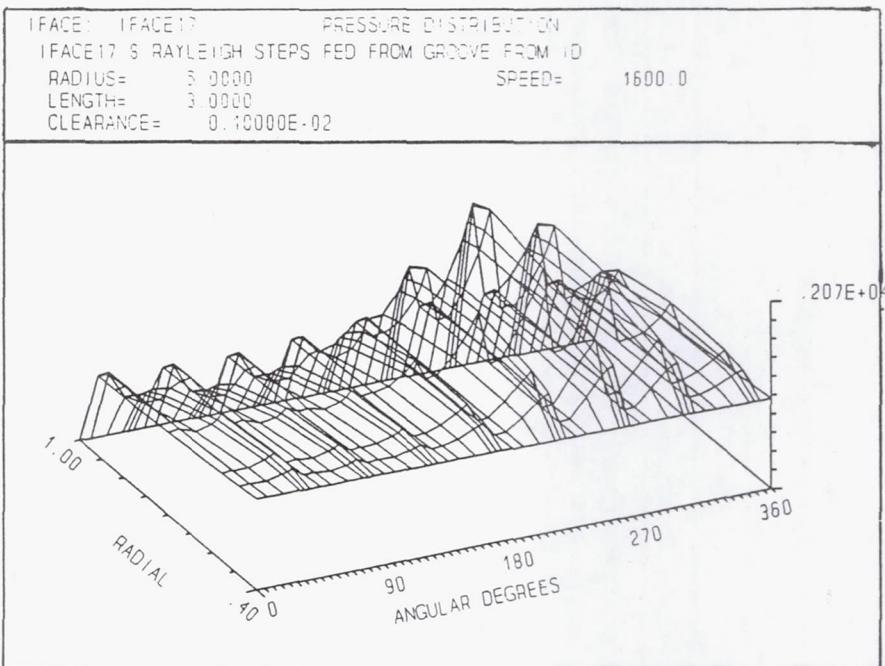
Figure 20   Pressure distribution for sample 17.

4– Pocket Face Seal with Prescribed Moments
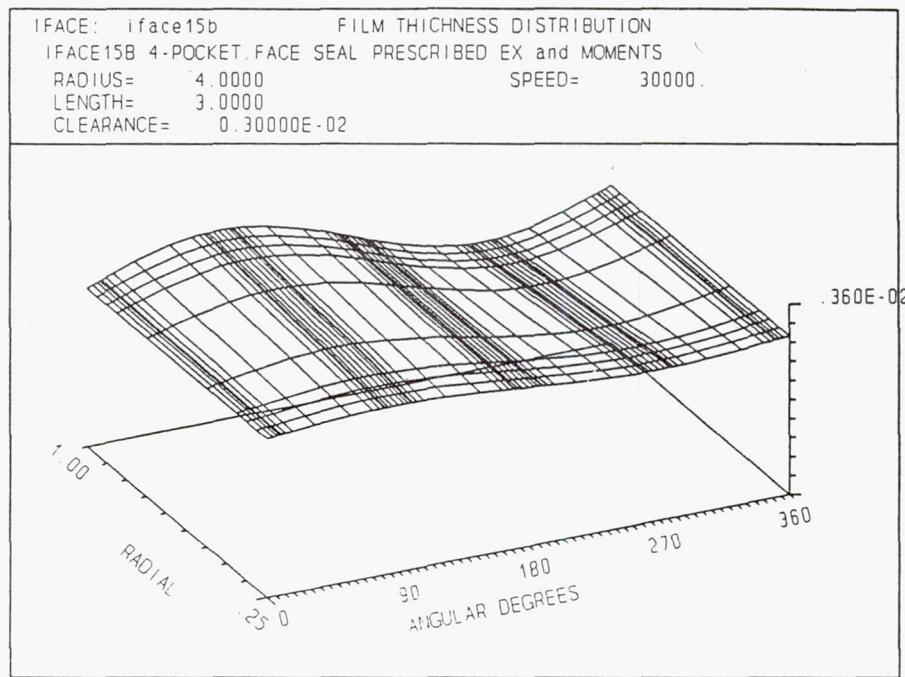
Figure 21   Film thickness distribution for sample 15B.
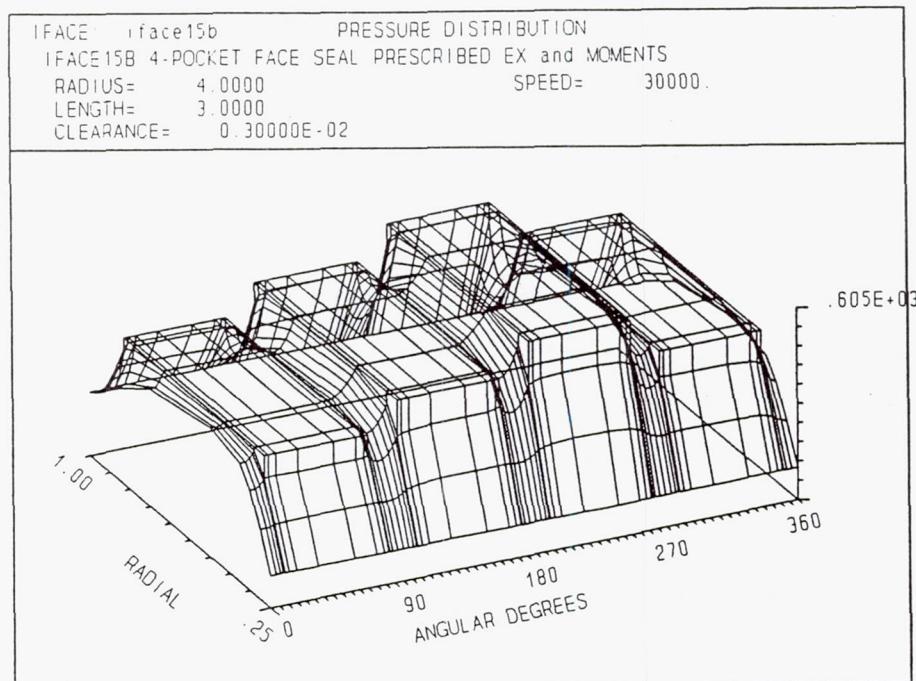
Figure 22   Pressure distribution for sample 15B.

Verification

	GBEAR	ICYL IFRIC=0	ICYL IFRIC=3	ICYL IFRIC=4
Recess flow (in^3/s)	25.75	25.21	20.931	22.316
Orifice diam. (in)	0.0833	0.0820	0.0752	0.0776
Torque (lb-in)	14.38	14.32	8.791	9.771
Power (Lb-in/s)	45,171	44,971	27,617	30,696
Fx (Lb)	3,694	3,358	3,352	3,477
Fy (Lb)	-3,488	-3,122	-3,083	-3,346
Kxx (10^6 Lb/in)	2.352	2.267	2.329	2.344
Kxy (10^6 Lb/in)	-1.461	-1.378	-1.280	-1.397
Kyx (10^6 Lb/in)	-1.998	-1.874	-1.871	-1.961
Kyy (10^6 Lb/in)	1.573	1.481	1.406	1.564
Bxx (Lb/in)	232.08	234.79	269.01	274.46
Bxy (Lb/in)	-175.53	-175.87	-194.38	-199.65
Byx (Lb/in)	-174.78	-174.10	-192.40	-200.56
Byy (Lb/in)	173.87	173.79	187.57	196.53

Table 5   Comparison against GBEAR.

RELATIVE PERFORMANCE COMPARISON BETWEEN BASELINE LABYRINTH AND DUAL-BRUSH COMPRESSOR DISCHARGE SEALS IN A T-700 ENGINE TEST

Robert C. Hendricks
NASA Lewis Research Center
Cleveland, Ohio

Thomas A. Griffin
Vehicle Propulsion Directorate
U.S. Army Research Laboratory
NASA Lewis Research Center
Cleveland, Ohio

Kristine R. Csavina
Sverdrup Technology, Inc.
NASA Lewis Research Center Group
Brook Park, Ohio

and

Arvind Pancholi and Dvandra Sood
General Electric Corporation
Lynn, Massachusetts

ABSTRACT

In separate series of T–700 engine tests, direct comparisons were made between the forward-facing labyrinth and dual-brush compressor discharge seals. Compressor speeds to 43 000 rpm, surface speeds to 160 m/s (530 ft/s), pressures to 1 MPa (145 psi), and temperatures to 680 K (765 °F) characterized these tests. The wear estimate for 40 hr of engine operations was less than 0.025 mm (0.001 in.) of the Haynes 25 alloy bristles running against a chromium-oxide-coated rub runner. The pressure drops were higher for the dual-brush than for the forward-facing labyrinth seal, implying better seal characteristics and engine performance for the brush seal. Modification of the secondary flow path requires that changes in cooling air and engine dynamics be accounted for.

Preceding Page Blank

INTRODUCTION

Labyrinth seals are efficient, readily integrated into designs, and generally easy to install into engines but are inherently unstable (Hendricks et al., 1992). However, installing a simple swirl break significantly enhances the stability margin and mitigates this drawback (Childs et al., 1989). Details of theory, experiments, and design methods for labyrinth seals and configurations are provided by Trutnovsky (1977). Forward-facing labyrinth tooth configurations with a variety of rub interfaces (e.g., honeycomb) were studied in detail by Stocker et al. (1977) under a U.S. Air Force contract with codes developed by Morrison and Chi (1985), Demko et al. (1988), and Rhode et al. (1988) and by Rocketdyne (internal Rocketdyne report). Optimization procedures are available from MTI Inc. (private communication from W. Shapiro) and are being implemented into the NASA seals codes program.

Brush seal systems are efficient, stable, contact seals that are usually interchangeable with labyrinth shaft seals but require a smooth rub runner interface and an interference fit upon installation. The major unknowns and needed research are tribological (e.g., life or interface friction and wear) because of the following performance demands: pressure drops over 2.1 MPa (300 psi), temperatures to over 1090 K (1500 °F), and surface speeds to 460 m/s (1500 ft/s). Current research supported by the Navy (private communication from W. Voorhees), the U.S. Army (private communication from R. Bill and G. Bobula), and the U.S. Air Force's Wright Patterson Air Force Base is addressing these issues and shows promise in meeting these demands.

In this paper we compare the relative pressure drop differences between the baseline labyrinth and dual-brush compressor discharge seals at compressor discharge pressures to 1 MPa (145 psi) and temperatures to 680 K (765 °F) with operating speeds to 43 000 rpm.

ENGINE FLOW PATH

The power stream airflow through the compressor and the secondary airflow leakage past the compressor discharge seal are illustrated in Fig. 1. The compressor discharge seal package and associated drain tube are located immediately downstream of the impeller and labeled CDS. The drain tube was opened after a series of runs and swabbed for debris.

COMPRESSOR DISCHARGE SEAL

Labyrinth Seal System

The nominal 71-mm (2.8-in.) diameter forward-facing labyrinth seal system is illustrated in Fig. 2. The labyrinth teeth rub into a felt-metal type of interface, forming the seal system. Note that the teeth are not all forward facing and are used in different ways to satisfy different engine operating requirements. A simulated exploded view of the seal system is given in Fig. 3 and clearly illustrates the forward-facing teeth of the rotor. However, the housing shown in the figure is for the brush seal.

Brush Seal System

The brush seal system replacement package is illustrated in Fig. 4. The dual brush, nominally 71 mm (2.8 in.) in diameter, runs against a chromium-oxide-coated rub runner interface as shown schematically. The basic seal system was envisioned by General Electric and manufactured by Cross Mfg. Ltd. (Flower, 1990). It has 0.071-mm (0.0028-in.) diameter, Haynes 25 bristles angled 43° to 50° to the interface with approximately 98 to 99 per millimeter of circumference (2500 per inch of circumference) and a nominal interference fit of 0.127 mm (0.005 in.) at installation. Figure 5 gives a post-test exploded view of the brush seal system with associated instrumentation lines (cut after testing). Figure 6 provides a side-by-side comparison of the forward-facing labyrinth seal (right) and the chromium-oxide-coated rub runner replacement (left); these represent the rotating interface.

APPARATUS AND INSTRUMENTATION

Pretest and post-test photographs of the dual brush and its installation in the seal system are shown as a series in Fig. 7. Figure 8 depicts the dual brush prior to testing. Figure 7(a) shows the upstream view of the instrumented housing; four thermocouples are attached to the side plates with upstream and downstream pressure taps. Figure 7(b) shows a direct view from the downstream side, and Fig. 7(c) is an isometric view showing the "shiny" nature of the bristle interface. Actual brush seal dimensions, rub runner coating, and installation of instrumentation are proprietary.

ENGINE SEAL INSTALLATION AND OPERATIONS

The T–700 compressor section was first assembled with the labyrinth seal and run as a baseline for comparison. After a test series was completed, the engine was shipped to the Corpus Christi overhaul facility. The compressor discharge seal labyrinth system was removed and the brush seal system was installed. The brush seal system was installed without special waxes, which can lead to bristle distortions and irregular bristle voidage. These waxes hold the bristles off the rotor during installation and readily "burn out" at a low temperature.

Operations consisted of the standard break-in procedures with data taken primarily under steady conditions. The engine was operated a total of 20 hr, including break-in, from ground to flight idle. Compressor speeds were to 43 000 rpm with seal housing temperatures to 680 K (765 °F). Local conditions at various compressor discharge pressures are given in Table I. The compressor discharge seal leakage was vented through the drain tube (Fig. 1) and metered by using a calibrated orifice. Because leakage data results were noisy, pressure drop was judged a more reliable indicator of leakage. The debris collected in the drain tube was a "lubricant powder," but the spectra indicated several contaminant metals from elsewhere in the engine. Rotor roughness, brush construction, and upstream debris generation play a major role in determining the spectrum. Although neither radial nor axial rotor positions were monitored, such position sensors should be an integral part of the engine dynamics.

RESULTS

Post-test measurements of the brush and inspection of the bristles revealed a smooth bristle interface with some characteristic shear wear (Fig. 9) but little other visible damage. The brush wear patterns (Figs. 10 and 11) were attributed to the engine dynamics although no dynamic tracking instrumentation was available. The patterns are interesting in that they are 15° from the antirotation pin. (GE is to provide clocking and determine if that point is associated with a compressor bearing position or loading point.) The patterns for the upstream seal differed from those for the downstream seal (see also Fig. 4), indicating a differential in pressure drop across each of the seals. It is anticipated that about 40 percent of the total pressure drop across the dual brush occurred across the first brush and 60 percent across the second brush (Flower, 1990, and private communication from R. Flower of Cross Mfg. Ltd.). Such loading resulted in stiffer bristles in the second brush and implies a greater bristle wear. Preload and operational loads are important design life parameters (private communication from Wright Patterson Air Force Base), but data to quantize these parameters are not available.

Another variation in the wear pattern is attributed to the rotor machining or coating variations (Fig. 11). The rotor showed a small eccentricity and was investigated for metallic transfer, but no significant transfer was found. The chromium oxide interface was worn smoother by the rubbing brush bristle interface, implying some form of wear or material smearing without significant transfer of the chromium oxide (CrO).

During the test series the drain pipe (Fig. 1) was swabbed for debris. When these samples were in turn investigated with a scanning electron microscope (SEM), nickel, chromium, and tungsten lines were observed along with other unexplainable peaks of salts (e.g., Fig. 12). The nickel, chromium, and tungsten lines characterize bristle materials and some possible coating wear. The debris was fine and difficult to locate and isolate within the tube. Other metal sources and rubbing surfaces could have also produced such debris, but we attributed it to bristle wear.

The CrO-coated rub runner exhibited slight wear scars but no spallation or coating degradation otherwise. These wear bands are readily visible in Fig. 6, where the upper band is associated with the upstream (high-pressure side) brush; see also Fig. 5. The upstream wear surface is characterized by Fig. 13(a) and the downstream wear surface by Fig. 13(b). The CrO coating is characterized by light and gray areas, and the energy spectrum shows the light areas to be an NiCr composition and the gray areas to be predominantly Cr. The light and gray areas of the matrix or unrubbed material between the bands is illustrated in Figs. 13(c) and (d). Similarly, for the upstream wear band in Figs. 13(e) and (f) and for the downstream wear band in Figs. 13(g) and (h). There appears to be no material transfer from the bristles to the rotor and only minor scarring and polishing.

The result of interest here is that the initial design interference was 0.127 mm (0.005 in.) and the post-test estimate of interference was 0.101 mm (0.004 in.), or perhaps a maximum wear of 0.025 mm (0.001 in.).

Although direct flow measurements were not available, the pressure drops for each comparable compressor discharge pressure setting were higher for the brush seal system than for the labyrinth seal system (Tables I and II). The implication is that for the same engine

operating conditions the dual-brush system leaked less than the baseline forward-facing labyrinth seal system. Also implied is enhanced engine efficiency.

It is important to recognize that more efficient seals cannot simply be installed without computing and accounting for the secondary airflows necessary for the cooling and engine dynamics associated with the seal leakage modifications.

SUMMARY

In a series of T–700 engine tests, direct comparisons were made between a forward-facing labyrinth seal configuration and a dual-brush compressor discharge seal. The nominal seal diameter was 71 mm (2.8 in.). The test conditions included compressor discharge pressures to 1 MPa (145 psi), temperatures to 680 K (765 °F), operating speeds to 43 000 rpm, and surface speeds to 160 m/s (530 ft/s) with the working fluid being nominally dry ambient air. The bristle wear was estimated to be less than 0.025 mm (0.001 in.) in 40 hr of engine operations.

Direct flow measurements were not available. The pressure drops at each comparable compressor discharge pressure setting were higher for the brush seal system than for the labyrinth seal system, implying that for the same engine operating conditions the dual-brush system leaked less than the baseline forward-facing labyrinth seal system. Also implied is enhanced engine efficiency.

More efficient seals cannot simply be installed into an engine without computing and accounting for the secondary airflows necessary for the cooling and engine dynamics associated with the seal leakage modifications.

ACKNOWLEDGMENTS

REFERENCES

Childs, D.W., Ramsey, C.J., and Pelletti, J.M., 1989, "Rotordynamic-Coefficient Test Results for the SSME HPOTP Turbine Interstage Seal for the Current and Improved Swirl Brake," NASA Lewis Grant NAG3–181, Turbomachine Laboratories Report 338–TL–3–89, Texas A&M University, College Station, TX 77843.

Demko, J.A., Morrison, G.L., and Rhode, D.L., 1988, "The Prediction and Measurement of Incompressible Flow in a Labyrinth Seal," AIAA Paper No. 88–0190.

Flower R., 1990, "Brush Seal Development Systems," AIAA Paper 90–2143.

Hendricks, R.C., Carlile, J.A., and Liang, A.D., 1992, "Some Sealing Concepts—A Review. Part A–Industrial, Proposed, and Dynamic; Part B–Brush Seal Systems," Presented at the ISROMAC–4, The Fourth International Symposium of Transport Phenomena and Dynamics of Rotating Machinery, Honolulu, Hawaii, U.S.A., Apr. 5–8.

Morrison, G.L., and Chi, D., 1985, "Incompressible Flow in Stepped Labyrinth Seals," ASME Paper No. 85–FE–4.

Rhode, D.L., Ko, S.H., and Morrison, G.L., 1988, "Numerical and Experimental Evaluation of a New Low Leakage Labyrinth Seal," AIAA/ASME/SAE/ASEE 24th Joint Propulsion Conference, July 11–13, 1988, Boston, MA, Paper No. 88–2884.

Stocker, H.L., Cox, D.M., and Holle, G.F., 1977, "Aerodynamic Performance of Conventional and Advanced Design Labyrinth Seals With Solid-Smooth, Abradable, and Honeycomb Lands," NASA CR–135307.

Trutnovsky, K., 1977, "Contactless Seals. Foundations and Applications of Flows Through Slots and Labyrinths," NASA TT F 17352.

TABLE I.—T–700 COMPRESSOR DISCHARGE SEAL

AND ENGINE TEST PARAMETERS

(a) On way up

Configuration	Compressor speed, rpm	Turbine speed, rpm	Compressor discharge pressure, psia	Compressor discharge low-pressure-cavity exhaust (CDLPCE) temperature, °F	Impeller aft cavity pressure, psia	CDLPCE pressure, psia	Pressure difference, psia
Baseline	29 600	10 500	50	348	37.5	16.2	21.3
Brush				321	39.5	15.4	24.1
Difference							2.8
Baseline	35 500	14 000	70	498	46.7	17.0	29.7
Brush[a]			79	458	53.1	16.3	36.8
Difference							7.1
Baseline	38 300	17 400	90	578	57.5	18.4	39.1
Brush				502	59.2	16.8	42.4
Difference							3.3
Baseline	41 300	20 000	120	688	74.2	21.2	53.0
Brush	40 400	20 000		599	76.0	18.7	57.3
Difference							4.3
Baseline	43 190	19 000	145	765	87.6	23.9	63.7
Brush	42 340	20 000		673	89.9	20.8	69.1
Difference							5.4
Baseline and brush	43 090	19 700	155	710	95.6	21.8	73.8

(b) On way down

Configuration	Compressor speed, rpm	Turbine speed, rpm	Compressor discharge pressure, psia	Compressor discharge low-pressure-cavity exhaust (CDLPCE) temperature, °F	Impeller aft cavity pressure, psia	CDLPCE pressure, psia	Pressure difference, psia
Baseline and brush	42 500	20 000	145	683	89.9	20.9	69.0
Baseline	41 400	20 000	120	690	74.1	21.2	52.9
Brush				605	76.4	18.9	57.5
Difference							4.6
Baseline	38 400	17 400	90	581	57.7	18.5	39.2
Brush	37 800	18 100		516	59.1	16.9	42.2
Difference							3.0
Baseline	35 600	14 000	70	----	46.8	16.9	29.9
Brush	34 800	14 600		473	48.2	16.0	32.2
Difference							2.3
Baseline	29 700	10 500	50	378	37.6	16.1	21.5
Brush	31 700	10 500	59	379	42.9	15.8	27.1
Difference							5.6

[a]rpm overshot and then backed down to "run through" the compressor critical speed. (Note: this is not the case on the way down.)

TABLE II.—RELATIVE PRESSURE DROPS FOR BASELINE COMPRESSOR DISCHARGE LABYRINTH AND BRUSH SEAL SYSTEMS

(a) On way up

Compressor discharge pressure, psia	Pressure difference, $\Delta P_{brush} - \Delta P_{baseline}$, psi
50	2.8
[a]70, [b]79	7.1
90	3.3
120	4.3
145	5.4

(b) On way down

120	4.6
90	3.0
70	2.3
[a]50, [b]59	5.6

[a]Baseline.
[b]Brush.

Compressor discharge (CDP)
seal low-pressure tube

Flowmeter

CDP

Airflow

(a) Airflow schematic.

CDP low-
pressure tube

CDP flowmeter

C-93-1435
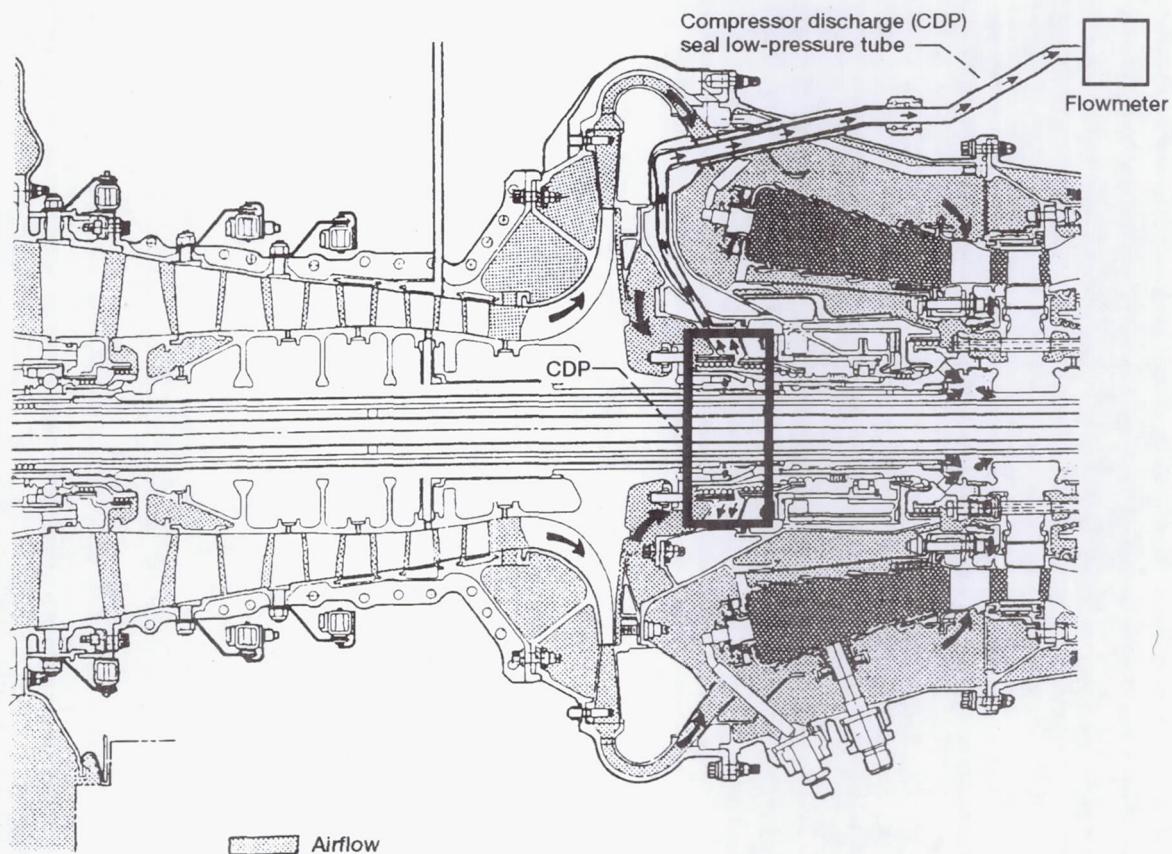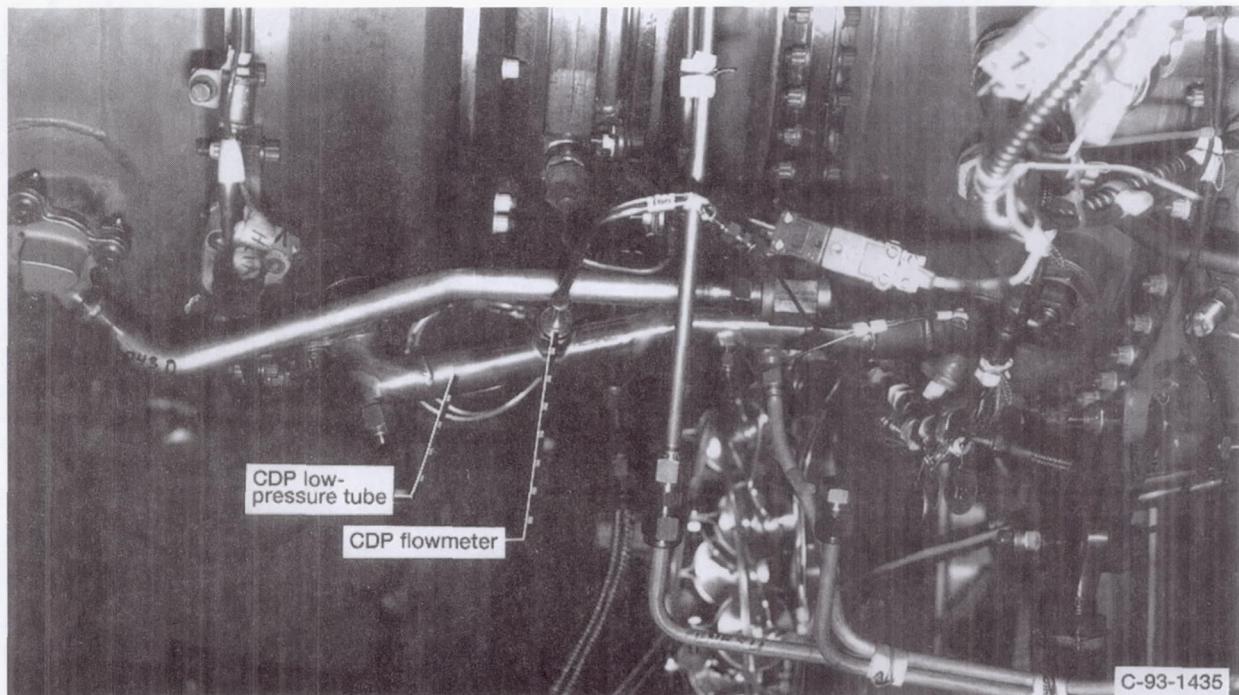
(b) Location of CDP flowmeter.

Figure 1.—Schematic of engine airflow and location of flowmeter.

313

2.583
2.553

2.247
2.237

1.847
1.837

1.452

0.798
0.788

5 teeth
(angled)
equally
spaced

0.020-
0.060 R

0.360
equally
spaced

0.146 →

0.480

0.200

0.125
0.115

0.040
0.020

2.8005
2.7995
diam

2.7005
2.6995
diam

2.5305
2.5295
diam

2.3305,
2.3205
diam

2.4267,
2.4263
(diam A)

1.9415,
1.9411
(diam B)

2.4305,
2.4295
diam

0.015
0.005
typ.

36°
34°

0.120
ref.

46°
44°

16° all teeth
except 14°
front five

0.040
0.020 R
typ.

Radius
4 places

No step allowed

No
step
allowed

Angled teeth

Straight teeth

Figure 2.—Schematic of labyrinth compressor discharge seal system. (Seal teeth and axis established by diameters A and B to be concentric within 0.003 full indicator reading. No steps allowed on tooth face or at fillet radius. All dimensions are in inches.)

C-93-04723
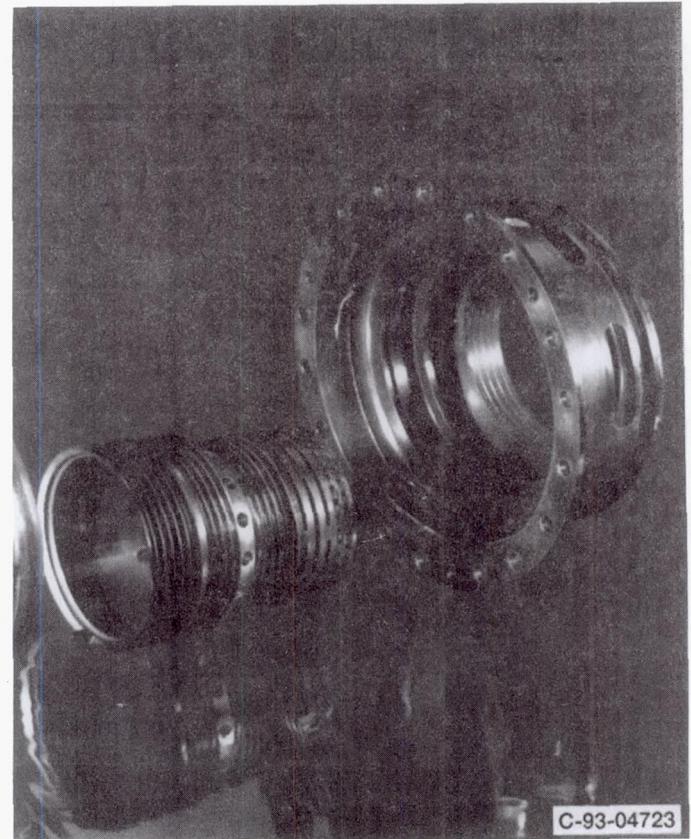
Figure 3.—Simulated exploded view of labyrinth compressor discharge seal system.

314

(a) Brush seal package and airflow.

Flow →

10 mm
(0.4 in.)

88.2-mm
(3.47-in.) diam

92.3 mm
(3.75 in.) diam

Chromium-carbide
rub runner

8

80 mm
(2.795 in.)

0.178-0.25 mm
(0.007-0.010 in.)

1.4 mm
(0.055 in.)

73-mm
(2.875-in.)
diam

4.83 mm
(0.19 in.)

C-92-05587

(b) Illustration of dual-brush compressor discharge seal system.
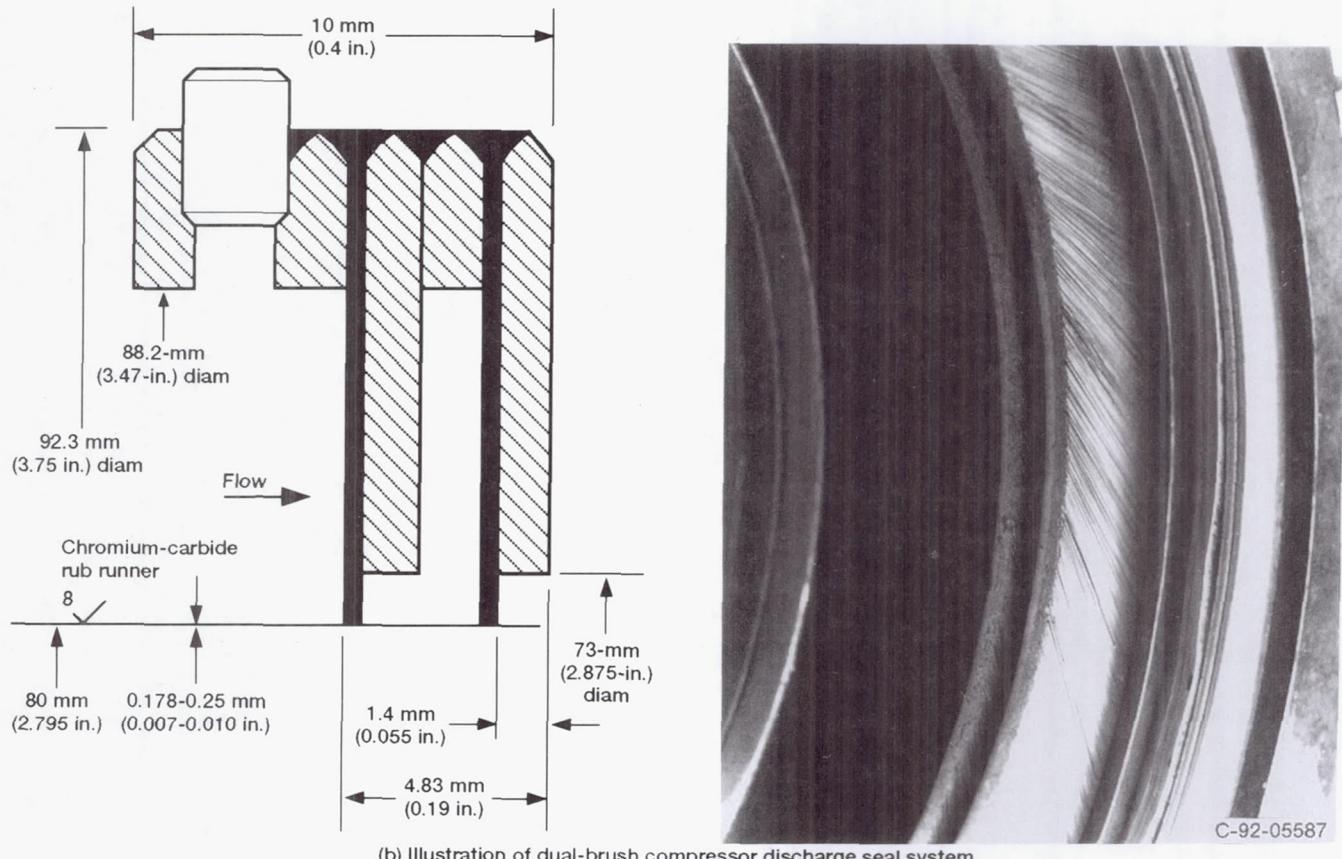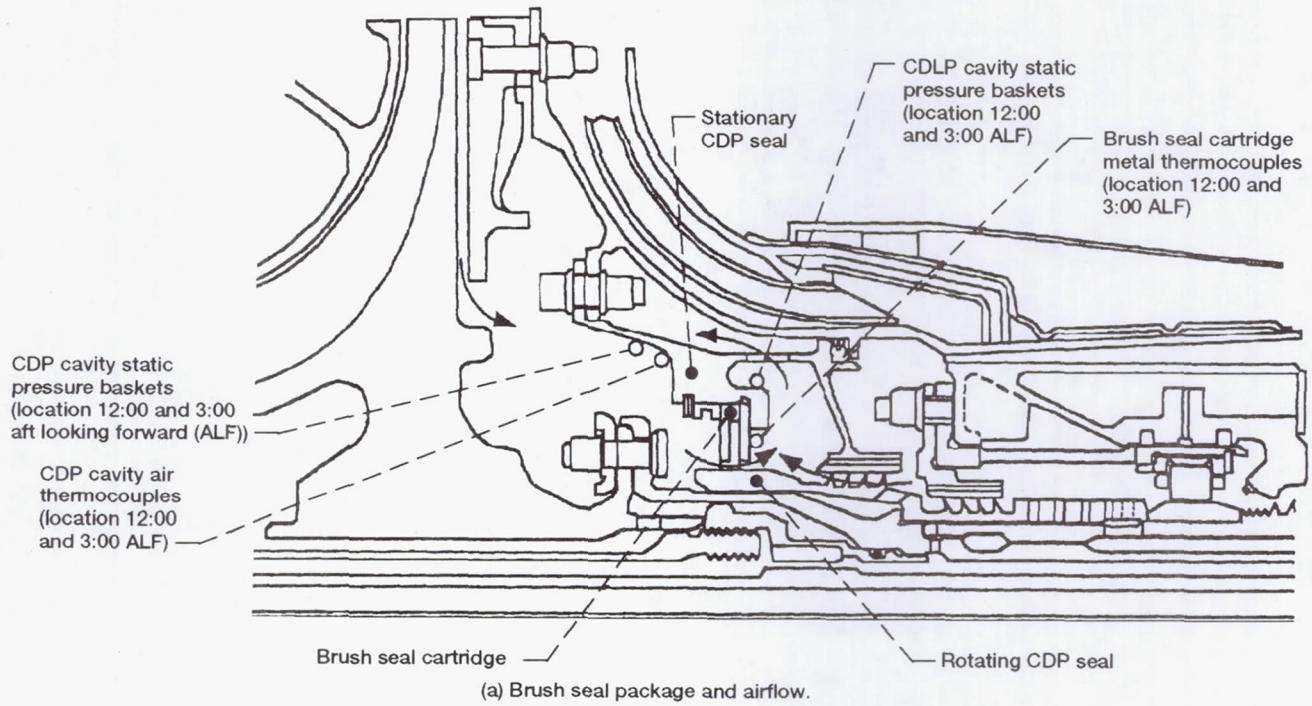
Figure 4.—Dual-brush compressor discharge seal system and schematic of airflow.

315
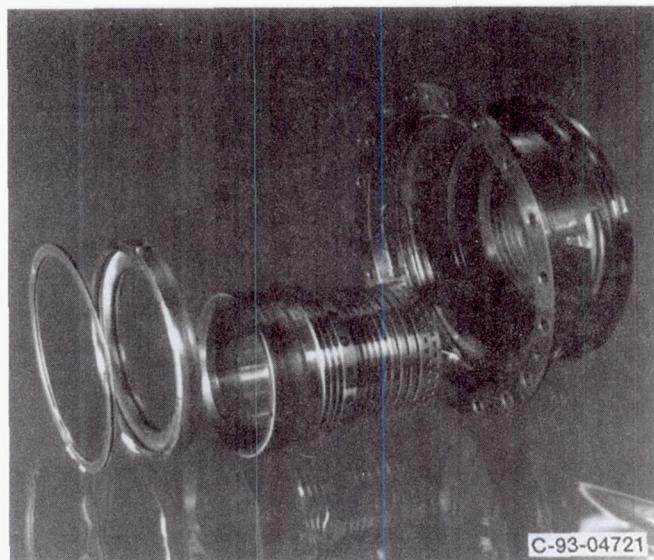
Figure 5.—Exploded view of dual-brush compressor discharge seal system (after test).

Figure 6.—Compressor discharge seal rotors for labyrinth seal (right) and brush seal (left).
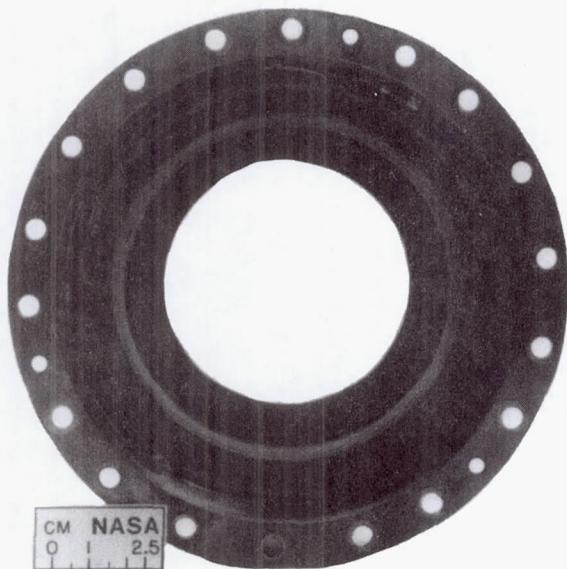
C-93-02710

(a) Upstream view.
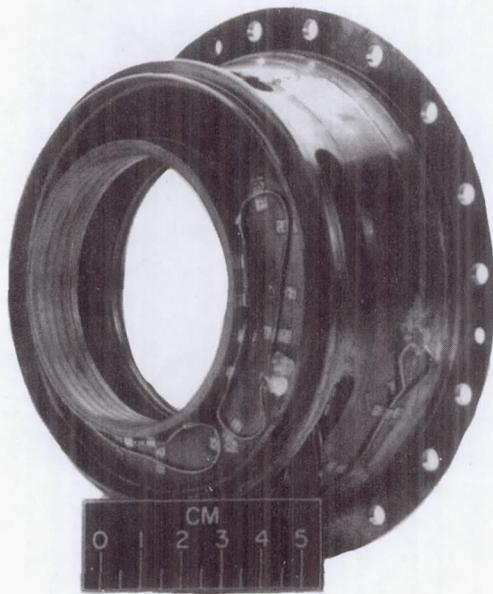
C-93-02712

(b) Downstream view.
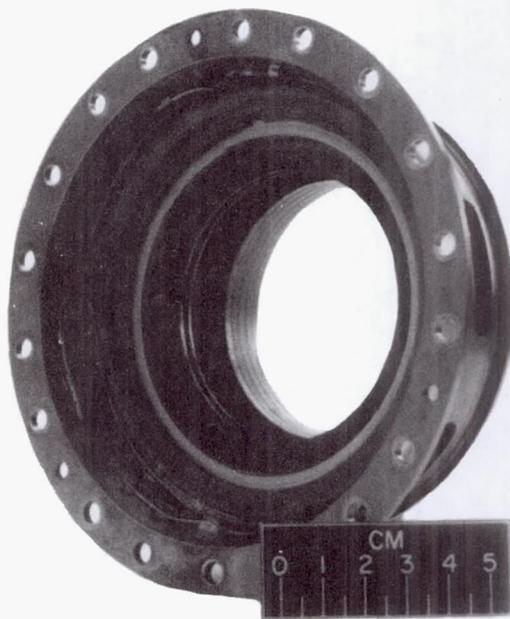
C-93-02711

(c) Isometric view.

Figure 7.—Dual-brush compressor discharge seal system after testing.
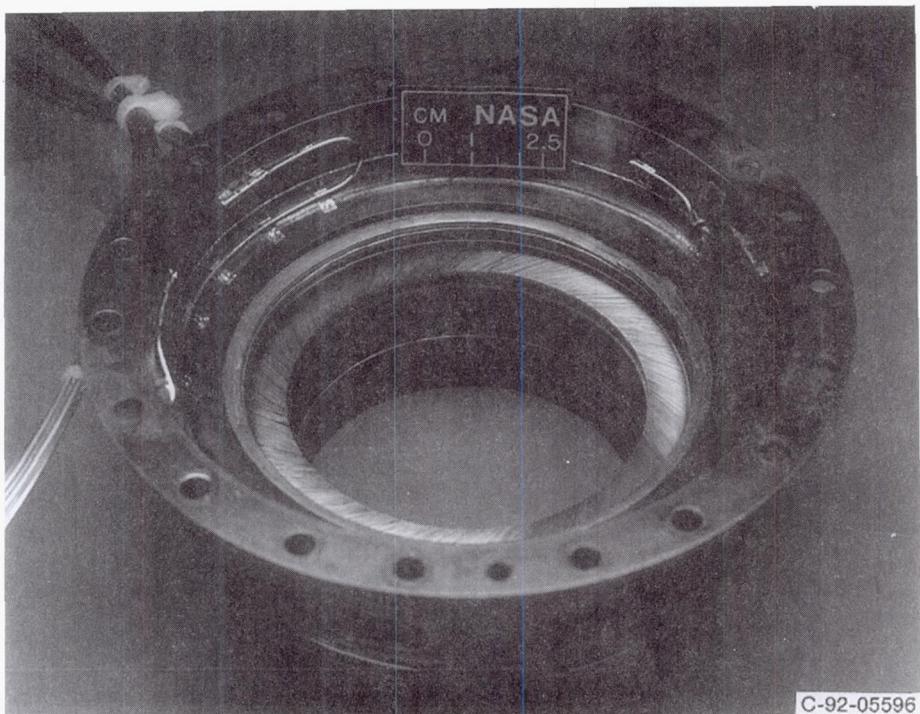
(a) Dual-brush seal.
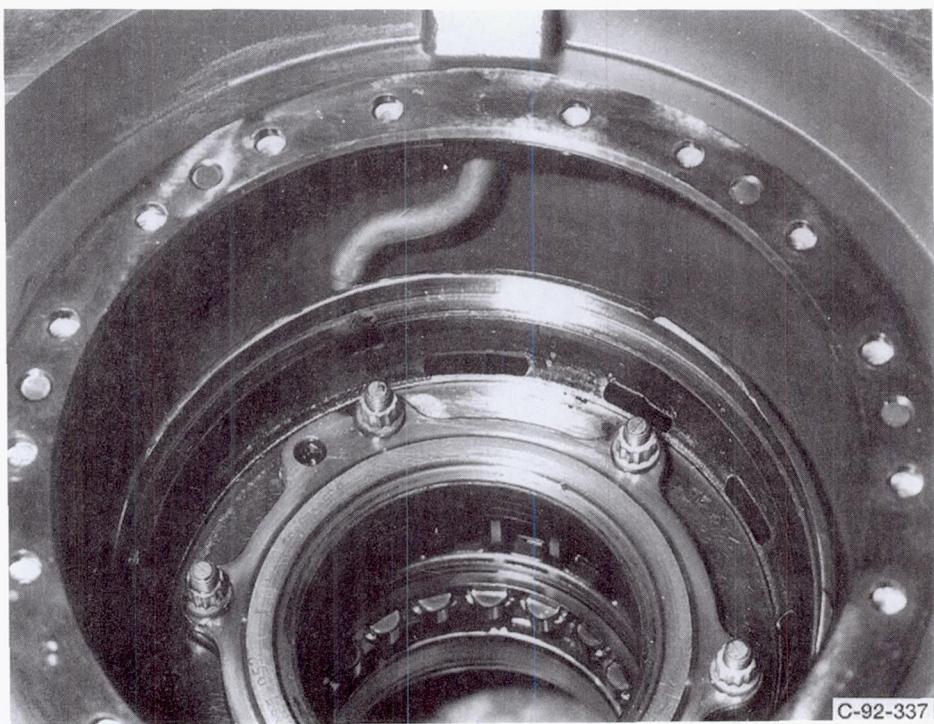
(b) Seal package cavity and housing.

Figure 8.—Dual-brush seal package installation.
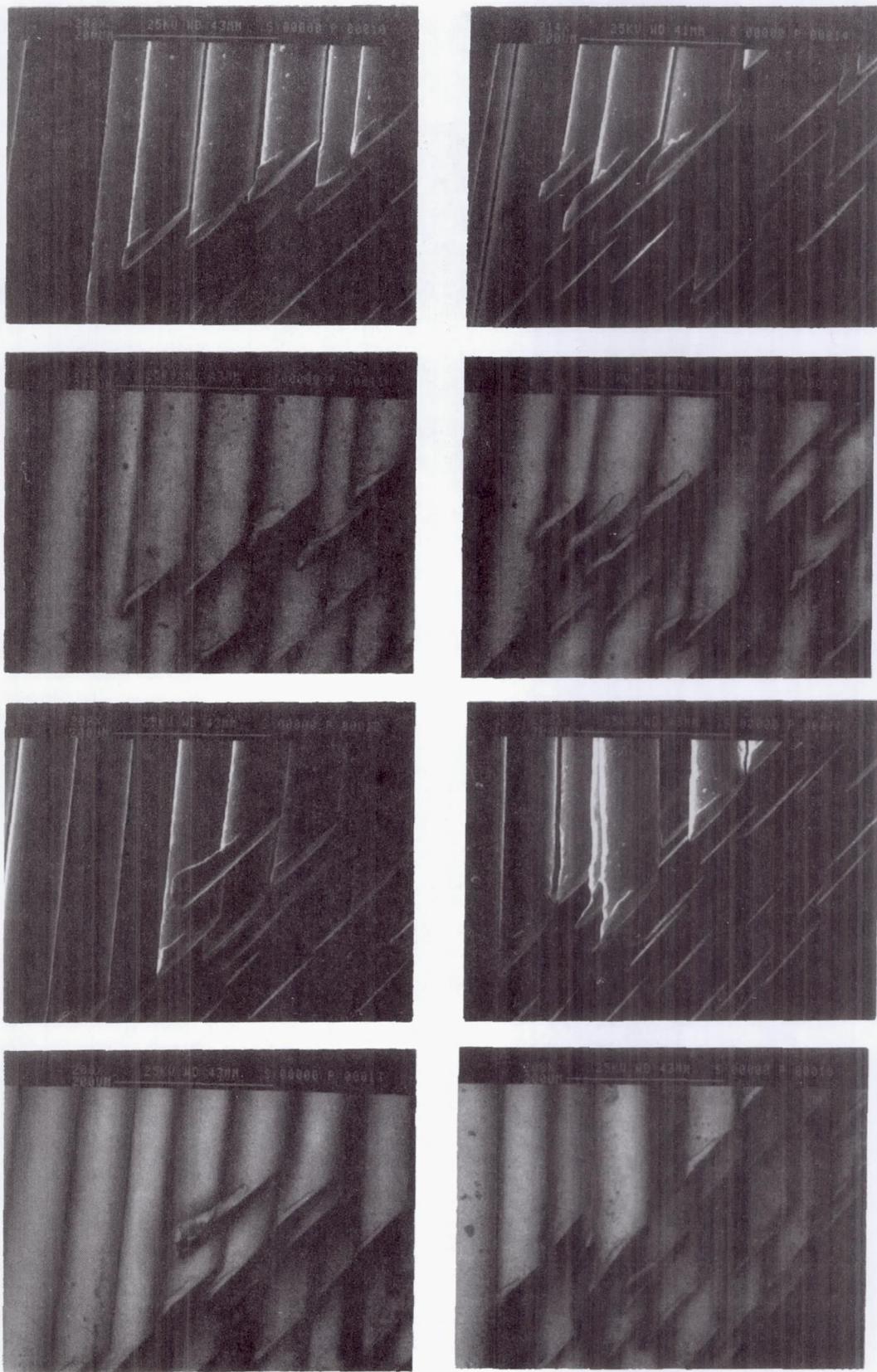
Figure 9.—Closeup views of bristles.

319
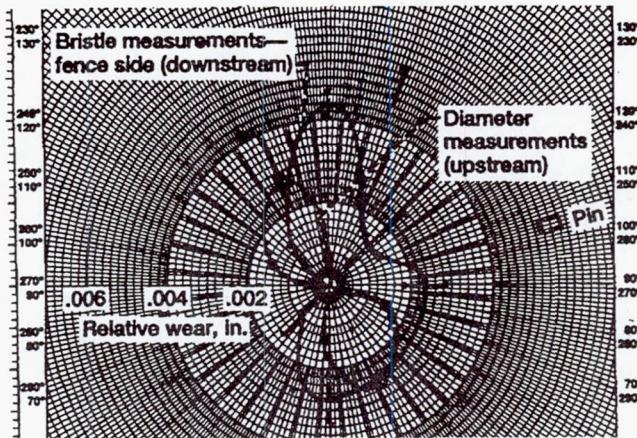
Figure 10.—Wear pattern for compressor discharge seal upstream brush.
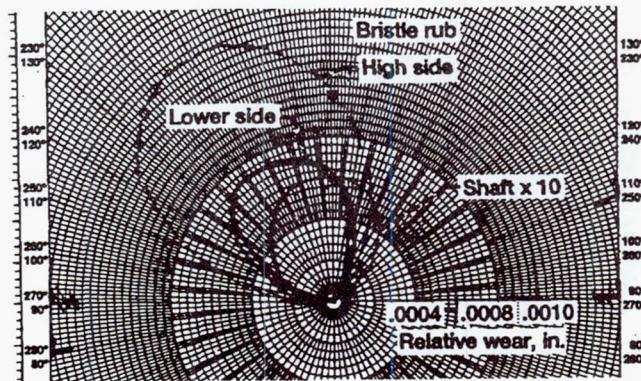
Figure 11.—Coating wear pattern for compressor discharge seal rub runner.
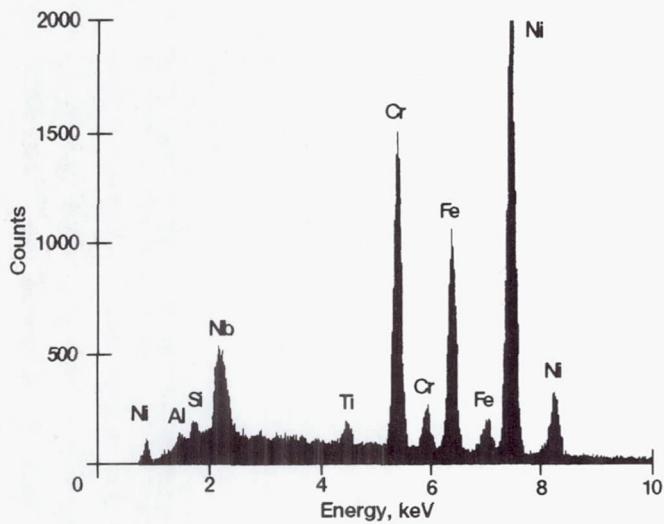
(a) Particle A.
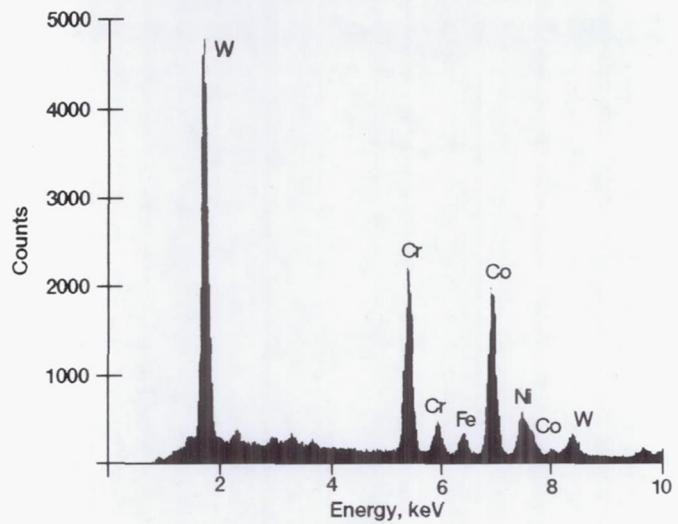
(b) Particle B.
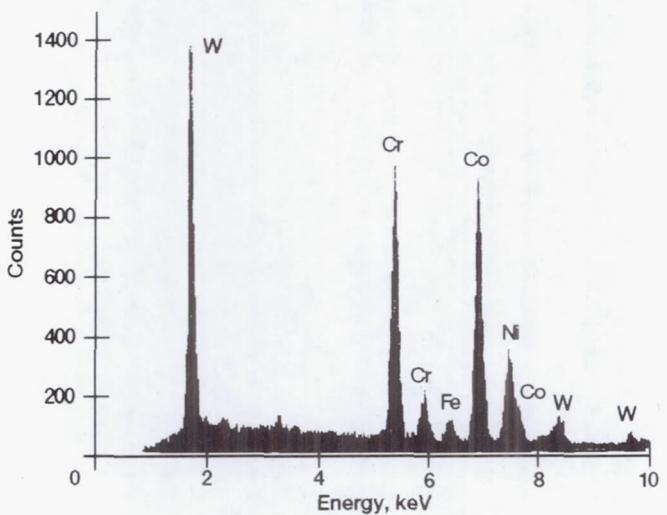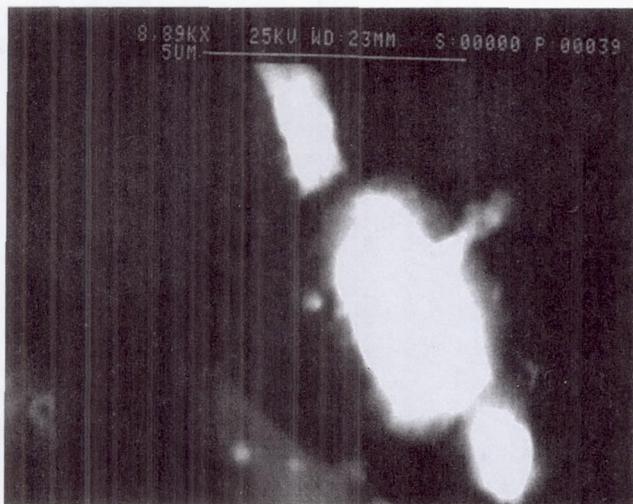
(c) Particle C.

Figure 12.—SEM peaks associated with drain pipe debris.

321

Flow

Upper wear band
Lower wear band
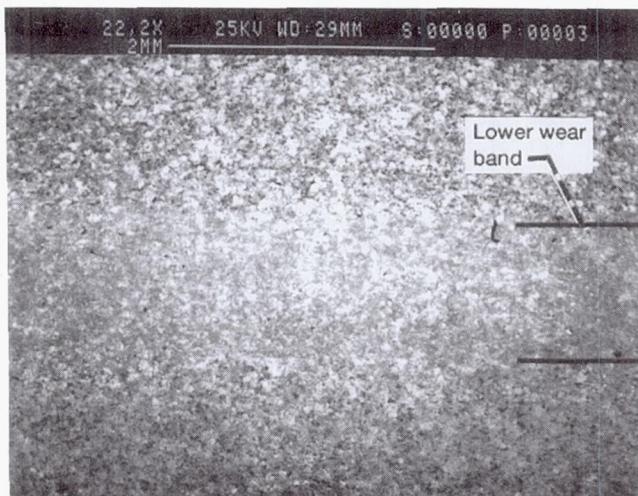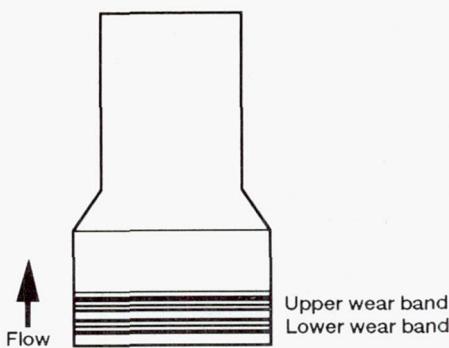
(a) Upstream (lower) wear band.
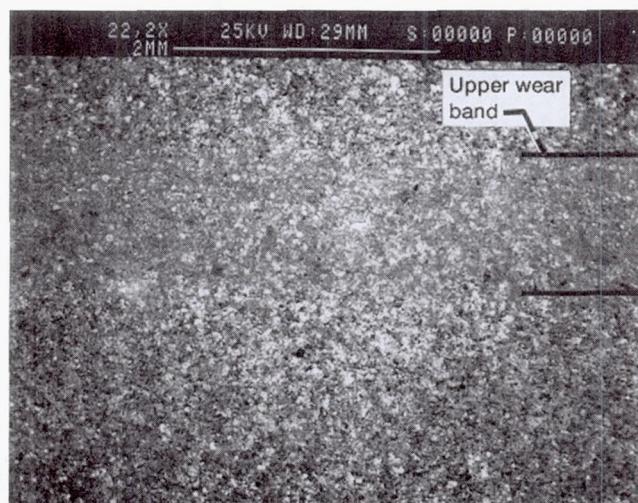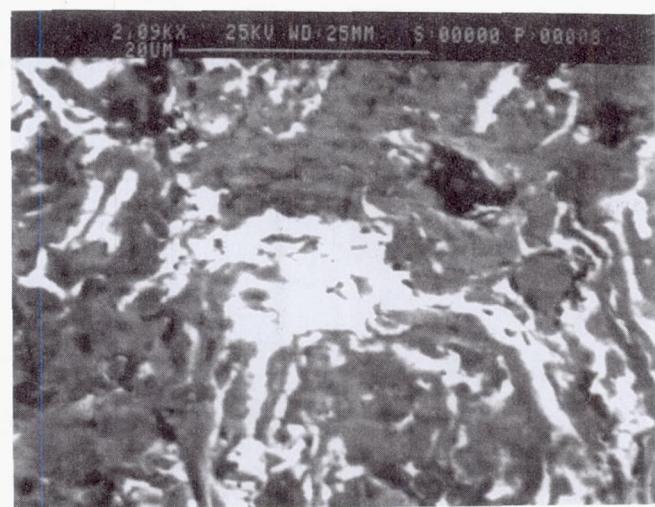
(b) Downstream (upper) wear band.
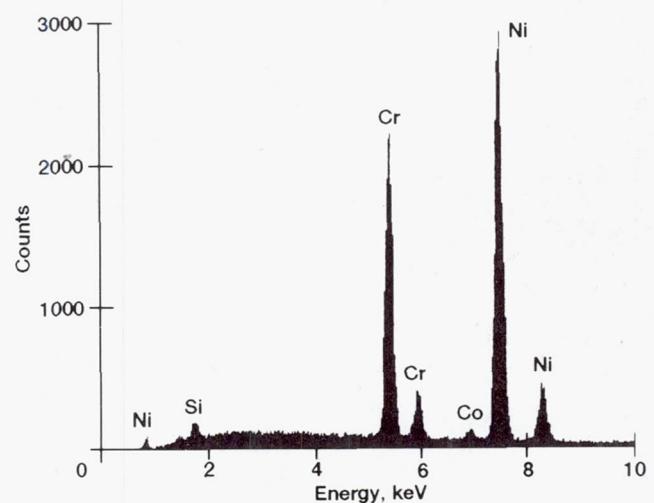
(c) Light area in coating matrix between bands.

Figure 13.—SEM peaks associated with chromium-carbide-coated rub runner.

(d) Gray area in coating matrix between bands.

(e) Light area in upstream (lower) wear band.

(f) Gray area in upstream (lower) wear band.
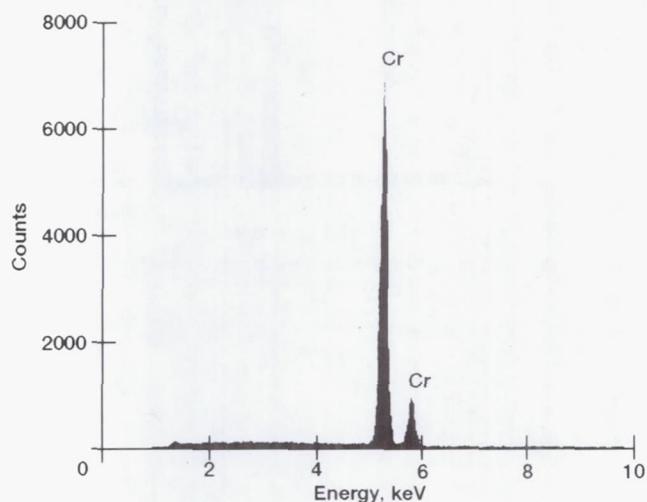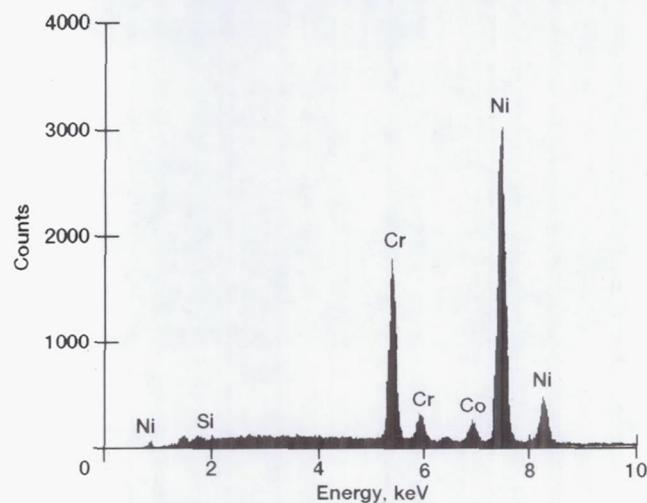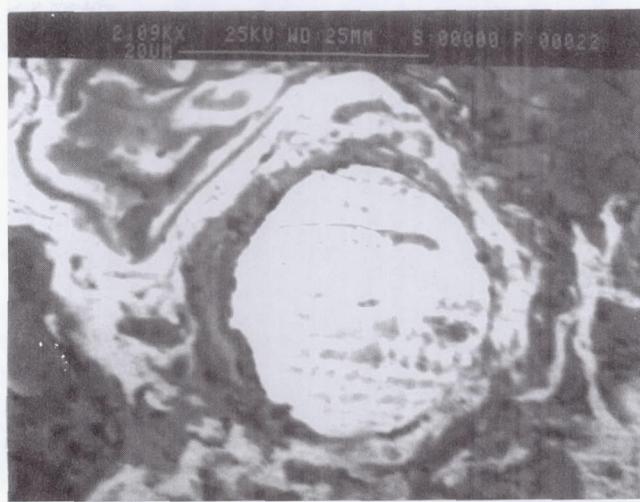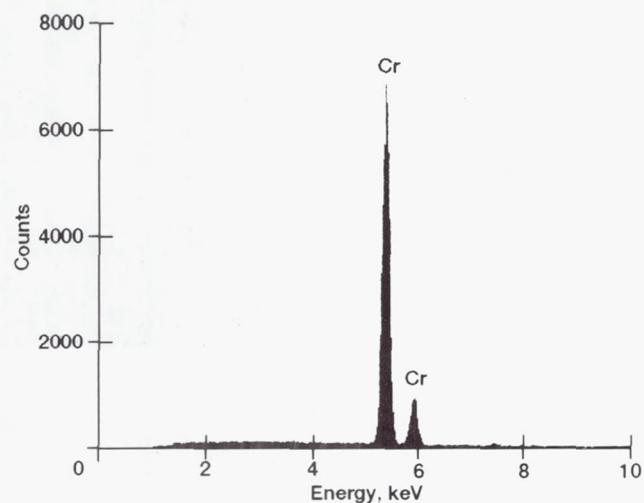
Figure 13.—Continued.

323
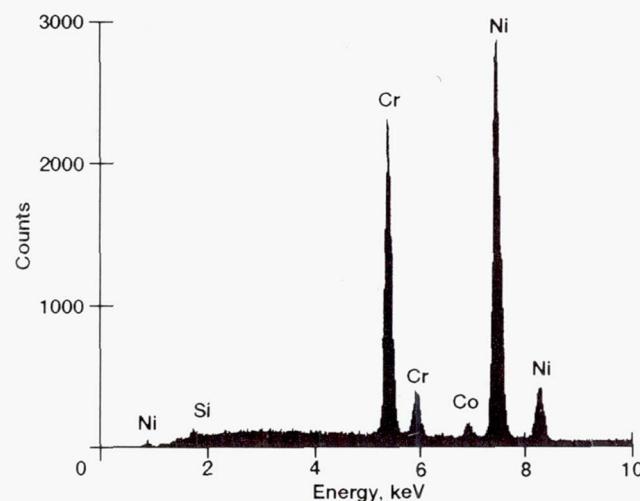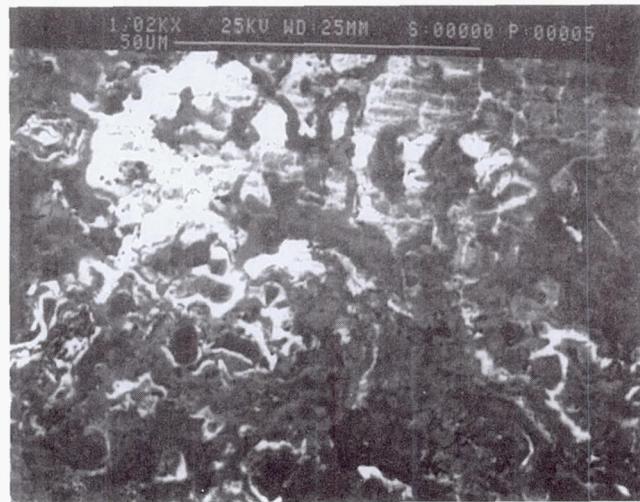
(g) Light area in downstream (upper) wear band.
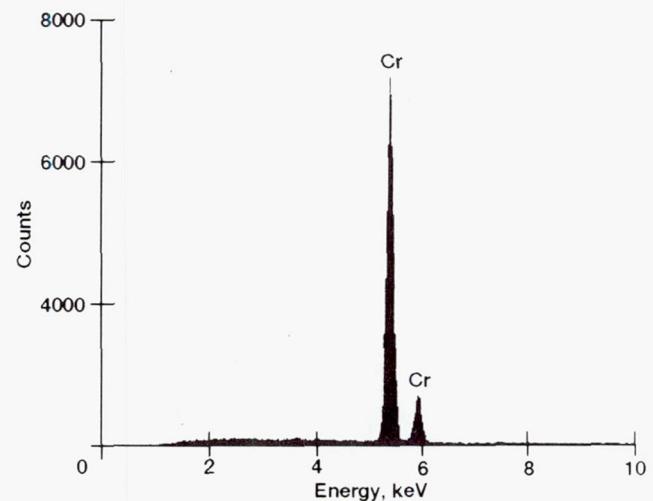
(h) Gray area in downstream (upper) wear band.

Figure 13.—Concluded.

SOME METALLOGRAPHIC RESULTS FOR BRUSH BRISTLES AND BRUSH SEGMENTS OF A SHROUD RING BRUSH SEAL TESTED IN A T-700 ENGINE

Robert C. Hendricks
NASA Lewis Research Center
Cleveland, Ohio

Thomas A. Griffin, George A. Bobula, and Robert C. Bill
Vehicle Propulsion Directorate
U.S. Army Research Laboratory
NASA Lewis Research Center
Cleveland, Ohio

David R. Hull
NASA Lewis Research Center
Cleveland, Ohio

and

Kristine R. Csavina
Sverdrup Technology, Inc.
Lewis Research Center Group
Brook Park, Ohio

SUMMARY

Post-test investigation of a T-700 engine brush seal found regions void of bristles ("yanked out"), regions of bent-over bristles near the inlet, some "snapped" bristles near the fence, and a more uniform "smeared" bristle interface between the first and last axial rows of bristles. Several bristles and four brush segments were cut from the brush seal, wax mounted, polished, and analyzed. Metallographic analysis of the bristle near the rub tip showed tungsten-rich phases uniformly distributed throughout the bristle, no apparent change within 1 μm of the interface, and possibly a small amount of titanium, which would represent a transfer from the rotor. Analysis of the bristle wear face showed nonuniform tungsten, which is indicative of material resolidification. The cut end contained oxides and internal fractures; the worn end was covered with oxide scale. Material losses due to wear and elastoplastic deformation within the shear zone and third-body lubrication effects in the contact zone are discussed.

INTRODUCTION

The preliminary results of T-700 engine brush seal testing have been reported in reference 1, and the post-test metallographic work on that same seal is described herein. The split-ring brush seal was fabricated, installed between two labyrinth-honeycomb shroud seals, and tested in the fourth-stage turbine of a T-700 engine (fig. 1, ref. 1).

Brush Seal Geometry

The brush seal was made up of 0.0028-in. (0.071-mm) diameter Haynes 25 bristles angled 43° to 50° to the interface with about 2500 per inch of circumference (98.4 per millimeter of circumference) (fig. 2(a)). The backing washer was angled 19° to match the slope of the turbine shroud (fig. 2(b)). The design clearance was −0.02 in. (−0.51 mm) but could range to −0.05 in. (−1.27 mm) diametral (the uncertainty reflecting that of the engine geometry) with an outside diameter of 13.146 in. (333.9 mm) and an inside diameter of 12.690 in. (322.3 mm).

Operating Conditions and Interface Geometry

The annealed Haynes 25 bristles rubbed directly against the nonconditioned, irregular René 80 turbine blade shroud surface. Turbine speeds were 10 000 and 20 000 rpm, and average fourth-stage turbine shroud temperatures were 850 and 1050 °F (455 and 566 °C), respectively. The turbine inlet temperatures were about 250 deg F (139 deg C) higher.

The turbine assembly has 50 shrouded blades with irregularities (radial, to 0.009 in. (0.023 mm); circumferential, to 0.003 in. (0.076 mm); and axial, to 0.002 in. (0.0051 mm)) representing protrusions into the brush and the spaces between the blade pairs. It is not known how many cycles were required to "free the bristles," but at 10 000 rpm and with 50 irregular asperities impacting each bristle (4000 impacts/s at a surface speed of 550 ft/s (168 m/s)), it is assumed that brush break-in was rapid.

A total of 21 hr of cyclic and steady-state data were taken with surface speeds to 1100 ft/s (335 m/s) and shroud temperatures to 1150 °F (620 °C). Wear appeared to be rapid initially, with a orange flash of hot brush fragments during the first engine startup, but decreased to none in less than 10 hr of operation.

Tribological Pairing

Derby and England (ref. 2) reported minimal brush and coating wear using an Alloy A bristle with Triboglide coating. Alloy A (a solid-solution-strengthened, nickel-chromium-aluminum-based superalloy) is being used in gas turbine hot spots and develops a tenacious chromia (Cr_2O_3) and alumina (Al_2O_3), yttria-modified oxide layer. Triboglide is a chromium carbide (CrC) containing a total of 12 wt % barium and calcium fluoride solid lubricants. Triboglide is based on the work of Harold Sliney at NASA Lewis Research Center but has no silver additive. The tests were performed with 1200 °F (650 °C) air.

Atkinson and Bristol (ref. 3) reported less wear for a cobalt-based alloy rubbing against CrC at room temperature than for a nickel-based alloy but nearly equivalent wear for either alloy at 480 °C (900 °F). However, the cobalt combination proved to leak less under dynamic conditions and wear less at room temperature. The tests were conducted to simulate a CT7-9 compressor discharge seal. The brush was 5.08 in. (129 mm) in diameter and of standard Cross Mfg. construction.

Hendricks et al. (ref. 1) reported the results of a T-700 engine test. Details of the bristles (fig. 3(a)) show an ingrained wear pattern that is characteristic of a high spot in the rotor which cuts a shallow groove as the rotor wears the brush. The rotor also ran eccentric with respect to the seal, and the blind installation made it difficult to assess intermediate states of wear or the health of the brush and the turbine shroud/brush interface.

Metallographic results illustrate some material migration along the bristle and material transfer both from and to the rotor surface (fig. 3(b)). Material smears seem to be in line with the softer brush material rubbing a harder material; the sacrificial bristles appear to be oxidized, pitted, and rubbed by line-to-line contact. It is not clear how the interface irregularities affected these results, but it is clear that materials were transferred and that they probably melted upon initial rub-in due to the high interface temperature.

Before the brush seal for the T–700 engine test was manufactured and installed (ref. 1), a 40-tooth rotor was used to gather debris, wear, and cycle information in an attempt to simulate the harsh geometric environment of the engine test. The bristles did wear significantly, produced only powder-like debris, and had no failures in over 10^9 flexure cycles of operation (ref. 4).

Tribological pairing is important and references 1 to 4 provide an initial look at the problem. It is apparent that the compositions of both the coating and the bristles need to be characterized with respect to the working fluid, the operating conditions, and the component life requirements. Also, the importance of surface conditions must be emphasized, noting that wear decreases after operation both because the brush rubs a smoother surface and because bristle wear decreases line loading.

Herein, we provide further details of the results of the brush seal engine testing described in reference 1.

ANALYSIS AND DISCUSSION

Several bristles (wires) and four sections of the brush seal tested in a T–700 engine (ref. 1) were cut, wax mounted, polished, and analyzed. The bristles and sections were mounted in a low-melting-point wax, rough lapped with 3-μm diamond grit, polished with 1-μm diamond grit, and coated with palladium for light optic and scanning electron microscope viewing.

Bristles Cut From Brush Seal

Bristle tip irregularities caused by the rub interface (fig. 4) indicate some form of material transfer and material smearing. However, metallographic analysis of the bristle near the rub tip showed tungsten-rich phases distributed throughout with no apparent change within 1 to 2 μm of the interface. Figure 5 shows a bristle wear surface and little or no evidence of a redistribution of tungsten indicative of resolidification. From the Blok problem (ref. 5) the temperature was sufficient to melt the bristles, but the materials may fail in shear before melting (like pulling a taffy), form oxides and pits, transfer to the interface or form layers less than 1 μm thick, wear away, or all of the preceding.

Figure 6 illustrates a wear surface, although because the tip is embedded and angled, the photograph does not always provide a true representation of the surface. From 2 μm to several millimeters from the interface, there appears to be no change in tungsten composition. Green dots are near the edge (micrometer range) and red is away from the edge (millimeter range), showing little or no change in tungsten distribution, but the surface appears to be coated (oxides are discussed later).

The wear marks and the pocked bristle tip (fig. 6) were examined at higher magnification (fig. 7). Backscatter images show heavy atomic particles as bright spots and lighter weight elements as dark spots. Secondary electron images show tungsten but at a lesser brightness. Backscatter tends to change with geometry and higher magnification and wax mounting effects must be differentiated, but the interface wear marks show clearly. The bright spots are tungsten rich as noted by the element spectra, and the

spot on figure 7 is a beam concentration spot obtained by energy-dispersive spectroscopy of a bright tungsten-rich region.

At resolutions of 10 000X, there is no apparent change in tungsten at the bristle edge but there is possibly a small amount of titanium, which would represent a transfer from the rotor (rotor scrappings are discussed later). Again little evidence of resolidification but more evidence of oxide scale is noted.

Oxide scale formation on the bristle (fig. 8) was most likely chromium oxide, which can form, rub (flake), and reform thus providing a third-body lubrication effect. Such surfaces are also noted in figures 6 and 7. A scale formation noted as a dark region (lower atomic number) showed decreases in tungsten and cobalt with significant increases in oxygen. A more detailed analysis was conducted on bristles also cut from the post-test brush seal. Micrographs of a cut end and a rubbed (worn) end are shown in figure 9 with the associated element spectra in figures 10 and 11, respectively. The cut end contained oxides and internal fractures (figs. 10(a) and (b)). The worn end was covered with scale that at 5000X appears to be oxide scale (figs. 11(a) and (b)). The oxygen level from the cut to worn ends increased from 5.7 to 12.7 percent; the cobalt level decreased from 32.5 to 22.0 percent; and the chromium level dropped from 24.4 to 22.3 percent.

The bristle element spectra are dominated by cobalt, chromium, and tungsten lines representative of a cobalt-based alloy such as Haynes 25 (table I). Most spectra show oxide scale and little material transfer from the René 80 rotor (table I) to the bristles. However, increases in nickel and molybdenum (fig. 12) illustrate that some material transfer from the rotor to the bristle tips did occur. Nevertheless, scrapings from the René 80 rotor-bristle wear track (fig. 13; see also fig. 3(b)) were rich in cobalt, which is characteristic of Haynes 25 transfer to the rotor. Therefore, the sacrificial elements were the Haynes 25 bristles, as designed.

With significant material transfer to the rotor and oxide scale formation over the bristle surface, an examination of a bristle tip (fig. 14) showed wear traces, pitting, and material transfer. Figure 15 illustrates that although the base material appears as Haynes 25, the distribution of tungsten differs as noted in the element spectra. Therefore, some form of resolidification must have occurred right at the bristle–rub runner interface.

Note that these tests were conducted in the fourth stage of a shrouded turbine disk where the fluids to be sealed were combustion gases, with cooling air to 1200 °F (650 °C). The principal elements of such gases are oxygen, steam, carbon dioxide, and nitrogen. In the tests conducted at GE (ref. 3) and at EG&G (ref. 2) the working fluid was probably air (0.8 N_2 and 0.2 O_2 approx.) at temperatures to 1200 °F (650 °C) (equivalent to our shroud temperatures) at EG&G and to 480 °C (895 °F) at GE. Both are above the transition temperature for cobalt (ref. 2). Also, note that the T–700 engine was probably fuel rich on startup and lean on shutdown so that oxide scaling could occur by engine air cooling of the heated bristles and by steam corrosion. Also, the GE tests were for 100 hr, the EG&G tests were for 1.5 hr, and the T–700 tests were for 30 hr.

Some additional micrographs illustrated carbon spots on the bristle surfaces (fig. 16). Bristle tips and irregular bristles found in the exhaust duct of the T–700 engine are shown in figures 17 and 18. Oxide scaling is noted but also apparent is a form of resolidification. The events associated with bristle loss at engine startup are discussed in reference 1. In this regard the reader is reminded that the brush was installed and disassembled "blind" (ref. 1).

Brush Segments Cut From Brush Seal

Sections were taken along the bristles of four segments of the T–700 brush. None of these showed evidence of melting at or near the interface. All showed material distortion due to both shearing and abrasive wear, with suspected material softening at elevated temperatures as a major contributor. All exhibited oxide formation, which presumably would scale off at some later time or embrittle the entire wire causing fracture. There was some evidence of melting and debris near the pinch washer interface, which after T–700 testing was close to the bristle–rub runner interface. A few bristles were sectioned along the length, but in general the bristle geometry did not conform to a uniform array. The reason was partially the construction method, partially the misalignment of the bristles and polishing plane used, and mostly the engine operations and the abusive nature of the segmented turbine blade rub interface.

Oxide formation at elevated temperatures and shear flow of materials appears to have caused the interface to smear, forming "mudflat" segmented structures (fig. 19) rather than the uniformly spaced elliptical footprints of the preinstallation grinding.

One segment evidenced some material transferred from the backing plate and rubbed into the brush. At this location the rotor did rub the backing plate, and the bristle stubble was nearly line to line with the backing plate. But the transfer could have resulted from electron beam discharge cutting of the seal.

Figure 20 illustrates brush segment 1, which was cut from the seal at the maximum bristle stubble location; see figure 3(a). A critical analysis was not done on this section, but a closeup of the fence surface is given as figure 20(a).

Some of the pitting in brush segment 2 (fig. 21) may be due to electric discharge cutting of the sections, with the bristles investigated too near that interface. The polishing plane and the bristle planes are not all aligned and bristle tips are shown along with some bristles in the polishing plane. It is evident that the last bristle row is bent under the fence, but not so evident is when it happened. Backscattering electron photographs show uniform distribution of tungsten spots, some oxide formation, and some local fracturing of the smeared bristle tip. Color element traces show tungsten-rich white spots, oxide formation and the bristle matrix. The chromium diminished as the oxide increased or was leached out of the matrix. A closeup of the fence surface is shown as figure 21(b).

Brush segment 3 (fig. 22) shows some evidence of melting and material debris from the backing plate or from the weld interface. The melt region is rich in redistributed tungsten, a factor that may have to be reevaluated as a manufacturing procedure. The color element traces show oxide formation between two bristles.

In brush segment 4 (fig. 23) the polishing plane and the bristle planes differ, yet oxides and smeared materials are apparent. The color element traces show the composition of the backing plate materials and the oxide that is formed on the bristle tip and around the bristle. Also observed is a bead that mimics the composition of the backing plate and may have come from the rubbed interface or the disintegration cutting of the ring.

Brush Seal Configuration

The post-test brush seal was examined by using a micro-video system. Several irregularities associated with installation were noted. One region was void of bristles (fig. 24(a)); perhaps they were yanked out. Adjacent bristles were all bent over (fig. 24(b)) on the leading edge but not in the core. One bristle of

original length was kinked at the tip and appeared to be approximately 2.5 times as long as the remaining bristles (fig. 24(c)). A closer look revealed some "snapped" bristles in that region (fig. 24(d)), perhaps from forcing the brush into position or from catching bristles within the turbine blade gaps. The snapped bristles were very close to the pinch washer. Bristles near the pinch washer were broken and/or bent, but deeper into the brush bristle pack (N_x) the bristles were straight and worn (fig. 24(e)). The appearance of the first three rows N_x of the brush showed erratic rubbed wires, probably due to installation deformations. For $N_x > 3$ the appearance is more uniform for the next nine rows. Higher magnification of the interface shows "smearing" of the bristle tips (fig. 24(f)). Each bristle appeared to have some scale covering it (fig. 24(g)) as evidenced from wire highlights and differential coloring, like air-quenched steel.

Other effects of the rubbing interface are discussed in references 1 and 4.

CONCLUSIONS

Post-test evaluation of brush bristles and brush sections cut from the brush shroud seal run in the fourth-stage shrouded turbine disk of a T–700 engine provided the following information.

Cut Bristles

1. Bristles cut from the brush showed little or no evidence of tungsten redistribution, indicating that little or no resolidification had occurred over the bristle length.

2. Bristles exhibited surface oxidation, pitting, color differentials, and scaling over their lengths with significant oxidation at the rub interface. Bristle tips were irregular in shape.

3. Rotor scrapings showed material transfer from the Haynes 25 brush to the René 80 rotor. The brush was sacrificial, as designed.

4. The bristle tips showed irregular distribution of tungsten, which is indicative of resolidification in a very thin layer at the rubbing interface.

Cut Sections

5. Oxides formed on bristle surfaces, with significant material losses at the interface. Bristles became more brittle.

6. Material dislocation and bristle distortion were high at and near the interface. Wear was high owing to the extreme test conditions.

7. The uniform distribution of tungsten indicated that no melting had occurred at or near the interface. Material softening with attendant shear deformation is postulated as a material smearing mechanism; see also the fourth conclusion.

8. Post-test investigation revealed the "mudflat" appearance of the interface in contrast to the "polished," distinct elliptical bristle ends noted before the test.

Seal Configuration

9. "Blind" installation and forcing the brush onto segmented rotors can lead to distortion of the first few and last bristle rows and to local pullout.

10. Bristle tip smearing at the rub interface was commonplace, with mudflat cracking but with a uniform wear track.

11. Some formation of bristle debris at startup was noted.

12. The mechanical aspects of the brush survived the harsh test environment.

REFERENCES

1. Hendricks, R.C., et al.: Integrity Testing of Brush Seal in Shroud Ring of T–700 Engine. ASME Paper 93–GT–373, 1993. (Also, NASA TM–105863, 1992.)

2. Derby, J.; and England, R.: Tribopair Evaluations of Brush Seal Applications. AIAA Paper 92–3715, 1992.

3. Atkinson, E.; and Bristol, B.L.: Effects of Material Choices on Brush Seal Performance. Lubr. Eng., vol. 48, no. 9, Sept. 1992, pp. 740–746.

4. Hendricks, R.C.; Carlile, J.A.; and Liang, A.D.: Brush Seal Bristle Flexure and Hard Rub Characteristics. NASA TM–105864, 1992.

5. Carslaw, H.S.; and Jager, J.C., eds.: Condition of Heat in Solids. Clarendon Press, Oxford, Second ed., 1959, p. 269.

TABLE I.—COMPOSITION OF RENÉ 80 AND HAYNES 25

Composition, wt %	
René 80	Haynes 25
60 Ni[a]	50 Co[a]
14 Cr	20 Cr
4 W	15 W
9.5 Co	10 Ni
4 Mo	3 Fe
3 Al	1.5 Mn
5 Ti	0.1 C
0.17 C	
0.015 B	
0.03 Zr	

[a]Balance.

TABLE II.—SUGGESTED BRUSH SEAL SYSTEM TRIBOPAIRS

Bristle materials	Rub runner	Lubricated runner or bristle

SiC
Al_2O_3
Haynes 25
L605 AMS5796
Haynes 188
AMS5801
Haynes 214
Haynes 230
MA 754
MA 956
In X750
Waspalloy
Lubricating
  coatings
	Inconel X750
	Inconel 718
	Al_2O_3:
	  Union Carbide LA2
	  Metco 105NS, 105SF
	TiN
	Cr_2O_3
	WC (Union Carbide)
	CrC (Union Carbide):
	  LC–1–B
	  LC–1–C
	Diamond
	Allison 250–C30 material
	CrCo
	MoC
	Wear Cote CF_x/EN
	YSZ
	Ion implantation
	  combinations
		Triboglide
		PS 212
		Wear Cote
		$YSZ + BaTiO_2$

Operations goals	Material	Temperature, K (°F)	Surface velocity,[a] m/s (ft/s)
1	Metallic	4 to 1090 (−455 to 1100)	0 to 350 (0 to 1100)
2	Metallic/ceramic	4 to 1145 (−455 to 1600)	0 to 395 (0 to 1300)
3	Ceramic	4 to >1370 (−455 to >2000)	0 to 457 (0 to 1500)

[a]May be achieved with metallic configurations with line-to-line contact, but rubbing will sacrifice the interface with attendant leakages.

332
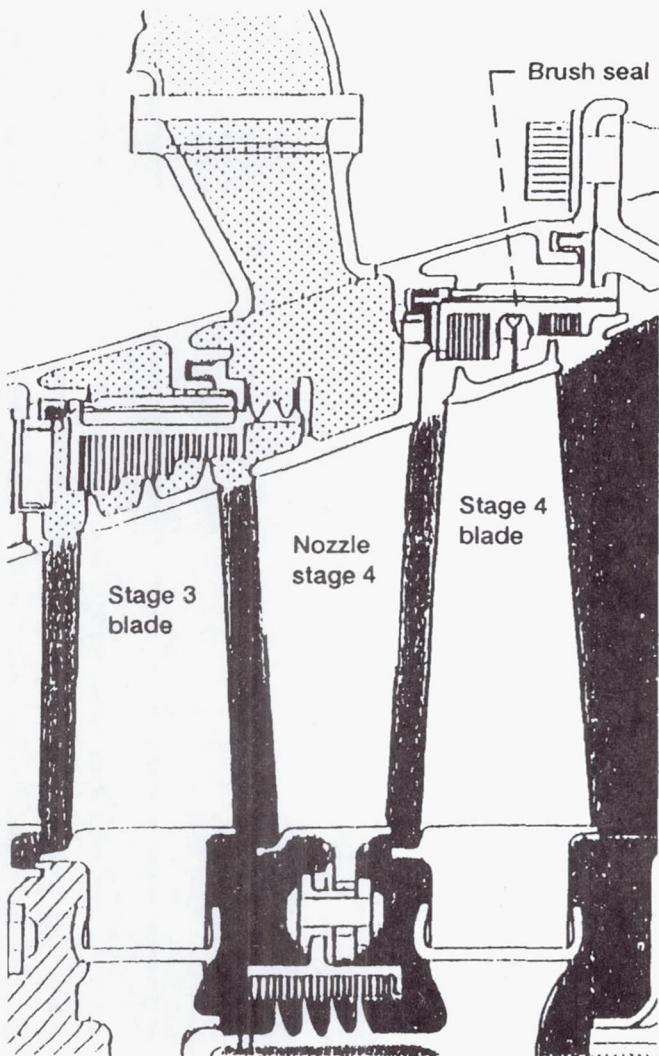
Figure 1.—Schematic of power turbine. From reference 1.
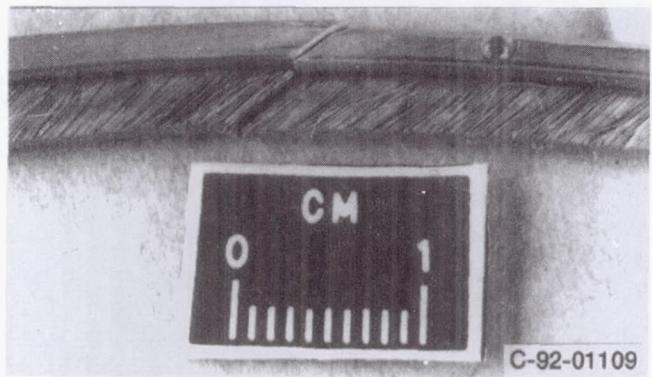
(a) Overview.

(b) Cross section

Figure 2.—Split-ring brush seal. From reference 1.
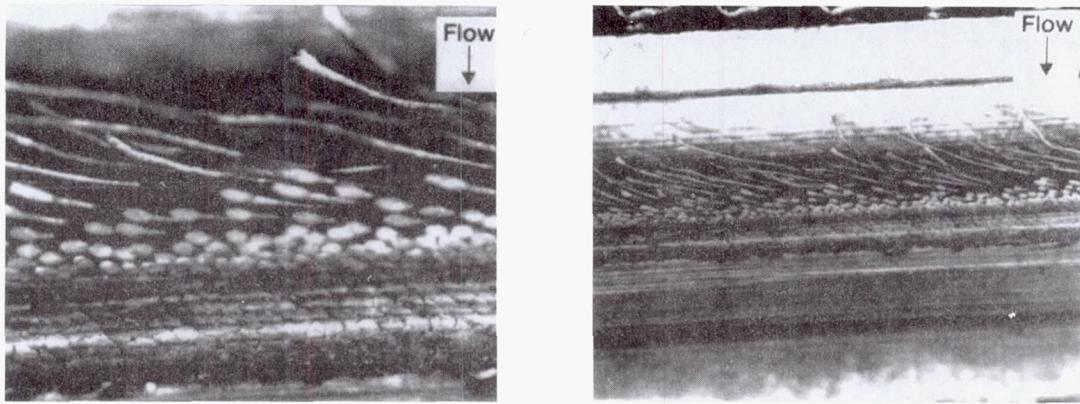
(i) Wear track and fence rub.
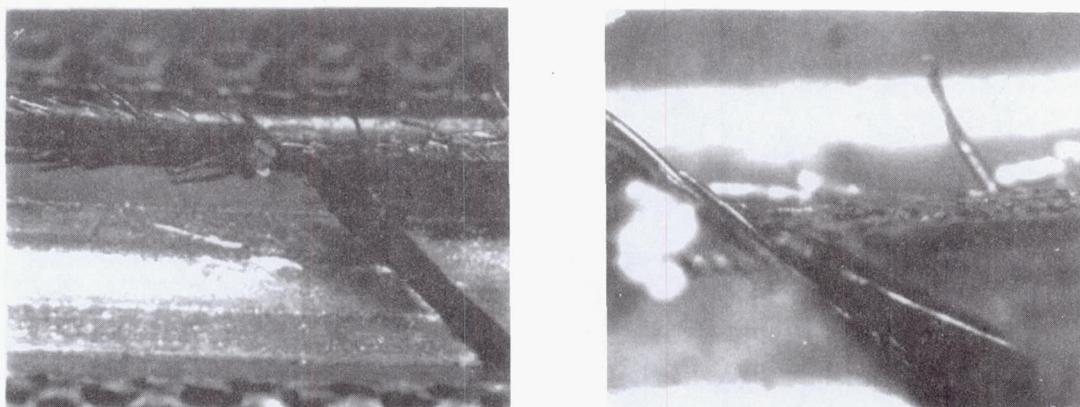
(ii) Joint wear track.
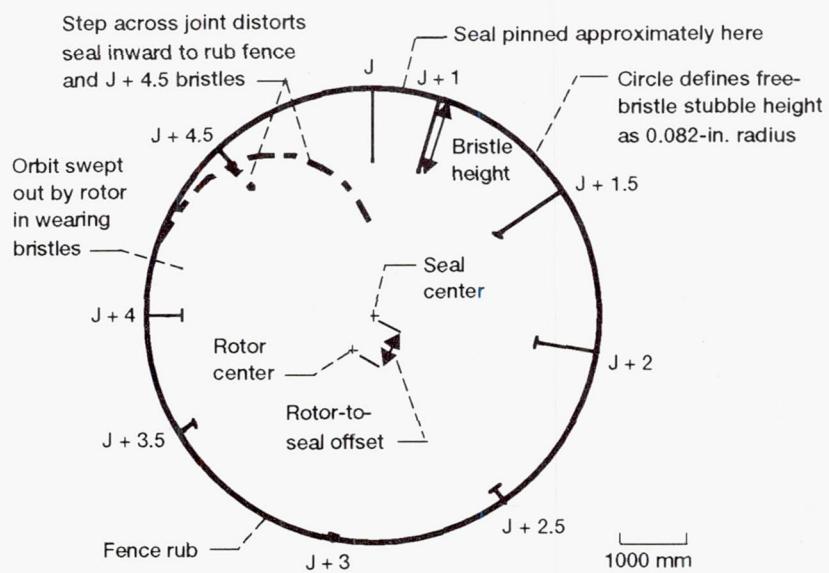
(iii) Bristle heights.

(a) Bristle heights, wear track and fence rub, and joint wear track.

Figure 3.—Post-test turbine shroud wear pattern. From reference 1.

334
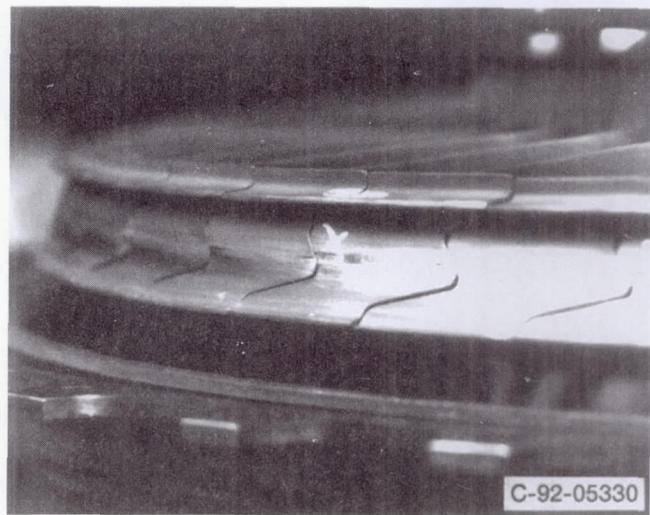
(b) Rotor scars.

Figure 3.—Concluded.
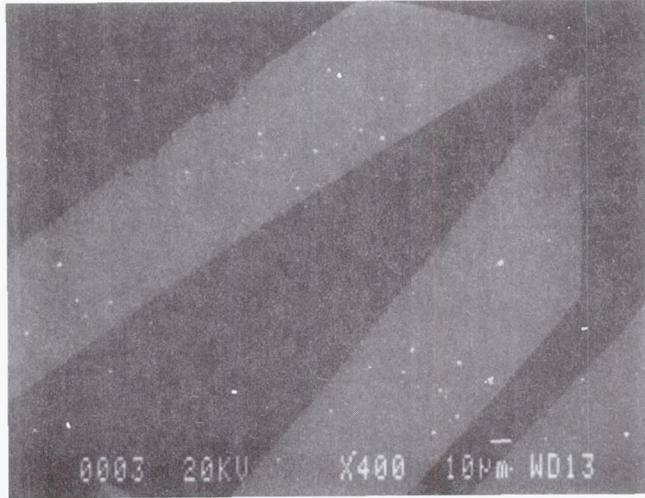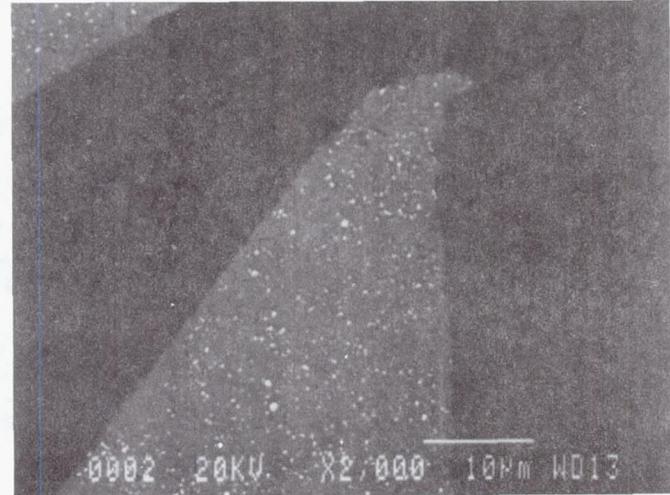
(a) Bristle tips.

(b) Enlargement of (a).
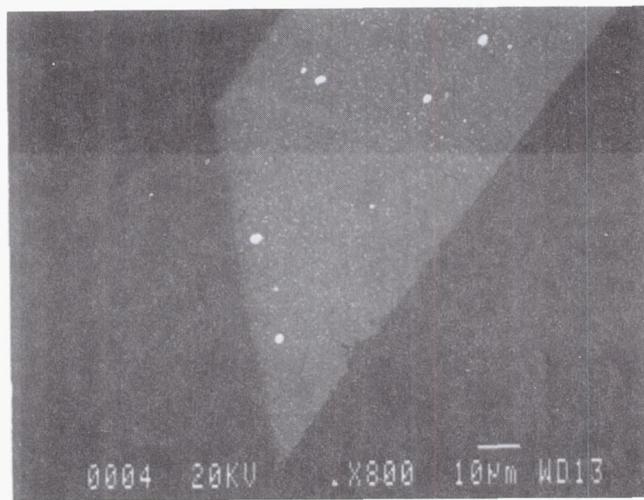
(c) Worn bristle tip.
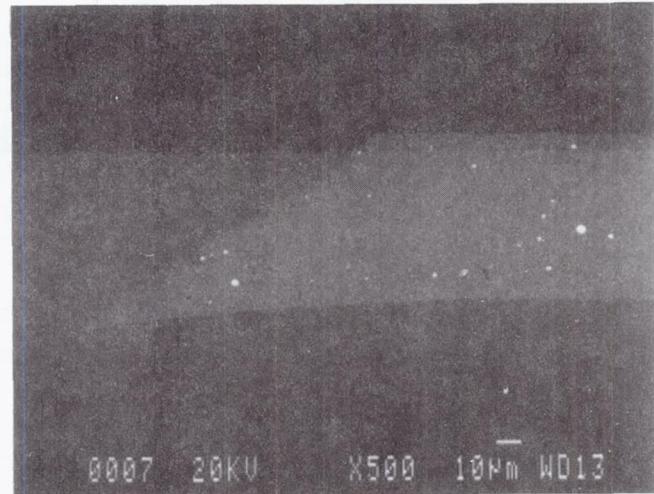
(d) Tip with possible transfer material.

Figure 4.—Post-test analysis of bristles cut from brush seal, showing irregular tips.
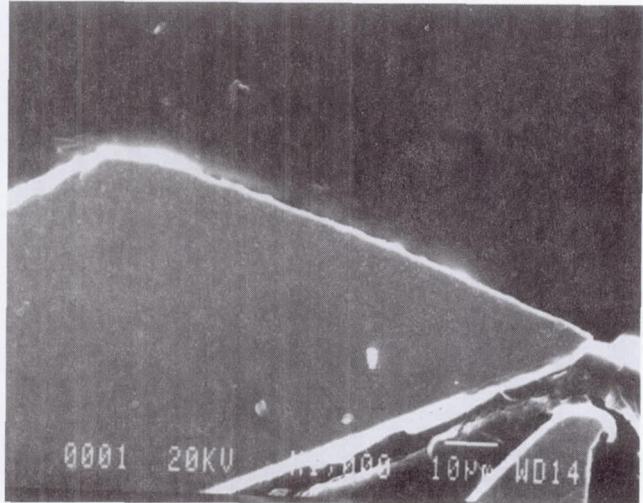
(a) Bristle tip.
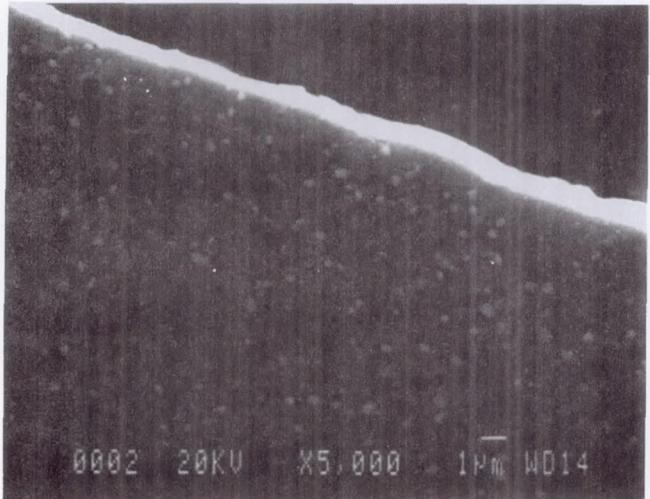
(b) Enlargement of bristle surface.
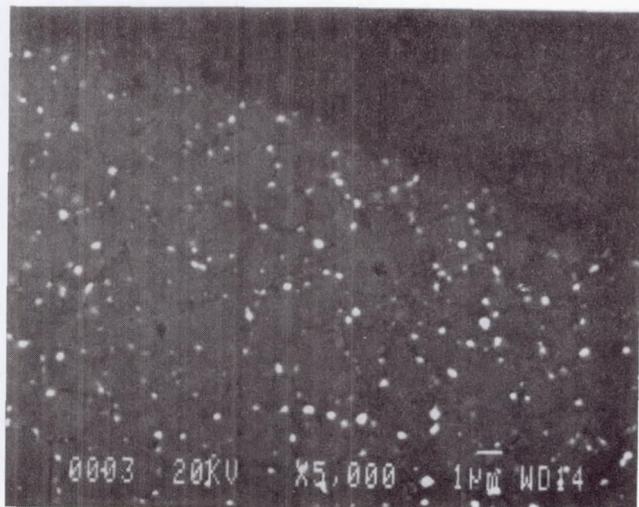
(c) Tungsten spots near interface.
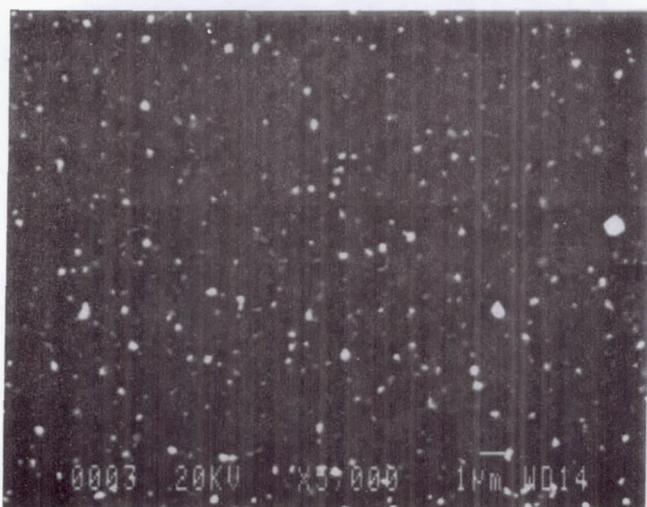
(d) Tungsten spots in interior.

Figure 5.—Etched surface structure, illustrating tungsten distribution.
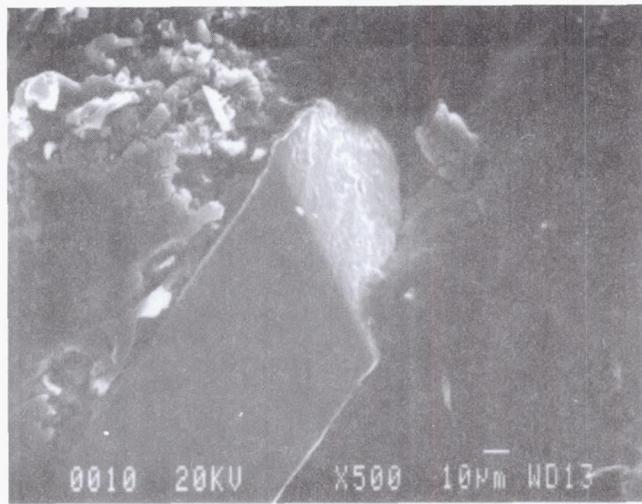
(a) Plan and end view.
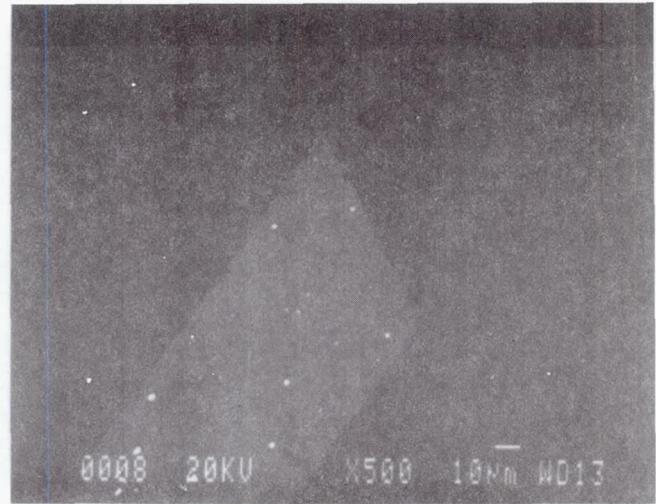
(b) Tungsten distribution.
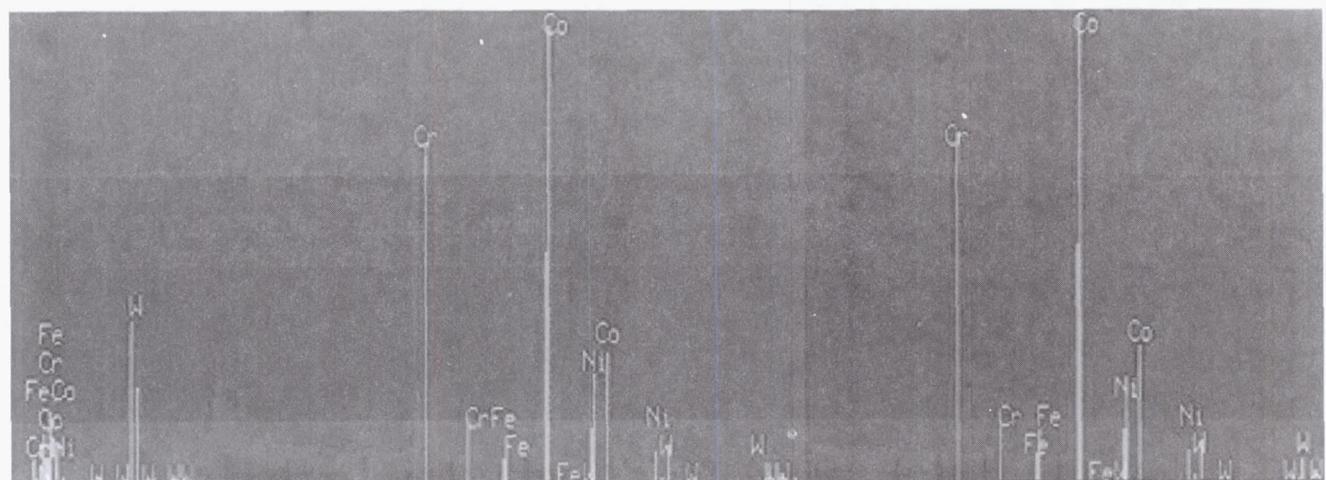
(c) Energy spectra.

(d) Selected region of (c).
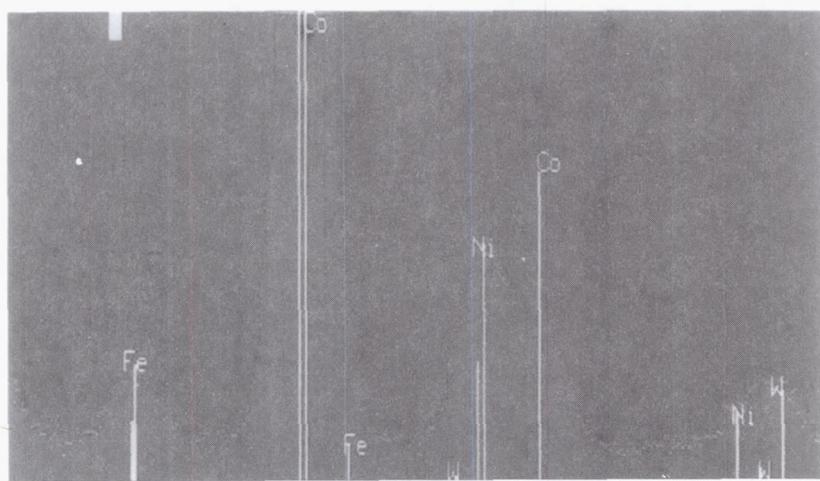
(e) Enhanced view of (d).

Figure 6.—Bristle tip wear surfaces, oxidation, and element composition.
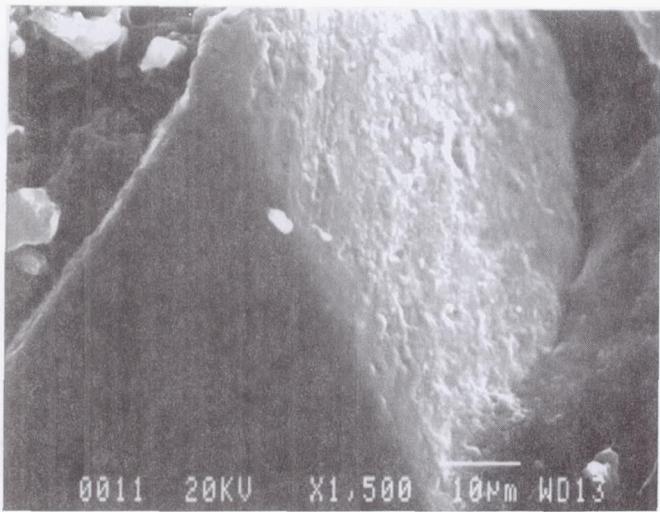
(a) Enlarged view of fig. 6(a).
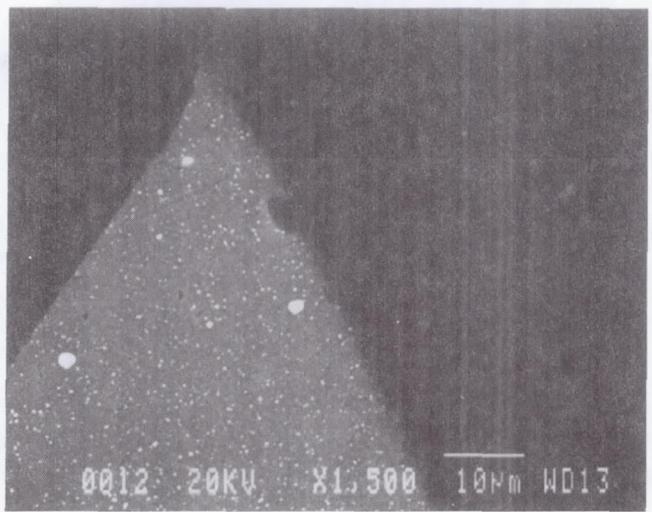
(b) Enlarged view of fig. 6(b).
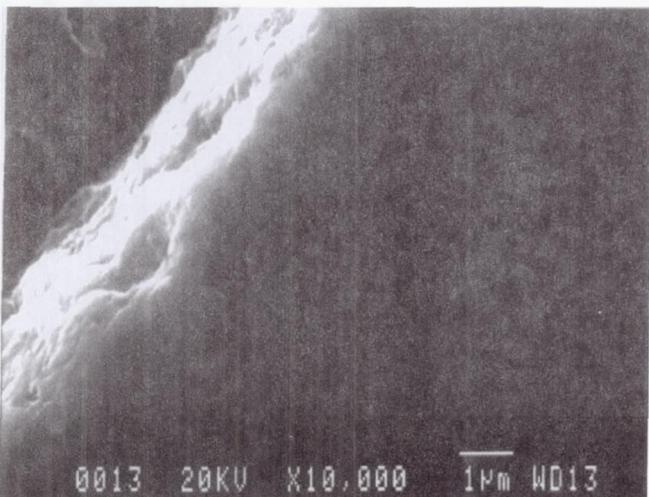
(c) Further enlargement of fig. 6(a).
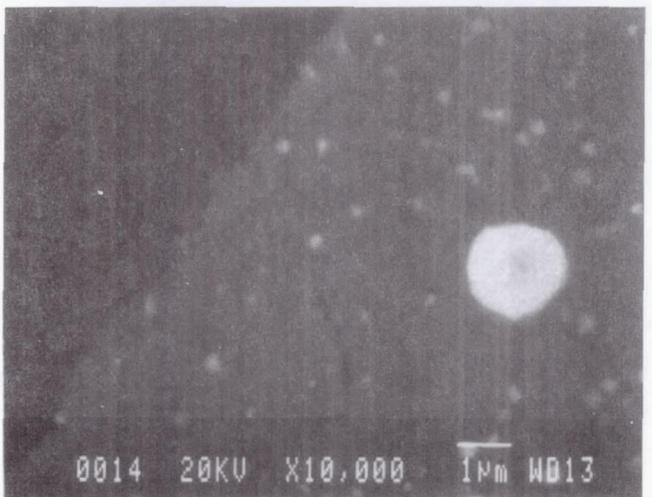
(d) Further enlargement of fig. 6(b).
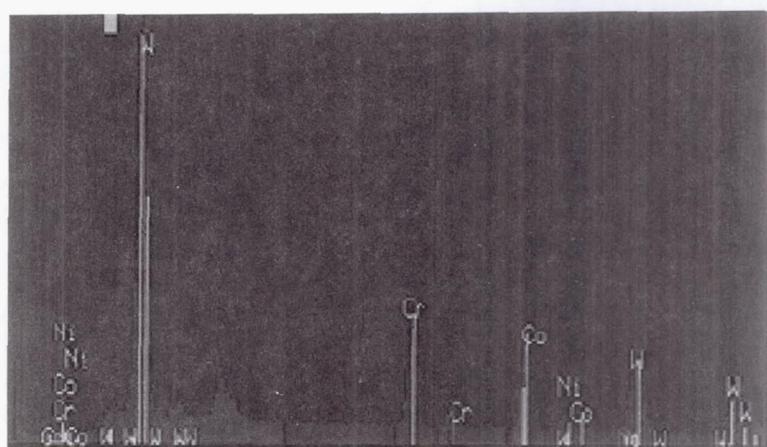
(e) Energy spectra of (d).

Figure 7.—Magnification of bristle tip wear surface and element composition.
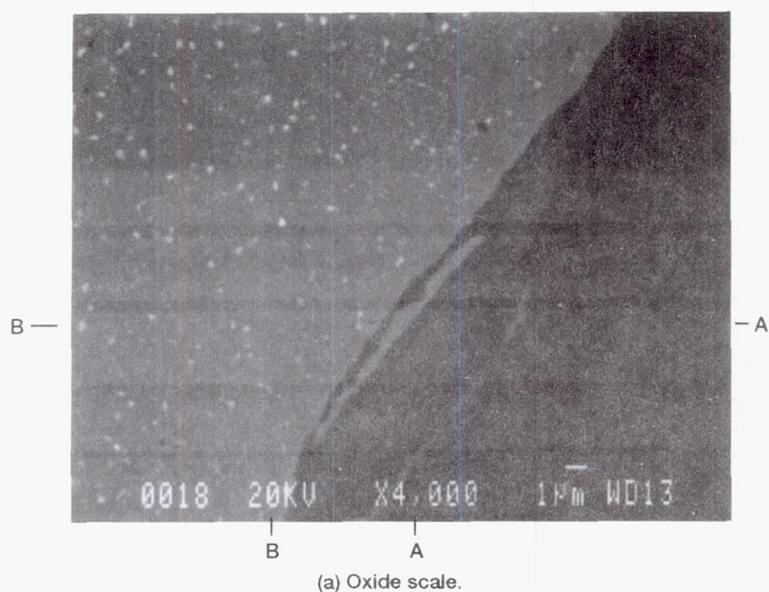
(a) Oxide scale.
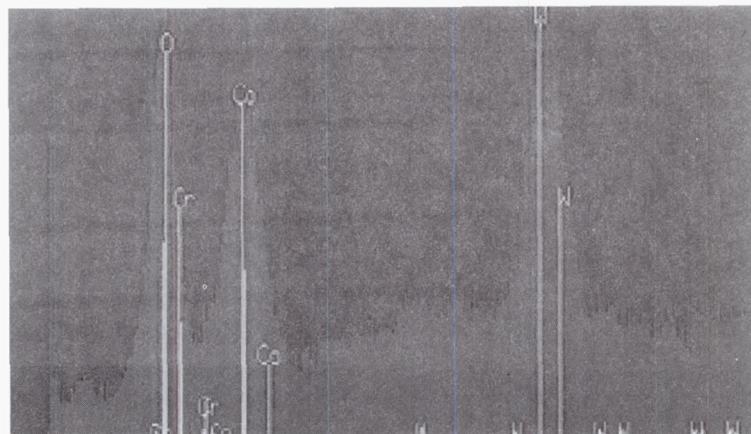
(i) Coordinates A–A.
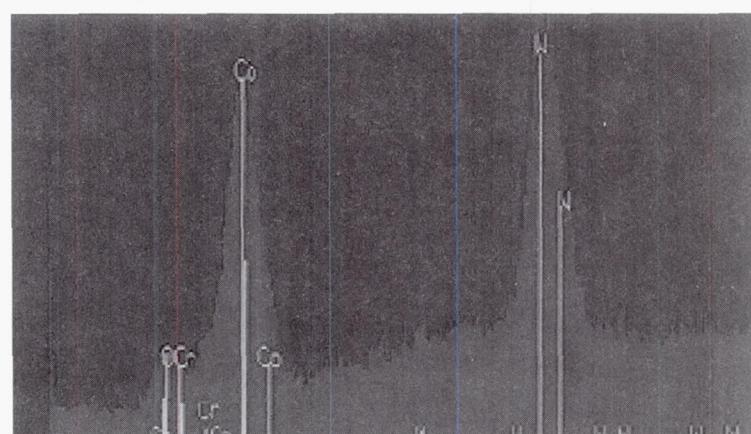
(ii) Coordinates B–B.

(b) Energy spectra.

Figure 8.—Oxide scale on bristle.
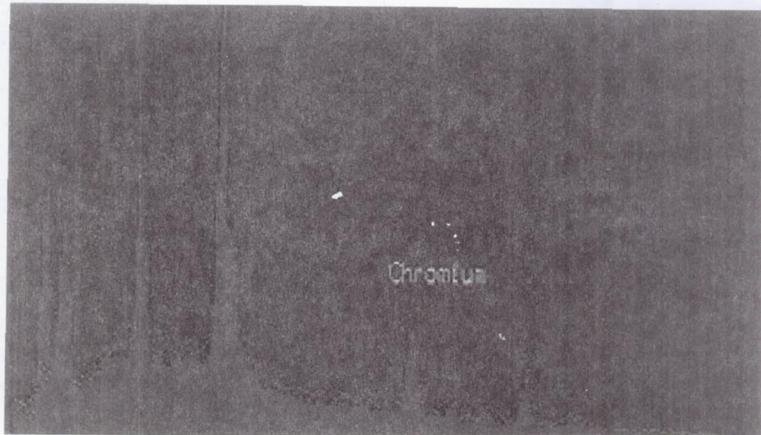
(c) Energy spectra comparison (oxide to matrix).
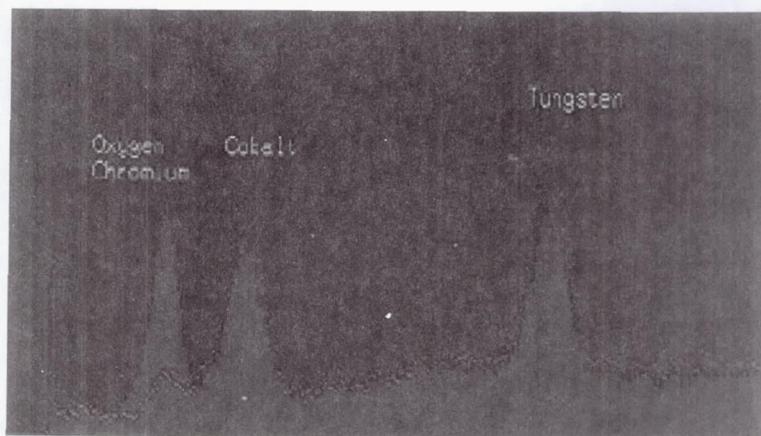
(d) Enlarged view of (c).

Figure 8.—Concluded.
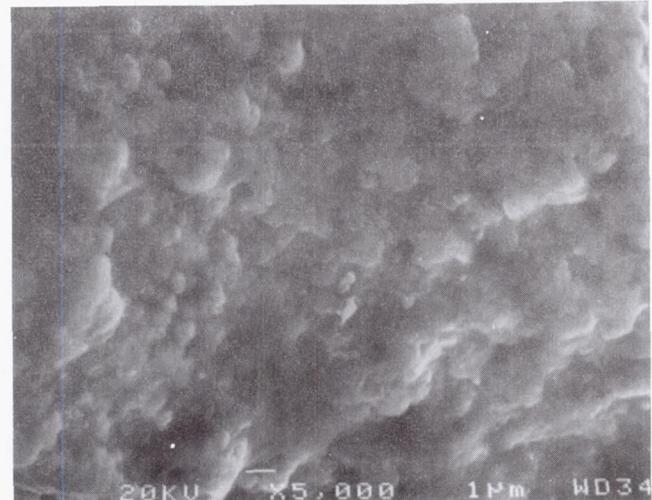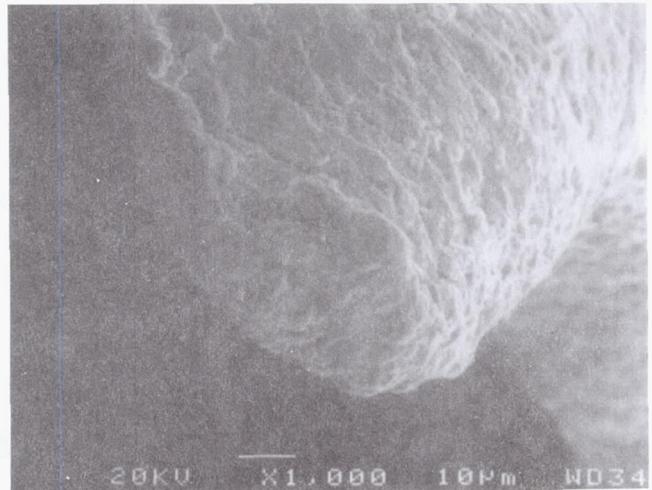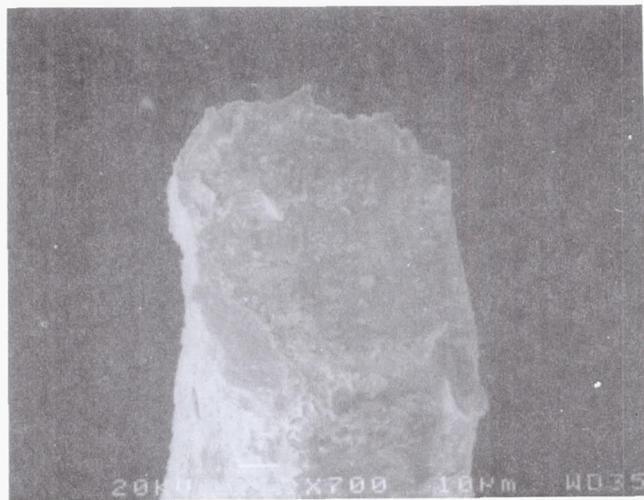
(a) Cut end.

(b) Worn end, showing oxide formation.

Figure 9.—Bristle cut and worn ends.

	Centroid, keV	Net area	Intensity
CKa	0.225	21 066	2.8
OKa	0.510	43 463	5.7
CoLa	0.780	29 633	3.9
WMa	1.800	65 602	8.6
CrKa	5.430	185 248	24.4
MnKa	5.955	39 090	5.1
FeKa	6.435	14 062	1.9
CoKa	6.945	246 707	32.5
NiKa	7.500	86 818	11.4
NiKb	8.385	21 442	2.8
WLb	9.660	6 573	0.9
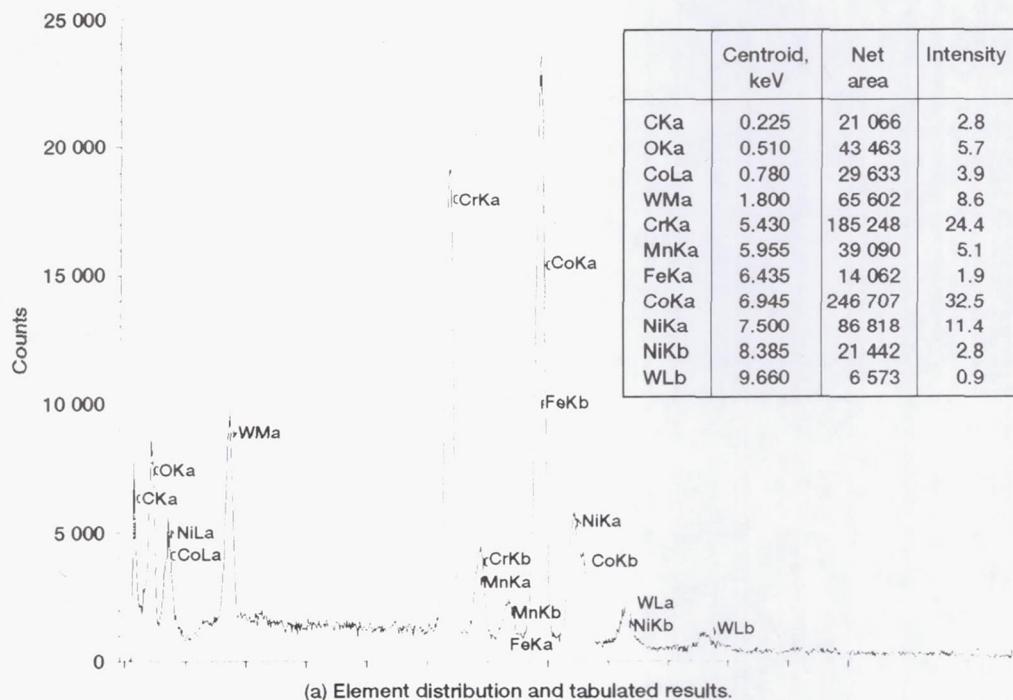
(a) Element distribution and tabulated results.
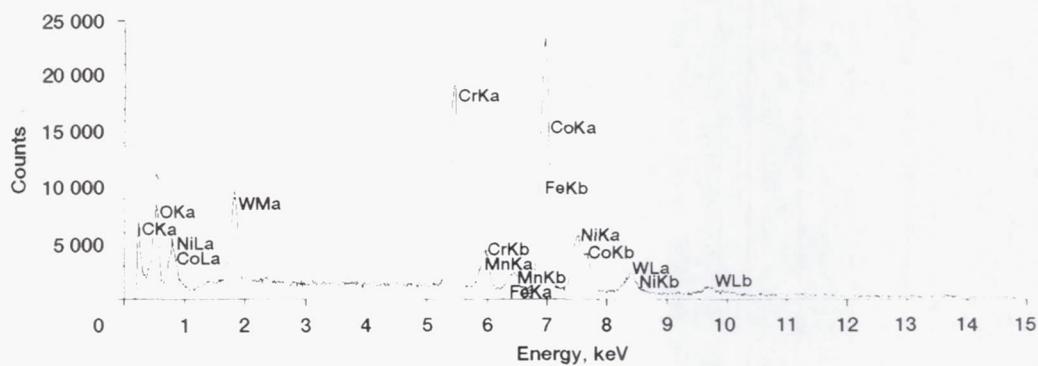
(b) Rescaled distribution.

Figure 10.—Composition of bristle cut end. Beam current, 0.3 mA; count time, 200 s; accelerating potential, 20 kV; beam spot magnification, 2000.

	Centroid, keV	Net area	Intensity
CKa	0.225	60 331	4.1
OKa	0.525	186 241	12.7
CoLa	0.795	70 556	4.8
AlKa	1.485	17 820	1.2
WMa	1.785	142 782	9.7
MoLa	2.295	17 680	1.2
CaKa	3.720	7 399	0.5
CrKa	5.415	327 186	22.3
MnKa	5.955	67 861	4.6
FeKa	6.435	39 110	2.7
CoKa	6.930	322 523	22.0
NiKa	7.485	165 926	11.3
WLa	8.415	38 395	2.6
WLb	9.690	4 725	0.3

(a) Element distribution and tabulated results.

(b) Rescaled distribution.
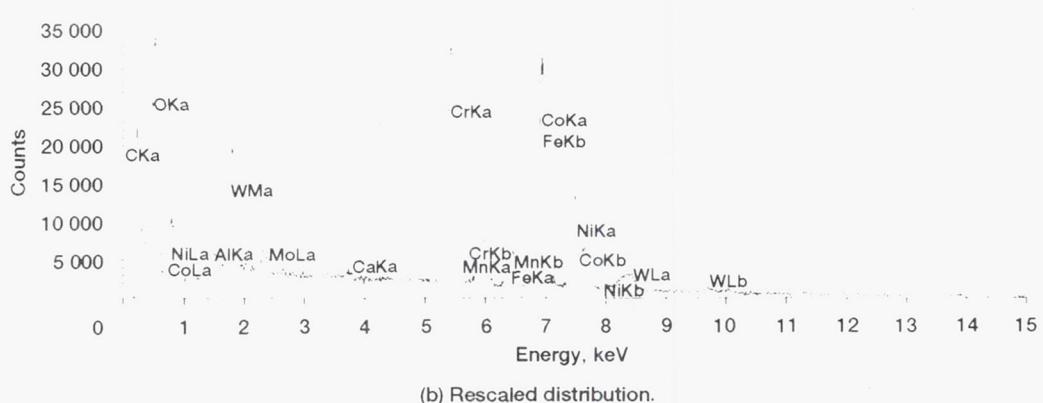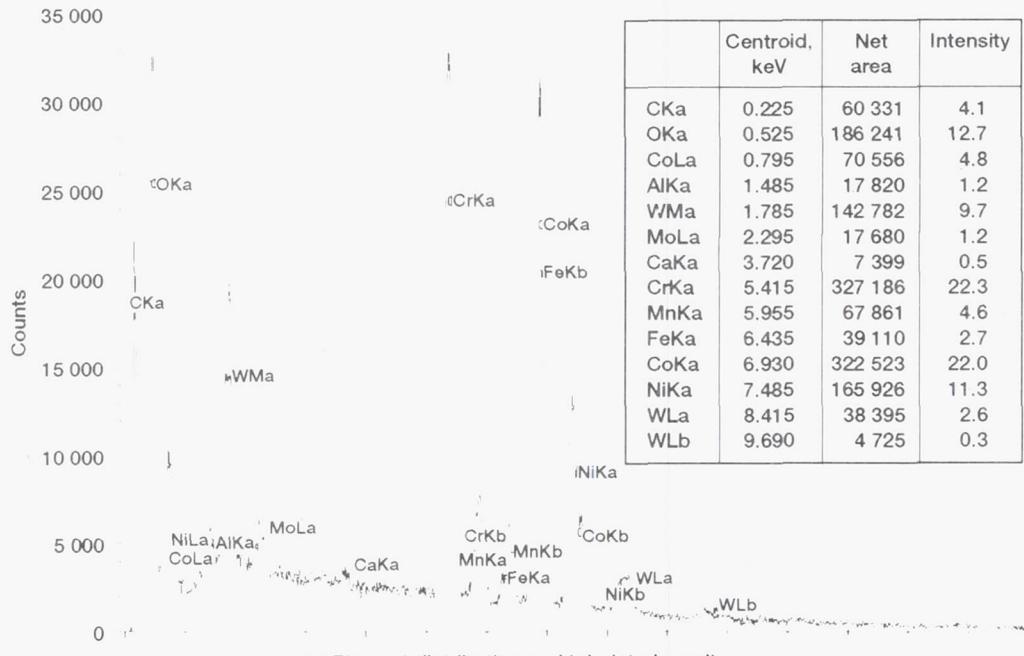
Figure 11.—Composition of bristle worn end. Beam current, 0.3 mA; count time, 200 s; accelerating potential, 20 kV; beam spot magnification, 5000.

344
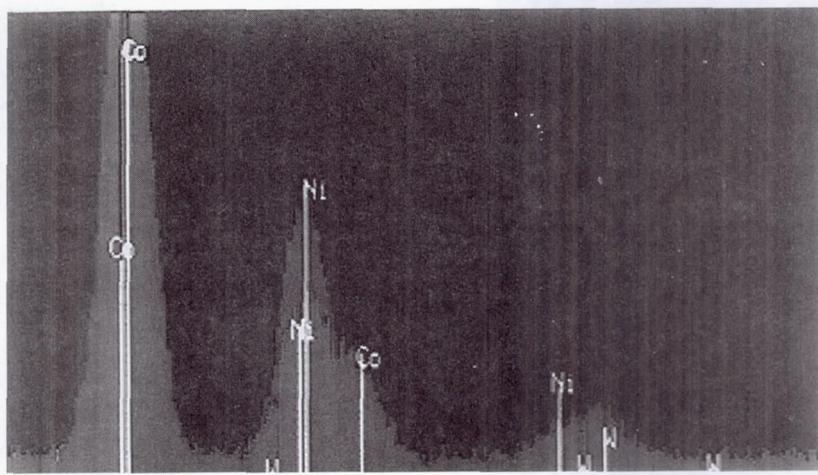
Figure 12.—Material transfer from René 80 rotor to Haynes 25 bristle.
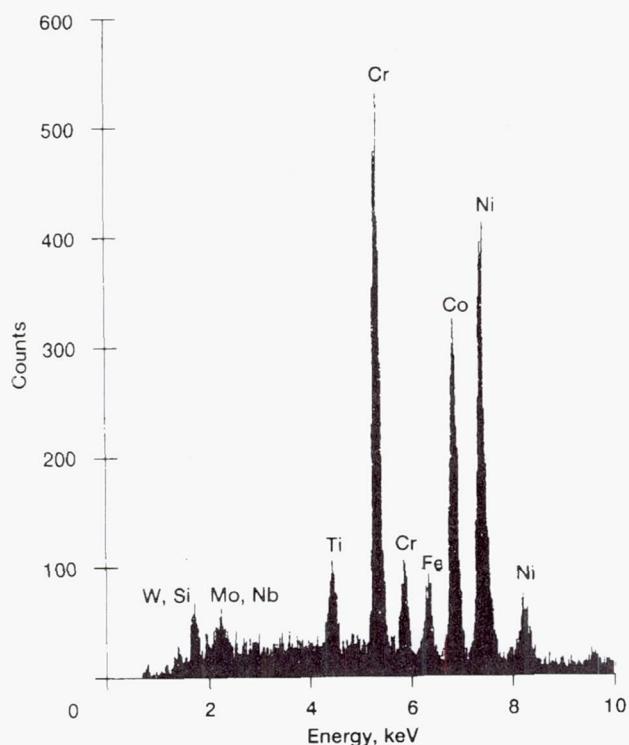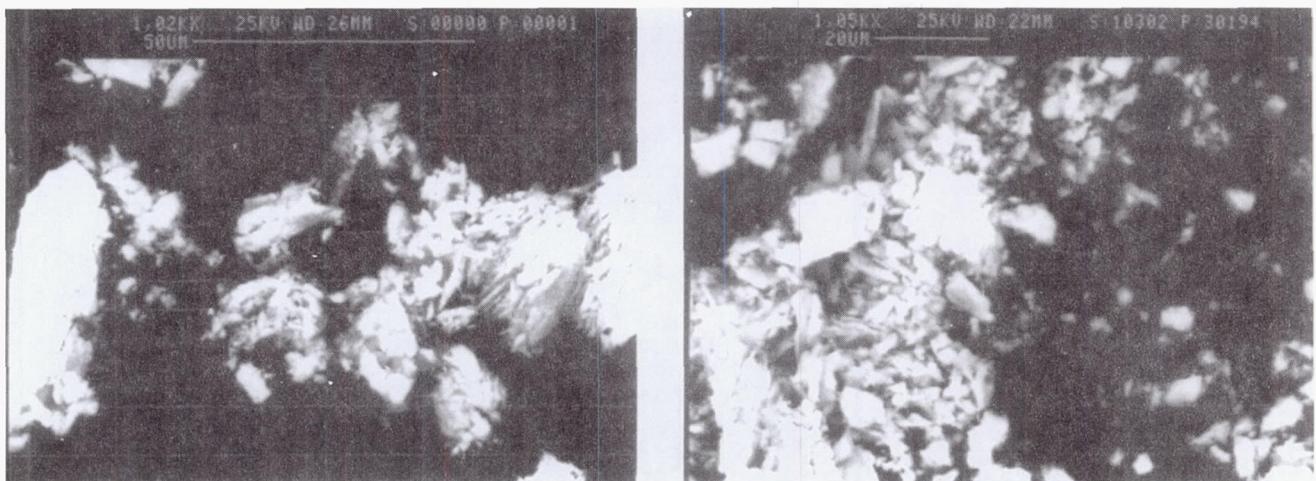
(a) Particle WS1A.
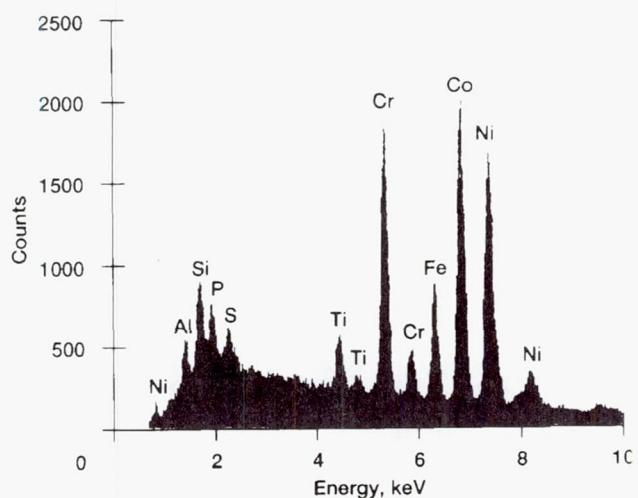
(b) Particle WS111A.

Figure 13.—Typical element spectra of post-test material scraped from René 80 rotor.

346
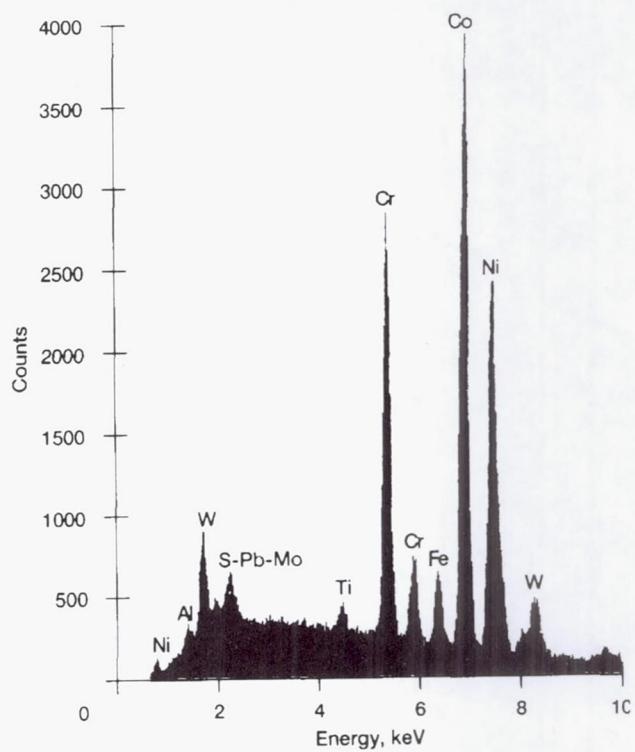
(c) Particle WSVA.

Figure 13.—Concluded.

347
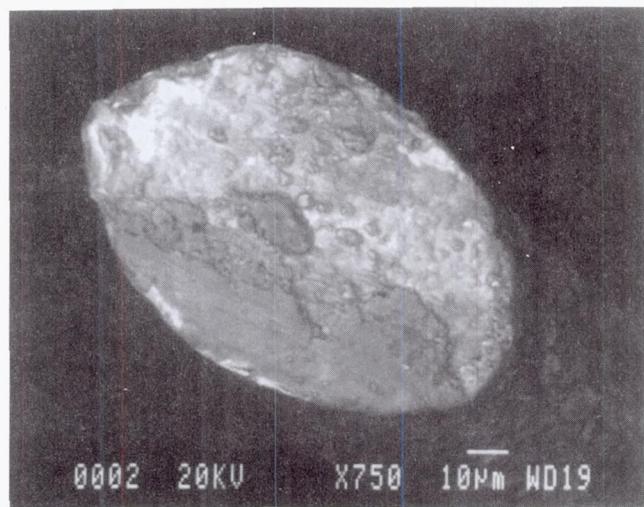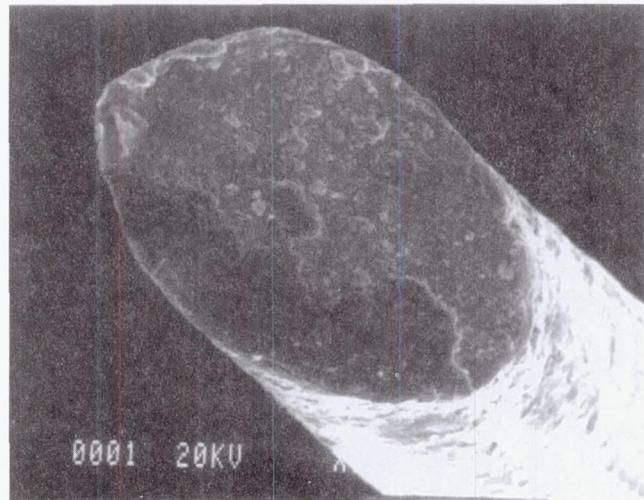
Figure 14.—Material transfer at bristle tip.
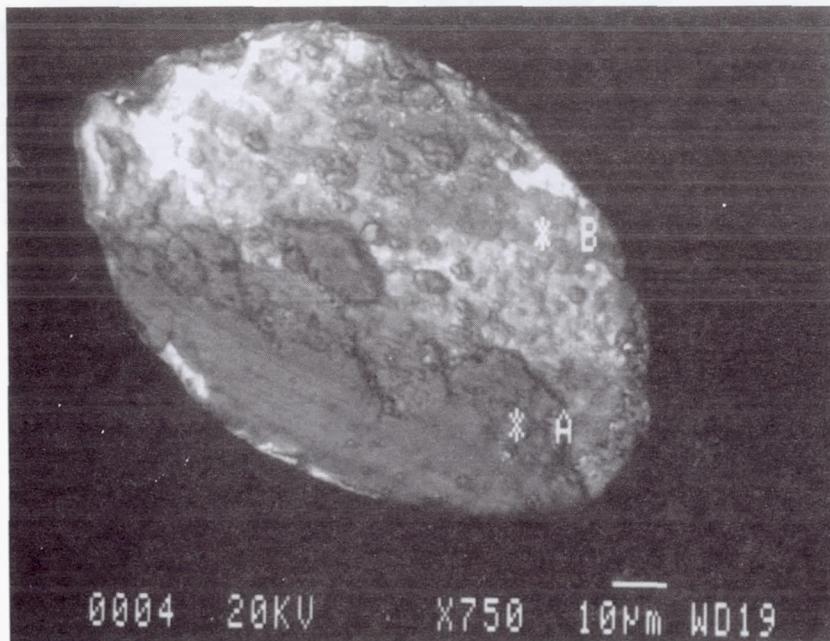
(a) Bristle tip spectra locations A, B, and C.
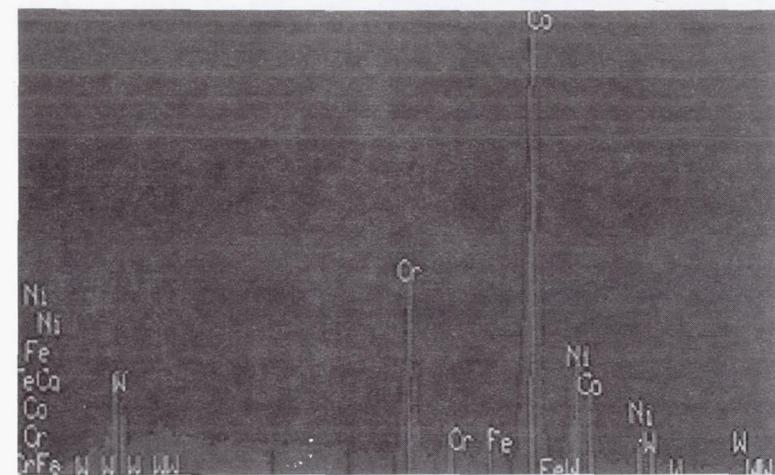
(b) Spectra location A.
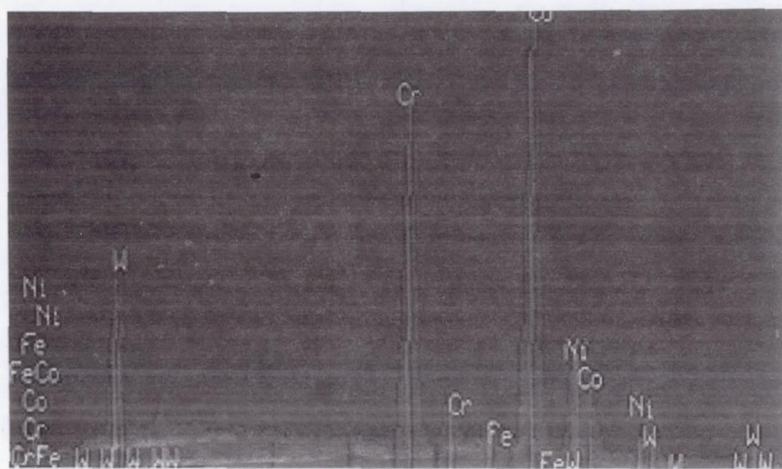
(c) Spectra location B.
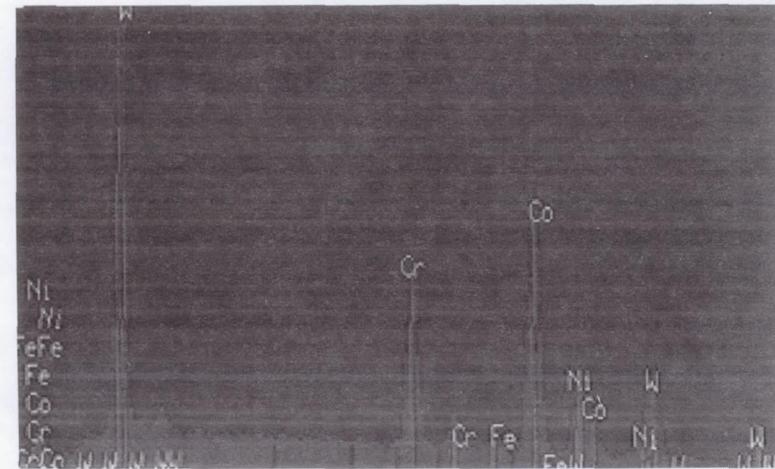
(d) Spectra location C.

Figure 15.—Variations in tungsten over bristle tip.
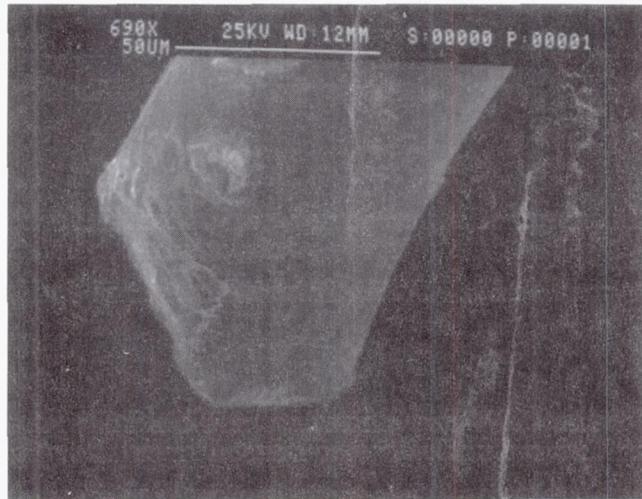
(a) Bristle end.
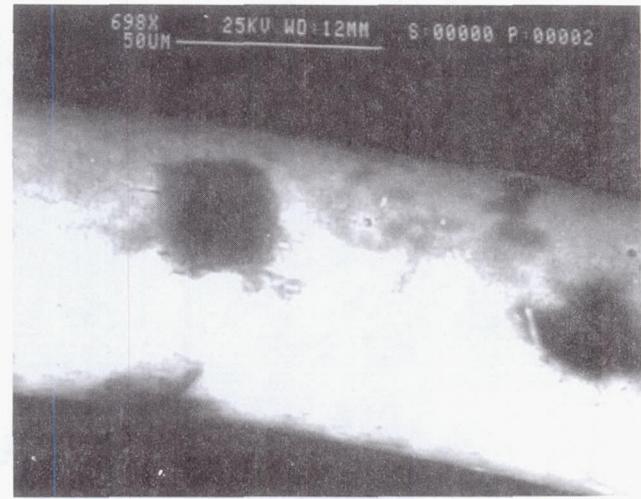
(b) Local spots.
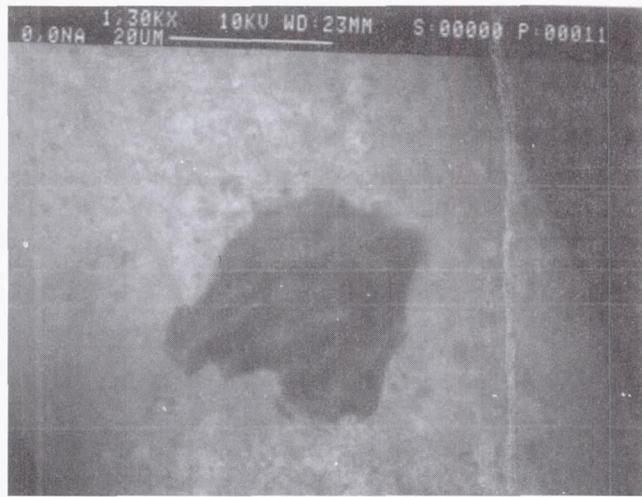
(c) Surface spot.
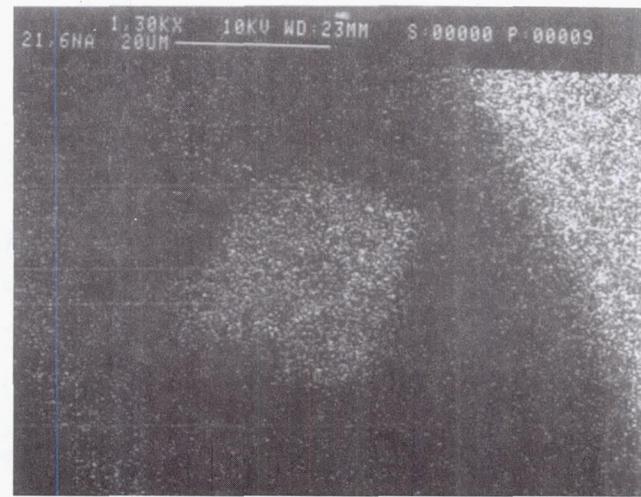
(d) Carbon dots of (c).

Figure 16.—Carbon distribution within spot on bristle tip.
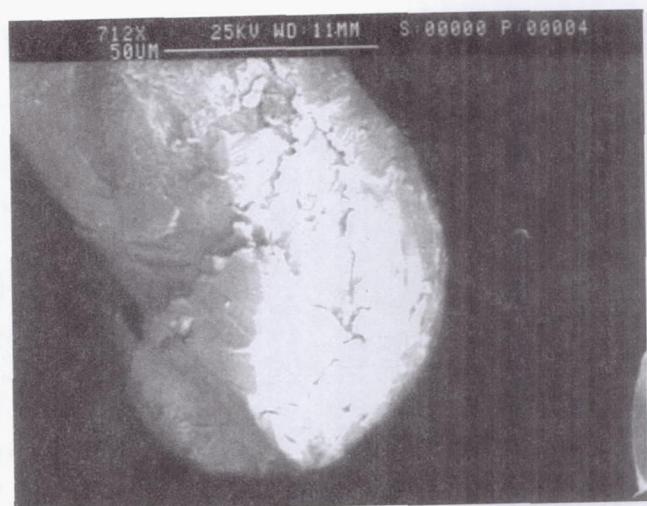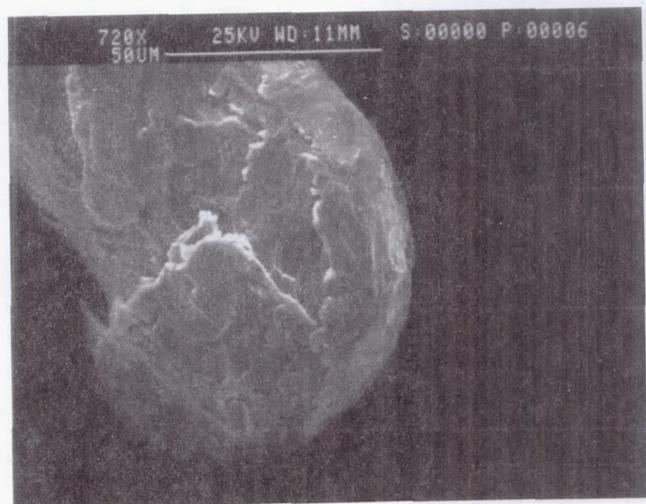
Figure 17.—Typical bristle tip collected in T–700 exhaust duct.
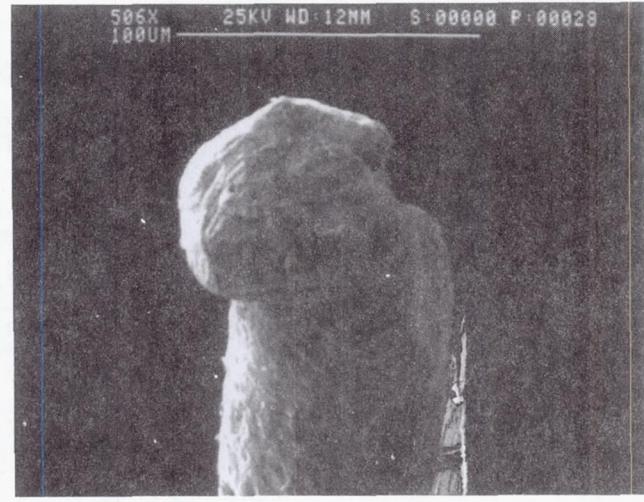
(a) Bristle tip 1 (two exposures).
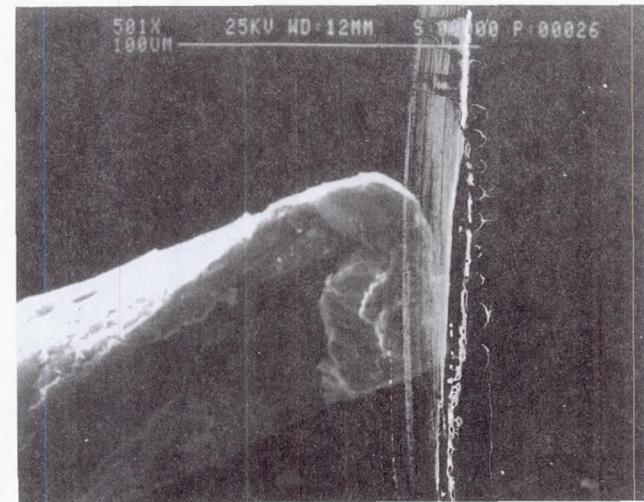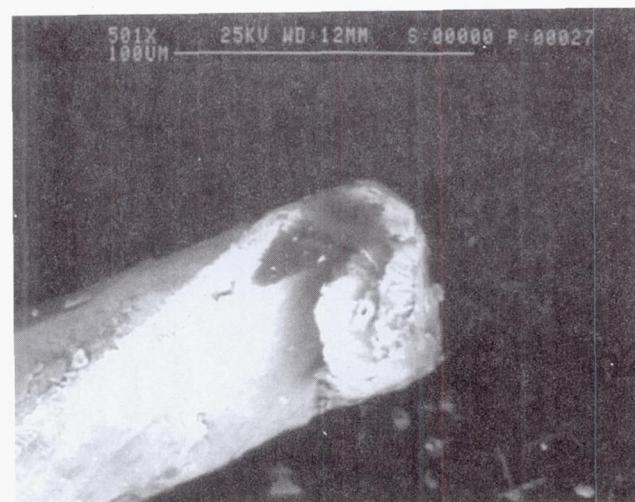
(b) Bristle tip 2 (two exposures).

Figure 18.—Typical bristle tip collected in T–700 exhaust duct, showing possible rubbed and quenched interface.
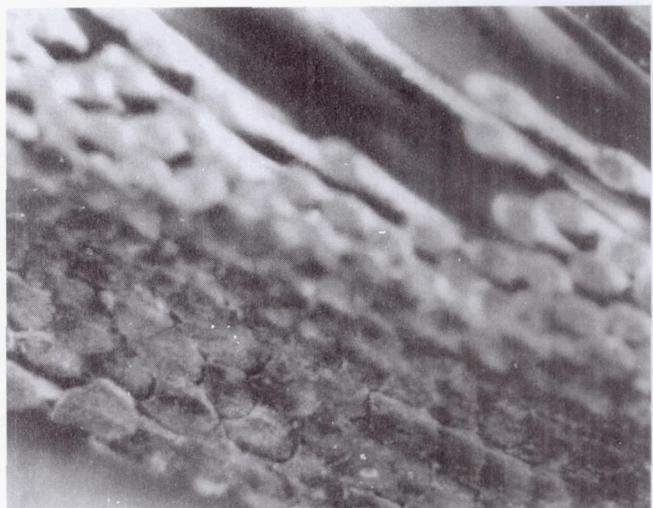
(a) Section 1.
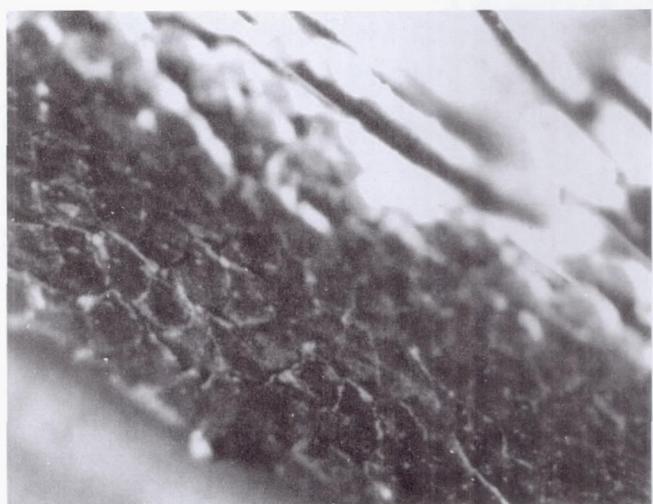
(b) Section 2.

Figure 19.— Bristle smearing (mudflat cracks) characteristic of rub interface.
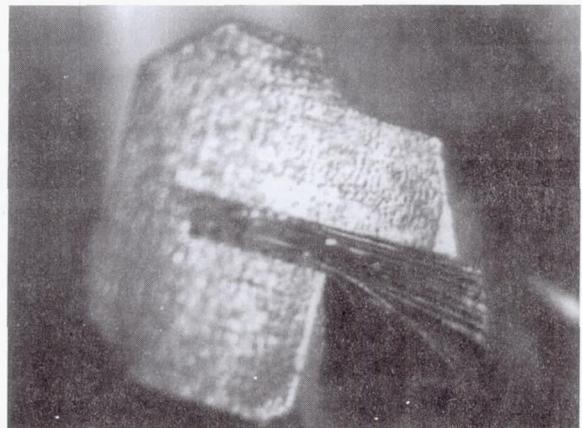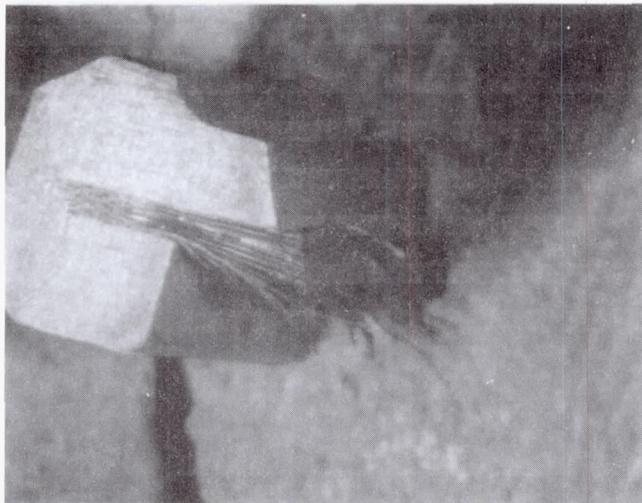
(a) Overview of bristles (seal section 1).
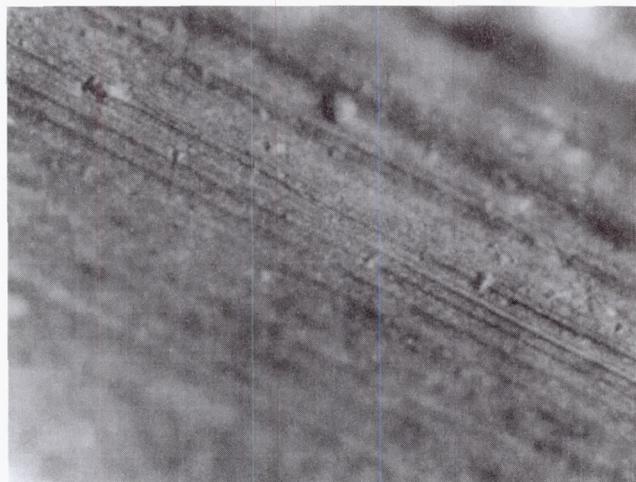
(b) Section of brush seal fence surface.

Figure 20.—Sets of information for brush segment 1.
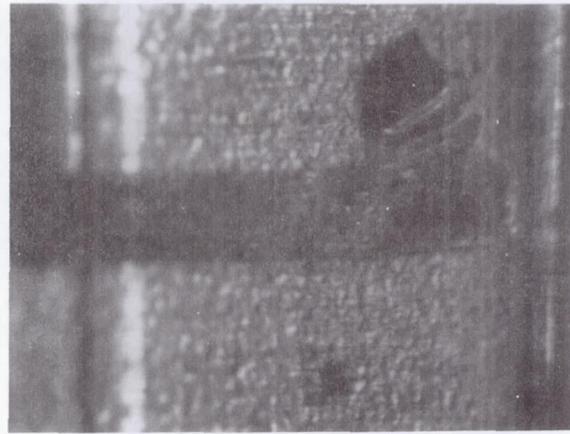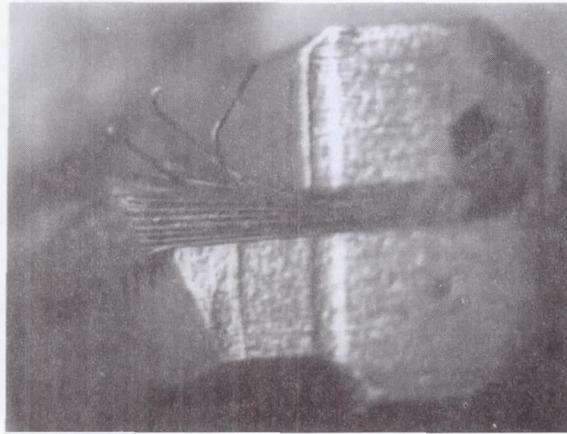
(a) Overview of bristles (seal section 2).
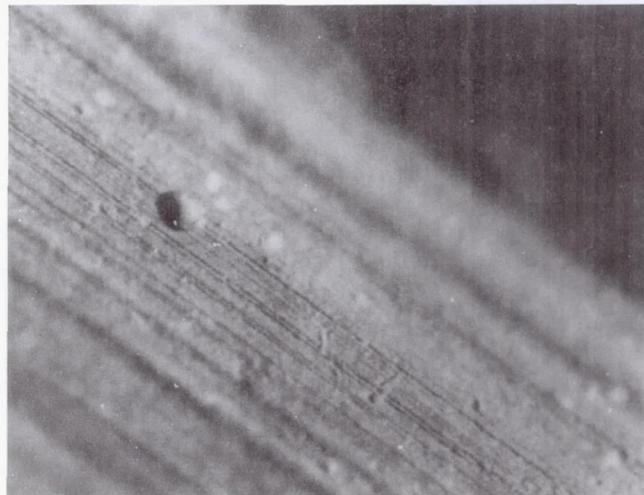
(i) Overview.
(b) Section of brush seal fence surface.

Figure 21.—Sets of information for brush segment 2.
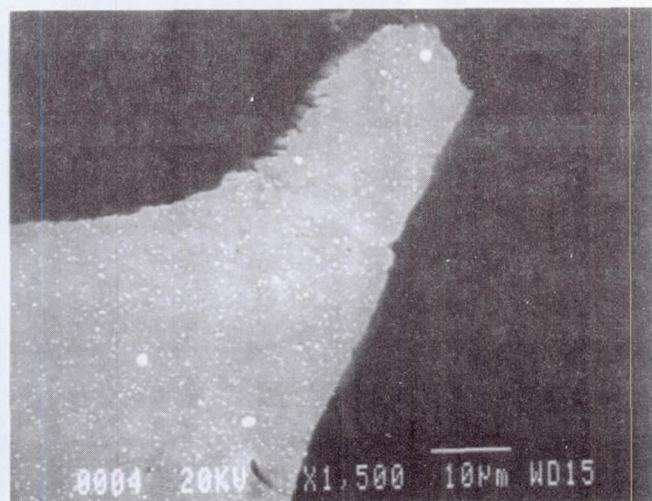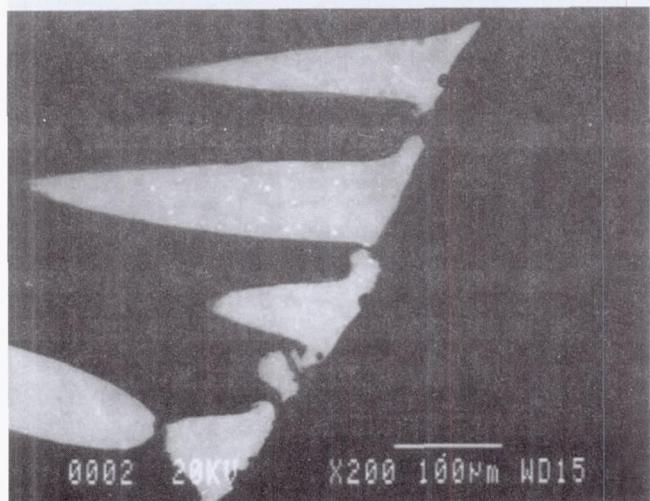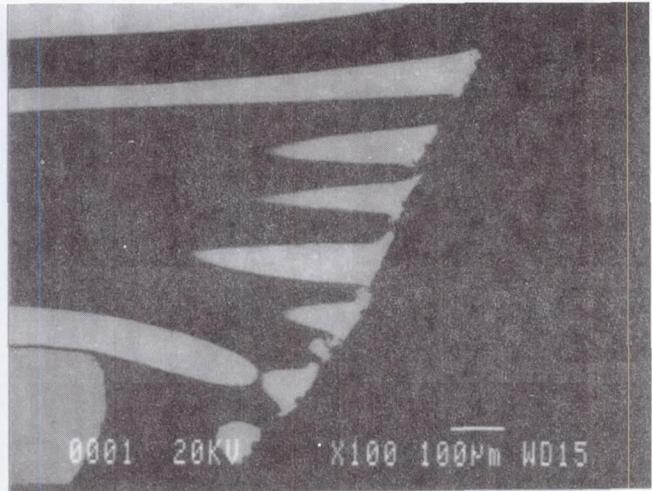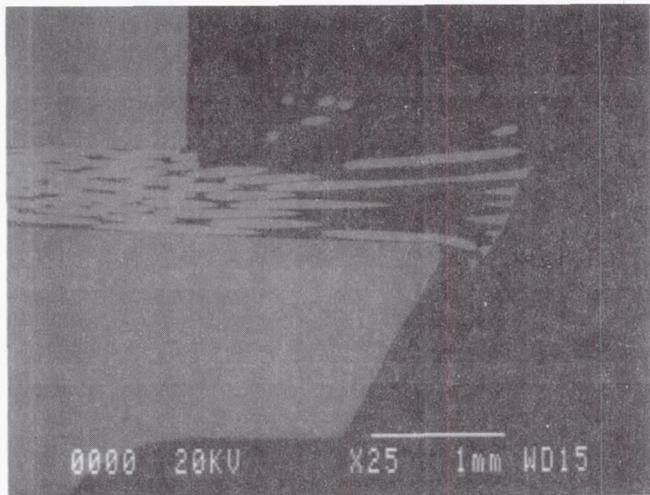
(ii) Enlargements of section view.

(b) Concluded.

Figure 21.—Continued.
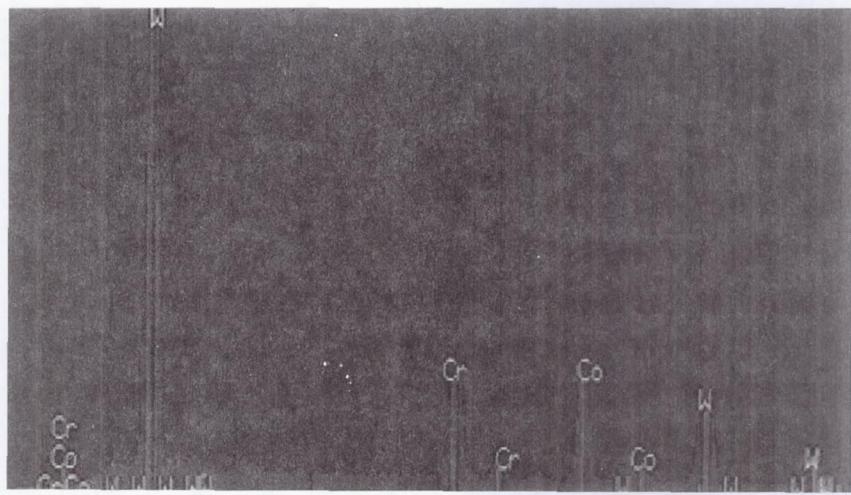
(i) White spot.
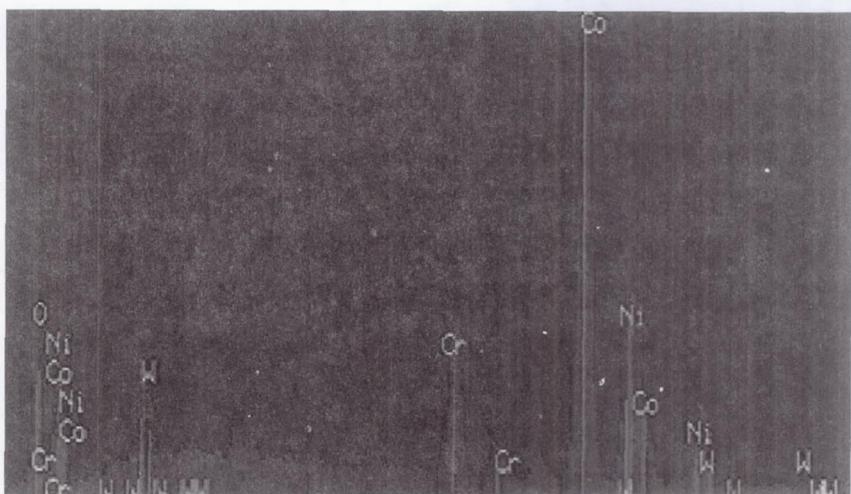
(ii) Oxide.
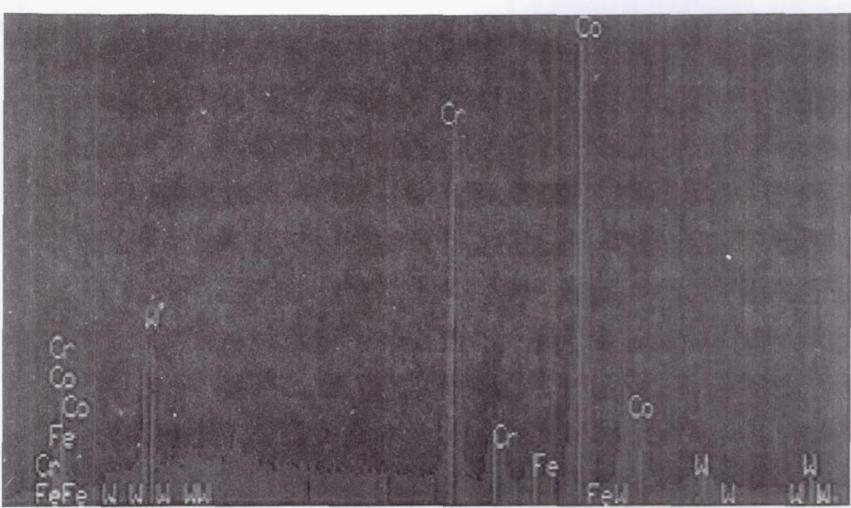
(iii) Matrix.

(c) Sets of element traces.

Figure 21.—Concluded.
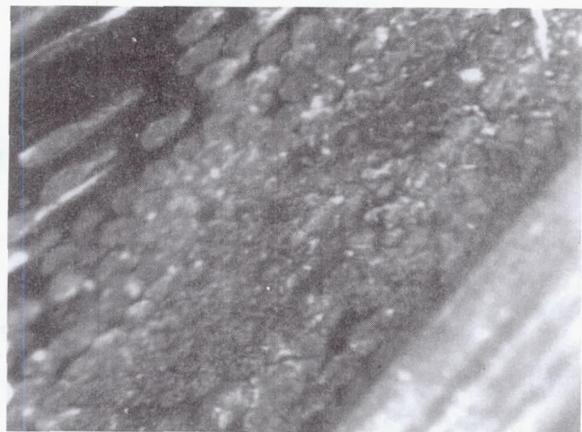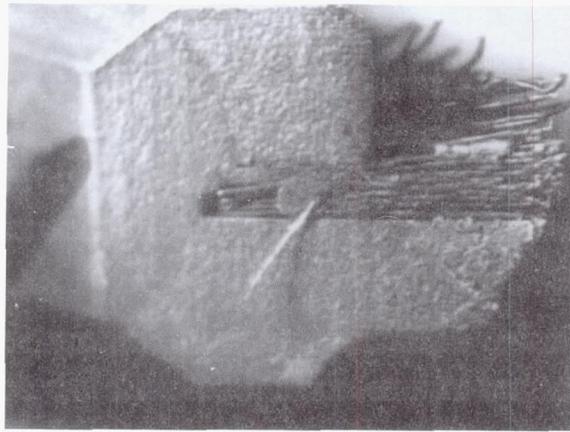
(a) Overview of bristles (seal section 3).
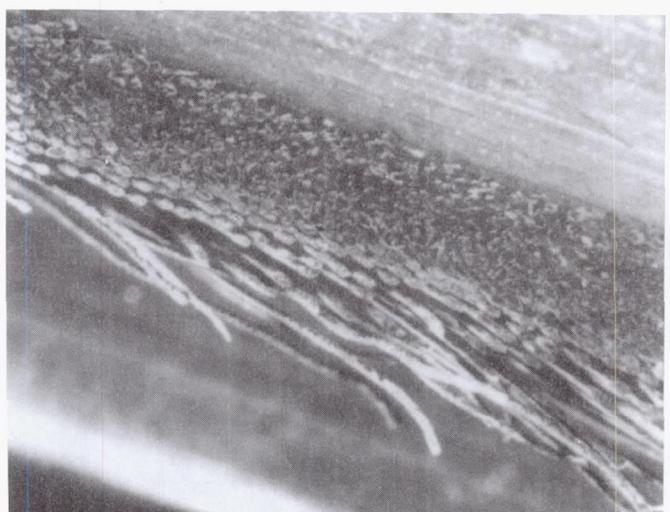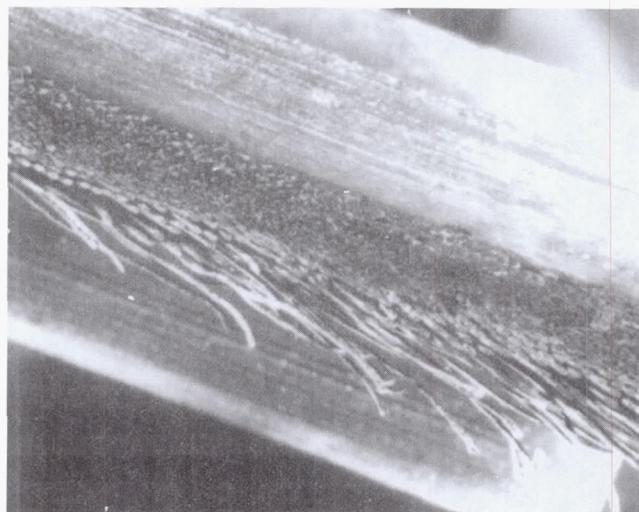
(i) Overview.

(b) Section of brush seal.

Figure 22.—Sets of information for brush segment 3.
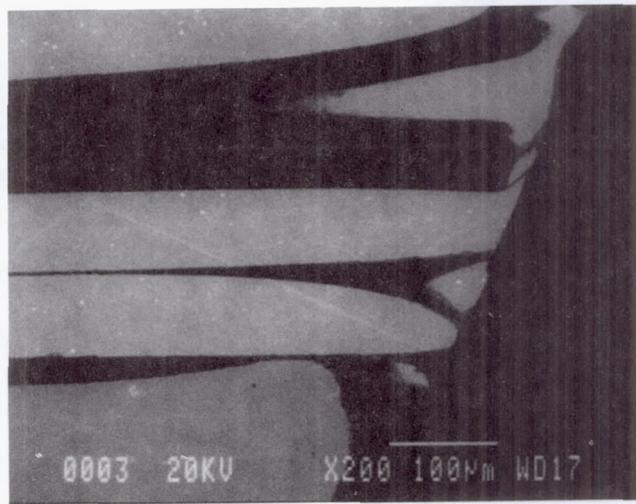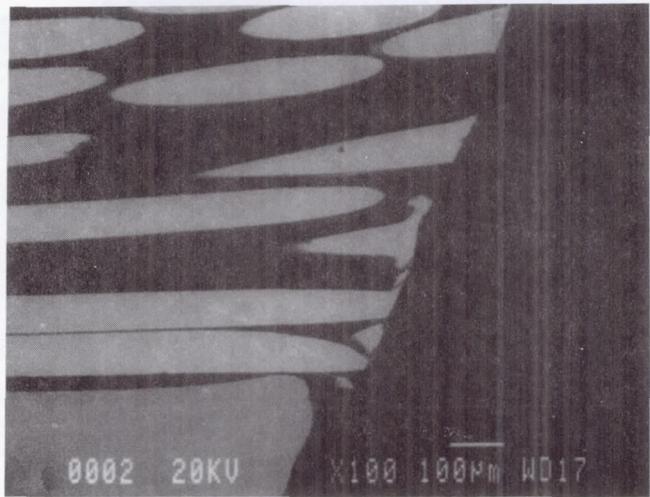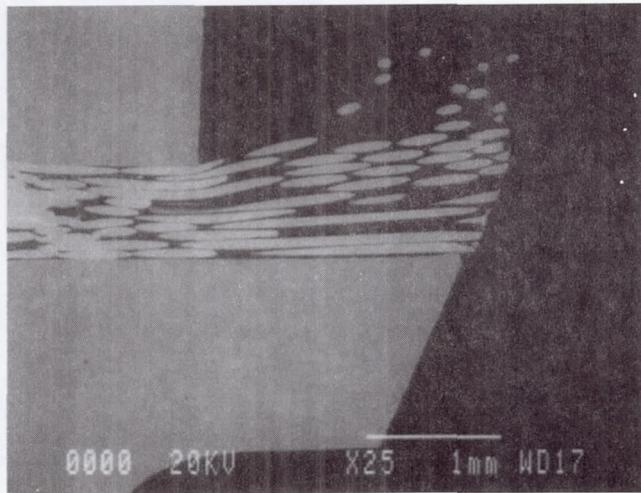
(ii) Enlargement of section view.

(b) Continued.

Figure 22.—Continued.
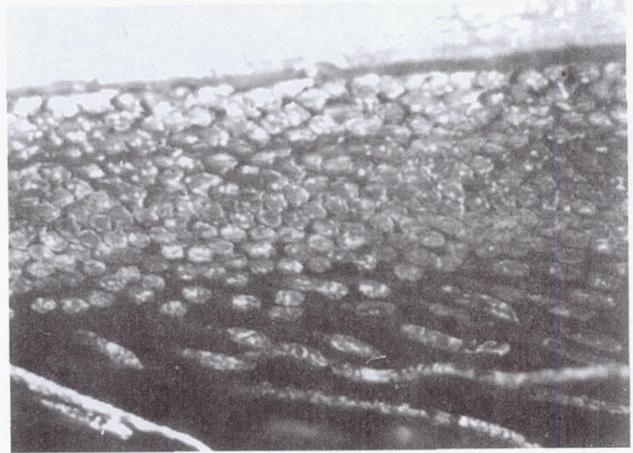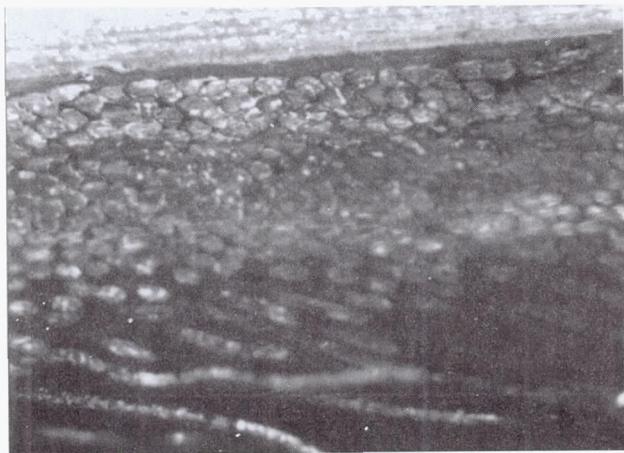
(iii) Enlargement of (i).

(b) Concluded.

Figure 22.—Continued.
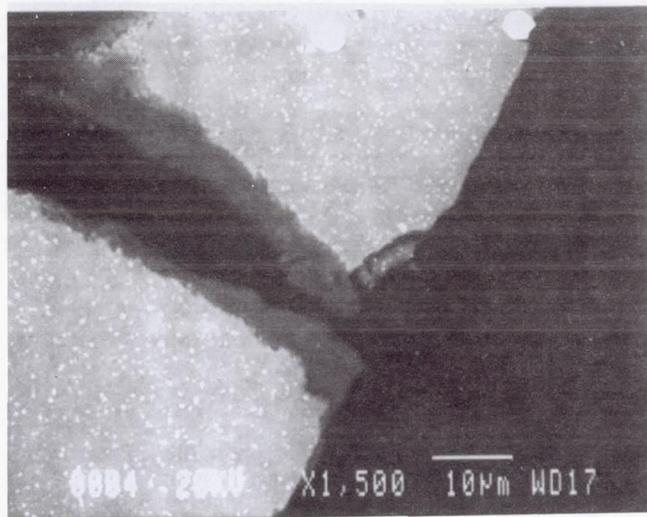
(i) Oxide.
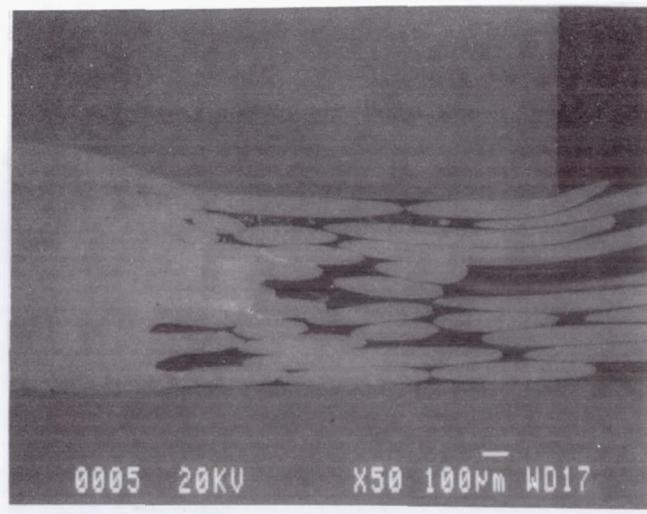
(ii) Melt near bristle attachment.

(c) Sets of element traces.

Figure 22.—Continued.
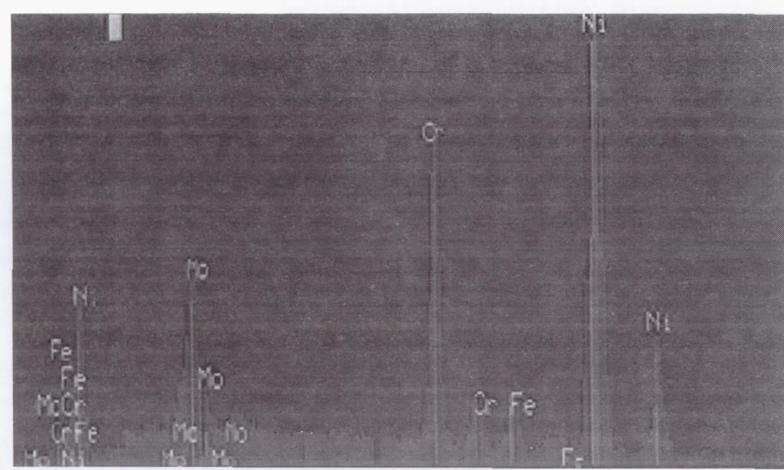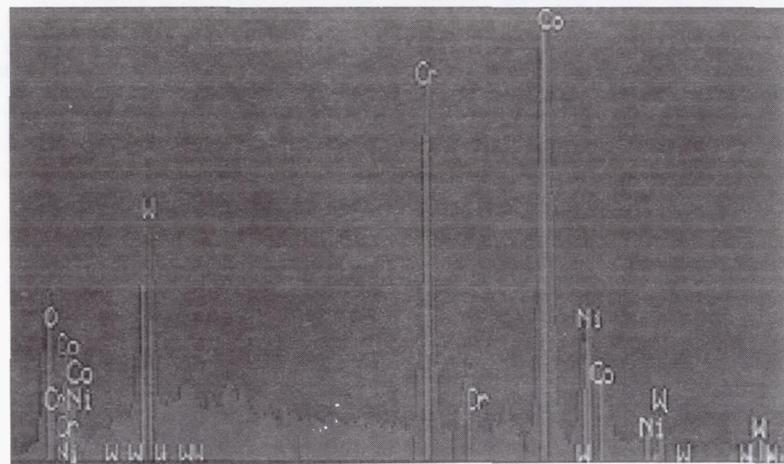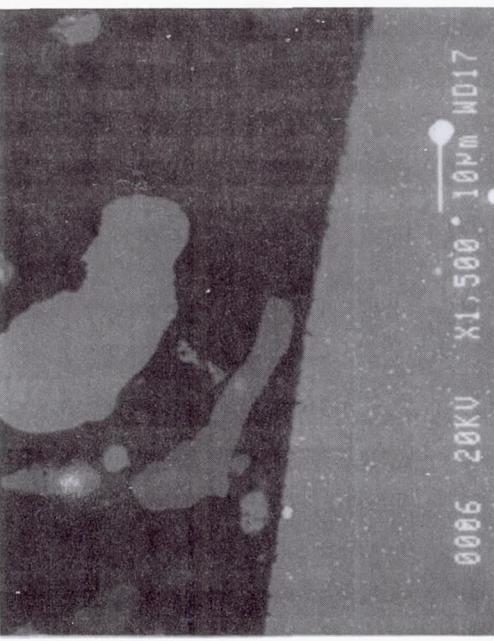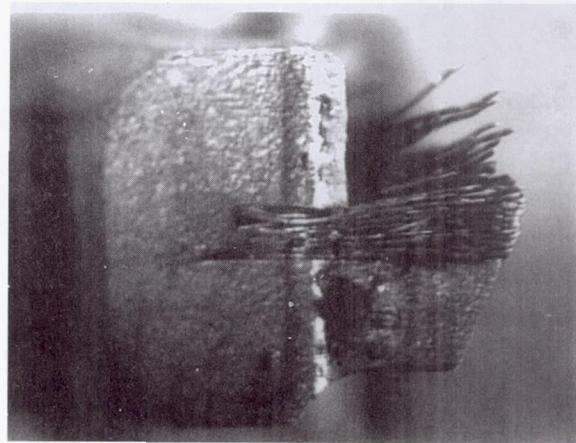
(iii) Foreign particle.
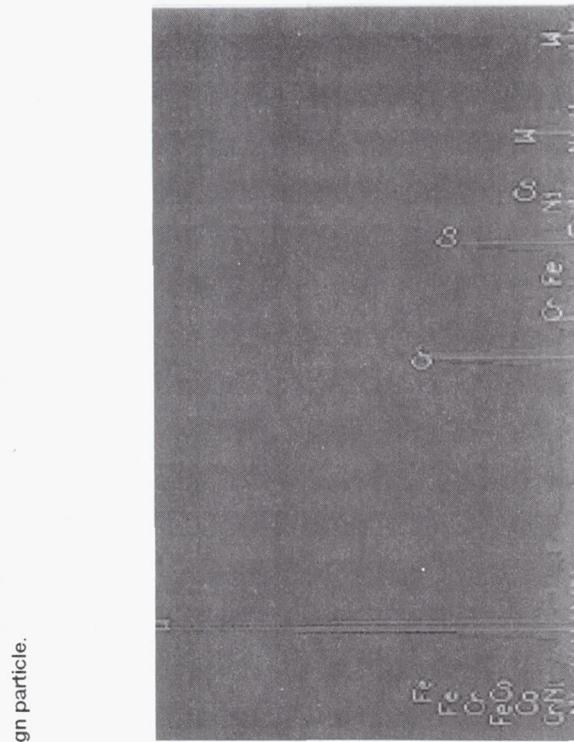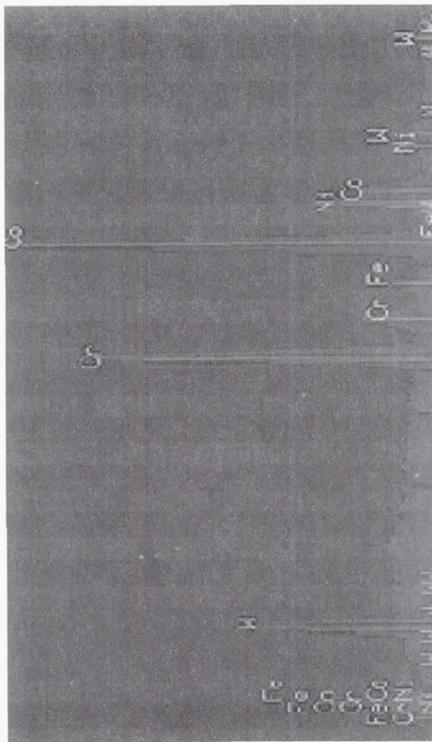
(iv) Resolidification of tungsten.

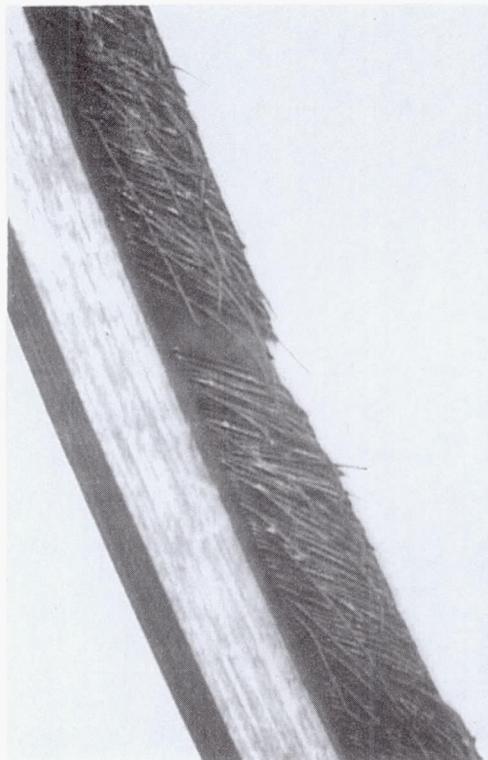(c) Concluded.

Figure 22.—Concluded.

362
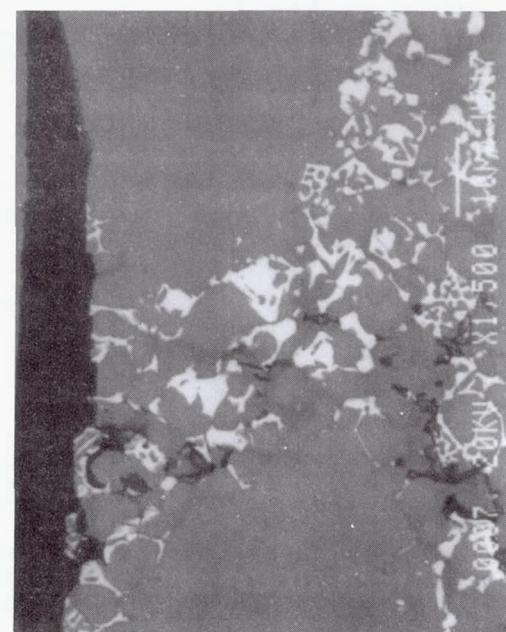
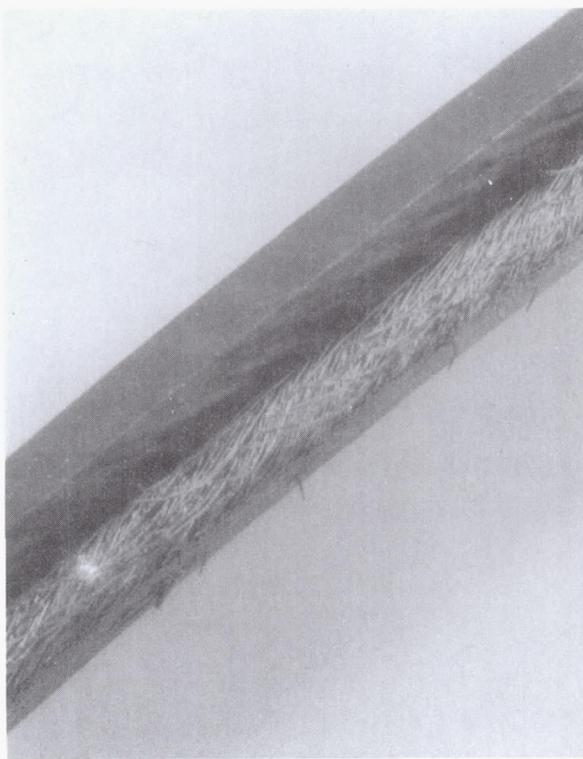(a) Overview of bristles (seal section 4).
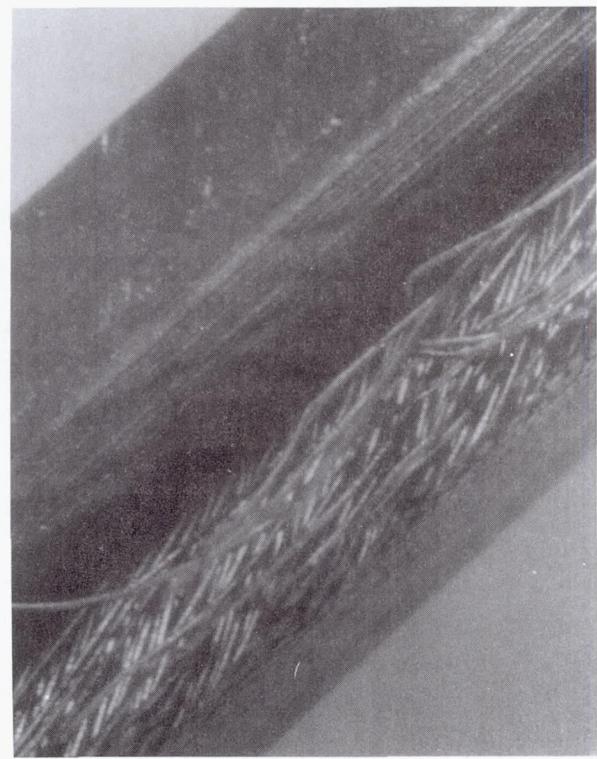

(b) Section of brush seal.

Figure 23.—Sets of information for brush segment 4.
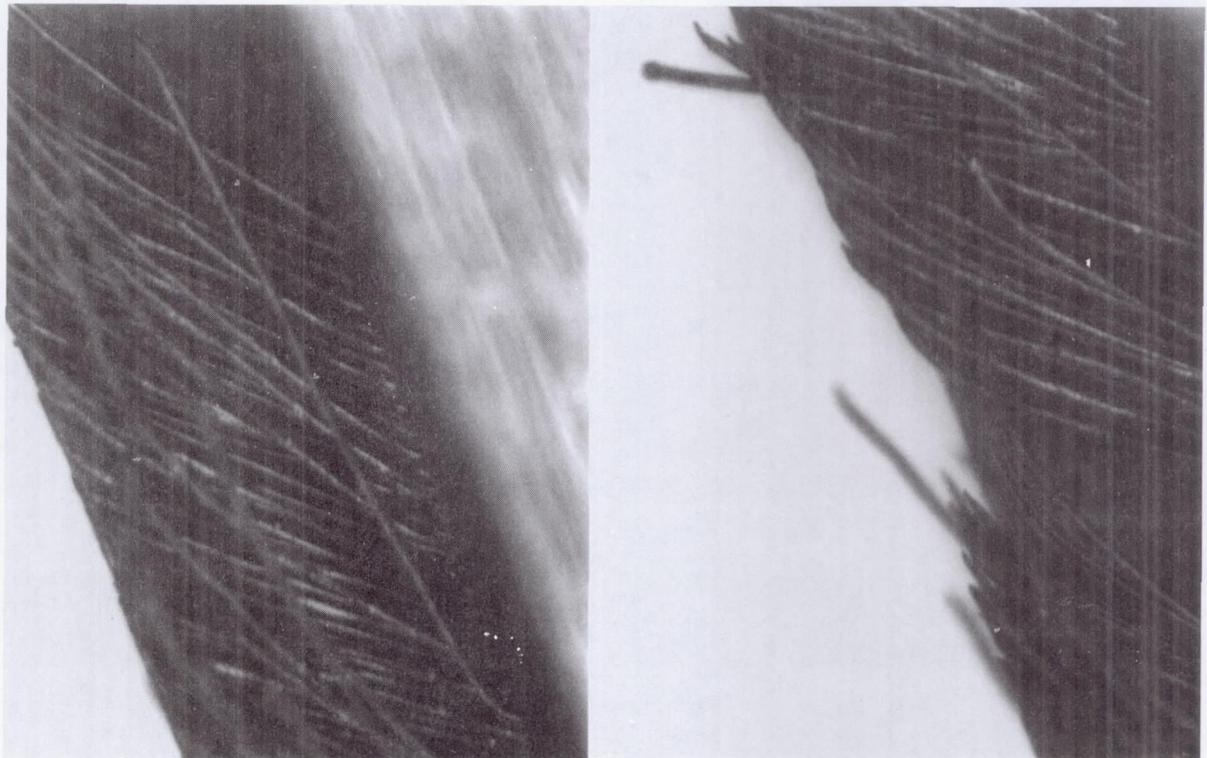
(a) Region void of bristles.

(b) Bent-over bristles (on leading edge but not in core).
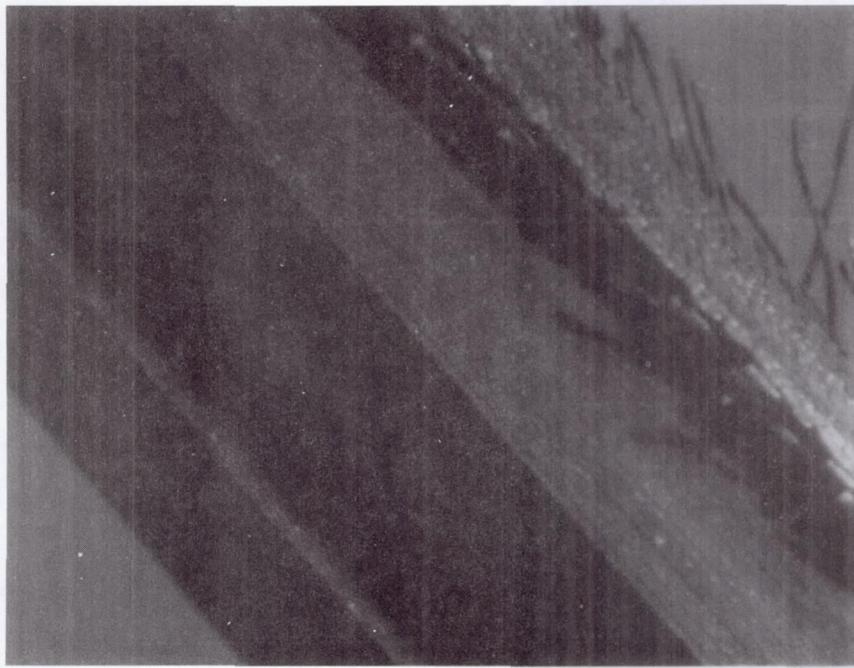

(c) Bristles kinked at tips (appear about 2.5 times as long as remaining bristles).

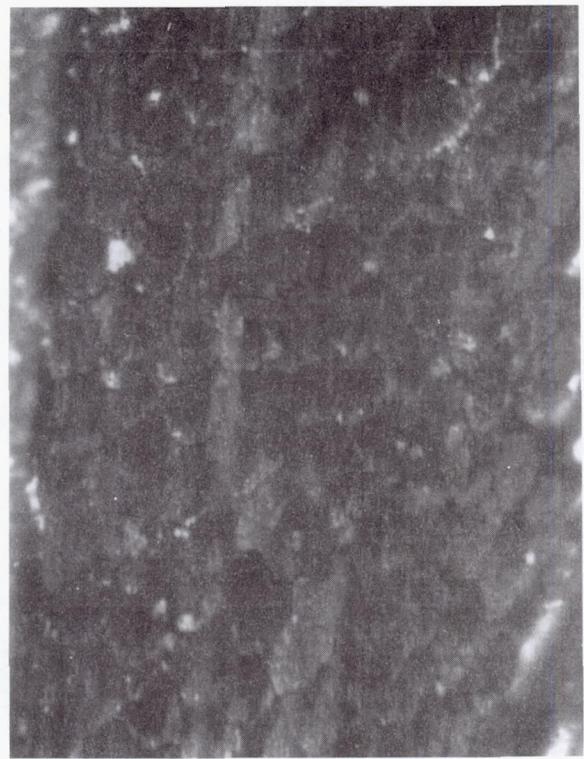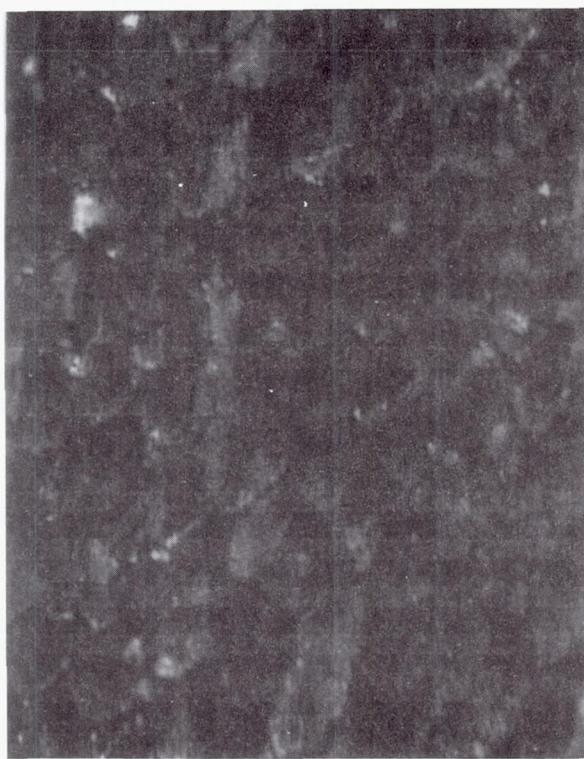Figure 24.—Geometry associated with installation, noted in post-test evaluation.

(d) Bristles caught within turbine blade gaps.

(e) Bristles straight and worn within brush.

Figure 24.—Continued.

(f) "Smearing" of bristle tips.

(g) Oxide scale on bristle.

Figure 24.—Concluded.

NON-CONTACTING GAS LUBRICATED FACE SEALS FOR HIGH p · v – VALUES

J. Glienicke, A. Launert, H. Schlums, and B. Kohring
Institute für Maschinenelemente und Fördertechnik
Technische Universität Braunschweig
Braunschweig, Germany

Abstract

The authors inform about recently developed mathematical fundamentals concerning the calculation of non–contacting gas lubricated face seals. They carried out extensive experiments using three different designs at pressures up to 10 MPa and sliding velocities up to 110 m/s. A comparison between the experimental results and the calculations indicates that a stable operation without wear can be ensured in all cases, provided that the materials and geometrical parameters of the seal have been properly chosen.

Introduction

Extreme operating conditions in gas process industry (high pressure, high surface velocity, hazardous and toxic gases) require dry running seals of high reliability with low leakage and minimal wear. Hence self–stabilizing face seals were developed, which are balanced aerostatically and controlled aerodynamically when in operation (refs. 1–9). To achieve a stable clearance between the rotating and the stationary face a self–acting geometry, similar to a narrow aerodynamic thrust bearing, is incorporated into one of the seal faces (ref. 10). As the shaft begins to rotate, the bearing generates a very thin gas film with high stiffness and an opening force, which separates the seal faces. Usually the self–acting geometry is located on the high pressure side.

The operational principle of such a self–stabilizing non–contacting face seal is illustrated in fig. 1: Any deviation in gap width from the position of equilibrium *(index 1)* causes changes in the pressure profile, which determines the opening force. If gap width increases *(2)*, the aerodynamic opening force decreases and vice versa *(3)*. This causes the gap width to automatically return to its equilibrium position. At present three self–acting surface patterns as shown in fig. 2 are used in industrial applications.

There has been a growing interest in these seals as components for process industry and other ranges (turbo compressors, expansion and cooling turbines etc.) in the last 15 years, but nevertheless there have been a certain lack of design fundamentals until recently. Therefore research projects were performed to obtain reliable, experimentally verified fundamentals for the design and calculation of gas lubricated face seals used at high p·v – values.

Theoretical Fundamentals

The isothermal compressible fluid flow in a sealing/lubricating gap is described by
  - the Navier – Stokes – equation,
  - the equation of continuity and
  - the equation of state (ideal gas)

with the boundary conditions and the simplifications commonly used in aerodynamic lubrication theory being applied. The generalized Reynolds equation results from this system of equations and is solved numerically to determine the pressure distribution in the sealing gap as well as the static and dynamic characteristics of gas lubricated face seals (ref. 11, 12).

Turbulence in the lubricating film may occure at very high surface velocities and high pressure differences. The effect of turbulence is represented by the two turbulence correction factors K_Θ and K_R, which are based on empirically derived turbulence models developed by Ng and Elrod as well as Constantinescu (ref. 13).

The generalized Reynolds differential equation is:

$$\frac{1}{r}\frac{\partial}{\partial\Theta}\left(\frac{\rho h^3}{\eta K_\Theta}\cdot\frac{\partial p}{\partial\Theta}\right)+\frac{\partial}{\partial r}\left(\frac{r\rho h^3}{\eta K_R}\cdot\frac{\partial p}{\partial r}\right)=6\omega r\frac{\partial\left(\rho h\right)}{\partial\Theta}+12r\frac{\partial\left(\rho h\right)}{\partial t} \qquad (1)$$

with:
p – pressure	ω – angular velocity
h – gap width	Θ – angular cordinate
η – dynamic viscosity	r – radial coordinate
ρ – density	t – time.

In solving the Reynolds equation numerically the mean film thickness and the pressures at the boundaries are held constant in each iteration. The pressure distribution $p(\Theta, r, t)$ is calculated whereby the stationary and transient contributions of the solution are computed separately. A conservative Finite – Difference – Method is used because of the discontinuities in the gap between the stationary and the rotating seal ring.

The gap opening force given by the integration of the pressure distribution is iterated, varying film thickness, until the equilibrium of opening and closing force is achieved (ref. 14). The friction force F_R is calculated by integrating the wall shear stress with respect to the seal face. The leakage (mass flow $\dot{m}$) results from the exit velocity times exit area and density. The linearized stiffness and damping coefficients (c_a, d_a) are determined by applying the method of small perturbation to the Reynolds equation.

Additionally the commercial FEM – program ANSYS (ref. 15) is coupled to this flow analysis program to estimate the influence of seal deformations on the characteristics.

For the design of gas lubricated face seals the effect of pressure and speed on leakage and gap width is of great importance. In the following the calculated characteristics of a gas lubricated face seal with spiral grooves and high pressure on the outer diameter are

presented. In this example it is assumed that the gas flow in the sealing gap is laminar and that the seal faces are parallel. The process medium is air.

The leakage of this spiral groove face seal shows nearly a linear increase with operating pressure and speed, fig. 3a. As shown in fig. 3b, the sealing gap decreases slightly with increasing pressure and increases with growing speed. At maximum operating pressure, $p_{op,max} = 10$ MPa, and max. speed, $n_{max} = 22\,000$ rpm, the gap width is $h = 2.5\ \mu$m. The resulting leakage mass flow of $\dot{m} = 1.45$ g/s is comparatively low. The seal is closed at low pressure difference and $n = 0$.

During operation an angular misalignment of the rotating seal ring and an axial shaft movement are always present. To provide good dynamic tracking ability between the stationary and the misaligned rotating ring the flexible support of the stationary ring in the housing allows angular and axial movements. To ensure stable operation it is essential, that the axial and angular stiffnesses of the gas film are very high and that the damping of the film is positive. With the chosen spiral groove design these requirements are met as shown in fig. 4.

Experimental Investigations

To verify the reliability of the developed design fundamentals series of comparative experiments using different complete gas lubricated face seals were carried out. The tests were performed with three seal designs at operating pressures p_{op} up to 10 MPa and sliding velocities v up to 110 m/s.

In fig. 5 the cross-section of the test rig is shown. The shaft is supported in ball bearings additionally equipped with a squeeze film damper on the side of the sealing unit. The test seals are arranged symmetrically to compensate the axial pressure force. Various sizes, designs and materials were tested for the seal rings, as well as different pattern for the self–acting structure and different balance ratios.

Test seal A (John Crane) is patterned with spiral grooves. The stationary face is manufactured from carbon – graphite and the rotating seal ring (outer diameter 148 mm) from tungsten carbide. The measured total leakage volume flow $\dot{V}_{tot}$ (fig. 6) increases very strong with speed and operating pressure and coincides quite well with the calculated values. The measured total power consumption P_{tot} (fig. 7) varies progressively with speed n and about linearly with pressure p; at a maximum speed of $n_{max} = 16\,000$ rpm and a maximum pressure of $p_{max} = 8$ MPa it reaches a value of $P_{tot} = 4$ kW. This high power consumption is due to highly turbulent flow at the surfaces of the rotating elements inside the pressurized chamber.

Test seal B (Pacific Wietz) uses a self – acting structure of symmetrical T – grooves. The material of the stationary ring is silicon carbide filled with graphite and that of the rotating ring is tungsten carbide (outer diameter 98 mm). The leakage characteristics (mass flow $\dot{m}$) of this seal (fig. 8a) are similar to those of seal A above, but the influence of speed is very small. To measure gap width during operation the stationary and rotating ring were modified. At the inner diameter of the stationary ring (atmospheric pressure side) two capacitance probes were mounted. The measured gap width h (fig. 8b) ranges from 2μm to 3.5μm across the entire operating range. The intersection of the measured lines is caused by deformations of the stationary ring. The results of calculation, which also takes into account the deformation of the sealing rings, agree quite well with the measurements.

The self–acting structure of test seal C (Feodor Burgmann) consists of circular V – grooves, which reach wedge shaped inwards (grooves depth is not constant). Here again the stationary ring is made of carbon and the rotating ring of silicon carbide (outer diameter 118 mm). As illustrated in fig. 9a the speed n very strongly influences the leakage $\dot{V}$ due to the high aerodynamic forces generated by the V – grooves. The effect of the operating pressure on leakage is at first very strong for low pressures (p_{op} <4 MPa) and decreases with higher pressures. The film thickness between the seal faces was measured by a capacitive probe. One of its electrodes was sputtered on the sealing face of the stationary ring (Al_2O_3). With no pressure difference across the seal it runs like a gas lubricated aerodynamic thrust bearing. For increasing operational pressure the film thickness decreases, fig. 9b. In operation the gap width h usually varies between the limits 2μm and 6μm.

Summary

In the investigated gas lubricated face seals a very narrow non–contacting sealing gap is realized, which is self–stabilizing. The theoretical fundamentals for a reliable design and optimization of the static and dynamic characteristics of these seals have been developed and are presented here, as well as in other recent publications (refs. 14, 16). The reliability of the method for calculating the characteristics of non–contacting gas lubricated face seals at high p·v – values has been verified by extensive comparative tests performed for three seal designs at operation pressures up to 10 MPa and sliding velocities up to 110 m/s. If the materials and geometric parameters of the sealing rings and the self–stabilizing patterns on the seal surface have been chosen properly, a non–contacting, stable and reliable operation without wear can be achieved.

Remarks

Some important problems of gas lubricated seals are not discussed here, for example: choked flow, energy dissipation, entrance and exit losses etc. These topics are discussed in other publications or else will be investigated in future projects.

Acknowledgements

References

1. Gabriel, R.P.: Fundamentals of Spiral Groove Noncontacting Face Seals.
   ASLE Preprint No. 78-AM-3D-1 (1978)

2. Pennink, H.: The Gas Lubricated Spiral Grooved Face Seal in the Process Industry.
   Proc. 14th Turbomachinery Symp., Texas 1985, pp. 59-64

3. Pugnet, J.M.; Bolusset, D.; Jehl, J.: The Application of Dry Seals and Active Magnetic Bearings to an Oil–Free Centrifugal Compressor.
   Proc. I. Mech. Engng. 201 (1987), pp. 35-42

4. Heinen, M.; Kotzur, J.; Turanskyj, L.: Experience with Gas–buffered Noncontacting Face Seals – GHH Design. Europ. Turbomachinery Symp., London 1986

5. Schöpplein, W.; Zeus, D.: Hochbelastete Gleitringdichtungen, öl– und gasgeschmiert, für Turboverdichter. VDI-Ber. Nr. 706, VDI-Verlag Düsseldorf 1988, pp. 129-153

6. Gasgeschmierte Gleitringdichtung John Crane Typ 28. John Crane GmbH, Fulda 1988

7. Pacific Gaspac – Gleitringdichtungen. Pacific Wietz GmbH & Co KG, Dortmund 1991

8. Netzel, J.P.: Seal Technology, a Control for Industrial Pollution.
   Lubr. Engng. 46 (1990), pp. 483-493

9. Müller, H.-K.; Falalejew, S.W.: Gasgeschmierte Gleitringdichtung als Lagerabdichtung für Flugtriebwerke. Konstruktion 43 (1991), pp. 31-35

10. Glienicke, J.; Launert, A.; Schlums, H.: Aerodynamische Lager für hohe Drehzahlen.
    Konstruktion 45 (1993), pp. 239-246

11. Launert, A.; Schlums, H.: Statische und dynamische Eigenschaften von Axialfederlagern und –gleitringdichtungen mit aerodynamischer Schmierung.
    Forsch.ber. Verbrennungskraftmasch. H. 460, Frankfurt/M. 1990

12. Hunger, H.: Berechnung der statischen und dynamischen Kennlinien aerodynamischer Federlager. Diss. Univ. Karlsruhe 1982

13. Constantinescu, V.N.: Basic Relationships in Turbulent Lubrication and Their Extension to Include Thermal Effects. Lubr. Technol. 95 (1973), pp. 147-154

14. Launert, A.; Schlums, H.: Grundlagen für die Weiterentwicklung von Axialfederlagern und –gleitringdichtungen mit aerodynamischer Schmierung. Forsch.ber. Verbrennungskraftmasch., Frankfurt/M. 1994

15. De Salvo, G.J.; Gorman, R.W.: ANSYS Engineering Analysis System – User's Manual. Swanson Analysis Systems Inc., Houston, Tex. 1989

16. Glienicke, J.; Launert, A.; Schlums, H.: Gasgeschmierte Axialgleitringdichtungen für hohe p·v – Werte. Konstruktion 46 (1994), pp. 17-23
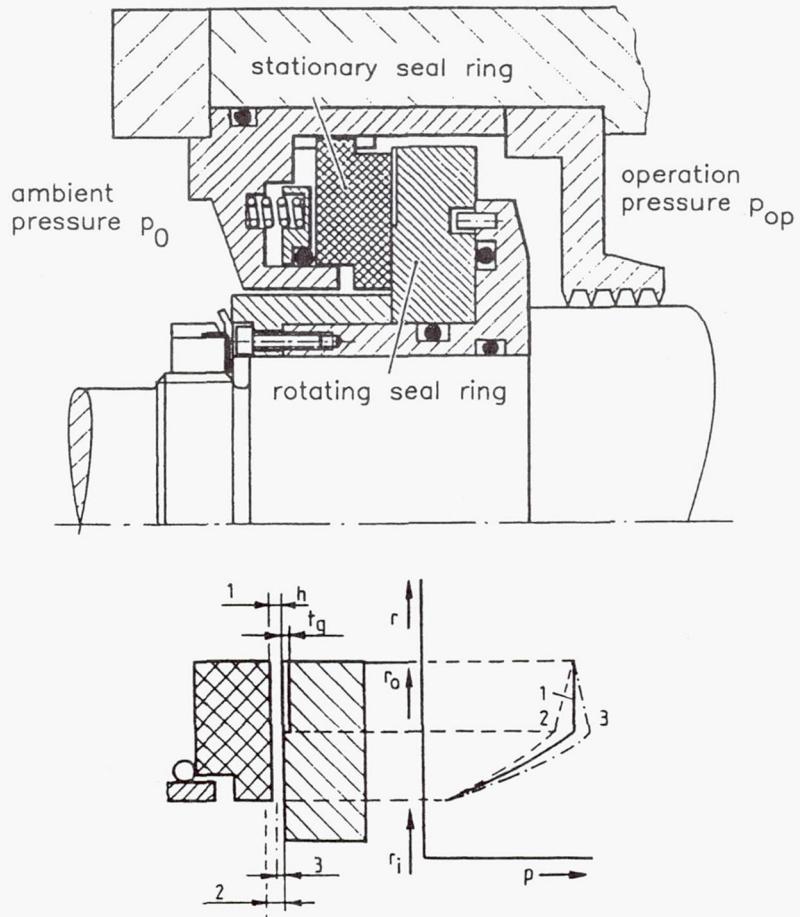
Figures

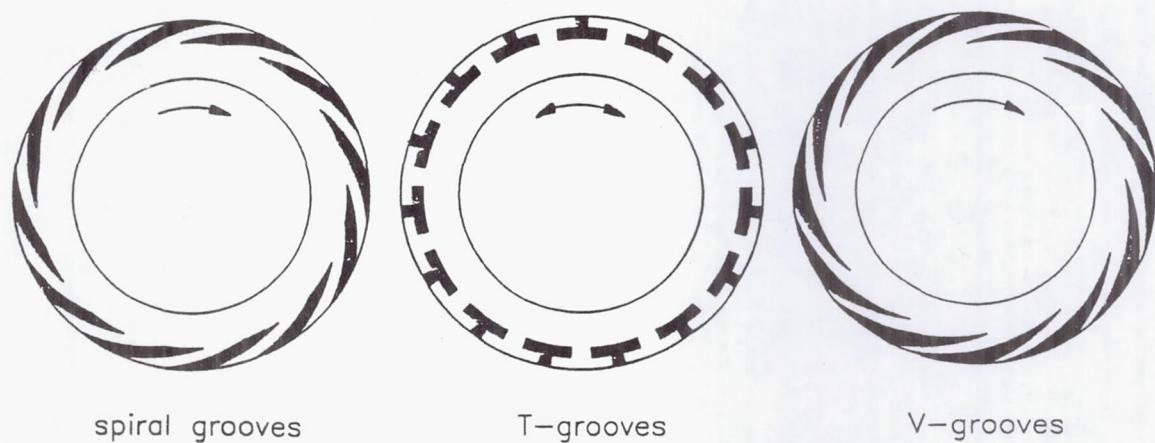Figure 1: Design and operational principle of gas lubricated face seals

spiral grooves   T–grooves   V–grooves

Figure 2: Self–acting geometries of gas lubricated face seals
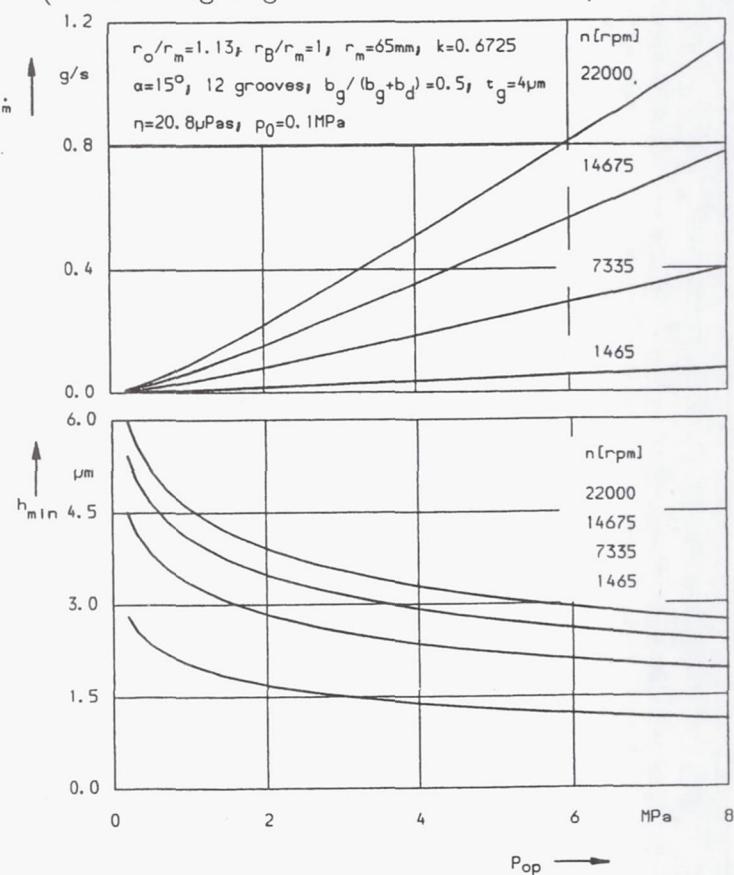($\longrightarrow$ Sealing ring's direction of rotation)

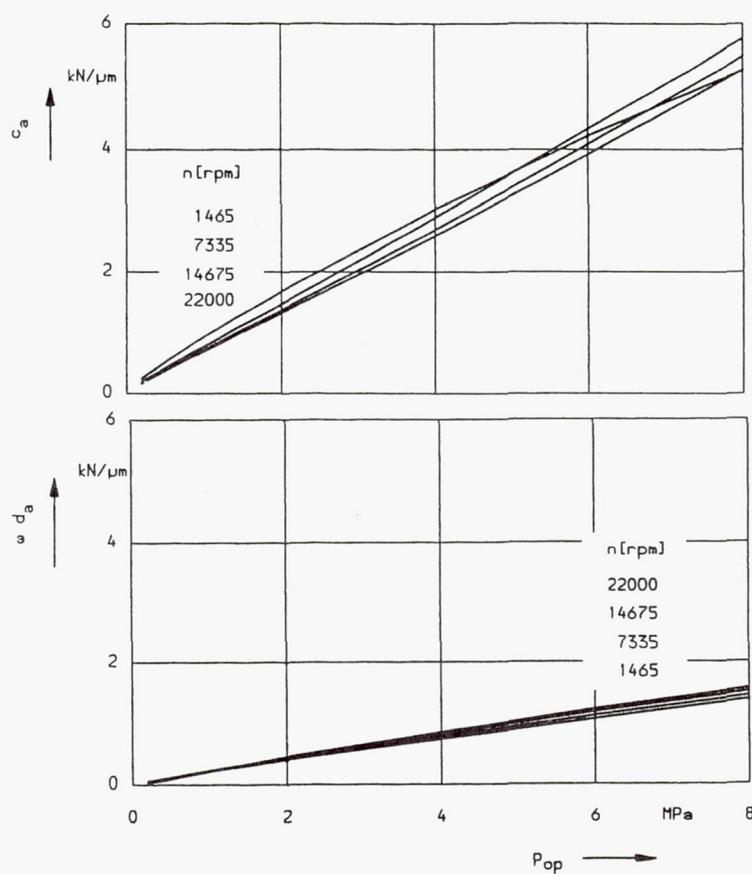Figure 3: Calculated leakage mass flow $\dot{m}(p_{op}, n)$ and film thickness $h(p_{op}, n)$ of a spiral groove face seal

Figure 4: Calculated axial stiffness $c_a(p_{op}, n)$ and
damping $d_a(p_{op}, n)$ (spiral groove face seal of fig. 3)

Buffer air

p_{op}
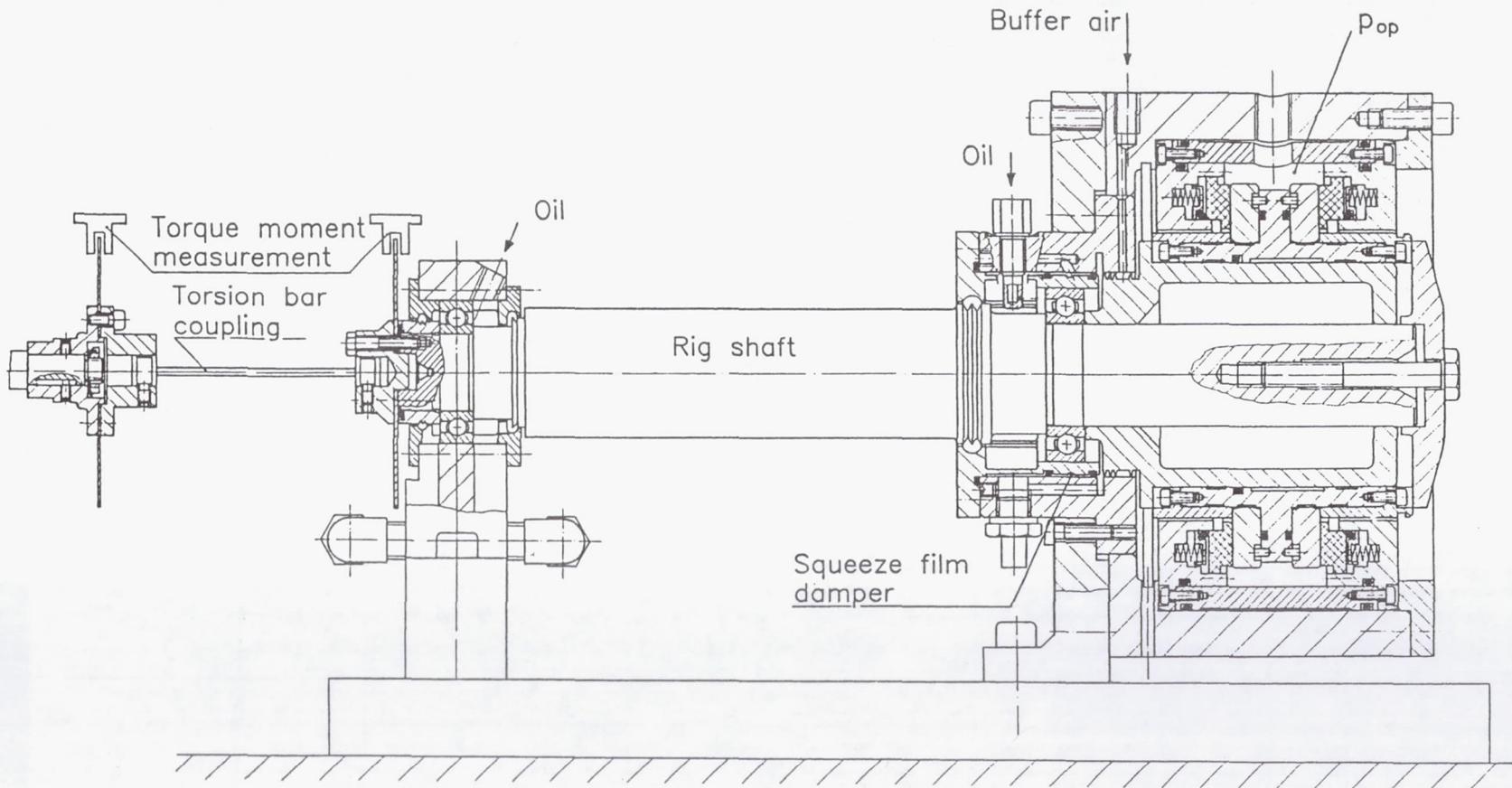
Oil

Oil

Torque moment
measurement

Torsion bar
coupling

Rig shaft

Squeeze film
damper

Figure 5: Test rig for gas lubricated face seals
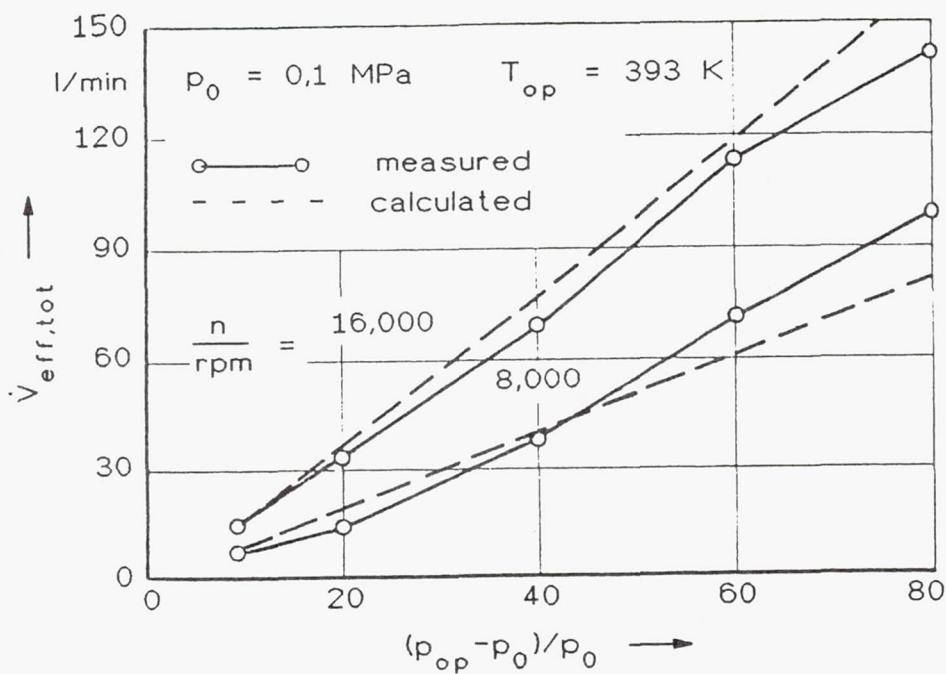($P_{max} = 7$ kW, $n = 0...30\,000$ rpm, $p_{op,max} = 10$ MPa)

Figure 6: Total leakage volume flow $\dot{V}_{tot}(p_{op}, n)$ of test seal A
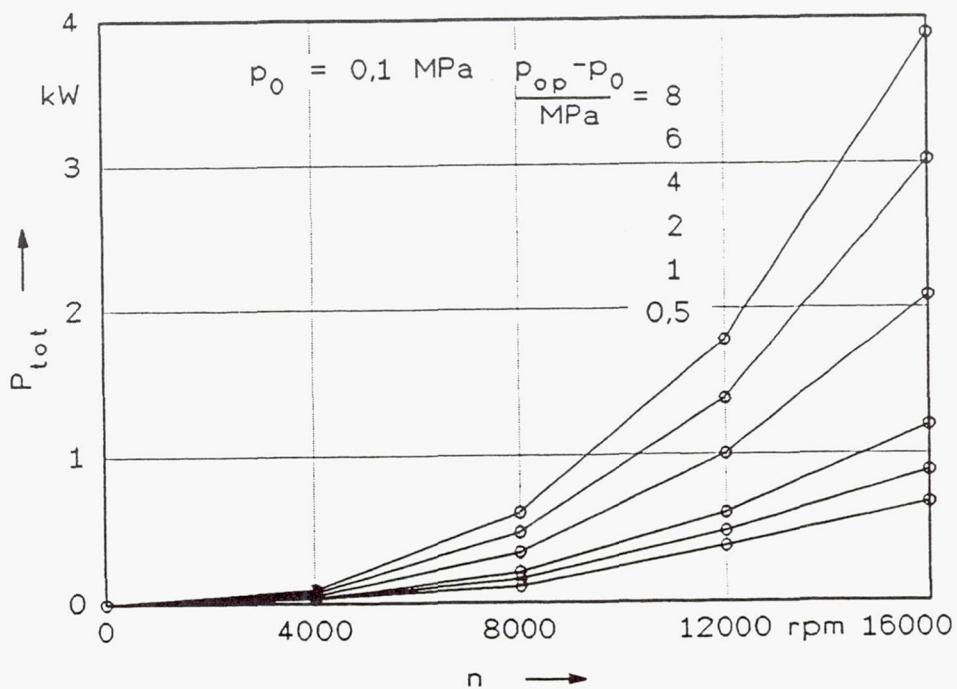

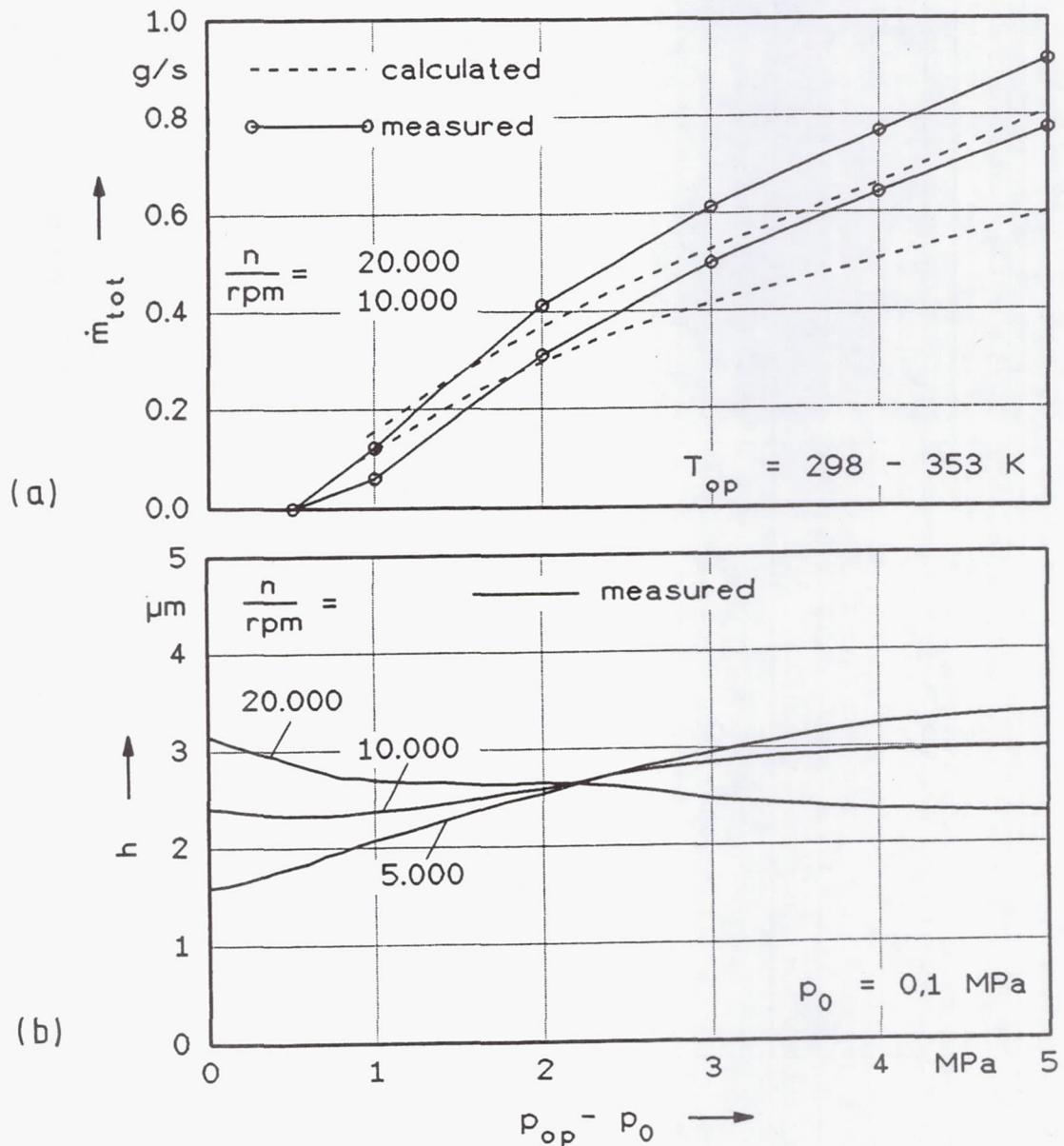Figure 7: Measured power consumption $P_{tot}(n, \Delta p)$ of test seal A

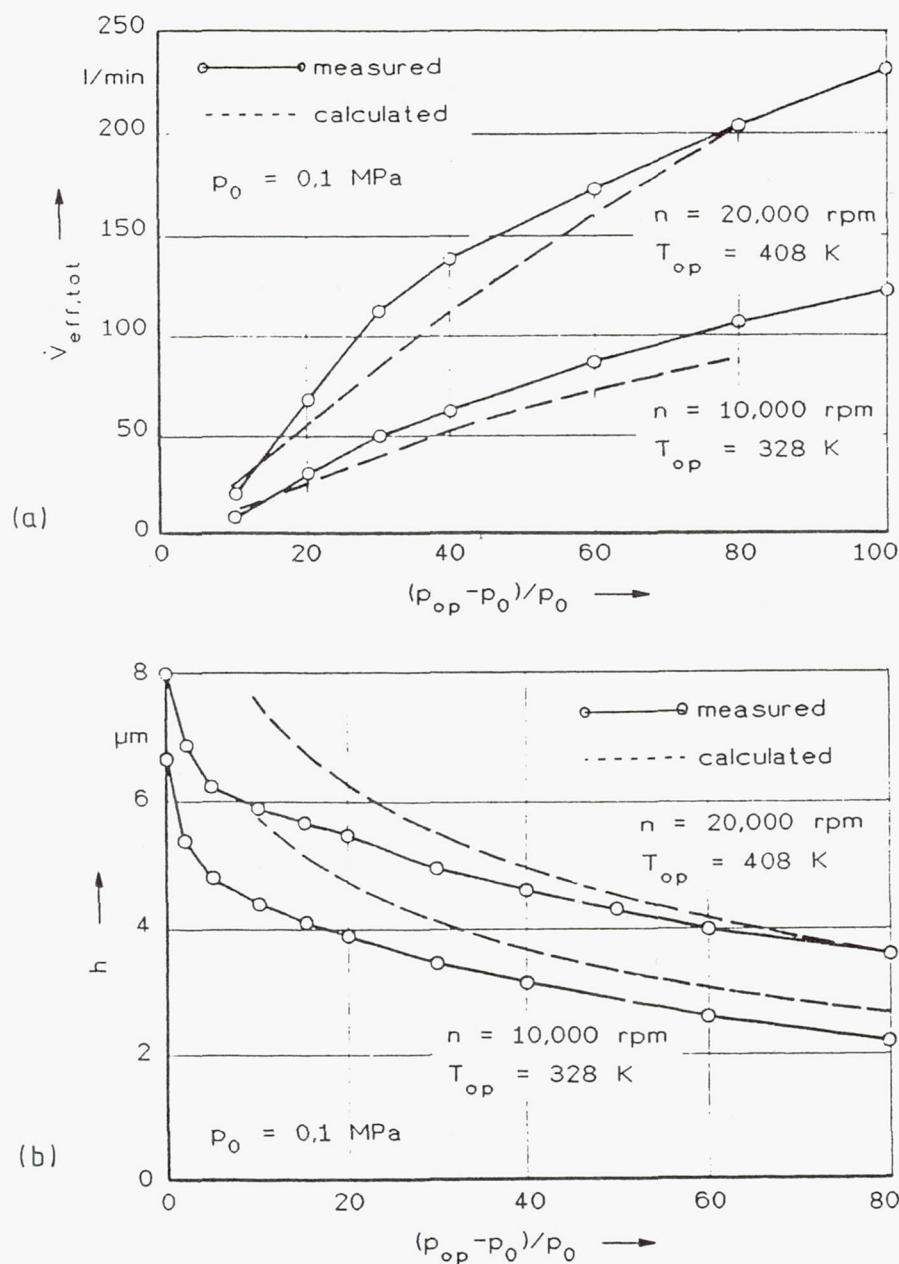Figure 8: Leakage $\dot{m}_{tot}(\Delta p, n)$ (a) and gap width $h(\Delta p, n)$ (b) of test seal B

Figure 9: Leakage $\dot{V}_{tot}(p_{op}, n)$ (a) and gap width $h(p_{op}, n)$ (b) of test seal C

REPORT DOCUMENTATION PAGE		Form Approved OMB No. 0704-0188

Public reporting burden for this collection of information is estimated to average 1 hour per response, including the time for reviewing instructions, searching existing data sources, gathering and maintaining the data needed, and completing and reviewing the collection of information. Send comments regarding this burden estimate or any other aspect of this collection of information, including suggestions for reducing this burden, to Washington Headquarters Services, Directorate for Information Operations and Reports, 1215 Jefferson Davis Highway, Suite 1204, Arlington, VA 22202-4302, and to the Office of Management and Budget, Paperwork Reduction Project (0704-0188), Washington, DC 20503.

1. AGENCY USE ONLY (Leave blank)	2. REPORT DATE July 1994	3. REPORT TYPE AND DATES COVERED Conference Publication

4. TITLE AND SUBTITLE

Seals Flow Code Development–93

5. FUNDING NUMBERS

WU–590–21–11

6. AUTHOR(S)

Anita D. Liang and Robert C. Hendricks, compilers

7. PERFORMING ORGANIZATION NAME(S) AND ADDRESS(ES)

National Aeronautics and Space Administration
Lewis Research Center
Cleveland, Ohio 44135–3191

8. PERFORMING ORGANIZATION REPORT NUMBER

E–8643

9. SPONSORING/MONITORING AGENCY NAME(S) AND ADDRESS(ES)

National Aeronautics and Space Administration
Washington, D.C. 20546–0001

10. SPONSORING/MONITORING AGENCY REPORT NUMBER

NASA CP–10136

11. SUPPLEMENTARY NOTES

Proceedings of a workshop held at NASA Lewis Research Center, Cleveland, Ohio. Responsible person, Robert C. Hendricks, organization code 5300, (216) 433–7507.

12a. DISTRIBUTION/AVAILABILITY STATEMENT

Unclassified - Unlimited
Subject Categories 16 and 99

12b. DISTRIBUTION CODE

13. ABSTRACT (Maximum 200 words)

Seals Workshop of 1993 code releases include SPIRALI—for spiral grooved cylindrical and face seal configurations; IFACE—for face seals with pockets, steps, tapers, turbulence, and cavitation; GFACE—for gas face seals with "lift pad" configurations; and SCISEAL—a CFD code for research and design of seals—cylindrical configuration. GUI (graphical user interface) and code usage was discussed with hands on usage of the codes, discussions, comparisons, and industry feedback. Other highlights for the Seals Workshop–93 include environmental and customer driven seal requirements; "what's coming"; and brush seal developments including flow visualization, numerical analysis, bench testing, T–700 engine testing, tribological pairing and ceramic configurations, and cryogenic and hot gas facility brush seal results. Also discussed are seals for hypersonic engines, dynamic results for spiral groove and smooth annular seals, and a three-wave journal bearing. Military engine goals include double thrust/weight, decrease SFC 40 percent, decrease secondary air flow leakage 60 percent, increase mainshaft speed 50 percent ; cited tests include 40 seals tested to 1200 °F, 1080 fps, 60 psid, and 0.0045 inch rotor runout with excursions to 0.019 inch for seals to 20 inches in diameter. Future activities will move toward face, lip, proprietary seals, and dynamics.

14. SUBJECT TERMS

Seals; Numerical; Code; Flow

15. NUMBER OF PAGES

393

16. PRICE CODE

A17

17. SECURITY CLASSIFICATION OF REPORT Unclassified	18. SECURITY CLASSIFICATION OF THIS PAGE Unclassified	19. SECURITY CLASSIFICATION OF ABSTRACT Unclassified	20. LIMITATION OF ABSTRACT

NSN 7540-01-280-5500

Standard Form 298 (Rev. 2-89)
Prescribed by ANSI Std. Z39-18
298-102